

**SOIL EROSION AND ITS MITIGATION: IMPROVEMENTS IN TESTING AND
MODELLING**

A Dissertation

by

ANNA SHIDLOVSKAYA

Submitted to the Graduate and Professional School of
Texas A&M University
in partial fulfillment of the requirements for the degree of

DOCTOR OF PHILOSOPHY

Chair of Committee,
Committee Members,

Head of Department,

Jean-Louis Briaud
Charles Aubeny
Mark Everett
Marcelo Sanchez
Zachary Grasley

December 2021

Major Subject: Civil Engineering

Copyright 2021 Anna Shidlovskaya

ABSTRACT

The objective of this research was to improve existing knowledge on soil erosion testing, modelling, classification, mitigation, and prediction of natural and improved soils for dam and levee engineering. An improved testing and data reduction procedure for the in-situ Borehole Erosion Test (BET) is proposed based on performing the BET at 13 locations. Nearly 250 erosion tests on natural and improved soils were performed in the Erosion Function Apparatus (EFA) in the Soil Erosion Laboratory at Texas A&M University to better understand the behavior of natural and improved soils under various conditions. Seventy-five tests out of the 250 EFA tests were performed on improved soils such as grass covered soils, lime-treated soils, enzyme-treated soils as well as riprap covered soils. All soils were classified for their erodibility including obtaining the entire erosion curve (erosion rate versus velocity and erosion rate versus shear stress), the critical shear stress and critical velocity, the erosion modulus. The efficiency of soil improvement methods was compared, and advantages and limitations for each method were identified. A new erosion model and erosion classification was developed and applied to natural and improved soils. The automated excel spreadsheet called TAMU-PEM (Prediction of Erosion Movement) was created which allows to estimate how much erosion can take place given the erosion function of the soil and the velocity vs time hydrograph for the water. The 250 erosion tests performed during this research were added to the existing TAMU-Erosion spread sheet along with an improved procedure. A

risk chart was proposed for earth dams, tailing dams, levees, and some other structures affected by erosion.

DEDICATION

I dedicate this dissertation to my father Valerij Kordakov, my mother, Tatiana Kordakova, and my daughter, Veronika Shidlovskaja, I am greatly indebted to you. Thank you for your constant support and unconditional love. I love you all dearly.

ACKNOWLEDGEMENTS

I would like to thank to my PhD advisor, Dr. Jean-Louis Briaud, for supporting me during this research. Dr. Briaud is one of the smartest people I know and the funniest advisor ever. I hope that I could be as intelligent, enthusiastic, and energetic as Dr. Briaud. Dr. Briaud has been supportive and has given me the freedom to pursue various projects during my education. Dr. Briaud has provided insightful discussions about the research. Moreover, he is my primary resource for getting my science and life questions answered. He is always cheering me up. I will forever be thankful to Dr. Briaud.

I wish to thank my other advisory committee members Dr. Charles Aubeny, Dr. Marcelo Sanchez, and Dr. Mark Everett for their contributions, valuable advice, excellent feedbacks, and insightful questions. I also would like to thank Dr. Hamn-Ching Chen from Department of Civil and Environmental Engineering and Ocean Engineering at Texas A&M University for his help and guiding on hydraulic part of research.

I also would like to thank many other people for their input and cooperation. They include Anna Timchenko, PhD student of Department of Civil and Environmental Engineering at Texas A&M University for her help with erosion testing and contributions to Sections 3.6 and 3.7. I would like to acknowledge Dr. Mostafa Bahmani, a former PhD student of Department of Civil and Environmental Engineering at Texas A&M University for his help with developing TAMU-PEM, the results of which are used in Section 9.4.

I wish to thank Mr. Todd Rivas and Mr. Jonathan AuBuchon from the U.S. Army Corp of Engineers, Dr. Paul Work and Dr. Daniel Livsey from the U.S. Geological Survey, and Dr. Eddy Langendoen from the U.S. Department of Agriculture for their contribution to Chapter 3 and continuous help and support throughout this research.

I would like to express my gratitude and appreciation to Dr. Chase Straw from the Department of Soil and Crop Sciences at Texas A&M University for providing help with grass sampling and testing as well as advising on the results.

I would also like to acknowledge Mr. Royal Marty from Substrata and Mr. Jon Sedgwick from Nature Plus, Inc. for providing enzymes for this research and for advising on conducting research, the College Station office of Terracon Consultants for helping with soil testing, and Mr. Weber from cbec eco engineering for help with the data used in Section 9.3. Finally, I would like to thank the staff and lab coordinators in the geotechnical engineering program at Texas A&M University, especially Ms. Laura Byrd Program Specialist in the Civil and Environmental Engineering Graduate Office, who helped during this research.

I am greatly indebted to my parents and my daughter, Veronika for their spiritually support in all the time of my education. I am very grateful to Cindy and Roy Robinson for providing emotional support and friendship that I needed, thank you. Thank all the horses, dogs, and cats for their unconditional love.

CONTRIBUTORS AND FUNDING SOURCES

The work was supported by a dissertation committee consisting of Professor Jean-Louis Briaud, Professor Charles Aubeny, Professor Marcelo Sanchez of the Zachry Department of Civil and Environmental Engineering, and Professor Mark Everett of the Department of Geology and Geophysics at Texas A&M University.

The Chapter 3 of this dissertation was performed as the Project “Assessing erosion resistance of bank materials on American and Sacramento Rivers” under the sponsorship of the United States Army Corps of Engineers (USACE), the United States Department of Agriculture, (USDA), and the United States Geological Survey (USGS).

The dissertation herein was supported by funds from the Buchanan Chair, the Soil Erosion Laboratory at Texas A&M University, the fellowship from Texas A&M University, the fellowships and scholarships from ASCE, DPI, and ADSC.

NOMENCLATURE

USGS	United States Geological Survey
USDA	United States Department of Agriculture
USACE	United States Army Corps of Engineers
FEMA	The Federal Emergency Management Agency
TAMU	Texas A&M University
NID	National Inventory of Dams
EPA	Environmental Protection Agency
ASCE	American Society of Civil Engineers
ASTM	American Society for Testing and Materials
ASDSO	Association of State Dam Safety Officials
CTNK	Contribution to New Knowledge
DPI	Deep Foundation Institute
ADSC	The International Association of Foundation Drilling

TABLE OF CONTENTS

	Page
ABSTRACT	ii
DEDICATION	iv
ACKNOWLEDGEMENTS	v
CONTRIBUTORS AND FUNDING SOURCES.....	vii
NOMENCLATURE.....	viii
TABLE OF CONTENTS	ix
LIST OF FIGURES.....	xiv
LIST OF TABLES	xxviii
1. INTRODUCTION.....	1
1.1. What is the problem?.....	1
1.1.1. Earth dams	3
1.1.2. Levees.....	6
1.1.3. Tailings dams	7
1.1.4. Bridges.....	8
1.2. Objectives of the research and approach.....	9
1.2.1. Task 1: Borehole Erosion Test	9
1.2.2. Task 2: Soil improvement	10
1.2.3. Task 3: New erosion model and classification	11
1.2.4. Task 5: Prediction of erosion movement.....	11
1.2.5. Task 6: TAMU-Erosion database.....	12
1.2.6. Task 7: Risk framework	12
2. BACKGROUND ON SOIL EROSION.....	14
2.1. Phenomenon of soil erosion	14
2.2. Some existing erosion tests	17
2.2.1. Laboratory Tests.....	18
2.2.2. In-situ Tests	26
2.3. Erosion models and erosion parameters.....	33

2.3.1. Erosion models	33
2.3.2. Erosion function	34
2.3.3. Slope of erosion function	35
2.3.4. Erosion rate.....	36
2.3.5. Critical velocity	36
2.3.6. Critical shear stress.....	37
2.3.7. Erosion category.....	39
3. EXPERIMENTAL RESEARCH ON SOIL ERODIBILITY	40
3.1. Existing knowledge on Borehole Erosion Test (BET).....	40
3.2. Field tests and sampling.....	44
3.3. Borehole Erosion Test (BET).....	47
3.3.1. Improved testing procedure.....	47
3.3.2. Improved data reduction procedure.....	52
3.4. Erosion Function Apparatus.....	59
3.4.1. Testing procedure	59
3.4.2. Data reduction procedure	61
3.5. Pocket Erodrometer Test	65
3.5.1. Testing procedure	65
3.5.2. Data reduction procedure	67
3.6. Erosion tests results.....	68
3.6.1. Erosion Function Apparatus (EFA).....	68
3.6.2. Pocket Erodrometer Test (PET).....	73
3.6.3. Borehole Erosion Test (BET).....	76
3.7. Summary and comparison of erosion tests.....	91
3.8. Precision, advantages, and limitations of BET	102
3.9. BET DOS and DON'T's	106
4. MITIGATION OF EROSION USING GRASS	109
4.1. Existing knowledge on grass erodibility	109
4.2. Obtaining shear stress equation.....	116
4.2.1. Manning versus Moody shear stress equation.....	116
4.2.2. Estimating Manning coefficient n	119
4.3. Grass characterization	125
4.4. Grass sampling	128
4.5. EFA test plan matrix	130
4.6. Results of EFA testing.....	133
4.6.1. Bermudagrass	133
4.6.2. St. Augustinegrass	136
4.6.3. Bahiagrass	139
4.6.4. Zoysiagrass	142
4.7. Summary of EFA grass testing.....	144

4.8. Effect of coverage on grass erodibility	150
4.9. Effect of health on grass erodibility	152
4.10. Effect of age on grass erodibility	154
4.11. Comparison of erodibility of grass and bare soil	157
4.12. Effect of roots on soil erodibility	160
4.13. Comparison of EFA results and full-scale levee overtopping test	162
5. MITIGATION OF EROSION USING ENZYMES	163
5.1. Existing knowledge on enzyme treatment	163
5.2. Materials and methods	170
5.3. EFA testing matrix	174
5.4. Results of EFA testing.....	178
5.5. Effect of PermaZyme and TerraZyme on soil erodibility	192
5.6. Effect of cure time on erodibility of enzyme-treated soil	193
5.7. Effect of the amount of clay particles on soil erodibility.....	195
6. MITIGATION OF EROSION USING ENZYMES	197
6.1. Existing knowledge on lime treatment.....	197
6.2. Materials and methods	201
6.3. EFA test plan matrix	203
6.4. Results of EFA testing.....	205
7. MITIGATION OF EROSION USING RIPRAP	211
7.1. Existing knowledge on riprap	211
7.2. Materials and methods	214
7.3. EFA test plan matrix	217
7.4. Results of EFA testing.....	219
7.5. Summary of EFA testing.....	228
7.6. Effect of compaction and wedging on soil erodibility	232
7.7. Effect of gravel/riprap thickness on soil erodibility.....	233
7.8. Effect of geotextile filter on soil erodibility.....	234
7.9. Comparison of EFA and full-scale tests.....	236
8. NEW EROSION MODEL AND APPLICATION	238
8.1. Existing knowledge on soil erosion models and classifications	238
8.2. Comparison of Hanson and Briaud erosion model and classification	242
8.3. New normalized power law model.....	245
8.4. New erosion classification chart	248
8.4.1. Shear stress	248
8.4.2. Velocity	254
8.5. Erosion classification	258

8.6. New erosion model for natural and improved soil.....	262
8.6.1. Clay	262
8.6.2. Silt	266
8.6.3. Sand.....	270
8.6.4. Grass	273
8.6.5. Riprap	276
8.6.6. Enzyme treated soil	279
8.6.7. Lime treated soil.....	282
8.7. Application of new erosion model	285
8.7.1. Prediction of levee erosion	287
8.7.2. Effect of overtopping cycling on erosion depth	294
8.7.3. Obtaining erosion depth for grass	295
8.7.4. Obtaining erosion depth for bare soil	296
8.7.5. Obtaining water velocity	297
9. PREDICTION OF EROSION MOVEMENT (TAMU-PEM).....	302
9.1. Existing knowledge on prediction of soil erosion.....	302
9.2. Procedure of TAMU-PEM (Prediction of Erosion Movement-Automated Excel Spread Sheet)	305
9.3. Procedure to obtain velocity hydrograph	309
9.3.1. Observed (past) hydrograph	310
9.3.2. Synthetic hydrograph	313
9.3.3. Synthetic/observed design hydrograph	314
9.4. Prediction of erosion movement by using TAMU-PEM	318
9.4.1. Silty Sand	318
9.4.2. Clay	319
9.4.3. Silt	320
9.4.4. Bermudagrass	321
9.4.5. Enzyme-treated soil.....	321
9.4.6. Lime-treated soil.....	322
9.5. Comparison of efficiency of remedial measures.....	323
9.6. Field calibration and scale factor	324
10. TAMU-EROSION DATABASE	327
10.1. Existing knowledge on TAMU-Erosion database.....	327
10.2. Structure of TAMU-Erosion	329
10.3. Advantages and limitations of TAMU-Erosion	331
10.4. New erosion tests	333
10.5. Improvement of TAMU-Erosion	333
11. RISK MANAGEMENT FOR EROSION OF DAMS AND LEVEES.....	338
11.1. Databases on case histories	338

11.1.1. Earth dams	338
11.1.2. Tailing dams	340
11.1.3. Levees.....	341
11.2. Risk and risk chart.....	343
11.2.1. General procedure to locate risk on risk chart.....	347
11.2.2. Procedure for risk location of earth dams	348
11.2.3. Procedure for risk location of tailing dams	351
11.2.4. Procedure for risk location of levees	353
11.2.5. Procedure for risk location of a set of structures subjected to hurricane....	355
11.2.6. Summary risk chart for dams and levees.....	357
11.3. Erosion risk category classification of dams.....	358
11.4. Recommendations for risk reduction	362
12. CONCLUSIONS, RECOMMENDATIONS AND CONTRIBUTIONS TO NEW KNOWLEDGE	364
12.1. Improvement of erosion testing and data reduction procedure	364
12.2. Mitigation of Erosion Using Grass	366
12.3. Mitigation of Erosion Using Enzymes.....	371
12.4. Mitigation of Erosion Using Lime	374
12.5. Mitigation of Erosion Using Riprap.....	376
12.6. Comparison between soil improvement methods	379
12.7. Advantages and limitations of soil improvement for erosion mitigation.....	382
12.8. New Erosion Model and Applications	383
12.9. TAMU-Prediction of Erosion Movement (TAMU-PEM)	384
12.10. Improvement of TAMU-Erosion Database.....	385
12.11. Risk Management for Erosion of Dams and Levees.....	385
12.12. Summary of contributions to new knowledge.....	386
OBJECTIVE I: Borehole Erosion Test.	386
OBJECTIVE II: Soil Improvement.	387
OBJECTIVE III: New Erosion Model and Classification.	387
OBJECTIVE IV: Prediction of Erosion Movement.....	388
OBJECTIVE V: TAMU-Erosion Database.	388
OBJECTIVE VI: Risk Framework.	388
REFERENCES.....	389

LIST OF FIGURES

	Page
Figure 1. Frequency of flooding along the United States coasts (adapted from www.epa.gov).....	2
Figure 2. Types of dams in the United State (modified from U.S. Army Corps of Engineers, “National Inventory of Dams,” 2020)	4
Figure 3. Causes of dam failures in the United States (modified from Association of State Dam Safety Officials, 2020).....	4
Figure 4. Some examples of failures of dams, levees, and bridges in the United States ...	5
Figure 5. Free body diagram of a soil particle or rock block in two different stages a) no-flow condition, b) with the water flow (adapted from Briaud, 2008)	15
Figure 6. Schematic diagram of the Erosion Function Apparatus and a photograph of the EFA (adapted from Briaud, 2013)	19
Figure 7. Erosion function for a sand and a low plasticity clay as measured in the EFA (adapted from Briaud, 2013).....	20
Figure 8. The photographs of laboratory version of JET (adapted from Wahl, 2010).....	21
Figure 9. A photograph of the sample setup (adapted from Briaud et al., 2019).....	23
Figure 10. A photograph of a Sedflume (reprinted from Briaud et al., 2019)	24
Figure 11. A schematic diagram of the BET (adapted from Briaud et al., 2017)	27
Figure 12. Borehole Erosion Test: (a) circulation of water in the borehole, (b) borehole caliper retracted and expanded (adapted from Briaud et al., 2017)...	27
Figure 13. A photograph of the PET device.....	28
Figure 14. ISEEP apparatus prototype at NCSU (adapted from Briaud et al., 2019)	30
Figure 15. A schematic diagram of the cutting head of the ISTD (adapted from Bergendahl and Kerenyi, 2016).....	31
Figure 16. Examples of erosion functions in natural scale.....	35
Figure 17. Erosion rate versus shear stress showing how to obtain slope of the erosion function (adapted from Briaud et al., 2019)	36

Figure 18. Erosion rate versus shear stress	37
Figure 19. Erosion rate versus shear stress showing critical shear stress definition (adapted from Briaud et. al., 2019).....	38
Figure 20. Erosion rate versus shear stress showing erosion category (adapted from Briaud et al., 2019)	39
Figure 21. Borehole radius profile at different stages during the BET for the clay site (adapted from Briaud et al., 2017).....	41
Figure 22. Borehole radius profile at different stages during the BET for the sand site (adapted from Briaud et al., 2017).....	42
Figure 23. Drilling site locations near Sacramento (adapted from USGS, 2020, https://www.usgs.gov/media/images/map-proposed-erosion-test-drill-sites) ..	45
Figure 24. General set up for the BET (Sacramento, April 2019)	48
Figure 25. BET testing procedure	49
Figure 26. Caliper calibration and installation in the borehole	50
Figure 27. Flowing the water for the BET	52
Figure 28. Moody chart for rough pipes (adapted from Munson, 2009).....	56
Figure 29. Extended Moody chart for very rough soil surfaces (modified from Moody 1944).....	56
Figure 30. The example of the BET data reduction Excel Spreadsheet (TAMU-BET) ..	58
Figure 31. Erosion Function Apparatus to measure erodibility (adapted from Briaud et al., 2001)	60
Figure 32. Example of EFA test result: erosion rate vs. velocity (SAC5A-Sample#25) .	62
Figure 33. Example of EFA test result: erosion rate vs. shear stress (SAC5A- Sample#25)	63
Figure 34. Calibrating the PET (adapted from Briaud, 2013).....	66
Figure 35. Snapshots of PET procedure (adapted from Briaud, 2013)	67
Figure 36. Erosion categories for soils based on the PET (adapted from Briaud et al., 2013).....	67

Figure 37. Erosion rate vs. velocity chart in natural scale (EFA tests results).....	68
Figure 38. Erosion rate vs. shear stress chart in natural scale (EFA tests results)	69
Figure 39. Erosion rate vs. velocity chart in log-log scale (EFA tests results)	69
Figure 40. Erosion rate vs. shear stress chart in log-log scale (EFA tests results).....	70
Figure 41. An example of erosion function for critical shear stress and slope definition.....	71
Figure 42. Slope of the EFA erosion function vs critical shear stress τ_c	72
Figure 43. Pocket Erodrometer Test results (velocity graph).....	75
Figure 44. Pocket Erodrometer Test results (shear stress graph)	76
Figure 45. BET radius profiles for “as drilled” and “after first flow run” (LAR2B).....	78
Figure 46. BET radius profiles for “as drilled” and “after first flow run” (LAR3B).....	78
Figure 47. BET radius profiles for “as drilled” and “after first flow run” (LAR5B).....	79
Figure 48. BET radius profiles for “as drilled” and “after first flow run” (LAR6B).....	79
Figure 49. BET radius profiles for “as drilled” and “after first flow run” (LAR7B).....	80
Figure 50. BET radius profiles for “as drilled” and “after first flow run” (LAR9B).....	80
Figure 51. BET radius profiles for “as drilled” and “after first flow run” (LAR10B).....	81
Figure 52. BET radius profiles for “as drilled” and “after first flow run” (LAR12B).....	81
Figure 53. BET radius profiles for “as drilled” and “after first flow run” (SAC1B).....	82
Figure 54. BET radius profiles for “as drilled” and “after first flow run” (SAC3B using water)	82
Figure 55. BET radius profiles for “as drilled” and “after first flow run” (SAC3B2 using mud)	83
Figure 56. BET radius profiles for “as drilled” and “after first flow run” (SAC7B).....	83
Figure 57. BET radius profiles for “as drilled” and “after first flow run” (SAC9B).....	84
Figure 58. Examples of radius, velocity, erosion rate, and shear stress profiles versus depth (TAMU-BET)	85

Figure 59. Erosion rate versus velocity chart for the first flow.....	86
Figure 60. Cluster of points from BET in each layer and back constructed erosion functions	87
Figure 61. Extending the erosion chart boundaries to create BET erosion function.....	87
Figure 62. Summary erosion chart for LAR1	93
Figure 63. Summary erosion chart for LAR2	94
Figure 64. Summary erosion chart for LAR3	94
Figure 65. Summary erosion chart for LAR4	95
Figure 66. Summary erosion chart for LAR5	95
Figure 67. Summary erosion chart for LAR6	96
Figure 68. Summary erosion chart for LAR7	96
Figure 69. Summary erosion chart for LAR9	97
Figure 70. Summary erosion chart for LAR10	97
Figure 71. Summary erosion chart for LAR12	98
Figure 72. Summary erosion chart for SAC1.....	98
Figure 73. Summary erosion chart for SAC3.....	99
Figure 74. Summary erosion chart for SAC5.....	99
Figure 75. Summary erosion chart for SAC7.....	100
Figure 76. Summary erosion chart for SAC8.....	100
Figure 77. Summary erosion chart for SAC9.....	101
Figure 78. Radius versus depth for drilling with water and mud	106
Figure 79. Critical velocity vs. time for poor, average, and good cover of grass (adapted from Hewlett et al., 1987).....	110
Figure 80. Erosion charts of bare clay and grass covered clay (adapted from Briaud, 2011).....	112

Figure 81. Full scale tests on a levee (adapted from Van der Meer, 2007).....	113
Figure 82. Full scale tests on a levee (adapted from Thornton, 2010).....	114
Figure 83. Full scale tests on a levee (adapted from Thornton, 2014).....	115
Figure 84. Shear stress by Moody versus shear stress by Manning	118
Figure 85. Moody friction factor f versus Manning value n	119
Figure 86. Erosion function for Bermudagrass with n -values	122
Figure 87. Erosion function for Bermudagrass with n -values and Moody roughness ...	123
Figure 88. Erosion function for BR7 with a range of Manning roughness n and Moody roughness.....	124
Figure 89. Mats of Bermudagrass and St. Augustinegrass	126
Figure 90. Sampling sites in College Station-Bryan (Texas).....	128
Figure 91. Sampling and measuring grass characteristics in College Station-Bryan (Texas)	129
Figure 92. Photographs of Bermudagrass	133
Figure 93. EFA testing of Bermudagrass (BR 7 and BR 6).....	134
Figure 94. Erosion functions in natural and logarithmic scale of Bermudagrass.....	135
Figure 95. Photographs of St. Augustinegrass	136
Figure 96. EFA testing of St. Augustinegrass (StA 3 and StA 5).....	137
Figure 97. Erosion functions in natural and logarithmic scale of St. Augustinegrass ...	138
Figure 98. Photographs of Bahiagrass.....	139
Figure 99. EFA testing of Bahiagrass (B3 and B4).....	140
Figure 100. Erosion functions in natural and logarithmic scale of Bahiagrass.....	141
Figure 101. Photographs of Zoysiagrass	142
Figure 102. EFA testing of Zoysiagrass (Z1 and Z3)	143
Figure 103. Erosion functions in natural and logarithmic scale of Zoysiagrass	143

Figure 104. Erosion rate versus velocity in natural scale of all grass types.....	146
Figure 105. Erosion rate versus shear stress in natural scale of all grass types	146
Figure 106. Erosion rate versus velocity in logarithmic scale of all grass types	147
Figure 107. Erosion rate versus shear stress in logarithmic scale of all grass types	147
Figure 108. Erosion thresholds of all grass types.....	148
Figure 109. Images of grass with showing percent coverage	150
Figure 110. Erosion rate versus shear stress of grass with different coverage.....	151
Figure 111. Critical velocity versus grass coverage.....	152
Figure 112. Bermudagrass of different quality/health in the EFA before testing	153
Figure 113. Erosion rate versus shear stress in logarithmic scale of green and brown Bermudagrass	154
Figure 114. Erosion rate versus shear stress in logarithmic scale of different age Bermudagrass	155
Figure 115. Erosion rate versus shear stress in logarithmic scale of different age Bermudagrass	156
Figure 116. Erosion rate versus shear stress in logarithmic scale of different age Zoysiagrass	157
Figure 117. Erosion rate versus shear stress in logarithmic scale of bare soil and grass	158
Figure 118. Summary erosion function showing erosion rate versus shear stress of bare soil and grass.....	158
Figure 119. Erosion rate versus shear stress in logarithmic scale of bare soil and reinforced soil with roots	161
Figure 120. Erosion rate versus shear stress for sand in 7 and 21 days (adapted from Shafii et al., 2018).....	167
Figure 121. Grain size distribution of soil for Experiment cluster 5 (ASTM D422 / ASTM C136)	171

Figure 122. Grain size distribution of soil for Experiment cluster 6 (ASTM D422 / ASTM C136)	171
Figure 123. Grain size distribution of soil for Experiment cluster 7 (ASTM D422 / ASTM C136)	172
Figure 124. Erosion functions of the experiment cluster 1	179
Figure 125. Erosion functions of the experiment cluster soil 2	179
Figure 126. Erosion functions of the experiment cluster soil 3	181
Figure 127. A photograph of the experiment cluster 3-AS-TZ-14	182
Figure 128. Erosion function of the kaolinite- and bentonite-based soil	184
Figure 129. Erosion functions of the untreated and enzyme-treated soils (Experiment cluster 2, Experiment cluster 3, and Experiment cluster 4)	185
Figure 130. Erosion functions of the untreated and enzyme-treated soils (Experiment cluster 5)	186
Figure 131. Erosion functions of the untreated and enzyme-treated soils (Experiment cluster 6)	187
Figure 132. Erosion functions of the untreated and enzyme-treated soils (Experiment cluster 7)	189
Figure 133. Erosion rate versus shear stress of TerraZyme-treated reconstituted soil (a) and PermaZyme-treated reconstituted soil (b)	192
Figure 134. Erosion rate versus shear stress of TerraZyme-treated natural soil (a) and PermaZyme-treated natural soil (b)	193
Figure 135. Erosion functions of the 7-days, 14-days, and 21-days TerraZyme-treated reconstituted soil (Experiment cluster 3)	194
Figure 136. Erosion functions of the 7-days, 14-days, and 21-days PermaZyme-treated reconstituted soil (Experiment cluster 3)	194
Figure 137. Erosion functions of the 7-days and 14-days TerraZyme- and PermaZyme-treated natural soil (Experiment cluster 7)	195
Figure 138. Erosion functions of the natural soil with 10% and 20% additional clay particles (Experiment clusters 6 and 7)	196

Figure 139. Erosion functions of untreated and lime-treated soil (adapted from Herrier, 2012b)	200
Figure 140. Erosion functions of the untreated and treated soil (adapted from Bennabi et al., 2016)	201
Figure 141. Erosion functions of the Experiment cluster 1-AS-LM.....	206
Figure 142. Critical velocity of lime-treated soil versus cure time	206
Figure 143. Erosion functions of the Experiment cluster 2-NS-LM.....	208
Figure 144. Critical velocity versus mean grain size (adapted from Briaud et al., 2008)	212
Figure 145. Critical shear stress versus mean grain size (adapted from Briaud et al., 2008)	212
Figure 146. Photograph of gravel used for EFA testing	215
Figure 147. Photograph of geotextile and sand used for EFA testing.....	215
Figure 148. Grain size distribution curve for clay	216
Figure 149. Erosion rate versus velocity for Experiment cluster 1	220
Figure 150. Erosion rate vs. velocity for Experiment clusters 1-R in logarithmic scale	221
Figure 151. Erosion rate versus velocity for Experiment cluster 1 (no filter).....	224
Figure 152. Photographs of the Experiment cluster 1-S-GTF1-1R. Test 1.....	225
Figure 153. Photographs of the Experiment cluster 1-S-GTF1-1R. Test 2.....	226
Figure 154. Photographs of the Experiment cluster 2-C-GTF1-1R	227
Figure 155. Erosion rate versus velocity for Experiment cluster 2 (with filter)	228
Figure 156. Erosion rate vs. velocity in natural scale for all EFA tests	229
Figure 157. Erosion rate vs. shear stress in natural scale for all EFA tests.....	230
Figure 158. Erosion rate vs. velocity in logarithmic scale for all EFA tests.....	230
Figure 159. Erosion rate vs. shear stress in logarithmic scale for all EFA tests	231

Figure 160. Difference between the “wedged” arrangement (a) and the loose arrangement (b).....	233
Figure 161. Erosion rate vs. velocity for Experiment clusters 1-S-1R/2R/3R in natural scale	234
Figure 162. Erosion rate vs. velocity for Experiment clusters 1-S-1R/2R/3R in logarithmic scale	234
Figure 163. Erosion rate vs. shear stress in logarithmic scale with no filter and with filter.....	235
Figure 164. Erosion rate vs. velocity in logarithmic scale with no filter and with filter	236
Figure 165. Critical velocity versus mean grain size (adapted from Briaud, 2008).....	237
Figure 166. Erosion function with erosion parameters	239
Figure 167. Erosion category based on critical shear stress (adapted from Hanson and Simon 2001).....	239
Figure 168. Erosion category chart with some parameters (adapted from Briaud, 2001)	240
Figure 169. Briaud chart with Hanson boundaries.....	243
Figure 170. Hanson boundaries on Briaud chart in natural scale.....	244
Figure 171. Hanson chart with Briaud boundaries (modified from Hanson and Simon, 2001)	245
Figure 172. Erosion function for the new erosion model (erosion rate vs. shear stress)	247
Figure 173. Erosion function for the new erosion model (erosion rate vs. velocity)	247
Figure 174. Erosion rate vs. shear stress (modified from Briaud 2001)	250
Figure 175. New erosion shear stress chart.....	251
Figure 176. Shear-based erosion modulus (α) vs. critical shear stress (τ_c) in semi-logarithmic scale	253
Figure 177. Erosion rate vs. velocity (modified from Briaud 2001).....	255
Figure 178. New erosion velocity chart	256

Figure 179. Velocity-based erosion modulus β vs. critical shear stress τ_c in semi-logarithmic scale	258
Figure 180. Different shapes of erosion function.....	261
Figure 181. New shear-based erosion classification chart for clay.....	264
Figure 182. New velocity-based erosion classification chart for clay	265
Figure 183. Shear-based erosion modulus (α) vs. critical shear stress (τ_c) in semi-logarithmic scale for clay.....	265
Figure 184. Velocity-based erosion modulus (β) vs. critical velocity (v_c) in semi-logarithmic scale for clay.....	266
Figure 185. New shear stress-based erosion classification chart for silt.....	268
Figure 186. New velocity-based erosion classification chart for silt	268
Figure 187. Shear stress-based erosion modulus (α) vs. critical shear stress (τ_c) in semi-logarithmic scale for silt	269
Figure 188. Velocity-based erosion modulus (β) vs. critical velocity (v_c) in semi-logarithmic scale for silt	269
Figure 189. New shear stress-based erosion classification chart for sand	271
Figure 190. New velocity-based erosion classification chart for sand.....	271
Figure 191. Shear stress-based erosion modulus (α) vs. critical shear stress (τ_c) in semi-logarithmic scale for sand	272
Figure 192. Velocity-based erosion modulus (β) vs. critical velocity (v_c) in semi-logarithmic scale for sand.....	272
Figure 193. New shear stress-based erosion classification chart for grass	274
Figure 194. New velocity-based erosion classification chart for grass.....	275
Figure 195. Shear stress-based erosion modulus (α) vs. critical shear stress (τ_c) in semi-logarithmic scale for grass	275
Figure 196. Velocity-based erosion modulus (β) vs. critical velocity (v_c) in semi-logarithmic scale for grass	276
Figure 197. New shear stress-based erosion classification chart for riprap	277

Figure 198. New velocity-based erosion classification chart for riprap.....	278
Figure 199. Shear stress-based erosion modulus (α) vs. critical shear stress (τ_c) in semi-logarithmic scale for riprap.....	278
Figure 200. Velocity-based erosion modulus (β) vs. critical velocity (v_c) in semi-logarithmic scale for riprap.....	279
Figure 201. New shear stress-based erosion classification chart for enzyme treated soil.....	280
Figure 202. New velocity-based erosion classification chart for enzyme treated soil ...	281
Figure 203. Shear stress-based erosion modulus (α) vs. critical shear stress (τ_c) in semi-logarithmic scale for enzyme treated soil	281
Figure 204. Velocity-based erosion modulus (α) vs. critical shear stress (τ_c) in semi-logarithmic scale for enzyme treated soil	282
Figure 205. New shear stress-based erosion classification chart for lime treated soil ...	283
Figure 206. New velocity-based erosion classification chart for lime treated soil	284
Figure 207. Shear stress-based erosion modulus (α) vs. critical shear stress (τ_c) in semi-logarithmic scale for lime treated soil.....	284
Figure 208. Velocity-based erosion modulus (α) vs. critical shear stress (τ_c) in semi-logarithmic scale for lime treated soil	285
Figure 209. Shear stresses on levee surface (adapted from Briaud et al., 2008).....	286
Figure 210. Shear stress over critical shear stress τ/τ_c versus time t	288
Figure 211. Depth of erosion versus overtopping time (Scenario 1)	289
Figure 212. Shear stress / critical shear stress versus overtopping time (Scenario 2 and 3)	290
Figure 213. Depth of erosion versus overtopping time (Scenario 2 and 3)	293
Figure 214. Shear stress vs. time (Scenario 2 and 3)	294
Figure 215. Levee overtopping problem (modified from Briaud, 2020)	299

Figure 216. Brazos River verification of prediction with field critical velocity of 0.83 m/s. (a) first matching period, (b) second prediction period (adapted from Briaud and Montalvo-Bartolomei, 2014)	304
Figure 217. Erosion function (erosion rate vs. velocity).....	306
Figure 218. Velocity hydrograph (after Briaud, 2020)	307
Figure 219. Erosion function (erosion rate vs. velocity) for SAC-5	308
Figure 220. Map of Sacramento showing a location of the stream gage USGS 11446500 American River Fair Oaks gage, California (adapted from USGS website, accessed 2020).....	311
Figure 221. Flow hydrograph for the stream gage USGS 11446500 (modified from USGS website, accessed 2020).....	312
Figure 222. Velocity hydrograph for LAR-7	313
Figure 223. An example of synthetic flow hydrograph.....	314
Figure 224. Velocity vs. discharge curve for LAR-7 (modified from M. Weber, received from Todd Rivas, 2020)	316
Figure 225. Synthetic flow hydrograph.....	317
Figure 226. Synthetic velocity hydrograph	317
Figure 227. Erosion curve (a) and erosion movement (b) for silty sand.....	319
Figure 228. Erosion curve (a) and erosion movement (b) for clay	320
Figure 229. Erosion curve (a) and erosion movement (b) for silt	320
Figure 230. Erosion curve (a) and erosion movement (b) for grass.....	321
Figure 231. Erosion curve (a) and erosion movement (b) for enzyme treated clayey sand	322
Figure 232. Erosion curve (a) and erosion movement (b) for lime treated soil	323
Figure 233. Erosion movement versus time for different remedial measures.....	324
Figure 234. Simplified cross-section using the 2006/2008 topo surface and the 2017 surface for LAR 7 (Courtesy of Todd Rivas, USACE, Sacramento District, 2020).....	325

Figure 235. An image of the introductory page of TAMU-Erosion (TAMU-Erosion, 2021)	328
Figure 236. An image of the TAMU-Erosion inventory page (TAMU-Erosion, 2021)	330
Figure 237. Normalized erosion rate versus normalized shear stress showing shear stress-based erosion modulus definition	335
Figure 238. Shear stress-based erosion modulus versus critical shear stress	335
Figure 239. Normalized erosion rate versus normalized velocity showing velocity-based erosion modulus definition	337
Figure 240. Velocity-based erosion modulus versus critical velocity	337
Figure 241. Civil engineering risk (adapted from Whitman 1984, Marr 1995, Christian, Baecher 2003, Briaud and Yao 2013, Gilbert 2017).....	345
Figure 242. Risk framework (adapted from USACE Levee Safety Portfolio Report 2018)	346
Figure 243. Risk chart for earth dams (for fatalities)	350
Figure 244. Risk chart for earth dams (for dollars lost)	351
Figure 245. Risk chart for world tailing dams (annual probability versus fatalities).....	353
Figure 246. Risk chart for levees (annual probability versus fatalities).....	354
Figure 247. Risk chart for levees (annual probability versus dollars lost).....	355
Figure 248. Risk chart for hurricane (annual probability versus fatalities).....	356
Figure 249. Risk chart for hurricane (annual probability versus dollars lost).....	356
Figure 250. Summary risk chart for earth and tailing dams, levees, and hurricane (annual probability versus fatalities)	357
Figure 251. Summary risk chart for earth and tailing dams, levees, and hurricane (annual probability versus dollars lost).....	358
Figure 252. An example of a dam showing the erosion categories.....	359
Figure 253. Cross section through Teton Dam (adapted from Seed and Duncan, 1981)	360

Figure 254. Erosion chart showing dams categories (adapted from Briaud, 2021)	362
Figure 255. Summary of erosion rate versus velocity in logarithmic scale of grass.....	366
Figure 256. Summary of erosion rate versus shear stress in logarithmic scale of grass	367
Figure 257. Summary of erosion rate versus velocity in logarithmic scale of enzyme-treated soil.....	371
Figure 258. Summary of erosion rate versus shear stress in logarithmic scale of enzyme-treated soil.....	372
Figure 259. Summary of erosion rate versus velocity of the lime-treated soil	375
Figure 260. Summary of erosion rate versus shear stress of the lime-treated soil.....	375
Figure 261. Summary of erosion rate versus velocity of riprap	376
Figure 262. Summary of erosion rate versus shear stress of riprap	377

LIST OF TABLES

	Page
Table 1. The advantages and limitations of the EFA (adapted from Briaud et al., 2019)	20
Table 2. The advantages and limitations of the JET (adapted from Briaud et al., 2019).....	22
Table 3. The advantages and limitations of the HET (adapted from Briaud et al., 2019)	23
Table 4. The advantages and limitations of the Sedflume (adapted from Briaud et al., 2019)	25
Table 5. The advantages and limitations of the BET	28
Table 6. The advantages and limitations of the PET (adapted from Briaud, 2013).....	29
Table 7. The advantages and limitations of the ISEEP (adapted from Briaud et al., 2019)	30
Table 8. Summary of the erosion tests (adapted from Briaud et al., 2019).....	32
Table 9. Some of erosion tests with information about their application setup (adapted from Briaud et al., 2019).....	32
Table 10. Flow, velocity, and time for the BET at clay site (adapted from Briaud et al., 2017)	41
Table 11. Flow, velocity, and time for the BET at sand site (adapted from Briaud et al., 2017)	43
Table 12. Samples tested in the EFA and PET	46
Table 13. BET testing borehole’s locations	47
Table 14. Critical shear stress and slope of erosion function measured in EFA tests.....	71
Table 15. Pocket Erodrometer Test (PET) results	74
Table 16. Critical velocity and critical shear stress inferred from BET.....	88
Table 17. Critical shear stress inferred from BET tests and corresponding EFA values	101

Table 18. Average values of the relative variation radius ratio RVR for all BET locations.....	103
Table 19. Average values of the relative variation flow ratio RVF for all BET locations.....	104
Table 20. Critical erosion parameter (adapted from Dean et al., 2010).....	111
Table 21. Values of Manning roughness n for grass.....	120
Table 22. Some characteristics and features of grass (adapted from Chalmers and McAfee; The LawnInstitute, 2020; Schery, R.W. 1973).....	127
Table 23. EFA test plan matrix	131
Table 24. Erosion parameters of Bermudagrass.....	136
Table 25. Erosion parameters of St. Augustinegrass	139
Table 26. Erosion parameters of Bahiagrass	141
Table 27. Erosion parameters of Zoysiagrass	144
Table 28. Summary of erosion parameters of all tested grass in the EFA	149
Table 29. Erosion parameters of grass with different coverage.....	151
Table 30. Erosion parameters of grass and bare soil.....	159
Table 31. Erosion parameters of bare soil and reinforced soil with roots.....	161
Table 32. Velocity detachment threshold for grass (modified from Thornton et al. 2010, 2014, Van der Meer 2007).....	162
Table 33. Matrix of EFA testing experiment clusters	174
Table 34. The properties of the untreated and enzyme treated soils	190
Table 35. Matrix of EFA testing experiment clusters	203
Table 36. Properties of the untreated and lime treated soils	209
Table 37. Properties of geotextile SoilTain PP 105/105DW (adapted from Huesker, 2020).....	215
Table 38. Properties of clay.....	217

Table 39. Matrix of EFA testing Experiment clusters.....	218
Table 40. Erosion parameters of all samples.....	232
Table 41. Threshold velocities and shear stress associated with each erosion category (adapted from Briaud, 2001).....	241
Table 42. Advantages and limitations of new erosion model	248
Table 43. Calculations for obtaining new erosion shear stress chart	251
Table 44. Calculations for obtaining new erosion velocity chart.....	256
Table 45. Classification of soils based on new model (shear stress chart)	260
Table 46. Classification of soils based on new model (velocity chart).....	260
Table 47. Summary classification of soils based on new model (shear stress and velocity charts).....	261
Table 48. Depth of erosion of the levee for different cases	293
Table 49. Discharge hydrograph for the stream gage USGS 11446500 American River Fair Oaks CA, USGS (15-25 February 1986).....	311
Table 50. Discharge and velocity for LAR-7 (obtained from M. Weber, 2020).....	315
Table 51. The erosion movement for different soils and grass (field and laboratory) ...	326
Table 52. The inventory of the EFA tests added to TAMU-Erosion	333
Table 53. Target risk levels for the United States (adapted from Briaud et al. 2012)....	345
Table 54. Target risk levels for the United States (adapted from Timchenko, Shidlovskaya, Briaud, 2021).....	350
Table 55. Description of the Teton Dams zone materials with proposed erosion categories (adapted from Briaud, 2021)	361
Table 56. Efficiency of soil improvement methods (based on three components)	380
Table 57. Advantages and limitations of soil improvement methods	382

1. INTRODUCTION

1.1. What is the problem?

Soil erosion is a major problem in civil engineering especially during floods and hurricanes. It is involved in bridge scour, meander migration, levee or dam overtopping, internal erosion of earth dams, surface erosion of embankments, and cliff erosion. The changes in the global climate have also resulted in greater fluctuations in temperature and precipitation causing acceleration of soil erosion by water. As the sea level rises, floods become more common, and the infrastructure elements suffer. According to the Environmental Protection Agency (EPA), the rate of flooding along the East and Gulf Coasts of the United States is increasing (www.epa.gov). Figure 1 shows the average number of days per year in which coastal waters rose above a local threshold. Every site shown has experienced an increase in coastal flooding since the 1950s. The New York Times (12 May 2021) published that in 2010s floods are at least three times more common than they were in the 1950s.

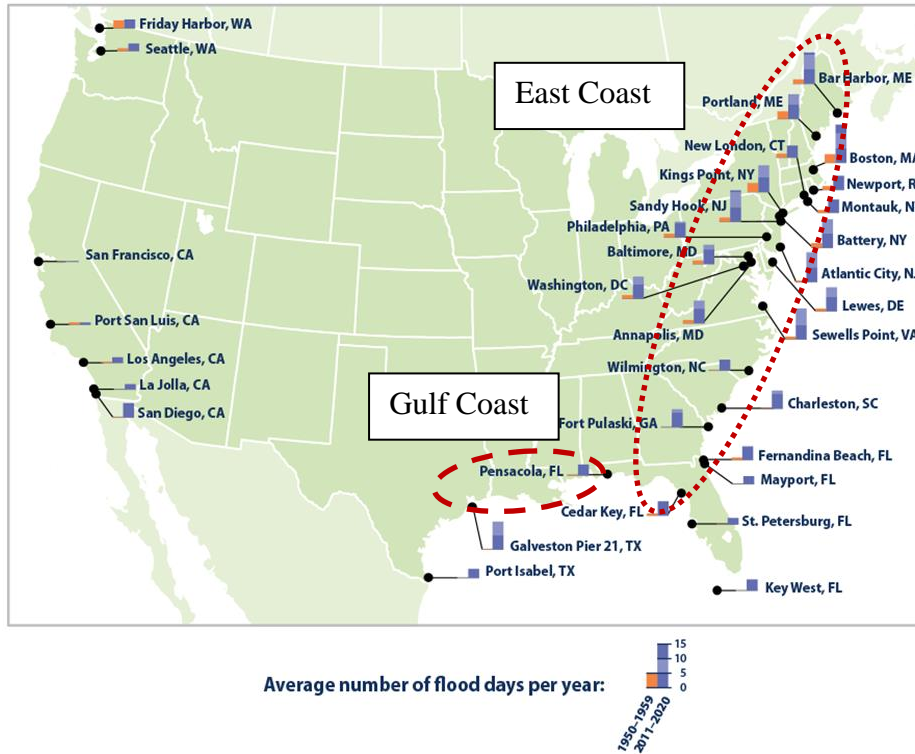


Figure 1. Frequency of flooding along the United States coasts (adapted from www.epa.gov)

The 2021 Infrastructure Report Card prepared by the American Society of Civil Engineers (ASCE) found that the national grade for infrastructure is a C- (American Society of Civil Engineers, 2021 Infrastructure Report Card). By comparison, the 2017 report cards issued infrastructures an overall grade of D+ (American Society of Civil Engineers, 2017 Infrastructure Report Card). In the 2021 report card, levees and dams get a grade of “D”, and bridges a grade of C. The average age of the Nation’s dams is 57 years. The ASCE 2021 report card shows that by 2030, seven out of ten dams in the country will be over 50 years old. The Nation’s levees are, on average, 57 years old. The average age of 42% of all bridges is at least 50 years old.

1.1.1. Earth dams

Based on the National Inventory of Dams maintained by U.S. Army Corps of Engineers, there are approximately 91,500 dams in the US, 79,700 of which are earth dams (Figure 2) (U.S. Army Corps of Engineers, “National Inventory of Dams,” 2020). According to the ASCE 2021 Infrastructure Report Card, about 15,600 dams in the United States are identified as high-hazard potential dams and approximately 11,340 dams are classified as significant-hazard potential dams. The failure of a high-hazard potential dam is anticipated to cause a loss of life. Meanwhile, a failure of a significant-hazard potential dams would likely cause significant economic damage but not necessary loss of life. The number of high hazard-potential dams has more than doubled since 2000s (American Society of Civil Engineers, 2021 Infrastructure Report Card).

According to the Association of State Dam Safety Officials (ASDSO), the main causes of dam failure are overtopping, pipping, and slope stability (Figure 3) (Association of State Dam Safety Officials, 2020). One of the most catastrophic earth dam failures was Canyon Lake Dam failure in South Dakota in 1972 (Figure 4). This failure was due to overtopping and led to 238 fatalities and US2020 \$1,021.6 million of losses (Association of State Dam Safety Officials, 2020).

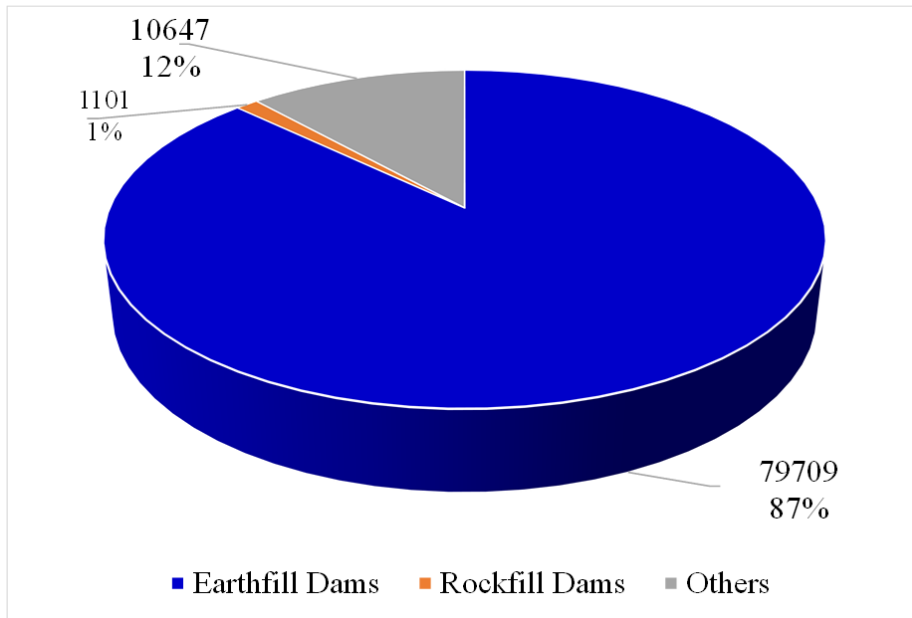


Figure 2. Types of dams in the United State (modified from U.S. Army Corps of Engineers, “National Inventory of Dams,” 2020)

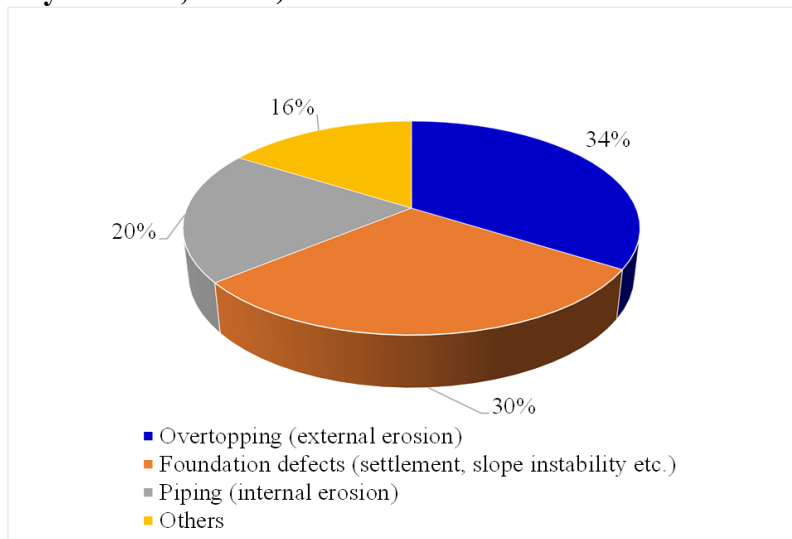


Figure 3. Causes of dam failures in the United States (modified from Association of State Dam Safety Officials, 2020)

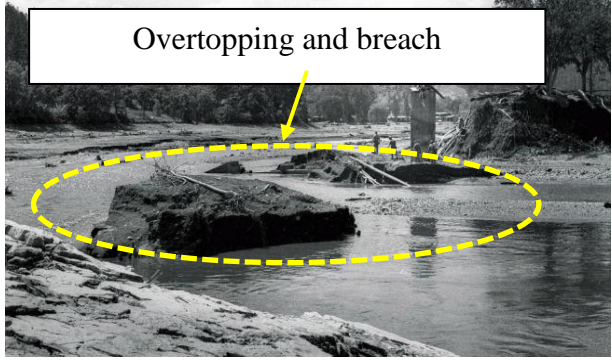




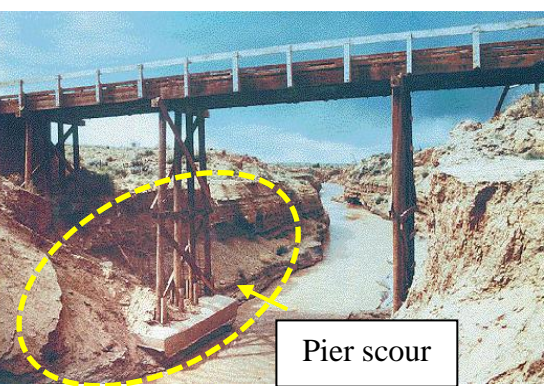
 <p>Overtopping and breach</p>	 <p>Bauxite residue</p> <p>Overtopping and breach</p>
<p>Canyon Lake Dam failure in South Dakota in 1972 (adapted from Association of State Dam Safety Officials, Lessons learned, 2020)</p>	<p>Tailing dam accident in Hungary in 2010 (adapted from 911 Metallurgist)</p>
 <p>Overtopping and breach of levee</p>	 <p>Inner Harbor Navigational Canal overtopping</p>
<p>The Mississippi River levee breach in 1993 (adapted from Mississippi River breaches Pin Oak levee in Winfield, flooding homes in Lincoln County, Missouri cbs8.com)</p>	<p>The New Orleans levee breach in 2005 (adapted from https://www.history.com/news/hurricane-katrina-levee-failures)</p>
 <p>Bridge scour and failure</p> <p>River flow</p>	 <p>Pier scour</p>
<p>Bridge failure in Maryland in 1995 (adapted from https://www2.usgs.gov)</p>	<p>Bridge scour in New Mexico (adapted from USGS Publication Repository, photo.jpeg (564×402) (usgs.gov))</p>

Figure 4. Some examples of failures of dams, levees, and bridges in the United States

1.1.2. Levees

Erosion is the number one “killer” of bridges through scour around bridge supports in rivers and overtopping of levees during floods. The USACE evaluates that there are approximately 7,100 levee systems, 40,200 kilometers of levees, 44,000 levee structures in the US (National levee database, 2021). Earthen embankments make up 97% of all levees, while the remaining 3% are made of concrete or rock and are steel floodwalls (Levees | ASCE's 2021 Infrastructure Report Card). A levee protects seventeen million people and \$2.3 trillion of property.

Levees are complicated structures to operate and maintain because they are long earthen systems built many years ago with a lack of knowledge of the construction materials. The USACE Levee Safety Portfolio Report 2018 names overtopping and breaching as the most common risk drivers in levee performance. Moreover, there is no national standard or requirement for levee design, construction, or operation and maintenance (USACE Levee Portfolio Report, 2018). In recent years, levee breaches were observed in major flooding events such as during the Great Flood of 1993 in Mississippi River Delta, Hurricane Katrina in New Orleans, Louisiana, in 2005 (Figure 4) and the Mississippi River flood in 2011.

The levee in New Orleans breached in more than 40 locations causing approximately 1,800 fatalities and ultimately \$160 billion in economic damage. The levees on the Mississippi and its tributaries were overtopped or breached in over 1,000 locations in 1993 with billions of dollars lost. In many of these cases, levee failed at least in part due to erosion (Briaud et al., 2008). The Federal Emergency Management Agency Hazard Mitigation Assistance (FEMA) estimated that during the Midwest flooding in spring 2019 over 80 levee systems were overtopped and breached and over 1,120 km of levees were damaged. The flooding cost twenty

billion dollars in damages (Levees | ASCE's 2021 Infrastructure Report Card). The USACE estimates that \$21 billion is needed to improve the moderate to high-risk levees in the country (ASCE 2021 Infrastructure Report Card). Around \$80 billion is needed in the next 10 years to maintain and improve the nation's system of levees (American Society of Civil Engineers, 2017 Infrastructure Report Card).

1.1.3. Tailings dams

When failure occurs during a tailing dam operation, it has a tremendous consequence for people and environment; a “famous” red mud tailing dam failure in Hungary in 2010 caused 10 fatalities and 406 injuries with billions of dollars loss (Figure 4) (Advancing Earth and Space Science, 2020). A total of 223 billion tons or 534 billion cubic meters of tailings has been accumulated worldwide from 1915 to 2019. It is estimated that about 40 – 50 billion tones or 95 – 120 billion cubic meters of tailings will be gathered by 2024. They are stored in active, inactive, and abandoned tailing facilities. The total number of tailings dams in the world roughly estimated as 29,000 – 35,000 (World Mine Tailings Failures portfolio, 2021).

Tailings dam failures result from a variety of mechanisms including overtopping, slope stability, seepage, foundation failure, liquefaction, or a combination of several. For example, can reduce slope stability to the point of failure. ICOLD (2001) reported the following causes of the tailing dam failure out of 135 cases (Tailings dam risk of dangerous occurrences, ICOLD, Bulletin 121):

- Slope stability - 23 %
- Overtopping - 21%
- Earthquakes (liquefaction) – 13 %
- Foundation failure – 9 %

- Seepage – 7.5 %
- Structural – 9%
- Others including unknown – 17.5 %

Erosion including overtopping and internal erosion is about 29 % of all tailing dam failures in the world (Center for science in public participation, 2021). Among other reasons of failure are poor management and regulation (Santamarina et al., 2019).

According to the World Mine Tailings Failures portfolio, the rate of tailing dam failures has increased significantly since 1950s. For example, the number of failures from 1950 to 2010 are:

- very serious failures per decade from 8 in the 1950s to 12 in 2010s
- serious failures per decade from 2 in the 1950s to 14 in the 2010s
- minor failures per decade from 3 in the 1950s to 19 in the 2010s

The number of fatalities increased 12 times from the 1950s to the 2010s. In 2019, a cumulative loss of almost 3000 lives took place (World Mine Tailings Failures portfolio, 2021) (Santamarina et al., 2019). Annually from 2 to 5 major tailings dam failures occur worldwide (Tailings dam risk of dangerous occurrences, ICOLD, Bulletin 121).

1.1.4. Bridges

More than 80 percent of all bridges in the United States (approximately 617,000 bridges across the country) are located over water; in 60 percent of the cases where bridge collapse has happened, the failure was due to the scour at and beneath the bridge supports (Briaud et al., 1999; Briaud et al., 2001). A 1973 national study for the Federal Highway Administration (FHWA) showed that 383 bridges failed due to catastrophic floods. The 1993 flood in the upper Mississippi basin caused 23 bridge failures for an estimated damage of \$15 million (The

Hydraulic Engineer Circular, HEC 18, 2012). In the 1994 flooding from storm Alberto in Georgia, there were over 500 bridges with damage attributed to scour. The scour depth varied from 4.6 to 6 m. Total damage to the highway system was approximately \$130 million (The Hydraulic Engineer Circular, HEC 18, 2012). One of the bridge scour failures occurred for a bridge crossing Enoree River in Maryland (Figure 4) in 1995 and a large scour depth was observed for a Rio Puerco River bridge in New Mexico (Figure 4).

1.2. Objectives of the research and approach

Research on improvement of testing and modelling of soil erosion and mitigation presented herein is comprised of several components including.

1.2.1. Task 1: Borehole Erosion Test

The goal is to develop a detailed testing procedure and data reduction procedure for the Borehole Erosion Test (BET). To accomplish this objective, the following steps are proposed:

Step 1. Evaluate and analyze the preliminary testing and data reduction procedure for the BET and identify missing recommendations and limitations (Briaud et al. 2016; Briaud et al., 2017). This step will consist of gathering data on the BET in a spread sheet which can be updated as more test results become available.

Step 2. Perform laboratory and field tests on levees to identify shortcomings and develop the detailed testing procedure for the BET. CTNK

Step 3. Propose the shear-based equation for the BET data reduction which did not exist in the preliminary data reduction procedure. CTNK

Step 4. Extend the Moody chart to very rough surfaces (for relative roughness $\epsilon/D > 0.05$). CTNK

Step 5. Develop the detailed data reduction procedure and spread sheet for the BET including the missing shear stress aspect of the procedure. CTNK

Step 6. Evaluate the BET precision, advantages and limitations compared to other erosion tests (e.g. EFA). Recommend optimum range of applications.

This knowledge is documented in the Chapter 3 of this dissertation.

1.2.2. Task 2: Soil improvement

The goal is to evaluate some soil improvements for erosion mitigation and their degree of efficacy. To accomplish this objective, the following steps are proposed:

Step 1. Review existing knowledge on soil improvement used for erosion mitigation and plan new tests to complement and advance knowledge in this area.

Step 2. Perform EFA testing on grass, riprap with a filter and without a filter, enzyme-treated and lime-treated soil. CTNK

Step 3. Obtain erosion function and parameters from EFA testing such as erosion function, critical velocity, critical shear stress, velocity-based erosion modulus, shear stress-based erosion modulus. CTNK

Step 4. Evaluate erosion performance of each modified soil or proposed material based on the EFA results. CTNK.

Step 5. Compare, to the extent possible, laboratory testing in the EFA with field (large-scale) testing or field performance as published in the open literature of each soil improvement method. CTNK

Step 6. Develop recommendations for using soil improvement methods for levees and dams depending on the purpose of usage, soil type, and site conditions (intensity of flood etc.). CTNK

The results of this knowledge are documented in the Chapters 4-7 of this dissertation.

1.2.3. Task 3: New erosion model and classification

The goal is to develop a new erosion function model and associated soil erosion classification to be applied for assessment of erodibility of soil for levees and dams. To accomplish this objective, the following steps are proposed:

Step 1. Analyze the existing erosion models including their shortcomings.

Step 2. Propose a new power law model to improve on the short comings (for velocity and shear stress) and satisfy the non-linearity of the erosion functions. CTNK

Step 3. Obtain the relationship between erosion modulus and critical shear stress/critical velocity needed to strengthen the new model. CTNK

Step 4. Prepare new erosion classification charts consistent with the new erosion model including a shear stress-based chart and a velocity-based chart. CTNK

Step 5. Apply the new erosion model for different types of soil, improved soil, and materials. CTNK

Step 6. Solve some practical erosion problems as examples of the application of the new erosion function model including levee overtopping problem by hand calculation. CTNK

This knowledge is documented in the Chapter 8 of this dissertation.

1.2.4. Task 5: Prediction of erosion movement

The goal is to develop TAMU-PEM, an automated Excel Spread Sheet, to predict of erosion movement for levees, dams, and riverbank erosion. To accomplish this objective, the following steps are proposed:

Step 1. Obtain the erosion functions for a soil from EFA testing.

Step 2. Select a flood velocity hydrograph for a given river location (velocity vs. time in hours). Use a synthetic hydrograph if necessary or an observed (past) hydrograph and a velocity hydrograph for the flood.

Step 3. Develop the equations to obtain the erosion movement for a series of increments of time and velocity from a velocity hydrograph.

Step 4. Develop the automated Excel Spread Sheet for obtaining the erosion movement and apply it to several examples. CTNK

Step 5. Calibrate the results by comparing the prediction with a field performance considering the lab/field scale factor. CTNK.

The results of this task are documented in the Chapter 9 of this dissertation.

1.2.5. Task 6: TAMU-Erosion database

The goal is to further improve and populate the TAMU-Erosion database with more than 200 new erosion test results. To accomplish this objective, the following steps are proposed:

Step 1. Input additional data (> 200 test results) in the existed TAMU-Erosion database.

Step 2. Analyze the new data and improve the existing database. CTNK

Step 3. Systemize the new data according to soil type, method or material of soil erosion improvement.

The knowledge on this task is documented in the Chapter 10 of this dissertation.

1.2.6. Task 7: Risk framework

The goal is to address erosion of dams and levees within a risk framework. To accomplish this objective, the following steps are proposed:

Step 1. Identify the risk associated with soil erosion of dams and levees and present the risk data on the risk chart. CTNK

Step 2. Develop a methodology to evaluate the erodibility of dams and levees by using the erosion categories. CTNK

The results of this task are documented in the Chapter 11 of this dissertation.

2. BACKGROUND ON SOIL EROSION

This chapter describes erosion phenomenon as well as some of the most common laboratory and field tests developed over the years to quantify soil erodibility and to obtain erosion parameters such as critical shear stress and critical velocity, erosion rate, erosion function, erosion function slope or coefficient of erodibility. The role of those parameters is essential in qualifying and quantifying soil erodibility.

2.1. Phenomenon of soil erosion

Soil erosion is a displacement of soil particles or soil aggregates by different agents such as water, ice, snow, air, plants and animal, and humans. This dissertation considers soil erosion by water flowing over a soil or/and through a soil. Erosion has three components involved: the soil or rock, the water, and the geometry of the barrier that the water is interacting with (Briaud, 2013). The resistance of soil to erosion is soil erodibility which can be qualitative and quantitative. The water is characterized by velocity and shear stress acting at the soil-water interface. The barrier is specified by its dimensions, for example, length and height for earth dams, the dimensions of a bridge pier.

Erosion is a complicated process; however, it can be illustrated by a free-body diagram of a soil particle showing the erosion phenomenon at the element level. The free-body diagram can be presented for no-flow and flow conditions to better illustrate erosion phenomenon. The free-body diagram for no-flow condition with forces acting on a particle is shown on Figure 5a. The water applies hydrostatic (normal) stress around the soil particle, the difference in which between the bottom and the top of a particle creates the buoyance force. This effect reduces the weight of the particle and the particle becomes easier to get detached when the water starts to flow over it.

The free-body diagram for flow condition is shown on Figure 5b. The water flow creates shear stress at the interface between the particle and the water, decreases the normal stress on the top of the particle, thereby developing the uplift force, and generates the turbulence which can contribute significantly to the erosion (Briaud, 2013). The combination of the shear force, the uplift force, and the water turbulence acts together to remove the soil particle or clusters of particles and initiate erosion. This phenomenon can be observed and visually identified during the erosion testing in the Erosion Function Apparatus (EFA). Briaud (2013) suggested that the erosion of unsaturated soil is closely related to apparent cohesion which can increase the resistance of soil to erosion. This phenomenon should be considered for levees which are typically designed to stay “dry” between the floods. However, an increase in the rate of flooding reported by EPA in 2021 forces a levee to be saturated for a prolonged period which would change an approach to a levee design and would emphasize the importance of soil erosion.

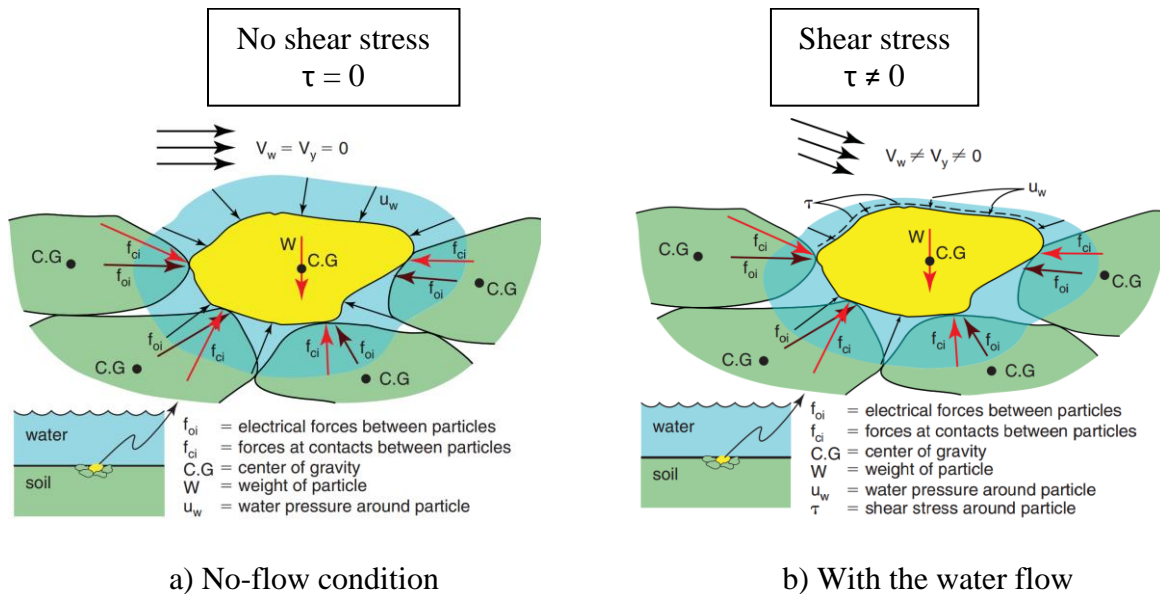


Figure 5. Free body diagram of a soil particle or rock block in two different stages a) no-flow condition, b) with the water flow (adapted from Briaud, 2008)

Soil erosion phenomenon can occur through two different types and mechanisms:

- 1) Internal erosion which is essential for embankment dams, its foundations, and levees.
- 2) Surface (external) erosion which is important for bridge scour, overtopping of levees, dams, highway embankments, and for meander migration.

The term “internal erosion” is used by Reclamation and United States Army Corps of Engineers (USACE) to describe erosion of soil particles by water passing through a body of soil. One of the most common form of internal erosion is piping which is initiated by backward erosion, or erosion in a crack or high permeability zone. Piping results in the formation of a continues tunnel called a pipe between the upstream and the downstream side of the embankment or its foundation (Fell and Fry, 2007). Internal erosion is not considered in this dissertation.

Surface erosion occurs on the surface of the soil including riverbeds and riverbanks, during overtopping flow of levee and dam embankments, wave action in coastal zones. Similar to the erosion shown in Figure 5, the surface erosion happens as a result of developing of the shear stress at the boundary of the soil-water interface, decreasing in normal stress on the top of the particle, and the turbulence in the water.

Soil erosion is a phenomenon affected by many different factors. Among these factors are gravitational forces, grain size distribution, physical and chemical soil properties as well as interaction of pore water and eroding fluids. Several attempts were made to obtain a relationship between soil properties and soil erodibility including the NCHRP Project 915 (Briaud et al., 2019). In many cases these attempts did not show reliable results, especially for clayey soil. Geotechnical parameters of soils such as shear strength and dry unit weight have not proved useful for erosion prediction (Briaud et al., 2019).

Another mechanism of soil loss different from erosion is flaking or soaking when soil loss immersed in water; this process can be observed even under no shear stress acting on the soil surface. Some soil can completely disintegrate in water and the rate of soil loss of partially saturated clayey samples can be very high. Moriwaki and Mitchell (1977) observed different mechanisms of clay disintegration in water depending on clay mineral type and fluid chemistry.

Since levees are designed as “dry” structures meaning they are not supposed to interact with between flooding, the effect of immersed water should not be underestimated.

Erosion is a complex process and direct testing is greatly preferred whenever possible. The following section is discussed the existing laboratory and field erosion tests.

2.2. Some existing erosion tests

Many erosion tests have been proposed over the last 30 years starting with laboratory tests (EFA, Sedflume and other flume tests, JET, HET etc.) and more recently with in-situ tests (BET, PET, JET etc.) (Briaud et al., 1999, 2001; Trammel, 2004; Shan et al., 2015; McNeil et al., 1996; Roberts et al., 2003; Gibbs, 1962; Lyle and Smerdon, 1965; Kandiah and Arulanandan, 1974; Arulanandan and Perry, 1983; Shaikh et al., 1988; Ghebreiyessus et al., 1994; Hanson and Cook, 2004; Hanson and Hunt, 2007; Hanson and Simon, 2001; Al-Madhhachi et al., 2013; Hanson et al., 2002; Dunn, 1959; Moore and Masch, 1962; Chapius and Gatien, 1986; Sherard et al., 1976; Sheppard et al., 2004, 2006; Lefebvre et al., 1985; Wan and Fell, 2002; Wahl et al., 2009; Chang and Zhang, 2011; Richards and Reddy, 2010; Briaud et al., 2016; Briaud et al., 2017; Gabr et al., 2013; Ham et al., 2016; Shidlovskaya et al., 2016; Shafii et al., 2016). The best way to predict the erodibility of a soil is to measure it directly on a site-specific basis by in-situ testing in the field complementary combined with testing samples in the laboratory.

All existing erosion tests are described in details in Briaud et al. (2019). In this section, the most common existing erosion tests are summarized. The advantages and limitations of the most common testing devices and methods are identified. The erosion tests can be performed in the field or in the laboratory:

- 1) Laboratory erosion testing
- 2) Field erosion testing

It should be noted that some of the erosion tests such as Jet Erosion Test and Pocket Erodrometer Test, have both applications, the laboratory, and the field. Some laboratory tests are briefly described below.

2.2.1. Laboratory Tests.

2.2.1.1. Erosion Function Apparatus (EFA)

The Erosion Function Apparatus (EFA) was developed by Briaud at Texas A&M University in 1991 (Briaud et al., 2001). Since that, the EFA is being manufactured by Humboldt, Inc. and used by many engineering companies and institutions worldwide. The ASTM standard for the EFA is in development (ASTM Standard WK67195, 2019).

Figure 6 shows a schematic diagram as well as a photograph of the EFA device. The principle is to go to the site where erosion is being investigated, collect samples within the depth of concern, bring them back to the laboratory and test them in the EFA. A standard Shelby tube with a 76.2-mm outside diameter (ASTM Standard D1587) which is also a testing tube containing the sample is brought back to the laboratory and placed through the bottom of the conduit where water flows at a constant velocity (

Figure 6). The soil is pushed out of the sampling tube only as fast as it is eroded by the water flowing over it. The velocity is measured with a flow meter and the erosion rate is the

piston rate of advancement. The erosion rate and the corresponding velocity give a point on the erosion function. A shear stress is calculated using Moody's chart (Moody, 1944). Point by point the erosion function (erosion rate vs velocity or erosion rate vs shear stress) is obtained. Examples of erosion functions for a fine sand and for a low plasticity clay are shown in Figure 7. Note that for the same average velocity of 1 m/s in the EFA test conduit, the rate of erosion for the sand is about 1000 times faster than for the clay. This indicates that the rate of erosion can be very different for different soils. The advantages and limitations of the EFA are shown in Table 1. The detailed testing and data reduction procedure of the EFA is described in Chapter 3, Section 3.4. The EFA is operated in the Soil Erosion Laboratory at Texas A&M University among the other erosion tests.

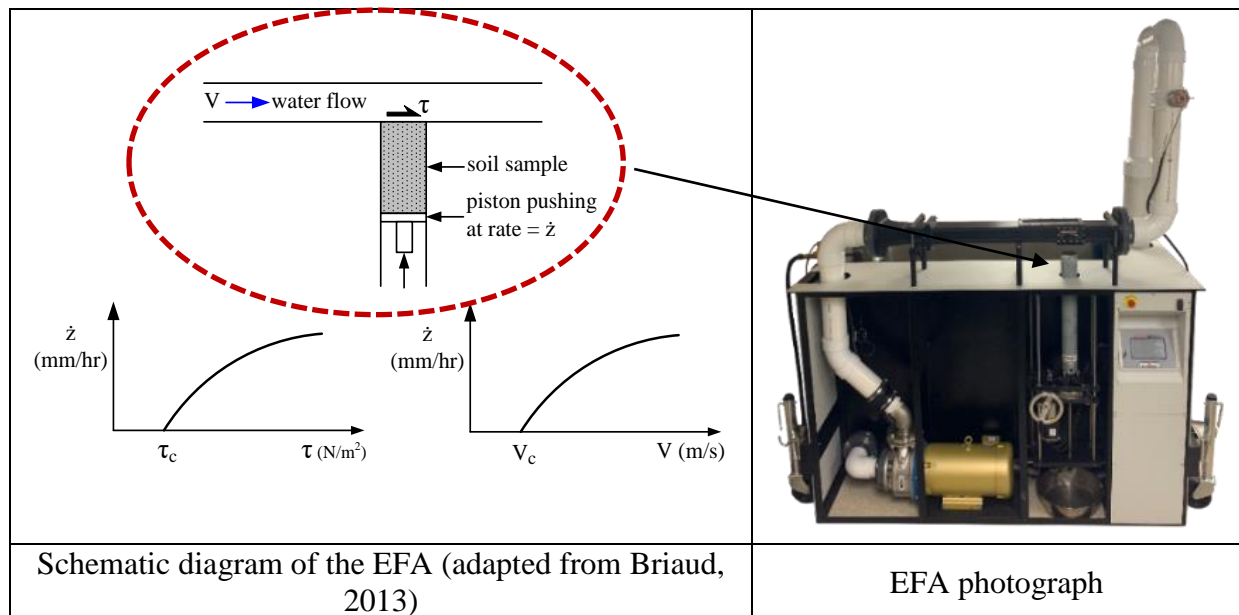


Figure 6. Schematic diagram of the Erosion Function Apparatus and a photograph of the EFA (adapted from Briaud, 2013)

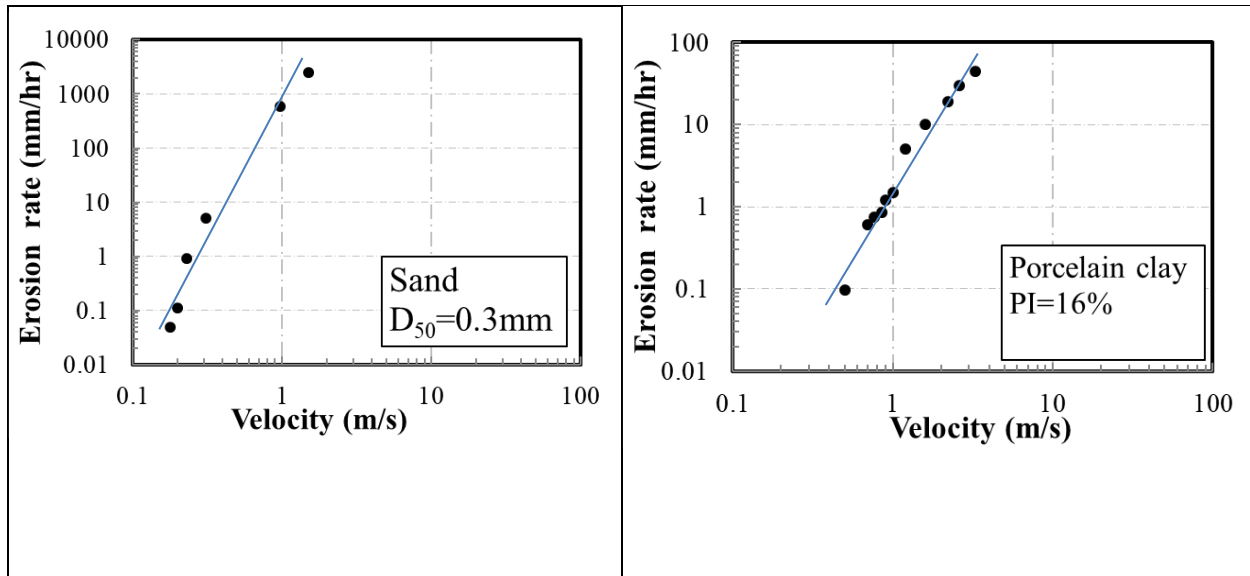


Figure 7. Erosion function for a sand and a low plasticity clay as measured in the EFA (adapted from Briaud, 2013)

Table 1. The advantages and limitations of the EFA (adapted from Briaud et al., 2019)

Advantages	Limitations
<ol style="list-style-type: none"> 1. Can be used for a wide range of soils including soft and hard natural soils, artificially reconstituted soils, improved soils, and grass. 2. Soil can be tested directly in the Shelby tubes obtained in the field, minimum disturbance. 3. Gives the entire erosion function for a range of stress-strain conditions. 4. Wide range of velocity can be modelled from 0.5 m/s to 6.5 m/s. 5. The erosion parameters such as critical velocity, critical shear stress, erosion rate, erosion slope or modulus can be obtained. 6. The results can be directly used as input to the TAMU-SCOUR, TAMU-Erosion database, TAMU-PEM to predict erosion (Chapter 6 and Chapter 7). 7. Can be beneficially used with the BET for a more precise evaluation of soil erodibility. 	<ol style="list-style-type: none"> 1. Shear stress is measured from velocity using Moody chart which might not be accurate. 2. The erosion rate is visually inspected; therefore, it can be not very accurate. 3. In some cases, the samples should be transferred from the sampling tube to the testing tube which can cause additional sample disturbance. 4. Soil with large particles such as 40 mm and larger cannot be tested with confidence as the diameter of the testing tube is 75 mm. 5. The EFA is an expensive device (around \$70,000). 6. One EFA test is \$1,500.

Recently, Ham et al. (2016) have developed an ultrasonic P-wave reflection monitoring method to quantify the erosion rate in the EFA. They proposed to monitor the erosion rate using ultrasonic transducers mounted above a soil surface. This technique was aimed to improve the measurements of the erosion rate; however, the authors found the same tendency and magnitude of erosion of fine and coarse grain soils as it can be measured by visual inspection.

2.2.1.2. Jet Erosion Test (JET)

The Jet Erosion Test is a field technique as well as a laboratory erosion test. First JET was invented by Hanson and developed at the USDA-ARS to measure erodibility of cohesive soil (Hanson, 1990; Hanson, 1991). The JET test is described in details in ASTM Standard D5852. This test can be performed in situ on exposed soils (Hanson et al. 2002; Hanson et al., 2004) as well as in the laboratory using tube samples or remolded samples in compaction molds (Hanson and Hunt 2007). The test can be carried out on samples as small as 75-mm. The apparatus jets the soil by a 6.35-mm diameter nozzle initially positioned between 6 and 30 nozzle diameters from the soil surface (Wahl et al. 2009). The schematic diagram of the JET of the laboratory version is shown in Figure 8.

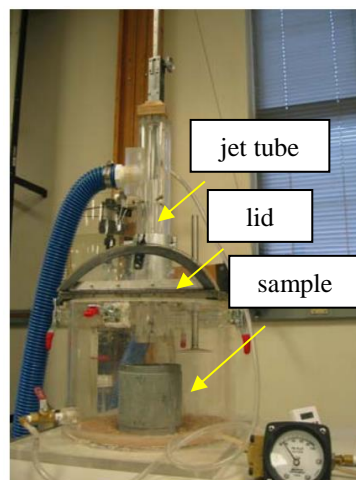


Figure 8. The photographs of laboratory version of JET (adapted from Wahl, 2010)

The latest version of the JET test is a miniature jet and was used by Al-Madhhachi et al. (2013). The JET has been applied for overtopping problems as well as for riverbank erosion. The advantages and limitations of the JET are summarized in Table 2.

Table 2. The advantages and limitations of the JET (adapted from Briaud et al., 2019)

Advantages	Limitations
<ol style="list-style-type: none"> 1. Laboratory and field versions. 2. Simple and quick to prepare and run as well as cost effective. 3. Can be performed on any surface vertical, horizontal, and inclined (Wahl, 2010). 4. Soil erodibility parameters such as critical shear stress and coefficient of erodibility can be obtained. 	<ol style="list-style-type: none"> 1. Can be performed only in cohesive soils or self-supporting soil (lab version). 2. Might not be appropriate in clayey soil with large coarse particles (for example, moraine). 3. The JET is limited to testing the soil at the surface; cannot be performed at depth (field version). 4. The flow mechanism is complex and difficult to analyze. 5. The data reduction is complicated.

2.2.1.3. Hole Erosion Test (HET)

The HET can be conducted in the laboratory on undisturbed samples as well as on a soil compacted into a Standard Proctor mold (Wahl et al., 2009). This test consists of drilling a 6.35 mm diameter hole through a soil and flowing water through that hole under a constant hydraulic head if flow can be maintained (Figure 1Figure 9). The measurements of the tests are the flow rate, the initial and final diameter of the hole which are used to compute the erosion rate and shear stress. The HET has been applied mostly to problems of internal erosion such as piping. The advantages and limitations of the HET are shown in Table 3.

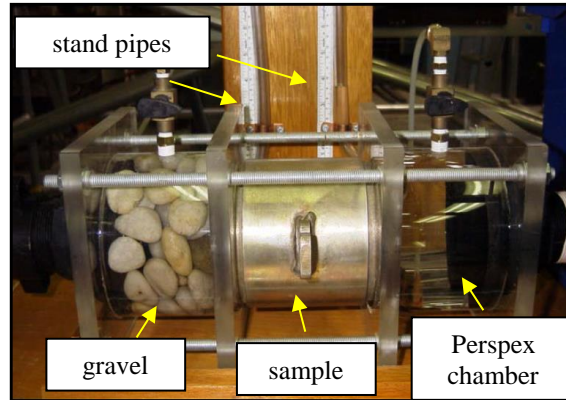


Figure 9. A photograph of the sample setup (adapted from Briaud et al., 2019)

Table 3. The advantages and limitations of the HET (adapted from Briaud et al., 2019)

Advantages	Limitations
<ol style="list-style-type: none"> 1. The test allows to model piping erosion in earth dams. 2. A wide range of pressure heads and hydraulic shear stress at the soil-water interface can be applied to model different flow conditions. 	<ol style="list-style-type: none"> 1. The soil needs to be strong enough to stand under its own weight (self-supporting). 2. Works better with soils of medium erodibility which can be eroded easy. 3. Difficult and time-consuming to prepare and run. 4. The erosion rate needs to be extrapolated and inferred, not direct measurements. 5. The hydraulic shear stress is inferred, and not directly measured. 6. The flow mechanism is complex and difficult to interpretate.

2.2.1.4. Slot Erosion Test (SET)

Slot Erosion Test was developed by Wan and Fell (2002) and it is very similar to the HET except the size of the soil sample which is bigger. The testing and data reduction procedure are almost the same except the shear stress calculation. The advantages and limitations of the SET are same as the ones discussed for the HET.

2.2.1.5. Sediment Erosion at Depth Flume (Sedflume)

The Sedflume was developed for the purpose of measuring the sediment erosion at high shear stress (McNeil et al., 1996). The U.S. Army Corps of Engineers High Shear Stress flume (Sedflume) is designed for evaluation of erodibility of fine grain as well as a mix of fine- and coarse grain soil. The Sedflume exists in laboratory and field version. The primary application of this device is a coastal erosion.

The idea of the apparatus is to flow the water through the channel of the flume which is 120 cm long and has the rectangular cross section of 10 cm × 2 cm (Figure 10). The soil sample has to be 1 m long and has cross section dimensions of 15 cm × 10 cm. The sample is placed on a piston with a hydraulic jack which allows to push the sample and adjust its height. The Sedflume follows the same procedure as the EFA when the sample needs to be flush with the flume surface. The flow rate during the test is controlled by a flowmeter and water powered by a pump and then flows into the flume. The advantages and limitations are given in Table 4.

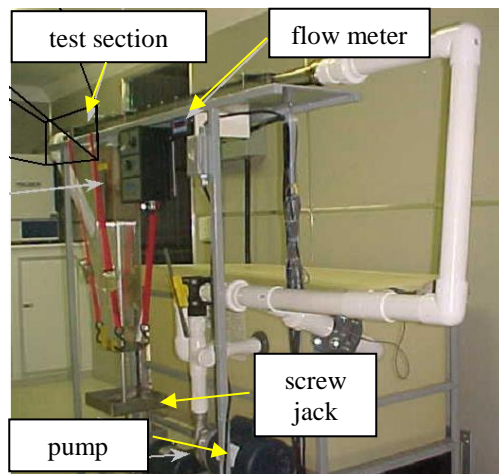


Figure 10. A photograph of a Sedflume (reprinted from Briaud et al., 2019)

Table 4. The advantages and limitations of the Sedflume (adapted from Briaud et al., 2019)

Advantages	Limitations
1. Field version of the apparatus allows to test the soil in in-situ stress and flow condition and minimize soil disturbance. 2. Soil samples from the site as well as reproduced soil in the lab using a sediment slurry can be tested.	1. The shear stress is calculated from the Moody chart and not directly measured. 2. The lab version is costly, testing is time consuming. 3. Can be performed on disturbed or reconstituted samples. 4. Difficult to prepare a sample in a complicated in situ environment.

Among the other laboratory erosion tests and techniques which are not considered above are the following (Briaud et al., 2019).

1. Flume tests and methods including the ones invented and conducted by Gibbs (1962), Lyle and Smerdon (1965) from Texas A&M University, Kandiah and Arulanandan (1974), Arulanandan and Perry (1983), Shaikh et al. (1988), Ghebreiyessus et al., (1994), Soil Protrusion Apparatus (SPA) by Jayaratne et al. (Salim et al., 2011).
2. Jet apparatus to measure the tractive resistance of cohesive channel beds Dunn (1959), submerged jet test proposed by Moore and Masch (1962) at the University of Texas.
3. Rotating cylinder apparatus developed by University of Texas for a scour purposes by Moore and Masch (1962) which allows directly estimate the shear stress using the induced torque on the side surface of the remolded sample; improved rotating cylinder test by Chapius and Gatien (1986) allowing to test not only remolded samples but also intact soil; Rotating Erosion Test Apparatus (RETA) invented by Sheppard et al. (2006) and Bloomquist et al. (2012) which can be used in soil and rock.
4. Hole tests such as Pinhole Test developed by Sherard et al. (1976), Drill Hole Test by Lefebvre et al. (1985) and used mostly for prediction of internal erosion.
5. Stress-Controlled Erosion Apparatus proposed by Chang and Zhang (2011) for internal erosion testing.

6. True Triaxial Piping Test Apparatus (TTPTA) developed by Richards and Reddy (2010) to study the internal erosion in a variety of soils.

The most common and promising field erosion tests are described below. Full-scale (in-situ) overtopping tests such as Wave Overtopping Simulator (Netherlands) and Full-scale Overtopping Test (Colorado) are presented in Chapter 4, Section 4.1.

2.2.2. In-situ Tests

2.2.2.1. Borehole Erosion Test (BET)

The Borehole Erosion Test, or BET, was developed by Briaud at Texas A&M University in 2014 (Briaud et al., 2016; Briaud et al., 2017). BET is a field in-situ test designed to make use of conventional drilling equipment to obtain the continuous erodibility profile of a soil deposit as a function of depth. It is to erosion what the cone penetration test is to soil strength profiling and stratigraphy. It consists of drilling a borehole approximately 100 mm in diameter to a depth covering the zone of interest for the erosion problem, removing the drilling rods from the hole and making an initial profile measurement of the borehole diameter with a caliper, lowering the rods and circulating fluid down the rods and up the annulus between the rods and the borehole wall thus eroding the soil (Figure 11). A mechanical caliper is preferable in soil while an acoustic caliper works well for rock because of the sharp stiffness discontinuity at the borehole wall (Briaud et al., 2017). After a chosen time, the flow is stopped, the rods are removed, and an eroded profile of the borehole diameter is measured with the caliper (Figure 12). The increase in borehole radius or diameter divided by the amount of time the fluid has been flowing gives the radial erosion rate and the test yields the erosion rate as a function of depth. Repeating the tests for different water flow velocities gives the erosion function which is erosion rate vs. velocity,

for each soil layer in the profile (Briaud et al, 2016, Briaud et al. 2017). The advantages and limitations of the BET are shown in

Table 5. The detailed and improved testing as well as data reduction procedure is described in Chapter 3, Section 3.3 of this dissertation.

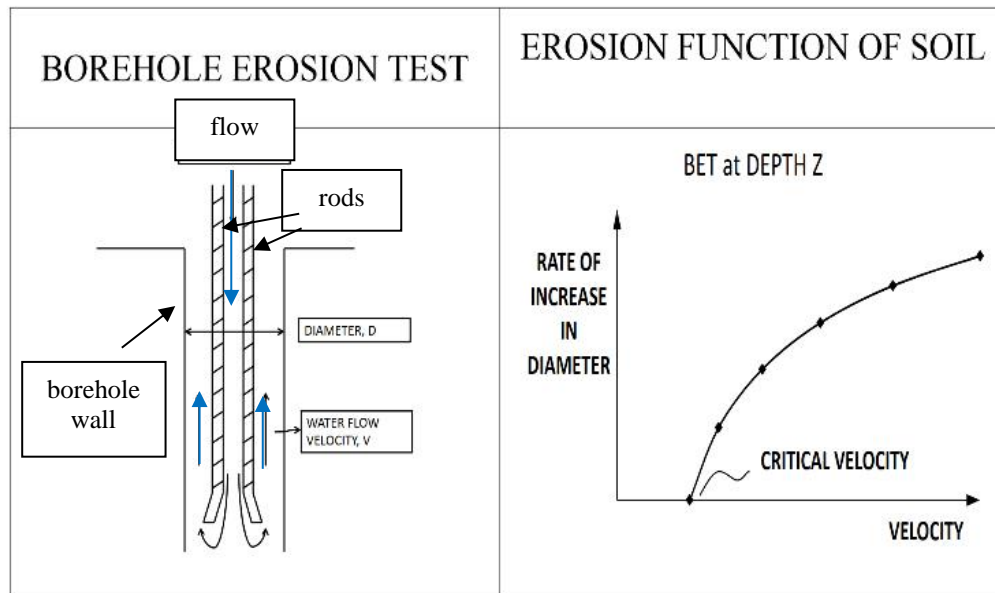


Figure 11. A schematic diagram of the BET (adapted from Briaud et al., 2017)

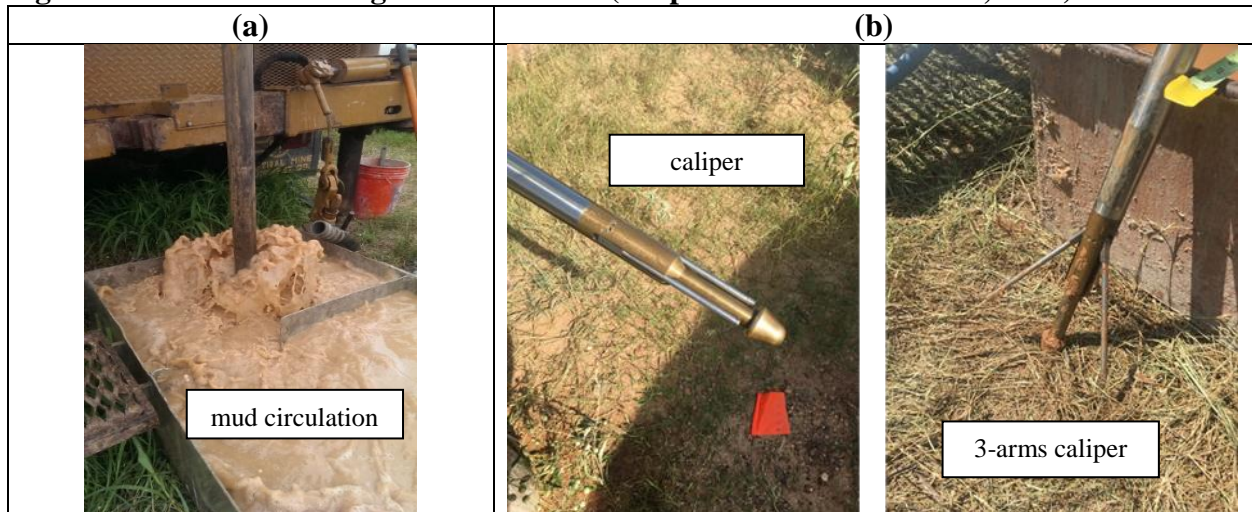


Figure 12. Borehole Erosion Test: (a) circulation of water in the borehole, (b) borehole caliper retracted and expanded (adapted from Briaud et al., 2017).

Table 5. The advantages and limitations of the BET

Advantages	Limitations
<ol style="list-style-type: none"> 1. Continuous profile of erodibility throughout a borehole depth. 2. Erosion testing in situ stress conditions. 3. Commonly available equipment (drill rig, pump, caliper etc.). 4. Potentially can be used for lateral and bottom erosion as well. 5. Economically advantageous: one BET test cost \$5,000-\$6,000 per 10 m borehole. 	<ol style="list-style-type: none"> 1. Difficult to perform in coarse and collapsible soil because of the instability of the borehole walls. 2. Shear stress is not measured directly, it is obtained from Moody chart. 3. Might be limited for flow depending on an available pump on the drill rig. 4. The borehole diameter measurements with the caliper may not be accurate due to material sloughing off.

2.2.2.2. Pocket Erodrometer Test (PET)

The Pocket Erodrometer Test (PET) was invented by Briaud in 2011 as a quick laboratory or field erosion test (Briaud et al., 2012). PET is a mini jet-test which generates a water impulse from the nozzle of about 0.5 mm in diameter at 8 m/s aiming horizontally at the vertical face of the sample. PET allows to preliminary estimate erodibility of soil before or in parallel with other erosion tests, for example EFA and BET. Figure 13 shows the schematic diagram of the PET, along with a photograph from the test (Briaud, 2013). The advantages and limitations of the PET are shown in Table 6.

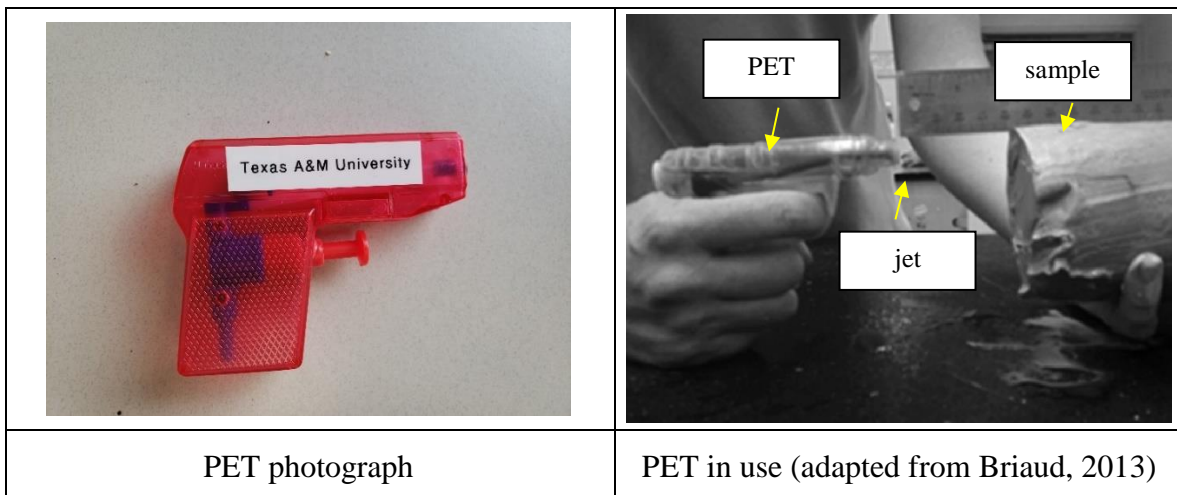


Figure 13. A photograph of the PET device

Table 6. The advantages and limitations of the PET (adapted from Briaud, 2013)

Advantages	Limitations
1. Very low price (\$0.80)	1. Very small scale
2. Very simple to operate both in the field and in the laboratory	2. Only gives the erosion category, no erosion function, no critical shear stress, or critical velocity can be obtained
3. Gives a quick and crude estimate of soil erodibility	3. Only useful for preliminary evaluation or in a combination with other erosion tests
	4. Not good for design purposes

2.2.2.3. In-situ Erosion Evaluation Probe (ISEEP)

The In-situ Erosion Evaluation Probe (ISEEP) was developed by Gabr et al. (2013) at North Carolina State University. The test can estimate the erodibility of any soil in-situ if the probe can penetrate the soil by erosion. This test can be also used at any depth for scour purposes. The test utilizes jetted water to advance a rod into the soil while measuring the rate of advancement setup (Briaud et al., 2019). The rate of advancement of the probe provides an indication of soil erodibility and represents the erosion rate. The results of the ISEEP are given in terms of the stream power. The bed shear stress can be calculated with some assumptions and limitations (Kayser, 2014). Figure 14 shows a photograph of the ISEEP and the probe. The advantages and limitations of the ISEEP are shown in Table 7.

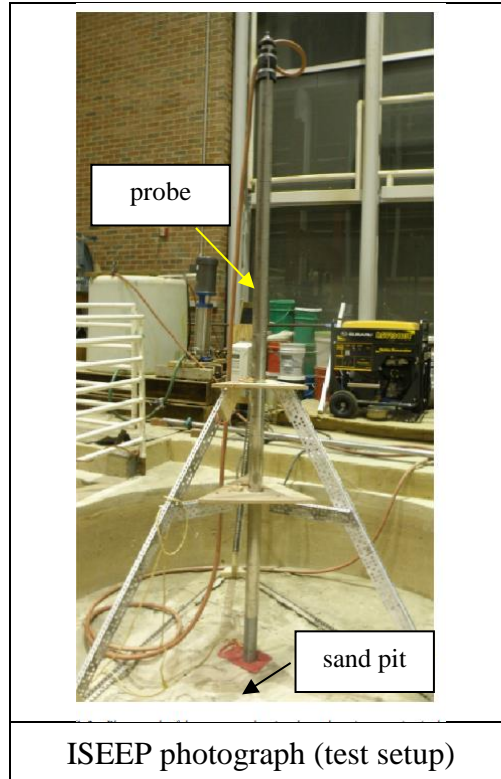


Figure 14. ISEEP apparatus prototype at NCSU (adapted from Briaud et al., 2019)

Table 7. The advantages and limitations of the ISEEP (adapted from Briaud et al., 2019)

Advantages	Limitations
<ol style="list-style-type: none"> 1. In-situ erosion testing. 2. Can be used in almost any soil at any depth. 3. Does not require the use of a power rig. 	<ol style="list-style-type: none"> 1. The penetration may be limited if the probe fails to erode the soil. The test was mostly used in sandy soil. 2. No critical shear stress can be measured. 3. The use of the stream power makes it difficult to compare this device with other erosion devices.

2.2.2.4. In-situ Scour Testing Device (ISTD)

In-situ Scour Testing Device (ISTD) was developed and patented by Bergendahl and Kerenyi at the U.S. Federal Highway Administration (FHWA) in 2016. The main purpose of the device is to determine the scour depth in fine grain soils by using a columnar containment vessel driven into the soil. The device has a cylindrical shape and potentially can be used in a boring

test rig and fit into the steel casing of hollow stem augers. The ISTD simulates the horizontal flow into the tested soil at the bottom of the borehole. Figure 15 shows a schematic diagram of the cutting head of the ISTD.

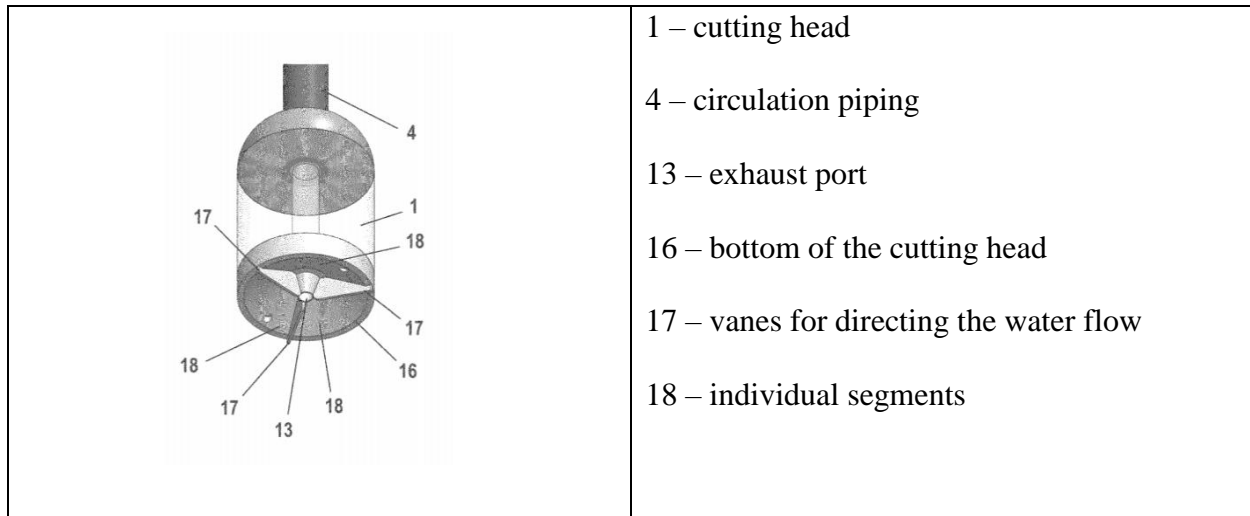


Figure 15. A schematic diagram of the cutting head of the ISTD (adapted from Bergendahl and Kerényi, 2016)

Briaud et al. in the NCHRP Project No. 24-43 presents a summary of the laboratory and in-situ erosion tests in terms of their application (Table 8). Table 9 indicates some of the most common erosion tests with information regarding their application in different soils, ability to measure shear stress, and the \cos . However, it should be noted that the existing erosion tests provide different quantitative estimates of the key erosion parameters. For example, a comparison between the JET and the HET tests showed that the difference in erosion rate can be one or more orders of magnitude, the difference in critical shear stress can be two or more orders of magnitude (Wahl, 2010).

Table 8. Summary of the erosion tests (adapted from Briaud et al., 2019)

Laboratory erosion tests	In-situ erosion tests
<ul style="list-style-type: none"> • Erosion Function Apparatus (EFA) • Flume tests such as SedFlume • Lab Jet Erosion Test (JET) • Hole Erosion Test (HET) • Pinhole Erosion Test • Drill Hole Erosion Test • Slot Erosion Test (SET) • Rotating Cylinder Test (RTC) and some improved versions. • Rotating Erosion Testing Apparatus (RETA) • Stress-controlled Erosion Apparatus • True Triaxial Piping Test Apparatus (TTPTA) • Constant Gradient Piping Test Apparatus 	<ul style="list-style-type: none"> • Borehole Erosion Test (BET) • Pocket Erodrometer Test (PET) • In-situ Scour Evaluation Probe (ISEEP) • Field Jet Erosion Test (JET) • In-site Scour Testing Device (ISTD) • Field Flume Tests • Wave Overtopping Simulators (Netherlands) • Full-scale Overtopping Tests (Colorado)

Table 9. Some of erosion tests with information about their application setup (adapted from Briaud et al., 2019)

Erosion Tests	Range of soil types that can be tested	Range of shear stress that can be applied	Cost of the Device (\$)	Reliability of Results
Lab JET	Sands to clays	< 100 Pa	5,000 – 15,000	Good
In situ JET	Sands to clays	< 500 Pa	15,000 – 30,000	Good
EFA	Sands to clays	< 165 Pa	≥ 30,000	Good
HET	Clayey soils	Up to 800 Pa	≥ 30,000	Good
SET	Clayey soils	Up to 400 Pa	≥ 30,000	Medium
RETA	Clayey soils	< 100 Pa	≥ 30,000	Medium
PET	Sands to clays	< 20 Pa	< 5,000	Medium
ISEEP	Sands to clays	< 650 Pa	≥ 30,000	Good
BET	Sands to clays	< 600 Pa	15,000 – 30,000	Good

2.3. Erosion models and erosion parameters

Soil erosion is a complex process on the boundary between geotechnical and hydraulic engineering. Erosion can be described by erosion models and quantified by erodibility parameters such as critical velocity and critical shear stress, erosion rate, slope of erosion function, and erosion category. These parameters can be obtained by performing laboratory or/and in-situ/field tests which are briefly described in Section 2.2 of Chapter 2.

2.3.1. Erosion models

The erodibility of a soil defined as the relationship between the erosion rate \dot{z} and the velocity of the water v or the erosion rate \dot{z} and the shear stress τ and can be presented as

$$\dot{z} = f(v) \text{ or } \dot{z} = f(\tau) \quad (1)$$

The water velocity is assumed to be mean velocity. This definition has a limitation because water velocity varies in vertical and horizontal direction of the flow (Briaud, 2013). In fact, water velocity is zero at the soil-water interface. Therefore, a more sophisticated and advanced approach to evaluate soil erodibility is the relationship between the erosion rate \dot{z} and the shear stress τ at the soil-water interface (Eq. 1) (Briaud, 2013).

The erosion function represents the constitutive law of the soil for erosion problems (Briaud, 2013). The simplest form of Eq. 2 is a linear function:

$$\dot{z} = k_d(\tau - \tau_c) \quad (2)$$

where k_d is a slope of the erosion function, τ is the shear stress, τ_c is the critical shear stress.

Eq. 2 is a linear function which does not fit many erosion tests performed in the Erosion Function Apparatus (EFA) (See Chapter 3 for more details). The erosion functions measured in the EFA fit better a nonlinear power law function the equation Eq. 3 for which is:

$$\dot{z} = a(\tau - \tau_c)^b \quad (3)$$

The nonlinear power law function becomes a linear if $b = 1$ and a is the erosion slope.

The parameters a and b are unit dependent. A more detailed model is (Eq. 4) (Briaud, 2013):

$$\frac{\dot{z}}{u} = \alpha \left(\frac{\tau - \tau_c}{\rho u^2} \right)^m + \beta \left(\frac{\Delta\tau}{\rho u^2} \right)^n + \gamma \left(\frac{\Delta\sigma}{\rho u^2} \right)^p \quad (4)$$

where \dot{z} is the erosion rate (m/s), u the water velocity (m/s), τ the hydraulic shear stress, τ_c the threshold or critical shear stress below which no erosion is detected, ρ the mass density of water (kg/m^3), $\Delta\tau$ the turbulent fluctuation of the hydraulic shear stress applied to the particle, and $\Delta\sigma$ the turbulent fluctuation of the net uplift normal stress applied to the particle. This model is not in a practical use because of its complexity. The most common existing erosion models and classifications as well as their advantages and limitations are discussed in more details in Chapter 5. The new erosion model and erosion classification are proposed in Chapter 8 of this dissertation.

2.3.2. Erosion function

Erosion function is essential for evaluation of soil erodibility to capture the erosion resistance of the soil at different velocities and shear stresses. The erosion function is the relationship between the erosion rate and velocity or the erosion rate and shear stress and can be presented in natural or logarithmic scale. While the natural scale is a good option to show the results for an individual soil, the logarithmic scale allows to present the results for a group of soils with different erodibility. The examples of the erosion functions in the natural scale obtained in the EFA are shown on Figure 16. The effect of the entire erosion function on the erosion movement is discussed in Chapter 9, Section 9.4. Also, erosion functions are input in the TAMU-Erosion Database (Chapter 10).

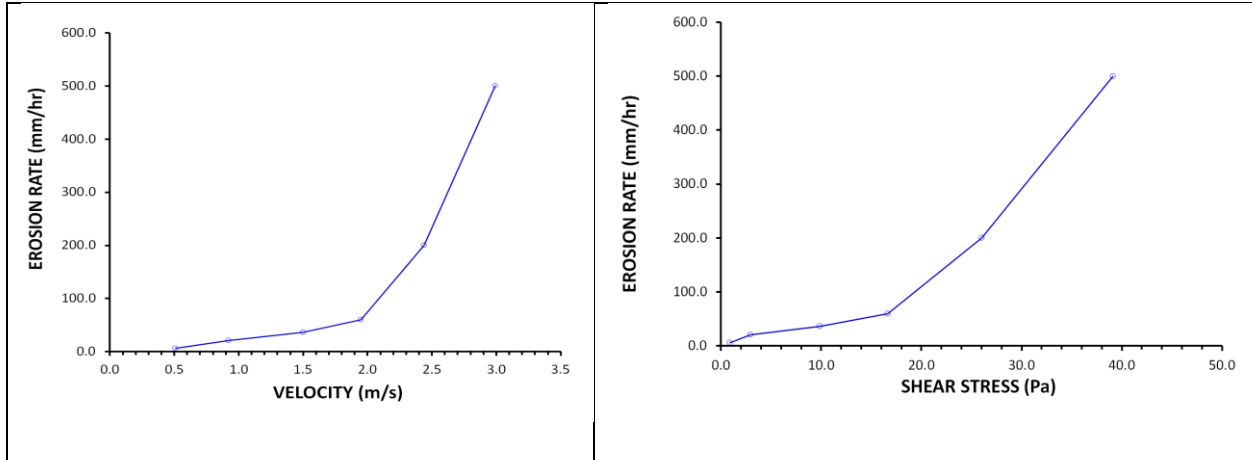


Figure 16. Examples of erosion functions in natural scale

2.3.3. Slope of erosion function

Slope of the erosion function is defined by the shape of the erosion function. As shown in Figure 17, the slope of erosion function can be expressed in terms of the slope of the erosion rate versus shear stress (E_{τ} (mm/hr)/Pa) in logarithmic scale as well as the slope of the erosion rate versus velocity (E_v (mm/hr)/(m/s)). One of the limitations of the definition is that the slope is a dimensional parameter. It means that the units must be considered in all erosion data analysis which is not convenient and also may cause errors if units are not the same such as American and metric units. For example, Hanson suggests that the slope of the erosion function (erosion rate versus shear stress) is to be called the erodibility coefficient k_d (Eq. 5). It is obtained from the erosion function as the intercept of the straight line and shear stress axis (Hanson and Cook, 2004)

$$k_d = \frac{\dot{z}}{\tau - \tau_c} \quad (5)$$

where τ is the shear stress corresponding to the hydraulic problem at hand, τ_c is the critical shear stress, and \dot{z} is the erosion rate. The S.I. units for k_d are $\text{m}^3/\text{N}\cdot\text{s}$ or $\text{cm}^3/\text{N}\cdot\text{s}$.

The slope of the erosion function can also be dimensionless if the normalization process is applied Figure 17. The details of the proposed model and dimensionless parameters are discussed in Chapter 5.

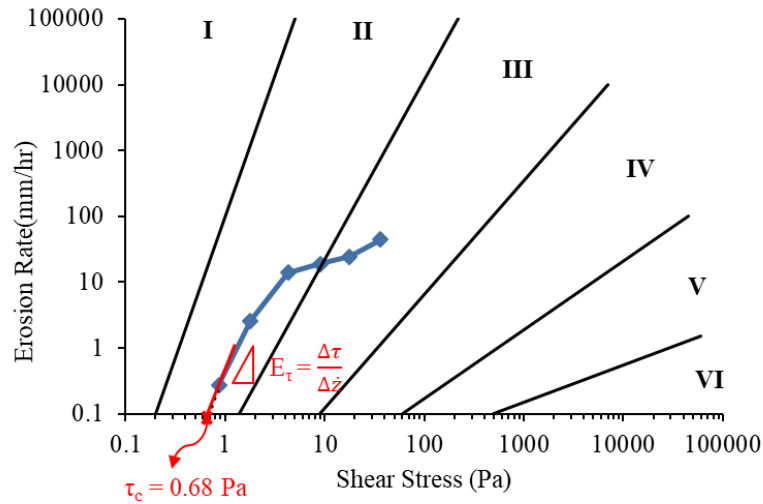


Figure 17. Erosion rate versus shear stress showing how to obtain slope of the erosion function (adapted from Briaud et al., 2019)

2.3.4. Erosion rate

The erosion rate of a soil is a soil reaction to a specific hydraulic shear stress induced by the eroding fluid. It can be expressed in terms of rate of change in depth of a soil surface, rate of change in soil volume, and rate of change in soil mass. In this dissertation, the erosion rate is defined as a rate of change in soil surface depth and expressed in mm/hr. This definition is derived from EFA testing (

Figure 6).

2.3.5. Critical velocity

The critical or the threshold velocity (m/s) is the mean depth water velocity below which no erosion occurs. This definition refers to the initiation of the erosion process and shows the

maximum velocity that the soil can resist without getting eroded. The critical velocity can be obtained from the erosion testing in the laboratory or in-situ knowing a flow rate and the geometry of an obstacle. For example, in the EFA, the velocity is computed as the flow rate divided by the area of the conduit through which the water flows (See Chapter 3 for more details).

2.3.6. Critical shear stress

The critical or the threshold shear stress (Pa or N/m^2) is the shear stress acting at the soil-water interface below which no erosion occurs. Typically, it is obtained from the erosion function as the intercept of the straight line drawn through the erosion curve and shear stress axis. In many cases, it is a challenge to define the straight line because the erosion functions can show a non-linearity between the erosion rate and the shear stress at the low shear stress (Figure 18).

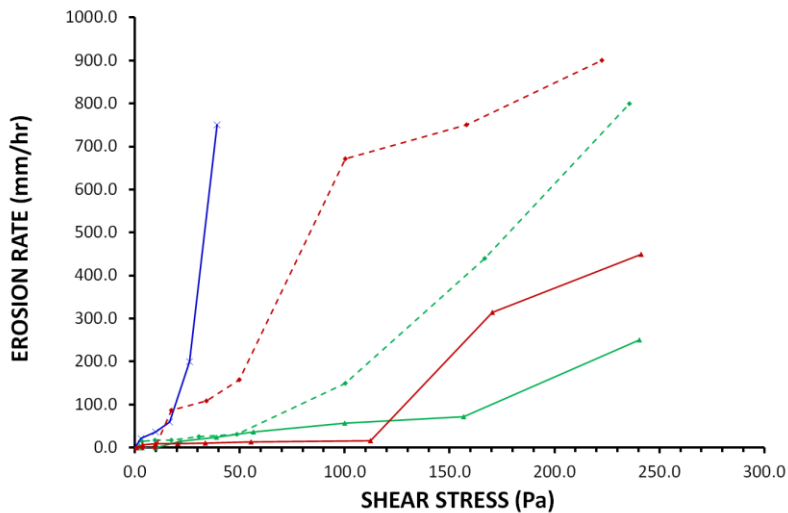


Figure 18. Erosion rate versus shear stress

In this dissertation, the critical shear stress is defined as the highest shear stress applied to the soil before any erosion was detected in the EFA while the velocity was gradually increased (Figure 19). This definition of the critical shear stress corresponds to the erosion rate of 0.1 mm/hr at which erosion can be neglected. If erosion is detected for the lowest velocity that can be applied in the EFA (0.3 m/s), the critical shear stress can be obtained by extending the erosion function until it intersected the shear stress axis with the erosion rate of 0.1 mm/hr (Figure 19). When it is not possible, the erosion rate of 0.1 mm/hr is used and the corresponding value of the shear stress is defined as the critical shear stress.

The critical shear stress is one of the two input parameters chosen for the probabilistic numerical simulations using the Bank Stability and Toe Erosion Model (BSTEM) by the United States Army Corps of Engineers (USACE) for prediction of erodibility of the riverbanks and levees in Sacramento, California (Rivas et al., 2021).

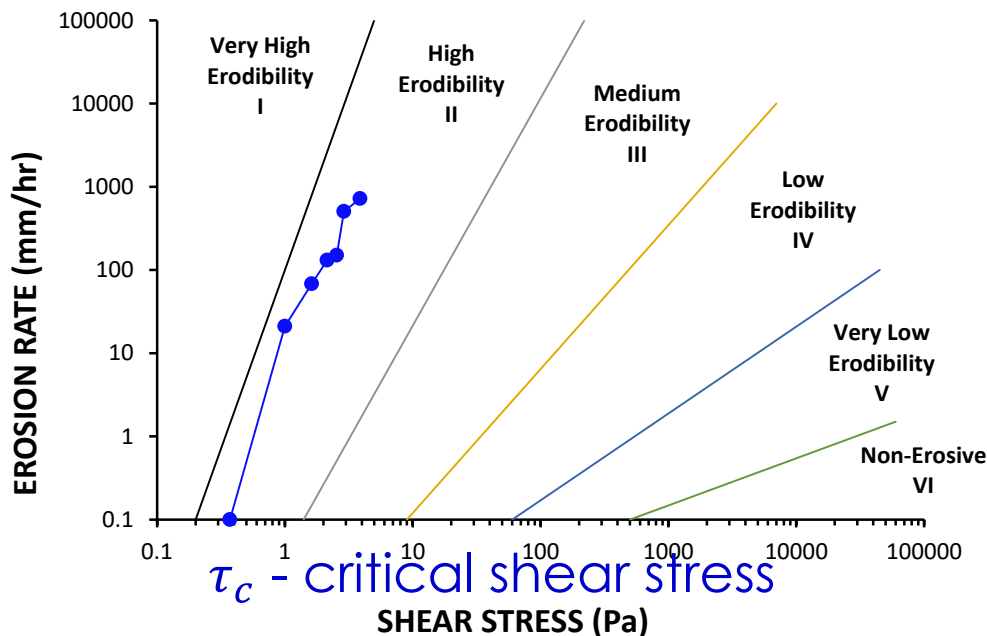


Figure 19. Erosion rate versus shear stress showing critical shear stress definition (adapted from Briaud et. al., 2019)

2.3.7. Erosion category

The erosion category is proposed as the median point in the erosion curve (Briaud et al., 2019). This approach has advantages and limitations. The advantages are its simplicity and dimensionless. However, the erosion category depends on the location of the median point on the erosion curve. Therefore, the limitation is that the number of points on the erosion function can impact the choice of erosion category. It is recommended to have at least six points in the erosion curve for better definition of erosion category. Figure 20 shows an example of how erosion category can be obtained from the entire erosion function. The solid and dash lines represent the erosion categories on the erosion chart. The median point in the erosion function corresponds to the erosion category of 2.25. The erosion category is useful for classifying dams or levee erodibility consisting of several zones or layers of soils of different erodibility (See Chapter 11, Section 11.3 for more details).

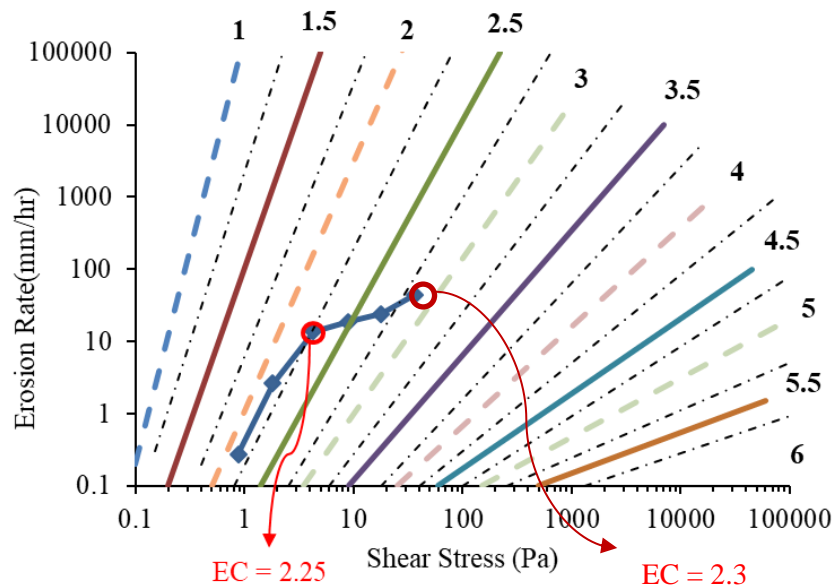


Figure 20. Erosion rate versus shear stress showing erosion category (adapted from Briaud et al., 2019)

3. EXPERIMENTAL RESEARCH ON SOIL ERODIBILITY

3.1. Existing knowledge on Borehole Erosion Test (BET)

The Borehole Erosion Test (BET) was developed by Briaud at Texas A&M University in 2014. The test is briefly described in Section 2.2. While two previous papers have been published on the BET (Briaud et al., 2016, Briaud et al., 2017), the BET is progressing, and new improvements need to be made.

In 2014 and 2015, as a part of a research project sponsored by Texas A&M Transportation Institute (TTI), a few shallow BET tests were performed at the RELIS Campus Sand and Clay sites at Texas A&M University (Briaud et al., 2016; Briaud et al., 2017). The depth of the borehole was 4.3 m at the clay site and 3.6 at the sand site. The clay site was predominately made of high plasticity clay (CH) and the sand site was made of clayey sand (SC). Figure 21 illustrates the borehole radius versus depth for the clay site before flushing and after flushing or three flow runs (caliper reading 1, 2 and 3). First flow run was 7.9 m³/hr (35 gpm), second – 4.8 m³/hr (21 gpm), third – 7.5 m³/hr (33 gpm). Table 10 gives the flow rates, velocities, and time of application of each velocity for the BET at the clay site.

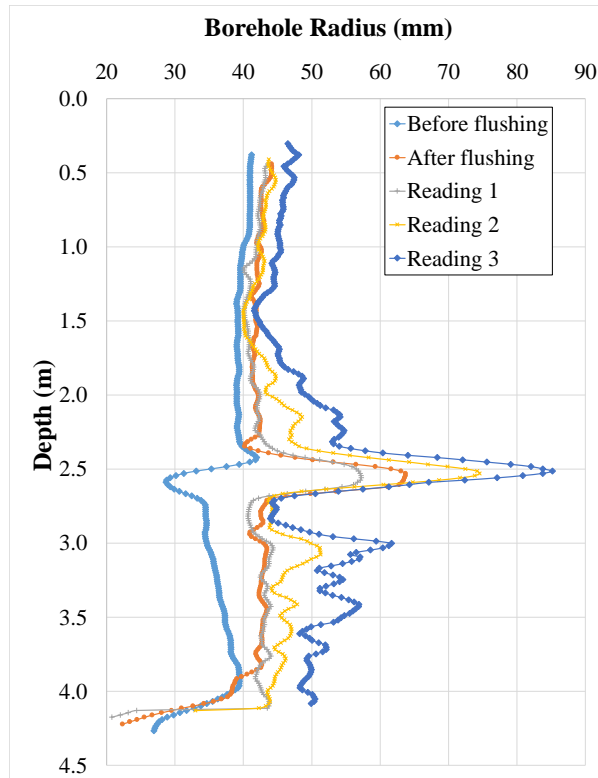


Figure 21. Borehole radius profile at different stages during the BET for the clay site (adapted from Briaud et al., 2017)

Figure 22 shows the borehole radius versus depth for the sand site before flushing and after flushing or two flow runs (caliper reading 1 and 2). First flow run was 7.7 m³/hr (34 gpm) and second – 8.6 m³/hr (38 gpm). Table 11 shows the flow rates, velocities, and time of application of each velocity for the BET at the sand site.

Table 10. Flow, velocity, and time for the BET at clay site (adapted from Briaud et al., 2017)

Depth (m)	Flow (m ³ /s)	Velocity (m/s)	Duration (min)	Change in profile
0.61 – 1.21	0.002271	1.967	1	before flushing to after flushing
	0.002208	1.308	10	After flushing to reading 1
	0.001325	0.773	10	Reading 1 to reading 2
	0.002082	1.063	10	Reading 2 to reading 3
1.21 – 1.81	0.002271	2.639	1	before flushing to after flushing
	0.002208	1.444	10	After flushing to reading 1
	0.001325	0.967	10	Reading 1 to reading 2
	0.002082	1.431	10	Reading 2 to reading 3

Depth (m)	Flow (m ³ /s)	Velocity (m/s)	Duration (min)	Change in profile
1.81 – 2.41	0.002271	2.450	1	before flushing to after flushing
	0.002208	1.280	10	After flushing to reading 1
	0.001325	0.669	10	Reading 1 to reading 2
	0.002082	0.687	10	Reading 2 to reading 3
2.41 – 3.01	0.002271	N/A	1	before flushing to after flushing
	0.002208	0.596	10	After flushing to reading 1
	0.001325	0.418	10	Reading 1 to reading 2
	0.002082	0.433	10	Reading 2 to reading 3
3.01 – 3.61	0.002271	2.242	1	before flushing to after flushing
	0.002208	1.188	10	After flushing to reading 1
	0.001325	0.621	10	Reading 1 to reading 2
	0.002082	0.712	10	Reading 2 to reading 3

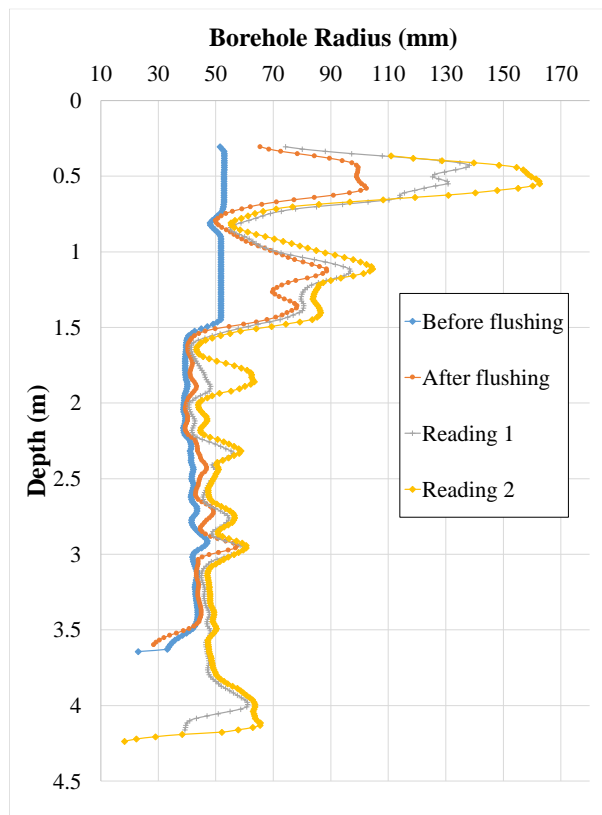


Figure 22. Borehole radius profile at different stages during the BET for the sand site (adapted from Briaud et al., 2017)

Table 11. Flow, velocity, and time for the BET at sand site (adapted from Briaud et al., 2017)

Depth (m)	Flow (m ³ /s)	Velocity (m/s)	Duration (min)	Change in profile
0.31 – 0.91	0.002334	0.518	0.5	before flushing to after flushing
	0.002145	0.147	7	After flushing to reading 1
	0.002397	0.102	7	Reading 1 to reading 2
0.91 – 1.51	0.002334	0.548	0.5	before flushing to after flushing
	0.002145	0.179	7	After flushing to reading 1
	0.002397	0.162	7	Reading 1 to reading 2
1.51 – 2.11	0.002334	2.453	0.5	before flushing to after flushing
	0.002145	1.555	7	After flushing to reading 1
	0.002397	1.191	7	Reading 1 to reading 2
2.11 – 2.71	0.002334	1.652	0.5	before flushing to after flushing
	0.002145	0.988	7	After flushing to reading 1
	0.002397	0.721	7	Reading 1 to reading 2
2.71 – 3.31	0.002334	1.207	0.5	before flushing to after flushing
	0.002145	0.769	7	After flushing to reading 1
	0.002397	0.647	7	Reading 1 to reading 2

The previous BET testing and data reduction procedure allowed to obtain only the borehole diameter and erosion rate versus depths but did not allow to compute shear stress. The interface shear stress was obtained from the Computational Fluid Dynamics (CFD) numerical simulations performed by Dr. Chen (Briaud et al., 2016). The results of the numerical simulations performed in 2016 indicate the surface roughness can have a major impact on the interface shear stress and that the shear stress is about 10 times higher on the bottom of the borehole than it is on the walls of the borehole (Briaud et al., 2017). The shear stress can be obtained by using the Moody chart (Moody, 1944) for the relative roughness ε/D less than 0.05 where ε is the soil surface roughness and D is the pipe diameter for the EFA. For the BET, Moody chart is limited and needs to be extended to the relative roughness $\varepsilon/D > 0.05$.

BET performed in 2014 and 2015 was very encouraging. An effort made to compare the BET results and the EFA results indicated that comparable values were obtained however further

testing was desirable to obtain a scale factor between testing a sample and running an in-situ test, to improve BET testing and data reduction procedure.

3.2. Field tests and sampling

Sections 3.2 to 3.8 come from the report to the USACE (Briaud et al., 2020). The City of Sacramento is home to the confluence of the Lower American River and the Sacramento River. Populated areas exist on both sides of these two large rivers that are bordered by levees. During high water events, the levees reduce the risk of flooding of these areas. In 2019, the US Army Corps of Engineers (USACE) initiated an erosion study of the riverbanks and levees in collaboration with US Geological Survey, the US Department of Agriculture, and Texas A&M University to improve the levees against erosion.

Several locations were selected for testing near the levees in the vicinity of Sacramento along the Sacramento River and the Lower American River. Accordingly, the sites were designated SAC (Sacramento River) sites and LAR (Lower American River) sites. A map showing drilling site locations is shown in

Figure 23. At several of the locations two borings were drilled: one to collect samples for soil properties including erosion study in the laboratory and one for performing in situ erosion testing. A series of field and laboratory tests to study erodibility of the riverbanks and levees were performed by Texas A&M University in 2019-2020. Among the tests were the Borehole Erosion Test (BET), the Erosion Function Apparatus (EFA), and the Pocket Penetrometer Test (PET).

The BET, a field in-situ test, was performed at 12 sites. At one BET location two tests were performed (SAC-3B water and SAC3B2 drilling mud): one with water and one with drilling mud. So, there were a total of 13 BET tests. Drilling took place to obtain the soil

stratigraphy and to collect samples for engineering properties prior to BET. Shelby tubes and bulk samples were collected in the field for testing in the EFA and PET at Texas A&M University. In total, 36 EFA and PET tests corresponding to 16 sites were performed.

The borings for samples collection and BET were 2-3 m apart from each other. The soil stratigraphy presented in this Chapter and used to correlate with erosion properties is based on the boring drilled for soil properties.

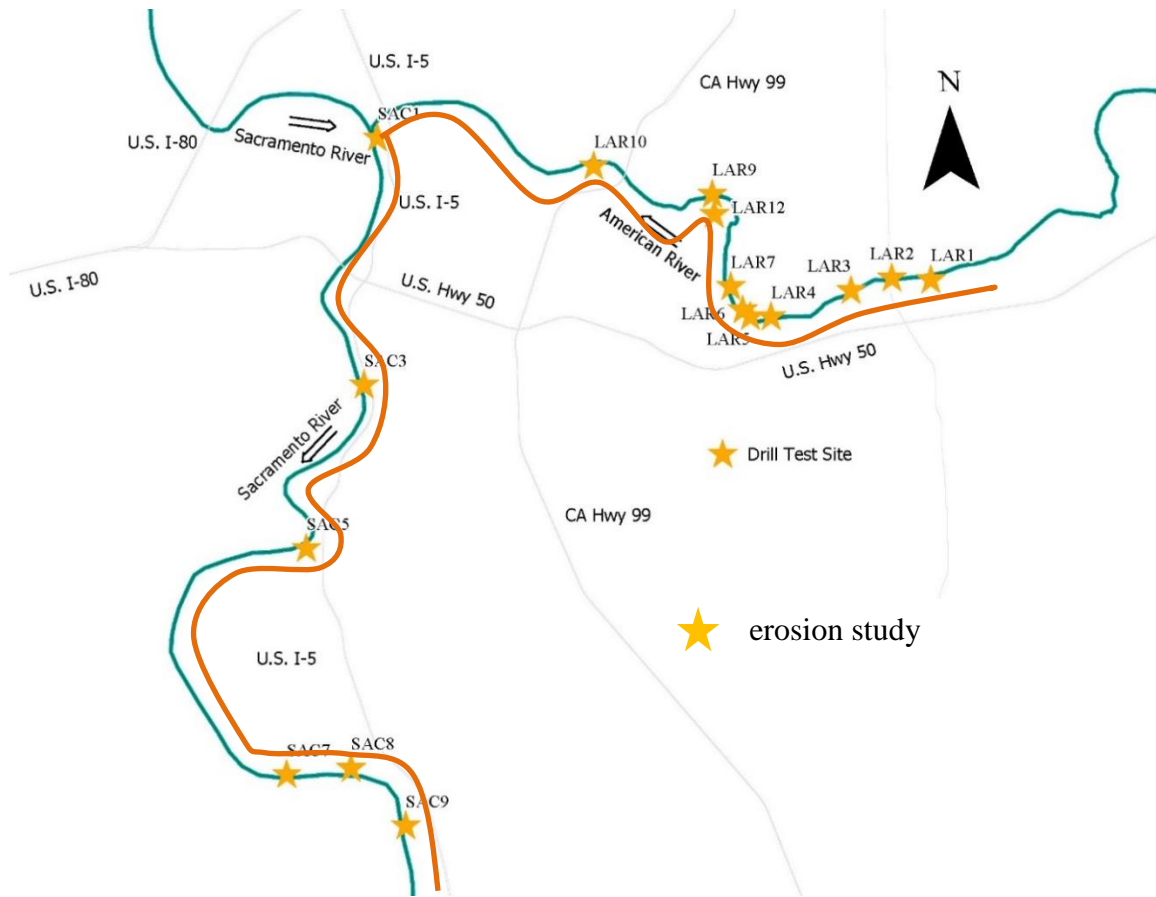


Figure 23. Drilling site locations near Sacramento (adapted from USGS, 2020, <https://www.usgs.gov/media/images/map-proposed-erosion-test-drill-sites>)

Next Sections presents the testing and data reduction procedure of the BET, EFA, and PET followed by discussion on their results including a comparison between these erosion tests.

The soil erosion category charts and classification charts are prepared and summary on erodibility of soils together with recommendations are made. The summary on soil samples tested in EFA and PET is given in Table 12. There were 12 samples in 76.2 mm (3-inch) outside diameter thin wall steel (Shelby) tubes and 24 bag samples of sand and gravel soils from the SPT sampler; they came from 16 borings. Table 13 shows the BET locations.

Table 12. Samples tested in the EFA and PET

#	Sample	Sample description	Site Location
1	Shelby tube	2F-19-LAR9A-ST2 11-13 ft	Lower American River
2	Shelby tube	2F-19-LAR9A -ST1 9-11 ft	Lower American River
3	Shelby tube	2F-19-LAR 6A-ST1 34-35 ft	Lower American River
4	Shelby tube	2F-19-SAC5A 53-55 ft	Sacramento River
5	Shelby tube	2F-19-SAC7A-ST2 15-17 ft	Sacramento River
6	Shelby tube	2F-19-SAC7A-ST1 9-11 ft	Sacramento River
7	Shelby tube	2F-19-SAC8A-ST2 47-49 ft	Sacramento River
8	Shelby tube	2F-19-SAC8A-ST-1 27-28.67 ft	Sacramento River
9	Shelby tube	2F-19-SAC9A-ST2 15-17 ft	Sacramento River
10	Shelby tube	2F-19-SAC9A-ST1 9-11 ft	Sacramento River
11	Shelby tube	2F-19-SAC1A-ST-6 29-31 ft	Sacramento River
12	Shelby tube	2F-19-SAC1A-ST-2	Sacramento River
13	Sand bags	2F-19-LAR9A Sand Sample #9	Lower American River
14	Sand bags	2F-19-LAR9A Sand Sample #8	Lower American River
15	Sand bags	2F-19-LAR7A Sand Sample #7	Lower American River
16	Sand bags	2F-19-LAR7A Sand Sample #6	Lower American River
17	Sand bags	2F-19-LAR7A Sand Sample #5	Lower American River
18	Sand bags	2F-19-LAR7A Sand Sample #4	Lower American River
19	Sand bags	2F-19-LAR7A Sand Sample #3	Lower American River
20	Sand bags	2F-19-LAR 6A – Sample # 11 (gravel)	Lower American River
21	Sand bags	2F-19-LAR6A Sand Sample #10	Lower American River
22	Sand bags	2F-19-LAR1A Sand Sample #12	Lower American River
23	Sand bags	2F-19-LAR12A Sand Sample #2	Lower American River
24	Sand bags	2F-19-LAR12A Sand Sample #1	Lower American River
25	Sand bags	2F-19-LAR4A–Sand Sample #24 (silty sand)	Lower American River
26	Sand bags	2F-19-LAR 10A – Sample # 16 (silty sand from 29 to 32.5 ft)	Lower American River
27	Sand bags	2F-19-LAR 10A – Sample # 14 (silty sand from 25 to 28.5 ft)	Lower American River

#	Sample	Sample description	Site Location
28	Sand bags	2F-19-LAR 3A – Sample #18 (silty sand from 11 to 16.5 ft)	Lower American River
29	Sand bags	2F-19-LAR 3A – Sample #17 (silty sand from 5 to 10.5 ft)	Lower American River
30	Sand bags	2F-19-SAC5A – Sample #25 (silty clay from 27 to 30 ft)	Sacramento River
31	Sand bags	2F-19-SAC5A – Sample #26 (silty sand from 42.5 to 48 ft)	Sacramento River
32	Sand bags	2F-19-SAC 3A – Sample #22 (sand from 15 to 18.5 ft)	Sacramento River
33	Sand bags	2F-19-SAC 8A – Sample #19 (sand from 9 to 12.5 ft)	Sacramento River
34	Sand bags	2F-19-SAC 8A – Sample #20 (sand from 7 to 8.5 ft)	Sacramento River
35	Sand bags	2F-19-SAC 3A – Sample #21 (silty sand from 3 to 10.5 ft)	Sacramento River
36	Sand bags	2F-19-LAR A1 – Sample #13 (silty sand from 23 to 26.5 ft)	Lower American River

Table 13. BET testing borehole’s locations

#	Borehole Number	Site Location
1	LAR2B	Lower American River
2	LAR3B	Lower American River
3	LAR5B	Lower American River
4.	LAR6B	Lower American River
5.	LAR7B	Lower American River
6.	LAR9B	Lower American River
7.	LAR10B	Lower American River
8.	LAR12B	Lower American River
9.	SAC1B	Sacramento River
10.	SAC3B (water)	Sacramento River
11.	SAC3B2 (drilling mud)	Sacramento River
12.	SAC7B	Sacramento River
13.	SAC9B	Sacramento River

3.3. Borehole Erosion Test (BET)

3.3.1. Improved testing procedure

As it was mentioned above, the Borehole Erosion Test (BET) has been already performed in 2014 and in 2015 in Texas, and in 2019 in California, Sacramento. In 2021, BET aims to be

performed in Netherlands. As the use of the borehole erosion test is increasing worldwide, lessons are being learned and the procedures are being updated and refined while dos and don'ts are encountered. This section describes the improved testing procedure for optimizing the result of the BET and the improved data reduction procedure for obtaining the erosion parameters such as shear stress. This is done considering some recent the BET results from Sacramento site. The general set up of the BET testing site is illustrated in Figure 24.



Figure 24. General set up for the BET (Sacramento, April 2019)

Recent tests have led to modifying the BET procedure as follows:

1. Decide on a site and a depth of erosion interest for a given structure such as a dam, a levee, a bridge pier or abutment, a river meander etc.
2. Set a casing down to a small depth, for example 0.6 m, with a known diameter, for example 100 mm. This will serve as an additional calibration for the caliper as it passes the casing. Seal the casing so the fluid used for drilling would return to the mud pit.

3. Drill a borehole by the wet rotary method over the depth of interest (Figure 25). The diameter of the drill bit is typically between 75 and 100 mm and the rods outside diameters should be 75% or less than the drill bit diameter ($OD_{rod} < 0.75 \times OD_{drill\ bit}$). For example, for 75 mm diameter of the borehole, the rods should have an outer diameter of about 50 mm so that the annulus is about 12.5 mm wide. The inside diameter of the rods is not critical. The size of the annulus will have an impact on the velocity that can be generated by the pump on the drilling rig. The drill rigs typically have pumps that can generate a maximum flow of about 50 m³/h or 220 gpm. Do not “clean” the borehole by repeated passages of the drill bit.

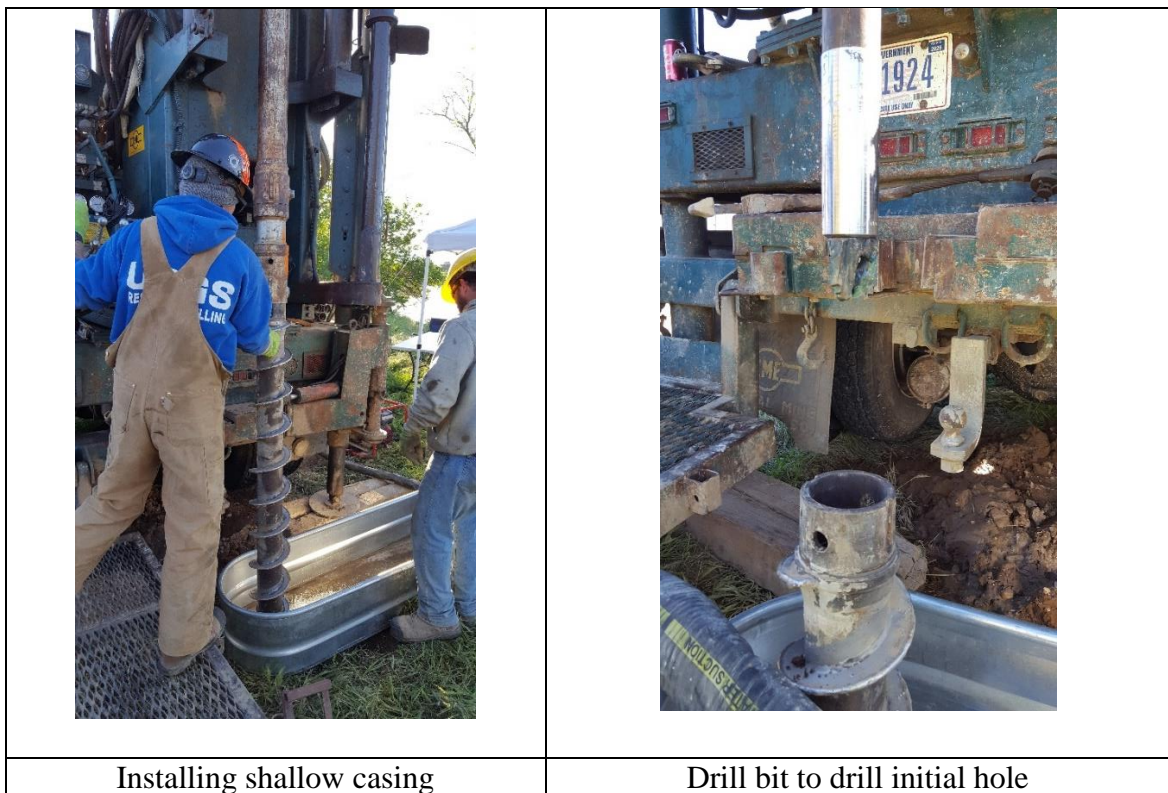


Figure 25. BET testing procedure

4. Remove the drilling rods and drill bit from the borehole.

5. Lower the caliper device to the bottom of the hole. A calibration of the caliper should be done before inserting (Figure 26). A 3-arms mechanical caliper works well for the BET. Figure 26 shows the caliper inserted in the borehole. Measure the depth of the bottom of the hole precisely. The caliper should be able to measure the diameter within 1 mm or better so the erosion rate is known with sufficient precision.



Figure 26. Caliper calibration and installation in the borehole

6. Once at the bottom of the borehole, deploy the arms of the caliper until they are in contact with the borehole wall. Pull the borehole caliper up the hole while recording the borehole diameter. The caliper arms, three at least, follow the hole and give a continuous record of its

average diameter. This gives the first borehole diameter profile D0. Repeat the caliper logging a couple of times for a better precision as the hole may not be completely circular.

7. Pull the caliper out of the hole.

8. Insert the drilling rods without the drill bit such that the bottom of the drilling rods is 0.15 m from the bottom of the borehole.

9. Start the pump and set it at a chosen flow rate (Figure 27). In doing so, the discharge at the bottom of the rods is vertical downward. The bottom of the hole can be tested as a jet erosion test; therefore, it is important to precisely measure the depth of the hole before and after the flow.

10. This flow rate should be calculated so that it corresponds to a chosen initial velocity V_1 in the annulus. The pump of the drilling rig is usually used for this purpose and maximum flow rates in the range of 55 to 109 m³/hr (200 to 400 gpm) are typical. The ability to generate velocities in the range of 0.5 to 4.0 m/s is desirable.

11. Maintain the flow for 10 minutes and record the flow as a function of time (1-minute intervals but continuous is best) (Figure 27).



Figure 27. Flowing the water for the BET

12. Stop the flow and remove the drilling rods from the borehole.
13. Repeat steps 5,6, and 7. This gives the diameter profile after water flow run 1 (D1). The difference between the initial diameter profile D0 and the diameter after flow run 1 D1 gives the increase in borehole diameter due to the 10-minute water flow at the chosen velocity.
14. Repeat steps 8 to 13 for different velocities. This gives data of velocities V2, V3, V4 and so on corresponding to diameter profiles D2, D3, D4 and so on.
15. Seal the borehole as required.

3.3.2. Improved data reduction procedure

This section describes a detailed data reduction procedure for the BET including shear stress calculation missing in the previous data reduction in 2014 and 2015. For that purpose, an automated Excel spreadsheet called TAMU-BET was developed by Shidlovskaya (2019). This spread sheet was provided to the Sacramento district of the US Army Corp of Engineers together

with the report “Assessing Erosion Resistance of Bank Materials on American and Sacramento Rivers”.

The Borehole Erosion Test (BET) data reduction consists of the following steps.

1. Input the field data which includes the site location, the site elevation and coordinates, the borehole number and diameter, the depths at which the caliper reading are taken, the corresponding borehole diameter (caliper reading) for each caliper run, the flow rate as a function of time, the time duration of the flow, and the outside radius of the rods.
2. Calculate the average radius versus depth profile for the borehole before any flow takes place. This requires making an average at any depth of the caliper diameter measurements recorded right after drilling the borehole. The radius is used because the erosion rate is the increase in radius divided by the elapsed time of flow. Indeed, several caliper diameter profiles are often recorded in the same borehole.
3. Calculate the average radius versus depth profile for the borehole after the first 10 minutes of flow. This requires making an average at any depth of the caliper diameter measurements recorded right after the 10 minutes of flow. Indeed, several caliper diameter profiles are often recorded in the same borehole.
4. Calculate the difference in radius between the profiles of step 1 and step 2 and record it as the radial erosion increment as a function of depth.
5. Calculate the erosion rate at any depth by dividing the radial erosion increment by the duration of the flow (10 minutes). This gives the erosion rate profile for the first flow velocity.
6. Repeat steps 2 to 5 for the other chosen flow rates.
7. During the first flow rate application, the flow rate varies, and an average value

has to be calculated. Calculate the average flow rate for the duration of the flow (10 minutes).

8. Repeat step 7 for all flow rates applied during the BET.

9. For each one of the flow rates Q , calculate the associated velocity by dividing the flow rate by the area available for the water to flow. This area varies with depth and is taken as the area of the annulus between the outside diameter of the rods and the diameter of the borehole at that depth. The diameter of the borehole at a given depth during the 10 minutes of flow is taken as the average of the annulus area before the flow start and after the flow stops. This step gives the velocity V profile for the first average flow rate (Eq. 6).

$$V = \frac{4Q}{\pi(R_{borehole}^2 - R_{outsiderod}^2)} \quad (6)$$

where Q is the flow rate, $R_{borehole}$ is the radius of the borehole, $R_{outsiderod}$ is the outside radius of the rods.

10. Repeat step 9 for all other flow rates.

11. Calculate the shear stress associated with the velocity as described in the following steps.

12. The Eq. 7 is to be used for the shear stress τ calculation from basic hydraulic engineering dimensional analysis (Munson, 2009) is:

$$\tau = \frac{1}{8} f \rho V^2 \quad (7)$$

where τ is the hydraulic shear stress at the water-soil interface, f is the friction factor, ρ is the density of water (1000 kg/m^3), and V is the mean flow velocity (m/s).

The following is the step-to-step procedure to obtain the shear stress.

a. Calculate the Reynolds Number Re as follows (Eq. 8).

$$Re = \frac{VD_h}{\nu} \quad (8)$$

where V is the velocity, D_h is the hydraulic diameter of the annulus space between the rods and the wall of the borehole and ν is the kinematic viscosity of water ($10^{-6} \text{ m}^2/\text{s}$ at 20°C).

- b. Obtain the hydraulic diameter D_h for an annulus as follows (Eq. 9):

$$D_h = \frac{4A_{cr}}{P_w} \quad (9)$$

where A_{cr} is the cross-sectional area of flow, P_w is the wetted perimeter.

The hydraulic diameter after simple calculations is happened to be just a difference between the outside diameter D_o (diameter of the borehole) and inside diameter D_i (diameter of the rods). Therefore, $D_h = D_o - D_i$. At any depth, the outside diameter D_o is taken as the average of 2 times the borehole radius before the flow and 2 times the borehole radius after the flow. The inside diameter D_i is equal to 2 times the outside radius of the rods.

- c. Calculate the friction factor f for the circular pipe using Moody chart or Haaland equation (Haaland, 1983). Moody (1944) developed a chart which gives the friction factor as a function of the relative roughness $\frac{\varepsilon}{D_h}$ and the Reynolds Number. The existing Moody chart (Figure 28) can be used for the relative roughness not more than 0.05. For the BET, the relative roughness can exceed 0.05 and can reach 0.1 and more. That is why Moody chart was extended (Figure 29) for rough soil with relative roughness more than 0.05. Extended Moody chart allows to use much higher relative roughness to obtain friction factor. Moody chart works for circular pipes and leads to the following equation proposed by Haaland (1983) (Eq. 10).

$$\frac{1}{\sqrt{f}} = -1.8 \log \left[\left(\frac{\varepsilon/D_h}{3.7} \right)^{1.11} + \frac{6.9}{Re} \right] \quad (10)$$

where ε is the roughness or the mean depth of the asperities along the borehole wall. Note that the roughness of the outside wall of the pipe is much smoother and so would the associated shear stress but since the quantity of interest is the shear stress on the soil surface, the roughness of the

soil surface is the one used here.

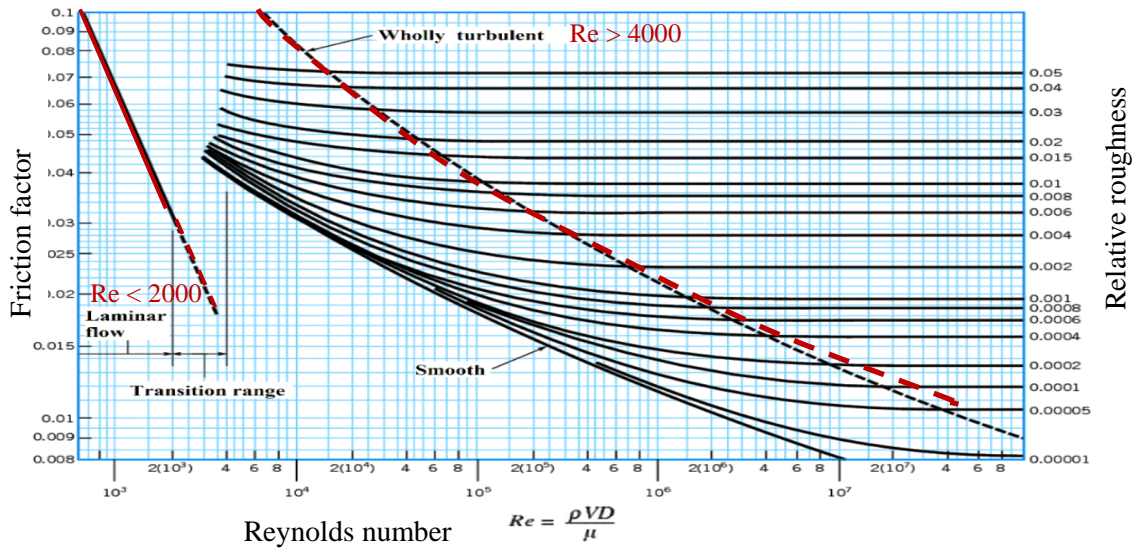


Figure 28. Moody chart for rough pipes (adapted from Munson, 2009)

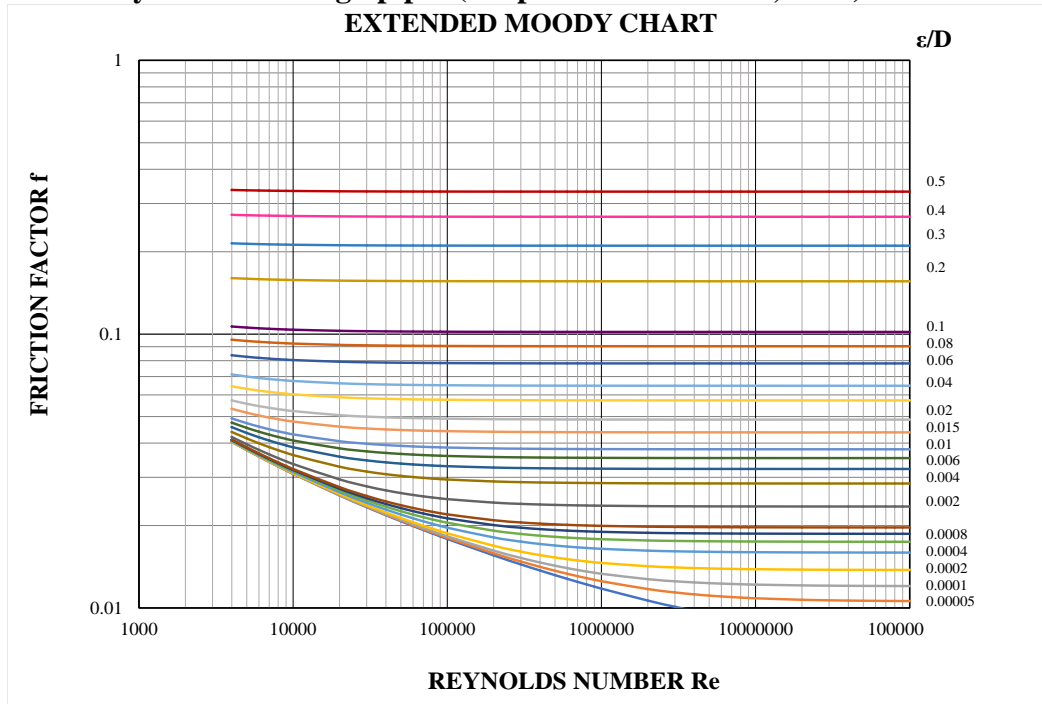


Figure 29. Extended Moody chart for very rough soil surfaces (modified from Moody 1944)

d. Obtain the friction factor for the annulus using the friction factor for the open pipe and the coefficient to go from the circular pipe to the annulus pipe. For the open pipe, the

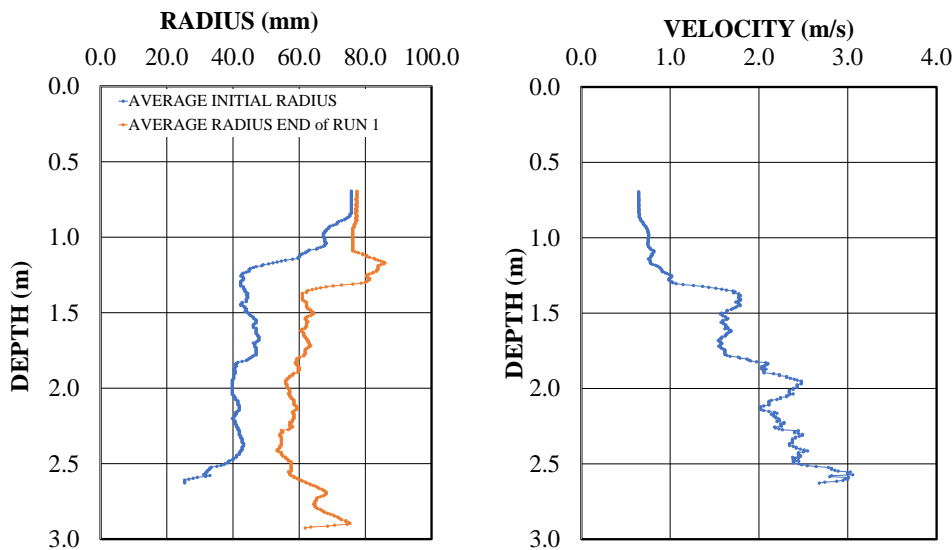
coefficient $C = fRe = 65$ (from the Moody chart for laminar flow). For the annulus pipe, the coefficient $C = fRe = 95.6$. The ratio between the friction factor for annulus and the friction factor for the open pipe is $95.6/65=1.5$. Therefore, use the coefficient 1.5 to go from the open circular pipe to the annulus pipe as $f_{\text{annulus}} = 1.5 f_{\text{pipe}}$.

e. The roughness ϵ is generated as a profile by considering a rolling depth equal to 0.1 m of the eroded radius profile and calculating for each one of those 0.1 m depth the mean depth of the asperities.

f. Now all the elements are set to calculate the shear stress from the velocity as follows (Eq. 6). At any depth, obtain the velocity using, then the fluid density, then the roughness, then the hydraulic diameter of the annulus (Eq. 8), then Reynolds Number (Eq. 7), then the friction factor (Figure 29), and then the hydraulic shear stress (Eq. 6).

g. Prepare a profile of shear stress versus depth.

h. Use the profiles of radius vs depth, erosion rate vs depth, velocity vs depth, and shear stress vs depth to generate for each stratigraphic layer the erosion functions of erosion rate vs velocity and erosion rate vs. shear stress. The examples of the profiles are shown in Figure 30.



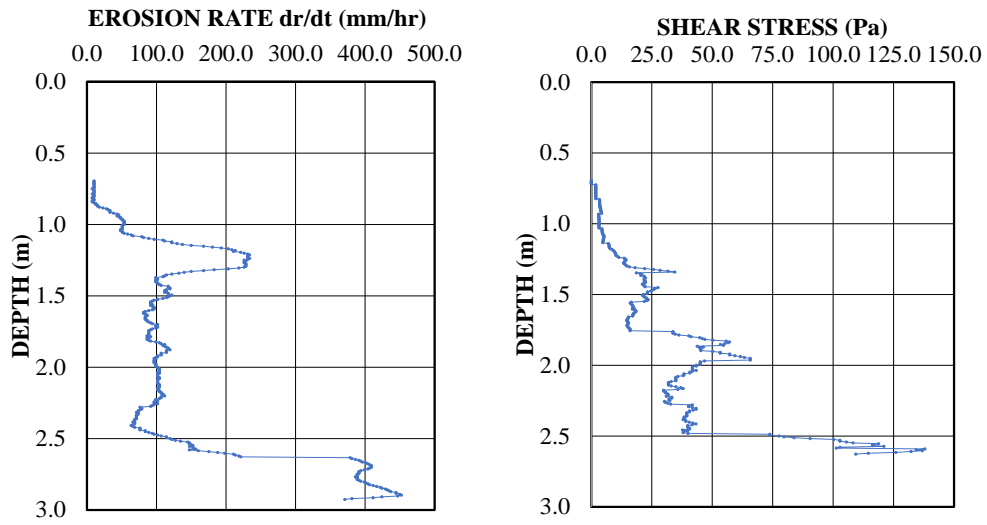


Figure 30. The example of the BET data reduction Excel Spreadsheet (TAMU-BET)

3.4. Erosion Function Apparatus

3.4.1. Testing procedure

The brief information about the Erosion Function Apparatus or EFA is presented in Chapter 2, Section 2.2.1. The testing procedure for the EFA is presented below.

1. Remove the end caps of the sampling Shelby tube.
2. Extrude and cut off a sample length equal to 1 cm from the end of the sample.

This end is the bottom of the sample (larger depth). This was done for twelve fine grain soil samples received in sampling Shelby tubes.

3. Collect a sample piece for water content determination prior to erosion testing (called water content before EFA testing).
4. Perform a pocket penetrometer test on the surface of the sample.
5. Perform a mini hand vane test on the end of the sample.
6. Perform a pocket erodometer test on the sample surface.
7. Push the sample far enough (about 8-10 cm) to describe and visually identify the soil type and to then cut off that zone disturbed by the testing in steps 3 to 6 above.
8. Extrude the sample from the sampling tube and transfer it into the testing tube. Before placing the sample into the testing tube, weigh the testing tube. Then, after transferring the sample in the testing tube, weigh the testing tube with the sample. Measure the length of the sample in the testing tube as well as the internal diameter of the testing tube. This will be used for the unit weight determination later on.
9. Bring the testing tube with the sample to the EFA machine.

10. Place the testing tube through the bottom of the conduit where the water will flow over the sample (Figure 31). Set the soil sample surface to be flush with the bottom of the conduit.

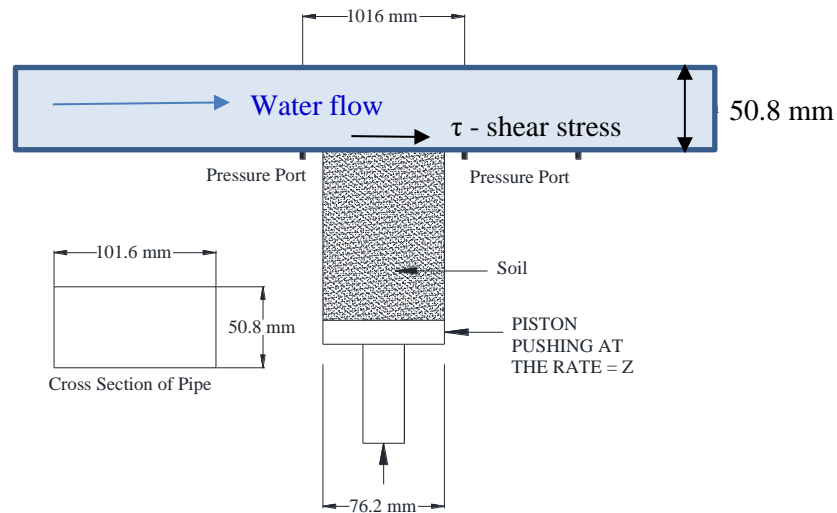


Figure 31. Erosion Function Apparatus to measure erodibility (adapted from Briaud et al., 2001)

11. Bring the piston up to meet with the bottom of the soil sample and stop when the sample starts to move up into the conduit.

12. Start the water flow at a chosen velocity (for example 0.3 m/s). Maintain that velocity and observe if any erosion occurs.

13. If erosion occurs advance the piston only as much as needed to bring it flush with the bottom of the water conduit. Sometimes the sample surface is rough, and judgement is needed to estimate the amount of push necessary to achieve the “flush with the bottom” concept. Sometimes at high velocities, the erosion rate can be faster than the maximum speed of the

piston. In this case the test is stopped, and the piston pushes the soil to be flush with the bottom before the test resumes.

14. If erosion does not occur, do not advance the piston.
15. Maintain the flow at that velocity for a minimum of 10 minutes or 10 mm of piston movement, whatever comes first.
16. Repeat steps 12 to 15 for other chosen velocities until the erosion function is well described (usually 6 velocity points on the erosion curve).
17. Stop the test, retrieve the sample and take a water content sample from the sample surface (called water content after EFA testing)
18. Secure the sample back into the humidity room if any soil is left.
19. A special procedure was used to prepare the EFA sample from the bag samples of coarse grain soils collected with the split spoon sample used in a Standard Penetration Test. The samples were reconstituted in a testing tube for EFA testing. For this, measurements collected at the site such as Standard Penetration Test (SPT) blow count were used. The estimated in situ unit weight became the target unit weight.

3.4.2. Data reduction procedure

1. The raw data results for the EFA test are the piston travel as a function of time and the flow rate or the velocity as a function of time. The test results consist of the erosion rate \dot{z} versus shear stress τ curve and erosion rate \dot{z} versus mean flow velocity V curve (Figure 32 and Figure 33). For each flow velocity V , the erosion rate \dot{z} (mm/hr) is obtained by dividing the length h of sample eroded taken equal to the piston travel length by the time t required to do so (Eq. 11).

$$\dot{z} = \frac{h}{t} \quad (11)$$

2. The velocity V is obtained by measuring the flow Q given by the flowmeter and dividing Q by the flow area A of the EFA water conduit (50.8 mm high by 101.6 mm wide). This works for the first versions of the EFA manufactured by Humboldt. Note that the latest version of the EFA given the velocity and not the flow rate.

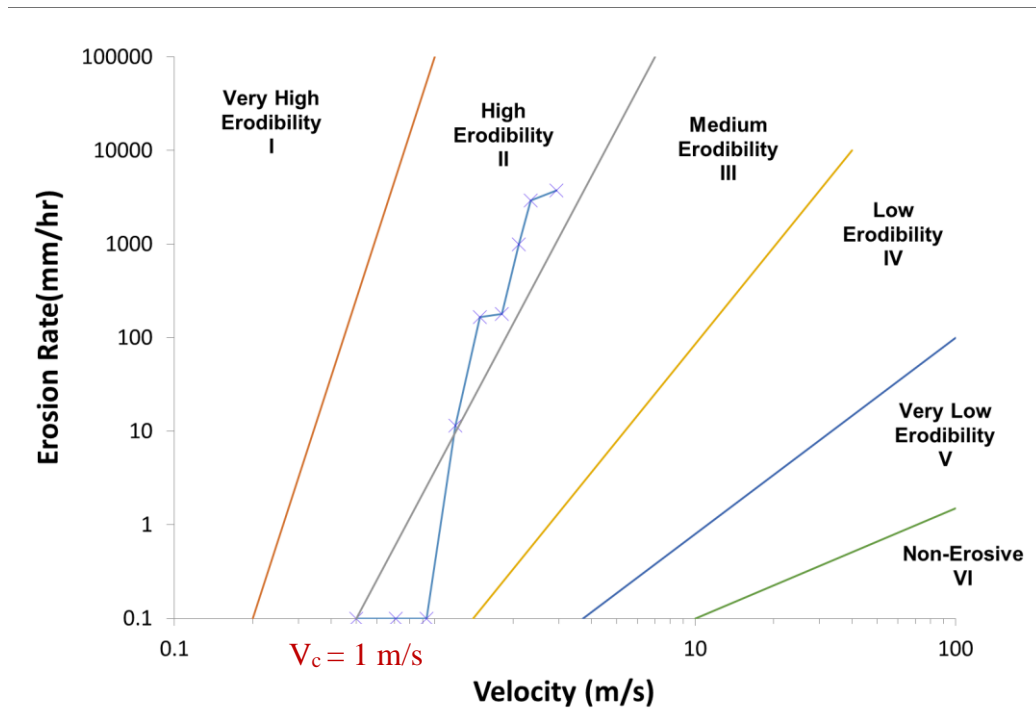


Figure 32. Example of EFA test result: erosion rate vs. velocity (SAC5A-Sample#25)

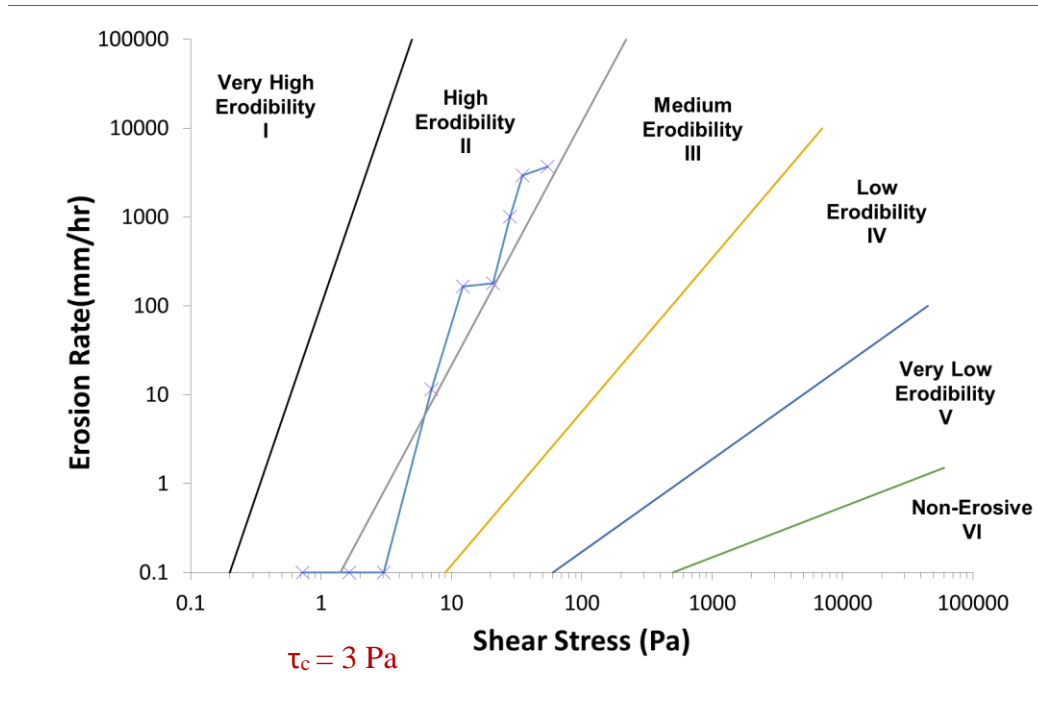


Figure 33. Example of EFA test result: erosion rate vs. shear stress (SAC5A-Sample#25)

The procedure to obtain the shear stress is the follows.

1. The shear stress τ is obtained from the basic hydraulic engineering for pipe flows (Munson, 2009) (Eq. 12).

$$\tau = \frac{1}{8} f \rho V^2 \quad (12)$$

where τ is the shear stress on the wall of the pipe in the EFA (conduit), f is the friction factor obtained from the Moody Chart (see Chapter 3.3.2.), ρ is the mass density of water (1,000 kg/m³), and V is the mean flow velocity in the conduit.

2. The friction factor f can be obtained from Moody chart or the Haaland equation (See Chapter 3.3.2).

3. The Reynolds Number is shown (Eq. 13)

$$R_e = \frac{VD_h}{\nu} \quad (13)$$

where D_h is the pipe hydraulic diameter and ν is the kinematic viscosity of water (10^{-6} m²/s at 20°C). Since the pipe in the EFA has a rectangular cross section, D is taken as the hydraulic diameter $D = 4A/P$ where A is the cross-sectional flow area, P is the wetted perimeter, and the factor 4 is used to ensure that the hydraulic diameter is equal to the diameter for a circular pipe. For a rectangular cross-section pipe (Eq. 14):

$$D_h = \frac{2ab}{a+b} \quad (14)$$

where a and b are the dimensions of the sides of the rectangle. The parameter D is 67.7 mm for the EFA conduit.

4. The relative roughness ε/D is the ratio of the average height ε of the sample roughness over the pipe diameter D . The average height of the sample roughness ε is taken equal to $0.5D_{50}$ where D_{50} is the mean grain size for the soil. The factor 0.5 is used because it is assumed that the top half of the particle protrudes into the flow while the bottom half is buried in the soil mass. For fine-grain soils, the roughness is taken as one half of the depth of the asperities on the sample surface. In many cases, this sample roughness is larger than $0.5D_{50}$ and the value of the relative roughness ε/D is larger than the largest value in Moody's chart set at 0.05. For this reason, Moody's chart was extended to cover larger values of ε/D by using Haaland's equation (see Chapter 3.3.2).

5. The result of an EFA test are a couple of erosion functions for the soil sample tested. They consist of the relationship between the erosion rate and the velocity on one hand and between erosion rate and shear stress at the interface between the fluid and the soil on the other hand. A set of 6 points at least is recommended to define the erosion curve.

On Figure 32, the critical velocity v_c was defined as the velocity below which no erosion occurred. On Figure 33, the critical shear stress τ_c corresponding to the critical velocity measured in the EFA was defined as the shear stress below which no erosion occurred. The slope of the erosion function can be determined as the slope of the linear regression line through the measured erosion rate vs shear stress points plotted on natural scales (See Section 2.3.).

3.5. Pocket Erodrometer Test

3.5.1. Testing procedure

The Pocket Erodrometer Test was invented by Briaud in 2011 as a quick laboratory or field erosion test (Briaud et al., 2012). The general idea of the PET is described in Section 2.2.7. This section provides the detailed testing procedure which was used in the current erosion study.

1. Fill the PET with tap water. Use other liquid or water of a certain chemistry if needed.
2. Calibrate the exit nozzle velocity to be 8 m/s. For doing that, the Pocket Erodrometer should be placed at a chosen height, aimed horizontally, and a water impulse is imparted.
3. Apply a definition of velocity and its horizontal component to obtain the particle motion equation (Figure 34) as follows (Eq. 15).

$$x = v_{0x} t \quad (15)$$

where x is a horizontal distance or displacement of water point, v_{0x} is the horizontal nozzle velocity, t is the time elapsed since the trigger is squeezed and the water portion leaves the nozzle.

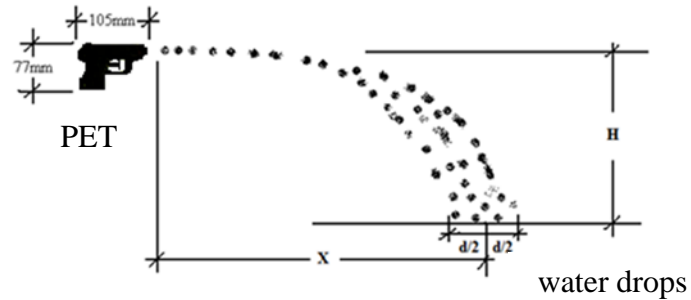


Figure 34. Calibrating the PET (adapted from Briaud, 2013)

4. Use a definition of velocity and its vertical component (Eq. 16).

$$H = \frac{1}{2}gt^2 \tag{16}$$

where H is the height of the PET, g is the acceleration due to gravity.

The acceleration due to gravity is $g = d^2z/dt^2$. After first integration $dz/dt = gt + V_0 = V_{\text{vertical}}$. But since $V_{\text{vertical}} = 0$ at $t = 0$ (no vertical velocity when the nozzle is squeezed) then $V_0 = 0$ and the equation is $dz/dt = gt$. After integration one more time $z = 0.5gt^2 + z_0$. Since the start elevation is 0, then $z_0 = 0$ and the equation is $z = 0.5gt^2$. For a chosen time at which the water molecule hits the ground surface, $z = H$, the equation is $H = 0.5gt^2$.

5. Eliminating t between Eq. 14 and 15 gives Eq. 17.

$$v_{0,x} = \frac{x}{\sqrt{\frac{2H}{g}}} \tag{17}$$

6. Calibrate the squeezing of the trigger of the PET to obtain the desired nozzle velocity of 8 m/s. The trigger should be squeezed 20 times at a rate of 1 squeeze per second. A mark should be made at the two ends of most of the water on the floor surface because of scatter (Figure 34). These end values of x should be used in Eq. 16. Place the PET nozzle 5 cm from the

sample surface (Figure 35) and impart 20 jet applications aiming the same spot on the sample surface.

7. Measure the depth of the hole eroded in the surface of the sample with a caliper.

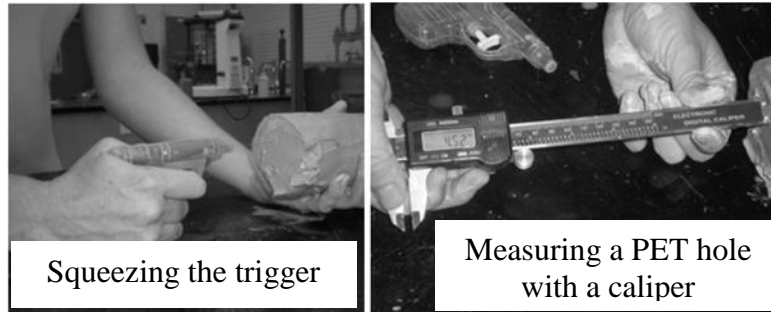


Figure 35. Snapshots of PET procedure (adapted from Briaud, 2013)

3.5.2. Data reduction procedure

The following data reduction procedure was used.

1. Measure the depth of the hole after running the PET with a caliper (Section 3.5.1.).
2. Use the PET erosion chart which gives the PET soil erosion categories to classify a soil erodibility (Figure 36).

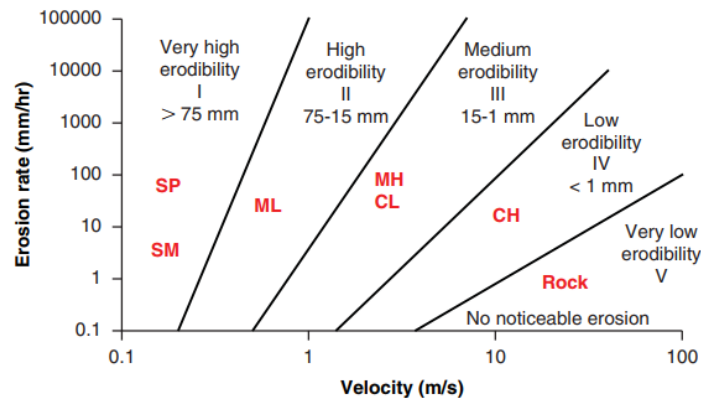


Figure 36. Erosion categories for soils based on the PET (adapted from Briaud et al., 2013)

The detailed data reduction procedure can be found in Briaud et al. (2012).

3.6. Erosion tests results

In this Section, the erosion tests result and analysis for all erosion tests (BET, EFA, and PET) are presented. The erosion parameters obtained from the erosion testing are critical velocity, critical shear stress, the slope of the erosion function in natural scale obtained from all the erosion testing. The data reduction procedure for each test described in the previous Sections.

3.6.1. Erosion Function Apparatus (EFA)

Figure 37 - Figure 40 show the EFA results regrouped on one erosion chart. The different figures are combinations in terms of velocity or shear stress versus erosion rate in natural and log-log scale. These charts include a total of 36 EFA tests performed on fine and coarse grain soils. Overall, the soils tested fit in the high erodibility category on the chart with very a few of them in the very high erodibility category and some of them landing on the medium erodibility category.

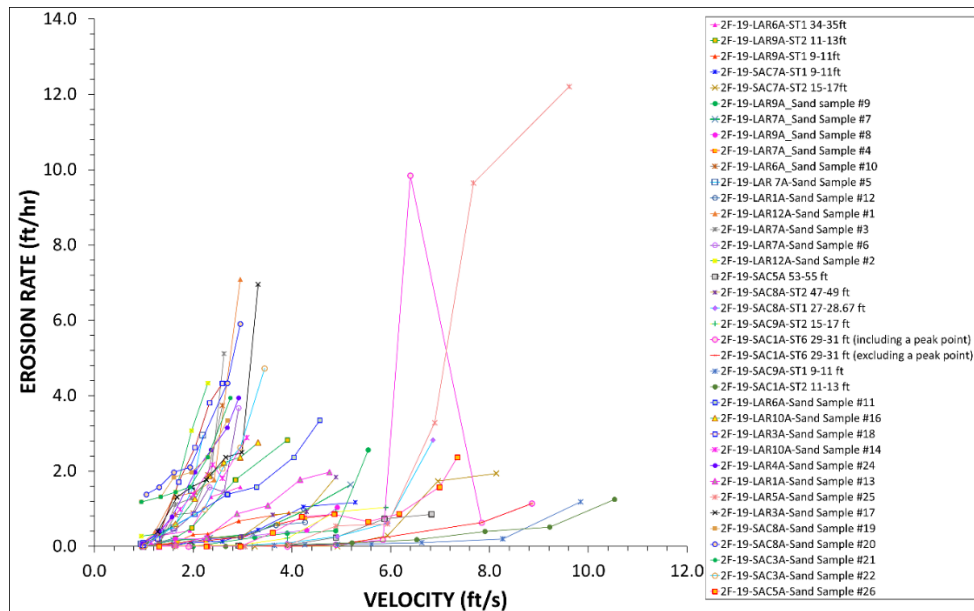


Figure 37. Erosion rate vs. velocity chart in natural scale (EFA tests results)

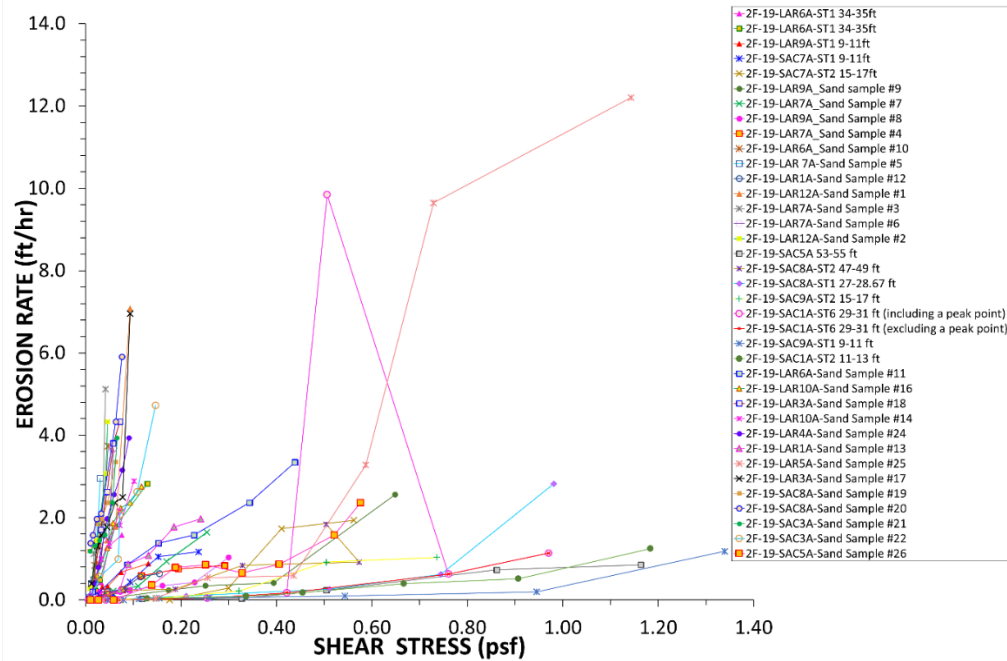


Figure 38. Erosion rate vs. shear stress chart in natural scale (EFA tests results)

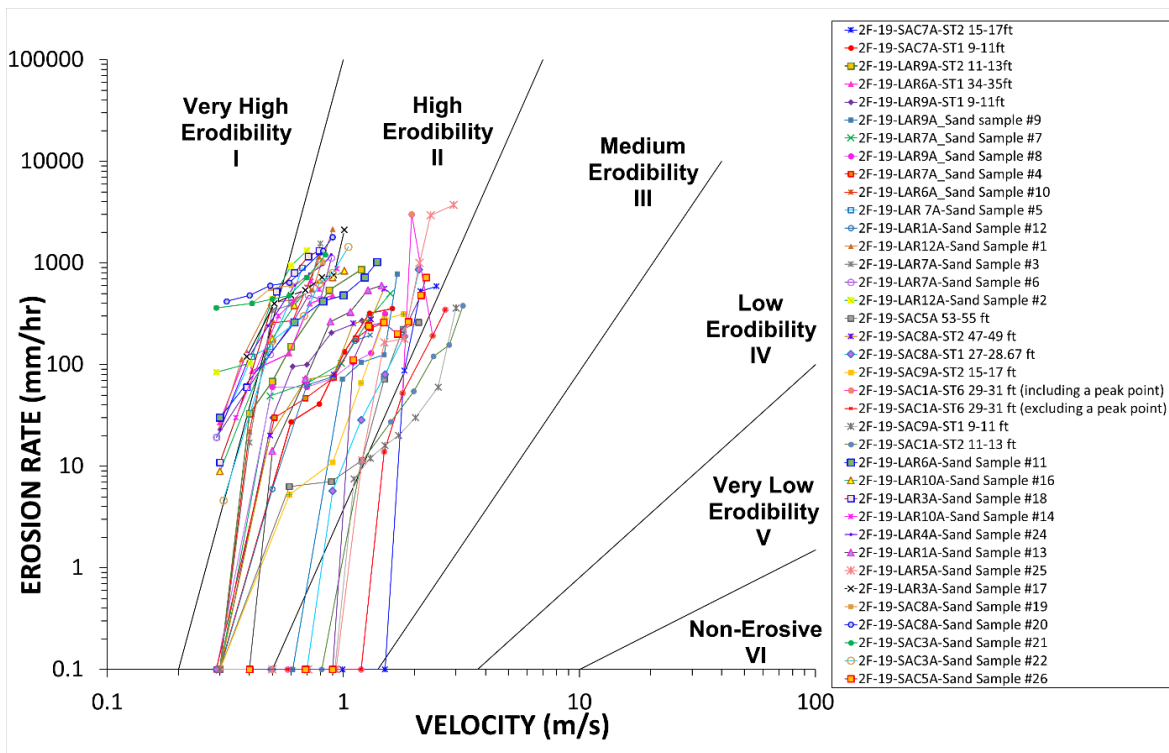


Figure 39. Erosion rate vs. velocity chart in log-log scale (EFA tests results)

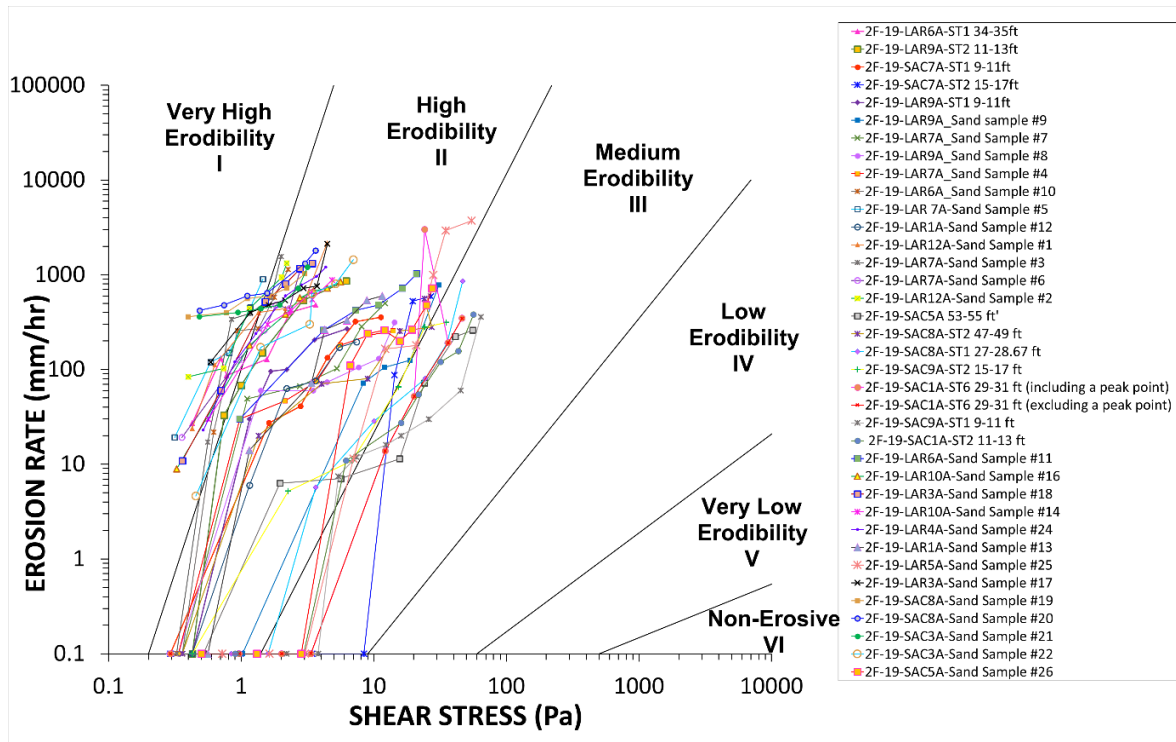


Figure 40. Erosion rate vs. shear stress chart in log-log scale (EFA tests results)

As it was described in Section 2.3.6, the critical shear stress is defined as the highest shear stress applied to the soil before any erosion was detected in the EFA test where the velocity was gradually increased. If erosion is detected for the lowest velocity that can be applied in the EFA (0.3 m/s) the corresponding value of shear stress is used as the critical shear stress.

The slope of the erosion function, called k_d , was determined as the slope of the linear regression line through the measured erosion rate versus shear stress points plotted on natural scales. An example showing the critical shear stress and the slope of the erosion function definition is presented in Figure 41. The individual values of critical shear stress τ_c , critical velocity v_c , and the slope of the erosion function k_d are shown in Table 14. The critical velocity measured in the EFA varied from 0.29 m/s to 1.5 m/s. The critical shear stress measured in the EFA varied from 0.293 Pa to 8.438 Pa.

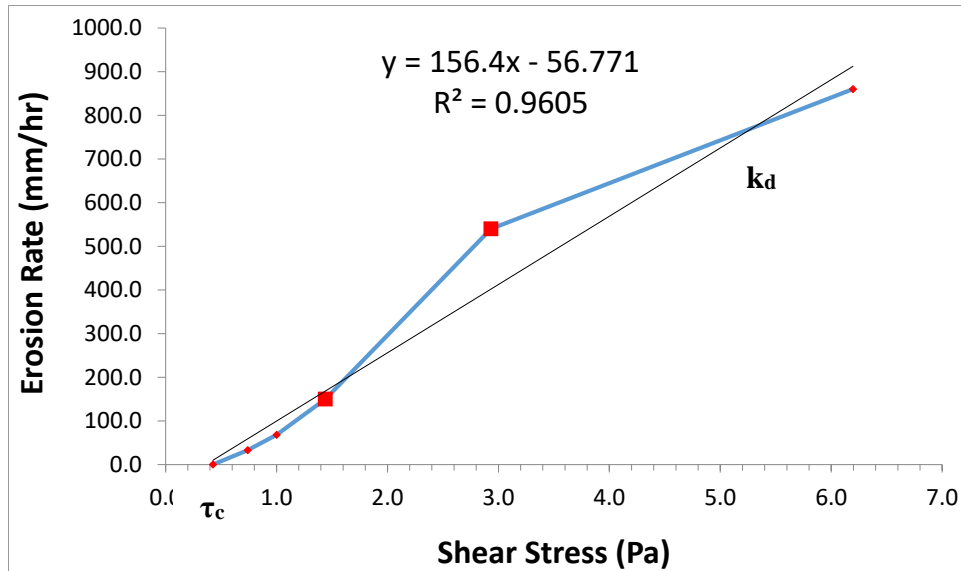


Figure 41. An example of erosion function for critical shear stress and slope definition

Table 14. Critical shear stress and slope of erosion function measured in EFA tests

#	Sample description	Site Location	v_c (m/s)	τ_c (Pa)	k_a ((mm/hr)/Pa)
1	2F-19-LAR9A-ST2	Lower American River	0.3	0.428	156.4
2	2F-19-LAR9A -ST1		0.3	0.428	66.102
3	2F-19-LAR 6A-ST1		0.3	0.428	142.59
4	2F-19-SAC5A	Sacramento River	0.3	0.518	5.11
5	2F-19-SAC7A-ST2		1.5	8.438	35.705
6	2F-19-SAC7A-ST1		0.3	0.293	36.676
7	2F-19-SAC8A-ST2		0.3	0.36	15.826
8	2F-19-SAC8A-ST-1		0.7	1.593	13.755
9	2F-19-SAC9A-ST2		0.3	0.428	10.169
10	2F-19-SAC9A-ST1		0.92	3.809	1.328
11	2F-19-SAC1A-ST-6		1.19	3.363	16.938
12	2F-19-SAC1A-ST-2		0.81	2.952	5.96
13	2F-19-LAR9A Sand Sample #9	Lower American River	0.61	1.023	7.137
14	2F-19-LAR9A Sand Sample #8		0.29	0.336	10.436
15	2F-19-LAR6A Sand Sample #7		0.3	0.36	40.796
16	2F-19-LAR7A Sand Sample #6		0.29	0.357	397.75
17	2F-19-LAR7A Sand Sample #5		0.29	0.315	742.08
18	2F-19-LAR7A Sand Sample #4		0.29	0.336	19.829
19	2F-19-LAR7A Sand Sample #3		0.3	0.326	793.01
20	2F-19-LAR 6A		0.3	0.979	45.413
21	2F-19-LAR6A Sand Sample #10		0.3	0.36	565.44
22	2F-19-LAR1A Sand Sample #12		0.3	0.428	30.091

#	Sample description	Site Location	v_c (m/s)	τ_c (Pa)	k_d ((mm/hr)/Pa)	
23	2F-19-LAR12A Sand Sample #2		0.29	0.399	754.04	
24	2F-19-LAR12A Sand Sample #1		0.3	0.428	459.99	
25	2F-19-LAR4A–Sand Sample #24		0.3	0.518	307.49	
26	2F-19-LAR 10A – Sample # 16		0.3	0.326	160.54	
27	2F-19-LAR 10A – Sample # 14		0.35	0.567	191.67	
28	2F-19-LAR 3A – Sample #18		0.3	0.36	458.02	
29	2F-19-LAR 3A – Sample #17		0.39	0.589	395.2	
30	2F-19-SAC5A – Sample #25		Sacramento River	0.93	3.027	72.409
31	2F-19-SAC5A – Sample #26			0.9	2.835	22.212
32	2F-19-SAC 3A – Sample #22			0.31	0.456	209.53
33	2F-19-SAC 8A – Sample #19	0.29		0.399	243.21	
34	2F-19-SAC 8A – Sample #20	0.32		0.486	424.46	
35	2F-19-SAC 3A – Sample #21	0.29		0.484	274.44	
36	2F-19-LAR A1 – Sample #13	Lower American River	0.4	0.560	59.72	

Figure 42 shows the correlation between the slope of the EFA erosion function k_d and the EFA critical shear stress τ_c . The Eq. 18 obtained after ignoring several outlier points is:

$$k_{dEFA} \left(\frac{mm/hr}{Pa} \right) = 42 (\tau_{CEFA}(Pa))^{-1.5} \quad (18)$$

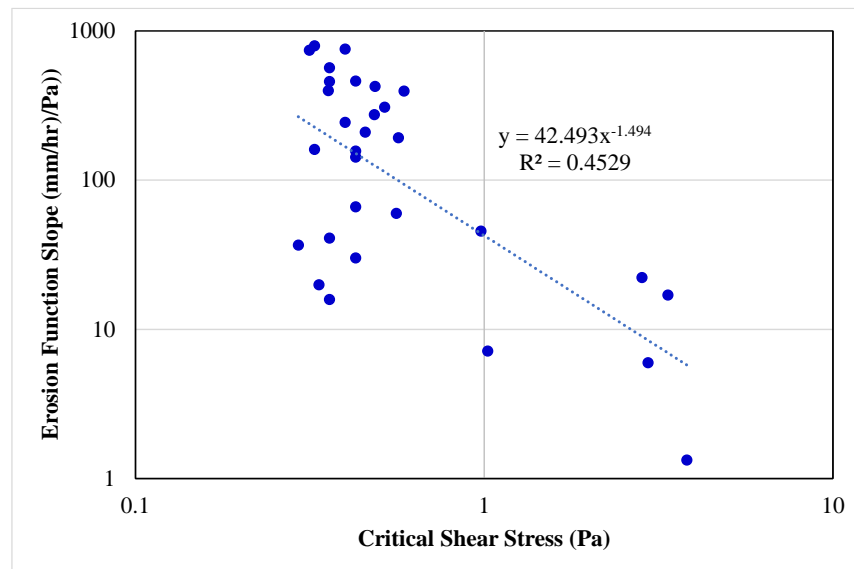


Figure 42. Slope of the EFA erosion function vs critical shear stress τ_c

Figure 42 shows that the slope of the erosion function and critical shear stress do not have a good correlation. However, the erosion function slope decreases with an increase in critical shear stress which is intuitive. The Hanson chart, in opposite, shows that the erosion parameter increases with critical shear stress which is counter intuitive as the slope decreases when the critical shear stress increases (Hanson, 2004).

3.6.2. Pocket Erodrometer Test (PET)

The Pocket Erodrometer Test (PET) was performed on the exposed sample surface prior to EFA testing. The result of a PET is the depth of the hole created in the sample surface after squeezing the nozzle 20 times at a velocity of 8 m/s (See Section 3.5.1.). The depth of the PET holes varies from 2.3 to 36 mm with an average of 16.2 mm and a standard deviation of 12.6 mm. Table 15 shows the depth of the PET holes and the corresponding erosion category.

Table 15. Pocket Erodrometer Test (PET) results

#	Sample Number	Sample Depth	Depth of Hole	Sample Description	Erosion Category
		(m)	(mm)		
Lower American River Site					
1	2F-19-LAR1A-Sand Sample #12	4.0-6.9	36	silty sand	2.2
2	2F-19-LARA1-Sand Sample #13	7.0-8.1	14	sand	2.6
3	2F-19-LAR3A-Sand Sample #17	2.1-3.2	9.35	silty sand	2.9
4	2F-19-LAR3A-Sand Sample #18	3.4-5.0	19.51	silty sand	2.4
5	2F-19-LAR4A-Sand Sample #24	5.2-6.9	12.51	sand	2.7
6	2F-19-LAR6A-Sand Sample #11	6.0-9.1	N/A	gravel	N/A
7	2F-19-LAR6A_Sand Sample #10	0.9-2.6	28	sand	2.3
8	2F-19-LAR6A-ST1 34-35ft	10.4-10.7	2.3	sandy silt	3.4
9	2F-19-LAR7A_Sand Sample #7	8.9-10.5	7.78	sand	3.0
10	2F-19-LAR7A_Sand Sample #4	3.6-4.5	30	clayey sand	2.3
11	2F-19-LAR 7A-Sand Sample #5	5.8-6.9	35	silty sand	2.2
12	2F-19-LAR7A-Sand Sample #3	0.3-2.0	5.6	silty sand	3.2
13	2F-19-LAR7A-Sand Sample #6	7.0-7.9	29.5	sand	2.3
14	2F-19-LAR9A-ST1 9-11ft	2.7-3.6	1.3	sandy lean clay	3.5
15	2F-19-LAR9A_Sand sample #9	6.4-7.8	17	silty sand	2.5
16	2F-19-LAR9A_Sand Sample #8	4.0-6.2	15.76	silty sand	2.5
17	2F-19-LAR9A-ST2 11-13ft	3.6-4.0	1.55	silty sand	3.5
18	2F-19-LAR10A-Sand Sample #16	8.9-9.9	13.51	sand	2.6
19	2F-19-LAR10A-Sand Sample #14	7.6-8.7	32.31	silty sand	2.2
20	2F-19-LAR12A-Sand Sample #1	2.1-4.3	16.7	sand	2.5
21	2F-19-LAR12A-Sand Sample #2	5.8-7.5	24	sand	2.4
Sacramento River Site					
22	2F-19-SAC1A-ST2	3.6-4.0	8.52	clayey sand	3.0
23	2F-19-SAC1A-ST6 29-31 ft	8.9-9.5	6.8	silty clay	3.1
24	2F-19-SAC3A-Sand Sample #21	1.5-2.6	3.5	clayey sand	3.3
25	2F-19-SAC3A-Sand Sample #22	4.6-5.0	38.7	silty sand	2.1
26	2F-19-SAC5A-Sand Sample #26	13-14.6	11	silty sand	2.7
27	2F-19-SAC5A 53-55 ft	16.2-17	9	silty sand	2.9
28	2F-19-SAC5A-Sand Sample #25	8.2-9.2	7.85	silty clay	3.0
29	2F-19-SAC7A-ST1 9-11ft	2.7-3.6	55	sandy lean clay	1.8
30	2F-19-SAC7A-ST2 15-17ft	4.6-5.2	10	layered clay with silt	2.9
31	2F-19-SAC8A-ST2 47-49 ft	14.3-14.9	10	silty clay	2.9
32	2F-19-SAC8A-ST1 27-28.67 ft	8.2-8.7	12.6	silt	2.6
33	2F-19-SAC8A-Sand Sample #19	2.7-3.8	13.5	silty sand	2.6
34	2F-19-SAC8A-Sand Sample #20	2.1-2.6	23	silty sand	2.4
35	2F-19-SAC9A-ST2 15-17 ft	4.6-5.2	4.2	silty clay	3.3
36	2F-19-SAC9A-ST1 9-11 ft	2.7-3.6	2.3	silty clay	3.4

This depth is then used together with the data reduction procedure described in Section 3.5.2 to obtain an erosion category number corresponding to the depth of the erosion hole. Erosion category numbers vary in the chart from Category I (Very High Erodibility) to Category VI (Non-erodible). The erosion category numbers for the samples tested varied from 1.8 to 3.5 with a mean of 2.7 and a standard deviation of 0.44 (Coefficient of Variation COV = 0.163) (Figure 43 and Figure 44). Each result of a PET test is represented by a dot on the erosion chart indicating the erosion category for that sample. The coordinates of the dots are meaningless as the erosion rate and the shear stress or velocity along the soil surface are not measured or calculated in this simple index test.

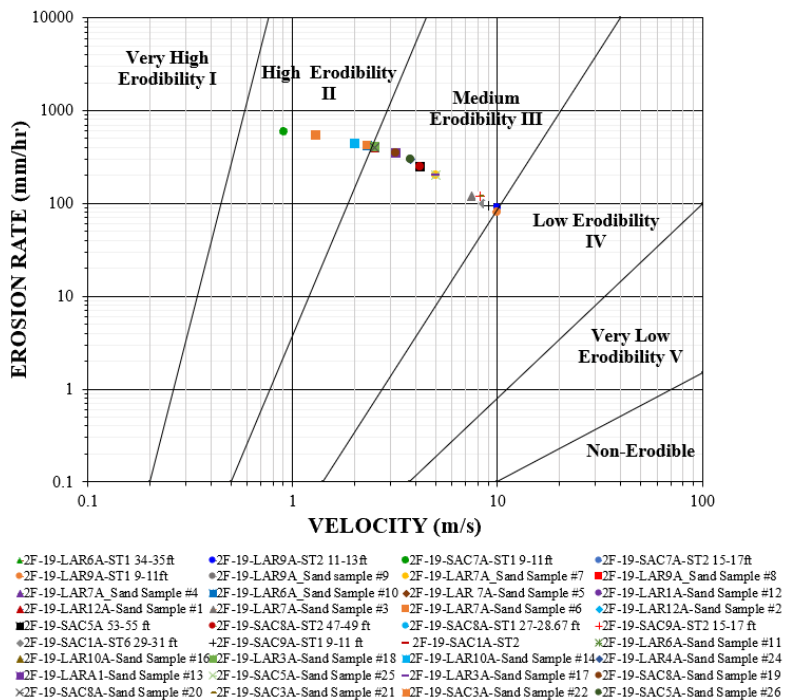


Figure 43. Pocket Erodometer Test results (velocity graph)

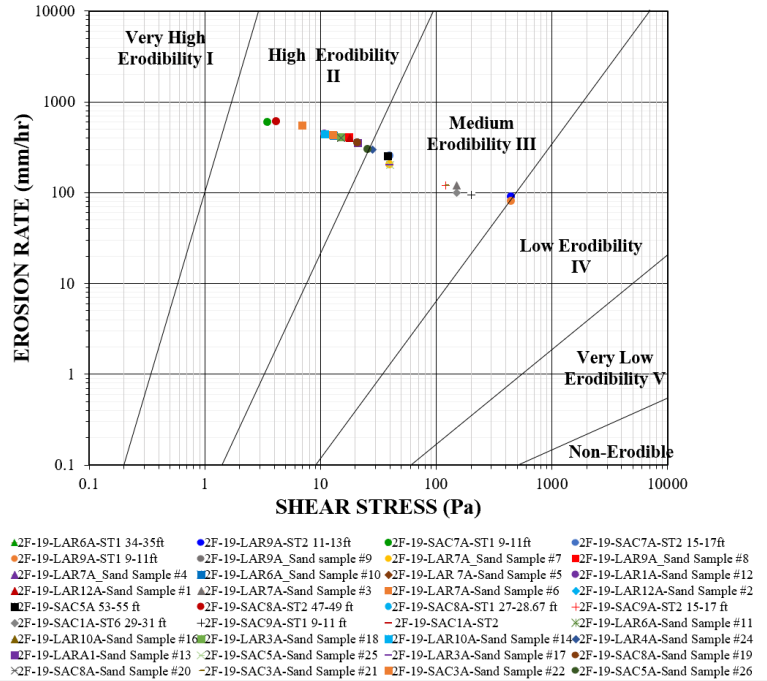


Figure 44. Pocket Erodrometer Test results (shear stress graph)

3.6.3. Borehole Erosion Test (BET)

This Chapter presents the results of the BET including a recommended procedure to reduce and optimize the data considering soil stratigraphy and mean values of velocity and shear stress. The results of the Borehole Erosion Test (BET) consist of a set of profiles:

- 1) the borehole radius as a function of depth
- 2) the velocity as a function of depth
- 3) the erosion rate profile as a function of depth
- 4) the shear stress profile as a function of depth
- 5) the erosion rate versus velocity chart in log-log space
- 6) the erosion rate versus shear stress chart in log-log space

The borehole radius versus depth profile is generated from the mechanical caliper readings and the velocity versus depth profile is generated from the flowmeter readings. The erosion rate versus depth profile is obtained from the radius change during the BET and time increment. The shear stress versus depth profile yields an average erosion rate for every 0.1 m of depth increment.

One of the most useful results of the BET is the borehole radius as a function of depth. This radius profile indicates which layers are likely to be more erodible than others so that attention can be focused accordingly. The radius profiles before and after the first flow run of all BETs are shown in Figure 45 -

Figure 57 along with the corresponding soil stratigraphy. The examples of velocity, erosion rate, and shear stress profiles versus depth are presented in Figure 58.

The erosion rate versus velocity and shear stress chart shows a cloud of points on both erosion charts because of a big number of data; the calculations of velocity and shear stress are done for every 6 mm of profile depth throughout a borehole depth (Figure 59 and Figure 60). To give a mean representation of the BET results for one distinct soil layer in the borehole stratigraphy, the cloud of points for that layer was reduced to one average point representing the cloud. For this layer and in the case of the erosion rate vs. shear stress cloud, the average of all erosion rate values was calculated, and the average of all shear stress values was obtained. This gave a representative point M for that layer on the shear stress erosion chart Figure 61.

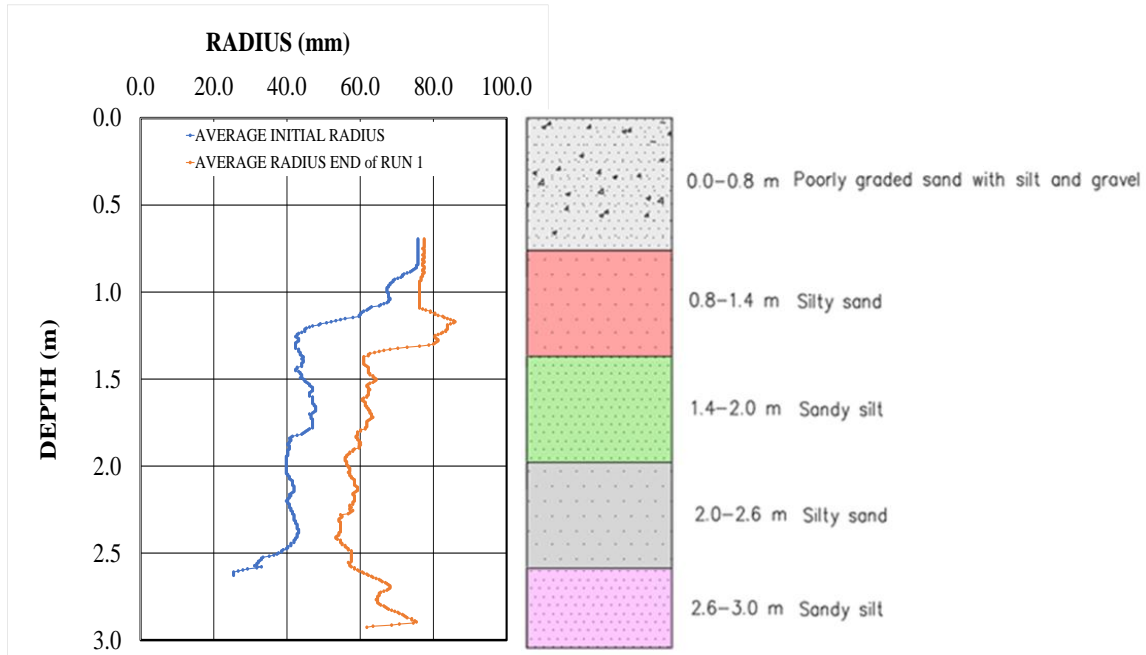


Figure 45. BET radius profiles for “as drilled” and “after first flow run” (LAR2B)

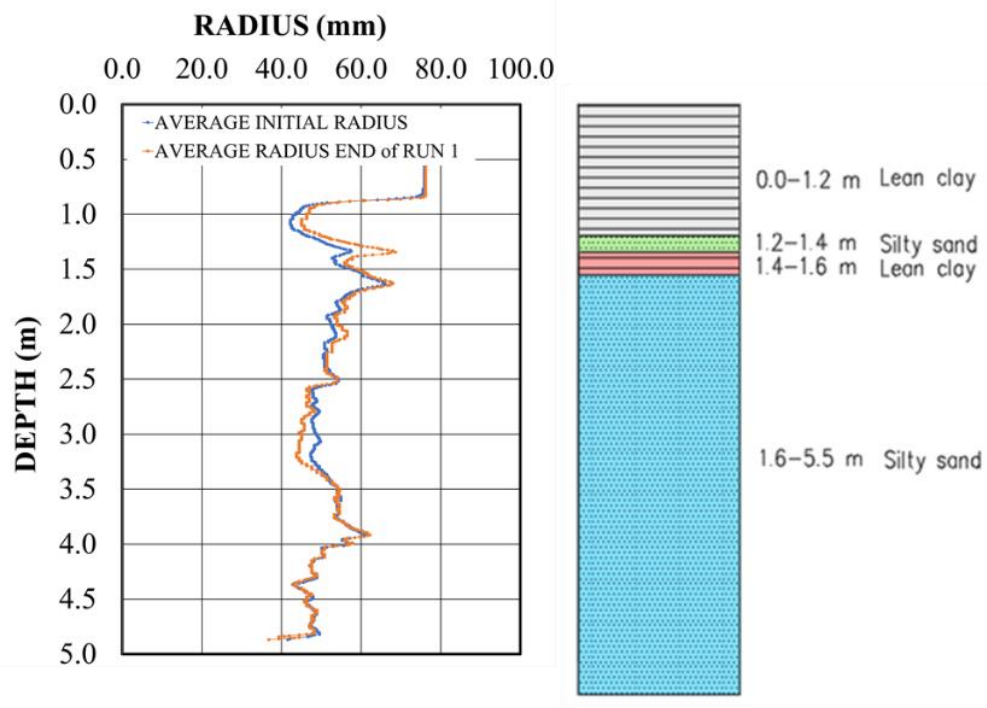


Figure 46. BET radius profiles for “as drilled” and “after first flow run” (LAR3B)

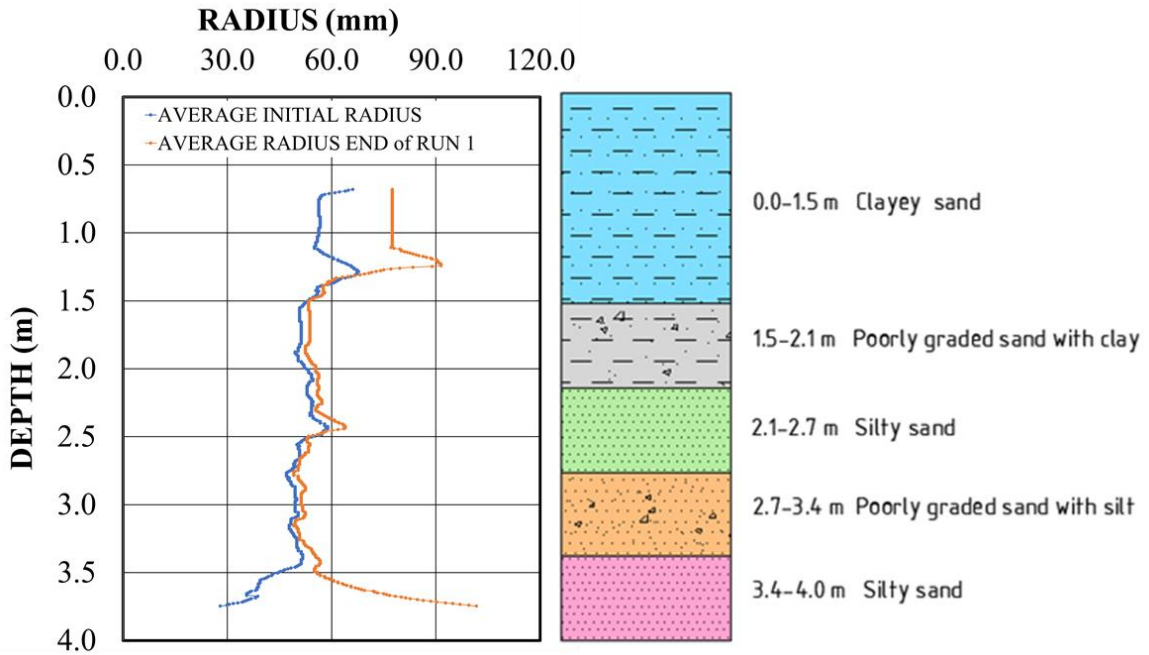


Figure 47. BET radius profiles for “as drilled” and “after first flow run” (LAR5B)

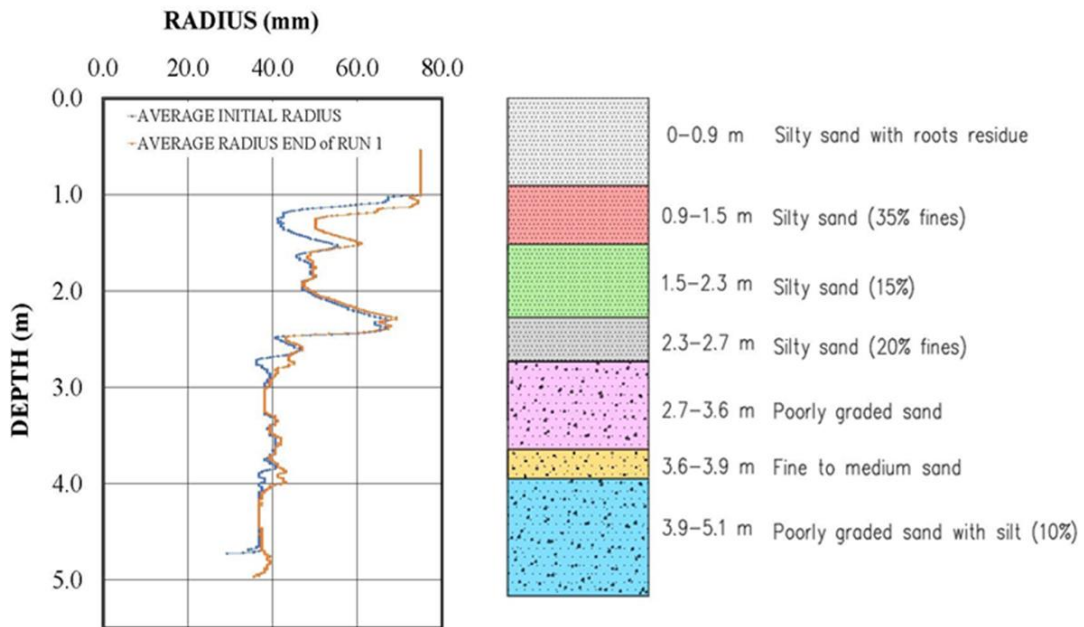


Figure 48. BET radius profiles for “as drilled” and “after first flow run” (LAR6B)

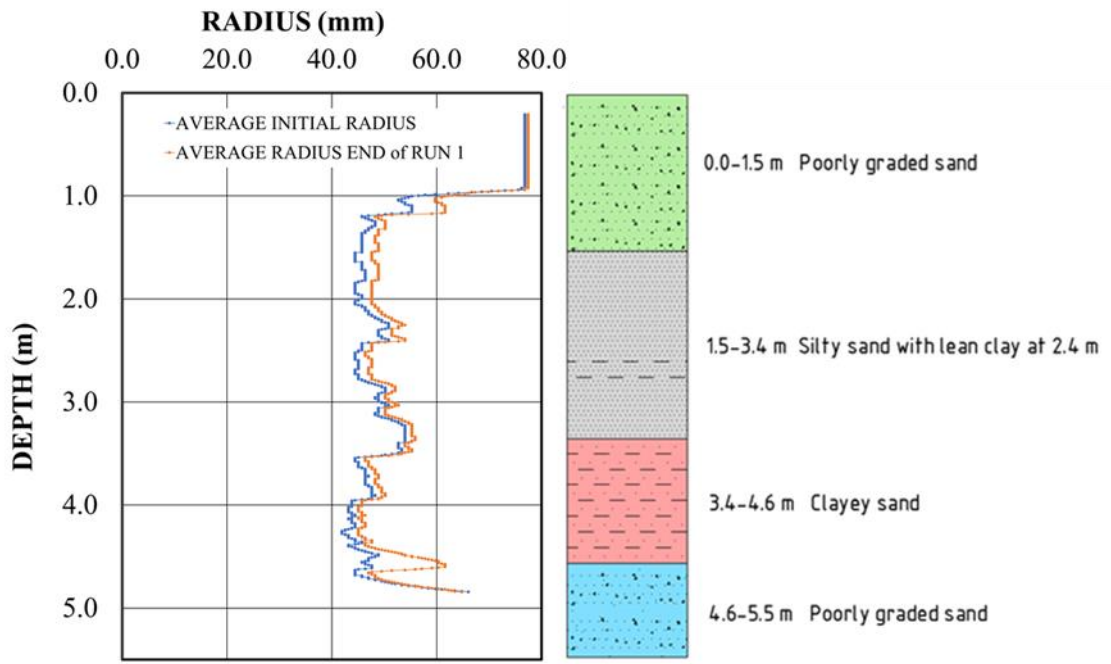


Figure 49. BET radius profiles for “as drilled” and “after first flow run” (LAR7B)

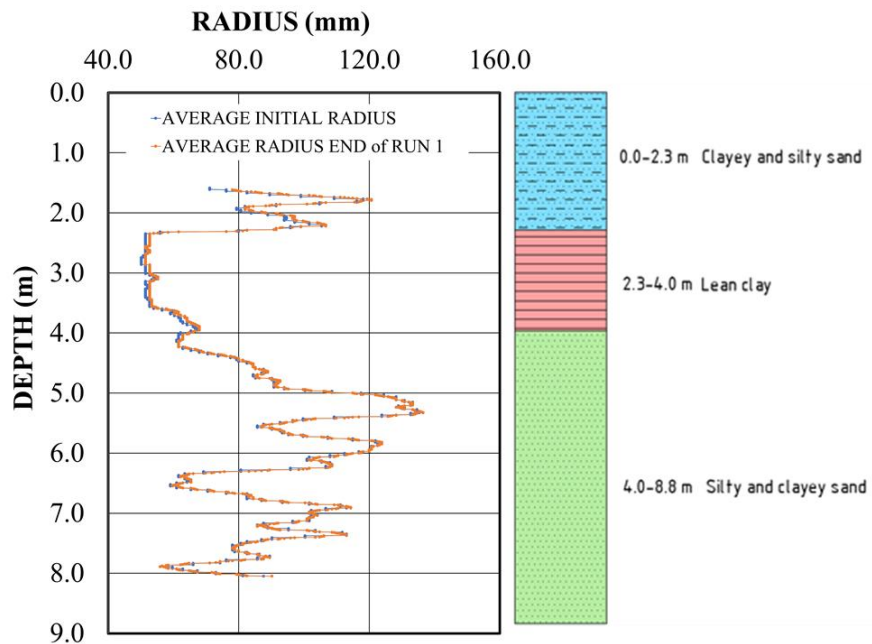


Figure 50. BET radius profiles for “as drilled” and “after first flow run” (LAR9B)

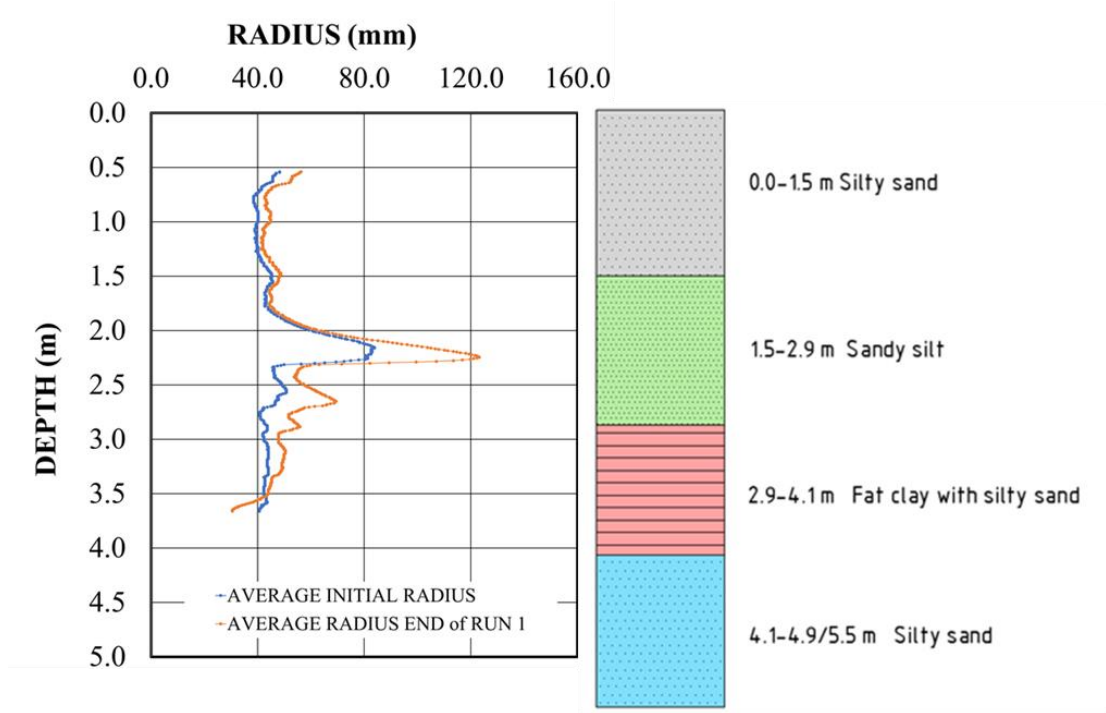


Figure 51. BET radius profiles for “as drilled” and “after first flow run” (LAR10B)

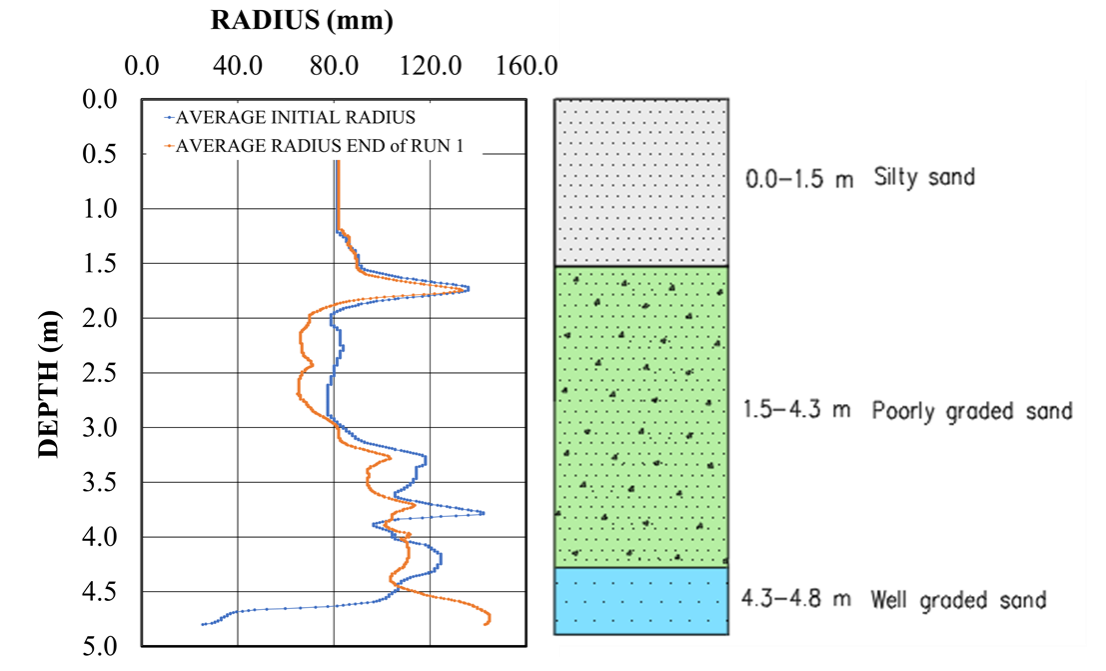


Figure 52. BET radius profiles for “as drilled” and “after first flow run” (LAR12B)

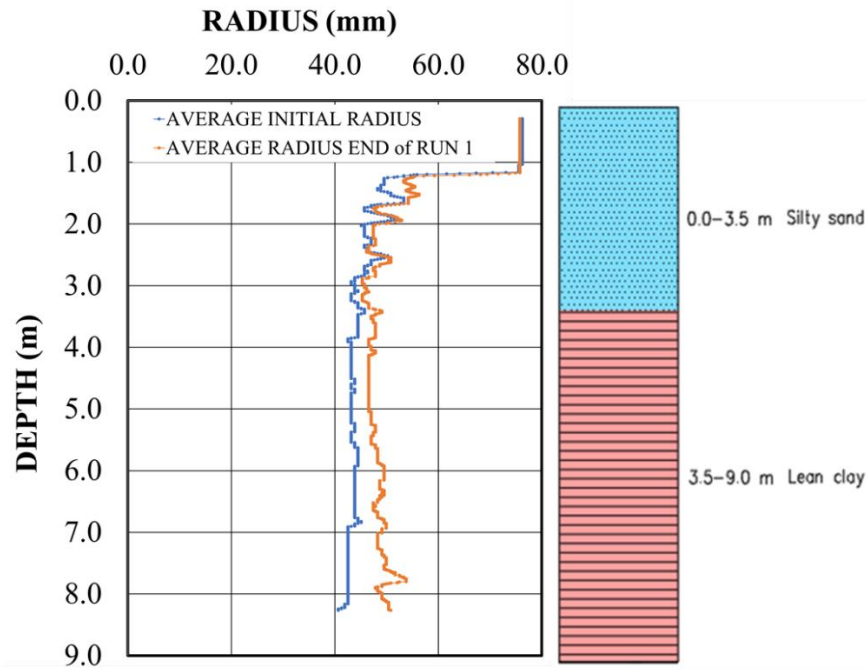


Figure 53. BET radius profiles for “as drilled” and “after first flow run” (SAC1B)

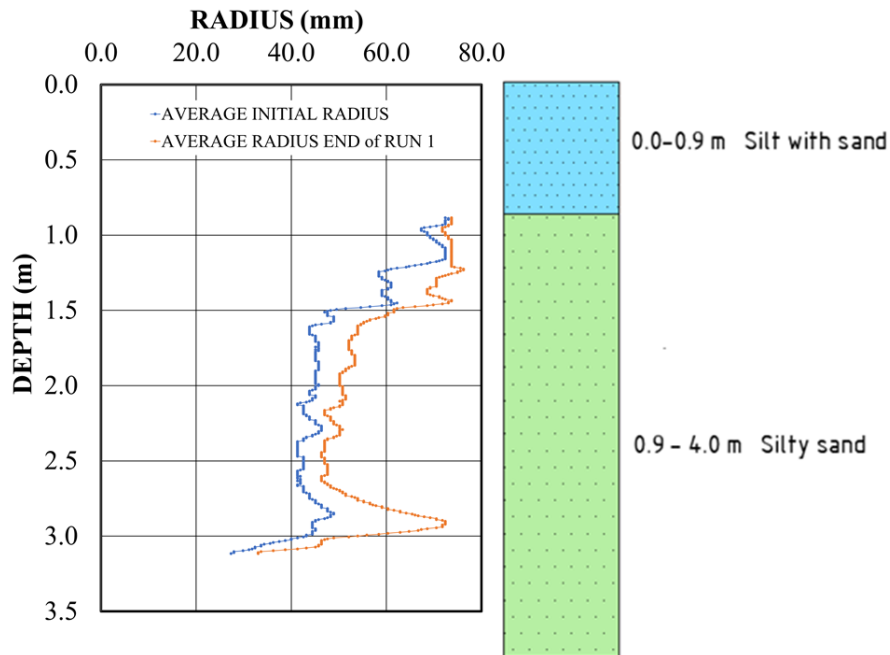


Figure 54. BET radius profiles for “as drilled” and “after first flow run” (SAC3B using water)

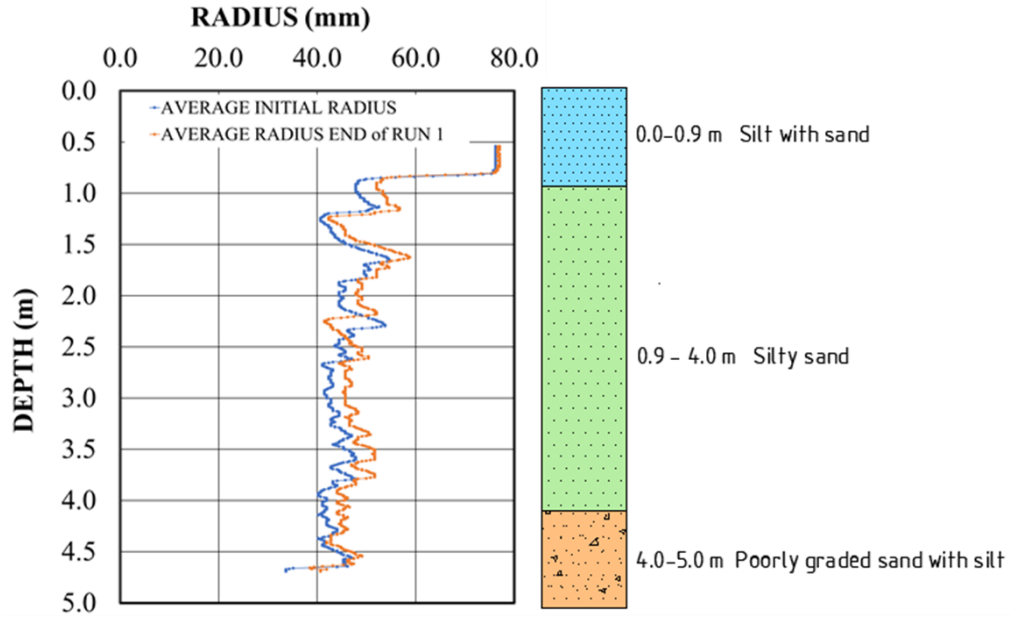


Figure 55. BET radius profiles for “as drilled” and “after first flow run” (SAC3B2 using mud)

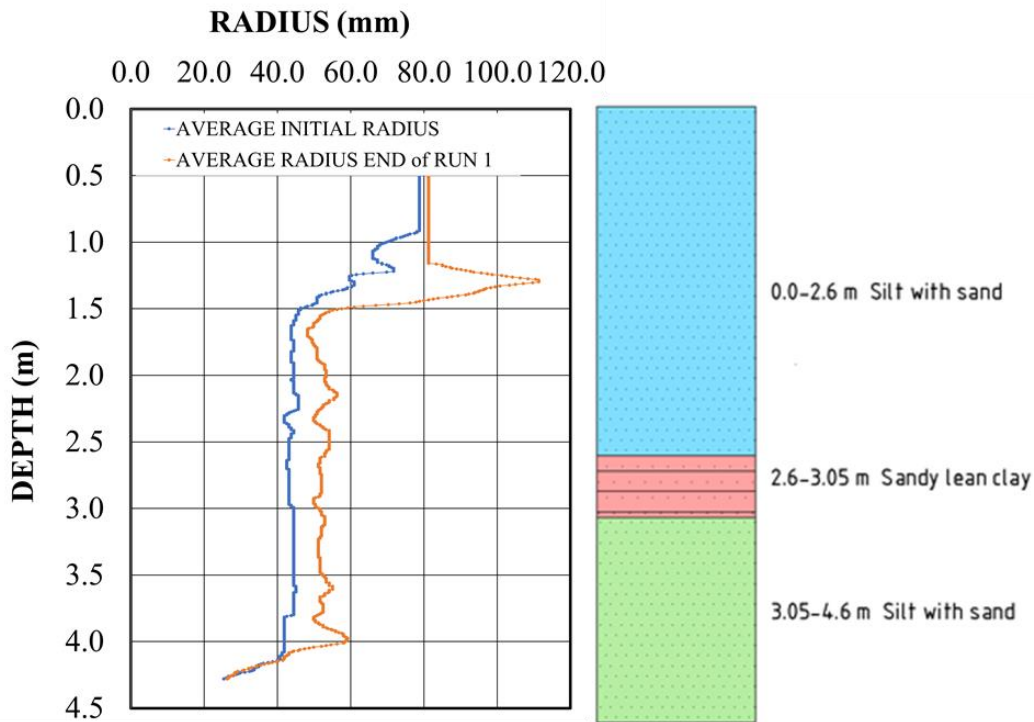


Figure 56. BET radius profiles for “as drilled” and “after first flow run” (SAC7B)

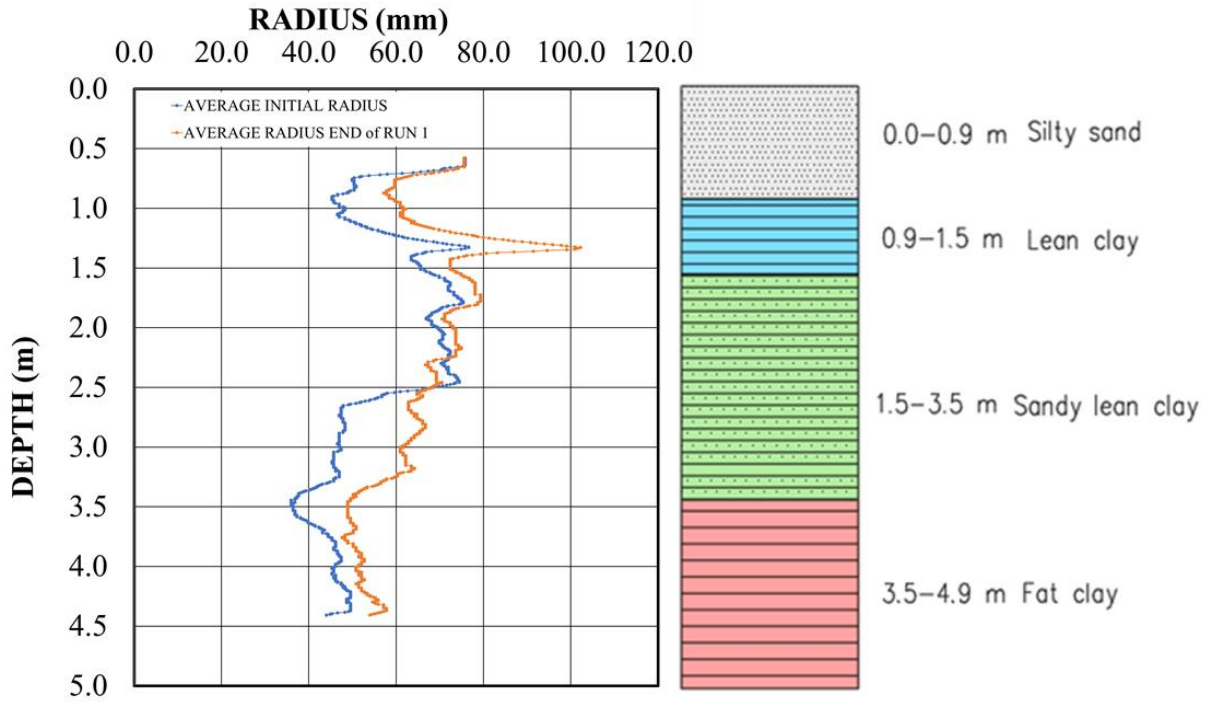
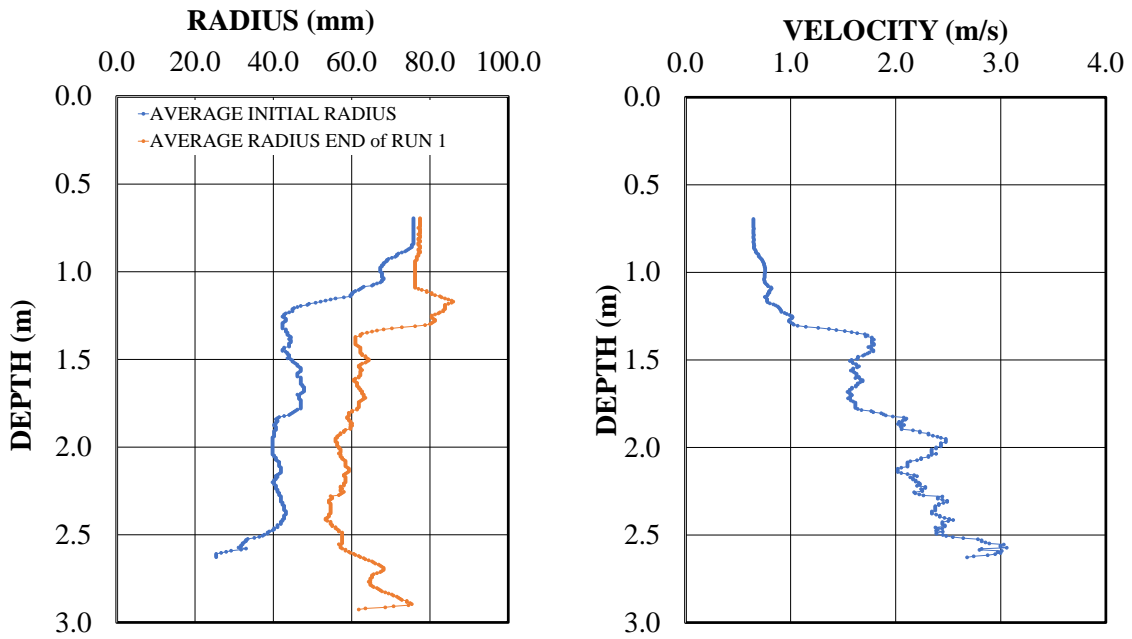


Figure 57. BET radius profiles for “as drilled” and “after first flow run” (SAC9B)



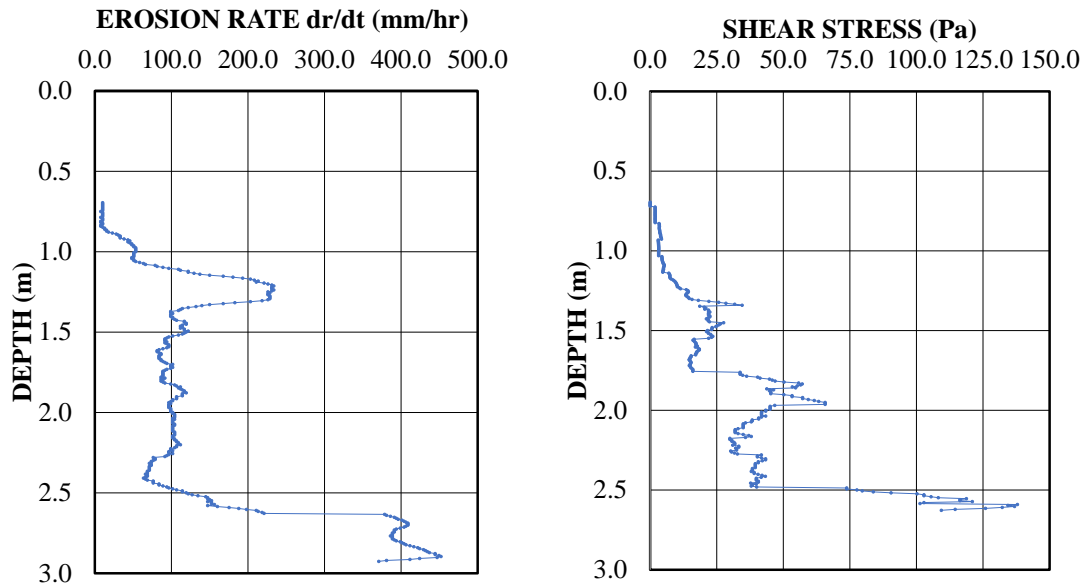


Figure 58. Examples of radius, velocity, erosion rate, and shear stress profiles versus depth (TAMU-BET)

Then to recreate an erosion function using that mean point M, the two boundary lines straddling the mean point on the shear stress erosion chart were extended until they intersected at a point O (Figure 61). The erosion function was then assumed to be the line OM. Because the soil stratigraphy of the borehole indicated several distinct layers, the cloud considered was always limited to the points on the BET profile corresponding to one stratigraphic layer. The clouds of BET points for each layer are shown on Figure 60 together with the back constructed log-log linear erosion functions. The legend on the Figure 59 and Figure 60 shows soil description, depth of the layers, mean velocity, mean shear stress, and mean erosion rate for each layer. These log-log linear erosion functions are back constructed according to Figure 61 as explained above. The erosion charts allow to evaluate soil erodibility for each layer and put the results on one plot which shows more and less erodible layers in soil profiles. Then, the EFA can be run in addition to verify soil erodibility at the sample level.

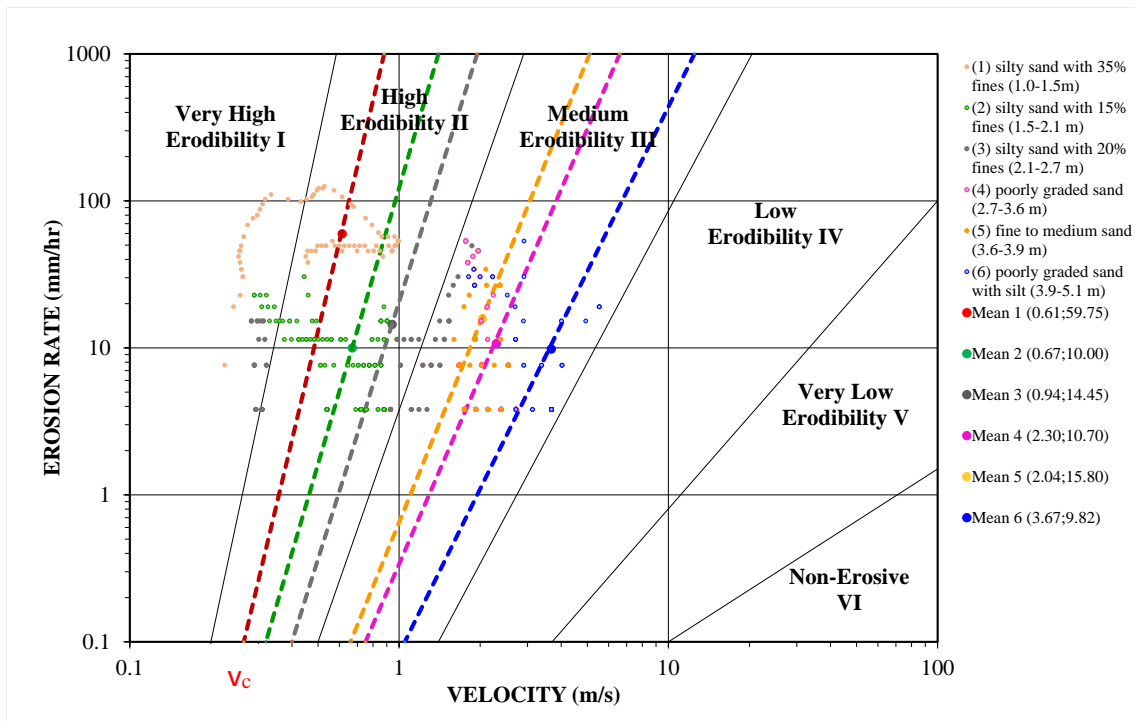


Figure 59. Erosion rate versus velocity chart for the first flow

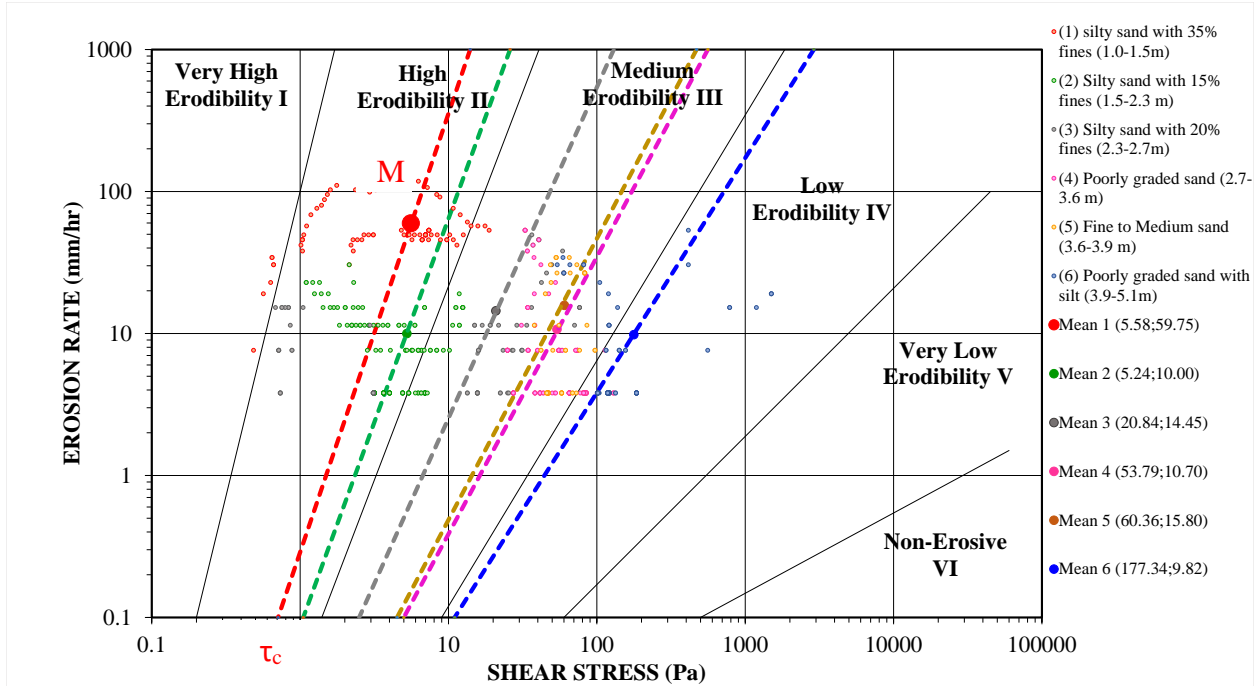


Figure 60. Cluster of points from BET in each layer and back constructed erosion functions

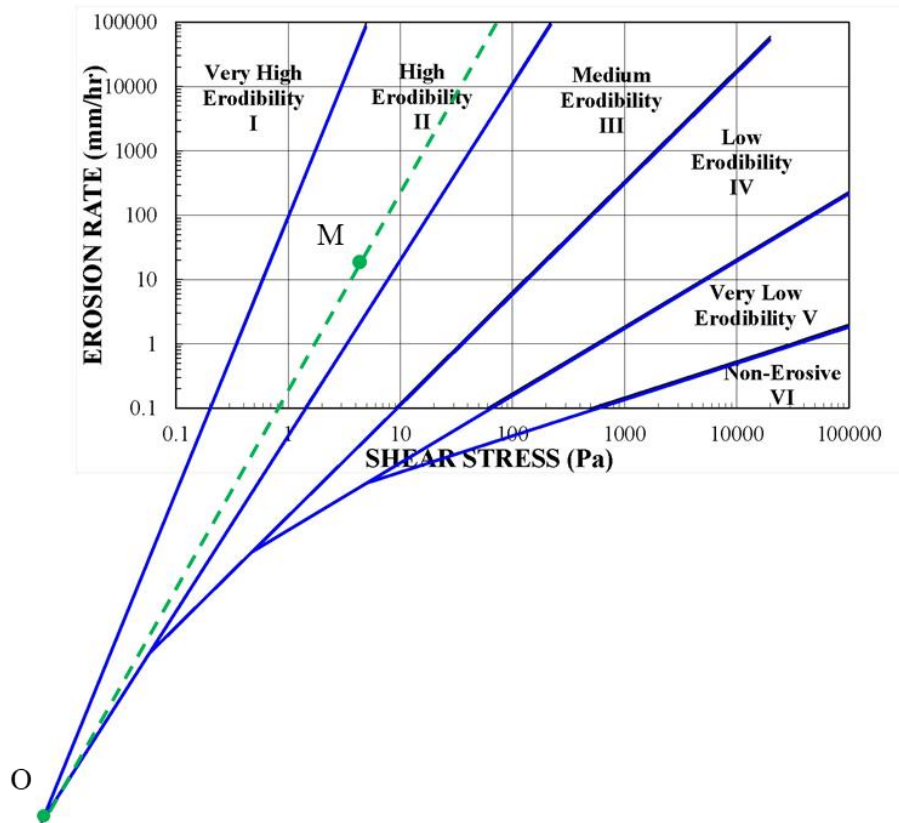


Figure 61. Extending the erosion chart boundaries to create BET erosion function

The erosion functions Figure 59 and Figure 60 give a BET critical velocity v_c and critical shear stress τ_c at the intersection with the 0.1 mm/hr erosion rate horizontal line. The critical velocity and critical shear stresses obtained in that fashion from the BET are listed in Table 16. The critical shear stress inferred from the BET varies from 0.18 Pa to 18 Pa with the average of 2.9 Pa. The critical velocity inferred from the BET varies from 0.16 m/s to 1.5 m/s with the average of 0.53 m/s.

Table 16. Critical velocity and critical shear stress inferred from BET

#	Site	Layer	Flow	τ_c (Pa)	Mean τ_c (Pa)	v_c (m/s)	Mean v_c (m/s)
1	LAR2B	Silty sand (0.8-1.4 m)	First	0.75	0.76	0.3	0.34
			Second	0.75		0.39	
			Third	0.78		0.34	
		Sandy silt (1.4 – 2 m)	First	1.8	1.33	0.49	0.42
			Second	1.0		0.36	
			Third	1.2		0.4	
		Silty sand (2 – 2.6 m)	First	2.7	2.53	0.58	0.50
			Second	1.7		0.46	
			Third	3.2		0.45	
		Sandy silt (2.6 – 3 m)	First	2.2	1.14	0.55	0.36
			Second	0.75		0.285	
			Third	0.48		0.25	
2	LAR3B	Lean clay (0 - 1.2 m)	First	5.5	3.2	0.63	0.51
			Second	2.3		0.49	
			Third	1.8		0.4	
		Silty sand (1.2 – 1.4 m)	First	2.2	1.8	0.41	0.37
			Second	1.5		0.36	
			Third	1.7		0.34	
		Lean clay (1.4 – 1.6 m)	First	2.0	2.26	0.46	0.47
			Second	2.0		0.44	
			Third	2.8		0.52	
		Silty sand (1.6 – 5.5 m)	First	4.5	4	0.7	0.69
			Second	3.0		0.63	
			Third	4.5		0.74	
3	LAR5B	Clayey sand (0 - 1.5 m)	First	0.7	0.75	0.3	0.29
			Second	0.8		0.28	
			First	2.0	2.15	0.57	0.59

#	Site	Layer	Flow	τ_c (Pa)	Mean τ_c (Pa)	v_c (m/s)	Mean v_c (m/s)		
		Poorly graded sand with clay (1.5 – 2.1 m)	Second	2.3	2.65	0.6	0.57		
		Silty sand (2.1 – 2.7 m)	First	2.5		0.57			
			Second	2.8	0.56				
		Poorly graded sand with silt (2.7 – 3.4 m)	First	3.5	3.5	0.67	0.66		
			Second	3.5		0.645			
		Silty sand (3.4 – 4 m)	First	1.5	1.4	0.4	0.37		
			Second	1.3		0.33			
		4	LAR6B	Silty sand-35% fines (1 - 1.5 m)	First	0.7	1.14	0.27	0.34
					Second	0.67		0.26	
					Third	1.7		0.44	
Forth	1.5				0.39				
Silty sand-15% fines (1.5 – 2.3 m)	First			1.0	1.3	0.32	0.41		
	Second			1.8		0.43			
	Third			1.2		0.46			
	Forth			1.2		0.44			
Silty sand-20% fines (2.3 – 2.7 m)	First			2.5	2.92	0.4	0.43		
	Second			2.8		0.41			
	Third			3.2		0.55			
	Forth			3.2		0.36			
Poorly graded sand (2.7 – 3.6 m)	First			5.0	5.7	0.75	0.78		
	Second			8.5		0.95			
	Third			3.8		0.7			
	Forth			5.5		0.7			
Fine to medium sand (3.6 – 3.9 m)	First			4.5	7.37	0.66	0.93		
	Second			5.5		0.76			
	Third			7.5		1.1			
	Forth			12.0		1.2			
Poorly graded sand with silt (3.9 – 5.1 m)	First	12.0	10.5	1.05	1.08				
	Second	18.0		1.5					
	Third	6.0		0.95					
	Forth	6.0		0.81					
5	LAR7B	Poorly graded sand (0 – 1.5 m)	First	0.9	1.2	0.325	0.36		
			Second	1.5		0.4			
		Silty sand (1.5 – 3.4 m) with lean clay at 2.4 m	First	1.3	2.95	0.4	0.56		
			Second	4.6		0.72			
		Clayey sand (3.4 – 4.6 m)	First	1.8	3.65	0.42	0.60		
			Second	5.5		0.77			
					First	1.4	2.95	NP	0.58

#	Site	Layer	Flow	τ_c (Pa)	Mean τ_c (Pa)	v_c (m/s)	Mean v_c (m/s)
		Poorly graded sand (4.6 – 5.5 m)	Second	4.5		0.58	
6	LAR9B	Silty and Clayey sand (0 – 2.3 m)	First	0.3	0.4	0.17	0.21
			Second	0.5		0.245	
		Lean clay (2.3 – 4 m)	First	1.8	2.25	0.48	0.53
			Second	2.7		0.57	
		Silty and clayey sand (4 – 8.8 m)	First	0.5	0.57	0.98	0.61
			Second	0.65		0.245	
7	LAR10B	Silty sand (0 – 1.5 m)	First	8.5	6.15	1.0	0.84
			Second	3.8		0.68	
		Sandy silt (1.5 – 2.9 m)	First	3.0	2.45	0.53	0.48
			Second	1.9		0.42	
		Fat clay with silty sand (2.9 – 4.1 m)	First	5.0	4.3	0.8	0.71
			Second	3.6		0.61	
8	LAR12B	Silty sand (0 – 1.5 m)	First	0.5	0.5	0.29	0.29
		Poorly graded sand (1.5 – 4.3 m)	First	0.28	0.28	0.18	0.18
		Well graded sand (4.3 – 4.8 m)	First	0.18	0.18	0.16	0.16
9	SAC1B	Silty sand (0 – 3.5 m)	First	3.0	2.97	0.57	0.55
			Second	3.7		0.61	
			Third	2.2		0.46	
		Lean clay (3.5 – 9 m)	First	4.0	2.93	0.69	0.61
			Second	2.5		0.59	
			Third	2.3		0.54	
10	SAC3B (water)	Silt with sand (0 – 0.9 m)	First	0.85	0.85	0.35	0.35
			Second	NP		NP	
			Third	NP		NP	
		Silty sand (0.9 – 4 m)	First	3.5	2.67	0.58	0.49
			Second	2.7		0.48	
			Third	1.8		0.41	
11	SAC3B2 (mud)	Silt with sand (0 – 0.9 m)	First	1.8	1.20	0.33	0.29
			Second	0.9		0.29	
			Third	0.9		0.26	

#	Site	Layer	Flow	τ_c (Pa)	Mean τ_c (Pa)	v_c (m/s)	Mean v_c (m/s)
		Silty sand (0.9 – 4 m)	First	4.5	4.13	0.65	0.66
			Second	5.0		0.68	
			Third	2.9		0.64	
		Poorly graded sand with silt (4.0-5.0 m)	First	8.0	7.17	0.8	0.74
			Second	9.5		0.9	
			Third	4.0		0.51	
12	SAC7B	Silt with sand (0 – 2.6 m)	First	1.8	1.22	0.44	0.36
			Second	1.0		0.32	
			Third	0.85		0.33	
		Sandy lean clay (2.6 – 3.05 m)	First	2.8	1.83	0.62	0.48
			Second	1.5		0.44	
			Third	1.2		0.39	
		Silt with sand (3.05 – 4.6 m)	First	2.7	1.80	0.66	0.50
			Second	1.4		0.44	
			Third	1.3		0.39	
13	SAC9B	Silty sand (0 – 0.9 m)	First	1.6	1.6	0.43	0.43
		Lean clay (0.9 – 1.5 m)	First	0.9	0.9	0.35	0.35
		Sandy lean clay (1.5 – 3.5 m)	First	1.0	1.0	0.48	0.48
		Fat clay (3.5 – 4.9 m)	First	3.2	3.2	0.72	0.72

The presented approach to obtain critical velocity and critical shear stress for BET is based on defining soil stratigraphy for a borehole, calculating a mean velocity and shear stress for each layer for each flow run, obtaining corresponding erosion curve, and reading critical values of velocity and shear stress when an erosion curve intersects the horizontal axis, and then computing a mean value of critical velocity and critical shear stress for each layer and for all flow runs. This approach can be used when many data are available.

3.7. Summary and comparison of erosion tests

In order to summarize and compare the results of all the erosion tests performed including BET, EFA, and PET, a one-page summary plot of the results is generated for each test

site Figure 62 - Figure 77). A total of 16 summary plot were created. For example, Figure 64 shows the location of the test site (Lower American River, Borehole 3, LAR-3), the soil stratigraphy from the sampling boring performed within 2-3 m from the BET boring, and erosion rate versus shear stress chart with all erosion functions available from the BET, EFA, and PET. The stratigraphy indicates the soil layers and where the EFA samples were collected. In the erosion classification chart, the EFA test results are shown in solid lines while the BET results are shown in dashed line. Each point on the BET lines corresponds to a mean point (see Section 3.6.3. for details) for the layer having the same color on the stratigraphy cross section. The PET dots are shown within the erosion category zones according to the erosion depth measured with the PET and following the process explained in Section 3.5. This is a unique way of representation of many erosion data. In many cases, EFA shows more erosion than EFA for the same soil (for example, purple curve for EFA and green for BET on Figure 64). The higher τ_c value is due to the advantage of testing the soil in in-situ stress environment while EFA is performed on disturbed samples. Therefore, BET can be run in parallel with a Table 17 shows a comparison between the critical shear stress obtained from the BET and from the EFA for the same conditions (soil, depth, borehole, site). Overall, the critical shear stress from the BET is higher than from the EFA except two cases (see Table 17). The average of all measured BET critical shear stresses ($\tau_{c(BET)}$) for which there was a corresponding value of the EFA critical shear stress ($\tau_{c(EFA)}$) was 2.18 Pa. The average of all corresponding values of the EFA critical shear stresses ($\tau_{c(EFA)}$) was 0.39 Pa. Thus, the BET gave critical shear stresses which were 5.6 times higher than the EFA critical shear stresses on average.

$$\tau_c(BET) = 5.6 \tau_c(EFA) \quad (19)$$

If it is argued that τ_{CBET} is more representative of in-situ conditions, then the reconstructed field erosion function would start at τ_{CBET} and follow the erosion function slope k_d measured in the EFA or given by using τ_{CEFA} (Chapter 3.6.1). Alternatively, it could be argued that the reconstructed field erosion function would start at τ_{CBET} and follow the erosion function measured in the EFA.

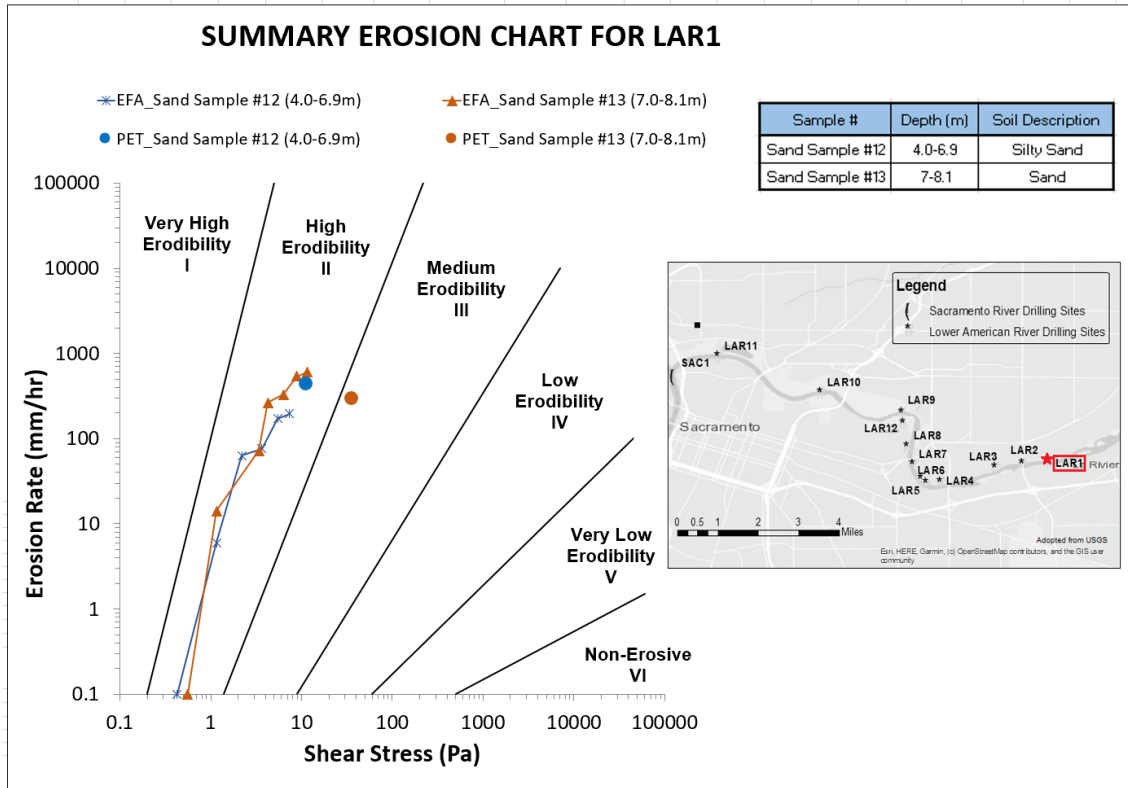


Figure 62. Summary erosion chart for LAR1

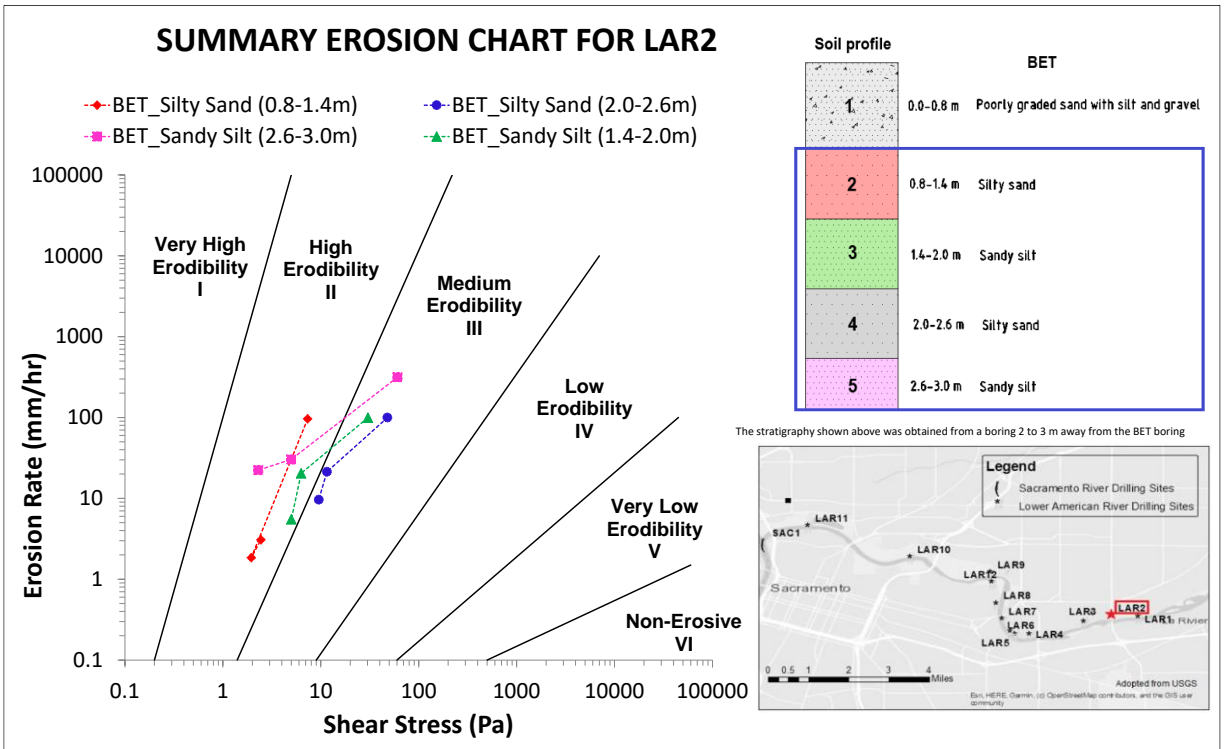


Figure 63. Summary erosion chart for LAR2

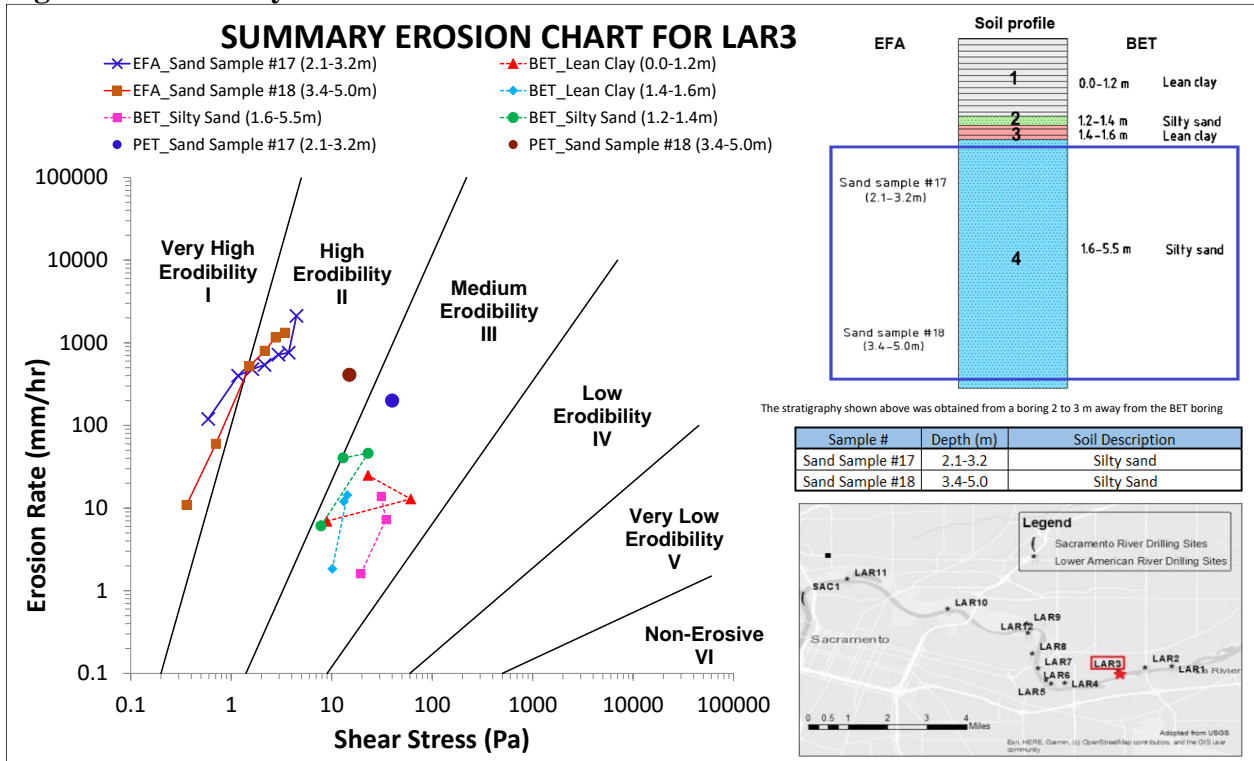


Figure 64. Summary erosion chart for LAR3

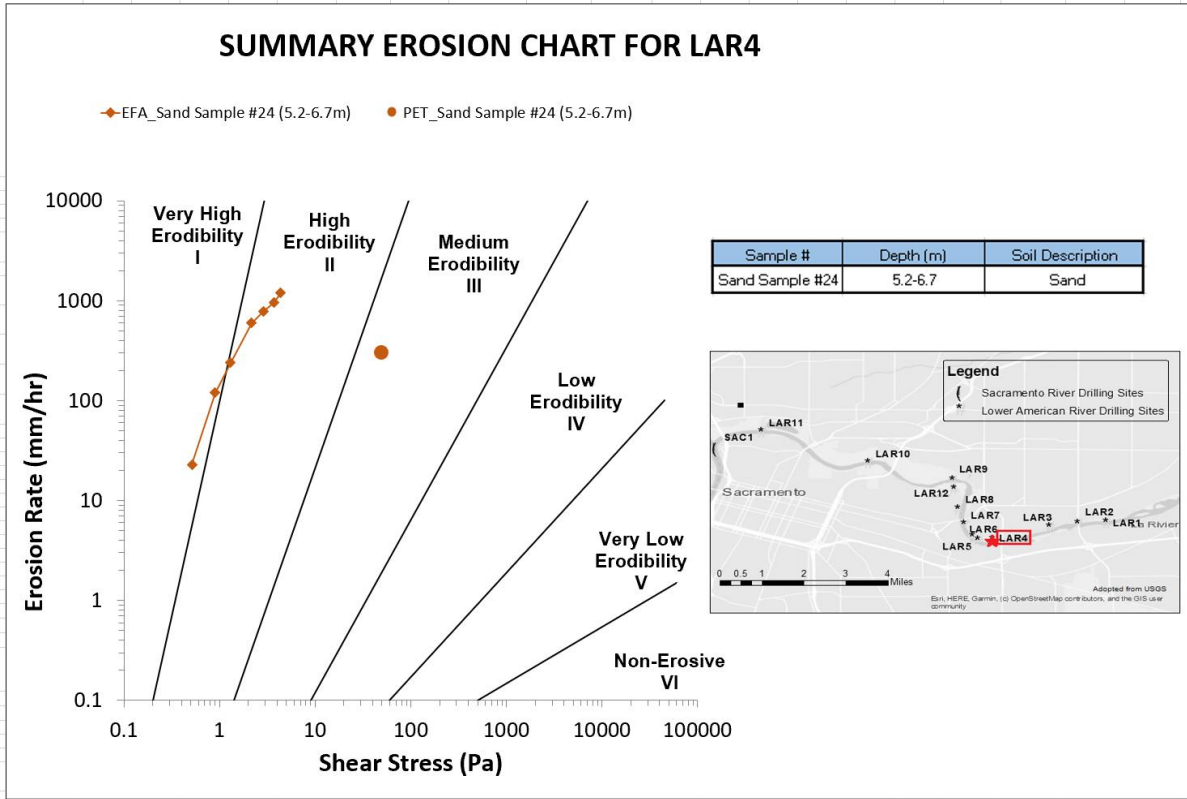


Figure 65. Summary erosion chart for LAR4

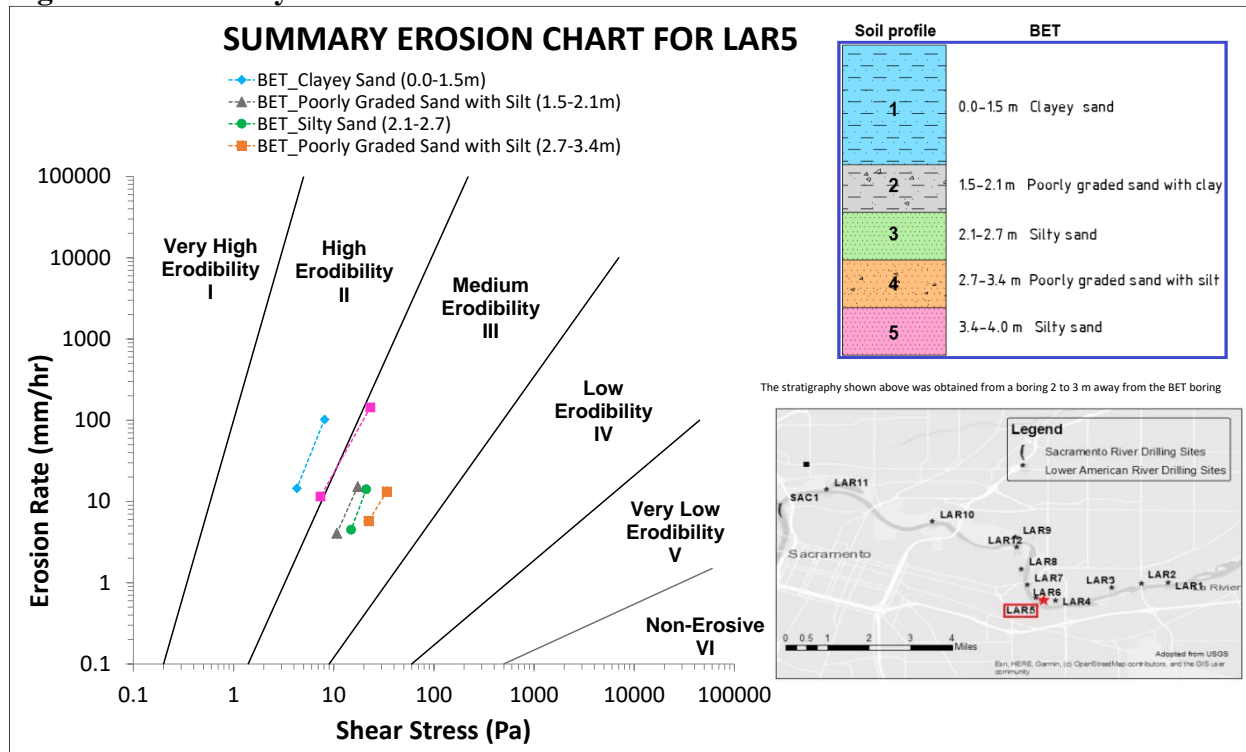


Figure 66. Summary erosion chart for LAR5

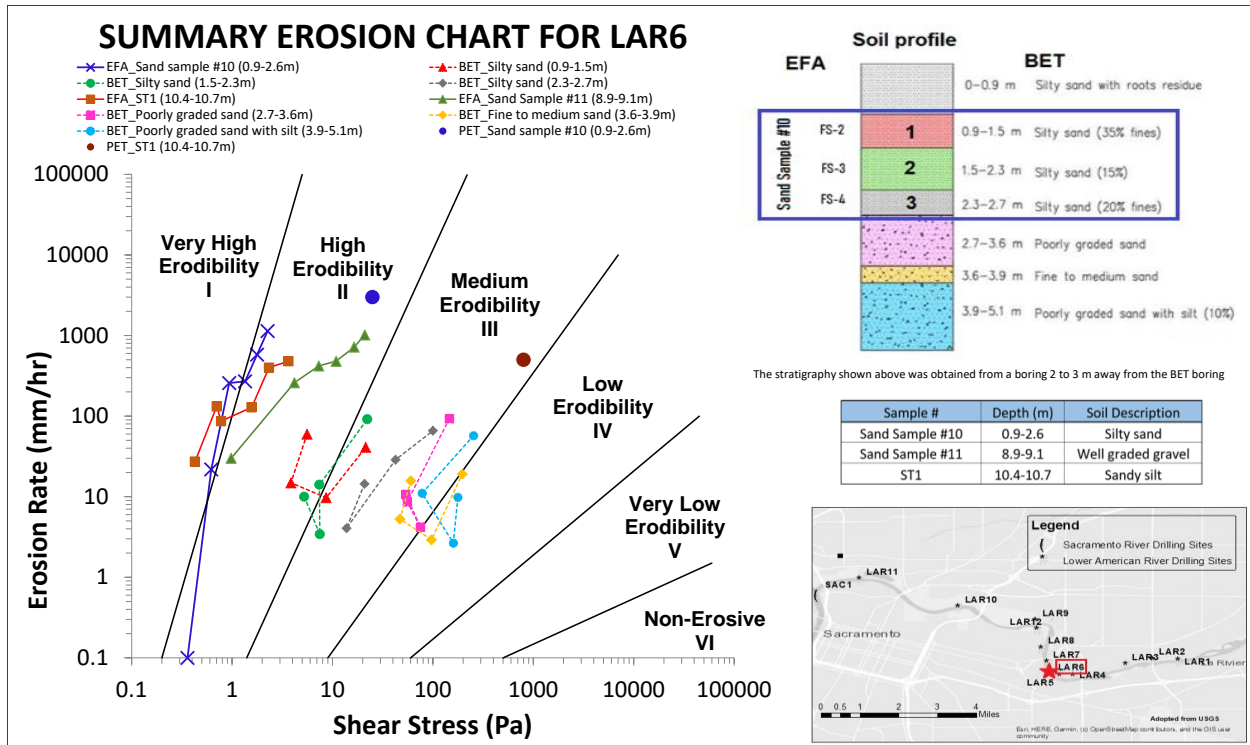


Figure 67. Summary erosion chart for LAR6

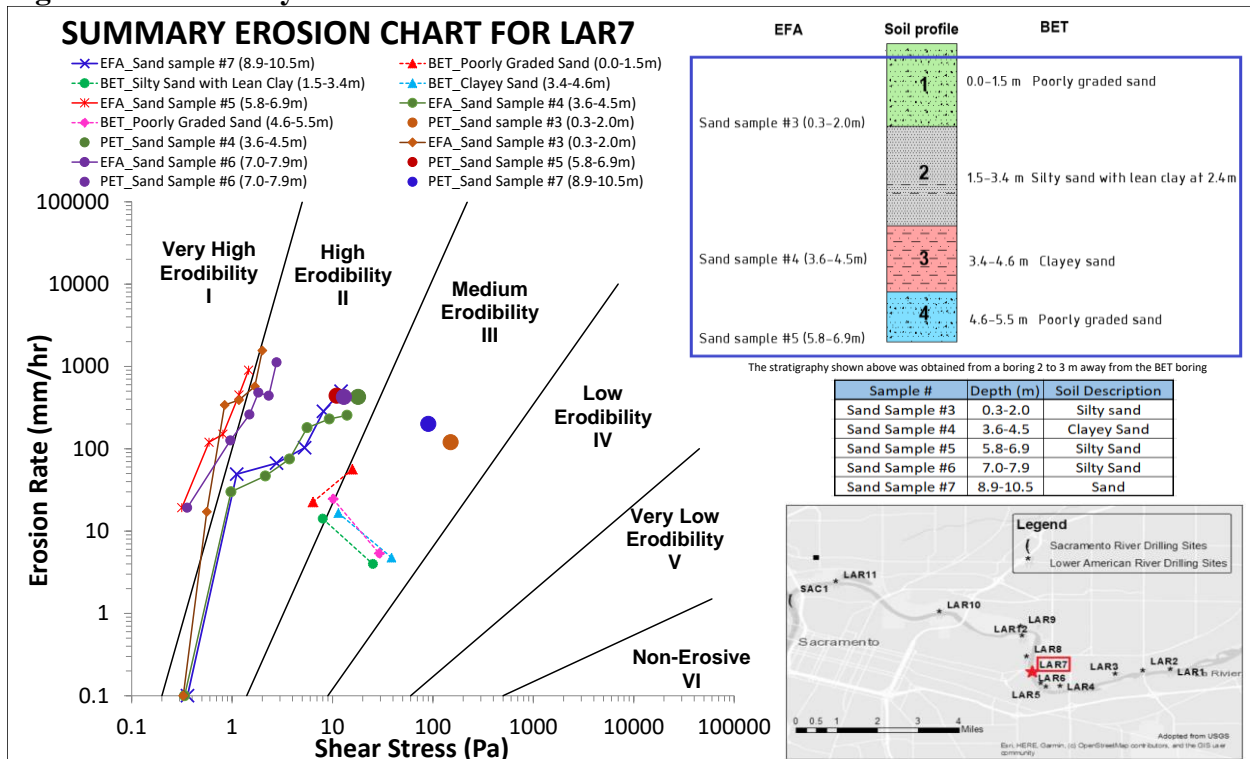


Figure 68. Summary erosion chart for LAR7

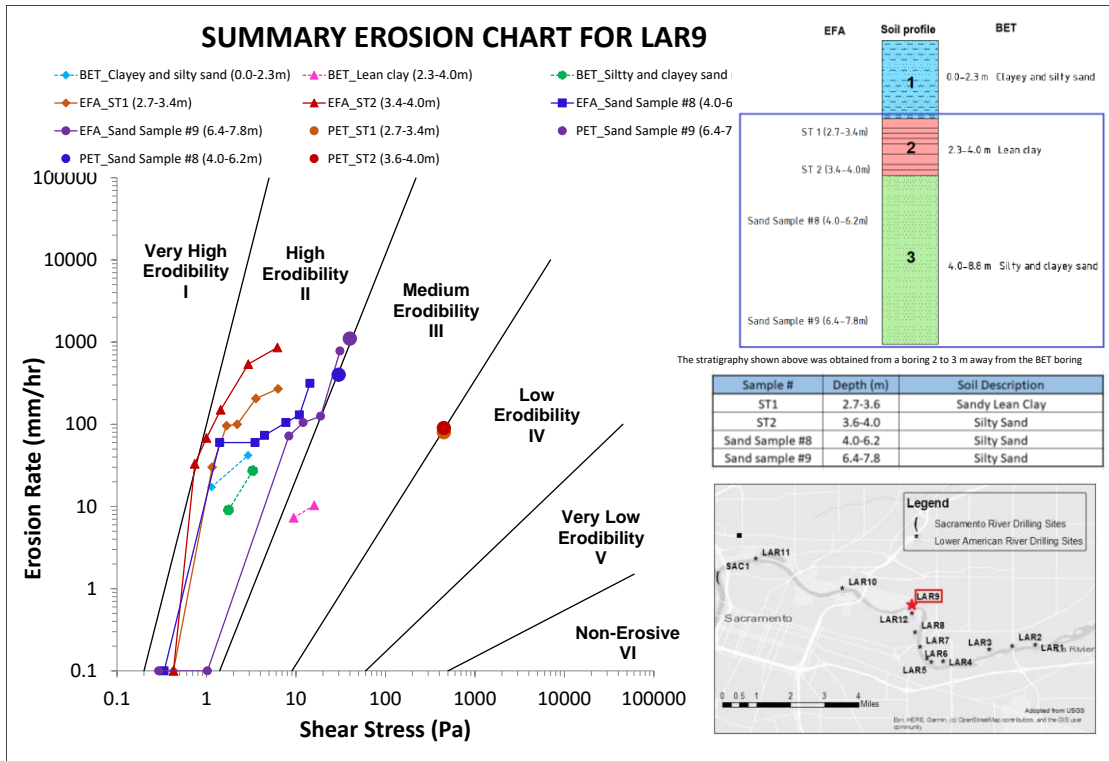


Figure 69. Summary erosion chart for LAR9

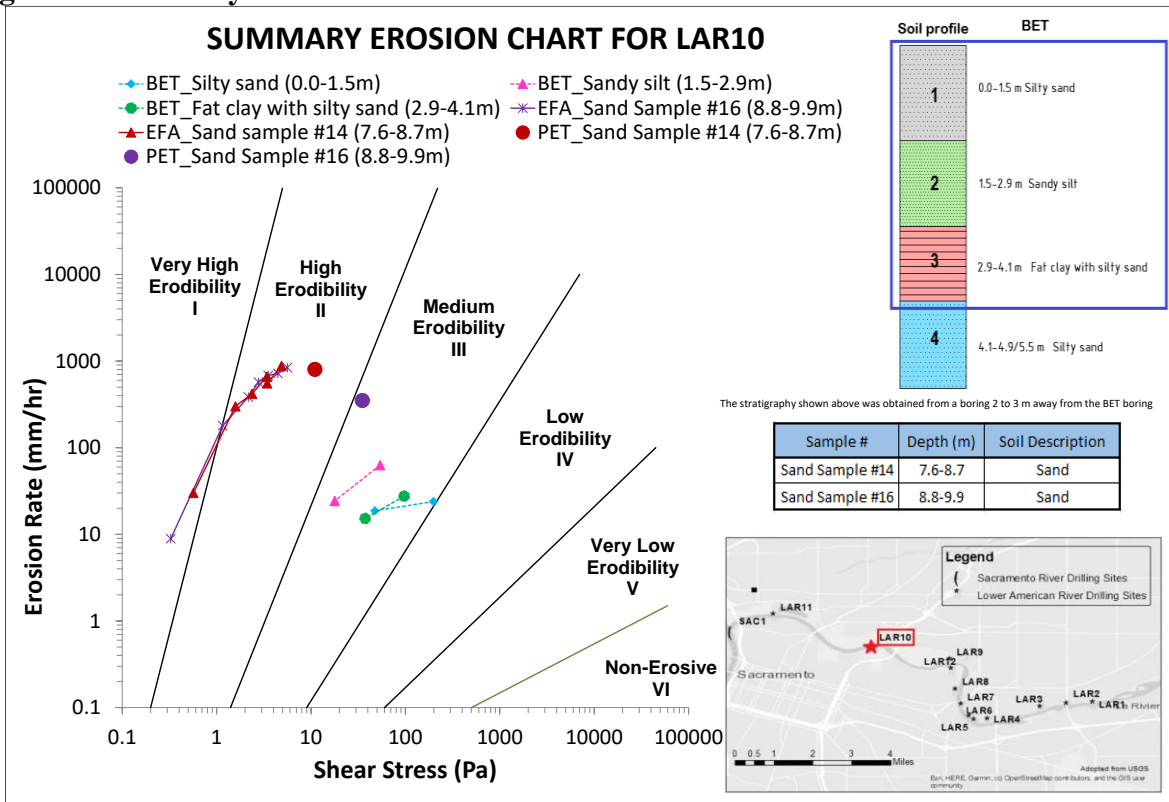


Figure 70. Summary erosion chart for LAR10

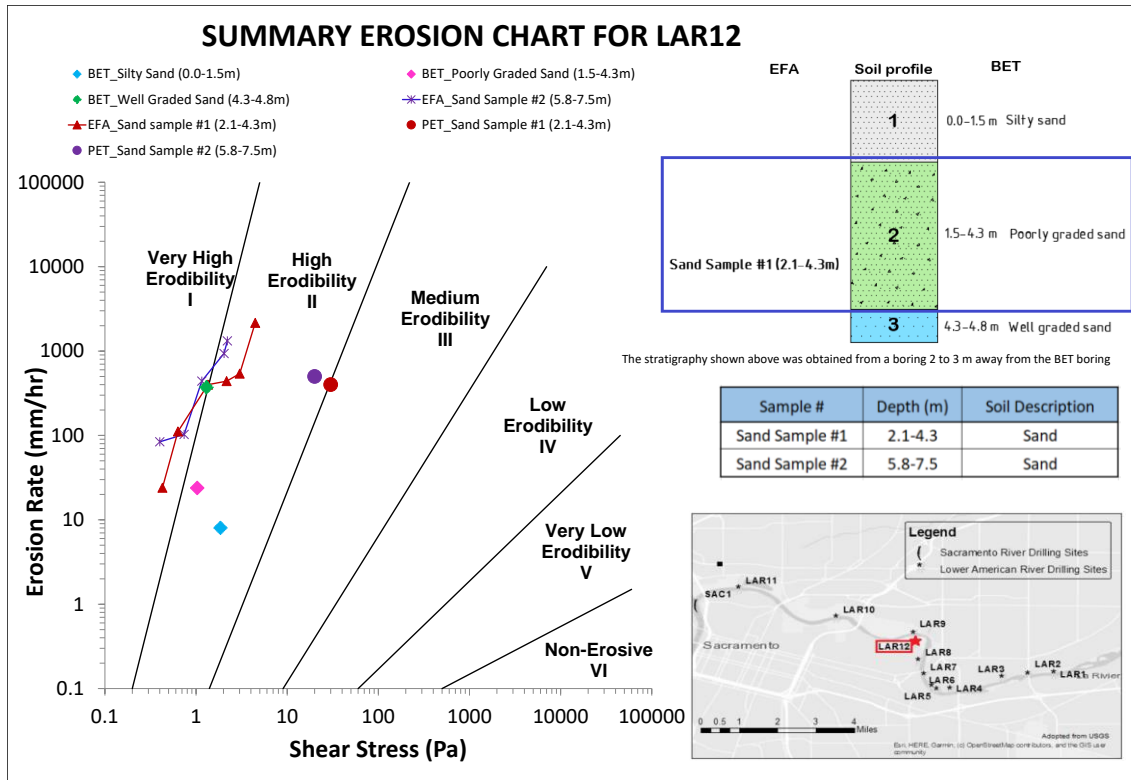


Figure 71. Summary erosion chart for LAR12

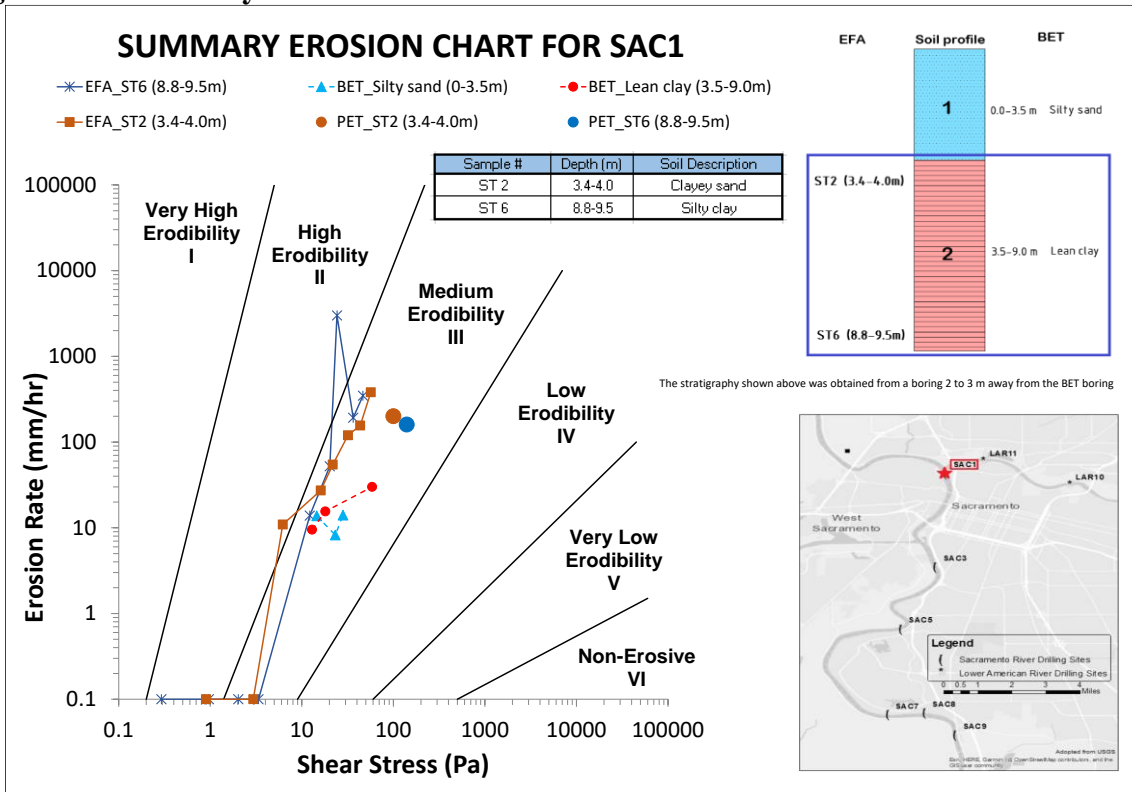


Figure 72. Summary erosion chart for SAC1

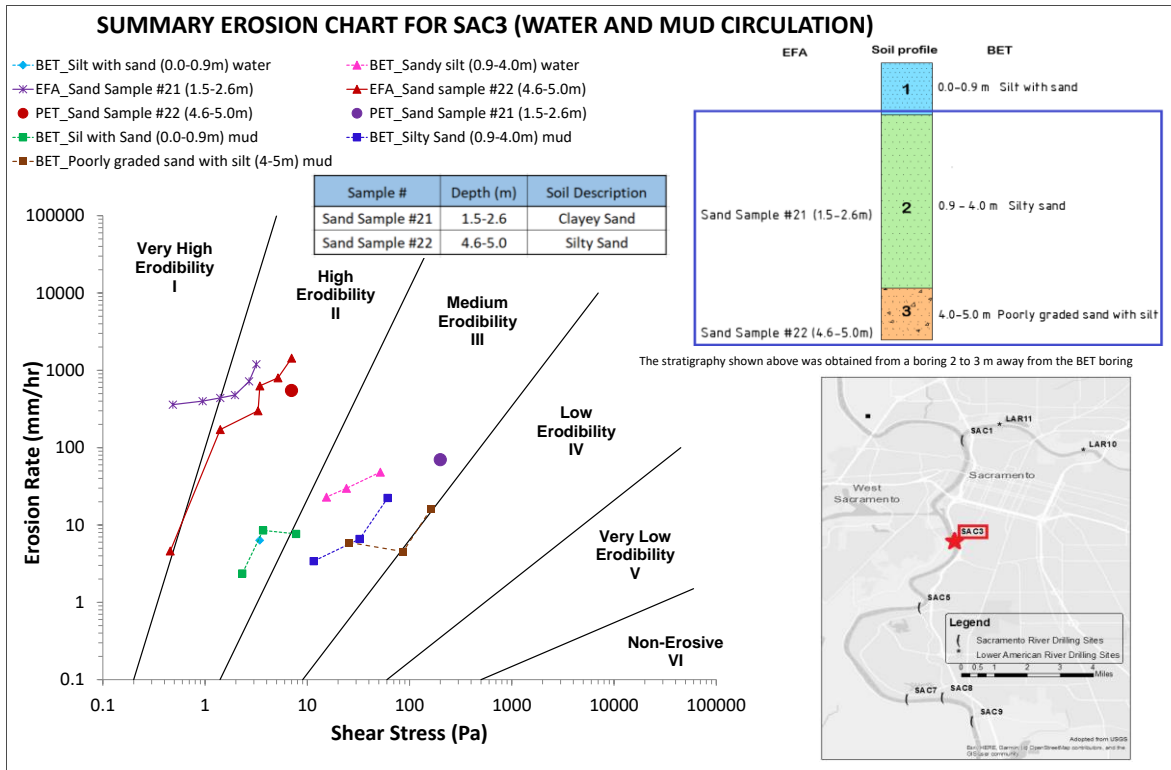


Figure 73. Summary erosion chart for SAC3

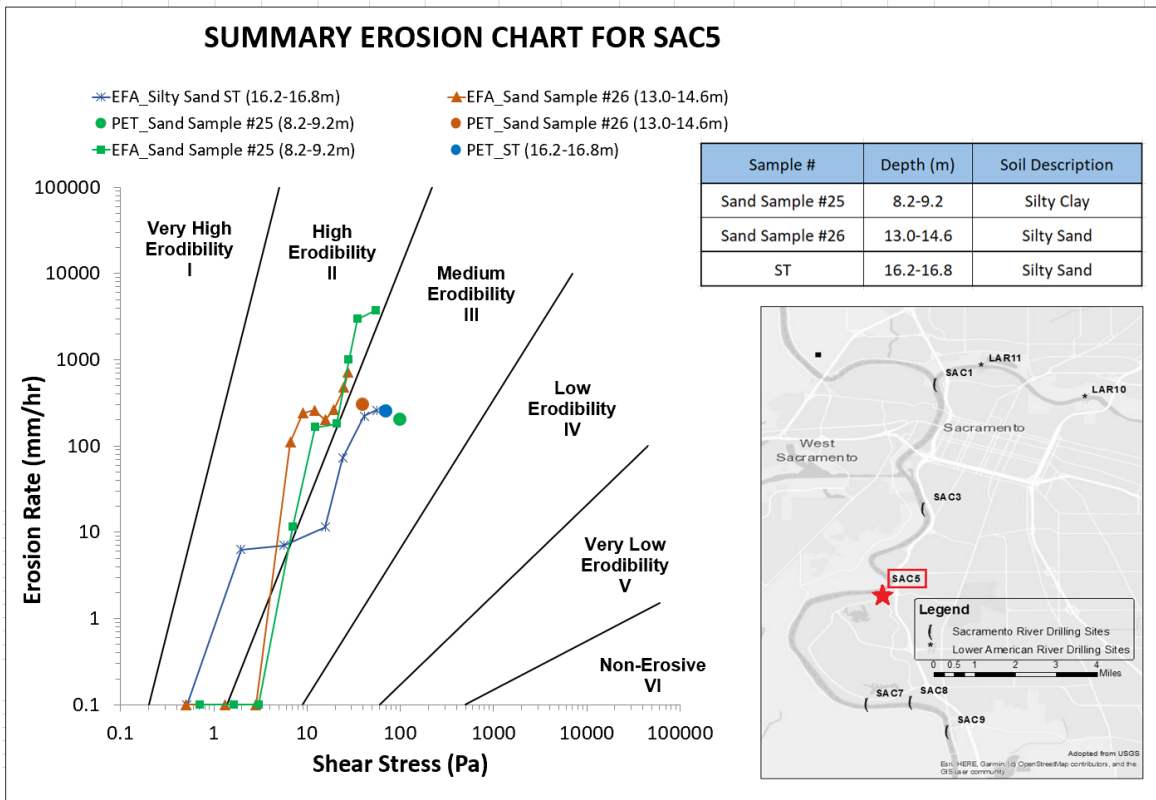


Figure 74. Summary erosion chart for SAC5

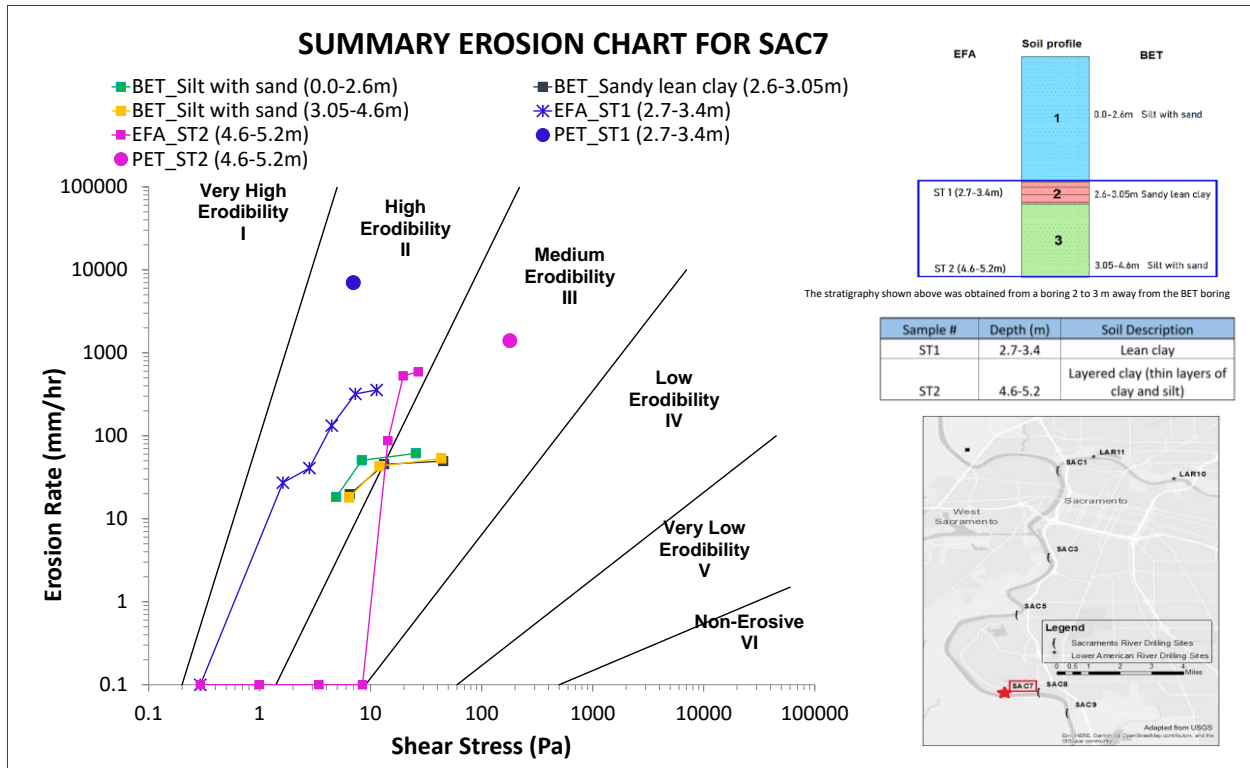


Figure 75. Summary erosion chart for SAC7

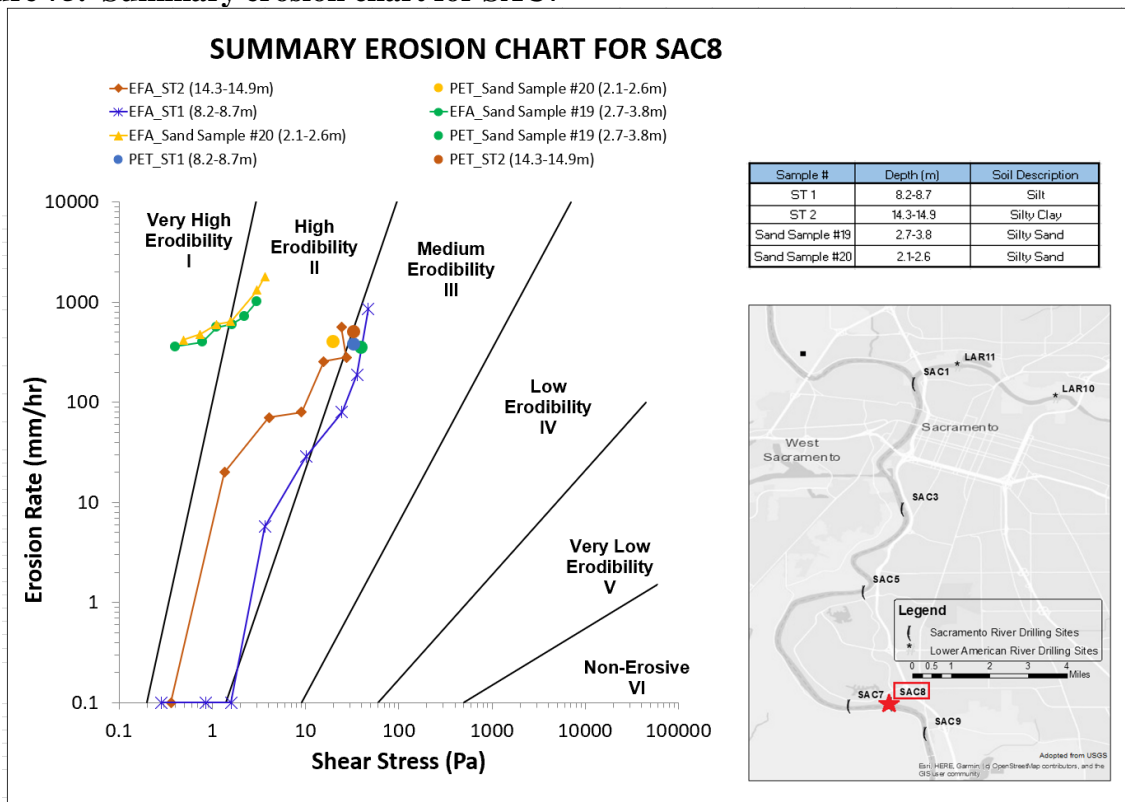


Figure 76. Summary erosion chart for SAC8

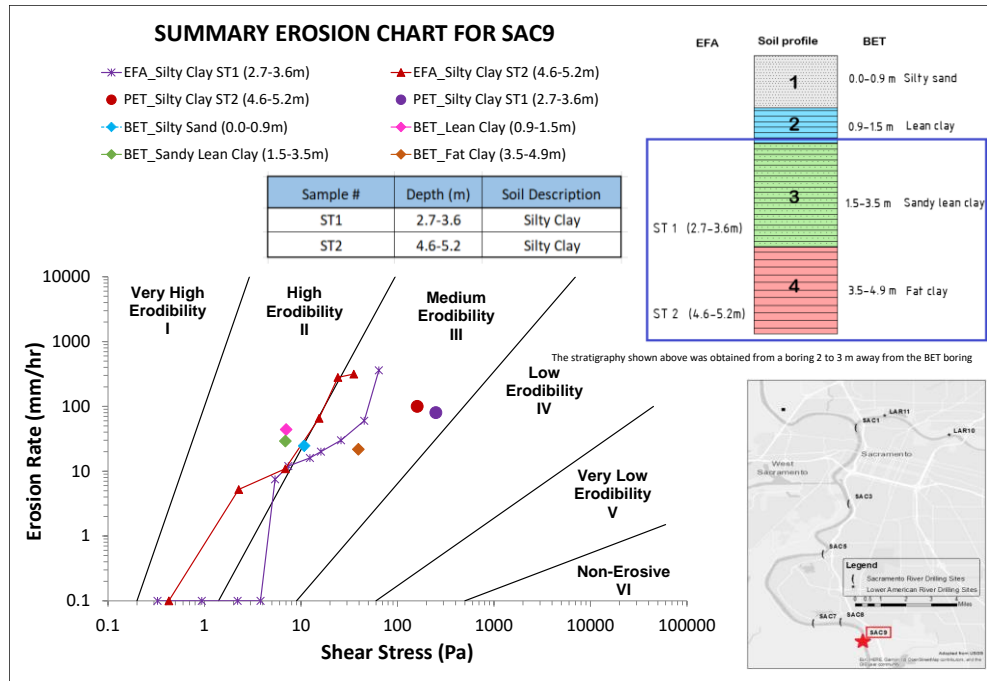


Figure 77. Summary erosion chart for SAC9

Table 17. Critical shear stress inferred from BET tests and corresponding EFA values

#	Site location	Layer	τ_c from BET (Pa)	τ_c from EFA (Pa)
1	LAR3B	Silty sand (1.6 – 5.5 m)	4.5	0.36
			3.0	0.589
2	LAR6B	Silty sand-35% fines (1 - 1.5 m)	0.7	0.979
		Silty sand-15% fines (1.5 – 2.3 m)	1.0	0.36
		Silty sand-20% fines (2.3 – 2.7 m)	2.5	0.428
3	LAR7B	Clayey sand (3.4 – 4.6 m)	1.8	0.326
		Poorly graded sand (4.6 – 5.5 m)	1.4	0.336
4	LAR12B	Poorly graded sand (1.5 – 4.3 m)	0.28	0.428
5	SAC3B (water)	Silty sand (0.9 – 4 m)	3.5	0.360
6	SAC7B	Sandy lean clay (2.6 – 3.05 m)	2.8	0.293
7	SAC9B	Sandy lean clay (1.5 – 3.5 m)	1	0.428

#	Site location	Layer	τ_c from BET (Pa)	τ_c from EFA (Pa)
		Fat clay (3.5 – 4.9 m)	3.2	3.809

3.8. Precision, advantages, and limitations of BET

This Chapter presents a procedure for precision calculation, advantages, and limitations of BET. For the BET, the uncertainty associated with the measurements is evaluated as follows. The caliper profiles are often repeated in the same borehole. The readings are not necessarily the same as the caliper orientation may be different in a borehole which, while theoretically circular, is in fact unlikely to be circular. To quantify this variation, the following was done.

1. Consider two caliper reading profiles (radius r_1 and r_2 and more if needed as a function of depth) recorded in the field within the same borehole at the end of a flow run.
2. Calculate the average caliper reading profile as $r_{av} = 0.5(r_1 + r_2)$ as a function of depth.
3. Calculate the differences Δr_1 and Δr_2 at any given depth between the radius given by each caliper reading (r_1 and r_2) and the average radius r_{av} calculated in step 2.
4. Calculate the sum of the absolute values of the differences Δr_1 and Δr_2 over the borehole depth.
5. The variation V_r is estimated as follows (Eq. 20).

$$V_r = \frac{\sum |\Delta r_1| + \sum |\Delta r_2|}{\sum (r_1 + r_2)} \quad (20)$$

The average values of the RVR in percent are presented in Table 18 for each BET location and each flow run. Overall, the values ranged from 0 % to 11.91 % and averaged 1.89 %.

Table 18. Average values of the relative variation radius ratio RVR for all BET locations

Flow	%	LAR 2B	LAR 3B	LAR 5B	LAR 6B	LAR 7B	LAR 9B	LAR 10B	LAR 12B	SAC 1B	SAC 3B	SAC 3B2	SAC 7B	SAC 9B
As drilled	$\Delta R_1/R_{av}$	3.42	6.17	3.25	0.75	1.98	0.87	7.37	0	0.58	0.98	2.44	1.44	4.69
	$\Delta R_2/R_{av}$	4.35	4.46	2.53	0.75	1.98	1.35	4.91		0.58	0.98	0.68	1.54	1.04
	$\Delta R_3/R_{av}$	5.27	4.69	4.47				11.91				0.21		3.49
	$\Delta R_4/R_{av}$	0	5.8											
End of flow 1	$\Delta R_1/R_{av}$	1.57	1.01	1.33	0.62	1.11	1.5	3.86	2.69	2.25	1.9	2.52	4.59	2.14
	$\Delta R_2/R_{av}$	0.66	1.44	0.57	0.62	1.11	1.5	1.4	2.69	0.73	1.8	1.22	0.94	1.96
	$\Delta R_3/R_{av}$	1.35		1.1				4.34		1.66		1.51	5.16	
End of flow 2	$\Delta R_1/R_{av}$	3.1	0.24	0.25	0.61	1.84	0.33	4.54		0.5	1.19	1.12	1.9	
	$\Delta R_2/R_{av}$	1.62	0.24	0.27	0.61	1.84	0.33	4.95		0.94	1.19	0.66	1.65	
	$\Delta R_3/R_{av}$	1.19		0.43				2.56				0.89		
End of flow 3	$\Delta R_1/R_{av}$	1.47	0.17		1.01					0.43	1.13	0.85	2.58	
	$\Delta R_2/R_{av}$	0.8	0.17		1.01					0.53	1.13	0.74	0.58	
	$\Delta R_3/R_{av}$	1.14										0.79		
End of flow 4	$\Delta R_1/R_{av}$				1.26									
	$\Delta R_2/R_{av}$				1.26									
	$\Delta R_3/R_{av}$													
Minimum	0													
Maximum	11.91													
Average	1.89													

The flow rate also varies during the flow duration. The variation is quantified as follows.

1. The difference between a flow value $Q(t)$ and the average flow value Q_{av} is calculated next for many time values, say every minute.

$$\Delta Q(t) = Q(t) - Q_{av} \quad (21)$$

2. The variation is quantified by the ratio of the sum of the absolute values of $\Delta Q(t)$ over the sum of the flow values for all time values. This ratio is called the relative variation flow ratio RVF.

$$V_Q = \frac{\sum |\Delta Q(t)|}{\sum Q(t)} \quad (22)$$

The average values of the RVF in percent are presented in Table 19 for each BET location and each flow run. Overall, the values ranged from 2.12% to 34.78% and averaged 10.31%.

Table 19. Average values of the relative variation flow ratio RVF for all BET locations

Borehole No	Flow Rate 1	Flow Rate 2	Flow Rate 3	Flow Rate 4
	%	%	%	%
LAR2B	6.53	9.71	4.55	
LAR3B	27.5	7.76	18.51	
LAR5B	11.66	10.6		
LAR6B	20	2.75	17.62	11.55
LAR7B	2.91	2.12		
LAR9B	10.44	6.62		
LAR10B	8.08	4.31		
LAR12B	3.22			
SAC1B	14.09	6.4	2.25	
SAC3B	4.99	3.59	5.32	
SAC3B2	22.86	34.78	15.63	
SAC7B	8.53	12.5	4.28	
SAC9B	8.35			
Minimum	2.12			
Maximum	34.78			
Average	10.31			

Some of the BET advantages and limitations are discussed in Section 3.3. The advantages and limitations summarized in this section have been updated because of the work presented in Chapter 3.

The BET advantages are:

1. Continuous profile of erodibility throughout a borehole depth
2. Erosion testing in situ stress conditions
3. Commonly available equipment (drill rig, pump, caliper etc.)
4. Calibration of laboratory data (for example, EFA)
5. Calibration of numerical simulation (for example, Computational Fluid

Dynamics numerical simulation)

6. Economically advantageous because one BET test may cost \$5,000-\$6,000 per 10 m borehole. For comparison, the EFA test performed on one sample cost \$1,500.

The BET limitations are:

1. Precision less than laboratory (for example, compare to the EFA)
2. BET shows less erosion than EFA (See Chapter 3.7. for more details)
3. Instability of the walls in coarse and collapsible soil
4. No slumping of material within the hole; it is assumed that all observed changes

are because of erosion caused by the water flowing through the annulus between the drilling rod and the hole.

For the one location (SAC3) on the Sacramento River, the BET was run with water and drilling mud (high solids powdered bentonite grout). The goal was to study the effect of two fluids on borehole radius and soil erodibility. Figure 78 shows the borehole radius versus depth for water and mud circulation. Comparison of two cases (for each of them two runs at different

fluid velocity were performed) shows that about 10% more erosion takes place when water is used (blue and green lines) compared to mud (orange and grey). Moreover, when water was used for wet drilling, the borehole was progressed down to 3 m and then collapsed in poorly graded sand with silt while for the case of mud, the borehole was drilled down to 4.5 m with no collapse.

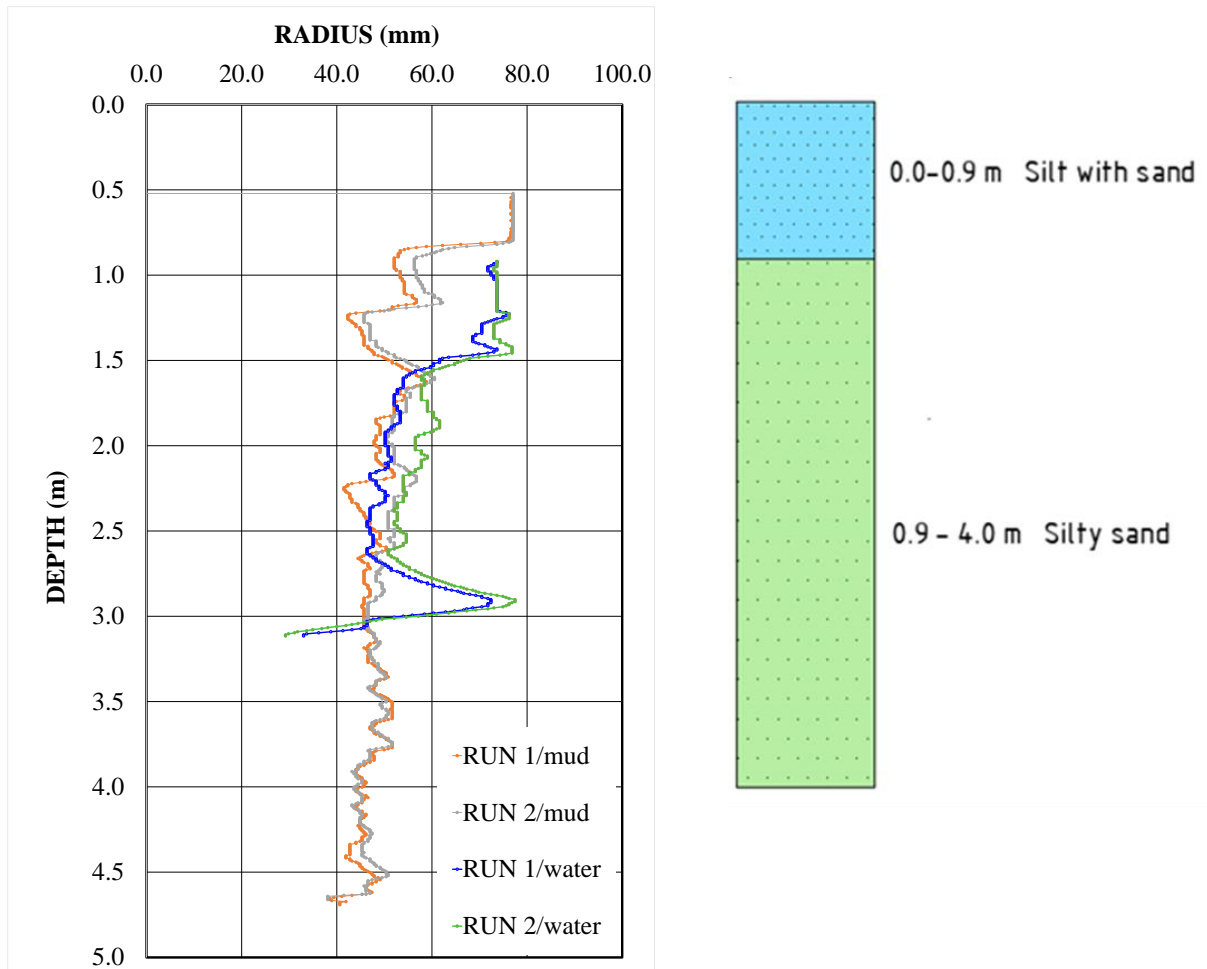


Figure 78. Radius versus depth for drilling with water and mud

3.9. BET DOS and DON'T's

DOS

1. Decide on the depth of interest and if available study the stratigraphy. Have that stratigraphy profile available at the site.

2. Prepare data collection forms.
3. Take pictures before and during testing.
4. Calculate the pump requirements and the borehole diameter to ensure that the velocity will be within the range required. The EFA pump reaches 450 gpm while large drill rigs may be limited to 200 gpm. This is not sufficient to generate 6 m/s velocity in the drilled annulus.
5. Use a mechanical caliper for soil with a minimum 3-arms. For rock, an acoustic caliper is likely better because it gives a 360-degree representation of the borehole geometry.
6. The caliper should be able to measure the diameter of the borehole precisely. The target precision is 0.1 mm, typical 1 mm is fairly coarse and leads to uncertainty in erosion rates.
7. Calibrate the caliper regularly in a known inside diameter pipe.
8. Bring two 1 m long sections of pipes with known inside diameters (~ 75 mm and 150 mm are suggested). These can be PVC pipes if the inside diameter is measured with a laboratory caliper.
9. Repeat the caliper logging a couple of times for a better precision as the hole may not be completely circular.
10. Mud is preferable as a drilling liquid for coarse grain soil because of the potential for borehole collapse.
11. If drilling mud is used, there is a need to measure the mud viscosity. Bring a viscosimeter to the site or store mud in bottles to measure the viscosity in the lab at a future date.
12. Have a readily source or location of water in case the borehole loses a lot of water.

13. Measure the depth of the bottom of the hole precisely as the bottom erosion can be used as a supplemental erosion test (jet test).
14. Keep notes on how fast the borehole is drilled because it may give some indication about the erodibility of the soil.
15. Reduce data in real time even if only in a coarse fashion for better decisions on the continuation of testing.
16. Collect samples in a parallel borehole.
17. Measure the flow with a flow meter in line with the pump.
18. Try to estimate how much water may be lost through the borehole walls during the test. This may require a crude permeability test where the water level in the hole is monitored versus time for a few minutes. This leads to a loss for volume per minute which can be considered in the data reduction.
19. Think of which velocity you wish to impose and decide whether to start with the high velocity or low velocity.

DON'TS

1. Do not “clean” the borehole while wet rotary drilling by repeated passages of the drill bit because it is increasing the borehole diameter, creates disturbance of the borehole walls and impact erodibility.
2. Do not leave the borehole open for any undue length of time as collapse likelihood will increase.
3. Do not keep the drilling bit on the rods when conducting the BET tests; this will change the erosion rate from a parallel flow to an impinging jet flow.

4. MITIGATION OF EROSION USING GRASS

The Chapters 4 -7 presents the results of soil improvement testing and analysis. Soil improvement is a promising method for erosion control. The following methods are typically used: concrete facing as rigid protection, riprap as flexible armor or reinforced with concrete, vegetation as soft armoring (FHWA Hydraulic Engineering Circular 23, HEC-23). Chemical stabilization using the traditional chemical stabilizers such as lime, cement, gypsum, bauxite residue and fly ash are not readily acceptable first because of their impact on environment as they change pH of soil and groundwater which often affects the vegetation and fauna. Most recently, researchers started to look for alternative to chemical but environmentally friendly soil stabilizers. Those alternative soil treatment are biocementation by microorganisms, enzyme-treatment, lignosulfonate, aminoacidic-treatment.

4.1. Existing knowledge on grass erodibility

The erosion of grass has been studied in the last 35 years or so. The most interesting erosion study was performed by Soil Conservation Center (Handbook of Channel Design for soil and water conservation, 1954), by Whitehead et al. (1976), Hewlett et al. (1987), Seiffert and Verheij (1999), Hughes and Thornton (2015), Thornton et al. (2014, 2010), Dean et al. (2010), Briaud et al. (2011). Mostly research has focused on the erosion of grass due to water overtopping and wave attack. Numerous studies have been conducted that discuss and describe erosion of vegetation-lined channels, grass covered earthen levees and embankments by overtopping. Among these studies are laboratory tests, full-scale tests, and fundamental modelling.

Hewlett et al. (1987) conducted full-scale steady overflow test and concluded that limiting velocity of grass is a function of overflow duration. Hewlett proposed a design chart to obtain the critical velocity depending on the grass quality (Figure 79). The critical velocity reaches its maximum value (approximately 4.5 m/s) for a grass with a good cover but then decreases with time. To enhance the erosion of grass, Hewlett et al. (1987) used a geotextile in a form of both mats and fabrics with small size openings. The critical velocity of geotextile-reinforced grass varies from 5 m/s to 6 m/s for one hour of flow duration and then increases down to 3.3-4.3 m/s with an increase in time (up to 50 hours).

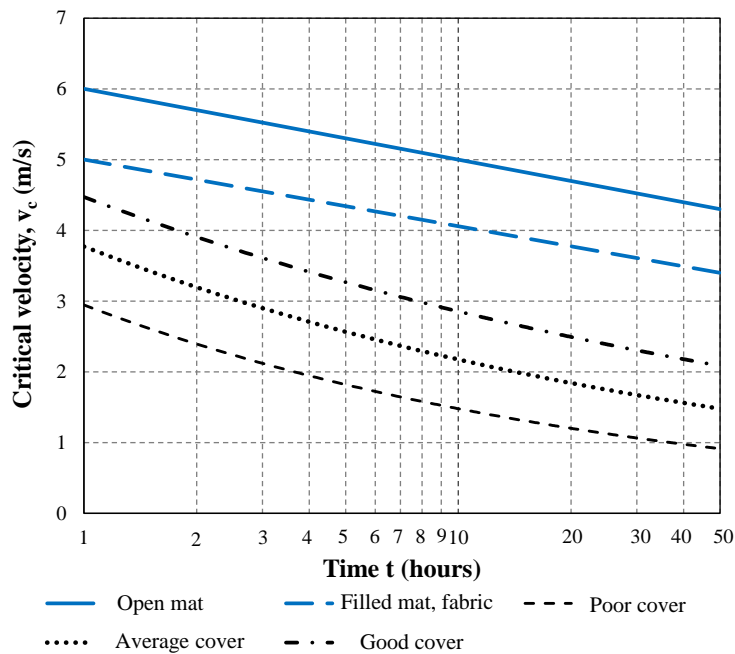


Figure 79. Critical velocity vs. time for poor, average, and good cover of grass (adapted from Hewlett et al., 1987)

Dean et al. (2010) obtained the critical velocities based on the Hewlett model (Table 20). The assumptions made by Dean et al. are steady flows on the land side of a levee and the mean water level is below the levee crest.

Table 20. Critical erosion parameter (adapted from Dean et al., 2010)

Grass Quality	Critical Velocity*, v_c (m/s)	Erosion Limit, G_F m^3/s^2
Good Cover	1.80	0.492×10^6
Average Cover	1.30	0.229×10^6
Poor Cover	0.76	0.10310^6

* Obtained on a basis of work above the critical value

The erosion of grass covered clay used in a levee (dyke) was studied by Seijffert and Verheij (1998) for a case of wave attack. The authors claimed that grass can resist up to a velocity of 2 m/s. Seijffert and Verheij (1998), by using the results and observations from large-scale wave tank experiments, obtained that the time required to remove grass turf (t_{max}) depends on the turf thickness, wave height, and quality of grass and can be estimated as the following:

$$t_{max} = \frac{d}{\gamma c_E H_s^2} \quad (23)$$

where d is the turf thickness (m), γ is the safety coefficient (dimensionless), H_s is the significant wave height (m), c_E is the coefficient used to describe grass quality ($m^{-1}s^{-1}$).

Erosion of grass armor prior to overtopping of the levees during Hurricane Katrina was studied by Storesund et al. (2010). The authors run simulation and obtained lateral erosion (m) due to wave attack for good, average, and no grass cover. The lateral erosion has been found in the wide range depending on the quality of grass, storm surge elevation, and time.

Hughes and Thornton (2015), emphasizing a lack of grass and soil erosion information, proposed to apply cumulative excess work concept for a measured or predicted discharge hydrograph. The authors obtained a relationship between peak overflow depth and overtopping duration which, as they claimed, can be used in risk analyses to evaluate the likelihood of grass failure associated with different floods. No other erosion parameters of grass such as critical shear velocity or erosion depth were not considered in their work.

Briaud et al. at Texas A&M University in 2011 conducted eight EFA tests on grass from the levee test section at Jackson State University. He also performed EFA tests on bare clay to compare erodibility of grass and bare soil. The results for both the grass and bare clay are shown in Figure 80.

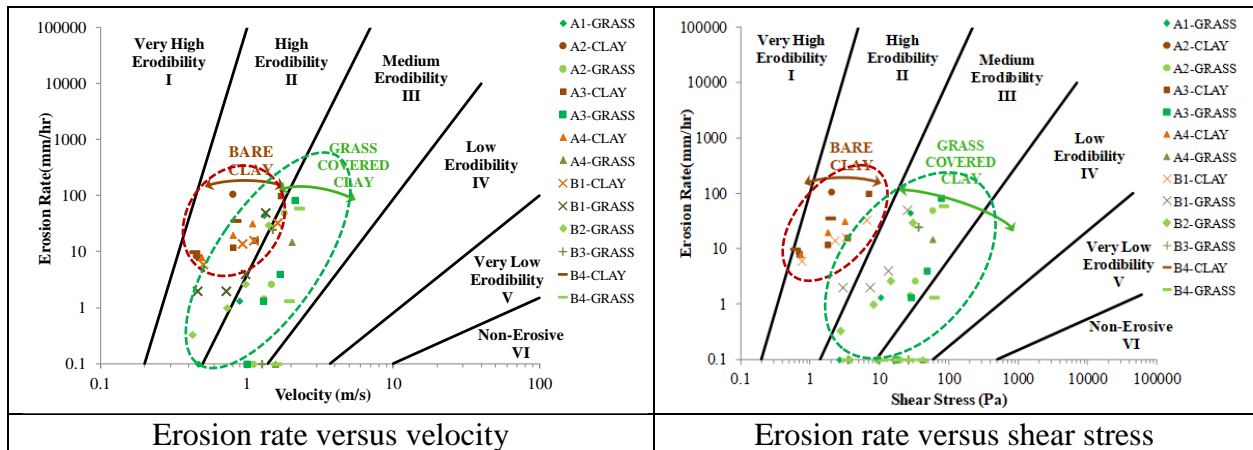


Figure 80. Erosion charts of bare clay and grass covered clay (adapted from Briaud, 2011)

The critical velocity for grass samples varied from 0.5 m/s to 2 m/s, while the critical velocity for the bare clay varied from 0.2 m/s to 0.5 m/s. The critical shear stress varied from 0.2 Pa to 1 Pa for the bare clay and from 1 to 50 Pa for the grass covered soil (Figure 80).

Van der Meer (2007) conducted some field experiments of overtopping on a levee (dyke) covered with natural grass. This study included construction and testing of the wave overtopping simulator at the dike at Delfzijl (Netherlands) with the measurements of velocity and flow depth during the testing. The 4 m wide and 3 m high wave overtopping simulator was installed on the crest and partly on the downstream slope of the levee. The pumps with a capacity of 700 – 1000 m³/hour was used for circulation of water. Figure 81 and Figure 82 show the overtopping test in progress. A certain number of events (waves) was simulated by releasing an exact volume of water (50; 150; 400; 700; 1000; 1500; 2500 and 3500 l/m width) on the levee during a certain

amount of time. The full-scale testing was started with an increasing an overtopping discharge from 0.1, 1, 10, 20, 30 and 50 l/s per m. The maximum number of overtopping waves in 6 hours reached 2159 with the maximum overtopping volume of 6364 l/m.

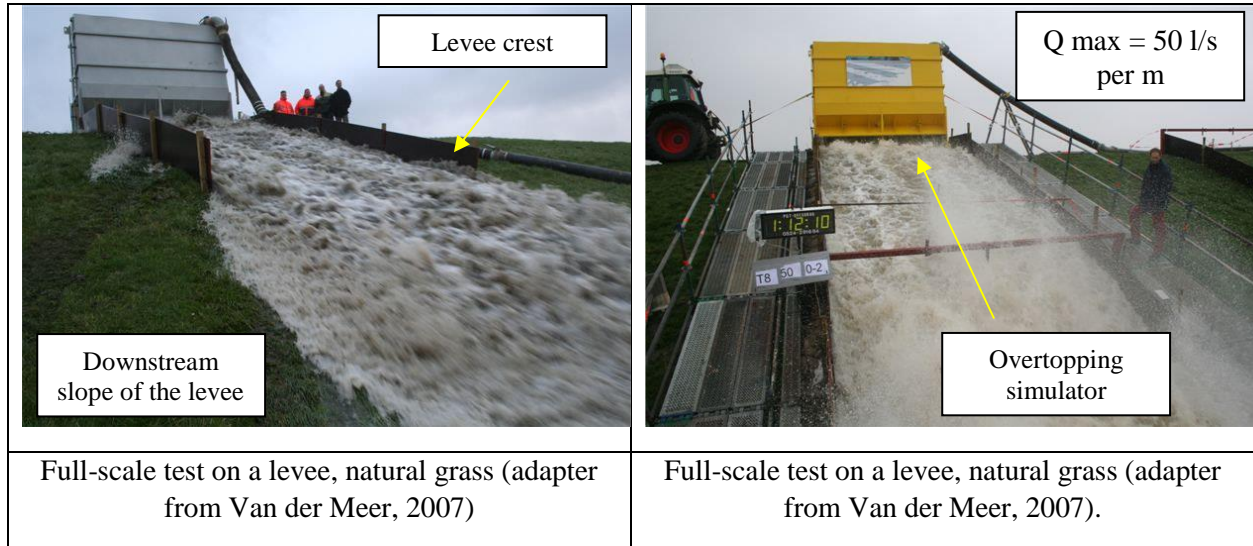


Figure 81. Full scale tests on a levee (adapted from Van der Meer, 2007)

The results indicate that the grass covered levee could resist flow up to about 6 m/s with no failure. Unfortunately, there is no information on type of grass used in this full-scale test.

In 2010, Thornton et al. at Colorado State University (CSU) performed a full-scale overtopping testing on a levee for the U.S. Army Corps of Engineers, New Orleans District. The testing was performed on Bermuda- and Bahiagrass as well as on a bare soil (lean to fat clay) for a comparison purpose. Four tests were run on a levee covered with Bermudagrass, four tests on Bahiagrass, and one test on a bare clay. However, testing program also included an overtopping test performed on a high-performance turf reinforcement mat (HPTRM), not to be considered in this dissertation. The upstream and downstream sections of a tray were 6 m long each, 1.8 m wide and 0.3048 m deep (Thornton et al., 2010).

Thornton et al. (2010) reported several failures of a bare clay (Figure 82). A catastrophic failure of clay was recorded in the upper 6 m of a tray in approximately 20 minutes into the second hour of testing when an average discharge rate was 0.11 m³/s (0.2 ft³/s per ft reported By CSU or 4 ft³/s for 20 ft length of an upper tray). Therefore, an estimated velocity at clay failure is 0.2 m/s (cross section area of a tray, A = 1.8 m x 0.3048 m = 0.55 m²).

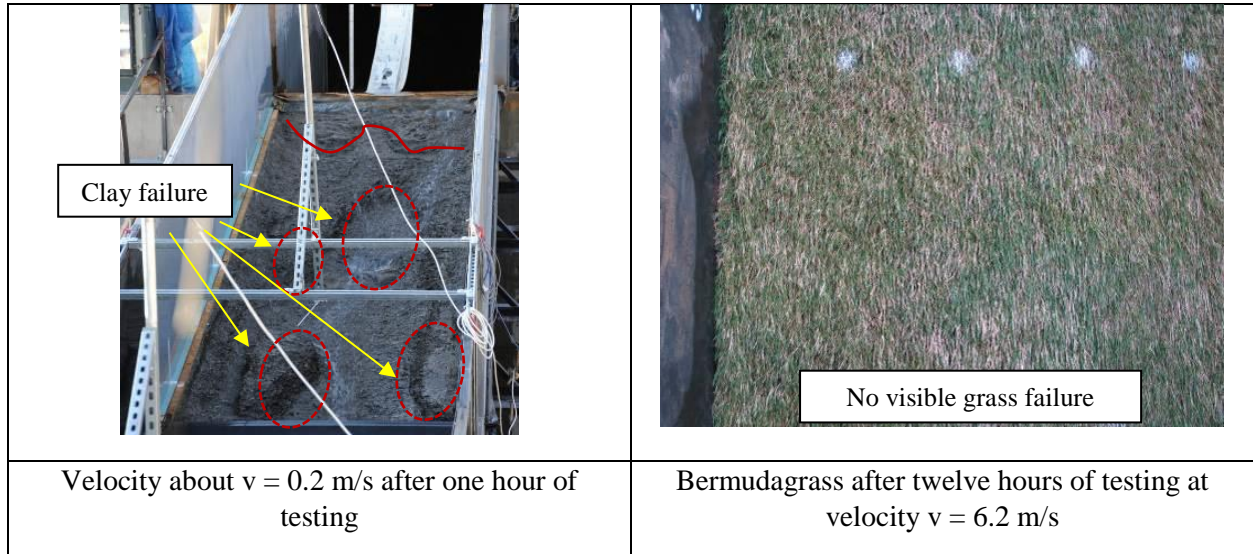


Figure 82. Full scale tests on a levee (adapted from Thornton, 2010)

The results of a full-scale overtopping tests indicate that Bermudagrass did not fail at velocity of 6.2 m/s (Figure 82).

In 2014, Thornton et al. reported the results of a serious of full-scale wave overtopping tests conducted Colorado State University (CSU) for the U.S. Army Corps of Engineers, Jacksonville District. The tests were performed on Jacksonville Bahiagrass sod grown for four months for the root system to establish. The grass grew in trays on sandy soils. The testing procedure consisted of running each one-hour test sequence for one hour and some for six minutes. Thornton et al. claimed five wave conditions used in overtopping tests with the wave heights ranging between 1.4 m to 2.4 m with the peak wave periods varied between 3.4 s and

7.7 s (Thornton, 2010). According to Thornton et al. (2014), grass failed in all tests exposing the underlying bare soil. Erosion depth varied from a several cm to 25 cm reaching the maximum values mostly down the flume slope where the velocity was maximum. Figure 83 shows grass failure in the trays after one hour of steady overtopping flow (cumulative time 6 hr at lower velocity). The reported velocity at grass failure was 3.6 m/s (12 ft/s reported by Thornton, 2014). The corresponding overtopping flow height is calculated as 5.5 cm.

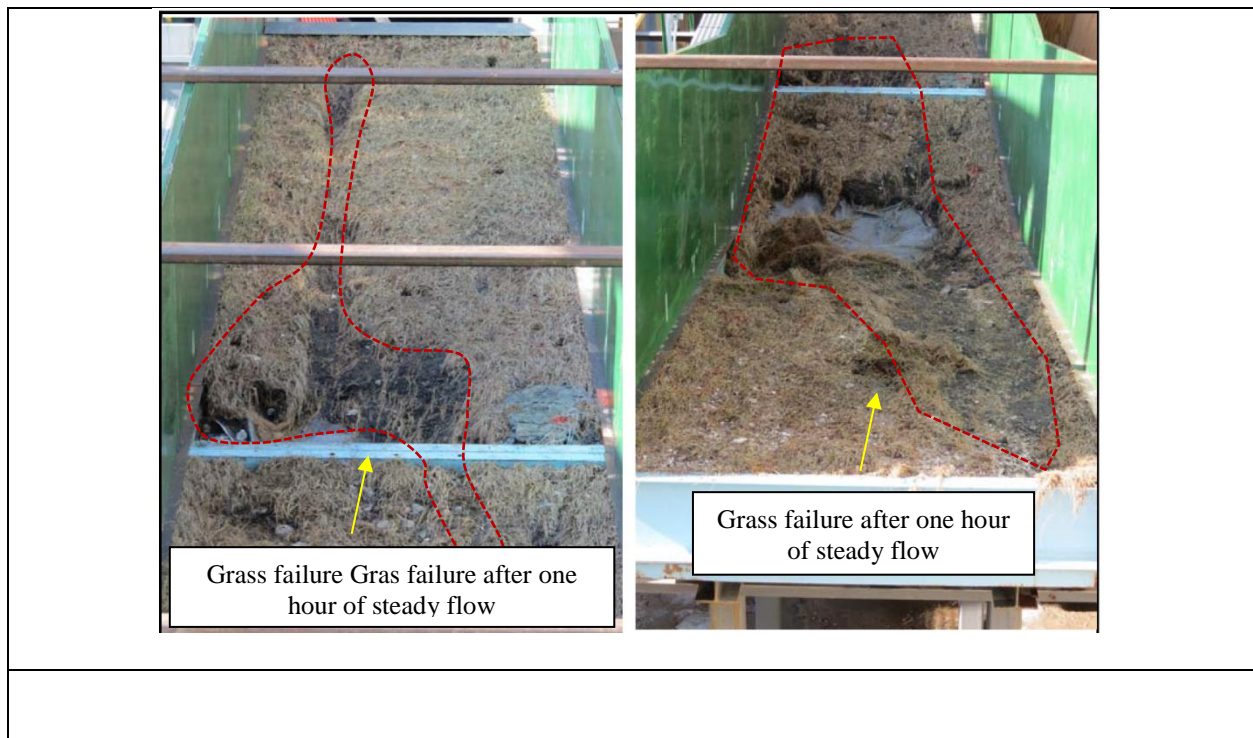


Figure 83. Full scale tests on a levee (adapted from Thornton, 2014)

Armstrong B (2016) in his master thesis studied the effect of grass root reinforcement on soil cohesion. In his research he planted two types of Bermudagrass and Bahiagrass. By running CPT and vane test, he observed an increase in strength in root reinforced soil compared to bare soil up to three times. He reported that the average total cohesion of the root reinforced soil and internal friction angle were 11000 Pa and 32° respectfully.

The erosion process can be significantly affected by the amount and type of vegetation on the riverbank, levee etc. and any obstacle which slows the flow down at the interface between the soil and the water. Vegetation can resist erosion to a degree, but that degree is not well known. No shear stress estimation was done based on the results of the full-scale tests described above. The full-scale field tests are informative but not cost-effective compared to the laboratory tests such as EFA. A full-scale test may cost \$35,000 or more and an EFA test costs \$1500. There is also a need to temporary measure while the grass grows.

4.2. Obtaining shear stress equation

4.2.1. Manning versus Moody shear stress equation

This Section describes the procedure of obtaining shear stress equation for grass. The hydraulic shear stress can be calculated by using the Moody chart approach and the Manning approach. The shear stress τ by Moody for pipe flows is (Eq. 24):

$$\tau = \frac{1}{8} f \rho V^2 \quad (24)$$

where τ is the shear stress on the wall of the pipe, f is the friction factor obtained from the Moody Chart, ρ is the mass density of water (1,000 kg/m³), and V is the mean flow velocity in the pipe. The friction factor f is a function of the pipe Reynolds Number Re and the pipe relative roughness ε/D . The relative roughness ε/D is the ratio of the average height ε of the sample roughness over the pipe hydraulic diameter D . For soils, the average sample roughness ε is taken equal to $0.5 D_{50}$, where D_{50} is the mean grain size for the soil. For grass, roughness is not well defined.

The following procedure with the assumptions has been made to obtain the shear stress equation for grass to be beneficially used for EFA testing.

1. For grass-lined open channel flows, the shear stress and friction factor are typically determined from the Manning coefficient n (Chen 2019, personal communication). Assume that flow is uniform and n does not vary with the flow conditions.

$$\tau_w = \gamma R S_0 = \frac{\gamma n^2 V^2}{C_m^2 R^{1/3}} \quad (25)$$

where γ is unit weight of water, $\gamma = 9810 \text{ N/m}^3$; R is the hydraulic radius of the EFA cross-section ($R = A/P$, where A is the cross-sectional area, $A = 5.16 \times 10^{-3} \text{ m}^2$ and P is the wetted perimeter, $P = 0.3048 \text{ m}$, therefore, $R = 0.01693 \text{ m}$); S_0 is the slope of energy line (flat surface in the EFA); n is the Manning roughness coefficient (dimensionless); V is the mean depth velocity; C_m is a constant which depends on the units ($C_m = 1$ for SI units). Note that for a circular pipe with a diameter D , the hydraulic radius R is equal to $D/4$ in Manning equation but equal to $D/2$ for Moody chart.

2. Obtain the slope of energy line S_0 from Eq. 26:

$$S_0 = \frac{n^2 V^2}{C_m^2 R^{4/3}} \quad (26)$$

where n is chosen for the following three arbitrary cases: $n = 0.01$ (smooth case), $n = 0.025$ (gravelly case), $n = 0.035$ (cobble case).

3. Determine the shear stress using Manning approach and Eq. 25.

4. Define the friction factor needed for the shear stress calculation using Moody approach. Note that the role played by the friction factor f in Moody chart is parallel to the role played by the Manning coefficient n .

5. Use the Chezy coefficient C and Manning equation (Chen 2020, personal communication):

$$C = \frac{R^{1/6}}{n} \quad (27)$$

For wholly turbulent flow at high Re, the friction factor f is directly related to the Manning n value through the following equations:

$$C = \frac{v}{\sqrt{RS_0}} \quad (28)$$

$$C = \sqrt{\frac{8g}{f}} \quad (29)$$

6. By equalizing and modifying Eq. 27, 29 and 29, the friction factor f can be expressed as:

$$f = \frac{8gn^2}{C_m^2 R^{1/3}} \quad (30)$$

where g is gravitational acceleration, $g=9.8 \text{ m/s}^2$.

7. Determine the shear stress using Eq. 25 and compare the shear stress by Moody with the shear stress by Manning. Figure 84 indicates good correlation between shear stress found by using Moody and Manning approaches.

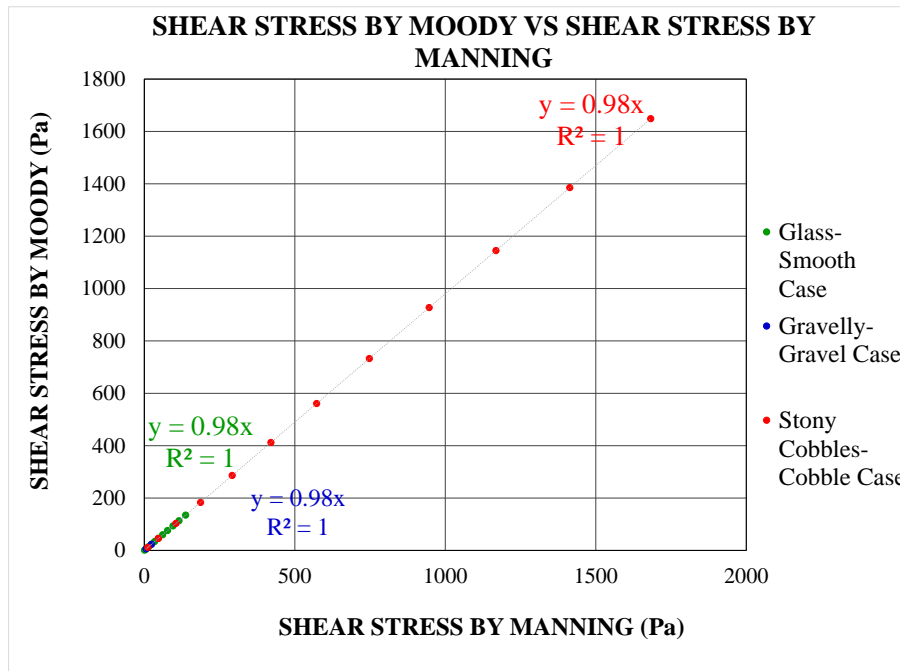


Figure 84. Shear stress by Moody versus shear stress by Manning

8. By equating the shear stress expression for the Moody approach (Eq. 24) and the Manning approach (Eq. 25), a relationship between the Moody friction factor f and the Manning coefficient n for three chosen n values below can be obtained (Figure 85).

- a) glass or smooth case.
- b) gravelly case or gravel with $D_{50}=5$ mm.
- c) stony cobbles or cobble with $D_{50}=200$ mm.

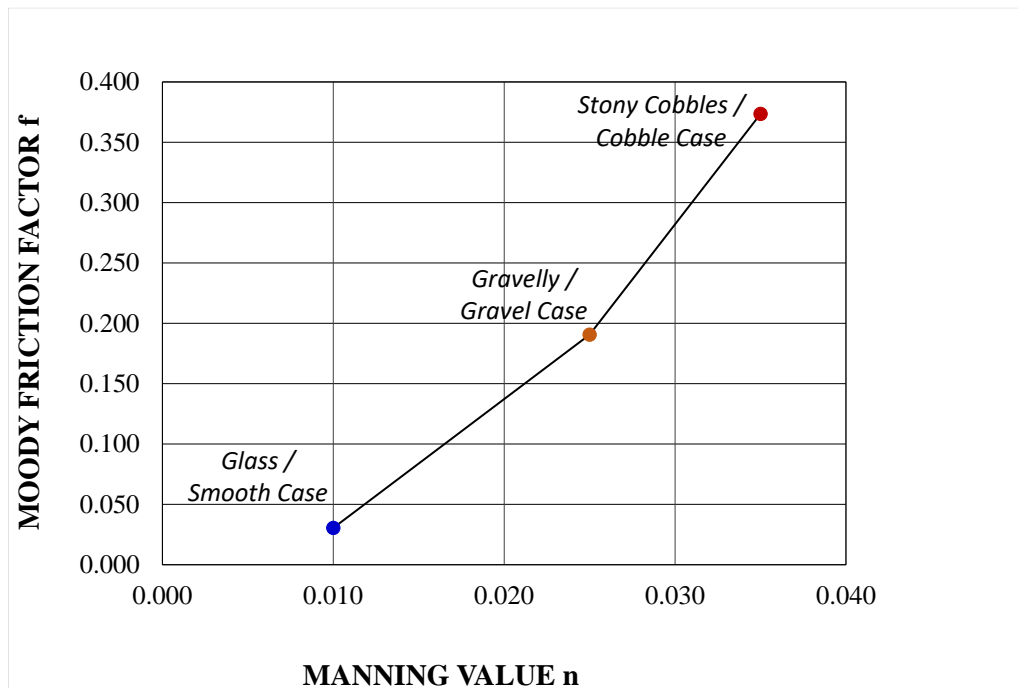


Figure 85. Moody friction factor f versus Manning value n

4.2.2. Estimating Manning coefficient n

This Section describes the procedure to be used to estimate grass roughness (Manning coefficient) for shear stress calculation. The proper estimation and selection of the Manning's roughness coefficient n for grass can be difficult because vegetation varies a lot depending on the type of grass, height of grass, grass species, type of soil, rain and flooding event, season etc.

The following procedure was developed to obtain the Manning coefficient n:

1. Review publications on Manning roughness n-values for grass.

Chen and Cotton (1988) have emphasized the importance of grass height and thickness on the hydraulic resistance. The following n-values were selected after inspecting many guidelines regarding the Manning n values (Table 21).

Table 21. Values of Manning roughness n for grass

Nº	Manning n-value	Channel Condition	Description	Reference
1.	0.002	Negligible	Grass, shrubs, or weeds were permanently laid over during flow	Phillips and Tadayon, 2007 (Modified from Cowen, 1956; and Chow, 1959)
2.	0.01	Small	Dense growths of flexible turf grass, such as Bermuda where the average depth of flow is at least two times the height of the vegetation where the vegetation is not laid over	Phillips and Tadayon, 2007 (Modified from Cowen, 1956; and Chow, 1959)
3.	0.0125	Medium	Moderately dense grass growing where the average depth of flow is from two to three times the height of vegetation	Phillips and Tadayon, 2007 (Modified from Cowen, 1956; and Chow, 1959)
4.	0.015	Medium	Moderately dense grass growing where the average depth of flow is from two to three times the height of vegetation	Phillips and Tadayon, 2007 (Modified from Cowen, 1956; and Chow, 1959)
5.	0.025	Medium	Moderately dense grass growing where the average depth of flow is from two to three times the height of vegetation	Phillips and Tadayon, 2007 (Modified from Cowen, 1956; and Chow, 1959)
6.	0.03	N/A	Short grass	Phillips and Tadayon, 2007 (Modified from Chow (1959) and Thomsen and Hjalmarson (1991))

Nº	Manning n-value	Channel Condition	Description	Reference
7.	0.035	N/A	High grass	Phillips and Tadayon, 2007 (Modified from Chow (1959) and Thomsen and Hjalmarson (1991))

2. Identify a range of Manning roughness n-values.

The n-value for grass as recommended in the guidelines shown in Table 21 varies from 0.002 to 0.035 with an average value of $n=0.019$. However, the selection of roughness for grass is typically based on field judgment and skill (Phillips and Tadayon, 2006).

3. Prepare erosion functions for a range of n-values (for a given case).

The erosion function (erosion rate vs. shear stress) of Bermudagrass for the range of n-values was chosen and then applied for eight values of Manning roughness n listed in Table 21 by using Manning equation (Eq. 25).

4. Choose the mean n-value and create the corresponding erosion function.

The erosion function for Bermudagrass with eight Manning roughness values including the mean $n = 0.019$ is plotted on Figure 86.

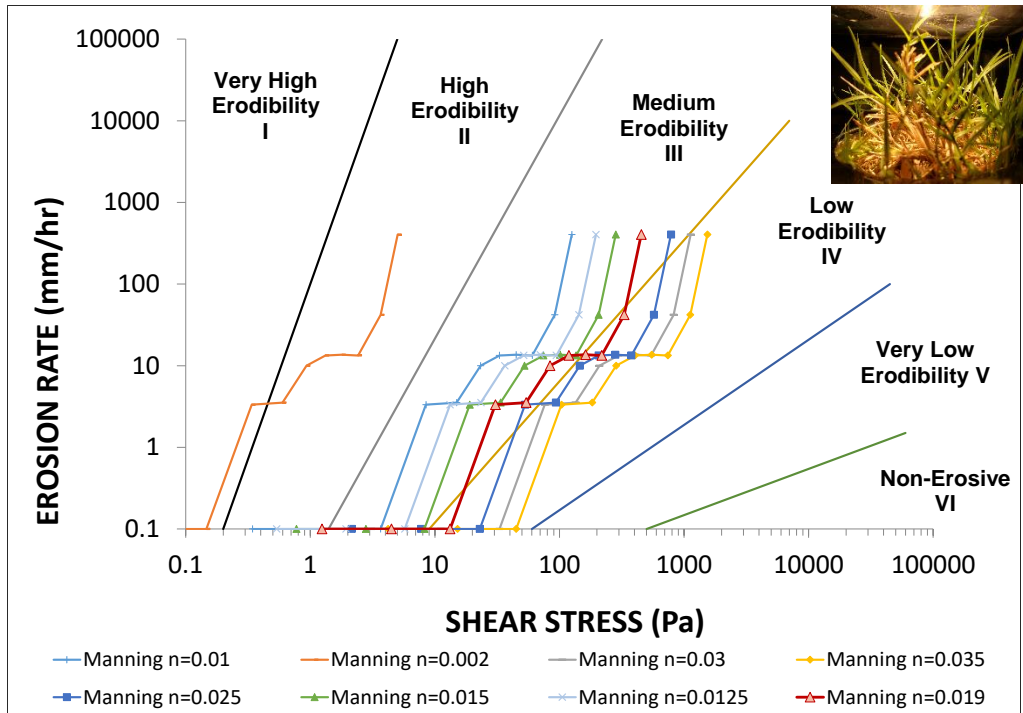


Figure 86. Erosion function for Bermudagrass with n-values

5. Match the erosion function from the previous step by using Moody roughness value.

It was found that the best match of the erosion function by using Manning approach with a mean value $n=0.019$ was obtained for a Moody chart roughness value $\epsilon = 5$ mm. The correspondence between the Moody roughness ϵ and the Manning n-values for Bermudagrass is shown in Figure 87.

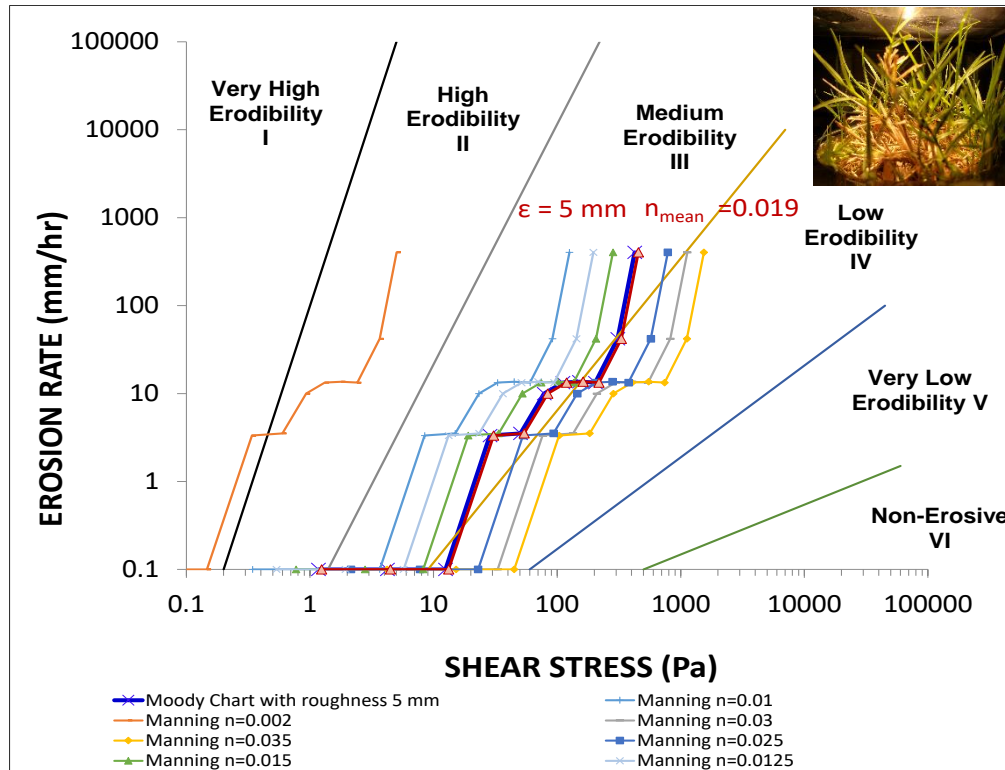


Figure 87. Erosion function for Bermudagrass with n-values and Moody roughness

6. Show the range of relative Moody roughness (ϵ/D) corresponding to the range of Manning n-values.

The range of relative Moody roughness (ϵ/D) corresponding to the range of Manning roughness n-values is shown in Figure 88. The range of Manning roughness n is set up between 0.002 and 0.035 and it shows that for Bermudagrass erosion category would change with a change in roughness from Very High (I) to Low Erodibility (IV) (Figure 88). The range of Moody roughness (ϵ) corresponding to the Manning roughness (n) varies between 0 and 50 mm. For that range, erosion function would fit into Medium Erodibility (III) to Low Erodibility (IV) as indicated by Figure 88 in the margin.

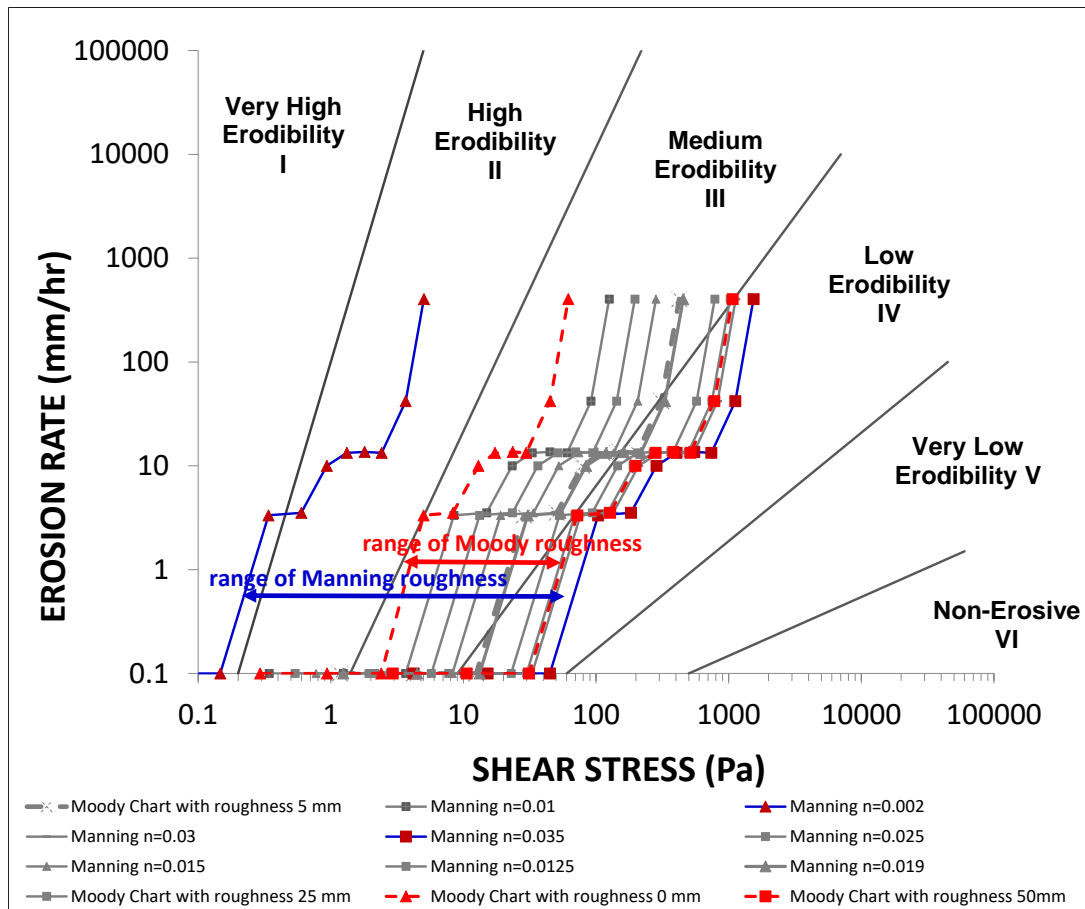


Figure 88. Erosion function for BR7 with a range of Manning roughness n and Moody roughness

7. Select the mean Moody roughness and use that roughness for all shear stress calculations using Moody chart.

Based on the approach described above, the grass roughness to be used in the EFA data reduction for all grass was chosen as $\epsilon = 5$ mm. This number matches reasonably well the mean Manning $n = 0.019$. While this roughness of 5 mm is an arbitrary choice, it has the advantage that anyone using the results in this Chapter knows what value was used and can modify the results if they think that a different value should be used. Note that a chosen Moody roughness of 5 mm for the EFA conduit corresponds to a friction factor $f(\epsilon/D) = f(0.005 / 0.068) = f(0.0735)$

~ 0.0868 (Figure 29). Manning friction factor above $f = 0.01$ was estimated by Hughes (2007) as a reasonable value for grass-covered slopes. Hewlett et al. (1987) suggested values of Manning n for grass-covered slopes depending on the slope stiffness as follows: $n = 0.03$ for slopes of 1:10, $n = 0.02$ for slopes of 1:3 and steeper.

4.3. Grass characterization

Grass is used for lining levees, open channel spillways and dam spillways, irrigation channels, bywash spillways etc. Engineers need to estimate of performance of grass during natural floods and obtain critical parameters such as critical velocity, critical shear stress etc. In soil and crops science, grass is often referred as turf and turfgrass. Turf is a thick mat consisted of (bottom to top) the upper stratum of soil bound by grass and plant roots (Webster's Seventh New Collegiate Dictionary, 2020). Turfgrass is a grass stratum in turf and made of grass only. In this Section, erosion would be considered in terms of erosion of turfgrass or grass and turf as a multicomponent system consisted of grass, roots, and soil.





Some grass profiles are shown on

Figure 89. Some grass, for example St. Augustinegrass, is made of mat, a thick above-ground stem with large open space between stems and a tall stiff canopy above the stems. Table 22 shows some characteristics and features of four types of grass such as Bermudagrass, St. Augustinegrass, Zoysiagrass, and Bahiagrass, chosen for erosion study in the EFA.



Figure 89. Mats of Bermudagrass and St. Augustinegrass

Table 22. Some characteristics and features of grass (adapted from Chalmers and McAfee; The LawnInstitute, 2020; Schery, R.W. 1973)

Description	Bermudagrass	St. Augustinegrass (<i>Stenotaphrum secundatum</i>)	Zoysiagrass	Bahiagrass (<i>Paspalum notatum</i>)
Grass adaptation*	Warm arid and semiarid region (irrigation necessary)			
	Cool semiarid region		Cool semiarid region	
	Warm humid region – Lower South (warm and wet)			
	Warm humid region (Upper South)		Warm humid region (Upper South)	
Maintenance	Tolerate some flooding, fast establishment	can become thatch, fairly acceptable to diseases and insects	May need regular dethatching	Can be seeded
Spreading/Establishment	Stolons & Rhizomes (rapidly)	Stolons	Stolons & Rhizomes	
Greatest growth	Late spring, summer, early fall			
Dormant	After first freeze, if moisture stresses during summer			
Drought Tolerance	Very good to excellent	Good to poor	Good	Good
Shade Tolerance	Very low to low	High	Light to moderate	
Traffic Tolerance	High	Low	Moderate	Moderate to low
Suggested Mowing Height (cm)	2.5 – 5.1	6.4 – 7.6	1.3 – 3.8 to 1.9 – 6.4 (coarse textured)	5.0 – 10.0
Varieties tested in the EFA	Tifway and Tahoma 31 (Hybrid or Vegetatively planted*)	Raleigh (Hybrid or Vegetatively planted*)	FAES (Hybrid or Vegetatively planted*)	N/A
Planting	Sods, seeds, sprigs or plugs	Sods (mostly)	Sods (better). Seed, sprigs and plugs	
Photo				

*Warm-season grasses turn straw-colored at the first frost and may go dormant during the winter

4.4. Grass sampling

Four types of grass were sampled during May-August 2020 in College Station-Bryan (Texas) at four different locations: Str. Augustinegrass (Raleigh sampled at Turf Research Facility and other unknown species sampled at Doherty Building), Bermudagrass (Tifway and Tahoma 31 sampled at Turf Research Facility and unknown species at Briaud Residence), Zoysiagrass (FAES sampled at Turf Research Facility), and Bahiagrass (unknown species at Allen Academy) (Figure 90). All grass samples were sampled at the sites where the grass had already grown for a certain number of years varying from one year to more than 30 years.

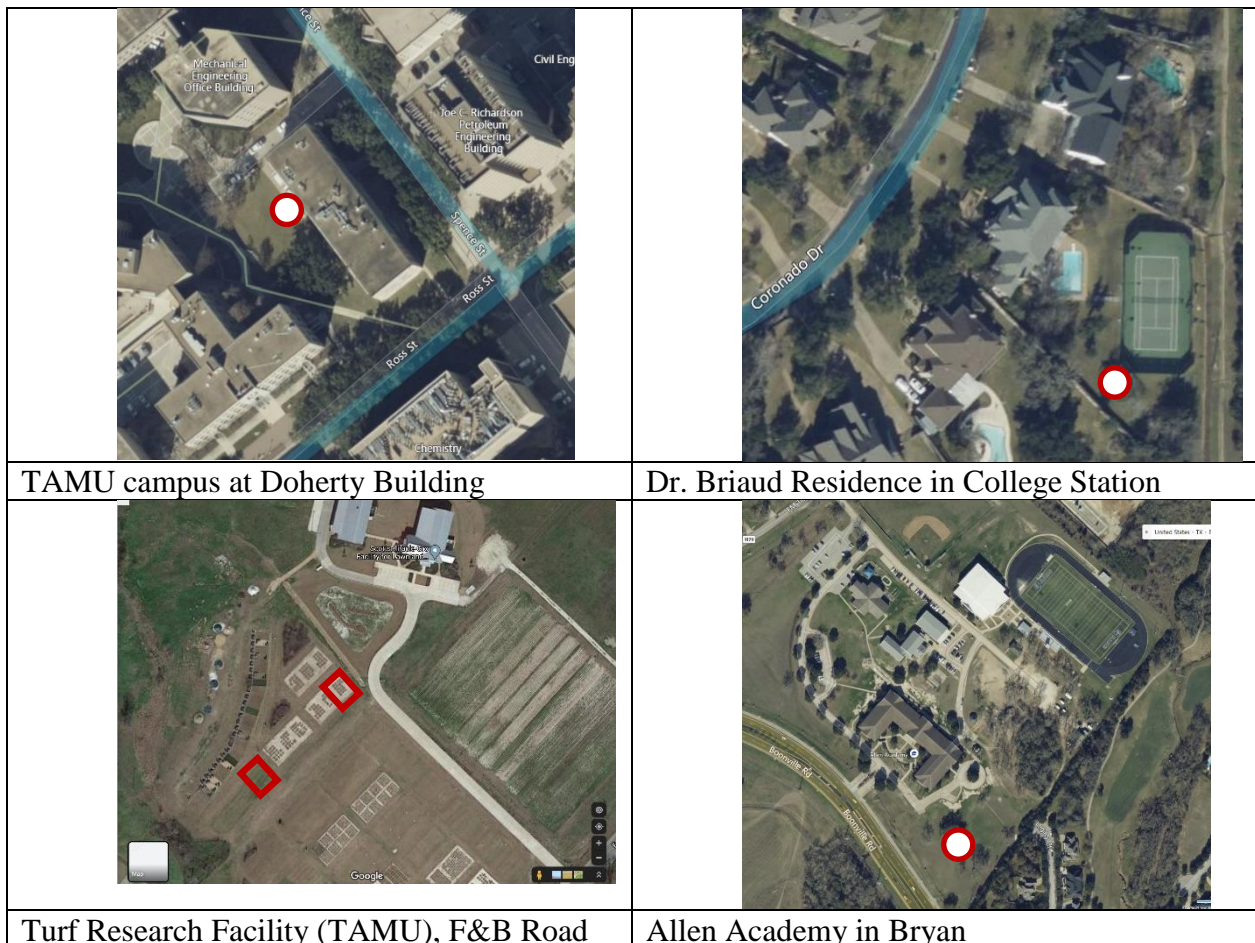


Figure 90. Sampling sites in College Station-Bryan (Texas)

Grass and bare soil samples were collected by driving the 7 cm diameter and 46 cm long Shelby tubes in grass very carefully with minimum disturbance. All grass sampled at the Turf Research Facility in summer 2020 are vegetative planted or Hybrid grass. There is no information on grass for other grass sites such as Briaud Residence, TAMU campus and Allen Academy. The general set up for grass sampling is shown in Figure 91. In the field, the measurements of Normalized Difference Vegetation Index (NDVI), a percentage of green cover, as an indicator of live green vegetation were taken.

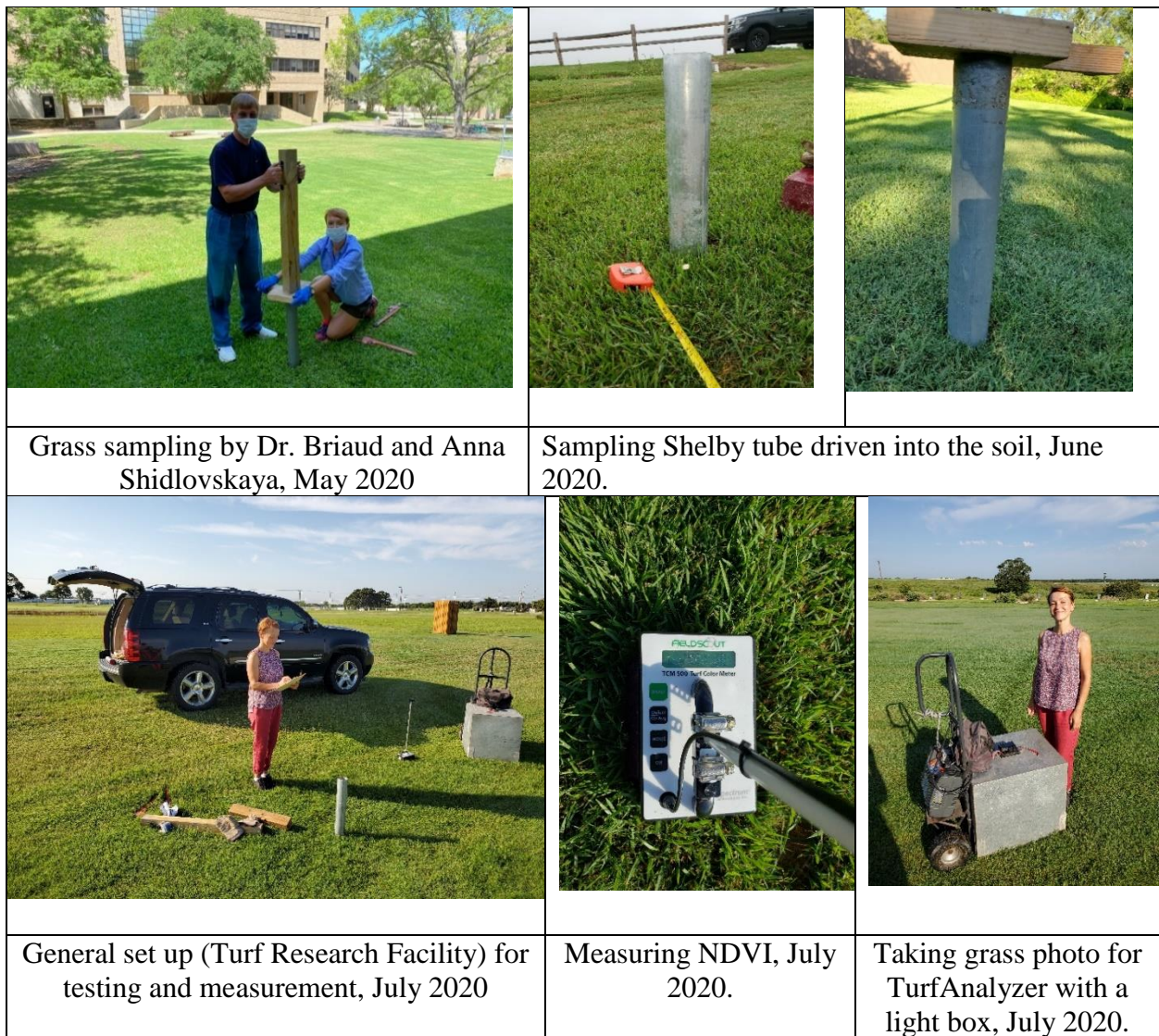


Figure 91. Sampling and measuring grass characteristics in College Station-Bryan (Texas)

4.5. EFA test plan matrix

Erosion testing have been carried out in the erosion lab at Texas A&M University during May-August 2020. The goal of EFA testing was to obtain erosion functions and erosion parameters of grass such as critical velocity and critical shear stress. The total number of tests performed on grass, soil with roots or bare soils was 28. The number of grass samples tested in the EFA was 17, the number of bare soil and soil containing roots was 11. Among grass samples were St. Augustinegrass (4 samples), Bermudagrass (6 samples), Zoysiagrass (3 samples), and Bahiagrass (4 samples). The samples were on average 12 cm long and 7 cm in diameter. The samples were delivered in steel Shelby tubes. Two soil samples were tested to be able to compare erodibility of grass and bare soil. Presumably, the length of the root system was bigger than the sample length. Table 23 shows the EFA test matrix showing index, species, sampling location, date of sampling and date of testing in the EFA.

The EFA test typically consisted of six to ten and more 10-min steps in which the overflowing velocity is constant. During the testing of the grass samples, the sample was placed slightly (about 2-3 mm) below the bottom of the conduit. Usually, before the end of the first-time step, the sample was pushed up to be level with the bottom of the conduit. This was done for two reasons: one was to allow the sample to saturate before testing; and the second was to prevent the initial flow inside the test section from pushing the sample over, but rather gradually inserting it into the flow level. During each step, qualitative and quantitative observations of erosion were taken. Table 23 shows the EFA test plan matrix. Note that all samples were sampled and tested in summer 2020.

Table 23. EFA test plan matrix

No	Index	Species	Location	Sampling	Testing	Notes
ST. AUGUSTINEGRASS						
	StA1	N/A	TAMU Campus	28 May	28 May	<i>“Fresh” grass - No EFA recorded data</i>
1	StA2				29 May	<i>“Fresh” grass, tested next day after sampling</i>
2	StA3				1 June	<i>StA2 recommenced 2 days later</i>
3	StA/R/S1				1 June	<i>StA2 recommenced the same day after grass failed (root system and soil)</i>
4	StA/R/S2				4 June	<i>StA/R/S1 recommenced 2 days later (root system and soil)</i>
5	StA4	Raleigh	Turf Research Facility	6 August	6 August	<i>3-4 years old grass, well established, 6 cm tall, sampled after rain</i>
6	StA5				6 August	<i>3-4 years old grass, well established, 6 cm tall, sampled after rain</i>
BERMUDAGRASS						
7	BR1	N/A	Briaud Residence	11 June	11 June	<i>Green grass</i>
8	BR/R/S1				12 June	<i>BR1 recommenced 1 day later (root system and red soil)</i>
9	BR/R/S2				12 June	<i>BR/R/S1 recommenced 1 day later after grass failed (root system and soil)</i>
10	BR2			12 June	15 June	<i>Sample kept in the Shelby tube for 3 days before testing in the EFA</i>
11	BR/R/S3			18 June	18 June	<i>BR2 recommenced 2 days later after grass failed (root system and soil)</i>
12	BR3			18 June	19 June	<i>Brown grass</i>
13	BR/R/S4			19 June	19 June	<i>BR3 recommenced after grass failed (root system and soil)</i>
14	BR5	Tahoma 31	Turf Research Facility	26 June	26 June	<i>Green grass, 1 year old</i>
15	BR6	Tifway		3 August	3 August	<i>3-4 years old green grass, well established, 6 cm tall, sampled after rain</i>
16	BR7					<i>3-4 years old green grass, well established, 6 cm tall, sampled after rain</i>

No	Index	Species	Location	Sampling	Testing	Notes
ZOYSIAGRASS						
17	Z1	N/A	Turf Research Facility	26 June	26 June	Green grass, 3.5 years old
18	Z2	FAES 1307		8 July	8 July	Green grass, 1 year old. Nitrogen in the soil (?). Seeded in Summer 2019.
19	Z3				9 July	Z2 recommenced 1 day later
20	Z/R/S1				9 July	Z3 recommenced the same day after grass failed (root system and soil)
BAHIAGRASS						
21	B1	N/A	Allen Academy	16 July	16 July	Green grass near the creek on the right side of the main entrance
22	B/R/S1			16 July	17 July	B1 recommenced 1 day later after grass failed (root system and soil)
23	B2			16 July	17 July	Green grass near the creek on the right side of the main entrance
24	B/R/S2			16 July	17 July	B2 recommenced 1 day later (root system and soil)
25	B3			21 July	21 July	Green grass (next day after mowing), 8-9 cm tall
26	B4			21 July	21 July	Green grass (next day after mowing), 8-9 cm tall
SOIL						
27	S1	N/A	Turf Research Facility	26 June	26 June	Soil sampled near Tahoma 31 BR5
28	S2			8 July	10 July	Soil sampled near Zoysia Z1

Notes: Tahoma 31 Bermudagrass is a Bermuda cultivar that was developed starting in 2007 at Oklahoma State University with the goal of producing an excellent quality Bermudagrass that was especially cold tolerant. FAES - Florida Agriculture Experiment Station.

4.6. Results of EFA testing

4.6.1. Bermudagrass

Bermudagrass is claimed to be one of the best choices for erosion control. Bermudagrass is uniform, has a good coverage and a dense relatively deep root system, produces a deep mat, and has an ability to reassume its normal growth and recovery from excessive deposition (Handbook of Channel Design for soil and water conservation, 1954). Bermudagrass was sampled for the further testing in the EFA at Briaud Residence in College Station (Texas) and at Turf Research Facility (F&B Road). Figure 92 show a good quality Bermudagrass with approximately 80% and 90% coverage.

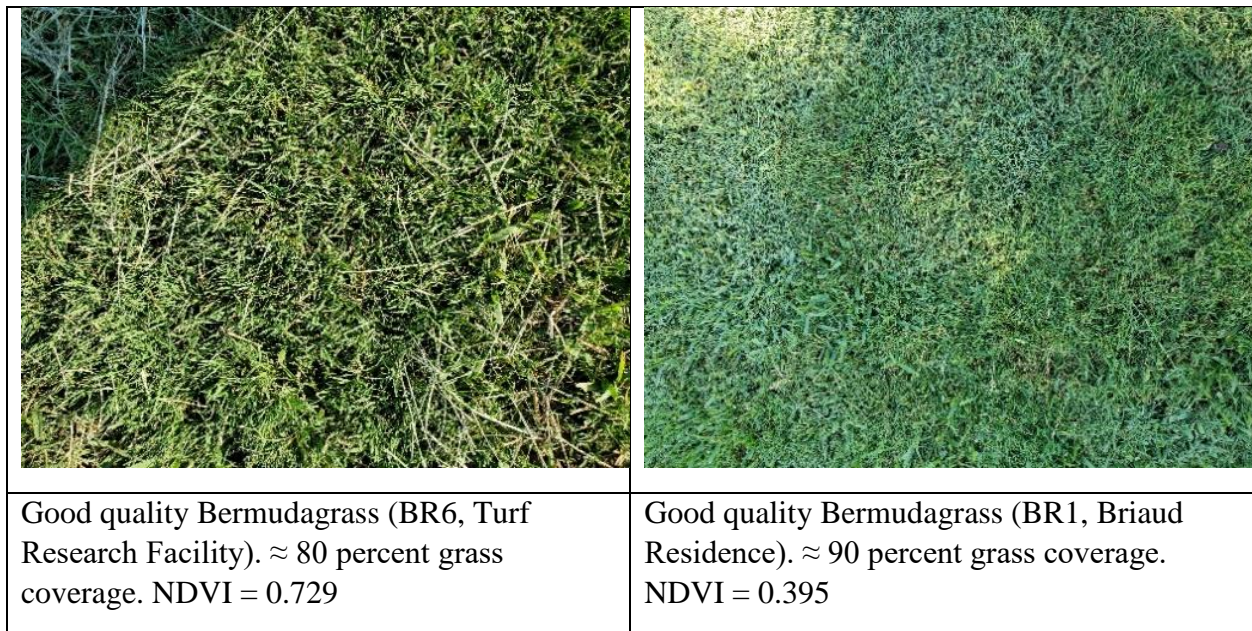


Figure 92. Photographs of Bermudagrass

Six samples of Bermudagrass (BR1, BR2, BR3, BR5, BR6, BR7) were tested in the EFA at the velocity varying from 0.25 m/s to 6.5 m/s (Table 23). Some grass mat failed at the end of the EFA test, and some did not fail (Figure 93).

Bermudagrass exhibits different erosion resistance. Figure 94 shows erosion functions in natural and logarithmic scales. All Bermudagrass except one-year old grass (BR5) is in medium erodibility based on the velocity and shear stress charts.







		
Before testing in the EFA (BR 7)	At $v = 4.9$ m/s (BR 7)	After testing in the EFA (BR 7)
		
Before testing in the EFA (BR 6)	At $v = 4.5$ m/s (BR 6)	After testing in the EFA (BR 6)

Figure 93. EFA testing of Bermudagrass (BR 7 and BR 6)

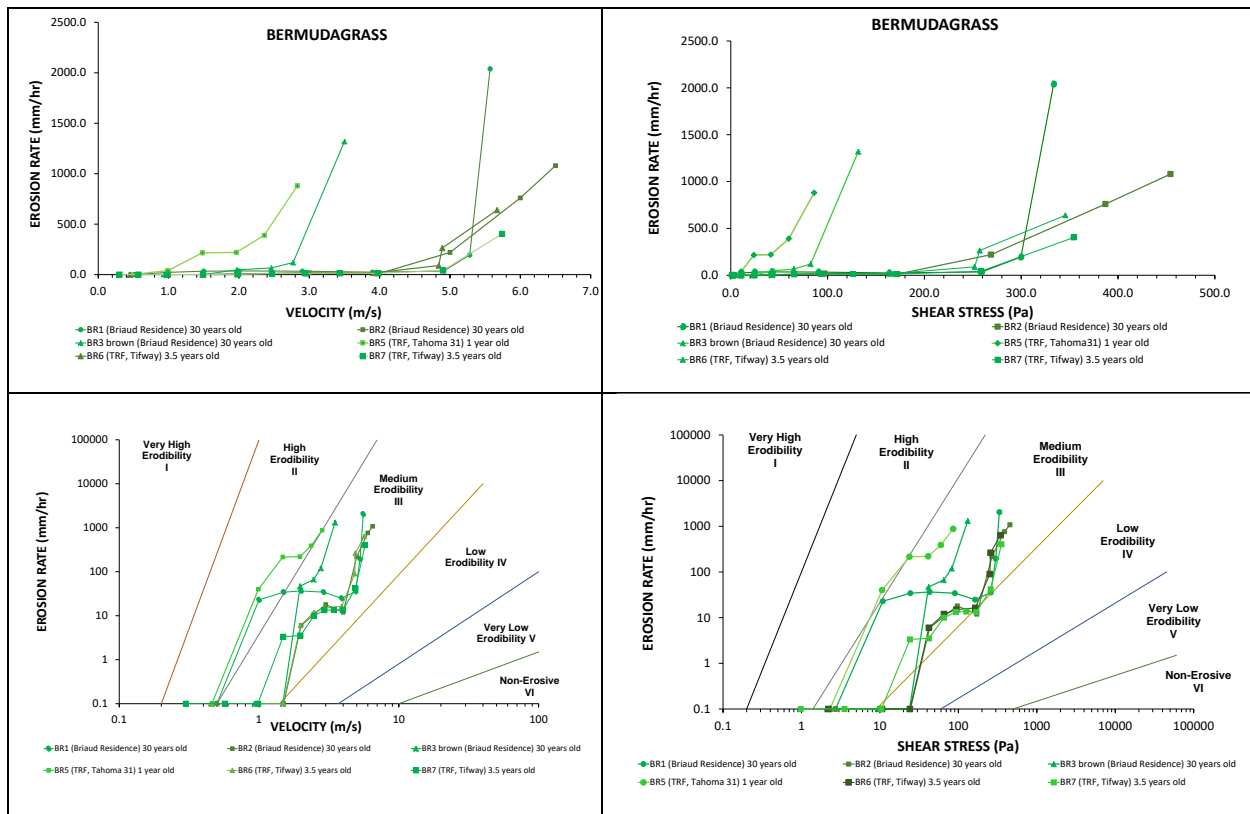


Figure 94. Erosion functions in natural and logarithmic scale of Bermudagrass

The erosion of Bermudagrass exhibits two thresholds. The first one is related to cleaning the grass mat and the second is associated with grass mat detachment. Table 24 shows two thresholds for Bermudagrass. Almost all Bermudagrass samples resist erosion well with not significant grass detachment up to 5 m/s except brown grass (BR3) and not well established one-year old grass (BR5). While the first threshold velocity for Bermudagrass varies from 0.5 m/s to 1.5 m/s, the second threshold velocity is between 1.48 m/s to 5.28 m/s (for fully or at least 50% of grass mat detachment). The first threshold critical shear stress changes from 2.719 Pa to 24.469 Pa while the second varies from 23.821 Pa to 299.693 Pa (for fully or at least 50% of grass mat detachment).

Table 24. Erosion parameters of Bermudagrass

	Critical velocities (m/s)		Critical shear stress (Pa)		Soil Type	Notes
	initiation	detachment	initiation	detachment		
BR1	0.5	5.28	2.719	299.693	Clayey sand, cemented (Fe ³⁺)	All grass detached
BR2	1.5	4.90	24.469	268.75		
BR3	1.48	2.48	23.821	65.055		
BR5	0.46	1.48	2.301	23.821	Silty sand	≈ 50% of grass detached
BR6	1.49	4.84	24.144	251.829		
BR7	0.98	4.90	10.444	258.108		
Range	0.5 – 1.5	1.48 – 5.28	2.719 – 24.469	23.821 – 299.693		
Average	1.07	3.98	14.65	194.54		

4.6.2. St. Augustinegrass

St. Augustinegrass was sampled at TAMU Campus, near Doherty Building (intersection of Ross and Spence St.) and at the Turf Research Facility on F&B Road. This type of grass forms a thick mat (stem) with a good coverage. Figure 95 illustrates a good quality grass with approximately 90% and 100% coverage.

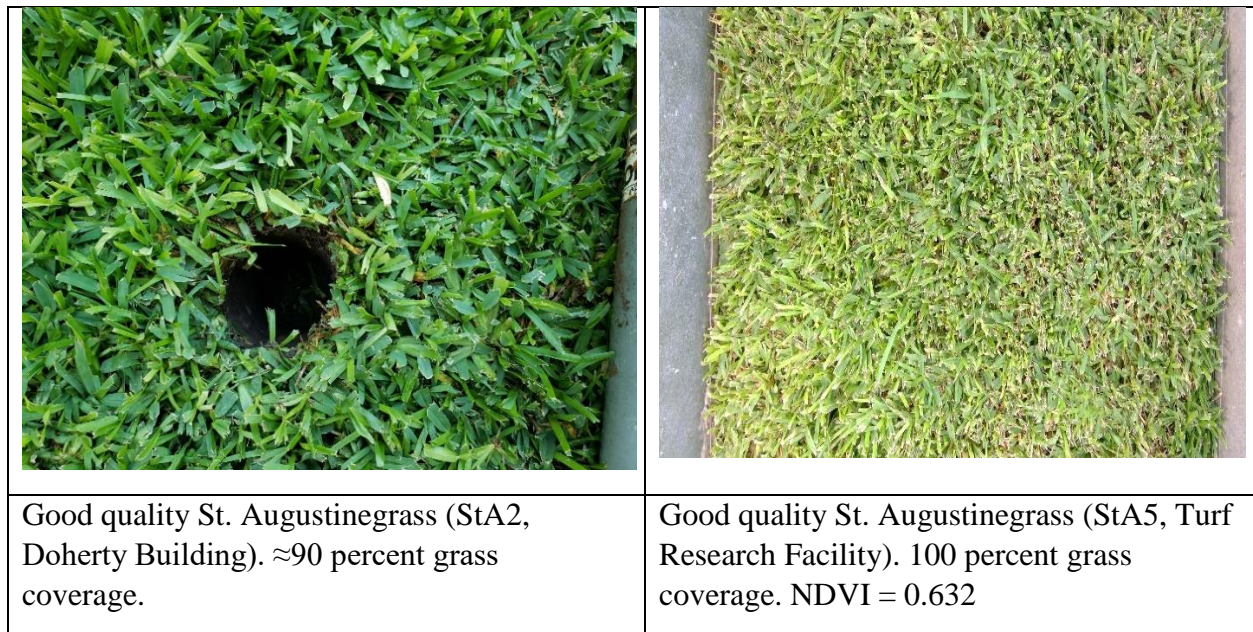


Figure 95. Photographs of St. Augustinegrass

Six samples of St. Augustinegrass (StA2, StA3, StA4, StA5) were tested in the EFA with the velocity varying from 0.25 m/s to 6.5 m/s (See Table 23). Sample StA3 was a sample StA2 re-commenced two days later after prior testing. Some grass failed during the testing while another one resisted erosion (Figure 96).

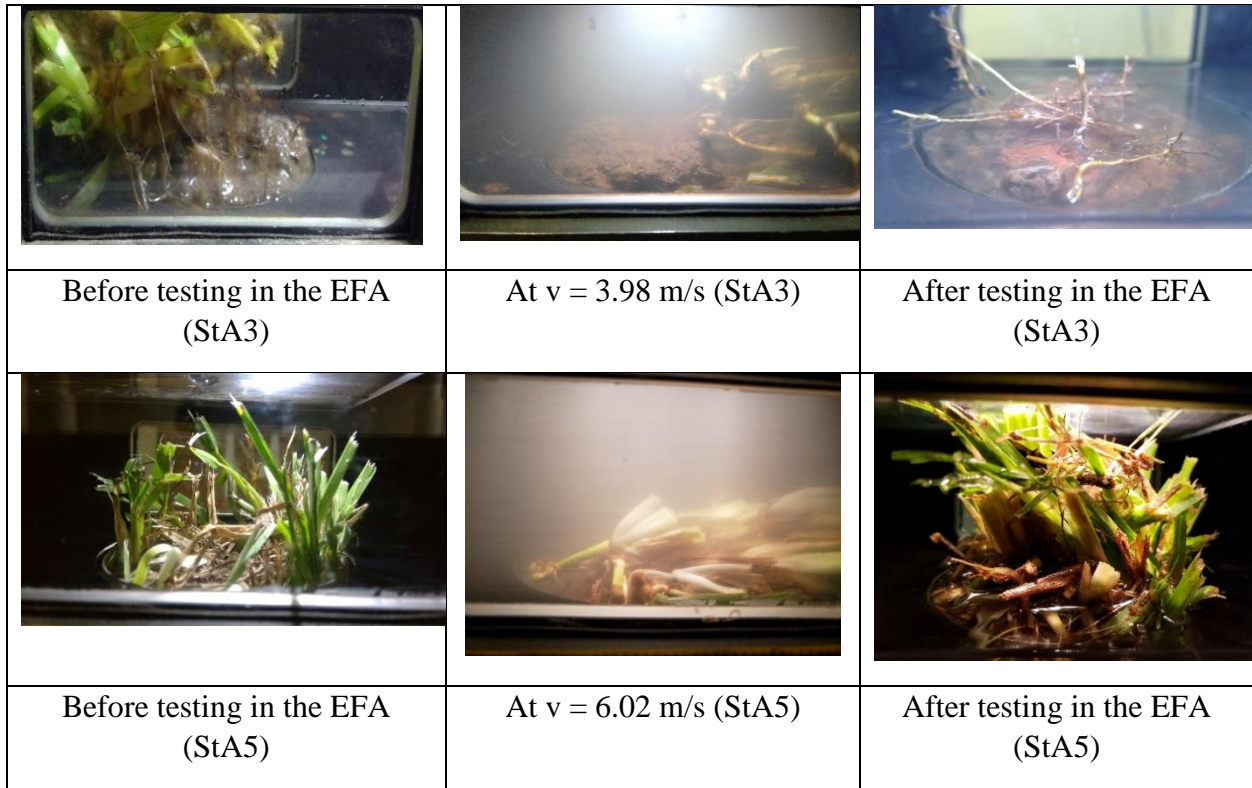


Figure 96. EFA testing of St. Augustinegrass (StA 3 and StA 5)

The erosion function of St. Augustine exhibits two thresholds (Figure 97). The first one corresponds to “cleaning” the grass of loose particles and dead blades of grass, while the second corresponds to partially or fully detachment of the grass mat. Despite some different erosion behavior, on logarithmic scale all St. Augustinegrass is in Medium Erodibility.

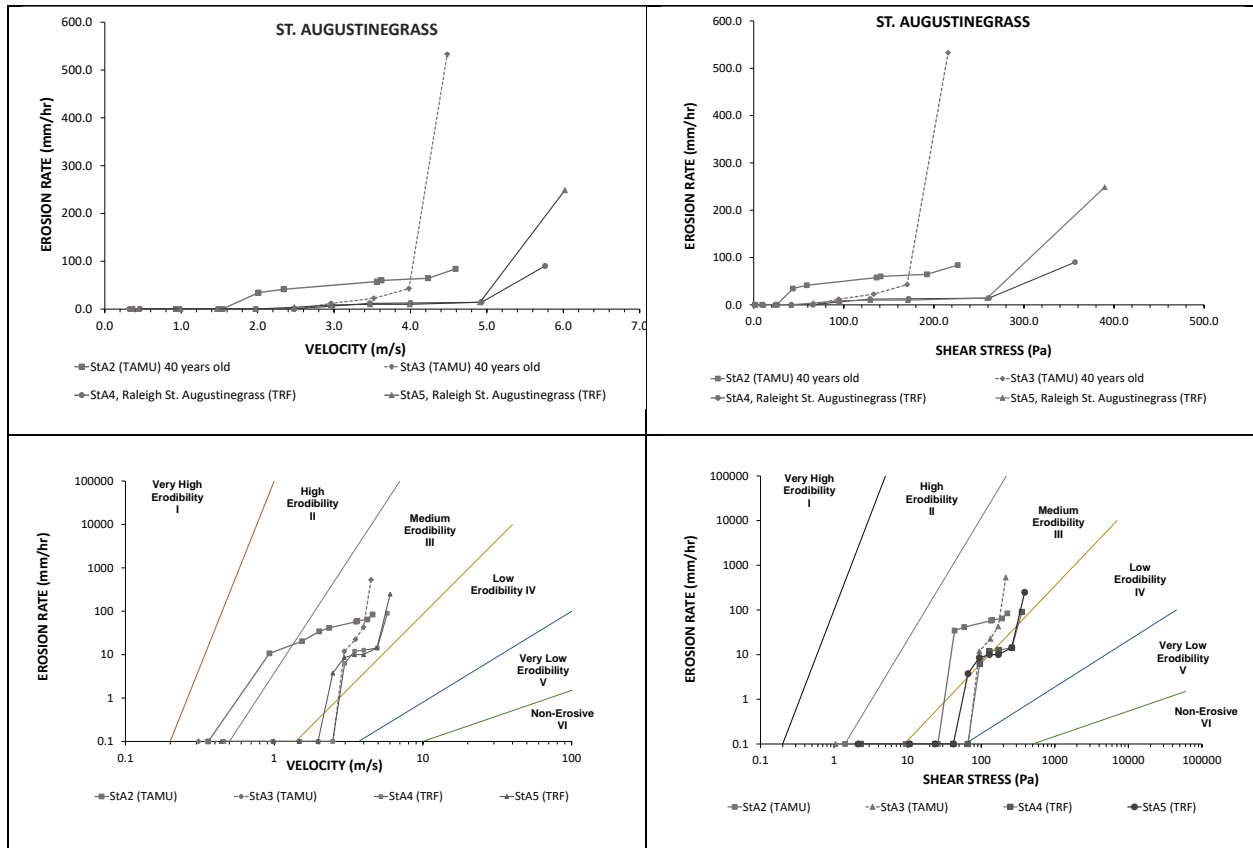


Figure 97. Erosion functions in natural and logarithmic scale of St. Augustinegrass

Table 25 shows two thresholds for velocity and corresponding shear stress. Overall, St. Augustinegrass is erosion resistant. Full grass detachment was observed only for StA3 sample after retesting the prior sample in several days. Critical velocities of grass vary from 1.54 m/s to 2.49 m/s (first threshold) and from 4.48 m/s to 6.02 m/s (second threshold, for fully or at least 70% of grass mat detachment). Corresponding critical shear stress is 25.791 Pa and 66.651 Pa (first threshold) and from 215.757 Pa to 389.584 Pa (second threshold, for fully or at least 70% of grass detached).

Table 25. Erosion parameters of St. Augustinegrass

	Critical velocities (m/s)		Critical shear stress (Pa)		Soil Type	Notes
	initiation	Detachment	initiation	detachment		
StA2	1.54	4.59	25.791	226.482	Clayey sand, cemented (Fe ³⁺)	50% of grass detached
StA3	2.49	4.48	66.651	215.757		All grass detached
StA4	2.47	5.76	65.585	356.659	Silty sand	No detachment
StA5	1.97	6.02	41.720	389.584		70% of grass detached
Range	1.54 – 2.49	4.48 – 6.02	25.791 – 66.651	215.757 – 389.584		
Average	2.12	5.21	49.94	297.12		

4.6.3. Bahiagrass

Bahiagrass was sampled for the further EFA testing at Allen Academy in Bryan (Texas).

Bahiagrass forms clumps and does not provide a good coverage. Figure 98 shows Bahiagrass with a coverage of approximately 75%.

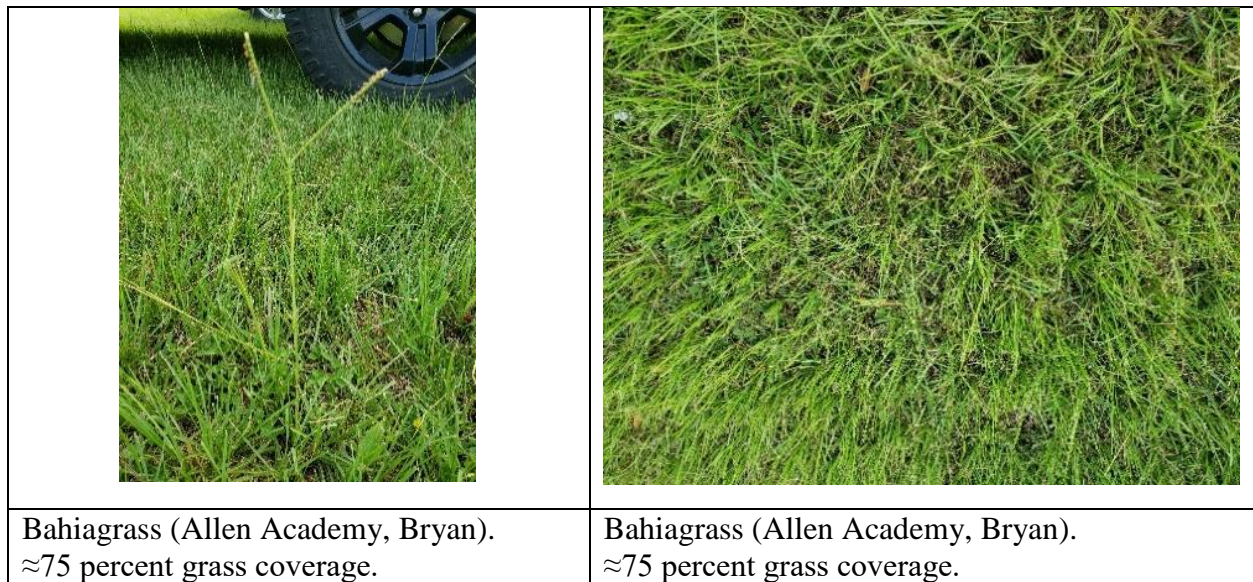


Figure 98. Photographs of Bahiagrass

Four samples of Bahiagrass (B1, B2, B3 and B4) were tested in the EFA at the velocity varying from 0.25 m/s to 6.5 m/s. Most of the samples failed during EFA testing (Figure 99). The erosion was observed in a form of clumps detachment. However, on the log-log scale erosion charts, all Bahiagrass is in medium erodibility (Figure 100).

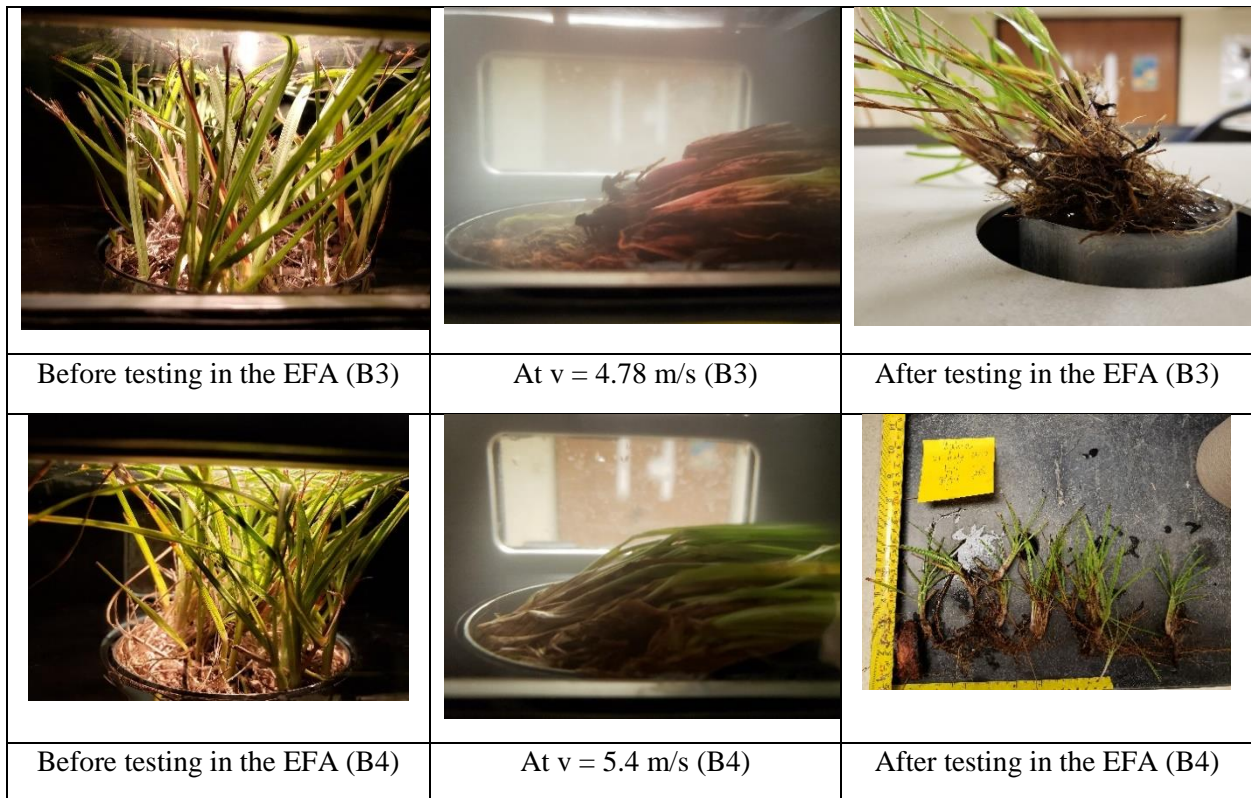
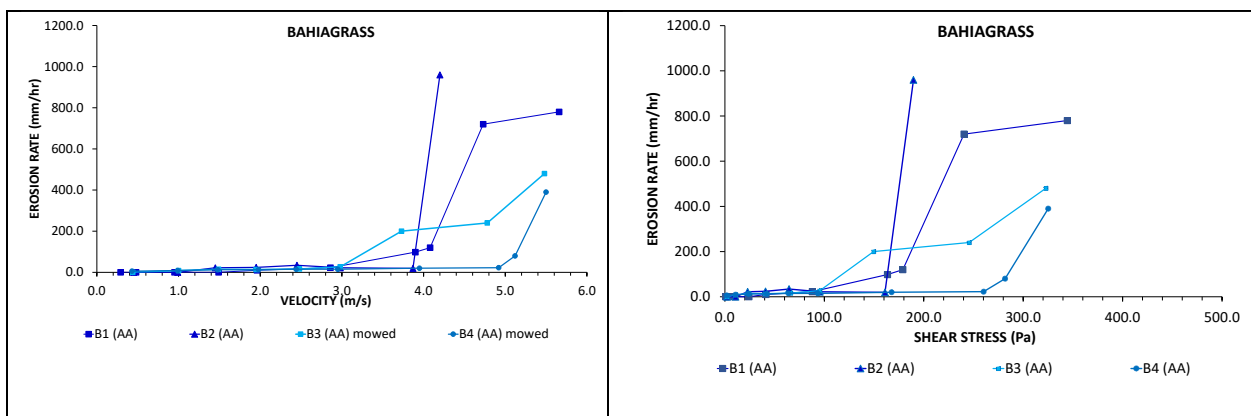


Figure 99. EFA testing of Bahiagrass (B3 and B4)



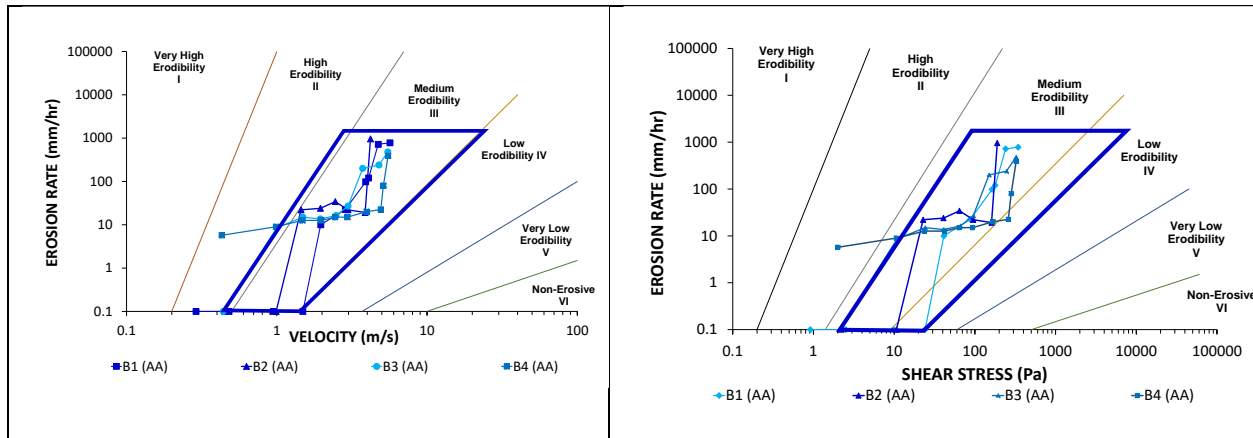


Figure 100. Erosion functions in natural and logarithmic scale of Bahiagrass

The erosion function of Bahiagrass on silty sand exhibits two thresholds like Bermudagrass and St. Augustinegrass. One of the differences is that Bahiagrass detaches clumps by clumps. Table 26 shows two thresholds for velocity and corresponding shear stress. First threshold of Bahiagrass varies from 0.43 m/s to 1.49 m/s, second - from 4.08 m/s to 4.92 m/s (for fully or at least 50% detachment). Critical shear stress ranges from 2.011 Pa to 24.144 Pa (first threshold) and from 178.949 Pa to 260.219 Pa (second threshold, for fully or at least 50% of grass detachment).

Table 26. Erosion parameters of Bahiagrass

	Critical velocities (m/s)		Critical shear stress (Pa)		Notes
	initiation	detachment	initiation	detachment	
B1	1.49	4.08	24.144	178.949	≈ 90% of grass detached at v=5.66m/s
B2	0.99	4.2	10.659	189.630	All grass detached at v=4.2 m/s
B3	0.44	4.78	2.105	245.620	≈ 50% of grass detached at v=5.4m/s
B4	0.43	4.92	2.011	260.219	≈ 80% of grass detached at v=5.5m/s
Range	0.43 – 1.49	4.08 – 4.92	2.011 – 24.144	178.949 – 260.219	
Average	0.84	4.5	9.73	218.6	

4.6.4. Zoysiagrass

Zoysiagrass was sampled for further testing in the EFA at the Turf Research Facility (F&B Road) in College Station (Texas). Figure 101 illustrates Zoysiagrass with approximately 85% of coverage.



	
<p>Zoysiagrass (Z1, Turf Research Facility, College Station), ≈85 percent grass coverage</p>	<p>Zoysiagrass (Turf Research Facility, College Station), ≈85 percent grass coverage</p>

Figure 101. Photographs of Zoysiagrass

Three samples of Zoysiagrass (Z1, Z2, and Z3) were tested in the EFA at the velocity varying from 0.25 m/s to 6.0 m/s. Sample Z3 was a re-commenced sample Z2 after grass did not fail during testing. The grass samples have different erosion resistance; the sample Z1 did not fail, however the sample Z3 failed in a form of a whole grass mat detachment (Figure 102). However, on the log-log scale erosion charts, all Zoysiagrass is mostly in Medium Erodibility zone (Figure 103).

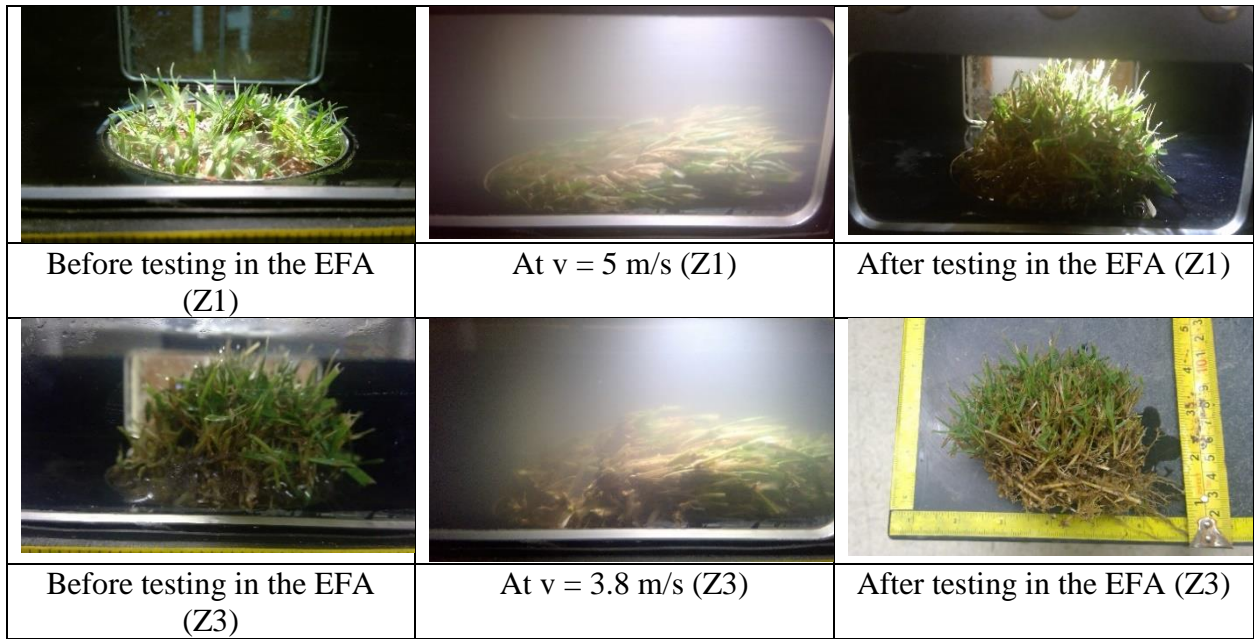


Figure 102. EFA testing of Zoysiagrass (Z1 and Z3)

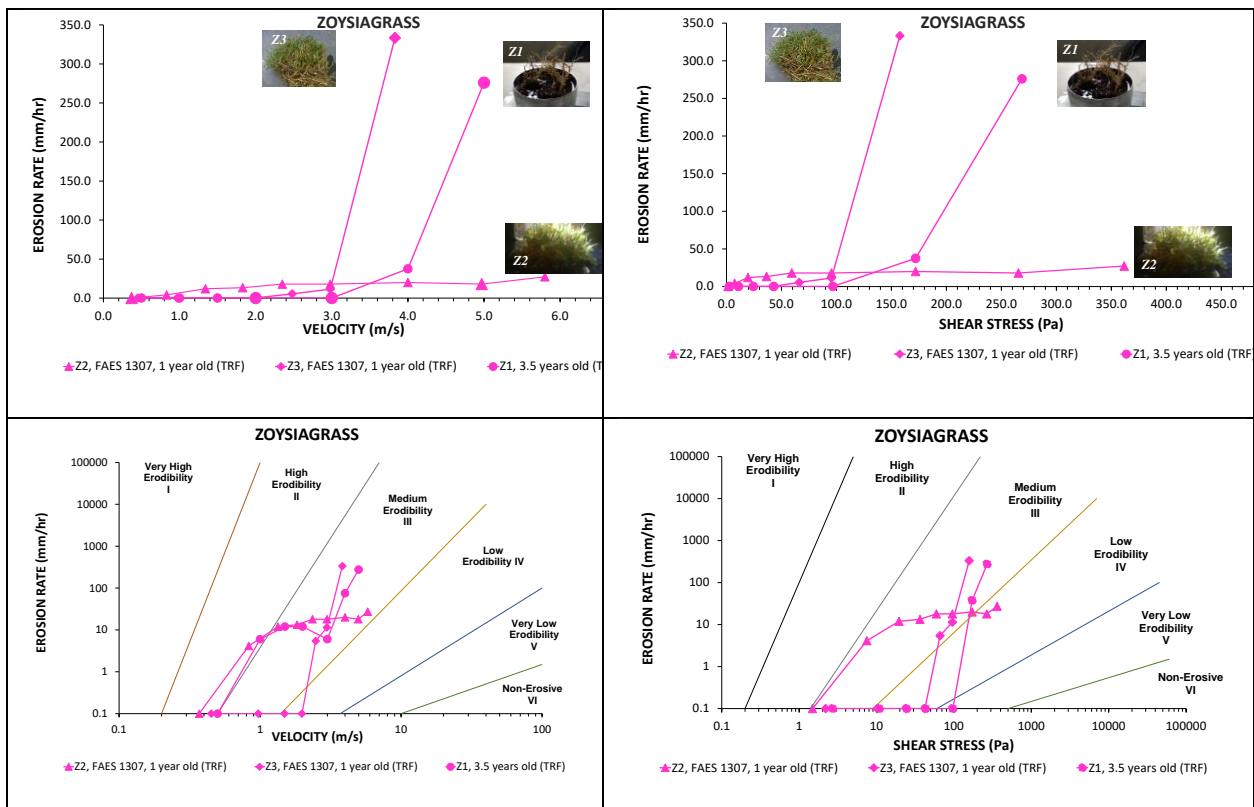


Figure 103. Erosion functions in natural and logarithmic scale of Zoysiagrass

The erosion function of Zoysiagrass exhibits two thresholds like Bermudagrass, St. Augustinegrass and Bahiagrass. Table 27 shows two thresholds for velocity and corresponding shear stress. First velocity threshold for Zoysiagrass varies from 0.5 m/s to 1.98 m/s; second threshold - from 2.98 m/s to 5.8 m/s (all grass detached). Critical shear stress ranges from 1.489 Pa to 42.144 Pa (first threshold) and from 95.464 Pa to 361.630 Pa (second threshold, all grass detached). EFA testing results allow to suggest that if the grass is subjected to a first flood and is not detached (Z2), that grass will not be as resistant as the first time is there is little time between floods (Z3). The second velocity threshold of Z3 is less than of Z2.

Table 27. Erosion parameters of Zoysiagrass

	Critical velocities (m/s)		Critical shear stress (Pa)		Soil Type	Notes
	initiation	detachment	initiation	detachment		
Z1	0.5	4.0	2.719	172.000	Silty sand	All grass detached at v=5 m/s
Z2	0.37	5.8	1.489	361.630		No grass detachment
Z3	1.98	2.98	42.144	95.464		All of grass detached at v=3.83 m/s
Range	0.5 – 1.98	2.98 -5.8	1.489 – 42.144	95.464 – 361.630		
Average	0.95	4.26	15.45	209.70		

4.7. Summary of EFA grass testing

To determine whether grass can be beneficially used, a series of test plots were prepared to evaluate its performance in controlling erosion. Figure 104 and Figure 105 show erosion rate versus velocity and erosion rate versus shear stress in natural scale for all grass samples. Figure 106 and Figure 107 illustrate erosion rate versus velocity and erosion rate versus shear stress in logarithmic scale for all grass samples.

The erosion functions presented on Figure 106 and Figure 107 indicate two thresholds. First threshold shows “cleaning” the grass of loose particles and dead blades of grass. It is shown as a blue ellipse. First threshold is associated with initiation of erosion. Second threshold is related to detachment of the grass mat. It is shown as a red ellipse. In some cases, grass mat did not fail, therefore, the second thresholds indicate a state when at least 50% of grass got detached. Erosion functions on Figure 106 and Figure 107 show low to high erosion rates until the detachment critical velocity. Erosion rate increases rapidly past that threshold. This means that less time will be available between failure of the grass cover and drastic erosion than in the case of soil alone. First threshold is higher for Bermudagrass and St. Augustinegrass than for Bahiagrass and Zoysiagrass. At the same time, Zoysiagrass and Bahiagrass exhibit about the same second threshold as the other two types of grasses when grass fails. Figure 104 shows that the highest critical velocity corresponding to grass mat detachment is 6.02 m/s (St. Augustinegrass) and the lowest critical velocity varies from 1 m/s to 1.48 m/s (one-year old Bermudagrass and brown Bermudagrass in a dormant state). The summary of the EFA results is shown in Table 28.

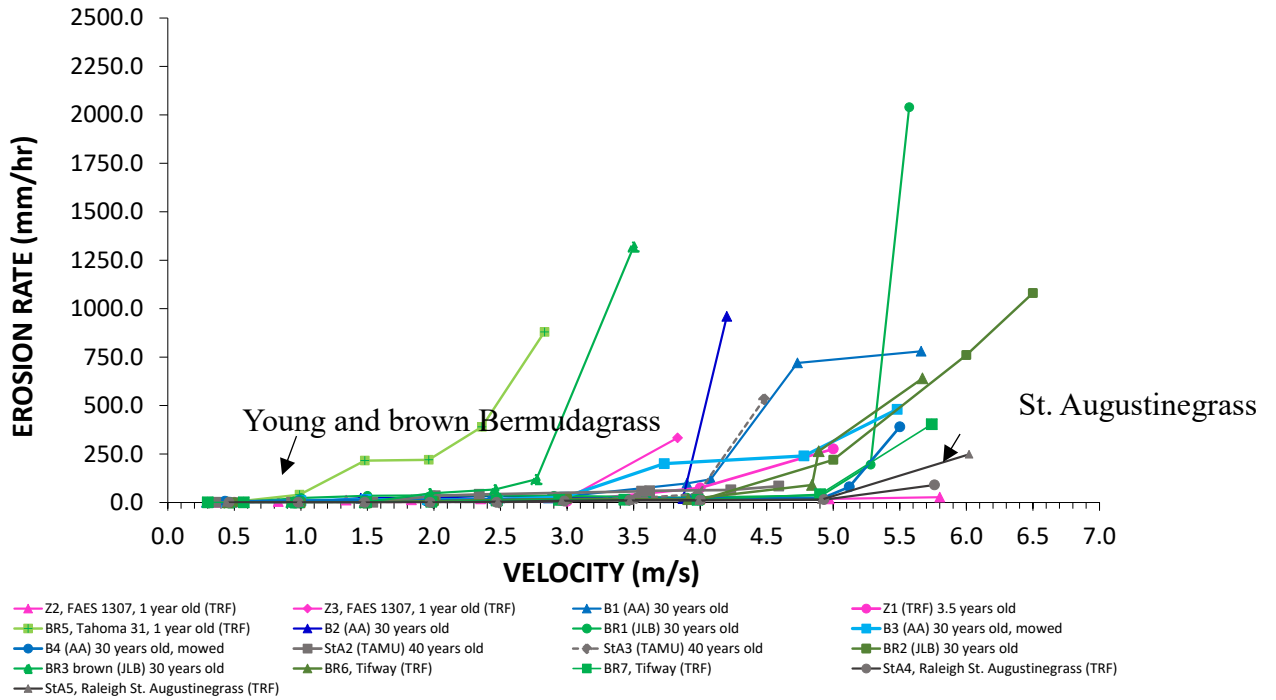


Figure 104. Erosion rate versus velocity in natural scale of all grass types

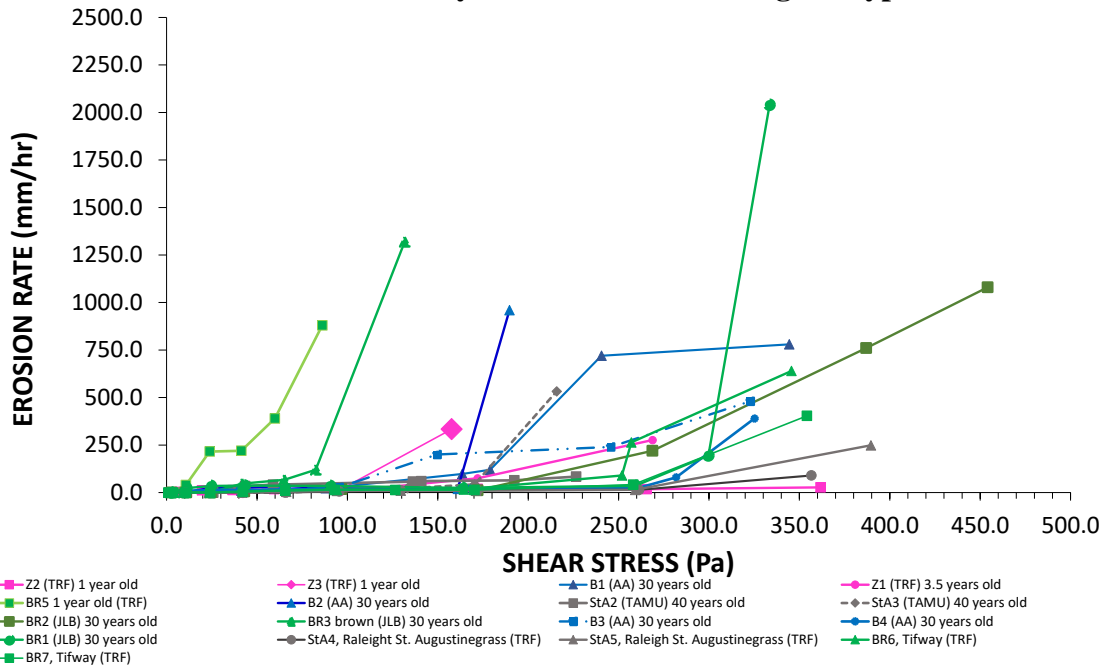


Figure 105. Erosion rate versus shear stress in natural scale of all grass types

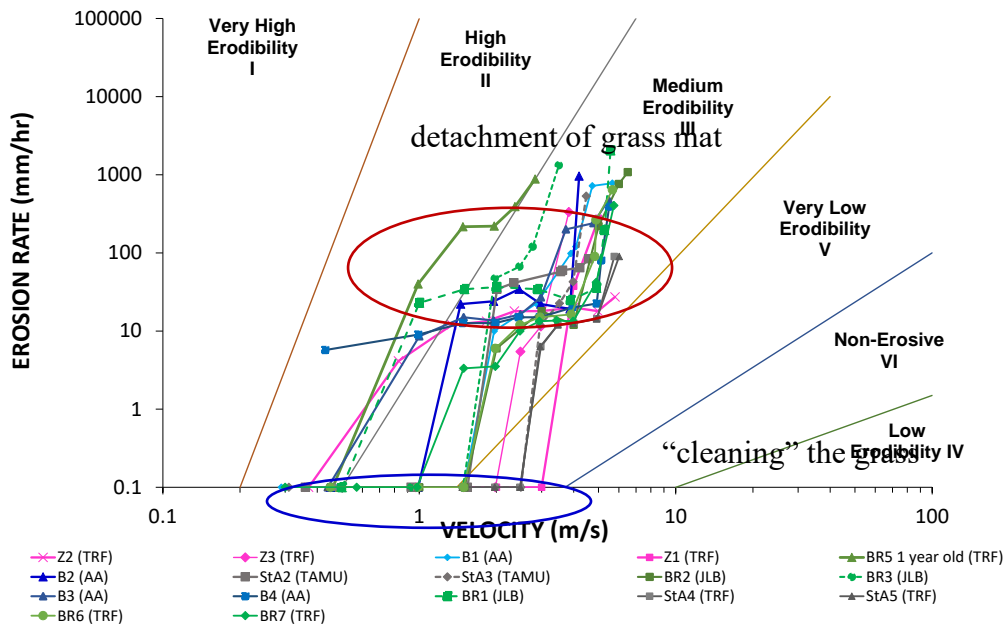


Figure 106. Erosion rate versus velocity in logarithmic scale of all grass types

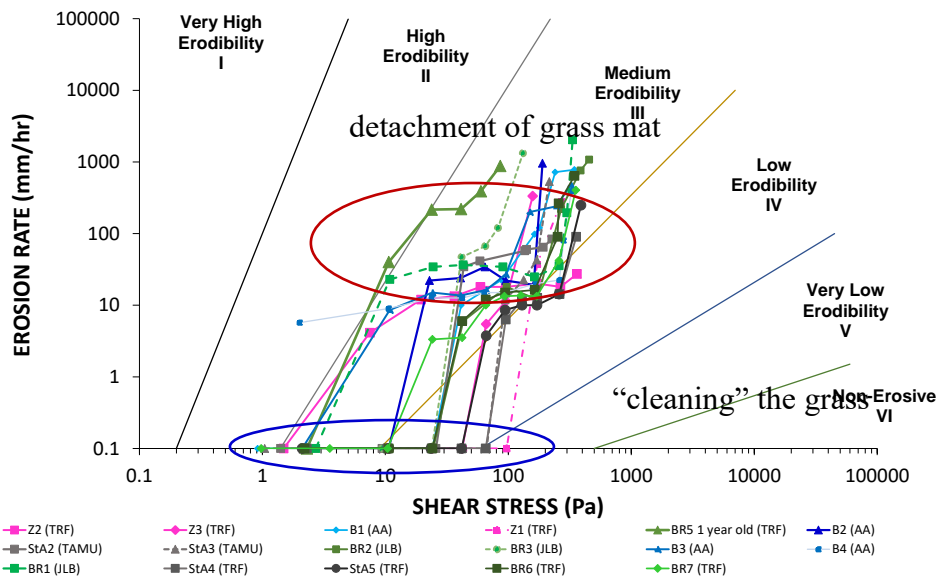


Figure 107. Erosion rate versus shear stress in logarithmic scale of all grass types

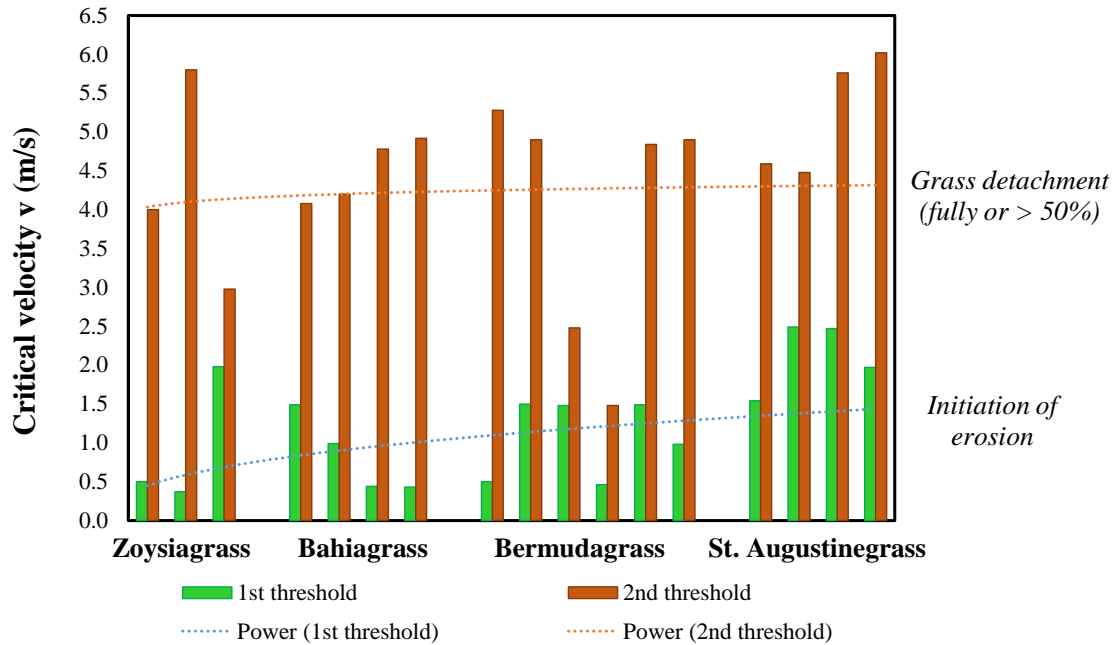


Figure 108. Erosion thresholds of all grass types

After the flow was stopped in the EFA at the end of the test, grass left after erosion together with roots was rolled back into position and covered an erosion “hole”. This would potentially allow grass to reestablish after flooding. For samples when grass mat did not fail, the EFA test was repeated in a few days to study erosion behavior. Individual erosion mechanism and erosion parameters for each type of grass are presented in more details below in Sections 4.6.1-4.6.4.

US Soil Conservation Service of USDA (1954) reported that grass does not form a protective shield by completely submerging and bending over in flowing water. Visual observations through the Plexiglas window during the EFA test confirmed that grass can sustain the flow by waving back and forth up a certain point which might not be associated with critical velocity in some cases. The ability of grass to remain up in the flow depends on flow velocity, depth of flow, grass and soil roughness etc. Above the critical point, grass starts to detach and wash away.

Table 28. Summary of erosion parameters of all tested grass in the EFA

Type of grass	Index	Age (yrs)	Height (cm)	Location	Soil type	Critical Velocity (m/s)		Critical Shear Stress (Pa)		NDVI *
						initial	failure	initial	failure	
Bermudagrass	BR1	≈30	9	Briaud Residence	Silty or clayey sand, well cemented with Fe ³⁺ (?)	0.5	5.28	2.719	299.693	0.667
	BR2		14			1.5	4.90	24.469	268.75	N/A
	BR3		10			1.48	2.48	23.821	65.055	0.434
	BR5	1	4	TRF	Silty sand with clay particles	0.46	1.48	2.301	23.821	0.710
	BR6	3+	5			1.49	4.84	24.144	251.829	0.729
	BR7	3+	5			0.98	4.90	10.444	258.108	0.729
	Range						0.5 – 1.5	1.48 – 5.28	2.719 – 24.469	23.821 – 299.693
Average						1.07	3.98	14.65	194.54	
St. Augustinegrass	StA2	30+	6	TAMU	Sandy clay with carbonate stones, brownish	1.54	4.59	25.79	226.48	N/A
	StA3	30+	6			2.49	4.48	66.65	215.76	N/A
	StA4	3+	6	TRF	Silty sand with clay particles	2.47	5.76	65.59	356.66	0.649
	StA5	3+	6			1.97	6.02	41.72	389.58	0.632
	Range						1.54 – 2.49	4.48 – 6.02	25.791 – 66.651	215.757 - 389.584
Average						2.12	5.21	49.94	297.12	
Bahigrass	B1	≈30	10-15	AA	Silty sand	1.49	4.08	24.144	178.95	0.572
	B2	≈30	10-15			0.99	4.2	10.659	189.63	0.572
	B3	≈30	9			0.44	4.78	2.105	245.62	0.572
	B4	≈30	9			0.43	4.92	2.011	260.22	0.572
Range						0.43 – 1.49	4.08 – 4.92	2.011 – 24.144	178.949 – 260.219	
Average						0.84	4.5	9.73	218.6	
Zoysiagrass	Z1	3+	6	TRF	Silty sand with clay particles	0.5	4.00	2.712	172.00	0.731
	Z2	1	2.5			0.37	5.8	1.49	361.63	0.670
	Z3	1	2.5			1.98	2.98	42.14	95.47	N/A
Range						0.5 – 1.98	2.98 -5.8	1.489 – 42.144	95.464 – 361.630	
Average						0.95	4.26	15.45	209.70	
Average for all grass						1.25	4.49	22.44	230	

4.8. Effect of coverage on grass erodibility

Grass coverage was estimated by using a software TurfAnalyzer which allows to calculate ground percentage covered by green turf (<https://www.turfanalyzer.com/turf-analyzer>). Grass coverage is widely used to quantify grass establishment, resistance to drought etc. The more value of grass coverage is the better coverage grass has. Six samples of Bermudagrass and Zoysiagrass were chosen to compare the effect of percent coverage on grass erosion. Figure 109 shows the images of six samples of grass and a percent cover for each of the samples. The erosion function of grass in natural scale indicates that one-year old Bermudagrass (BR5) with percent cover 72.673% is more erodible compared to 3+ years old Bermudagrass (BR7) with 84.886% cover (Figure 110). Table 29 indicates critical thresholds for grass. Figure 111 illustrates that critical velocity increases with an increase in percent coverage for the same site (Turf Research Facility) and same type of soil (silty sand).







		
Bermudagrass (BR5). Percent cover = 72.673 %	Bermudagrass (BR6). Percent cover = 84.212 %	Bermudagrass (BR7). Percent cover = 84.886 %
		
St. Augustinegrass (StA4). Percent cover = 72.567 %	Zoysiagrass (Z1). Percent cover = 85.251 %	Zoysiagrass (Z2). Percent cover = 57.639 %

Figure 109. Images of grass with showing percent coverage

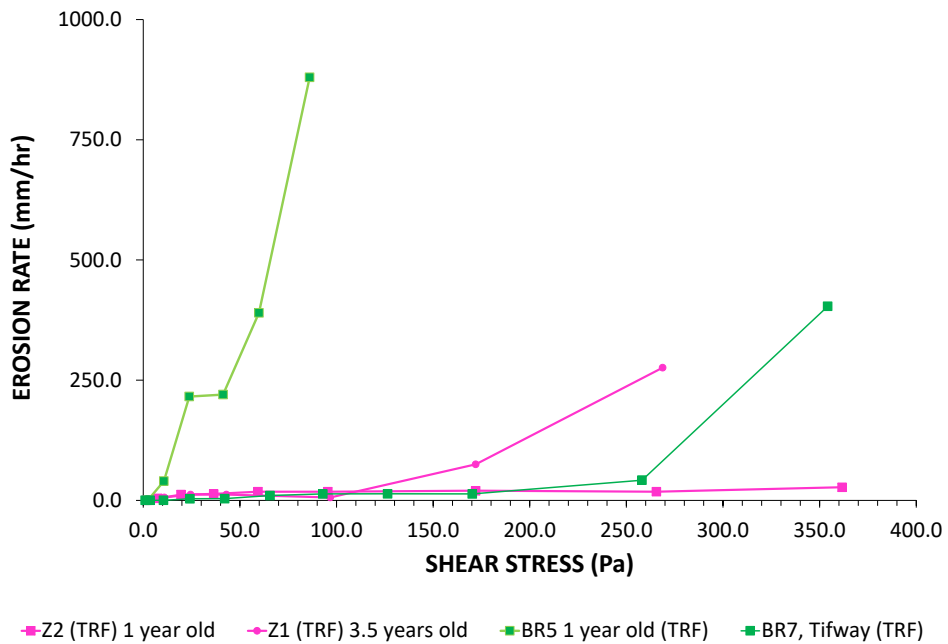


Figure 110. Erosion rate versus shear stress of grass with different coverage

Table 29. Erosion parameters of grass with different coverage

Grass	Percent coverage	Critical Velocity (m/s)		Critical Shear Stress (Pa)	
		1 st threshold	2 nd threshold	1 st threshold	2 nd threshold
BR5	72.673	0.46	1.48	2.301	23.821
BR7	84.886	0.98	4.9	10.444	258.108
Z1	85.251	0.5	4	2.719	172
Z2	57.639	0.37	5.8	1.489	361.63

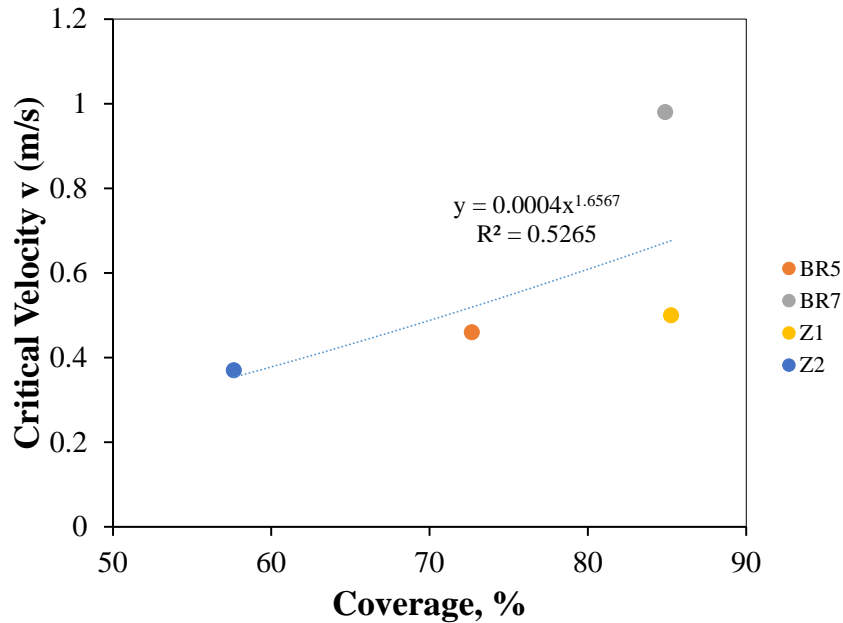


Figure 111. Critical velocity versus grass coverage

4.9. Effect of health on grass erodibility

In this Section, the effect of grass health such as green Bermudagrass versus brown Bermudagrass is considered. Green grass (sample BR1) and brown grass in a dormant grass (sample BR3) show different erodibility. Note that dormancy is a natural process and a normal response to the stress and drought. It is a state of reduced water usage when grass focuses resources on the roots. Most grass can stay in a dormant state for at least 3 to 4 weeks without the grass dying (The LawnInstitute, 2020). Figure 112 illustrates two samples of Bermudagrass (BR1 and BR3) sampled at Briaud Residence in summer 2020. The Normalized Difference Vegetation Index (NDVI) used to estimate a health of grass was obtained at the sampling site. The NDVI was 0.667 for the green Bermudagrass and 0.434 for the brown Bermudagrass. The brown grass is classified by lower NDVI compared to the green grass.

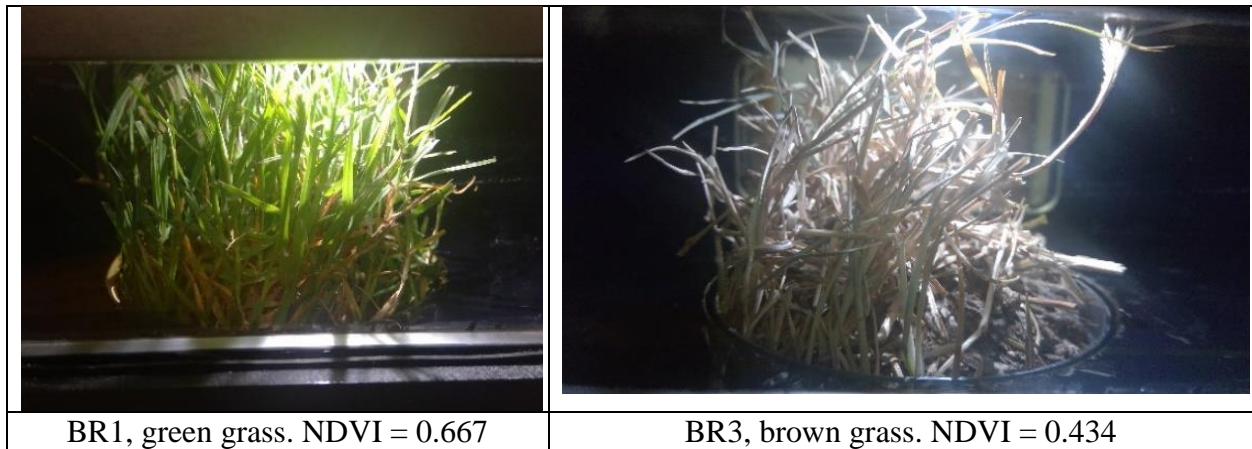


Figure 112. Bermudagrass of different quality/health in the EFA before testing

Erosion functions of green versus brown Bermudagrass are shown in Figure 113. On the erosion function chart green grass is in Medium Erodibility (III) and brown grass is in High (II) to Medium (III) Erodibility. For that case, NDVI (Normalized Difference Vegetation Index) is a good indicator of grass erodibility showing that brown grass with low NDVI (0.434) is less erosion resistant than green grass with higher NDVI (0.667). The velocity threshold corresponding to grass mat detachment is 2.48 m/s for brown grass and 5.28 m/s for green grass.

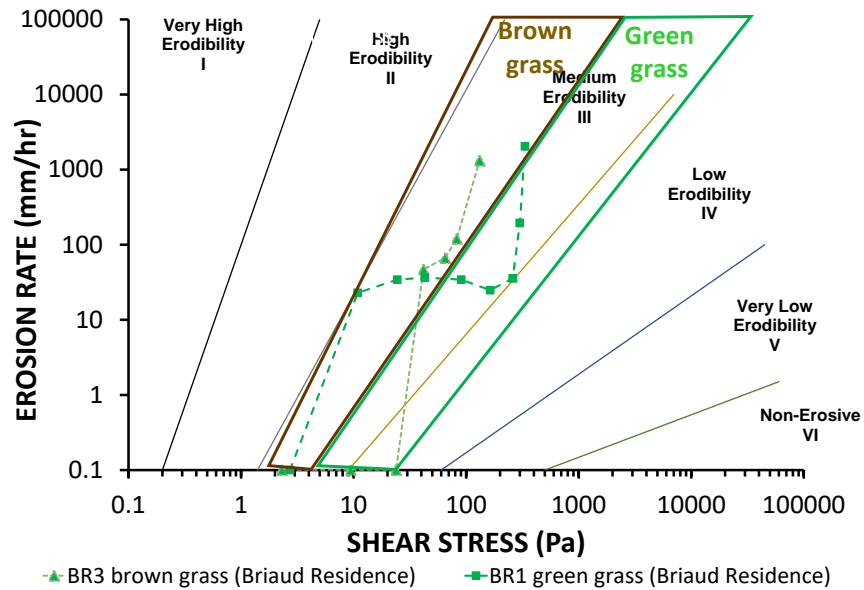


Figure 113. Erosion rate versus shear stress in logarithmic scale of green and brown Bermudagrass

4.10. Effect of age on grass erodibility

Some general tendency in Bermudagrass erodibility was obtained for grass of different age. One-year old Bermudagrass (BR5) exhibits higher erodibility (low critical velocity and low critical shear stress) compared to three and more years old grass (BR1, BR2, BR6, and BR7) (Figure 114). Thirty years old brown grass (BR3) is an exception that shows lower critical velocity and shear stress than green grass of the same age. It can be concluded that age has an effect on grass erosion; well established grass of three and more years is more erosion resistant than the younger not established grass.

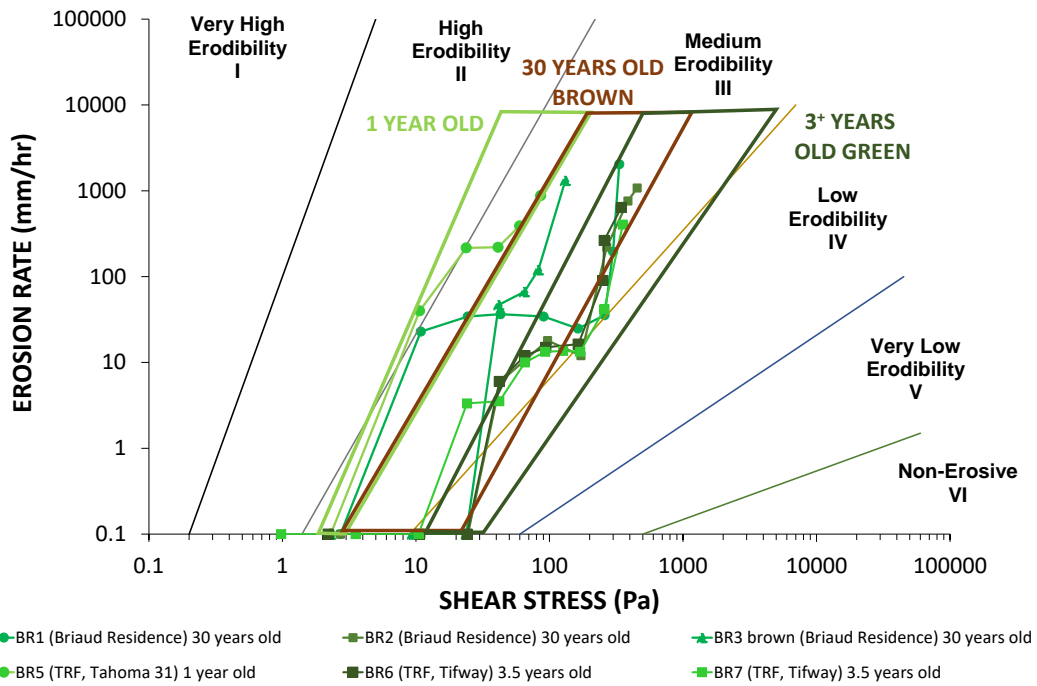


Figure 114. Erosion rate versus shear stress in logarithmic scale of different age Bermudagrass

To be more specific, the effect of age on Bermudagrass erodibility for the Turf Research Facility site is shown on Figure 115 that indicates the critical shear stress of one years old Bermudagrass is four to ten times lower than three years old Bermudagrass.

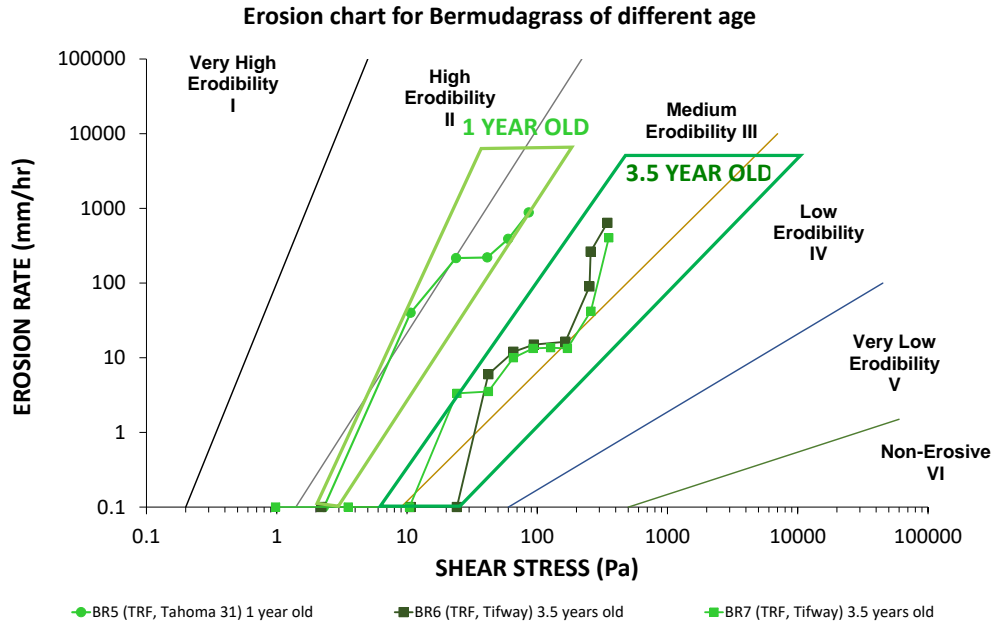


Figure 115. Erosion rate versus shear stress in logarithmic scale of different age Bermudagrass

The effect of age on grass erodibility was also studied for Zoysiagrass. Three samples of Zoysiagrass were tested in the EFA. Z1 sample is referred to three years old grass, Z2 is one-year old grass, and Z3 is a sample Z2 retested in two days. Note that Z2 did not fail in the EFA, so it was suggested to test the sample again in a few days. Figure 116 indicates that the critical shear stress is higher for a well-established three and a half years old Z1 compared to Z2 and Z3. EFA testing on Z1 shows that at 5 m/s only grass was detached, the roots kept in place and resisted erosion. One-year old grass, Z2 and Z3, not well-established compared to Z1, experienced more erosion compared to Z1. In fact, Z3 is the same sample as Z2 but retested in two days, the critical velocity of Z3 is much higher (up to 5 times) than Z2. This phenomenon might be related to more extensive erosion between the roots for Z2 compared to Z3 as well as “hardening” after the first EFA performed on Z2. However, the grass mat of Z3 was completely detached as one piece at the end of the test when the velocity was only $v=3.83$ m/s.

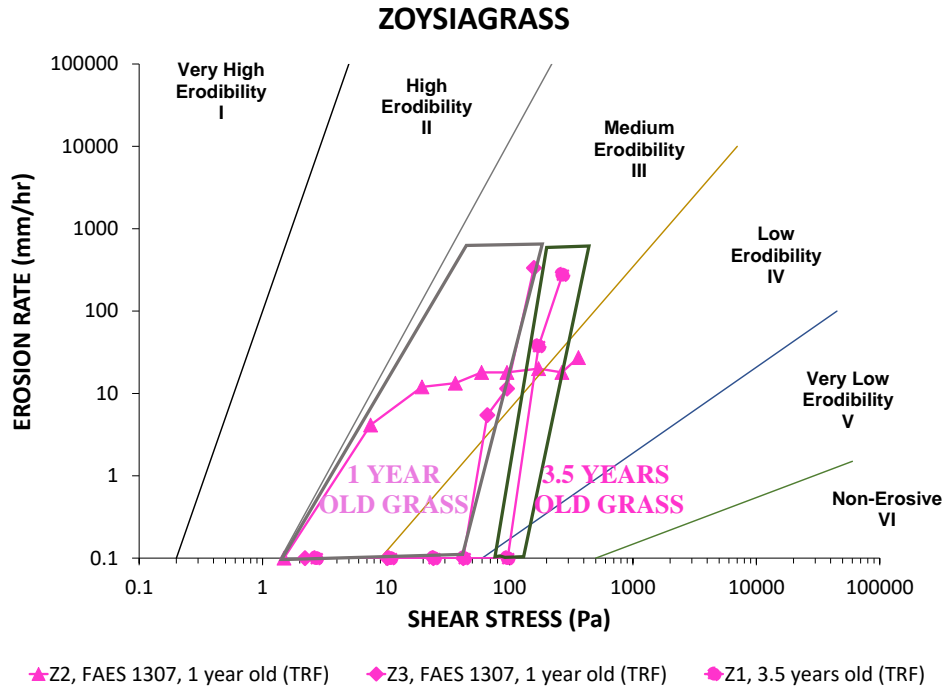


Figure 116. Erosion rate versus shear stress in logarithmic scale of different age Zoysiagrass

4.11. Comparison of erodibility of grass and bare soil

Two samples of silty sand with clay particles (S1 and S2) were sampled at the Turf Research Facility (Texas A&M University) and tested in the EFA to obtain erosion parameters and compare them with the grass samples. Note that the critical velocity of silty sand is below $v_c < 0.290 - 0.300$ m/s. Silty sand appears to fit into High Erodibility category (Figure 117).

To a comparison reason between erodibility of a bare soil and grass, a plot showing the erosion functions was prepared. Figure 118 indicates that soil is in High Erodibility (II) category, however the grass grown on the same soil is in Medium (III) to Low (IV) Erodibility category.

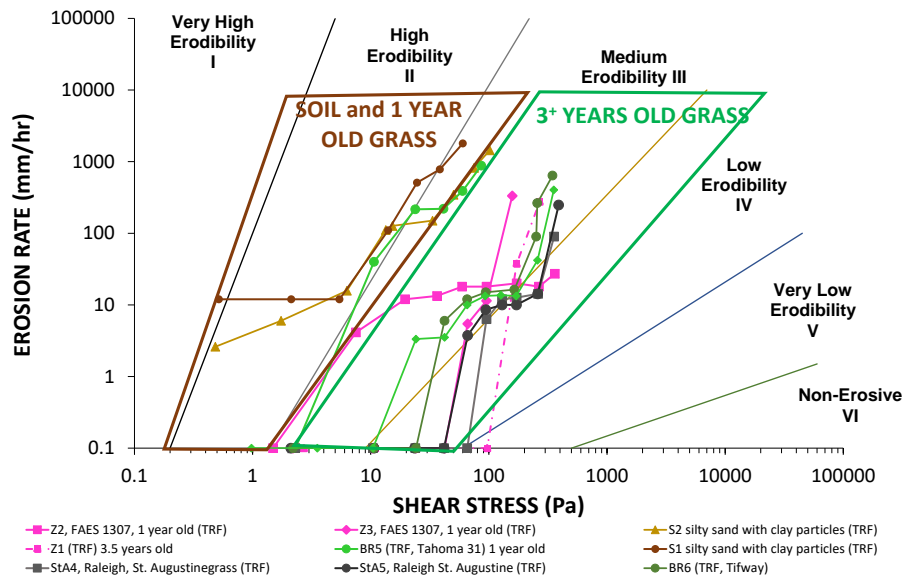


Figure 117. Erosion rate versus shear stress in logarithmic scale of bare soil and grass

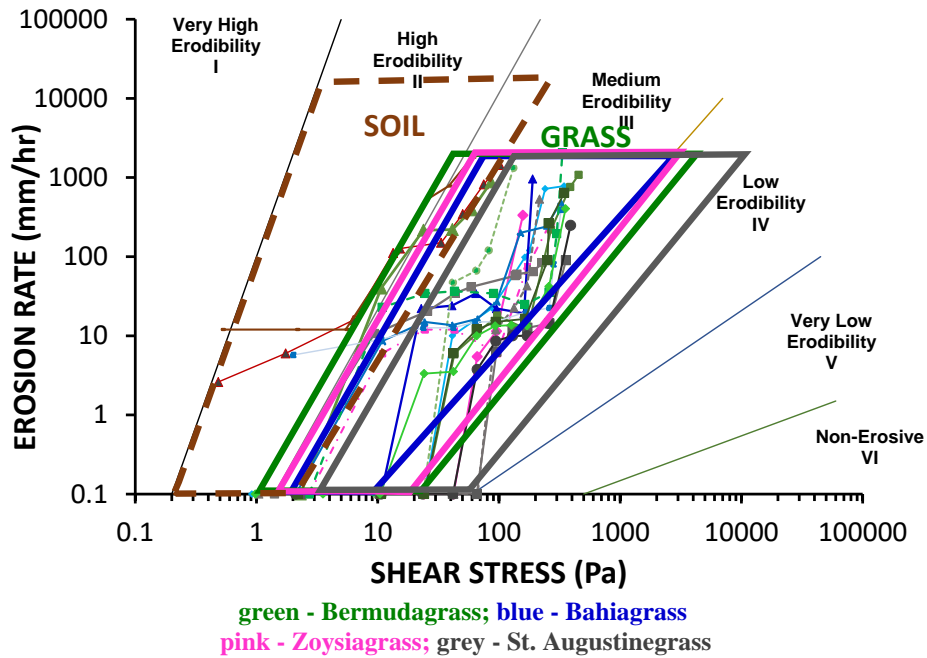


Figure 118. Summary erosion function showing erosion rate versus shear stress of bare soil and grass

The erosion rate versus shear stress chart presents that grass moves the erodibility of soil by one category to the right compared to soil with no vegetation. Table 30 gives a comparison of soil and grass erosion parameters. The critical velocity of silty sand is 7-8 times lower than first threshold of St. Augustinegrass, 1.5-5 times lower than Bermudagrass and 1.5-6.5 times lower than Zoysiagrass.

Table 30. Erosion parameters of grass and bare soil

	Critical velocities (m/s)		Critical shear stress (Pa)		Soil Type	Notes
	initiation	detachment	initiation	detachment		
Z1	0.5	4.0	2.719	172.000	Silty sand with clay particles	All grass detached at v=5 m/s
Z2	0.37	5.8	1.489	361.630		No grass detachment
Z3	1.98	2.98	42.144	95.464		All of grass detached at v=3.83 m/s
BR5	0.46	1.48	2.301	23.821		All grass detached
BR6	1.49	4.84	24.144	251.829		≈ 50% of grass detached
BR7	0.98	4.90	10.444	258.108		No grass detachment
StA4	2.47	5.76	65.585	356.659		≈ 70% of grass detached
StA5	1.97	6.02	41.72	389.58		62 cm of soil eroded
S1	0.30	N/A	0.518	N/A		161 cm of soil eroded
S2	0.29	N/A	0.484	N/A		

Overall, grass is in Category III (Medium Erodibility) to Category IV (Low Erodibility). Bare soil is in Category II (High Erodibility) (Figure 118). This finding is consistent with the EFA tests results performed on grass samples and bare clay in the EFA in 2011 (Briaud et. Al., 2011). It can be concluded that grass moves the erodibility of the soil by one category compared to the soil.

4.12. Effect of roots on soil erodibility

The following is an example that once the grass mat is detached or failed, the soil below is still reinforced by the root system and still more resistant to erosion than the soil alone (Figure 119). The sample Z/R/S1 is soil reinforced by roots after Zoysiagrass failed, B/R/S1 and B/R/S2 are soil samples reinforced by roots after Bermudagrass failed. The soil which is silty sand with clay particles is in High Erodibility category (II) compared to root reinforcement soil that is in Medium Erodibility category (III).

Table 31 Table 31 shows erosion parameters for bare soils and roots reinforced soils after

	Critical velocities (m/s)		Critical shear stress (Pa)		Soil Type	Notes
	initiation	detachment	initiation	detachment		
Z/R/S1	0.47	3.534	3.030	88.366	Silty sand	Root system detached at v=4.3 m/s
B/R/S1	0.43	2.958	2.79	83.679		Root system detached at v=3.5 m/s
B/R/S2	0.43	1.595	2.430	94.478		Root system detached at v=2.92 m/s
S1	0.30	N/A	0.518	N/A		62 cm of soil eroded
S2	0.29	N/A	0.484	N/A		161 cm of soil eroded

grass failed during EFA testing.

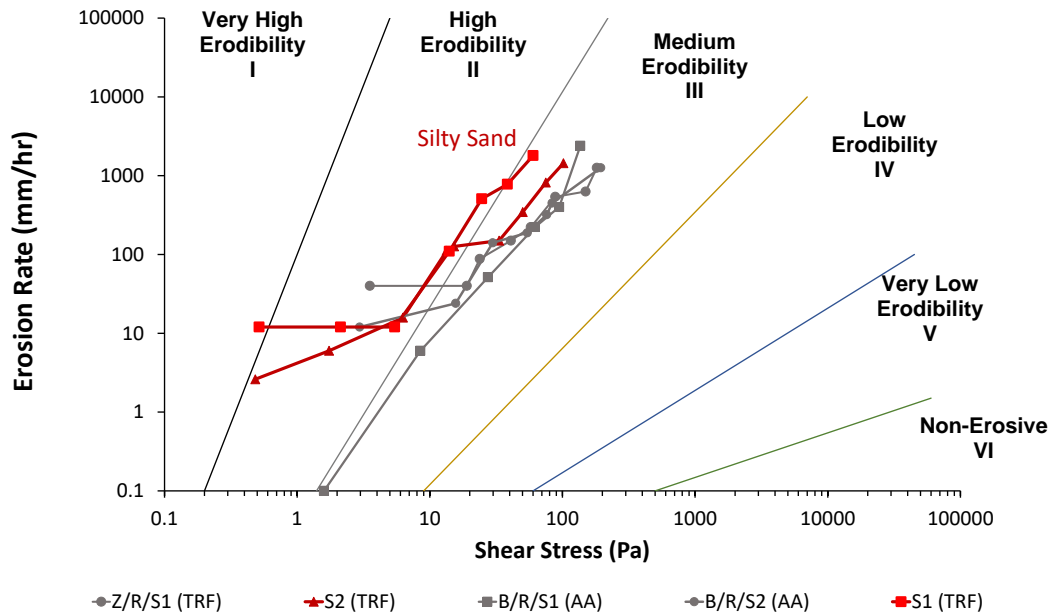


Figure 119. Erosion rate versus shear stress in logarithmic scale of bare soil and reinforced soil with roots

Table 31. Erosion parameters of bare soil and reinforced soil with roots

	Critical velocities (m/s)		Critical shear stress (Pa)		Soil Type	Notes
	initiation	detachment	initiation	detachment		
Z/R/S1	0.47	3.534	3.030	88.366	Silty sand	Root system detached at v=4.3 m/s
B/R/S1	0.43	2.958	2.79	83.679		Root system detached at v=3.5 m/s
B/R/S2	0.43	1.595	2.430	94.478		Root system detached at v=2.92 m/s
S1	0.30	N/A	0.518	N/A		62 cm of soil eroded
S2	0.29	N/A	0.484	N/A		161 cm of soil eroded

4.13. Comparison of EFA results and full-scale levee overtopping test

The critical velocity obtained in the EFA (2020) can be compared well with the ones obtained in the full-scale tests run by Thornton et al. at Colorado State University in 2010 and 2014; they also compared well with the results obtained by Van der Meer (2007) et al. in the Netherlands full-scale tests.

The average threshold velocity showing grass mat detachment for Bahiagrass obtained in the EFA can be compared well with the result of a full-scale test performed by Thornton in 2014. Bahiagrass in this full-scale test failed at velocity 3.6 m/s. Bahiagrass failed in the EFA at an average velocity of 4.5 m/s. The difference in critical velocity can be explained by a different species of Bahiagrass, sodded Jacksonville Bahiagrass in a full-scale test and unspecified Bahiagrass in the EFA test. No grass failure was observed in a full-scale test performed by Van der Meer (2007) and in a full-scale test performed by Thornton et al. in 2010. The maximum velocity reached in these tests were 6.5 m/s and 6.2 m/s (Table 32).

Table 32. Velocity detachment threshold for grass (modified from Thornton et al. 2010, 2014, Van der Meer 2007)

EFA tests (Texas A&M University)		CSU Full scale tests- Florida	CSU Full scale tests- New Orleans	Netherlands	
2020		2011	2014	2010	
2007					
Bermudagrass	Bahiagrass	Unknown	Bahiagrass	Bahia- and Bermudagrass	Unknown
2.48 – 5.28 with an average of 4.48 m/s*	4.08 – 4.92 with an average of 4.5 m/s	1.6	3.6 m/s	> 6 m/s (no failure below 6.2 m/s)	> 6 m/s (no failure below 6 m/s)

5. MITIGATION OF EROSION USING ENZYMES

5.1. Existing knowledge on enzyme treatment

This section discusses some information about commonly available enzyme products and techniques as well as the effect of enzymes on soil properties. Enzymes in general are soluble protein molecules which are comprised of a thread of amino acids. Enzymes are liquid organic compounds which are environmentally friendly and non-toxic. The size of enzyme proteins is of the order of 1 Angstrom or 10^{-10} m (Shafii et al., 2018). Velasquez et al. (2005) reported the protein concentration in the enzyme of 9230 mg/L.

One of the earliest applications of enzymes in civil engineering is to use them to build impermeable layers for tailings and dams in the 1960s. Enzymes has been used road construction since the 1980s. Enzymes have also been used in civil engineering in more than 40 countries for the past 30 years (Velasquez et al., 2005).

The effect of enzymes can be compared with the work done by termites and ants in Brazil; by using their saliva which has a lot of enzymes, they build hard and tall soil structures.

Enzymes act as a catalyst in soil and help to remove bind water, bring particles close enough so they can get chemically stabilized and gain stronger bonds. There are two mechanisms of enzyme acting in the soil.

1. Enzyme is adsorbed by the clay lattice, and in turn cations are released as an exchange, a process like cation exchange. This leads to a reduction in the thickness of diffuse double layer of the clay.

2. Enzymes bond with large organic molecules present in the soil, and together attract to the clay minerals' net negative surface charge. The large organic molecules surround the clay minerals, neutralize the negative charge, and reduce the affinity of clay to water.

Enzymes can also cause hydrophobization of clayey soil. As the particles come in a closer contact, the pores decrease, and the better compaction can be expected. It is also known that the enzyme works as a flocculant which aggregates particles. The aggregation effect can be beneficial for erosion control as erosion usually starts with individual particles detachment and then moves to aggregates detachment at higher velocity.

Soil improvement by enzymes, suggested by manufacturers to ensure maximum effect requires the following soil properties.

- a) Presence at least 15% but no more than 65% fines passing the #200 sieve (0.075 mm), with at least 6% clay particles.
- b) Liquid Limit (LL) of soil should be less than 40% and the Plasticity Index (PI) between 5 to 18%.
- c) Preferable soil pH of 4.5 - 9.5.

The amount of water needed depends on the soil type and aims to get the soil just below optimum moisture prior to compaction. Adding more enzymes than the recommended amount will help it cure faster but not necessarily make it stronger. If a curing time is less than six weeks, a more concentrated amount of enzyme could help the curing process move along faster. It is recommended that the enzyme will continue to cure for more than six weeks (Royal Marty, personal communication, 2020).

Enzymes can be used as an individual product, as well as an additive to other products. Below, several methods of possible enzyme treatment are presented.

Enzymes Soil Treatment (EST). Enzymes soil treatment is a technique which utilizes commercially available enzymes. This technique is called Enzymes Soil Treatment (EST). These enzymes are TerraZyme and PermaZyme formulated using vegetable extracts (PermaZyme, 2020; TerraZyme, 2020). Enzymes can be made from sugar beets, a fermenting process is like beer brewing, but it continues until everything is fermented (Velasquez et al., 2005). Enzymes have been known to improve engineering properties of soils such as plasticity, liquid limit, compressive strength, and shear strength, swelling and shrinking (Rajoria and Kaur, 2014; Khan and Sarker, 1993; Velasquez et al., 2005; Shafii et al., 2018; Sahoo et al., 2018; Santoni et al., 2002; Tingle and Santoni, 2003; Santoni et al., 2005; Tingle et al., 2007, Taha et al., 2013).

PermaZyme and TerraZyme are traditionally used in compaction for road base improvement. They increase density for a less compaction effort. PermaZyme is known as a “compaction” enzyme because it is blended with a biodegradable surfactant to reduce the surface tension and achieve higher density (Rajoria and Kaur, 2014; Velasquez et al., 2005). It is claimed that the treatment with PermaZyme is permanent and that the treated soil becomes impermeable. PermaZyme provides a much faster rate of compaction than it is required by nature. TerraZyme has been used in India to construct a state highway and several trial roads. The cost of construction using enzymes reduced up to 20-40 % due to reduction in the transportation of materials and use of onsite materials (Rajoria and Kaur, 2014). TerraZyme treatment increases soil density and reduces optimum water content by 1-2% (TerraZyme Specification, 2020). TerraZyme also decreases the ability of soil to swell and reduces permeability. In fact, enzymes reduce the absorbed water and bring the particles together forming agglomerates and as a result is the surface area reduction and a decrease in absorbed water, which in turn reduces the swelling capacity (Velasquez et al., 2005). Muguda and Nagaraj (2019) observed that TerraZyme

decreased the liquid limit of soil while increased plastic and shrinkage limits, reduced plasticity and shrinkage potential. Pooni et al. (2019) obtained that enzyme can effectively improve the strength and mitigate volume change and mass loss during wetting/drying cycles which can be beneficial for dams and levees application.

Khan and Sarker (1993) reported that a small amount of enzyme (about 5%) increased the unconfined compression strength of soil mixed with fly ash significantly. The strength of enzyme treated soil-fly ash mixture was found to be higher than the strengths of lime stabilized soil (Khan and Sarker, 1993). The authors also claimed that enzyme treated soil showed good performance in freeze-thaw testing. It shows that enzymes can be beneficially used in a combination with fly ash to enhance soil strength. Presumably, enzymes mixed with other byproducts, for example, bauxite residue would improve soil properties while allowing to reuse the residue.

Velasquez et al. (2005) showed that enzymes increased the shear strength of soil from 9% to 39% depending on the soil type and type of enzyme. However, their study indicated that at least four months of cure time needed to improve the shear strength.

The Engineer Research and Development Center (ERDC) used four enzymes to improve engineering properties of clayey and sandy soils (Santoni et al. 2002, Tingle and Santoni 2003, Tingle and Santoni 2003, Santoni et al. 2005, Tingle et al. 2007). Tingle and Santoni (2003) treated clayey soils with four different enzymes with a concentration of 0.019% to 0.2% by dry weight of soil. Enzyme treated clay exhibited the highest value of unconfined compressive strength of high-plasticity clay (CH) than lime-treated soils. However, for a low-plasticity clay (CL), enzymes demonstrated only a minor increase in the unconfined compressive strength.

However, all enzyme treated clay lost their strength after being soaked in water by a factor of three and more (Tingle and Santoni, 2003).

In most cases (Santoni et al. 2002), enzyme-treated silty sand indicated a disintegration after placing in water for 15-minutes. The unconfined compressive strength of the enzyme treated soil after soaking decreased by a factor of two compared to the strength of the dry soil. The results of the experiments show that the only cement treated soil (9%) provided excellent resistance to water, they did not lose any strength after being soaked (Santoni et al. 2002).

The idea of using enzyme for erosion control was developed from the application of enzyme products used to improve engineering properties of soils. However, the performance of enzymes for erosion has not yet been established well. The EFA tests on the soil samples treated with enzymes of different concentration (0.2% and 1%) were performed in the Erosion Laboratory at Texas A&M University in 2017 (Shafii et al., 2018; Shidlovskaya et al., 2019). The results show that enzymes increased the erosion resistance of the clayey and silty sand (SC-SM) (Figure 120).

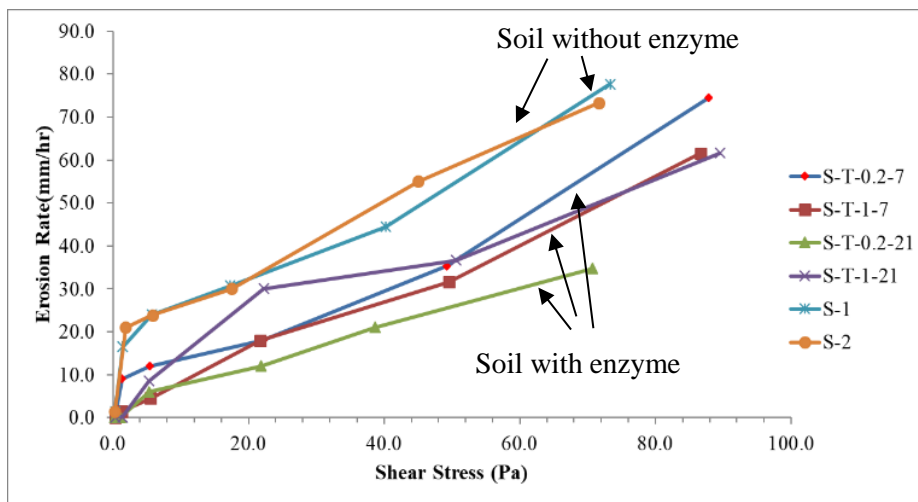


Figure 120. Erosion rate versus shear stress for sand in 7 and 21 days (adapted from Shafii et al., 2018)

The effect of enzymes on soil improvement is summarized below.

1. Reduces compaction effort.
2. Increased solid dry density.
3. Increased compressive strength and shear strength.
4. Lowered water permeability.
5. Reduced shrinkage and swelling.
6. Increased soil resistance to erosion by water and air.

MICP and EICP. One of the enzyme applications is Microbial-Induced Calcite Precipitation (MICP) technique which rely on ureolytic bacteria (usually *Sporosarcina pasteurii*) to produce calcium carbonate CaCO_3 that binds soil particles together (Mitchell and Santamarina, 2005; van Paassen, 2009; DeJong et al., 2006, 2009, 2010, 2011; Harkes et al., 2010; Mortensen et al. 2011; Ikuma, 2018; Hoang et al., 2018; Almajed, 2017, Almajed et al. 2019). Another technique which is like MICP is Enzyme-Induced Calcite Precipitation (EICP) that uses an aqueous solution comprised of urea, calcium chloride, and urease enzyme to produce calcium carbonate. USBR in 2019 performed a research on application of EICP for channel lining and erosion control (Application of Enzyme Induced Carbonate Precipitation (EICP) for Channel Lining and Repair, Low Volume Road Stabilization, Embankment Construction, and Erosion Control, 2019).

The MICP technique utilizes the urease enzymes while EICP is based on plant-derived urease enzyme (Hoang et al. 2018). Both, MICP and EICP, produce ammonium management of which is a problem whether ureolytic MICP or EICP is employed.

Research suggests that biocementation using MICP and EICP can address several important geotechnical problems including erosion control and scour (Kavazanjian and Karatas

2008; Kavazanjian et al., 2009; DeJong et al. 2010; Harkes et al. 2010; van Paassen et al. 2009; Jiang and Soga, 2019; Gao et al. 2018; Indraratna et al., 2008; Salifu et al., 2016). Salifu et al. (2016) used MICP for sandy embankment slopes reproduced in the laboratory. The MICP treated sandy slopes exhibited an erosion resistance.

Montoya et al. (2018) studied the erodibility of the MICP treated sand by running the jet test and found that the critical shear stress of the treated sand increased one to three orders of magnitudes than the same parameter of the untreated sand. The critical shear stress for lightly cemented sand did not exceed 0.2 Pa, for moderately cemented reached 2-8 Pa, and for heavily cemented sand increased to 20-80 Pa. Note that MICP is limited to coarse graded soils and particularly to “clean” medium to fine sand. Field application of MICP requires creating and maintaining the conditions needed for urease producing microbes which can be a challenge.

The erodibility of the MICP treated beach sand was studied by the Pocket Erodrometer Test (PET) (Chek et al., 2021). The erosion depth of the MICP-treated soil after running the PET varied from 23 to 27 mm. It should be noted that the PET can be used as a preliminary erosion test, and it does not allow to obtain the erosion functions or the erosion thresholds.

A series of laboratory tests were conducted by the Center for Bio-mediated and Bio-inspired Geotechnics (CBBG) at Arizona State University (ASU) and Bureau of Reclamation in 2018 to study wind erodibility of enzyme-improved sand. The results of the tests show that enzyme-treated sand with $D_{50} = 0.18$ mm can resist wind erosion up to 25 m/s and more (Hamdan, 2015). The resistance of enzyme-treated soil to water was not studied.

Improvement in erosion resistance of sand by microbial biopolymer formation was observed in the study performed by Ham et al. in the EFA (2018). The authors observed an increase in the critical velocity and the critical shear stress of the treated soil. The critical

velocity increased from 0.15 m/s to 0.24 m/s while the critical shear stress increased from 0.1 Pa to 0.23 Pa (Ham et al., 2018).

5.2. Materials and methods

This section discusses the material and methods used in this dissertation for enzyme treatment.

Soils. Enzymes would be expected to be soil specific (Tingle et al, 2007; Shafii et al., 2018). Therefore, several types of soils such as “artificial” soils reconstituted from locally available particles and natural soil from the field were chosen. The reconstituted soils (Experiment cluster 1, Experiment cluster 2, and Experiment cluster 3) were prepared from three groups of particles: kaolinite clay (0.003-0.005 mm size), finer sand (0.18-0.25 mm size, sieve #60-80), and coarser sand particles (0.85-2 mm size, sieve #10-20). The artificial soil (Experiment cluster 4) was prepared from bentonite particles instead of kaolinite clay. The natural soil from the Sacramento levee site were classified as clayey sand (SC, Experiment cluster 5), silty sand with 10 % additional kaolinite particles (SM, Experiment cluster 6), and clayey sand with 20% additional kaolinite particles. Note that the Experiment cluster 6 and 7 initially contained 1.2% clay particles which was not sufficient for enzyme treatment, therefore, additional clay particles was added to the soil.

It was ensured that the soil was pulverized using a wooden mallet to break the clods and then sieved through 4.75 mm sieve. It was also ensured that soils have at least 15 % fines (0.075 mm) to increase the efficiency of enzyme treatment. The soil grain size is shown in Figure 121 (Experiment cluster 5), Figure 122 (Experiment cluster 6), and Figure 123 (Experiment cluster 7). The description of each experiment cluster is given in Section 5.3.

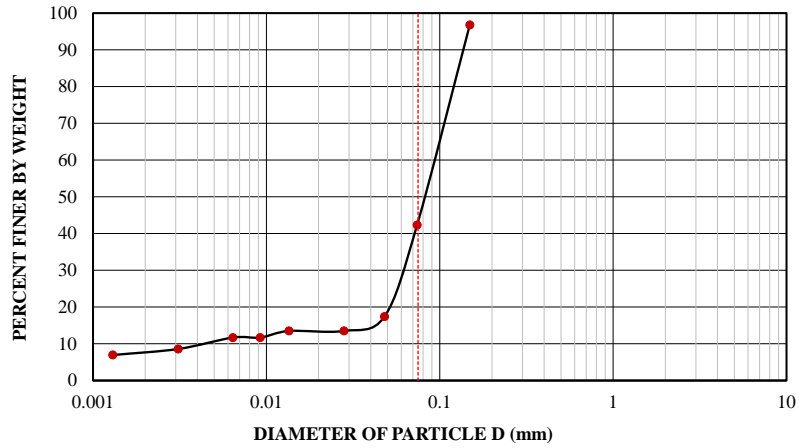


Figure 121. Grain size distribution of soil for Experiment cluster 5 (ASTM D422 / ASTM C136)

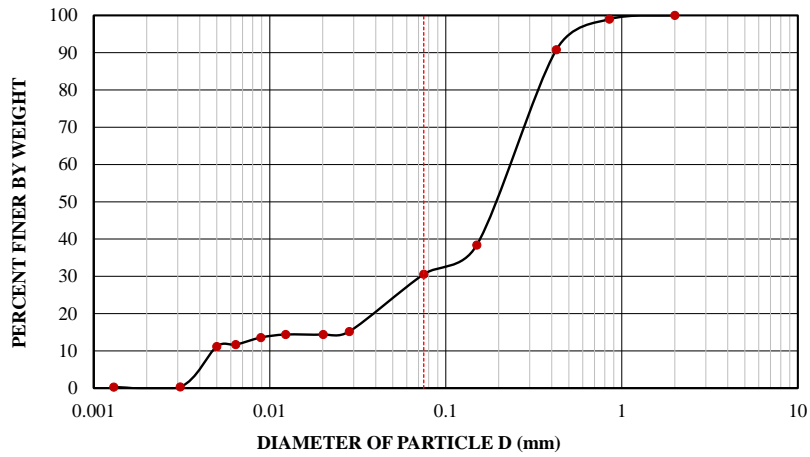


Figure 122. Grain size distribution of soil for Experiment cluster 6 (ASTM D422 / ASTM C136)

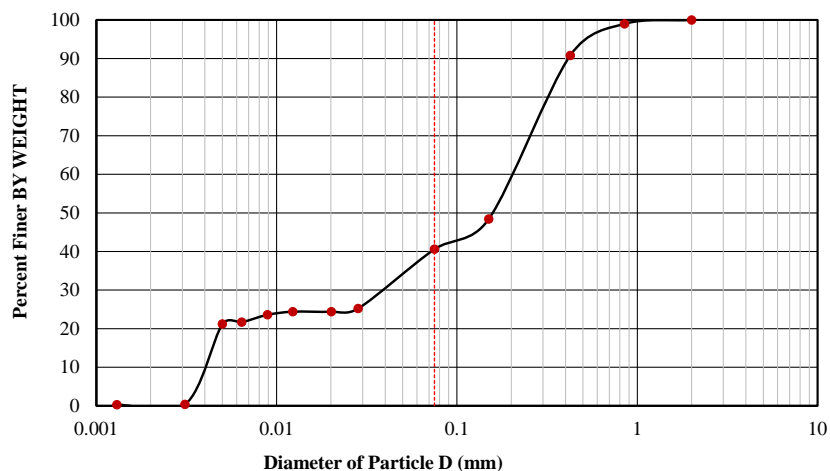


Figure 123. Grain size distribution of soil for Experiment cluster 7 (ASTM D422 / ASTM C136)

Enzymes. In this study, two commercially available enzymes, TerraZyme (product from Nature Plus, Stratford, Connecticut, USA) and PermaZyme (product from Substrata) were used to check if they can improve soil erodibility. Both, TerraZyme and PermaZyme, are in liquid form formulated using vegetable extracts. Both enzymes exhibited foaming when shaken because they consist of large macromolecules that resemble surfactants in chemical structure and behavior. They are soluble in water, brown in color, viscous, and non-toxic. The chemical composition is not revealed by the manufacturers.

Both enzymes, as suggested by the manufactures, require dilution in water before application. Since the enzymes act as a catalyst in initiating physical and chemical reactions in treated soil, they are recommended in small dosages. The TerraZyme Dosage Guidelines (2020) suggests that TerraZyme is used in a dosage depending on a plasticity index of soil and a percent of fines passing #200 Sieve with 0.075 mm openings. It is also recommended that TerraZyme

should be diluted in water depending on the soil density and a volume of soil to be treated before application to soil.

The dosage of TerraZyme and PermaZyme used in the present study was based on the recommended guidelines by the manufactures. However, to simplify the procedure for both enzymes and to compare the efficiency of the enzymes, it was decided to use 2 ml of concentrated enzyme for 1000 ml of water. The proposed dilution matches the recommendations of the manufacturers. Since it is reported that enzyme treatment has a time-related effect on soil properties, different ageing periods of 7, 14, 21, and 28 days were selected.

Methods. For each EFA test, 1 kg of the air-dried reconstituted and natural soils was used. One sample for each experiment cluster was made without enzymes to serve as a reference test. The TerraZyme and PermaZyme concentrate in the required dosage (2 ml to 1000 ml of water) were carefully extracted through a clinical micro syringe (1- and 2-ml maximum capacity), and then, injected to the tap water to be used for mixing. The selected amount of water was approximately near the optimum water content. Each mixture of soil with enzymes was thoroughly mixed with a spatula for more than 10 min and then one third of the total soil volume was inserted in the Shelby tube and compacted in the tube with a drop hammer (compaction test hammer). Twenty drops were chosen. Then the second and the last third of the sample were compacted by the same number of drops. It was ensured that the prepared sample was within tolerable limits of the target unit weight. The prepared samples were sealed in the steel tubes and left in the moisture room for different ageing periods such as 7-days, 14-days, 21-days, and 28-days. At the designated ageing periods, the tube with the sample was taken from the moisture room and tested for erosion in the EFA.

5.3. EFA testing matrix

The experimental program was taken up to study erodibility of the enzyme-treated soil in the EFA. The total of twenty-five EFA tests were carried out to study the effect of enzymes on soil erodibility. Seven tests were performed on reconstituted and natural soil to obtain soil erodibility without the effect of enzymes. The total of ten EFA tests were performed on the TerraZyme-treated soil and the total of eight EFA tests on the PermaZyme-treated soil. The testing matrix is given in Table 33. The soil type 1 is the reconstituted soil prepared from different fraction and it is referred to as (Artificially reconstituted soil). The soil type 2 is the natural soil and is called NS (Natural Soil). The abbreviation “TZ” means TerraZyme, the abbreviation “PZ” means PermaZyme, the abbreviation “NE” means no enzymes or untreated soil.

Table 33. Matrix of EFA testing experiment clusters

No	Experiment cluster	Soil Type		Enzyme			Curing Time, days			
		1	2	TZ	PZ	NE	7	14	21	28
1	Experiment cluster 1-AS-NE	+				+				
2	Experiment cluster 1-AS-TZ-14	+		+				+		
3	Experiment cluster 2-AS-NE	+				+				
4	Experiment cluster 2-AS-TZ-14	+		+				+		
5	Experiment cluster 2-AS-PZ-14	+			+			+		
6	Experiment cluster 3-AS-NE	+				+				
7	Experiment cluster 3-AS-TZ-7	+		+			+			
8	Experiment cluster 3-AS-TZ-14	+		+				+		
9	Experiment cluster 3-AS-TZ-21	+		+					+	
10	Experiment cluster 3-AS-PZ-7	+			+		+			
11	Experiment cluster 3-AS-PZ-14	+			+			+		
12	Experiment cluster 3-AS-PZ-21	+			+				+	
13	Experiment cluster 4-AS-NE (bentonite)	+				+				
14	Experiment cluster 5-NS-NE		+			+				
15	Experiment cluster 5-NS-TZ-14		+	+				+		
16	Experiment cluster 6-NS-NE		+			+				

No	Experiment cluster	Soil Type		Enzyme			Curing Time, days			
		1	2	TZ	PZ	NE	7	14	21	28
17	Experiment cluster 6-NS-TZ-7		+	+			+			
18	Experiment cluster 6-NS-TZ-14		+	+				+		
19	Experiment cluster 6-NS-PZ-7		+		+		+			
20	Experiment cluster 6-NS-PZ-14		+		+			+		
21	Experiment cluster 7-NS-NE		+			+				
22	Experiment cluster 7-NT-TZ-7		+	+			+			
23	Experiment cluster 7-NS-TZ-14		+	+				+		
24	Experiment cluster 7-NS-PZ-7		+		+		+			
25	Experiment cluster 7-NS-PZ-14		+		+			+		

The description of each experiment cluster including grain size composition, enzyme used for treatment, and cure time is given below.

1. Experiment cluster 1-AS-NE: artificial soil reconstituted from 40 % clay particles (0.003-0.005 mm size), 20 % finer sand particles (0.18-0.25 mm size, sieve #60-80), and 40 % coarser sand particles (0.85-2 mm size, sieve #10-20), untreated.
2. Experiment cluster 1-AS-TZ-14: same composition as Experiment cluster 1-AS-NE but treated with TerraZyme for 14 days.
3. Experiment cluster 2-AS-NE: artificial soil reconstituted from 20 % clay particles (kaolinite), 50 % finer sand particles (0.18-0.25 mm size, sieve #60-80), and 30 % coarser sand particles (0.85-2 mm size, sieve #10-20), untreated.
4. Experiment cluster 2-AS-TZ-14: the same composition as Experiment cluster 2-AS-NE but treated with TerraZyme for 14 days.
5. Experiment cluster 2-AS-PZ-14: the same composition as Experiment cluster 2-AS-NE but treated with PermaZyme for 14 days.

6. Experiment cluster 3-AS-NE: artificial soil reconstituted from 15 % clay particles (kaolinite), 50 % finer sand particles (0.18-0.25 mm size, sieve #60-80), and 35 % coarser sand particles (0.85-2 mm size, sieve #10-20), untreated.
7. Experiment cluster 3-AS-TZ-7: same composition as Experiment cluster 3-AS-NE but treated with TerraZyme for 7 days.
8. Experiment cluster 3-AS-TZ-14: same composition as Experiment cluster 3-AS-NE but treated with TerraZyme for 14 days.
9. Experiment cluster 3-AS-TZ-21: same composition as Experiment cluster 3-AS-NE but treated with TerraZyme for 21 days.
10. Experiment cluster 3-AS-PZ-7: same composition as Experiment cluster 3-AS-NE but treated with PermaZyme for 7 days.
11. Experiment cluster 3-AS-PZ-14: same composition as Experiment cluster 3-AS-NE but treated with PermaZyme for 14 days.
12. Experiment cluster 3-AS-PZ-21: same composition as Experiment cluster 3-AS-NE but treated with PermaZyme for 21 days.
13. Experiment cluster 4-AS-NE (bentonite): artificial soil reconstituted from 15 % bentonite clay particles, 50 % finer sand particles (0.18-0.25 mm size, sieve #60-80), and 35 % coarser sand particles (0.85-2 mm size, sieve #10-20), untreated.
14. Experiment cluster 5-NS-NE: natural soil described as clayey sand (SC), untreated.
15. Experiment cluster 5-NS-TZ-14: same composition as Experiment cluster 5-NS-NE but treated with TerraZyme for 14 days.

16. Experiment cluster 6-NS-NE: natural soil described as silty sand with 10 % by weight kaolinite clay particles (SM), untreated.
17. Experiment cluster 6-NS-TZ-7: same composition as Experiment cluster 6-NS-NE but treated with TerraZyme for 7 days.
18. Experiment cluster 6-NS-TZ-14: same composition as Experiment cluster 6-NS-NE but treated with TerraZyme for 14 days.
19. Experiment cluster 6-NS-PZ-7: same composition as Experiment cluster 6-NS-NE but treated with TerraZyme for 7 days.
20. Experiment cluster 6-NS-PZ-14: same composition as Experiment cluster 6-NS-NE but treated with TerraZyme for 14 days.
21. Experiment cluster 7-NS-NE: natural soil described as clayey sand with 20 % by weight kaolinite clay particles (SC), untreated.
22. Experiment cluster 7-NS-TZ-7: same composition as Experiment cluster 7-NS-NE but treated with TerraZyme for 7 days.
23. Experiment cluster 7-NS-TZ-14: same composition as Experiment cluster 7-NS-NE but treated with TerraZyme for 14 days.
24. Experiment cluster 7-NS-PZ-7: same composition as Experiment cluster 7-NS-NE but treated with PermaZyme for 7 days.
25. Experiment cluster 7-NS-PZ-14: same composition as Experiment cluster 7-NS-NE but treated with PermaZyme for 14 days.

5.4. Results of EFA testing

The results of EFA testing of the enzyme-treated and untreated soils are discussed below. The erosion of each EFA experiment cluster is analyzed and the erosion functions together with erosion parameters such as critical velocity and critical shear stress are derived. It was observed that if the critical velocity is low, the erosion, in some cases, remains low until much higher velocity. Therefore, this shows that it is critically important not to limit the evaluation of erosion to the use of the critical velocity but to include the entire erosion function to capture the erosion resistance of the material at different velocity and shear stress. The effect of the entire erosion function on the erosion movement is discussed in Chapter 9, Section 9.4.

Experiment cluster 1-AS-NE. The erosion of the untreated soil was initiated at the beginning of the first velocity step of 0.5 m/s. Therefore, the critical velocity is lower than 0.5 m/s. Meanwhile, the erosion rate remained low (around 10 mm/hr) until the velocity of 4 m/s and then slightly increased to 30 mm/hr at the velocity of 4.95 m/s. In this case, the erosion category would depend on the acting velocity of shear stress.

Experiment cluster 1-AS-TZ-14. The TerraZyme-treated soil cured for 14-days exhibits a slight increase in erosion rate with an increase in velocity. The treated soil shows a slight increase in critical velocity up to 0.56 m/s compared to the untreated soil (Figure 124). However, EFA testing shows no notable improvement in the TerraZyme-treated soil erodibility in 14 days except the improved value of the critical velocity.

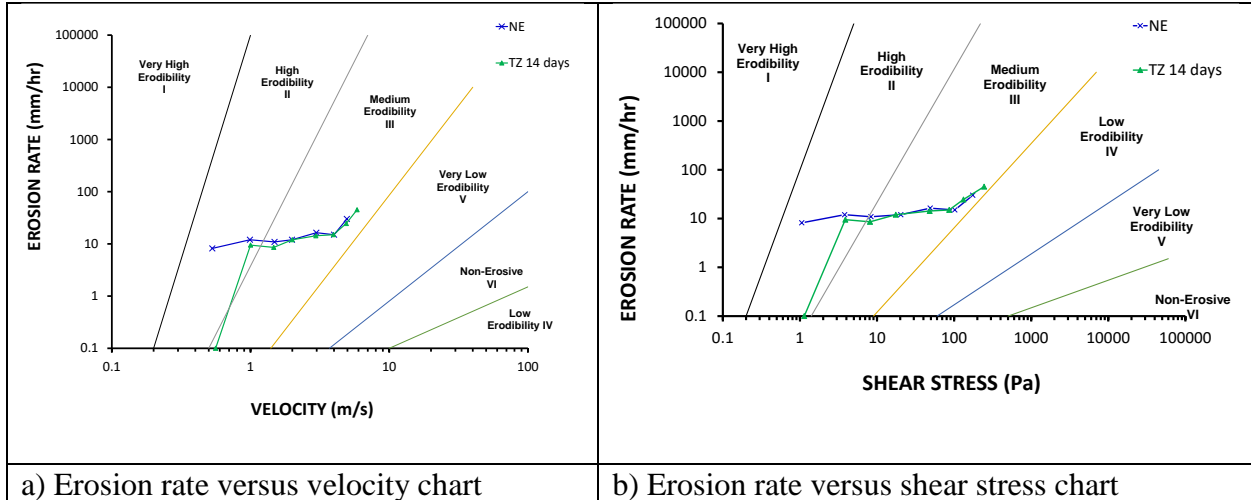


Figure 124. Erosion functions of the experiment cluster 1

Experiment cluster 2-AS-NE. The erosion of the untreated soil was detected during the first velocity step in a form of individual particles detachment at the low velocity and then as chunks of particles detachment at the higher velocities. The critical velocity of the soil was obtained as the value of velocity read from the intersection of the erosion function and horizontal axis and was 0.16 m/s (Figure 125). The critical shear stress was below 0.5 Pa. At the velocity of 2.99 m/s, a big portion of the sample got entrained by the flowing over and the erosion rate exceeded 3000 mm/hr. The soil exhibits a high erosion.

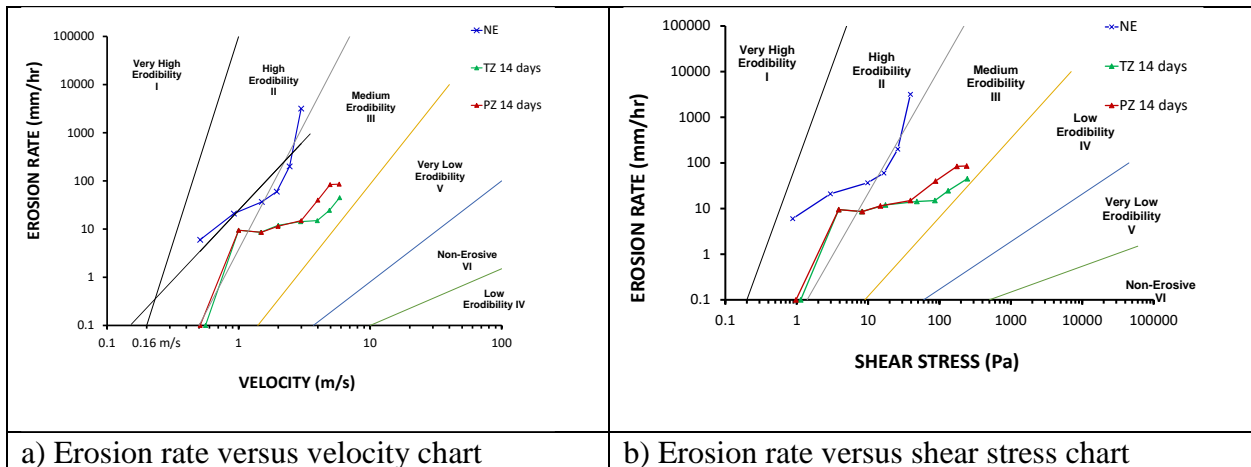


Figure 125. Erosion functions of the experiment cluster soil 2

Experiment cluster 2-AS-TZ-14. The critical velocity of the TerraZyme-treated soil with 14-days cure time was detected during the first velocity of 0.56 m/s (Figure 125) and the corresponding critical shear stress was 1.137 Pa. The soil resisted up to the velocity of 5.86 m/s at which the soil experiences the erosion rate of 45 mm/hr. Overall, EFA testing indicates an improvement in erosion of the treated soil compared to the untreated soil (Experiment cluster 2-AS-NE). Figure 125 shows that the treated soil is in Category III (Medium Erodibility), while the untreated soil is in Category II (High Erodibility).

Experiment cluster 2-AS-PZ-14. The critical velocity of the PermaZyme-treated soil with 14-days cure time was detected around $v_c = 0.51$ m/s and the corresponding critical shear stress was $\tau_c = 0.975$ Pa. The erosion rate maintained at the constant rate up to the velocity of 3 m/s and then increased 2 times with an increase in velocity from 4 m/s to 5 m/s. As can be seen on Figure 125, EFA testing shows a notable improvement in the PermaZyme-treated soil erodibility in 14 days compare to the untreated soil (Experiment cluster 2-AS-NE). The PermaZyme-treated soil is in Category III (Medium Erodibility).

Experiment cluster 3-AS-NE. The erosion of the untreated soil was detected during the first velocity step in a form of individual particles detachment at the low velocity and then as chunks of particles detachment at the higher velocities. The critical velocity of the soil was obtained as the value of velocity read from the intersection of the erosion function and horizontal axis and was 0.15 m/s. The higher velocity during the EFA test was 2.99 m/s and the corresponding shear stress was 39 Pa. The erosion rate at that velocity reached 3180 mm/hr which was connected to the detachment of the portion of the sample. This demonstrated high erodibility of the untreated soil. The erosion function of the untreated soil is shown on Figure 126 along with the treated soil.

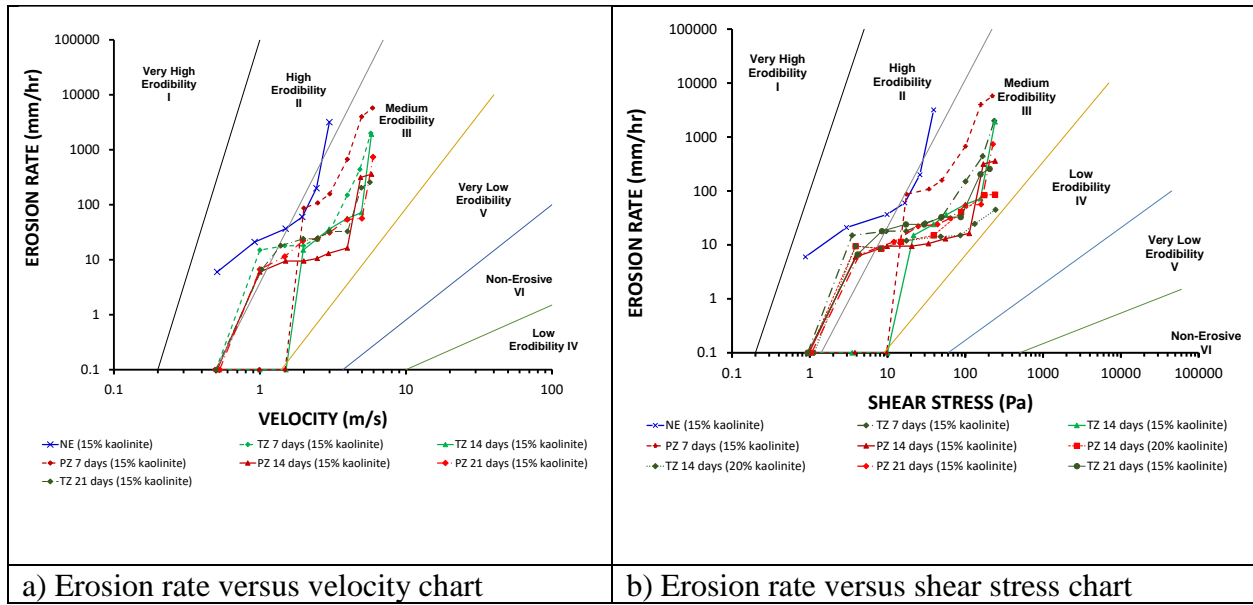


Figure 126. Erosion functions of the experiment cluster soil 3

Experiment cluster 3-AS-TZ-7. The erosion behavior of the TerraZyme-treated soil is like the behavior of the PermaZyme-treated soil with 7 days cure time except the values of critical velocity and critical shear stress. The slight erosion initiated at the lower velocity ($v = 0.5$ m/s) and shear stress of $\tau_c = 0.938$ Pa at which some particles started to detach. Hence, undermining was observed at the lower velocity of 3 m/s and then undermining erosion progressed with time and an increase in the velocity. At $v = 5$ m/s erosion took place around of the sample. The center part of the sample was not eroded as much as the edges. A big portion of sample, approximately 5 cm thick, got detached at the velocity of 5.75 m/s with the corresponding erosion rate of 2000 mm/hr. The treated soil is in Category III (Medium Erodibility) (Figure 126).

Experiment cluster 3-AS-TZ-14. The erosion initiated in a form of fine sand particles detachment at the velocity of 1.51 m/s when the corresponding shear stress reached 9.975 Pa. This indicates an erosion improvement of the 14-days treated soil compared to the 7-days treated

soil: the critical velocity increased up to 3 times. At the velocity of 5.81 m/s, the erosion rate reached 1920 mm/hr which was similar to the 7-days treated soil at matching velocity. This shows that TerraZyme increases the critical velocity of treated soil with an increase in curing time. Meanwhile, 7 and 14-days treated soils exhibit the same function with an increase in velocity (> 1.5 m/s). It shows the time-related tendency in soil erodibility. The treated soil is in Category III (Medium Erodibility) (Figure 127).

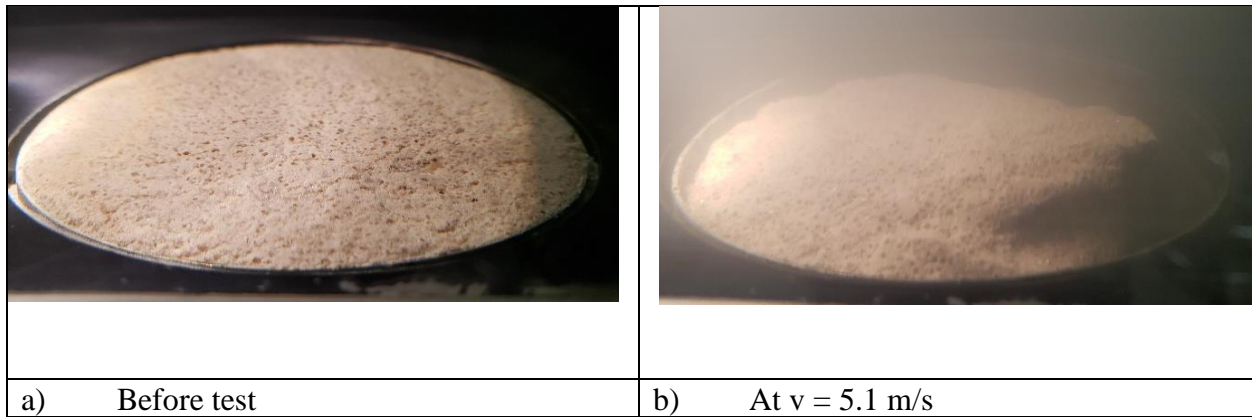


Figure 127. A photograph of the experiment cluster 3-AS-TZ-14

Experiment cluster 3-AS-TZ-21. The soil started to erode in a form of loose particles detachment at the velocity of 0.5 m/s. The erosion rates up to the velocity of 4.95 m/s did not exceed 33 mm/hr. However, at the velocity of 4.95 m/s and above, the erosion rate increased up to 5 and more times and reached more than 200 mm/hr. Meanwhile, the 21-days TerraZyme-treated soil exhibited less erosion rate and presuming less erosion compared to the 7-days and 14-days when the erosion rate at the same velocity reached almost 2000 mm/hr. It shows the time-related tendency in soil treatment by TerraZyme. The treated soil is in Category III (Medium Erodibility) (Figure 126).

Experiment cluster 3-AS-PZ-7. The erosion initiated with fine sand particles detachment at the velocity of 1.49 m/s. Aggregates of particles started to detach and washed

away as the velocity increased. At the velocity of 4 m/s, the undermining was initiated at the downstream of the sample. A big portion of sample got uplift at the velocity of 5.91 m/s which dramatically increased the erosion rate up to 5760 mm/hr. The erosion curve shown on the erosion classification chart is in Category III (Medium Erodibility) (Figure 126). Note that the 7-days treated soil exhibit less erosion compared to the untreated soil. PermaZyme has been proven to be time related improvement agent.

Experiment cluster 3-AS-PZ-14. The erosion was detected in a form of fine sand particles detachment at $v = 0.5$ m/s which was 3 times lower than the detachment velocity for the sample cured for 7 days. This shows that the critical velocity and critical shear stress do not improve with an increase in curing time. However, 14-days treated sample showed less erosion at higher velocity and higher shear stress. For example, at the velocity $v = 5.82$ m/s, the erosion rate of the 14-days soil was 360 mm/hr which is almost 10 times lower than for the 7-days soil. Also, no sample uplift was indicated at higher velocity. Overall, the 14-days sample showed better erosion resistance compared to the 7-days sample, excluding the low critical velocity. PermaZyme has shown time related improvement in soil erosion. The erosion curve moves to the right on the erosion classification chart on Figure 126. The treated soil is in Category III (Medium Erodibility).

Experiment Cluster 3-AS-PZ-21 days. The erosion initiated at the low velocity of 0.53 m/s when loose soil particles started to detach. The erosion rate maintained low up to the velocity of 3 m/s and did not exceed 30 mm/hr. However, it increased drastically and reached 738 mm/hr when a big portion of the sample (about 8 cm thick) got detached at the velocity of 5.96 m/s. The 21-days PermaZyme-treated soil does not improve its erodibility compared to the

14-days soil which contradicts the time-related tendency of TerraZyme-treated soil. The treated soil is in Category III (Medium Erodibility) (Figure 126).

Experiment cluster 4-AS-NE (bentonite). This experiment cluster was tested to compare the effect of clay mineralogy on soil erodibility. The erosion function shows that replacing kaolinite with bentonite allows to improve soil erodibility by one category to the right on the erosion chart (Figure 128). Overall, the sample exhibited not much erosion and it is in Category III (Medium Erodibility). The critical velocity of the bentonite-based soil (1 m/s) is two times higher than the critical velocity of the kaolinite-based soil (0.5 m/s). Kaolinite clay particles are less erosion resistance than bentonite clay. The erosion rate for soil with kaolinite is 10 times higher than for soil with bentonite. For the case of clay containing active minerals such as bentonite (presumably montmorillonite as well), the beneficial use of enzymes to improve soil erosion should be additionally studied.

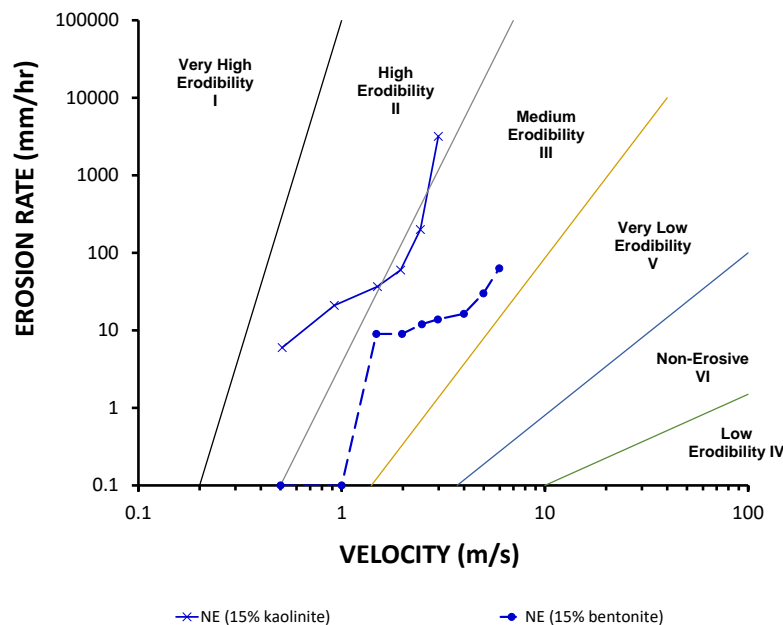


Figure 128. Erosion function of the kaolinite- and bentonite-based soil

The summary erosion functions of the experiment clusters 2, 3, and 4 are shown in Figure 129. It demonstrates that enzyme treatment allows to improve soil erodibility by one category.

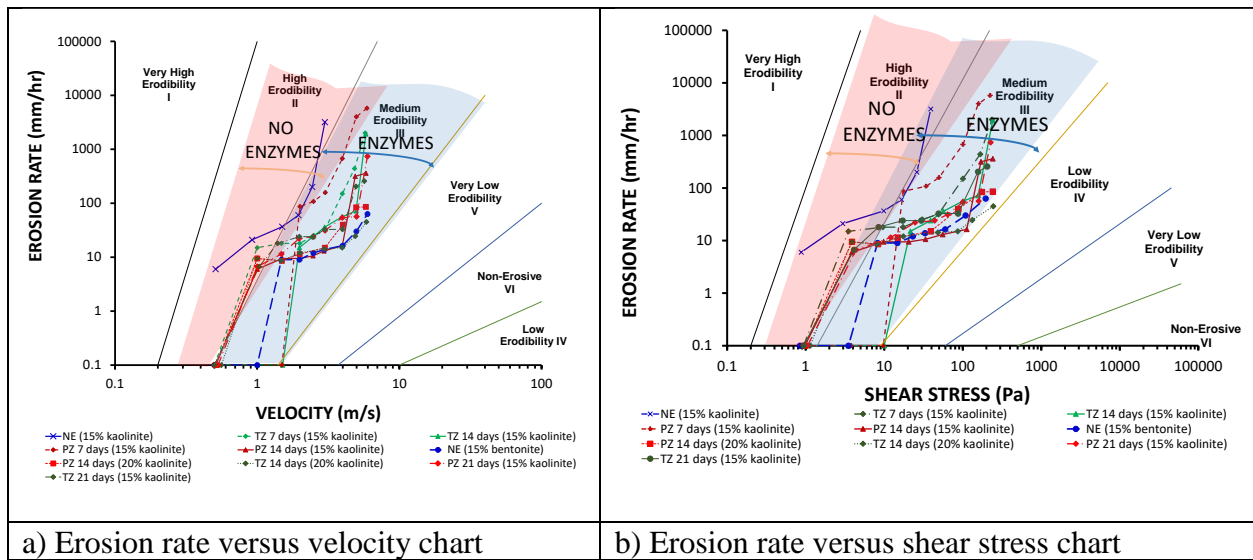


Figure 129. Erosion functions of the untreated and enzyme-treated soils (Experiment cluster 2, Experiment cluster 3, and Experiment cluster 4)

Experiment cluster 5-NS-NE. The erosion of the untreated clayey sand (SC) was detected during the first velocity step ($v = 0.5$ m/s). The critical velocity of the soil was obtained as the value of velocity read from the intersection of the erosion function and horizontal axis and was 0.1 m/s (Figure 130). At the velocity of 1.72 m/s, the erosion rate exceeded 2880 mm/hr because of detachment of a thick portion of the sample. This shows that the untreated soil is in Category II (High Erodibility).

Experiment cluster 5-NS-TZ-14. The erosion of clayey sand (SC) treated with TerraZyme for 14-days was initiated at the velocity 0.43 m/s which is 4 times higher than for the untreated soil. Moreover, less erosion rate was detected compared to the untreated soil with an increase in velocity. For example, the erosion rate did not exceed 66 mm/hr at the velocity 1.6 – 1.7 m/s which was 43 times less than for the untreated soil at the same velocity. However, the

treated and untreated soils are both in the same erosion category II (High Erodibility) (Figure 130). PermaZyme was not available at that time.

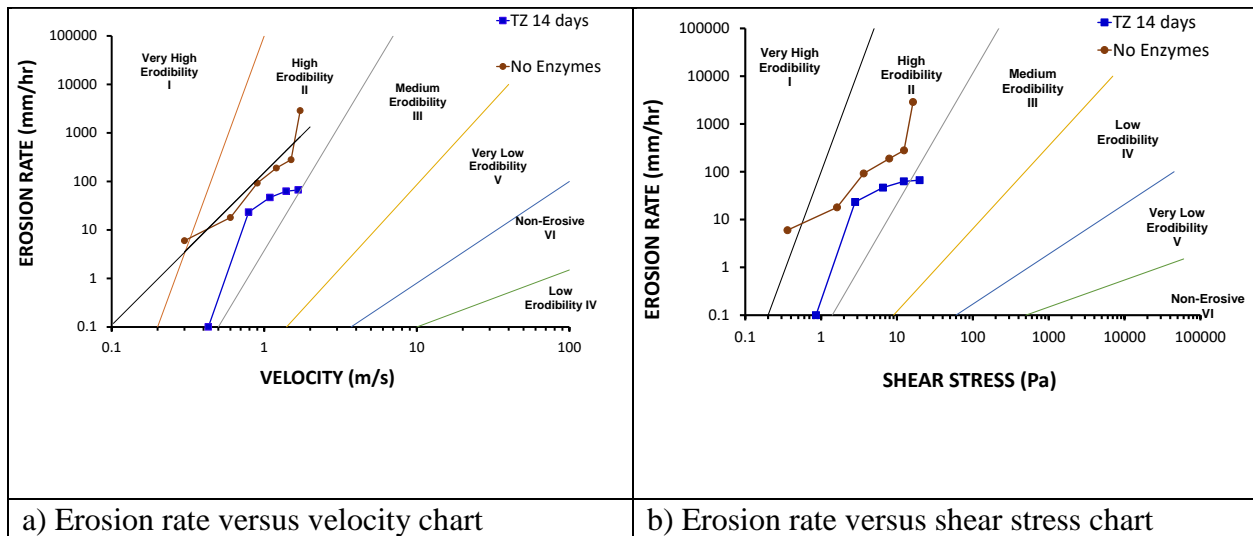


Figure 130. Erosion functions of the untreated and enzyme-treated soils (Experiment cluster 5)

Experiment cluster 6-NS-NE. The erosion in a form of loose fine particles detachment initiated during the first velocity step of 0.5 m/s when the erosion reached 66 mm/hr. At the velocity of 2.4 m/s, the erosion rate was 900 mm/hr which shows a high level of soil erodibility. The erosion category is High Erodibility (Category II).

Experiment cluster 6-NS-TZ-7/14. TerraZyme-treatment of the natural soil with 21% of fine particles and the cure time of 7 and 14 days does not significantly improve soil erodibility as can be seen on Figure 131 because treated soil is still in Category II (High Erodibility). The erosion of the treated soil initiated at the velocity of 0.5 m/s. However, the erosion rate of the 14-days treated soil at the velocity of 0.5 m/s is one order of magnitude less than the erosion rate of untreated soil at the same velocity. Meanwhile, the erosion rate of the treated soil is the same as

of the untreated soil at the velocity of 1.5 m/s and higher. The critical velocity and shear stress did not improve compared to the untreated soil.

Experiment cluster 6-NS-PZ-7/14. The treated natural soil by PermaZyme for 7 and 14 days showed almost the same results in erosion (Figure 131). The critical velocity of the treated soil has increased two times compared to the untreated soil, however, at the velocity of 1 m/s and higher, the erosion rate of the treated soil is the same as of the untreated which indicates no considerable improvement in erosion by enzymes. The treated soil is considered as high erodible on the erosion chart (Figure 131).

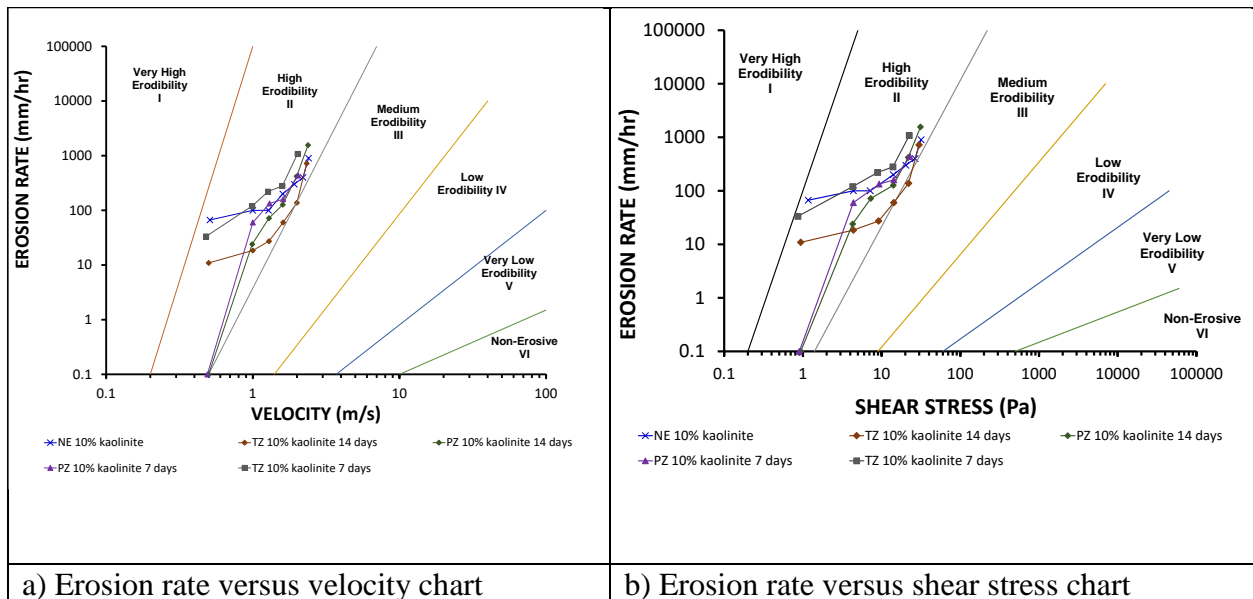


Figure 131. Erosion functions of the untreated and enzyme-treated soils (Experiment cluster 6)

Experiment cluster 7-NS-NE. The erosion was detected during the second velocity step. The critical velocity is 0.51 m/s and the critical shear stress is 0.975 Pa. At the velocity of 1.3 m/s, the erosion rate did not exceed 100 mm/hr. The erosion rate increased up to 3 times with an increase in velocity up to 3.2 m/s when the undermining was initiated at the downstream (Figure

132). The erosion chart shows that the soil exhibits high erodibility when the velocity did not exceed 2.4 m/s. Above that velocity, the erodibility is in Category III (Medium Erodibility).

Experiment cluster 7-NS-TZ-7. The 7-days TerraZyme cured soil exhibited less erosion than the untreated soil: the erosion rate is at least 6 times less and the critical velocity is two times higher. The erosion function of the treated soil is in Category III (Medium Erodibility) which is one category less erodible than the untreated soil (Figure 132).

Experiment cluster 7-NS-TZ-14. The 14-days TerraZyme-treated soil is more erosion resistant than 7-days treated soil, however the critical velocity and critical shear stress are the same as for the 7-days treated soil. Meanwhile, the erosion rate of the 14-days soil decreases by a factor of 5 to 6 above the critical point. Figure 132 shows that the 14-days soil has moved the erosion category to the right on the erosion chart.

Experiment cluster 7-NS-PZ-7. The 7-days PermaZyme treated soil shows that enzyme can be beneficially used to improve soil erodibility even in 7 cure days. The critical velocity is three times higher than of the untreated soil. The entire erosion function indicates that the erosion rate is at least 7 times less that of the untreated soil. The 7-days treated soil is in category III (Medium Erodibility) (Figure 132).

Experiment cluster 7-NS-PZ-14. PermaZyme is the time related enzyme because it improves erosion resistance by increasing the critical velocity and critical shear stress. The critical velocity increased by 100 % and the critical shear stress increased by a factor of 4 during the 7-days cure time. Figure 132 shown that the 14-days cure soil moves the erosion category to the right.

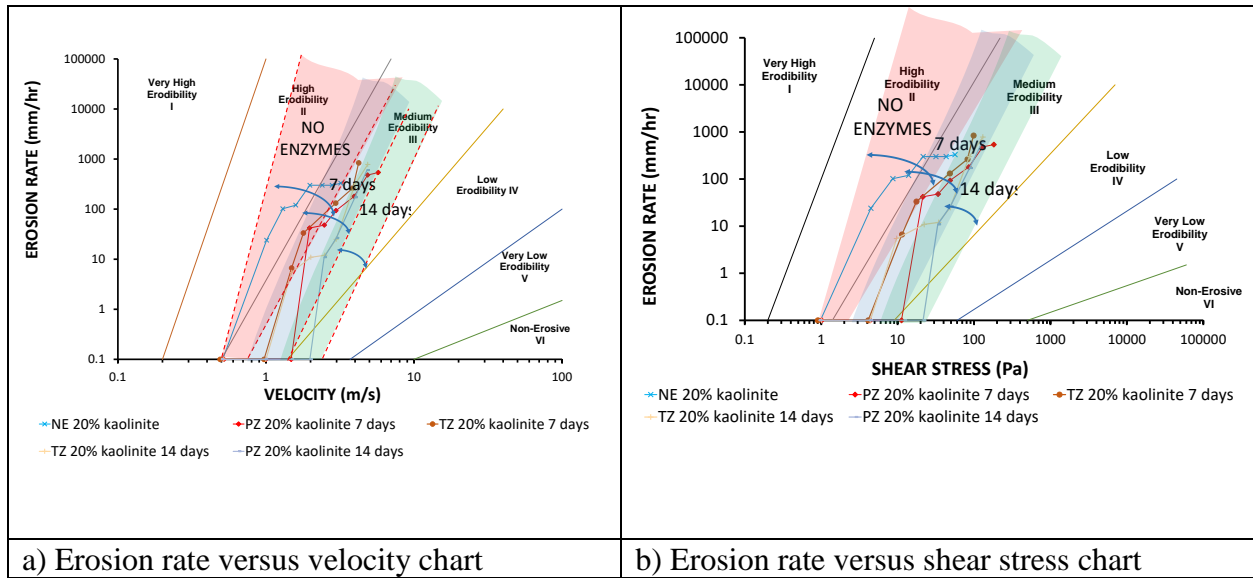


Figure 132. Erosion functions of the untreated and enzyme-treated soils (Experiment cluster 7)

Soil properties of the untreated and enzyme-treated soils such as water content, dry density, dry unit weight, undrained shear strength, critical velocity and critical shear stress are shown in Table 34.

Table 34. The properties of the untreated and enzyme treated soils

No	Experiment cluster	Soil Type	USCS	Particles (%)						Soil Properties					
				Fines (mm)	Clay (mm)	Silt (mm)	Sand (mm)			w_c (%)	ρ_d (kg/m ³)	γ_d (kN/m ³)	S_u (kPa)	v_c (m/s)	τ_c (Pa)
							0.075-2	0.18-0.25	0.85-2						
Experiment cluster 1. Artificial soil: clayey sand (SC) with 40% kaolinite clay particles															
1	Experiment cluster 1-AS-NE	Clayey Sand	SC	40	40	N/A	N/A	20	40	17	1852.2	18.17	N/A	< 0.5	< 1.0
2	Experiment cluster 1-AS-TZ-14			40*	40*	N/A	N/A	20*	40*	17	2004.1	19.66	N/A	0.56	1.137
Experiment cluster 2. Artificial soil: clayey sand (SC) with 20% kaolinite clay particles															
3	Experiment cluster 2-AS-NE	Clayey Sand	SC	20	20	N/A	N/A	50	30	10	1887.9	18.52	N/A	0.16**	< 0.5
4	Experiment cluster 2-AS-TZ-14			20	20	N/A	N/A	50	30	10	1987.8	19.5	N/A	0.56	1.137
5	Experiment cluster 2-AS-PZ-14			20	20	N/A	N/A	50	30	10	1967.4	19.3	N/A	0.51	0.975
Experiment cluster 3. Artificial soil: clayey sand (SC) with 15% kaolinite clay particles															
6	Experiment cluster 3-AS-NE	Clayey Sand	SC	15	15	N/A	N/A	50	35	9	N/A	N/A	10	0.15**	< 0.5
7	Experiment cluster 3-AS-TZ-7			15	15	N/A	N/A	50	35	9	1795.4	17.62	45	0.5	0.938
8	Experiment cluster 3-AS-TZ-14			15	15	N/A	N/A	50	35	9	1795.4	17.62	90	1.51	9.975
9	Experiment cluster 3-AS-TZ-21			15	15	N/A	N/A	50	35	9	1970.5	19.31	60	0.5	0.938
10	Experiment cluster 3-AS-PZ-7			15	15	N/A	N/A	50	35	9	1767.8	17.34	90	1.49	9.713
11	Experiment cluster 3-AS-PZ-14			15	15	N/A	N/A	50	35	9	1767.8	17.34	60	0.51	0.975
12	Experiment cluster 3-AS-PZ-21			15	15	N/A	N/A	50	35	9	2278.5	22.3	120* 30**	0.53	1.053
Experiment cluster 4. Artificial soil with 15% bentonite clay particles															
13	Experiment cluster 4-AS-NE (bentonite)	Clayey Sand	SC	15	15	N/A	N/A	50	35	27	1903.5	18.67	N/A	1.0	3.5

Experiment cluster 5. Natural soil: silty sand (SP-SM)															
14	Experiment cluster 5-NS-NE	Clayey Sand	SC	42.3	10.6	31.7	54.5	N/A	N/A	29.3	1569.83	15.40	35	0.1**	0.1**
15	Experiment cluster 5-NS-TZ-14			42.3*	10.6*	31.7*	54.5*	N/A	N/A	19.8	2080.5	20.41	60	0.43	0.86
Experiment cluster 6. Natural soil: silty sand with additional 10% kaolinite clay particles															
16	Experiment cluster 6-NS-NE	Silty Sand	SM	30.6	11.2	19.4	69.4	N/A	N/A	13.8	1785.3	17.5	7.5	<0.5	< 1.170
17	Experiment cluster 6-NS-TZ-7			30.6	11.2	19.4	69.4	N/A	N/A	13.8	1707.47	16.74	45	< 0.48	< 0.864
18	Experiment cluster 6-NS-TZ-14			30.6	11.2	19.4	69.4	N/A	N/A	13.8	1732.7	17	120** 45***	< 0.5	< 0.938
19	Experiment cluster 6-NS-PZ-7			30.6	11.2	19.4	69.4	N/A	N/A	13.8	1722.79	16.89	45	0.49	0.9
20	Experiment cluster 6-NS-PZ-14			30.6	11.2	19.4	69.4	N/A	N/A	13.8	1780.7	17.45	120/ 30	0.5	0.938
Experiment cluster 7. Natural soil: clayey soil with additional 20% kaolinite clay particles															
21	Experiment cluster 7-NS-NE	Clayey Sand	SC	40.6	21.2	19.4	59.4	N/A	N/A	16.25	1879.01	18.41	30 ** 22.5***	0.51	0.975
22	Experiment cluster 7-NS-TZ-7			40.6	21.2	19.4	59.4	N/A	N/A	16.25	1765.13	17.30	45	0.97	4.116
23	Experiment cluster 7-NS-TZ-14			40.6	21.2	19.4	59.4	N/A	N/A	16.25	1792.56	17.57	60	1.0	4.375
24	Experiment cluster 7-NS-PZ-7			40.6	21.2	19.4	59.4	N/A	N/A	16.25	1766.42	17.32	45	1.49	11.226
25	Experiment cluster 7-NS-PZ-14			40.6	21.2	19.4	59.4	N/A	N/A	16.25	1809.73	17.74	60	1.98	21.562

* estimated by using the trendline

** dry surface

*** wet surface

5.5. Effect of PermaZyme and TerraZyme on soil erodibility

Both, TerraZyme and PermaZyme, show that they can be beneficially used to improve erodibility at least one type of soil. Enzymes allow to reduce erodibility of the reconstituted soil (Experiment clusters 2 and 3) by one category on the Briaud chart. Figure 133 indicates that the untreated reconstituted soil exhibits high erodibility, meanwhile the TerraZyme and PermaZyme treated soils are in category III (Medium Erodibility). This conclusion is made on the entire erosion function obtained by running erosion test at different velocity to capture the erosion resistance of the soil. No significant erosion improvement is shown by natural soil with an additional 10% clay particles. However, the natural soil with an additional 20% kaolinite particles has proven the effect of both enzymes on soil erodibility (Figure 134).

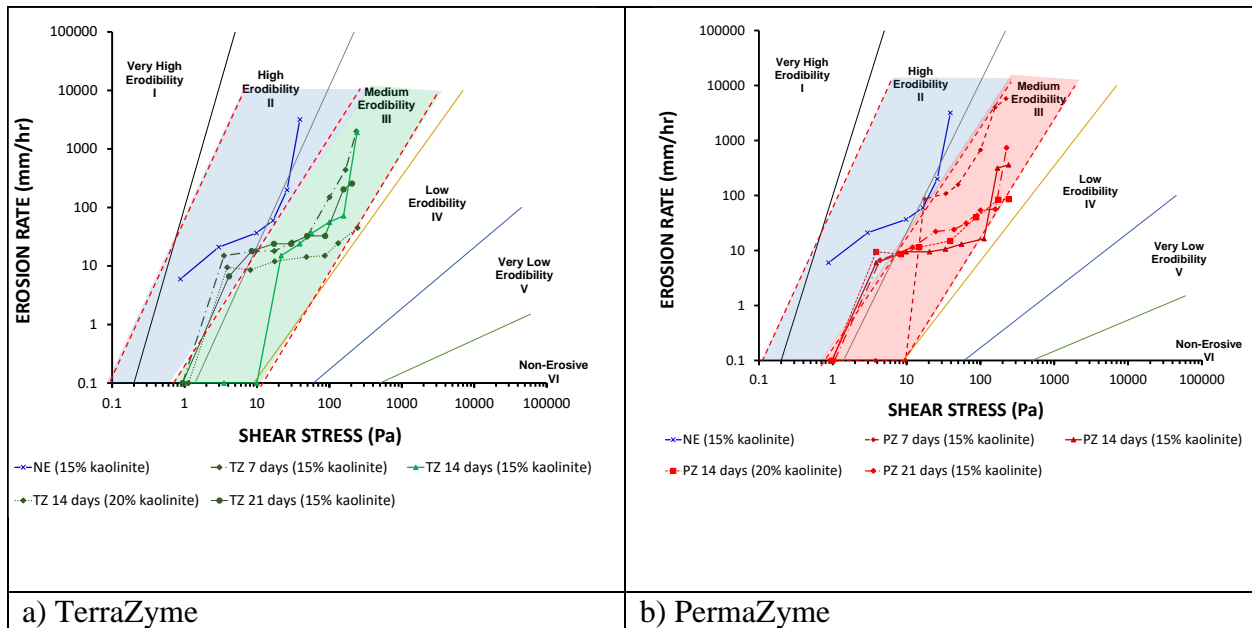


Figure 133. Erosion rate versus shear stress of TerraZyme-treated reconstituted soil (a) and PermaZyme-treated reconstituted soil (b)

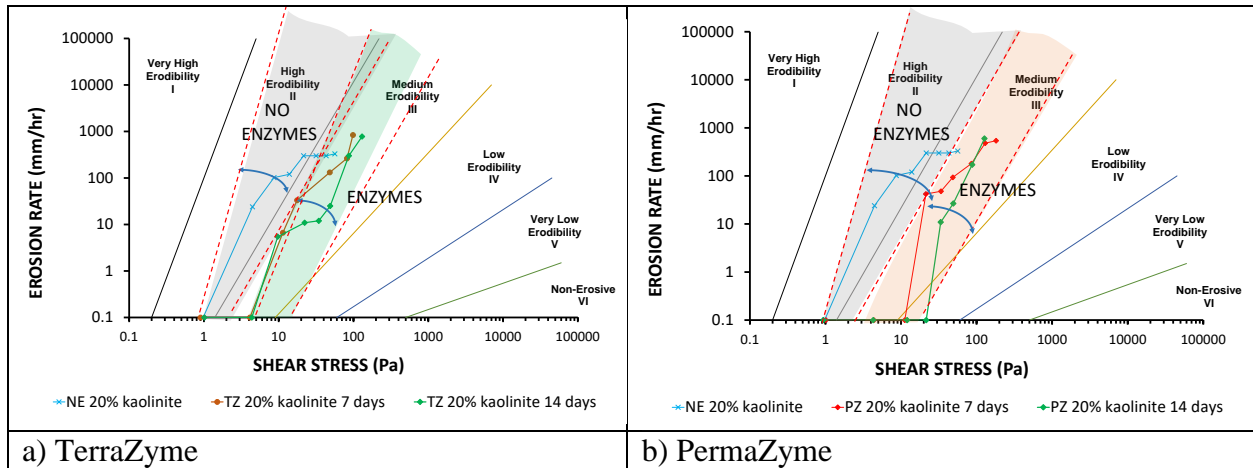
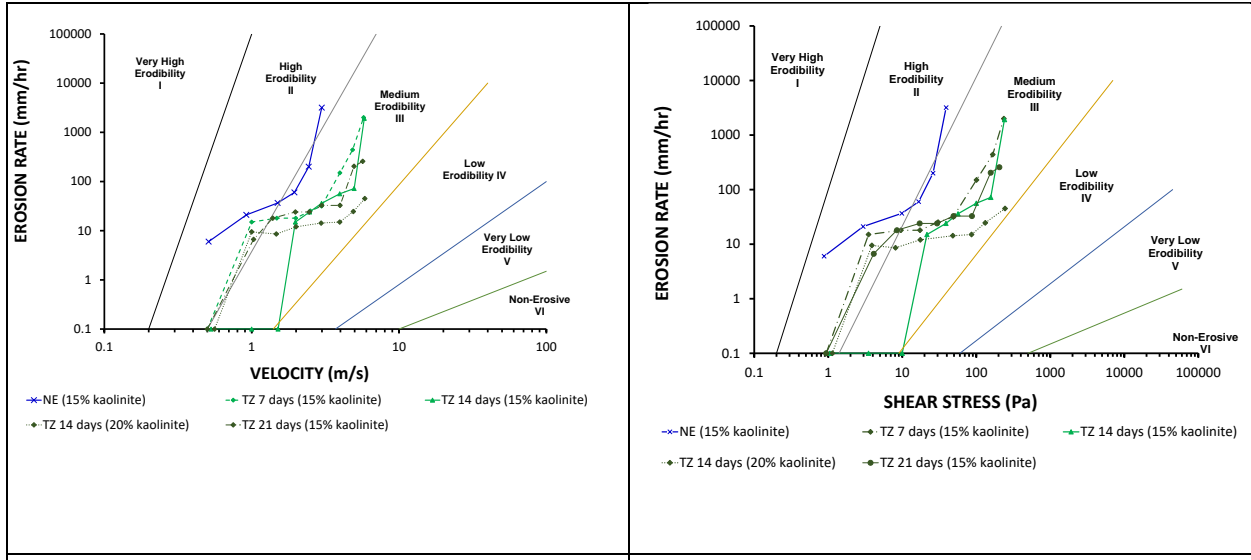


Figure 134. Erosion rate versus shear stress of TerraZyme-treated natural soil (a) and PermaZyme-treated natural soil (b)

It was also noticed from the Experiment 6 and the Experiment 7 that PermaZyme-treated soil typically exhibits less erosion than TerraZyme-treated soil.

5.6. Effect of cure time on erodibility of enzyme-treated soil

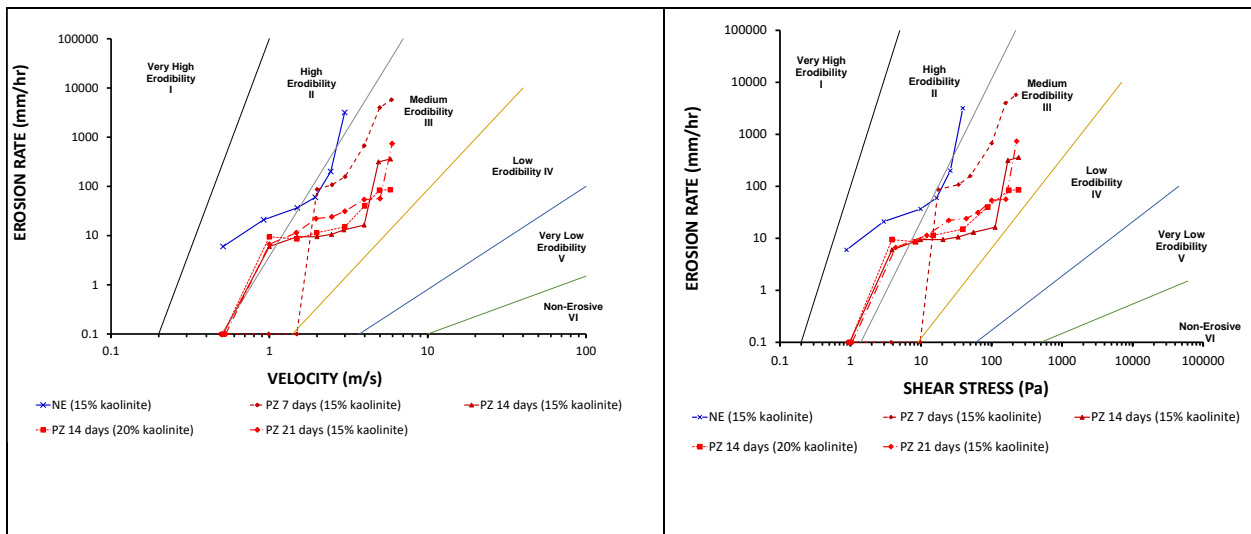
TerraZyme-treated reconstituted soil exhibits no change in erodibility with an increase in cure time: the erosion functions of 7-days, 14-days, and 21-days cured soil are very similar (Figure 135). The critical velocity for almost all tested soils is around 0.5 m/s except the soil treated for 14-days for which it is 1.5 m/s. Meanwhile, the erosion rate above 1.98 m/s is the same as of the 7-days and 21-days treated soil.



a) Erosion rate versus velocity b) Erosion rate versus shear stress

Figure 135. Erosion functions of the 7-days, 14-days, and 21-days TerraZyme-treated reconstituted soil (Experiment cluster 3)

The erodibility of PermaZyme-treated reconstituted soil also appears not to be related to the cure time. Figure 136 shows that the critical velocity of the 14-days and 21-days treated soil is the same (0.5 m/s). Only the 7-days cured soil shows an increase in critical velocity up to 1.5 m/s which is counterintuitive, but the erosion rate is higher than the erosion rate of the 14-days and the 21-days soils.



a) Erosion rate versus velocity b) Erosion rate versus shear stress

Figure 136. Erosion functions of the 7-days, 14-days, and 21-days PermaZyme-treated reconstituted soil (Experiment cluster 3)

In contrary to the reconstituted soil, natural soil with 20% additional clay particles (Experiment cluster 7) indicates an improvement in erosion resistance with the cure time. Both, TerraZyme and PermaZyme showed time-related erosion behavior (Figure 137).

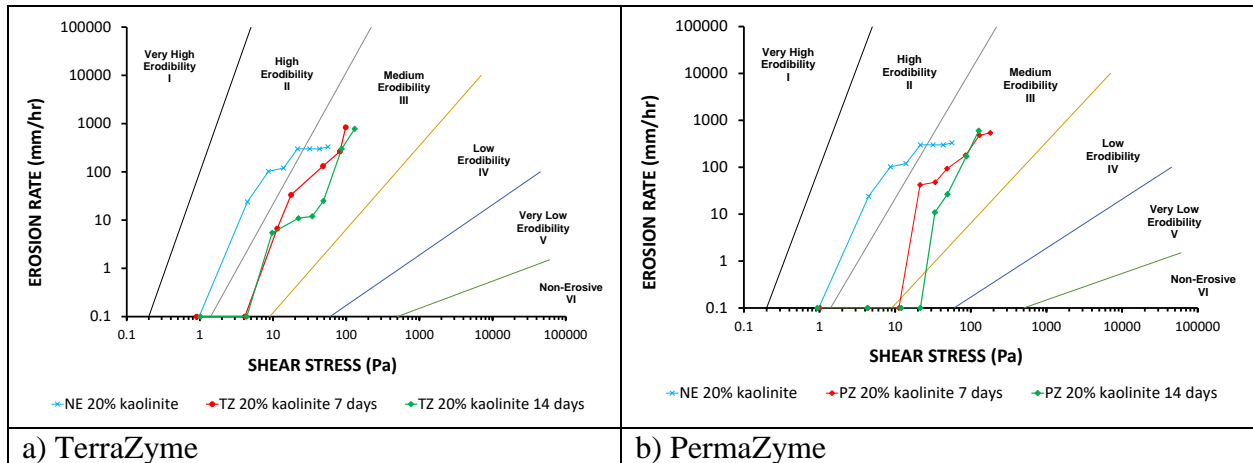


Figure 137. Erosion functions of the 7-days and 14-days TerraZyme- and PermaZyme-treated natural soil (Experiment cluster 7)

5.7. Effect of the amount of clay particles on soil erodibility

The effect of the amount of clay particles on soil erodibility can be seen by comparison the erodibility of the Experiment cluster 6 and the Experiment cluster 7 with the same enzymes and cure time. The cluster have the same composition except the amount of kaolinite clay particles: 10% additional clay particles were added to the soil of the Experiment 6 and 20% to the soil of the Experiment 7. An increase in clay particles from 10% to 20% allowed to improve soil erodibility from high to medium on the erosion chart as well as increase the critical velocity and critical shear stress by two times (Figure 138).

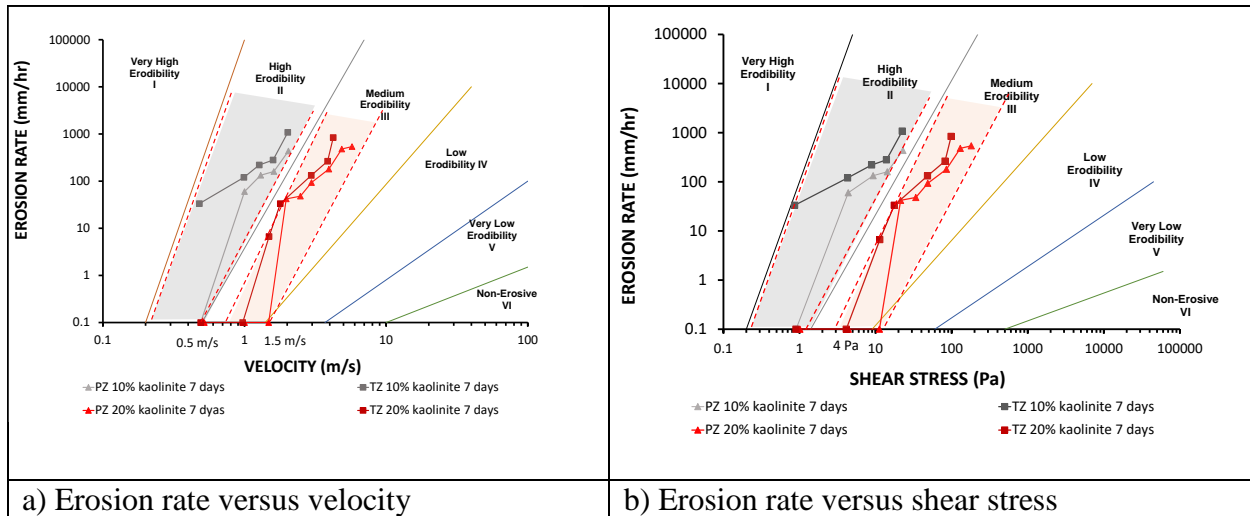


Figure 138. Erosion functions of the natural soil with 10% and 20% additional clay particles (Experiment clusters 6 and 7)

In addition to EFA testing, some samples after being tested in the EFA were placed in water to study the effect of soaking on the sample. It was observed that the samples started to disintegrate into their fine form. The samples were approximately 80% disintegrated in 6 hours. It shows that if the kaolin is exposed to liquid water, it will be reabsorbed and disintegrate into its fine particulate form. This transformation of kaolinite is not reversible due to permanent physical and chemical changes.

6. MITIGATION OF EROSION USING ENZYMES

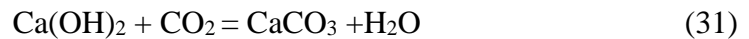
6.1. Existing knowledge on lime treatment

Lime treatment has been used for two major effects on soil: improvement the soil workability and increase the soil strength. Lime in a form of calcium oxide (quicklime) CaO and calcium hydroxide (hydrated lime) $\text{Ca}(\text{OH})_2$ can be applied to a range of soil; however, it performs better in fine-grained soil. According to some studies, a candidate soil for lime treatment of subgrades and bases should possess at least 25 % fine particles (< 0.075 mm) and have a plasticity index of at least 10 (Little, 1999). Lime can be effectively used for clayey soils; it is less effective for a fat clay.

There are two types of lime-treatment technique which lead to soil modification and soil stabilization. Modification occurs in many soils when a low percentage of lime is added, stabilization takes place only when a proper amount of lime is added to a soil to provide a required strength.

In general, lime acts in soil by four consecutive mechanisms: dehydration, cations exchange, pozzolanic reaction, and carbonation. Dehydration reduces the soil capacity to hold water and increases its stability. Cation exchange occurs between the calcium Ca^{2+} supplied by the lime and exchangeable cations supplied by the clay mineral in soil. Lime causes a significant increase in soil pH; in this alkaline environment, clay mineral surface is altered as it reacts with the Ca^{2+} to form cementitious products. As the results of this modification, soil experiences a reduction in plasticity and swelling. Pozzolanic reaction differs modification of soil from stabilization which provides a significant level of long-term strength of stabilized soil (Little, 1995; Little, 1999). Pozzolanic reaction occurs when Ca^{2+} from the lime reacts with the

aluminates and silicates from the clay to form cementitious products such as calcium-silicate-hydrates (CSH) and calcium-aluminate-hydrates (CAH). It was reported that pozzolanic reaction can take many years, if enough lime is present and the pH remains high (11.5-12.5) (Little, 1999). A carbonization occurs when calcium hydroxide Ca(OH)_2 reacts with carbon dioxide in the air and according to the following reaction (Eq. 31):



The key to pozzolanic reaction is a reactive soil and a good mix protocol. The result of lime stabilization is a significant increase in soil modulus (by a factor of 10 or more) and shear strength (by a factor of 20 or more) (Little, 1999). Some research suggests pozzolanic reactions may continue in the long-term for up to 10 years (Kavak and Baykal, 2012).

As a result, an improvement in the soil mechanical properties takes place. The effectiveness of the improvement depends on the amount of lime added, the nature of the soil and its properties, and the curing time (Le Runigo et al., 2011).

Lime can be used in a form of CaO and Ca(OH)_2 . Lime can be added to soils in a form of milk of lime or dry powder depending on the liquidity and plasticity of soils. Typically, 1% to 4% lime by dry weight of soil is used for soil modification (Lime-treated soil construction manual, 2004). To permanently stabilize the soil, up to 12% lime by dry weight of soil can be applied (Le Runigo et al., 2011).

Kavak and Baykal (2012) found that the unconfined compression strength of kaolinite clay stabilized by 4 % lime increased significantly and had a long-term effect. The UCS of improved soil in 28 days was 1,015 kPa, in 10 years - 2,640 kPa compared to pure kaolinite with the UCS of 125 kPa.

Lime-treatment can be considered as permanent and durable technique which has been widely used in road and embankment constructions; however, its use in dams and levees construction is not well studied. Lime-treated soil when they are subjected to water can experience leaching and hence loss of strength. Le Runigo et al. (2011) showed that interaction with water leads to a significant decrease in shear strength of lime-treated silt with 1% and 3% lime to weight. The durability of lime-treated soil used for levees and dams would depend on climate (dry or wet), hydraulic conditions, presumably duration of water flow, water velocity and shear stress at the interface between the water and the soil.

Lime has been used for improving the soils in levees and earth dams in the United States, Europe, and Australia (Herrier and Bonelli, 2015). Use of lime in soil improvement for hydraulic earthworks has been known since the 1970's (Perry, 1977; Garver, 1987; Gutschick, 1978; Gutschick, 1985; Howard and Bara, 1976; Knodel, 1987; Fleming et al., 1992; USBR, 1998; Stapledon, 2005; Nerinx et al. 2016; Bennadi et al., 2016). One of the examples of lime treatment for a hydraulic use is the Friant-Kern irrigation canal in California (Knodel, 1987). For that purpose, quicklime in a range of 2 % to 4 % was applied to the soil to form a lining. The unconfined compressive strength of the treated soil was reported to increase about 20 times compared to the unconfined compressive strength of the untreated soil. The plasticity index reduced from 40 to 10. Unfortunately, no erosion prediction was performed since the canal was supposed to be operated under water during 10 months of a year.

The treatment of soil with lime was reported to solve erosion problems for dispersive soils, to prevent the shrinking and swelling of clay, and, therefore, to stabilize the embankment slopes (Charles et al., 2012; Herrier et al., 2012; Herrier and Bonelli, 2015; Bennabi et al, 2016). The improvement of erosion resistance of a clayey silt treated with 2% lime was examined by

Herrier et al (2012). The soil contained 19% of sand and 30% of clay particles, with a plasticity index of 11. The critical velocity of the non-treated silt was 2 m/s (Figure 139). The critical velocity of the treated silt after 14 days of curing time was around 10 m/s indicating an improvement to erosion up to 5 times. The critical shear stress is found to increase from 53 Pa for the case of untreated soil to 190 Pa for the lime treated soil after 3 days of ageing and to 350 Pa after 14 days of ageing (Figure 139).

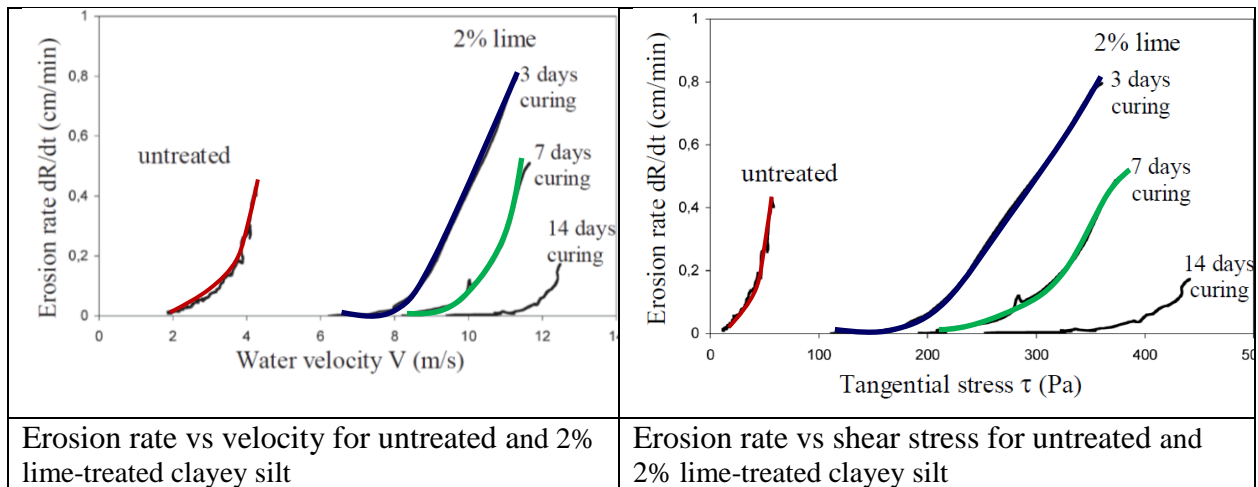


Figure 139. Erosion functions of untreated and lime-treated soil (adapted from Herrier, 2012b)

The erodibility of the lime-treated silty soil (2.5 % of lime) with a 12 % of clay fraction and plasticity index of 7-8 was estimated in the EFA (Bennabi et al., 2016). It was found that the critical shear stress increased from 15 Pa for the non-treated soil to 20 Pa for the treated soil in 7 days of ageing and to 30 Pa in 28 days of ageing (Figure 140). The critical velocity increased from 0.5 m/s for non-treated soil to 3 m/s for the treated soil; a very little difference in critical velocity was observed for the 7 days and 28 days of curing time (Bennabi et al., 2016) (Figure 140).

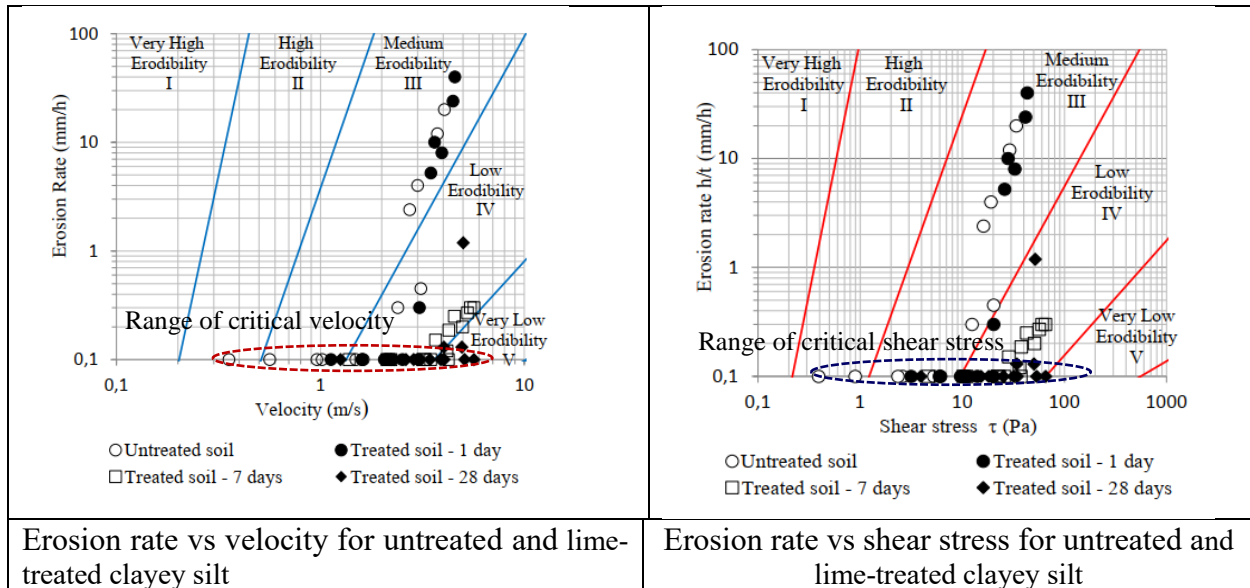


Figure 140. Erosion functions of the untreated and treated soil (adapted from Bennabi et al., 2016)

The erosion category of the silty soil is moved from Category II (High Erodibility) to Category III (Medium Erodibility) and to Category IV (Low Erodibility) and even, in some cases, to Category V (Very Low Erodibility).

An effort to estimate soil erodibility for the full-scale experimental dikes (levees) built out of the silty soil with the 2.5% lime was made in Belgium (Charles et al., 2012). A month later after construction, the critical shear stress increased by at least 7 orders of magnitude from 180 Pa to more than 1200 Pa compared to the non-treated section of the levee.

Lime treatment shows an erosion improvement of the treated soil. However, one should consider a possible lime leaching because of interaction with water containing CO₂.

6.2. Materials and methods

Soil. In this study, two types of soils such as artificially reconstituted soil from locally available particles and natural soil from the field were used to treat with lime. The reconstituted soil (Experiment cluster 1) was made of three groups of particles: 20% kaolinite clay (0.003-

0.005 mm size), 50% finer sand (0.18-0.25 mm size, sieve #60-80), and 30% coarser sand particles (0.85-2 mm size, sieve #10-20). The natural soil from the field (Experiment cluster 2) was classified as silty sand with clay particles. It was ensured that the soil was pulverized using a wooden mallet to break the clods and then sieved through 4.75 mm sieve. The detailed description of each experiment cluster is given in Section 6.3.

Lime. Hydrated lime or calcium hydroxide Ca(OH)_2 in a form of dry powder was used in this study. Hydrated lime is made of quicklime by adding water to turn oxides into hydroxides. Quicklime is a product of a series of physical and chemical processes such as crashing limestone to reduce its size, preheating, calcining, and cooling. Based on the literature review of using lime for erosion control, the lime content to the dry weight of the soil was chosen as 2.5 % for the reconstituted soil and 2.4 % for natural soil.

Methods. For each EFA test, 1 kg of the air-dried soil reconstituted from particles of different size and 1 kg of natural soil were used. One sample of each soil was made without lime to serve as a reference test. The lime and the tap water have been mixed into the soil and then compacted once the soil-lime mixture was considered friable enough. The mellow time, time between the mixing of the lime with the soil and the compaction of the soil-lime mixture, was less than 30 minutes. The untreated and treated samples were molded in the Shelby tubes, compacted with a drop hammer (compaction test hammer). The number of drops for each layer was 10 and the thickness of each layer was 2.5-3 cm. The compacted samples were left exposed to the air for the cure time.

Lime-treated artificially reconstituted soil was kept exposed to the air for a cure time, the elapsed time since the final compaction of the soil-lime mixture, such as 7-days, 14-days, 21-days, and 28 days. Lime-treated natural soil was kept in the Shelby tube in the moisture room

and then tested in the EFA by the end of a cure time such as 7-days, 14-days, 21-days and 28-days cure.

6.3. EFA test plan matrix

EFA testing was performed to study the erosion behavior of lime-treated soil under different velocity and shear stress. The total of ten EFA tests were carried out including two tests performed on untreated (reference) soils and eight on lime-treated soils. Artificial or reconstituted soil from groups of particles and natural soils were chosen for EFA testing.

Artificial soil (Experiment cluster 1) used in this study was reconstituted from locally available particles such as 20 % kaolinite particles, 50 % finer sand particles (0.18-0.25 mm size, sieve #60-80), and 30 % coarser sand particles (0.85-2 mm size, sieve #10-20). Natural soil (Experiment cluster 2) was sampled in the field. Both soils were treated with 2.5 % hydrated lime $\text{Ca}(\text{OH})_2$ and curried for 7, 14, 21, and 28 days. The testing matrix is given in Table 35.

Table 35. Matrix of EFA testing experiment clusters

No	Experiment cluster	Soil Type		Lime	Cure
		1	2	%	days
1	Experiment cluster 1-AS-NL	+		0	0
2	Experiment cluster 1-AS-LM-7	+		2.5	7
3	Experiment cluster 1-AS-LM-14	+		2.5	14
4	Experiment cluster 1-AS-LM-21	+		2.5	21
5	Experiment cluster 1-AS-LM-28	+		2.5	28
6	Experiment cluster 2-NS-NL (SAC5 53-55)		+	0	0
7	Experiment cluster 2-NS-LM-7		+	2.4	7
8	Experiment cluster 2-NS-LM-14		+	2.4	14
9	Experiment cluster 2-NS-LM-21		+	2.4	21
10	Experiment cluster 2-NS-LM-28???		+		28

Soil type: 1 = Artificially Reconstituted Soil (AS); 2 = Natural Soil (NS); NL = No Lime; LM = Lime; 7, 14, 21, 28 – number of curing days.

The description of each experiment cluster is given below.

1. Experiment cluster 1-AS-NL: artificial soil reconstituted from 20 % clay particles (0.003-0.005 mm size), 50 % finer sand particles (0.18-0.25 mm size, sieve #60-80), and 30 % coarser sand particles (0.85-2 mm size, sieve #10-20), untreated.
2. Experiment cluster 1-AS-LM-7: same composition as Experiment cluster 1-AS-NL but treated with hydrated lime for 7 days.
3. Experiment cluster 1-AS-LM-14: same composition as Experiment cluster 1-AS-NL but treated with hydrated lime for 14 days.
4. Experiment cluster 1-AS-LM-21: same composition as Experiment cluster 1-AS-NL but treated with hydrated lime for 21 days.
5. Experiment cluster 1-AS-LM-28: same composition as Experiment cluster 1-AS-NL but treated with hydrated lime for 28 days.
6. Experiment cluster 2-NS-NL: natural soil described as silty sand with clay particles (SM-SC), untreated.
7. Experiment cluster 2-NS-LM-7: same composition as Experiment cluster 2-NS-NL but treated with hydrated lime for 7 days.
8. Experiment cluster 2-NS-LM-14: same composition as Experiment cluster 2-NS-NL but treated with hydrated lime for 14 days.
9. Experiment cluster 2-NS-LM-21: same composition as Experiment cluster 2-NS-NL but treated with hydrated lime for 21 days.
10. Experiment cluster 2-NS-LM-28: same composition as Experiment cluster 2-NS-NL but treated with hydrated lime for 28 days.

6.4. Results of EFA testing

The erosion functions and the erodibility parameters such as critical velocity, critical shear stress, erosion rate for untreated and lime-treated soil were determined using ten EFA tests performed by the end of 7-days, 14-days, 21-days, and 28-days cure periods. The results of EFA testing for each experiment cluster showing the artificially reconstituted soil and the natural soil are discussed below. The erosion behavior of the soil in many cases is complicated and does not allow to properly determine the critical velocity and critical shear stress. Therefore, the entire erosion function to capture the erosion resistance of the material at different velocity and shear stress becomes to be very important. The common erosion behavior of the lime-treated soil is that the soil tends to erode at the edges first and then erosion moves towards the center of the sample. The erosion concentrates on the sample edges until it reaches a certain depth at which a sample or a part of the sample gets detached because of uplift. In some cases, the erosion initiates and progresses through the discontinuities (cracks, boundaries between the layers). This shows the importance of soil-lime mixing and compaction.

Experiment cluster 1-AS-NL. The erosion of the untreated soil was detected during the first velocity step in a form of individual particles detachment at the low velocity and then as chunks of particles detachment at the higher velocities. The critical velocity of the soil was obtained as the value of velocity read from the intersection of the erosion function and horizontal axis and was 0.16 m/s (Figure 141). The critical shear stress was below 0.5 Pa. At the velocity of 2.99 m/s, a big portion of the sample got entrained by the flowing over and the erosion rate exceeded 3000 mm/hr. This indicates a high erodibility of soil (Figure 141).

Experiment cluster 1-AS-LM-7/14/21/28 days. The erosion rate versus shear stress chart shows that lime makes a difference in reconstituted soil erodibility and improves it at least

one category to the right and there is no significant effect of cure time. Figure 141 indicates that the critical velocity of all treated soils is about 1.5 m/s with the corresponding shear stress of about 10 Pa. Figure 142 shows that the critical velocity does not depend on the cure time. The rate of erosion slowed down at the velocity of 2 m/s up to 5 m/s but at the velocity of 5 m/s a thick portion of the sample (about 5 cm thick) got detached and the erosion rate increased significantly up to 1000 mm/hr and more. In fact, all treated soils are in Category III (Medium Erodibility).

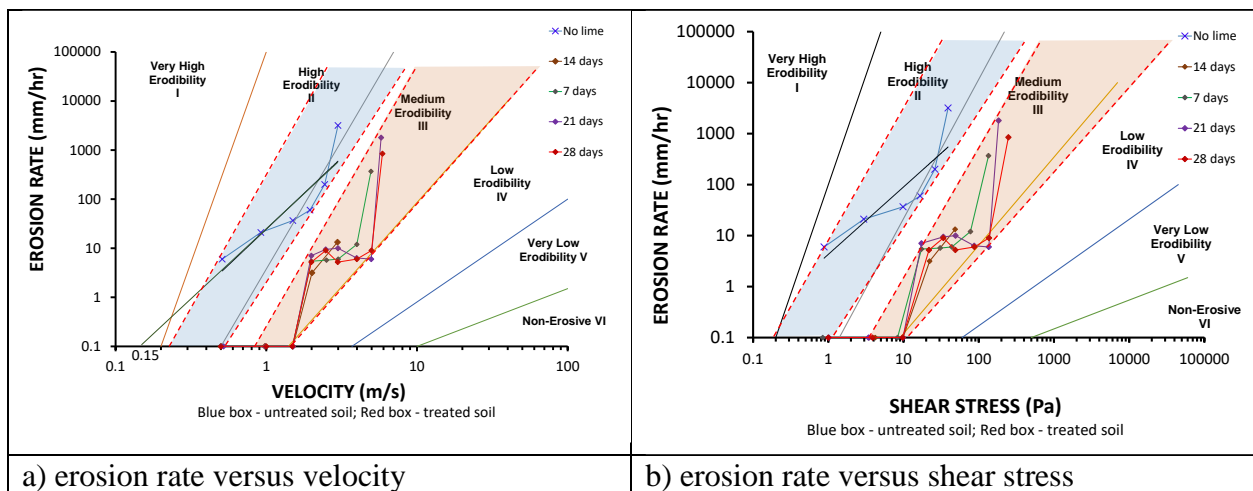


Figure 141. Erosion functions of the Experiment cluster 1-AS-LM

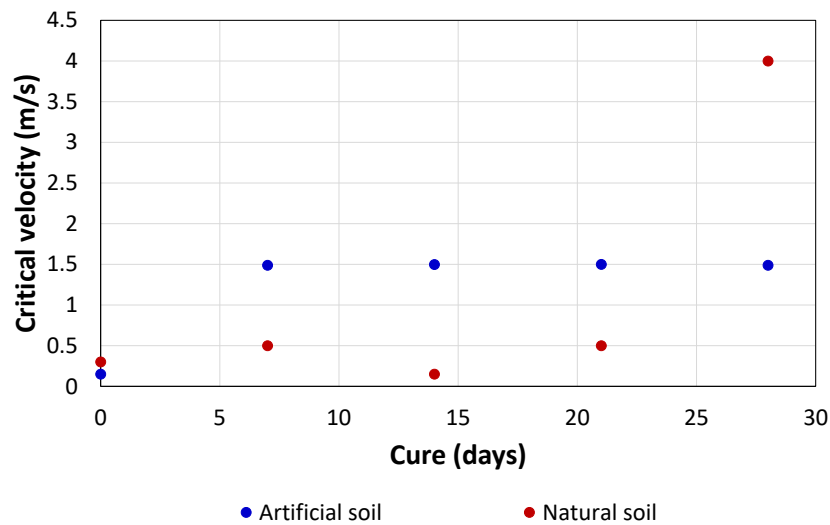


Figure 142. Critical velocity of lime-treated soil versus cure time

Experiment cluster 2-NS-NL. The erosion of the soil was detected at the lowest velocity of 0.3 m/s with the corresponding shear stress of 0.518 Pa in a form of individual particles detachment and mass wasting. The maximum velocity at which the soil was tested in the EFA was 2 m/s when the erosion rate reached about 200 mm/hr. Figure 143 shows the soil erosion surface at velocity of 2 m/s. The untreated soil is in Category II (High Erodibility).

Experiment cluster 2-NS-LM-7/14/21/28-days. Figure 143 shows the erosion function of the 7-days, 14-days, 21-days and 28-days lime treated silty sand. In most cases, the erosion rate decreases with an increase in cure time. No significant improvement for the 7, 14, and 28-days samples in critical velocity and critical shear stress can be concluded from the experiments (Figure 143). The critical velocity of 7-days and 21-days treated soil is the same (0.5 m/s). Meanwhile, the critical velocity of the 14-days cure soil is less than 0.5 m/s which is counterintuitive. This can be related to some disturbance of the sample which happened during the sample preparation and also the fact that the sample after the 7-days cure was left in the EFA and likely soaked in water which weakened the 14-days sample. The 28-days cured soil exhibited much less erosion than the 21-days soil (Figure 143). The 28-days treated soil resists velocity up to 4 m/s. This shows that lime is a slow acting agent when it comes to erosion improvement and can be beneficially used for erosion control after 28-days of cure. Overall, the erodibility of the treated soil is mostly in Category III (Medium Erodibility) (Figure 143).

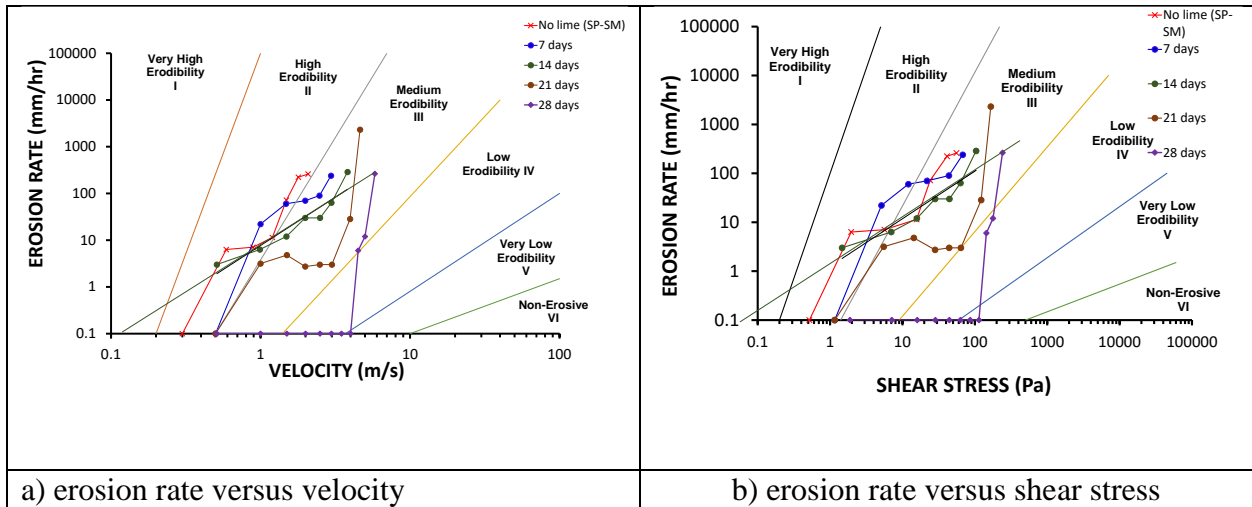


Figure 143. Erosion functions of the Experiment cluster 2-NS-LM

Soil properties of the untreated and lime-treated soils such as water content, dry density, dry unit weight, undrained shear strength, critical velocity and critical shear stress are shown in Table 36.

Table 36. Properties of the untreated and lime treated soils

* Assumed based on the trendline

No	Experiment cluster	Soil	USCS	Particles (%)						Soil Properties						Cure days	Lime %
				Fines (mm)	Clay (mm)	Silt (mm)	Sand (mm)			w _c (%)	ρ _d (kg/m ³)	γ _d (kN/m ³)	S _u (kPa)	v _c (m/s)	τ _c (Pa)		
							0.075-2	0.18-0.25	0.85-2								
Experiment cluster 1. Artificial soil: clayey sand (SC) with 40% kaolinite clay particles																	
1	Experiment cluster 1-AS-NL	Clayey Sand	SC	20	20	N/A	N/A	50	30	15	1692.82	16.61	30	0.15*	0.1*	0	0
2	Experiment cluster 1-AS-LM-7			20	20	N/A	N/A	50	30	15	1692.82	16.61	120	1.49	8.325	7	2.5
3	Experiment cluster 1-AS-LM-14			20	20	N/A	N/A	50	30	15	1692.82	16.61	> 135	1.5	9.831	14	2.5
4	Experiment cluster 1-AS-LM-21			20	20	N/A	N/A	50	30	15	1692.82	16.61	> 135	1.5	9.844	21	2.5
5	Experiment cluster 1-AS-LM-28			20	20	N/A	N/A	50	30	15	1692.82	16.61	> 135	1.49	9.713	28	2.5
Experiment cluster 2. Natural soil: clayey sand (SC) with 20% kaolinite clay particles																	
6	Experiment cluster 2-NS-NL	Silty sand with clay	SM-SC	N/A	N/A	N/A	N/A	N/A	N/A	26.7	1634.7	16.02	22.5	0.3	0.518	0	0
7	Experiment cluster 2-NS-LM-7			N/A	N/A	N/A	N/A	N/A	N/A	19.6	1478.7	14.49	45	0.5	1.156	7	2.4
8	Experiment cluster 2-NS-LM-14			N/A	N/A	N/A	N/A	N/A	N/A	19.6	1478.7	14.49	75	0.15*	0.1*	14	2.4
9	Experiment cluster 2-NS-LM-21			N/A	N/A	N/A	N/A	N/A	N/A	19.6	1478.7	14.49	> 135	0.5	1.156	21	2.4
10	Experiment cluster 2-NS-LM -28			N/A	N/A	N/A	N/A	N/A	N/A	19.6	1478.7	14.49	> 135	4.0	114	28	2.4

The other finding is that soaking the artificial soil for 2 hours caused sample disintegration up to 50 % of the initial volume. Continued soaking for 6 hours led to 80 % loss of the initial sample volume. Presumably, the bonds between kaolinite particles disintegrate when exposed to liquid water for a period of time. This loss of bonding in kaolinite soils is not reversible due to permanent physical and chemical changes.

Soaking the natural soil did not lead to the same extent of disintegration compared with the reconstituted soil.

7. MITIGATION OF EROSION USING RIPRAP

7.1. Existing knowledge on riprap

Riprap is commonly used for scour protection around bridge foundations, for reinforcement of shorelines, streambeds, for protection a dam during a small overtopping event etc. Riprap is rock or other material such as rubble, broken concrete slabs, preformed concrete shapes which is placed on the surface to protect it from erosion. In many instances, the riprap has not performed correctly, and failures do exist. At the bridge pier, this can be due to the soil below the riprap continuing to scour away. On the abutment slope or the downstream face of a dam, this can be due to the riprap failing the slope because of the added weight from the riprap. There is also a need to estimate an importance and a performance of a filter, granular or geosynthetic. Granular filter is chosen on a basis of grain size criterion which must prevent from piping. The function of geotextile filter fabric is to provide both drainage and filtration; it is found to be less expensive compared to a granular filter.

Briaud et al. (2008) summarized the EFA data combined with other soil erosion measurements to plot critical velocity and critical shear stress versus mean grain size for different soil and rock including riprap (Briaud et al., 2008). Figure 144 indicates that critical velocity v_c for 30 mm in size riprap would be approximately $v_c = 1.5$ m/s and for 270 mm - $v_c = 7$ m/s. The corresponding shear stress shown in Figure 145 is $\tau_c = 50$ Pa and $\tau_c = 130$ Pa.

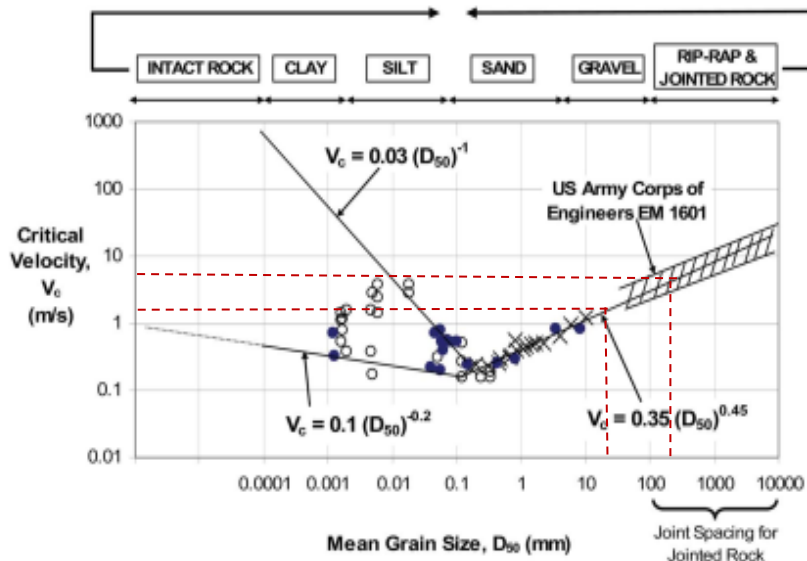


Figure 144. Critical velocity versus mean grain size (adapted from Briaud et al., 2008)

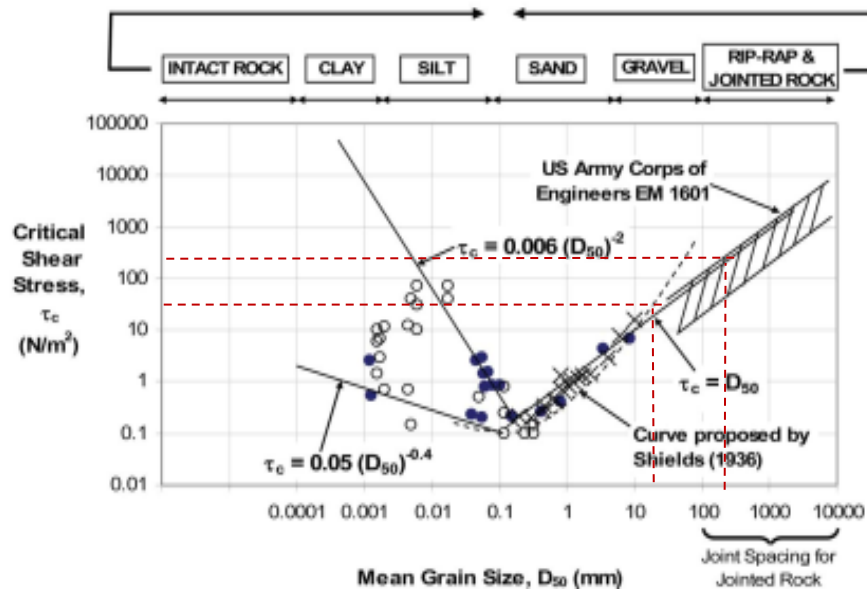


Figure 145. Critical shear stress versus mean grain size (adapted from Briaud et al., 2008)

A series of the full-scale field overtopping experiments with riprap was conducted at Colorado State University (CSU) (Abt et al., 1987; Abt and Johnson, 1991;

Frizell et al., 1997). In 1987 and 1988, overtopping testing was performed at the Engineering Research Center of Colorado State University (CSU) on the steep embankment slopes (> 0.10) and on flat surfaces (< 0.10). Riprap was placed on sand which was overlaid by the geofabric (Abt and Johnson, 1991). For the case of the flat surface (0.02), riprap of D50=2.6 cm and 7.6 cm thick failed at the flow rate varying from $0.00164 \text{ m}^3/\text{s}$ to $0.00689 \text{ m}^3/\text{s}$ which was calculated knowing that the flow at riprap failure was $q=0.1-0.42 \text{ m}^3/\text{s-m}$ and the length of the flume was 61 m (Abt and Johnson, 1991). For the case of steeper slope (0.10), riprap of D50 = 10.2 cm and 30.5 cm thick failed at the flow rate varying from $0.006-0.0064 \text{ m}^3/\text{s}$ (for $q = 0.33-0.35 \text{ m}^3/\text{s-m}$ and the flume length was 55 m).

In 1994, 1995, and 1997, more overtopping testing was performed in the Overtopping Facility at CSU in Fort Collins on riprap placed on the 2:1 slope (Frizell et al., 1998). In 1994, the riprap with D50 of 386 mm was placed 0.6 m thick over a 203-mm-thick gravel bedding material. In 1995, a 0.6 m thick layer of relatively uniformly graded rock with D50 of 655 mm was placed over the existing material left from the testing performed in 1994. Most rocks were dumped into the flume. In 1997, bedding with a D50 of 48.3 mm and riprap with a D50 of 271 mm was installed. The data provided for the testing performed in 1997 showed that the average interstitial velocity in riprap was 0.7 m/s. The critical velocity was approximately 1.5 m/s calculated using the discharge $0.2 \text{ m}^3/\text{s/m}$ for 3 m wide flume with a water depth of 0.8 m and the length of the riprap of 18 m.

Some laboratory testing on riprap with a goal to establish a depth-discharge relationship for riprap on a basis of a laboratory scale model channel was performed by Eli and Gray in 2008. Unfortunately, they do not provide the critical parameters for the riprap which can be used for comparison.

There is a need to estimate the critical velocity and critical shear stress of riprap with a filter and without a filter to make sure that riprap performs as planned which would allow to save money by avoiding sustained maintenance or replacement.

7.2. Materials and methods

The materials and soils chosen for the study and their characteristics are presented below.

Gravel/riprap. Since riprap cannot be tested in the EFA, gravel was chosen to represent riprap. It is referred as “gravel/riprap”. The biggest gravel used in the EFA was 30 mm gravel. Considering that the average riprap is about 0.5 m, a scale factor of gravel/riprap would be 1:16. Coarse gravel of sedimentary origin was used in EFA testing. The gravel passed 75-mm sieve and was retained on 19-mm sieve. The range of the gravel size varied from 25 mm to 30 mm. The dry unit weight of gravel was approximately 14.5 kN/m^3 . Figure 146 shows gravel in the Shelby tube before EFA testing.

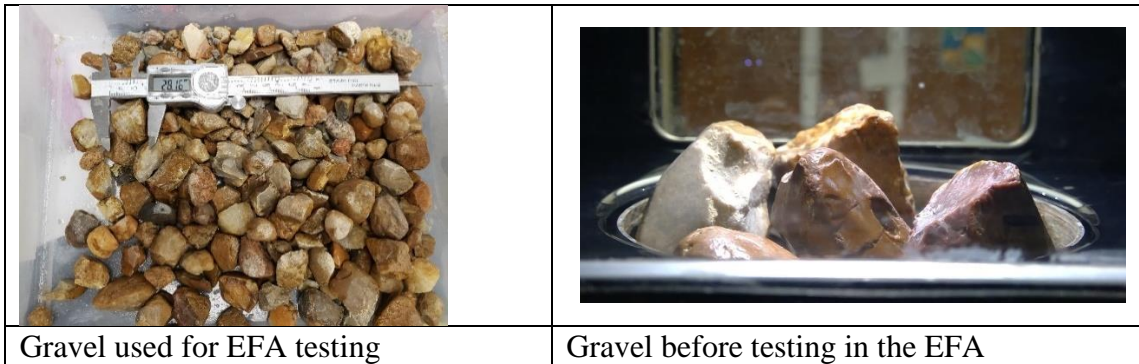


Figure 146. Photograph of gravel used for EFA testing

Geotextile filter. SoilTain PP 105/105DW, manufactured by Huesker, was available as a geotextile filter for EFA testing (Figure 147). Properties of geotextile SoilTain PP 105/105DW are given in Table 37. An effective opening size of the geotextile fabric was 0.24 mm; the permeability claimed by the manufacturer was 20×10^{-3} m/s. It is assumed that DW stands for DeWatering and PP stands for Polypropylene. Huesker recommends that SoilTain is used for coastal and bank protection and can be installed as a ballast layer or large-size geosynthetic containers filled with sand or other soil to prevent from erosion ([Huesker, 2020](#)). The geotextile filter was placed on the top of sand and clay. Note that the geotextile filter was not anchored in the soil below.

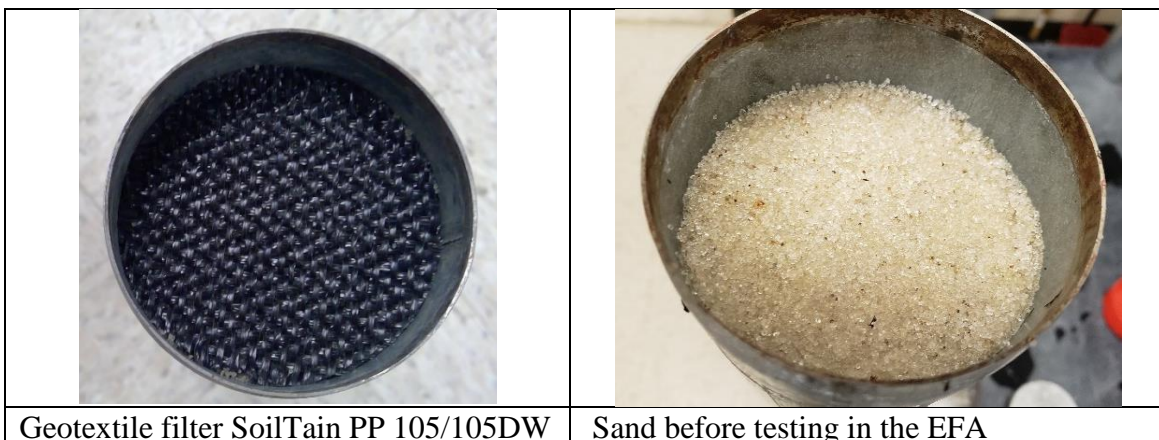


Figure 147. Photograph of geotextile and sand used for EFA testing

Table 37. Properties of geotextile SoilTain PP 105/105DW (adapted from Huesker, 2020)

Type of Geotextile	SoilTain PP 105/105DW
Material	Woven PP for dewatering applications, polypropylene
Opening Size	240 μm
Water Permeability Index Normal to the Plane	20×10^{-3} m/s
Standard Dimensions: Width x Length	5.20 x 200.0 m
Weight	≈ 440 g/m ²
Ultimate Tensile Strength: Longitudinal x Transversal	≥ 105 kN/m
Application	Dewatering, Tailings Dam Embankment Construction.

Sand. Sand was classified in accordance with USBR 3900 Standard Definitions of Terms and Symbols Relating to Soil Mechanics used for filed soil description as a medium sand passed No. 10 (2.00-mm) sieve and retained on No. 40 (425- μm) sieve (USBR, 1990). Sand was a clean dry and uniform slightly compacted by using a Proctor test, received 10 blow counts, and was built in 4-5 cm thick layers (Figure 147). The initial water content was 5 %.

Clay. Clay was a brownish lean clay with a grain size showing in Figure 148. The clay properties are presented in Table 38

Table 38.

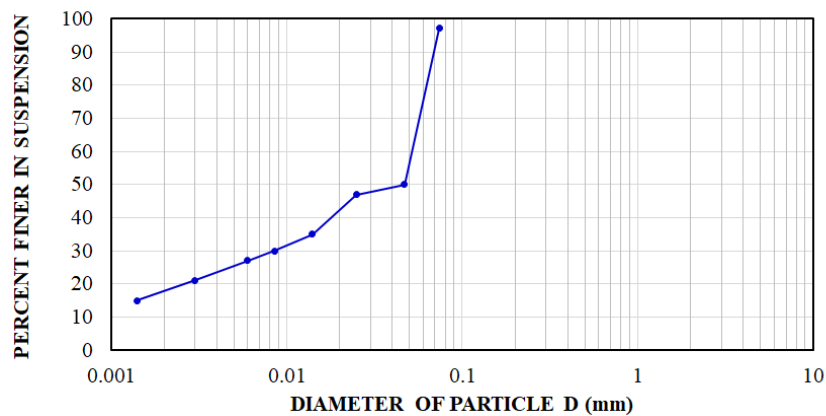


Figure 148. Grain size distribution curve for clay

Table 38. Properties of clay

Properties	Units	Lean Clay
Sand particles	%	2.6
Silt particles	%	72.2
Clay particles	%	25.0
Water Content (before EFA), w_c	%	36.8
Water Content (after EFA), w_c	%	51.4
Unit Weight, γ	kN/m ³	16.3
Liquid Limit		45
Plastic Limit		24
Plasticity Index, PI		21
Undrained Shear Strength (PPT) s_u	kPa	0
Undrained Shear Strength (PPT) s_u	kPa	10
PET (Pocket Erodrometer)	mm	1

7.3. EFA test plan matrix

The total of twelve EFA tests were carried out. Two tests as the reference erosion tests were performed on sand and clay only to determine their erosion parameters. Two reference tests were run on gravel only which was used to represent riprap in the EFA experiments. For the further examination, gravel was placed on sand and clay forming from one to several layers. One to three layers of gravel/riprap were used on sand. Only one layer of gravel/riprap was used on clay. To enhance the erosion of soil underneath the gravel/riprap, a geotextile filter was placed between the natural soil and gravel/riprap to either protect or stabilize the soil from erosion. To study the effect of a filter on soil erodibility, two tests were performed. First test was with one layer of gravel/riprap placed on a geotextile filter underlined by sand. Second test was carried out on one layer

of gravel/riprap placed on a geotextile filter underlined by clay. Table 39 shows the matrix.

Table 39. Matrix of EFA testing Experiment clusters

No	Experiment cluster	Soil Type		Geotextile Type	Gravel
		Sand	Clay		
1	Experiment cluster 1-S (sand)	+			
2	Experiment cluster 1-S-1R Test 1	+			1 layer +
3	Experiment cluster 1-S-1R Test 2	+			1 layer +
4	Experiment cluster 1-S-2R	+			2 layers +
5	Experiment cluster 1-S-3R	+			3 layers +
6	Experiment cluster 1-S-GTF1-1R Test 1	+		SoilTain PP 105/105DW	+
7	Experiment cluster 1-S-GTF1-1R Test 2	+		SoilTain PP 105/105DW	+
8	Experiment cluster 2-C (clay)		+		
9	Experiment cluster 2-C-1R		+		+
10	Experiment cluster 2-C-GTF1-1R		+	SoilTain PP 105/105DW	+
11	Experiment cluster 1-R (riprap) Test 1				+
12	Experiment cluster 1-R (riprap) Test 2				+

S = Sand; R = gravel-riprap (1R = 1 layer of riprap, 2R = 2 layers of riprap, 3R = 3 layers of riprap);

GTF – Geotextile Filter; C = Clay; Experiment cluster 1 = sand Experiment cluster; Experiment cluster 2 = clay Experiment cluster

The erosion testing followed the same procedure as those of other EFA testing described in Section 3.4. The constant velocity steps were chosen with 0.3 m/s increment in velocity until a failure was observed.

The erosion behavior of twelve experiment clusters was difficult to predict due to their complex structure consisted of a layer of natural soil (sand or clay), geotextile

filter, and layers of gravel/riprap. In this dissertation an effort is made to consider erodibility of the complex experiment clusters while considering erosion behavior of each layer.

7.4. Results of EFA testing

The purpose of EFA testing was not only to obtain erosion characteristics of Experiment clusters such as critical velocity, critical shear stress, erosion rate etc. but also to qualitatively study the erosion mechanism for each Experiment cluster. Visual observations were performed during each test which can be helpful for understanding the erosion phenomenon.

Experiment cluster 1-S: Sand

The Experiment cluster consisted of a 15 cm thick sand with an initial water content $w_c = 15\%$. Erosion occurred at the first velocity step ($v = 0.29$ m/s) and continued up to $v = 1.0$ m/s when the EFA test was stopped because of excessive erosion. A scour hole was initiated at $v = 0.6$ m/s and continued to increase at the higher velocity. During the EFA test, the erosion rate increased from 14 mm/hr to 1440 mm/hr with an increase in velocity. Excessive erosion of the sand was observed at $v=0.72$ m/s when the erosion rate reached 660 mm/hr and then gradually increased with an increase in velocity. The critical velocity of sand was less than $v_{cs} = 0.29$ m/s with a corresponding critical shear stress of $\tau_{cs} = 0.347$ Pa. The erosion function on Figure 149 shows that the sand is in the Category I (Very High Erodibility) to Category II (High Erodibility).

Experiment cluster 2-C: Clay

The Experiment cluster was formed of a 15 cm thick lean clay with a unit weight of 16.3 kN/m³. Erosion occurred at a velocity of $v_{cc} = 0.7$ m/s at which small flocks of clay particles (approximately 0.5 mm in size) started to detach from the erosion surface. At a velocity of $v = 0.9$ m/s, erosion progresses on bigger flocks and aggregates varying from 2 mm to 5mm. The corresponding critical shear stress of a lean clay was $\tau_{cc} = 1.96$ Pa. The erosion function on Figure 149 shows that the lean clay is in the Category II (High Erodibility).

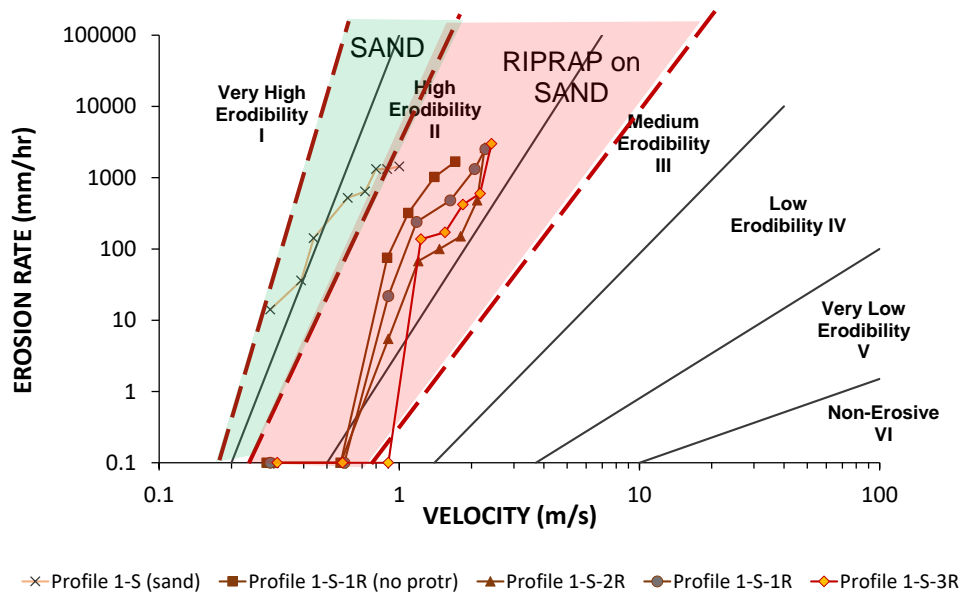


**Figure 149. Erosion rate versus velocity for Experiment cluster 1
Experiment cluster 1-R Test 1 and Test 2: Gravel/riprap**

The Experiment cluster was made of a 10 cm thick coarse gravel/riprap used to represent riprap. Two tests were run to check the repeatability of the tests. The conditions of Test 1 were repeated in Test 2. Figure 150 shows the erosion functions for gravel/riprap. The critical velocity at which the gravel/riprap got detached was $v_{cg} = 0.74$

m/s and $v_{cg} = 0.94$ m/s for Test 1 and Test 2 respectively. The corresponding critical shear stress of that gravel/riprap was $\tau_{cg} = 9.788$ Pa and $\tau_{cg} = 15.794$ Pa for Test 1 and Test 2 respectively. The gravel/riprap is intermediate between Category II (High Erodibility) and Category III (Medium Erodibility) (Figure 150).

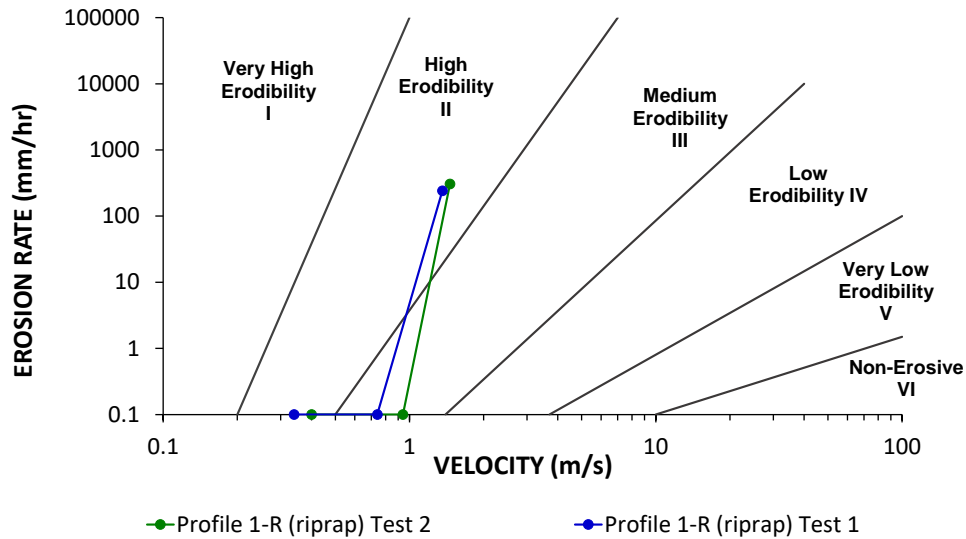


Figure 150. Erosion rate vs. velocity for Experiment clusters 1-R in logarithmic scale

Experiment cluster 1-S-1R/2R/3R: Sand+1-2-3 layers of gravel/riprap

These experiment clusters were made up of one to three layers of gravel/riprap placed on medium sand. The original goal of adding layers of gravel/riprap on sand was to check if additional layers of gravel/riprap would decrease and possibly arrest the erosion of the sand through the gravel/riprap. However, not much erosion improvement was obtained by adding layers of gravel/riprap. The critical velocity and the critical shear stress corresponding to the point at which erosion of the sand was initiated below the gravel/riprap (initiation of erosion) and the critical velocity and critical shear stress

corresponding to the point at which the gravel/riprap failed were determined (Figure 149).

In the case of one layer of gravel/riprap (approximately 30 mm thick) on top of the sand, the following observations were made. When the velocity reached a level twice as high as the critical velocity of the sand ($v_{cs} = 0.29$), some sand particles started to move up through the voids of the gravel/riprap and were eroded away. This process continued and intensified as the velocity increased. During that increase, the gravel/riprap started to shake and roll ($v = 0.9$ m/s). Then the flow velocity reached the critical velocity of the gravel/riprap at which point some got detached ($v_{cr} = 1.09 - 1.18$ m/s). Other gravel/riprap had sunk into the sand. In this case, the critical velocity at which the gravel/riprap failed was twice as high as the critical velocity at which the erosion on the sand particles was initiated.

In the case of two layers of gravel/riprap (approximately 60 mm thick) on top of the sand, the observations were very similar to the case above except the critical velocity was somewhat different. However, similar to the case of one layer of gravel/riprap on the top of the sand, the erosion occurred on sand particles first ($v_{cs} = 0.57 - 0.59$ m/s), then it progressed to the gravel/riprap ($v_{cr} \geq 0.9$ m/s). It shows that two layers of the gravel/riprap do not improve the erodibility of the sand and the gravel/riprap.

In the case of three layers of gravel/riprap (approximately 90 mm thick) on top of the sand, the observations were again similar with slightly different values of the critical velocity. The critical velocity of gravel/riprap was $v_{cs} = 0.9$ m/s and $v_{cg} = 1.23$ m/s. Even with three layers of gravel/riprap, the sand still erodes through the gravel/riprap. This

showed that when there is no filter, the sand would erode through the voids in the gravel/riprap.

Experiment cluster 2-C-1R: Clay + 1 layer of gravel/riprap

This Experiment cluster consisted of one layer of the gravel/riprap on top of the lean clay. Before a velocity of $v = 0.9$ m/s, no erosion was observed. At a velocity of $v_{cc} = 0.9$ m/s, small flocks of clay particles started to erode through the gravel/riprap which failed at a velocity of $v_{cr} = 1.78$ m/s. The critical velocity of the gravel/riprap on the top of the clay is happened to be higher than the critical velocity of the gravel/riprap on the top of the sand which varied from 0.9 to 1.23 m/s. The difference recorded between these two cases could be due to the cohesion between clay and gravel/riprap and/or the shape and arrangement of the gravel/riprap in the EFA tube. Erosion in the EFA is a surficial shearing process where the shearing area is determined at a contact area between gravel/riprap and clay. This Experiment cluster is in Category II (High) to Category III (Medium) Erodibility (Figure 151).

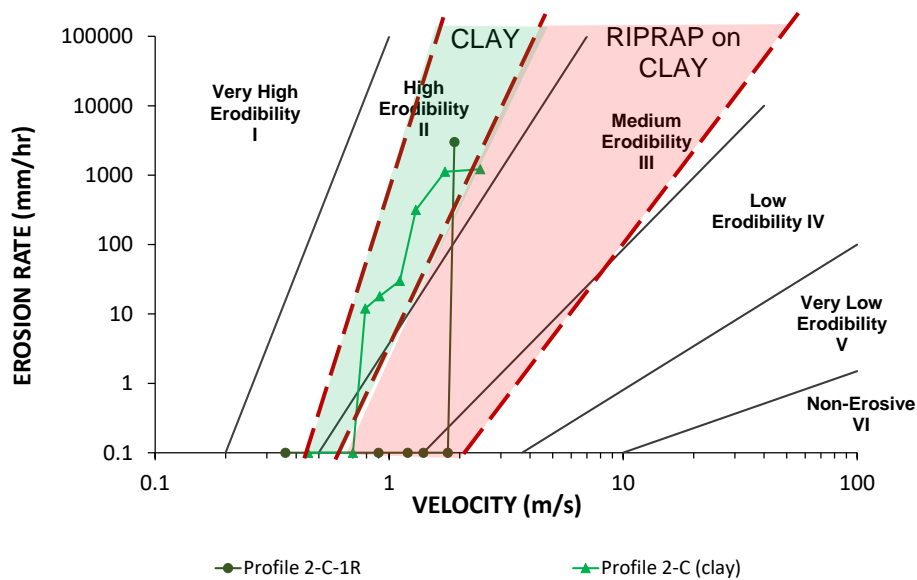


Figure 151. Erosion rate versus velocity for Experiment cluster 1 (no filter)

Experiment cluster 1-S-GTF1-1R-Test 1: Sand + Geotextile Filter + 1 layer of gravel/riprap

The Experiment cluster consisted of (bottom to top) a 10 cm thick sand, the geotextile filter SoilTain PP 105/105DW, and gravel/riprap with an average size of $D_{50} = 30$ mm. The gravel/riprap was placed in one layer (approximately 30 mm thick) consisting of five stones protruding in the flume about $\frac{1}{2}$ of their diameter above the floor of the EFA conduit. The gravel/riprap was forced, squeezed, and wedged into place solidly; this will be called the “wedged” arrangement.

No erosion was observed until a velocity $v_{cs} = 1.19$ m/s at which sand particles started to move through the openings of the geotextile filter. The erosion of sand was initiated at the center of the sample and continued slowly until the gravel/riprap failed followed by a filter uplift failure at a velocity $v_{cg} = 4.88$ m/s. The filter eroded away in

one piece due to the fact that it was not solidly anchored in the soil below. One of the reasons for the gravel/riprap to remain in place even at a high velocity is that the gravel/riprap ended up leaning against the wall of the steel Shelby tube (Figure 152). This significantly increased the value of the critical velocity and the critical shear stress.

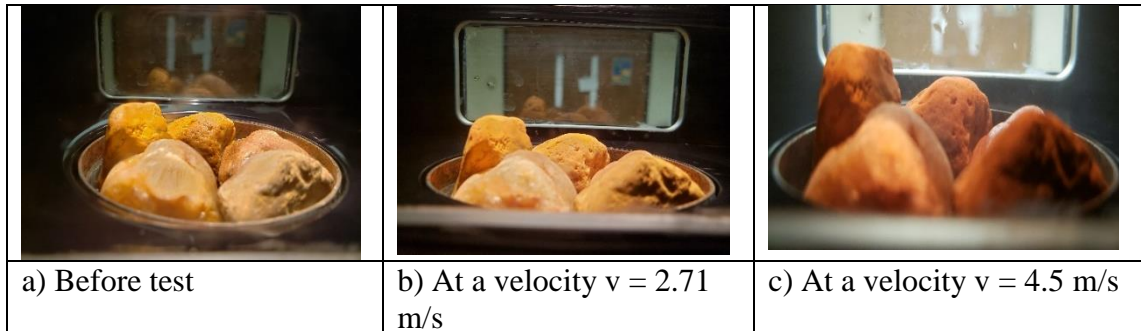


Figure 152. Photographs of the Experiment cluster 1-S-GTF1-1R. Test 1.

Experiment cluster 1-S-GTF1-1R-Test 2: Sand + Geotextile Filter + 1 layer of gravel/riprap

This Experiment cluster was similar to the Experiment cluster 1-S-GTF1-1R-Test 1 except the gravel/riprap had a loose arrangement as there was space between particles. A loosely placed piece of gravel/riprap was detached on the downstream face of the EFA tube and washed away when the flow was initiated at a velocity of 0.37 m/s. The other two pieces of gravel/riprap were detached at velocities of 1.15 m/s and 1.47 m/s. From a velocity of 1.47 m/s to 2.48 m/s, only one piece of gravel/riprap remained on the erosion surface until it got entrained followed by a geotextile filter failure. Failure of the gravel/riprap has been attributed to uplift on the geotextile filter at a velocity of $v = 2.88$ m/s (Figure 153). It is likely that the geotextile filter failed because it was not anchored solidly in the soil below. Drastic erosion of the sand occurred after the geotextile filter

failed and the test was stopped. It was observed during the erosion test that prior to failure, the gravel/riprap was shaking and rotating.

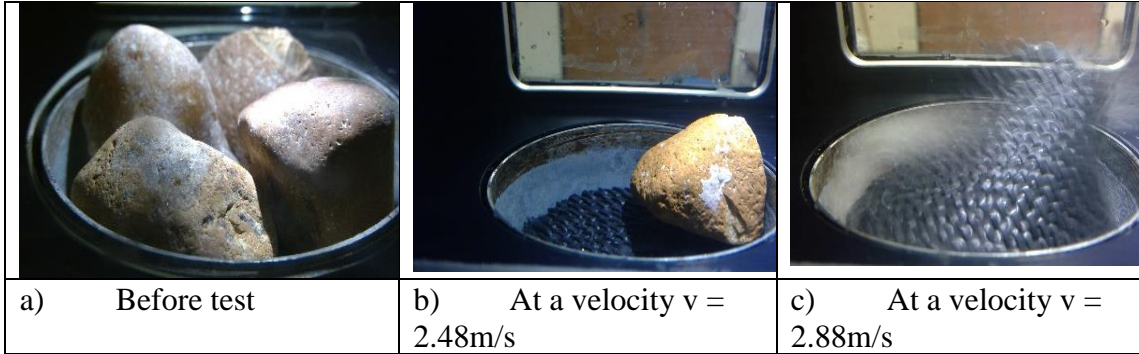


Figure 153. Photographs of the Experiment cluster 1-S-GTF1-1R. Test 2.

The two tests performed with the loose and “wedged” arrangement of gravel/riprap show the influence of the arrangement on the magnitude of the critical velocity. The loose arrangement gave a velocity of $v = 1.15 \text{ m/s}$ on average while the “wedged” arrangement gave a velocity of $v = 5.8 \text{ m/s}$.

Experiment cluster 2-C-GTF1-1R: Clay + Geotextile filter + 1 layer of Gravel/riprap

The Experiment cluster consisted of (bottom to top) 10 cm of lean clay, the geotextile filter SoilTain PP 105/105DW, and the gravel/riprap placed on the filter with an average size D_{50} of about 30 mm. The gravel/riprap was placed as one layer consisting of four stones protruding in the flume about $\frac{1}{2}$ of their diameter. The gravel/riprap was round shaped and placed in a loose arranged. Erosion of the clay occurred at a velocity of $v_{cs} = 0.9 \text{ m/s}$. The first stone of gravel/riprap got entrained at a velocity of $v_{cr} = 1.19 \text{ m/s}$; the second stone failed at $v = 1.49 \text{ m/s}$. The other two stones remained on the erosion surface until the geotextile filter got uplifted at a velocity of $v =$

5.44 m/s at the upstream where were no gravel/riprap support. The filter did not fail completely because of the gravel/riprap support at the downstream face of the sample. The last velocity of the test was $v = 6.48$ m/s. A hole in a form of a scour (approximately 9 cm deep) was measured after the test was stopped (Figure 154). It shows that erosion of clay took place under the filter, however, the filter did not fail. It is somewhat the engineers should be aware of while considering erosion of gravel/riprap and its design. Figure 155 indicates that geotextile filter allows to improve clay erodibility from high to low.

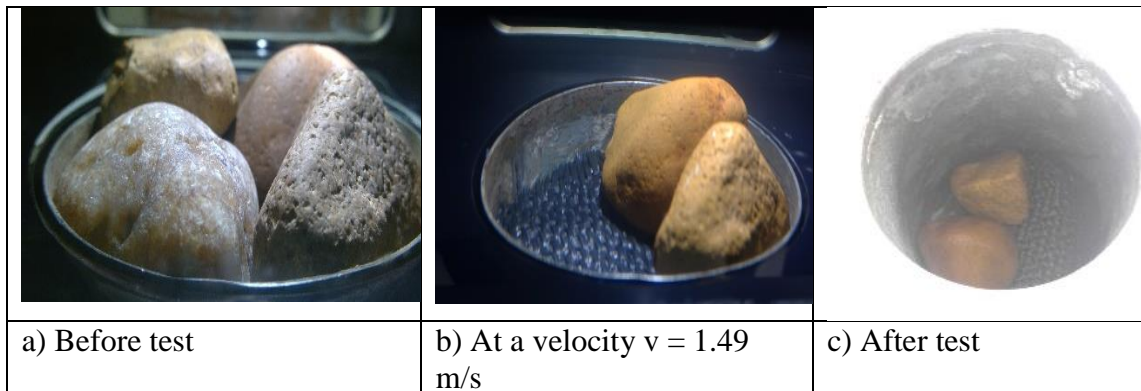


Figure 154. Photographs of the Experiment cluster 2-C-GTF1-1R

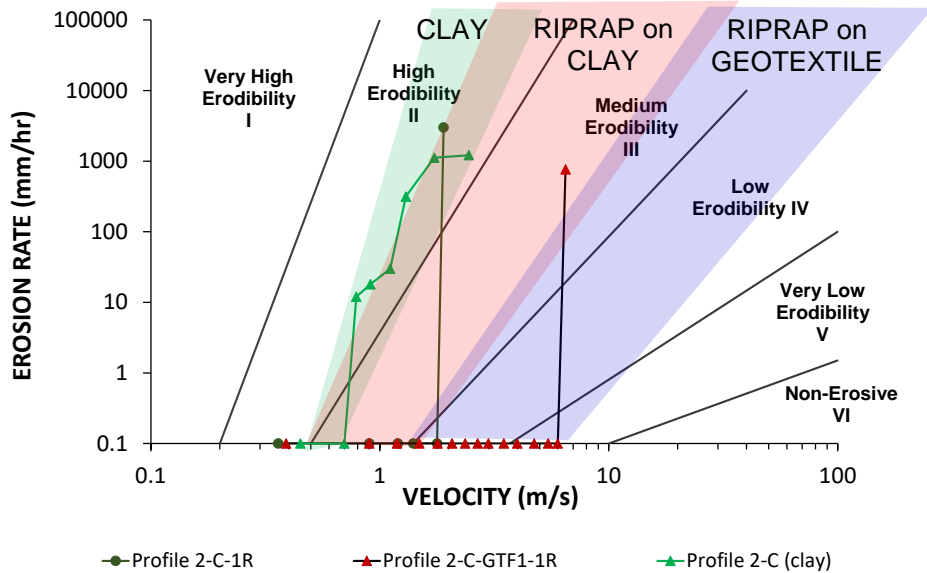


Figure 155. Erosion rate versus velocity for Experiment cluster 2 (with filter)

7.5. Summary of EFA testing

Most of the EFA tests indicate the same general behavior of the gravel/riprap experiment clusters: negligible to slight erosion in the beginning until erosion rate increases when the shear stress reaches its critical value at which erosion progresses rapidly and sample finally fails. One exception is the sand sample (Experiment cluster 1-S) which started to erode at the $v = 0.3$ m/s. Figure 156 and Figure 157 show erosion rate versus velocity and erosion rate versus shear stress in natural scale for all tests. Some erosion improvement while using gravel/riprap can be observed. However, much more improvement in erosion is demonstrated by using a geotextile filter and one layer of gravel/riprap.

The erosion functions are shown in Figure 158 and Figure 159. The green box is the sand by itself. The red box is the riprap on sand or clay with no filter. The blue box is

the gravel/riprap with geotextile filter on sand or clay. The results indicate that gravel/riprap improves erodibility of natural soil. However, a filter is needed to decrease erodibility of soil compared to a case with no filter. The Experiment clusters with the geotextile filter (1-S-GTF1-1R and 2-C-GTF1-1R) are in Medium (III) to Low (IV) Erodibility. The general behavior of soils with a geotextile filter allows to bring the erosion category from Category II (High) to Category III (Medium) and for some cases to Category IV (Low) Erodibility (Figure 158 and Figure 159).

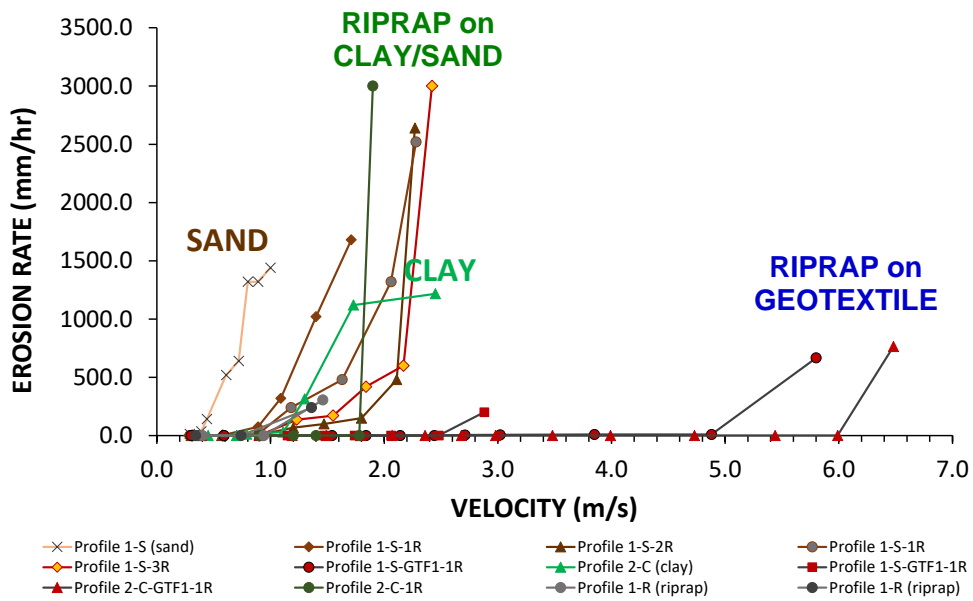


Figure 156. Erosion rate vs. velocity in natural scale for all EFA tests

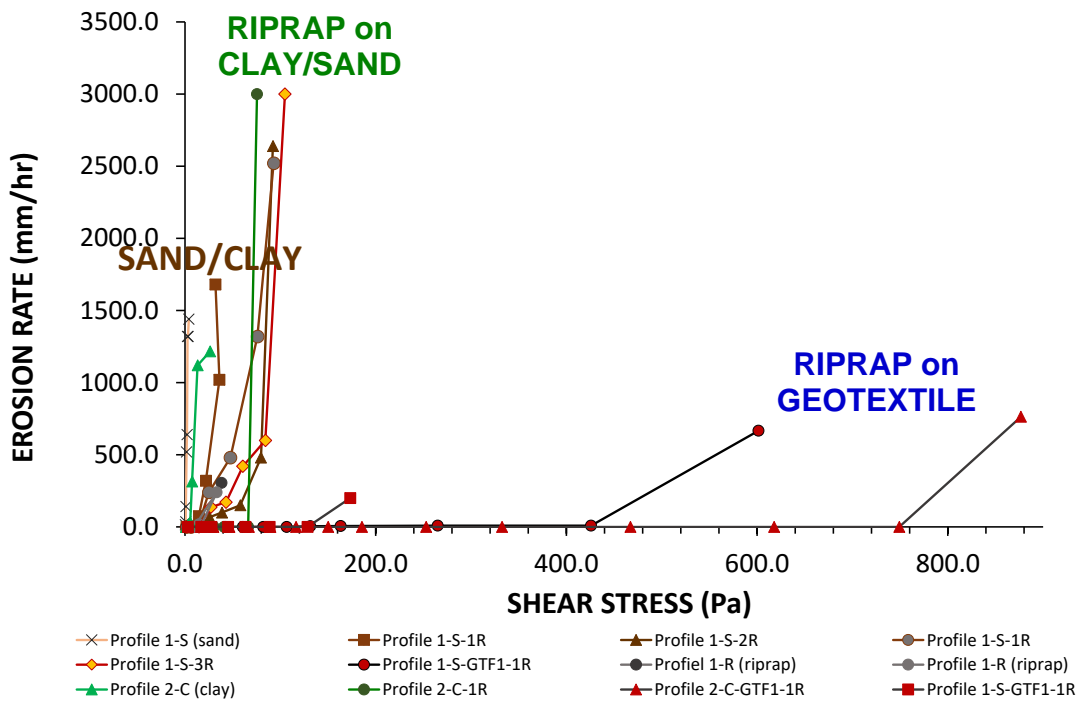


Figure 157. Erosion rate vs. shear stress in natural scale for all EFA tests

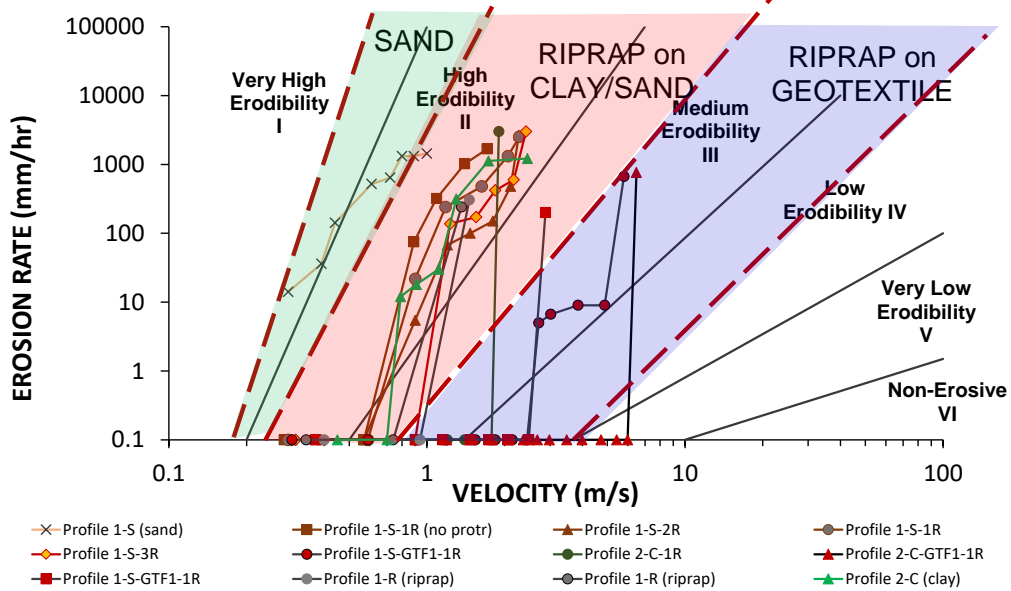


Figure 158. Erosion rate vs. velocity in logarithmic scale for all EFA tests

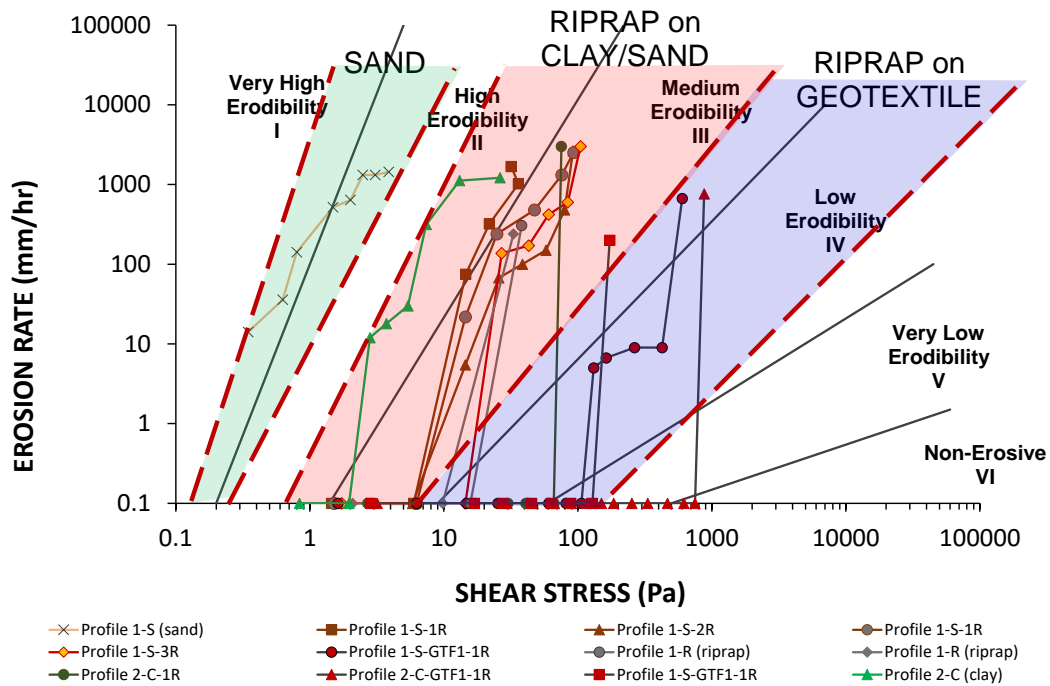


Figure 159. Erosion rate vs. shear stress in logarithmic scale for all EFA tests

Table 40 indicates the critical velocity and the critical shear stress for each test obtained for the points at which erosion was initiated on natural soils and when gravel/riprap followed by a filter failed. Initiation of erosion corresponds to a point when sand particles or clayey flocks were observed in the water above the erosion surface. At that point, the piston was not necessary pushed up unless it was a visual evidence of erosion and downward settlement of the sample during the test. Note that soil erodibility is not an exact number but a whole erosion function such as erosion rate versus velocity or erosion rate versus shear stress (Figure 158 and Figure 159).

Table 40. Erosion parameters of all samples

Experiment cluster	Duration (h)	Critical Velocity v_c (m/s)		Critical Shear Stress τ_c (Pa)	
		Initiation of Erosion	Riprap	Initiation of Erosion	Riprap or Geotextile Failure
Experiment cluster 1-S (sand)	0.47	0.29	-	0.347	-
Experiment cluster 1-S-1R Test 1	0.53	0.57	1.09	5.970	21.831
Experiment cluster 1-S-1R Test 2	0.38	0.59	0.9	6.266	14.479
Experiment cluster 1-S-2R	0.88	0.57	0.9	5.848	14.479
Experiment cluster 1-S-3R	0.4	0.9	0.9 - 1.23	14.479	14.479 - 27.043
Experiment cluster 1-S-GTF1-1R Test 1	1.47	1.19*	4.88	25.313	425.682
Experiment cluster 1-S-GTF1-1R Test 2	0.62	0.9*	1.15	16.909	27.607
Experiment cluster 2-C (clay)	1.00	0.70	-	1.96	-
Experiment cluster 2-C-1R	0.44	0.9**	1.78	16.909	66.140
Experiment cluster 2-C-GTF1-1R	1.43	0.9**	1.19	16.909	29.561
Experiment cluster 1-R (riprap) Test 1	0.44	-	0.94	-	15.794
Experiment cluster 1-R (riprap) Test 2	0.41	-	0.74	-	9.788

* slight erosion on sand particles; ** slight erosion on clay particles

7.6. Effect of compaction and wedging on soil erodibility

Two tests were performed with one layer of gravel/riprap on top of the geotextile filter which was placed on the top of the sand. The only difference between the two tests was the arrangement of the gravel/riprap. In the first test the gravel/riprap was tightly packed and had the “wedged” arrangement and in the second, gravel/riprap was loosely laid and had the loose arrangement (Figure 160). The critical velocities of the

gravel/riprap were $v_{cr} = 4.88$ m/s and $v_{cr} = 1.15$ m/s for the “wedged” and loose arrangement of the gravel/riprap respectively. Stability of the gravel/riprap appears to depend on the contacts between the stones. Failure cannot occur until these contacts are overcome; the critical velocity (detachment velocity) in this case reaches $v = 4.88$ m/s. Failure of the gravel/riprap with no interconnected contacts was observed at much less velocity $v = 1.15$ m/s.

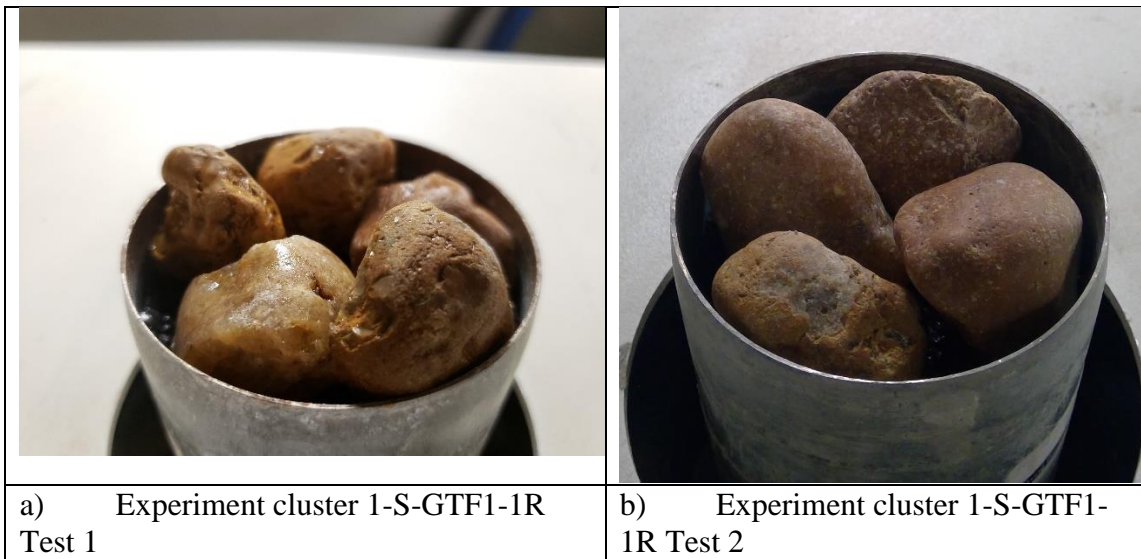


Figure 160. Difference between the “wedged” arrangement (a) and the loose arrangement (b)

7.7. Effect of gravel/riprap thickness on soil erodibility

Effect of thickness of gravel/riprap on its erodibility is shown in Figure 161. The erosion rate versus velocity chart indicates that even several layers of gravel/riprap do not prevent the sand from eroding through the riprap. Erosion of the sand initiated at $v_{cs} = 0.6 - 0.9$ m/s. The critical velocity of the sand with no gravel/riprap on top is $v_{cs} \leq 0.290$ m/s. Therefore, the gravel/riprap increases the critical velocity of sand but not much.

Erosion of gravel/riprap started at a velocity of $v = 0.9 - 1.23$ m/s. Figure 162 shows that

despite the thickness of gravel/riprap, it is in intermediate between Category II (High Erodibility) and Category III (Medium Erodibility).

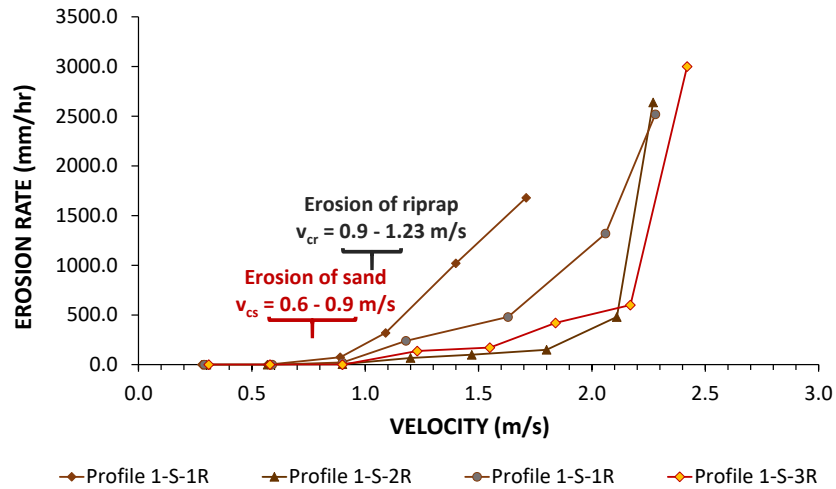


Figure 161. Erosion rate vs. velocity for Experiment clusters 1-S-1R/2R/3R in natural scale

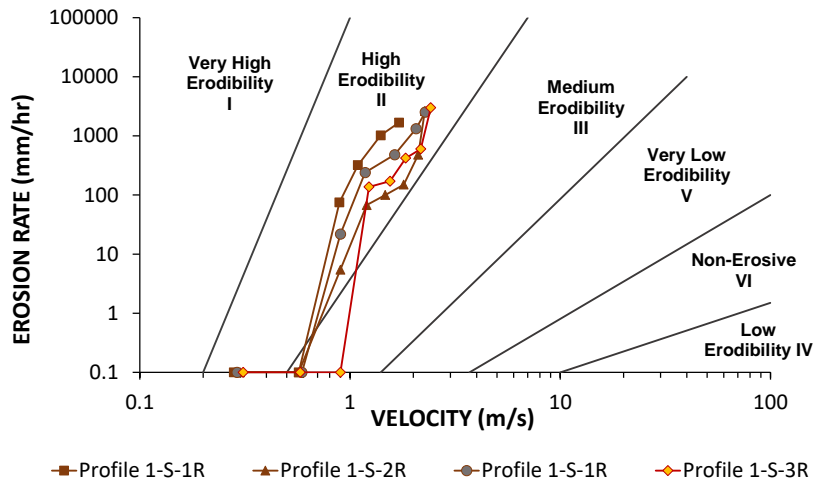


Figure 162. Erosion rate vs. velocity for Experiment clusters 1-S-1R/2R/3R in logarithmic scale

7.8. Effect of geotextile filter on soil erodibility

The effect of the geotextile filter placed on the top of the natural soil (sand or clay) and covered with one layer of the gravel/riprap was considered in the tests

Experiment cluster 1-S-GTF1-1R and Experiment cluster 1-C-GTF1-1R. Figure 163

shows a substantial improvement; indeed, using the geotextile filter reduces soil erodibility and can be successfully used to minimize soil erosion. Use of the geotextile filter allows to move erodibility from High Erodibility (II) to Medium Erodibility (III) and Low Erodibility (IV) (Figure 163 and Figure 164). However, to check whether the results of EFA testing are applicable to a field scale, full scale tests are needed. The conclusion is that the gravel/riprap without the filter does not work even with several layers of gravel/riprap. The geotextile filter under the gravel/riprap improves that problem. However, observations and results of EFA testing suggest that the risk of uplift failure of the filter becomes significant when the gravel/riprap is detached, and the average velocity of flow exceeds 5-6 m/s. In one case, the geotextile filter failed due to uplift; a velocity was 2.88 m/s after the gravel/riprap got entrained.

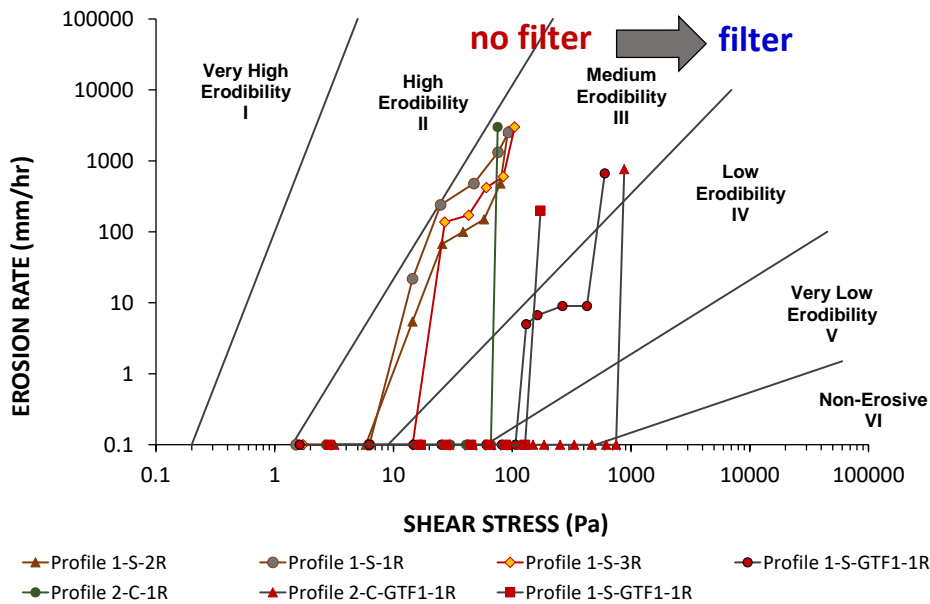


Figure 163. Erosion rate vs. shear stress in logarithmic scale with no filter and with filter

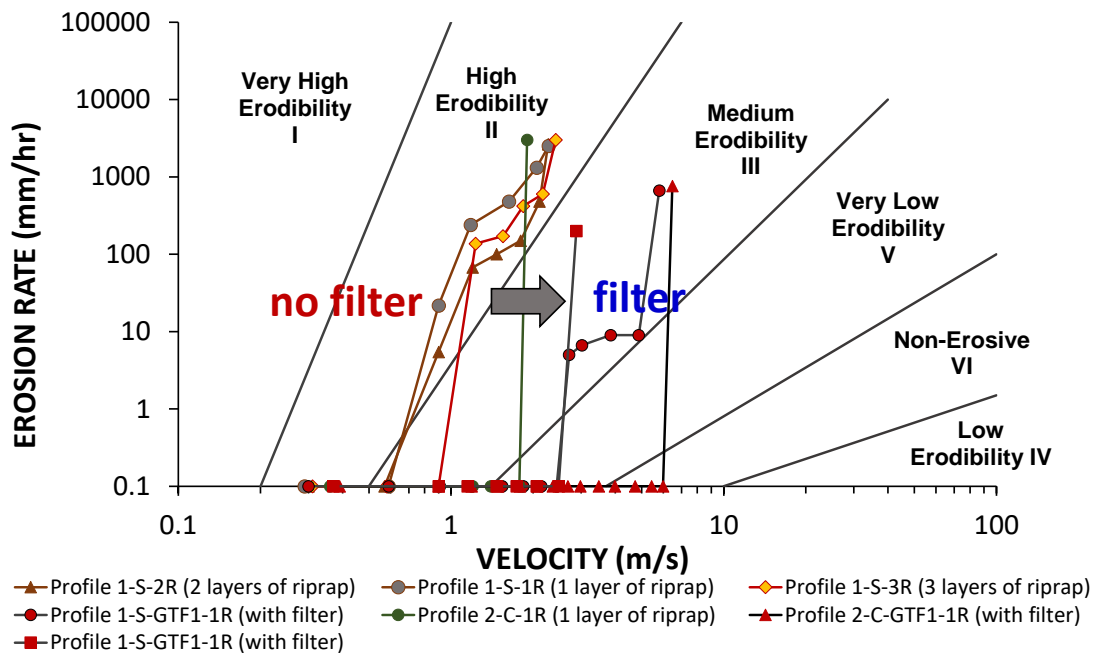


Figure 164. Erosion rate vs. velocity in logarithmic scale with no filter and with filter

7.9. Comparison of EFA and full-scale tests

In this Section, an effort is made to compare erodibility of gravel/riprap based on the EFA results with erodibility of riprap obtained from full-scale testing. There are limited data available for the comparison. Field full-scale testing of loosely arranged riprap on the 2:1 slope with the mean grain size of 271 mm was performed in the Overtopping Facility at Colorado State University in 1997. It was concluded (See Section 7.1. for more details) that the critical velocity of riprap was approximately 2.0 m/s. The critical velocity from Briaud chart (2008) for the same size gravel is 3 times higher than the one from the full-scale test. The critical velocity of gravel increases to 6 m/s (Figure 165). The difference in critical velocity from Briaud (2008) and the full-

scale test (1997) is likely to be the effect of the slope; in Briaud chart the slope is flat, in the full-scale test the slope was 2:1. However, more research should be done to verify the results.

Meanwhile, the critical velocity of gravel obtained from Briaud chart can be compared to the critical velocity of gravel/riprap from EFA testing for the same conditions. Briaud (2008) showed that the critical velocity of 30 mm gravel is $v = 1.5$ m/s, EFA testing of 30 mm gravel indicates the critical velocity $v = 1.15$ m/s (Figure 165).

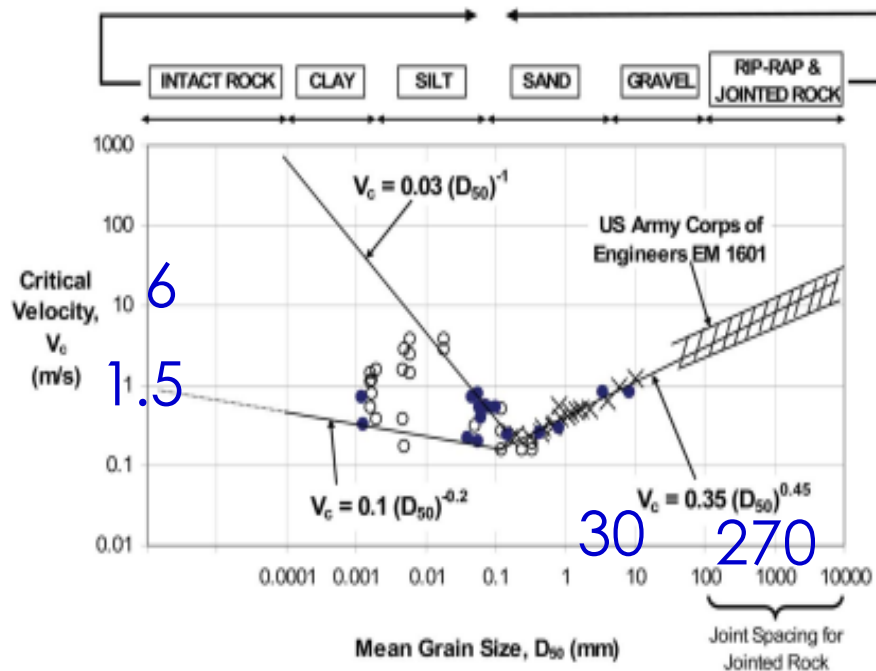


Figure 165. Critical velocity versus mean grain size (adapted from Briaud, 2008)

8. NEW EROSION MODEL AND APPLICATION

8.1. Existing knowledge on soil erosion models and classifications

The erosion models and erosion charts are useful to compare soil erosion classifications. Despite the number of existing soil models and classifications, no unified approach to classify soil erodibility has been achieved so far. There are two existing erosion models and classifications used to classify soil and rock erodibility: Hanson and Briaud.

The Hanson chart (Hanson and Simon, 2001, 2002) is based on recognizing that different soils have different erosion functions. It considers that these erosion functions can be represented by a linear model with a slope k_d and a critical shear stress τ_c (Figure 166).

$$\dot{z} = k_d (\tau - \tau_c) \quad (32)$$

where \dot{z} is the erosion rate (cm/s or mm/hr), k_d is the erodibility coefficient ($\text{cm}^3/\text{N}\cdot\text{s}$), τ_c is the critical shear stress (Pa).

The slope of the erosion function k_d and the critical shear stress τ_c are the parameters plotted on the chart and one erosion function is represented by one point on the chart (

Figure 167). The boundaries between soil erodibility on the Hanson chart are set as straight lines in the logarithmic space where k_d increases with τ_c which is counter intuitive as k_d should decrease when τ_c increases. The equations for the boundary lines are of the form:

$$k_d = n(\tau_c)^m \quad (33)$$

where m is the slope of the boundary line.

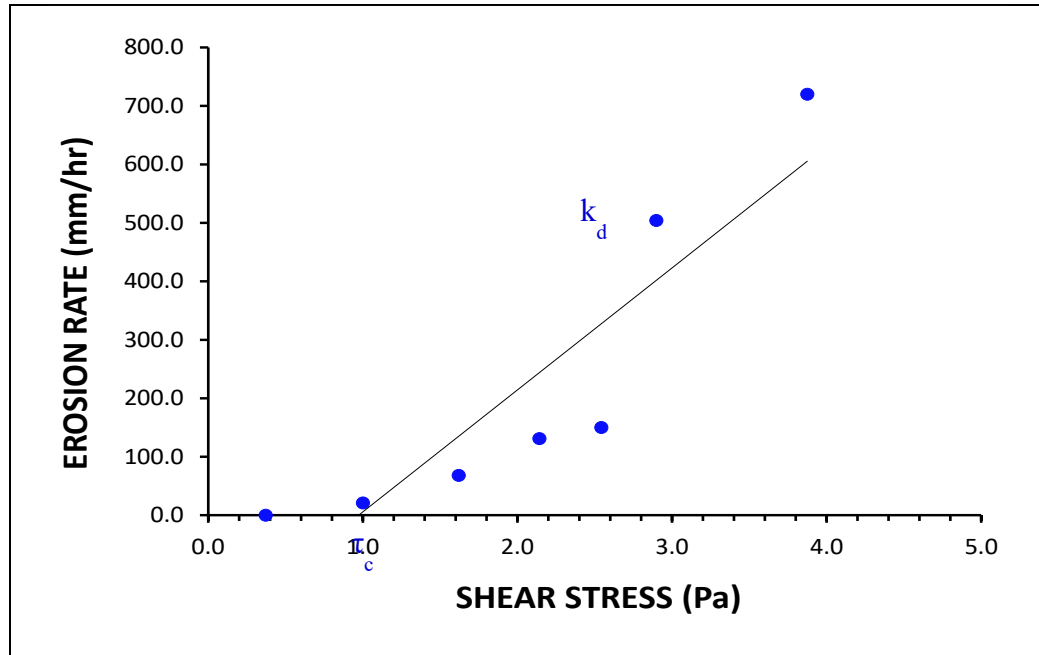


Figure 166. Erosion function with erosion parameters

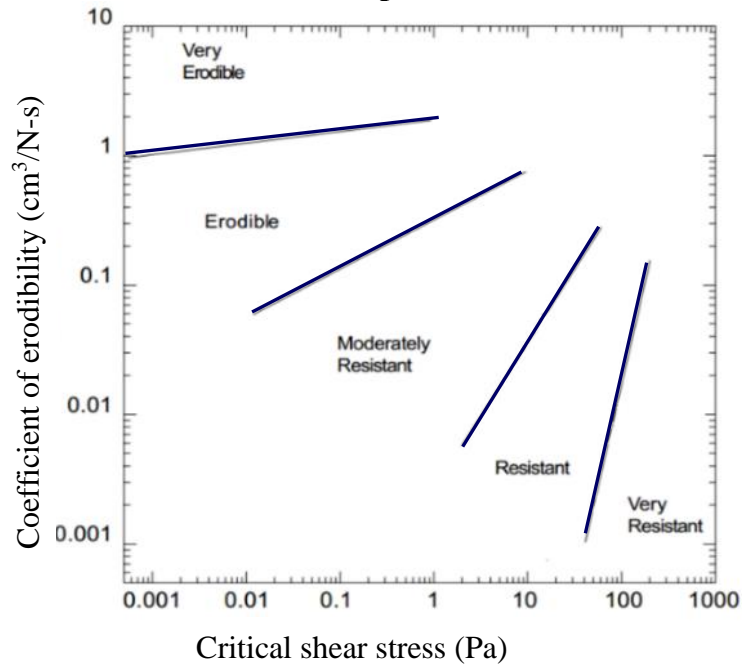


Figure 167. Erosion category based on critical shear stress (adapted from Hanson and Simon 2001)

The Briaud Chart (Briaud et al., 2001) is also based on recognizing that different soils have different erosion functions linking the erosion rate \dot{z} to the applied velocity or shear stress τ (Figure 168). It is set up in the erosion rate on the vertical axis and the shear stress or velocity on the horizontal axis. Because the erosion function varies significantly and it is non-linear, a log-log scale is selected to be able to recognize both very small and very large values with reasonable precision.

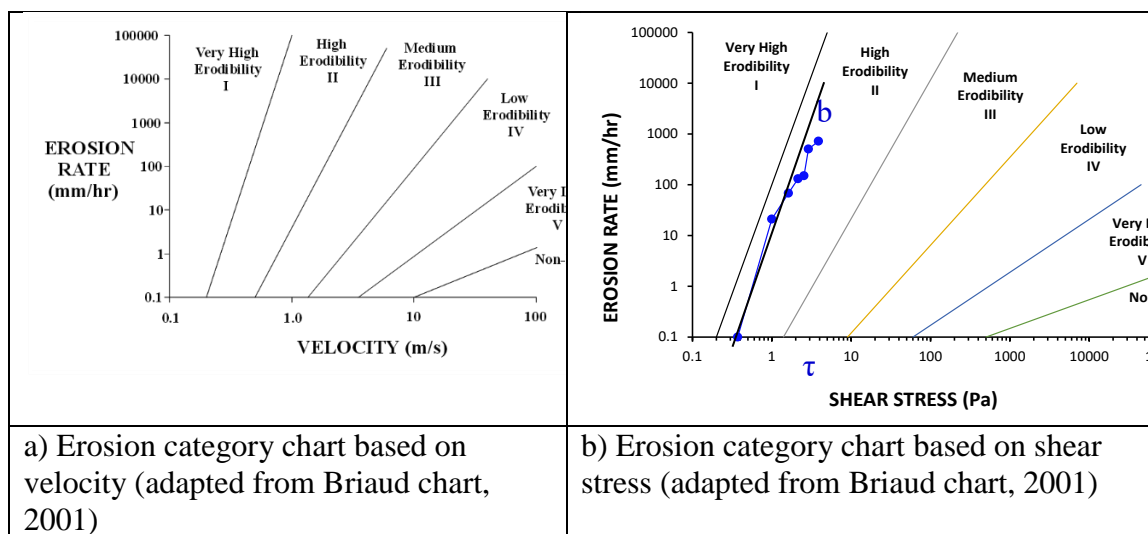


Figure 168. Erosion category chart with some parameters (adapted from Briaud, 2001)

This constant slope of the erosion function on log-log means that each boundary line is a power law model of erosion rate vs velocity or shear stress as in the following general equation:

$$\dot{z} = a(\tau - \tau_c)^b \quad (34)$$

$$\dot{z} = c(v - v_c)^d \quad (35)$$

where \dot{z} is the erosion rate (mm/hr), τ is the applied shear stress (Pa), τ_c is the critical shear stress (Pa), v_c is the critical velocity, v is the applied velocity, b and d are the slopes of a power law model (Figure 166).

The boundaries between soil erosion categories on Figure 168 are based on erosion functions which correspond to one critical shear stress and a constant slope on the log-log scale. This chart is based on many years of erosion testing at Texas A&M University.

Each boundary in the Briaud shear stress-based chart corresponds to a soil having a given critical shear stress τ_c and a given slope b of the erosion function in the log space. Table 41 shows the critical values for the velocity and the shear stress for each erosion category in Figure 168.

Table 41. Threshold velocities and shear stress associated with each erosion category (adapted from Briaud, 2001)

Category No.	Erosion Category Description	v_c (m/s)	τ_c (Pa)
I	Very high erodibility geomaterials	0.1	0.1
II	High erodibility geomaterials	0.2	0.2
III	Medium erodibility geomaterials	0.5	1.3
IV	Low erodibility geomaterials	1.35	9.3
V	Very low erodibility geomaterials	3.5	62.0
VI	Non-erosive materials	10	500

It is recognized that the models presented above have limitations. The limitations are that they either do not fit the data well or they use dimensional parameters. For example, Hanson chart considers that erosion function is a linear model where erosion rate linearly increases with an increase in shear stress which does not correspond to soil

behavior in the EFA. The non-linearity in soil erosion has been observed for many years in EFA testing and has been summarized in the TAMU-Erosion database (Briaud et al., 2019) as well as during EFA testing of different natural and improved soils for the purpose of this research. Hanson and Briaud charts use dimensional parameters. For example, Hanson chart utilizes erodibility coefficient k_d which is also the slope of the erosion function (erosion rate versus shear stress). Briaud power model has parameters a , b , and critical velocity or shear stress. The units must be considered in all erosion data analysis which is not convenient and may cause errors if units are not the same.

Therefore, there is a need in comparison of Hanson and Briaud charts to be used for development of the more advanced erosion model and classification which would combine the advantages of the two models and would have dimensionless parameters.

8.2. Comparison of Hanson and Briaud erosion model and classification

The comparison between the two classification charts can be done by placing the Briaud boundaries on the Hanson chart or placing the Hanson boundaries on the Briaud chart. First the Hanson boundaries were placed on the Briaud chart (Figure 169). This was done by selecting points on the Hanson boundaries and plotting the corresponding erosion functions on the Briaud chart. The complication was that the Hanson boundaries do not correspond to a single erosion function since they represent different combinations of the coefficient of erodibility k_d and critical shear stress τ_c . For a given Hanson boundary line (see

Figure 167), the first point and last point of the Hanson boundary line were selected and the $k_d - \tau_c$ linear model was plotted on the Briaud log-log space. Note that a

point on the Hanson chart is a straight line in the natural space of erosion rate versus shear stress and that straight line becomes a curve in the log-log space. It is indicated in Figure 169. This curve was drawn by selecting a few values of the erosion rate and calculating the corresponding shear stress according to the linear model. This led to a segmented curve in the log-log space which is shown in Figure 169. Then a hatched area was identified between the log-log space curves corresponding to the two extreme values of the $k_d - \tau_c$ Hanson chart boundary. In some cases, the Hanson boundaries or zones leave very little room between the zones for the erosion function to fit in. Figure 170 shows the erosion rate versus shear stress in natural scales and confirms that the Hanson boundaries are zones on the Briaud chart.

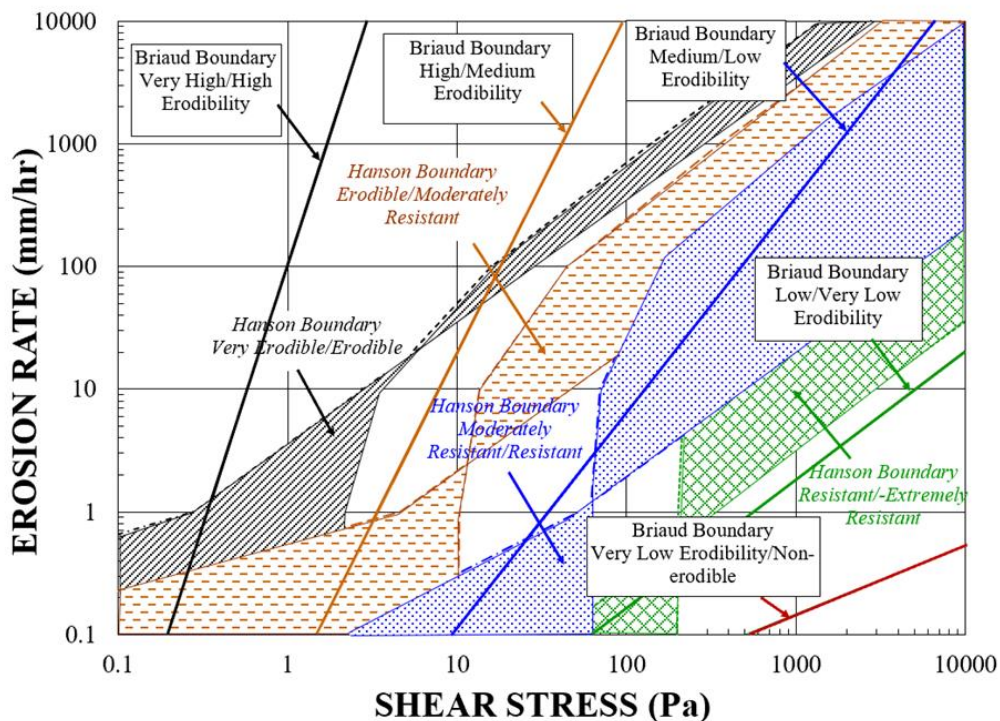


Figure 169. Briaud chart with Hanson boundaries

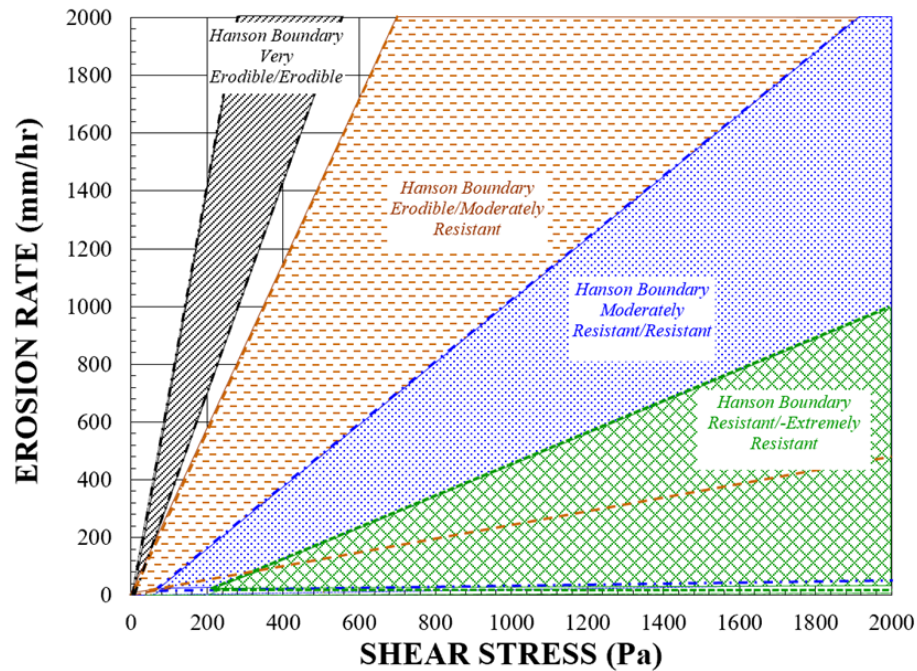


Figure 170. Hanson boundaries on Briaud chart in natural scale

Then the Briaud boundaries were placed on the Hanson chart. Each Briaud erosion boundary corresponds to one critical shear stress. Each Briaud erosion boundary also corresponds to one erosion function which is a straight line in the log-log space ($\log z$ vs. $\log \tau_c$). This is a nonlinear model which corresponds to many different linear slope k_d intersecting the nonlinear model. Therefore, each Briaud boundary corresponds to many different secant k_d values. Thus, the Briaud boundaries on the Hanson chart will be vertical lines (constant critical shear stress) exhibiting a range of k_d values (Figure 171). Briaud chart has six different erosion categories while Hanson has five. The only category which is in Briaud and not in Hanson is the non-erodible category associated with sound rock (Briaud, 2001). That comparison shows that the models fit well.

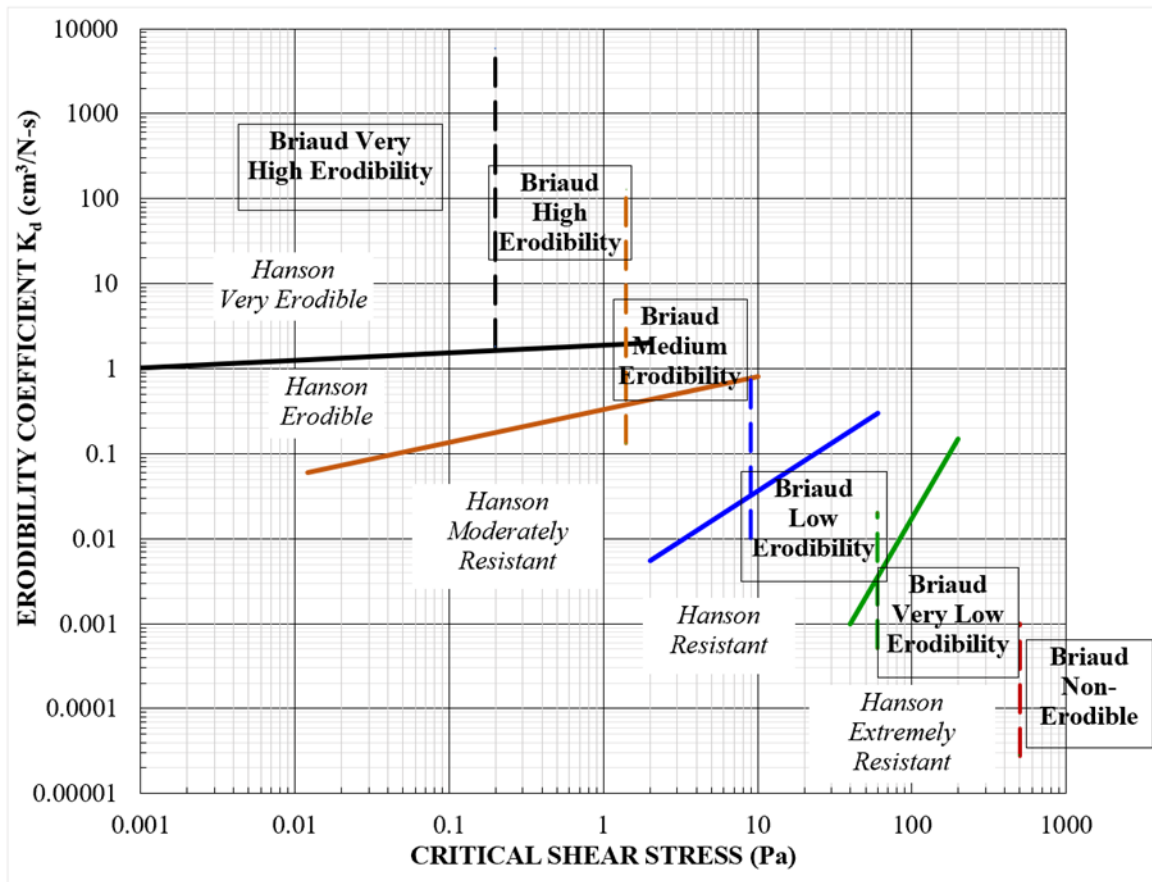


Figure 171. Hanson chart with Briaud boundaries (modified from Hanson and Simon, 2001)

8.3. New normalized power law model

This chapter develops a simple methodology (physical and simple mathematical level) for the new erosion model and the classification chart to be used to estimate soil erodibility. As was described in Section 8.1 and Section 8.2, the existing erosion models and classification charts have some limitations which can be improved based on soil erosion behavior obtained in the EFA.

One of the advantages of the Briaud model is that it is a nonlinear power law function which provides a better fit of the erosion functions measured in the EFA. This

model was chosen as a basis for the further development and improvement. This erosion model will be referred to as “previous” erosion model in this Section.

It is proposed to normalize the new model for the erosion rate, for the shear stress, and for the velocity which would allow to obtain the dimensionless parameters. The following erosion model referred to as the new erosion model is presented below.

$$\frac{\dot{z} \text{ (mm/hr)}}{0.1 \text{ mm/hr}} = \left(\frac{\tau}{\tau_c}\right)^\alpha \quad (36)$$

$$\frac{\dot{z} \text{ (mm/hr)}}{0.1 \text{ mm/hr}} = \left(\frac{v}{v_c}\right)^\beta \quad (37)$$

where \dot{z} is the erosion rate (mm/hr), 0.1 mm/hr is the erosion rate at which erosion is negligible, τ is the shear stress (Pa), τ_c is the critical shear stress (Pa), v is the velocity (m/s), v_c is the critical velocity (m/s), α and β are the slopes of a power law model. Note that for the purpose of the dissertation, the critical shear stress is defined as the highest shear stress applied to the soil before any erosion was detected in the EFA where the velocity was gradually increased (Figure 172).

Figure 172 and Figure 173 show the erosion function and the erosion parameters used for the new erosion model. This nonlinear model is reduced to two dimensionless parameters called shear stress-based erosion modulus α (Figure 172) and velocity-based erosion modulus β (Figure 173). The parameters α and β are the slope of erosion rate vs. shear stress or velocity line in a logarithmic scale and called erosion modulus. Both parameters, α and β characterize the rate at which the soil erodes. Note that the erosion rate is normalized with respect to the erosion corresponding to the detection of the shear stress. The rate of 0.1 mm/hr was chosen arbitrarily as a very small erosion rate to define

the point at which erosion is initiated considering the erosion detection limits of the EFA device.

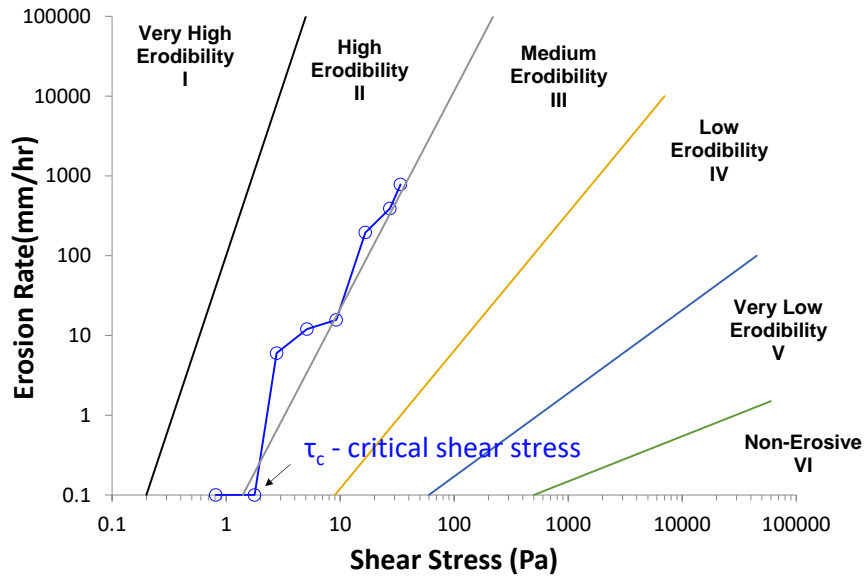


Figure 172. Erosion function for the new erosion model (erosion rate vs. shear stress)

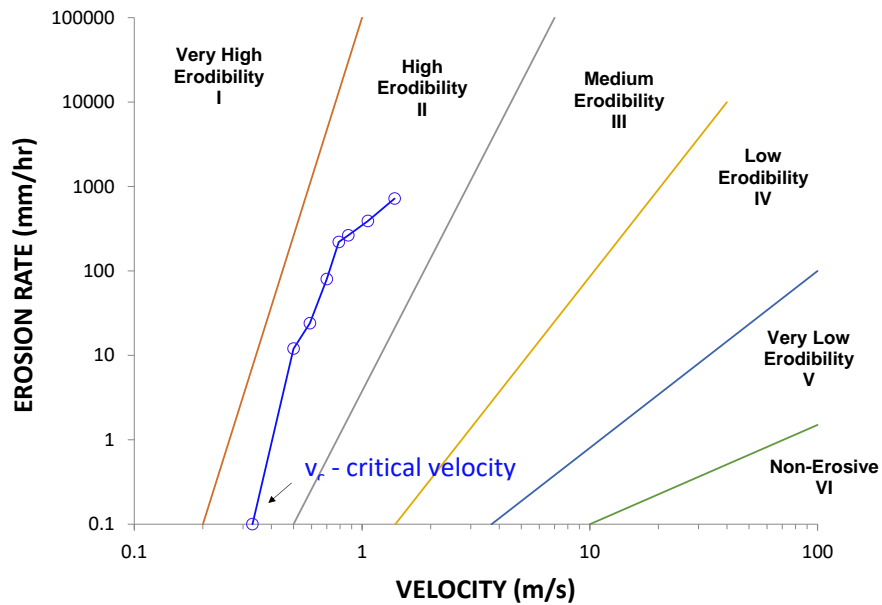


Figure 173. Erosion function for the new erosion model (erosion rate vs. velocity)

The new erosion model proposed in this Chapter:

1. Normalized for erosion rate and for velocity/shear stress.
2. It has only one dimensionless parameter which is a property of the soil

and called the erosion modulus (α and β).

3. It is still non-linear power law model.
4. It still fits the erosion functions well.
5. It still provides useful classification.
6. It is simpler to handle mathematically.

The advantages and the limitations of the previous and the new erosion models are shown in the Table 42.

Table 42. Advantages and limitations of new erosion model

Old model		New model	
Advantages	Limitations	Advantages	Limitations
Has been around a long time		New improved one	New, needs to be checked
Single soil categories	Single soil categories	Two separate erosion categories	
	Dimensional	Non-dimensional	
One chart			Two charts
Less complex		More refined	
	More difficult to handle mathematically	Simpler to handle mathematically	

8.4. New erosion classification chart

8.4.1. Shear stress

As it was described in Section 8.1, the previous erosion model has two charts: the erosion rate vs. shear stress and the erosion rate vs. velocity chart. Figure 174 shows the

previous erosion chart for shear stress developed Briaud (2001). It is proposed the new model is also developed for shear stress and velocity. Therefore, the new model can be graphically presented as the normalized erosion rate versus the normalized shear stress and the normalized velocity. The choice of scale representation is not connected to the choice of model. However, some models, such as a power law model, are more conveniently represented in a logarithmic scale the use of which has three reasons:

1. The model becomes a straight line on the normalized erosion rate vs. normalized shear stress in logarithmic scale (Figure 175).
2. It allows to show wide variations in parameters.
3. The data cloud is decreased in size.

The procedure to obtain the new shear stress erosion chart is:

- a. Use the previous erosion chart (erosion rate vs shear stress in logarithmic scale) to find the equations of the boundaries between erosion categories. Use power model for each boundary line (Figure 174). The exponent of each equation would be shear-based erosion modulus α .
- b. For each erosion category line, obtain the shear stress (Pa) which corresponds to the erosion rate $\dot{z} = 10000$ mm/hr chosen as an arbitrary number.
- c. For each erosion category line, read the critical shear stress from that chart corresponding to the erosion rate set as $\dot{z} = 0.1$ mm/hr.
- d. For each erosion category, find a ration of shear stress over critical shear stress $\frac{\tau}{\tau_c}$ and its logarithm.

- e. Take the erosion rate $\dot{z} = 10000 \text{ mm/hr}$ for the five erosion category lines.
- f. For each erosion category, find a logarithm of $\frac{\dot{z}}{0.1}$.
- g. Develop the erosion chart $\frac{\dot{z}}{0.1}$ vs. $\frac{\tau}{\tau_c}$ and show the boundary lines between erosion categories (Figure 175).
- h. Compute the erosion modulus α for each erosion category line and compare these numbers with the exponent of the previous power model (Figure 174).

Table 43 shows the results of calculations for obtaining the new shear stress erosion chart.

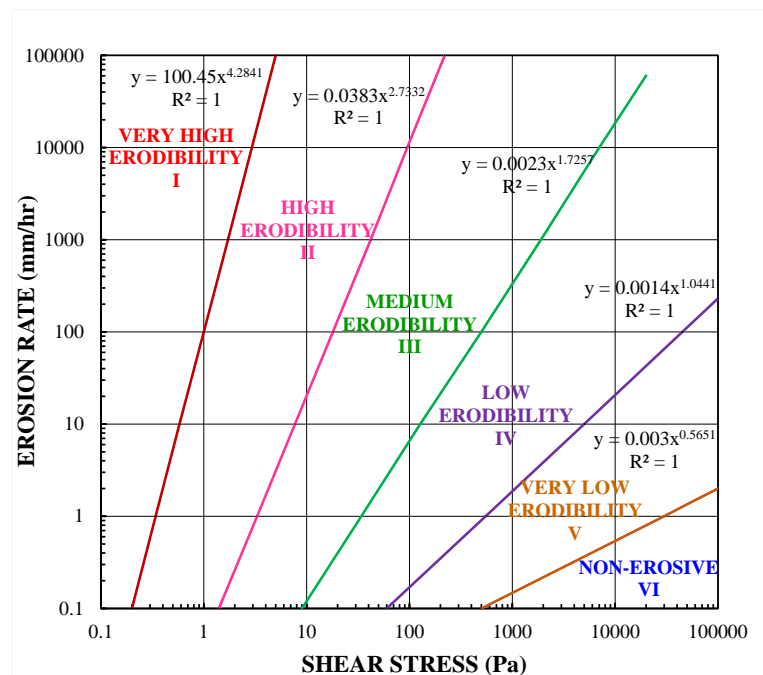


Figure 174. Erosion rate vs. shear stress (modified from Briaud 2001)

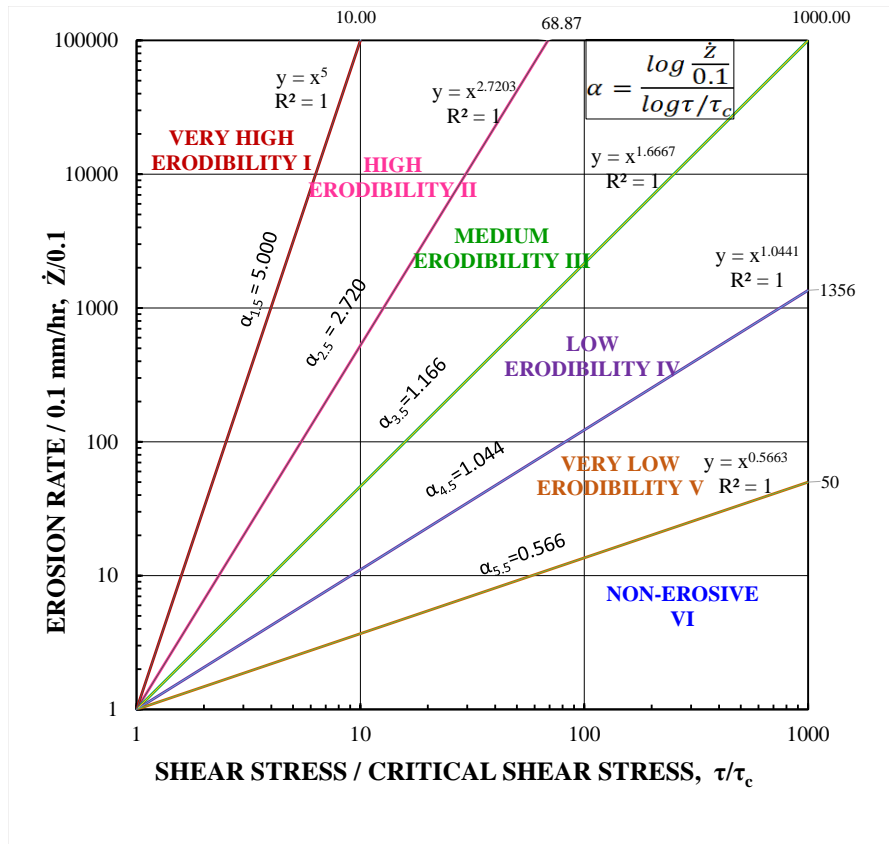


Figure 175. New erosion shear stress chart

Table 43. Calculations for obtaining new erosion shear stress chart

Category	τ (Pa) for $\dot{z}=10000$ mm/hr	τ_c (Pa)	$\frac{\tau}{\tau_c}$	$\log \frac{\tau}{\tau_c}$	\dot{z} (mm/h r)	$\log \frac{\dot{z}}{0.1}$	Erosion modulus (α)	
							Computed	Obtained from the chart
I-II	2.93	0.20	10.00*	1.00	10000	5.000	5.000	5.000
II-III	96.42	1.40	68.87	1.84	10000	5.000	2.720	2.7203
III-IV	6870.88	9.00	763.43	2.88	10000	5.000	1.734	1.667
IV-V	389141 5.9	60.00	1000.0 0	3.00	135.6	3.132	1.044	1.044
V-VI	2.778E +11	500.0 0	1000.0 0	3.00	4.96	1.695	0.565	0.566

Note. * $\frac{\tau}{\tau_c}$ chosen value

The new erosion function is shown in the Figure 175. It gives a relationship between $\frac{\dot{z}}{0.1}$ and $\frac{\tau}{\tau_c}$ in a logarithmic scale. Note that the new erosion chart starts at $\frac{\dot{z}}{0.1} = 1$ and $\frac{\tau}{\tau_c} = 1$. The axes are non-dimensional. The boundary lines split consecutive erosion categories. The slopes of the erosion line between categories are:

very high (I) and high erodibility (II) - $\alpha_{1.5} = 5.000$;

high (II) and medium erodibility (III) - $\alpha_{2.5} = 2.720$;

medium (III) and low erodibility (IV) - $\alpha_{3.5} = 1.667$;

low (IV) and very low erodibility (V) - $\alpha_{4.5} = 1.044$;

very low erodibility (V) and non-erosive (VI) - $\alpha_{5.5} = 0.566$;

However, there is a need for a separate classification and erosion chart because the critical shear stress is disappeared in the normalization process. An additional erosion chart showing shear-based erosion modulus α versus critical shear stress τ_c can be drawn. The shear-based erosion modulus α is the ratio of the logarithm of the erosion rate \dot{z} divided by a reference erosion rate arbitrarily chosen as 0.1 mm/hr to the logarithm of the shear stress (τ) divided by the critical shear stress (τ_c) (Eq. 38).

$$\alpha = \frac{\log \frac{\dot{z}}{0.1}}{\log \frac{\tau}{\tau_c}} \quad (38)$$

The boundaries lines between erosion categories are the lines of constant critical shear stress: $\tau_c = 0.2$ Pa; 1.4 Pa, 9 Pa, 60 Pa, 500 Pa. Note that these boundary lines are vertical lines on semi-logarithmic scale (Figure 176). The black line on Fig. 5.14 comes from the boundaries in Briaud erosion category chart. The shear-based erosion modulus α decreases with an increase in critical shear stress τ_c as indicated Figure 176. The

relationship between α and τ_c fits the relationship between erodibility coefficient k_d and critical shear stress τ_c obtained by Arulanandan et al. (1980).

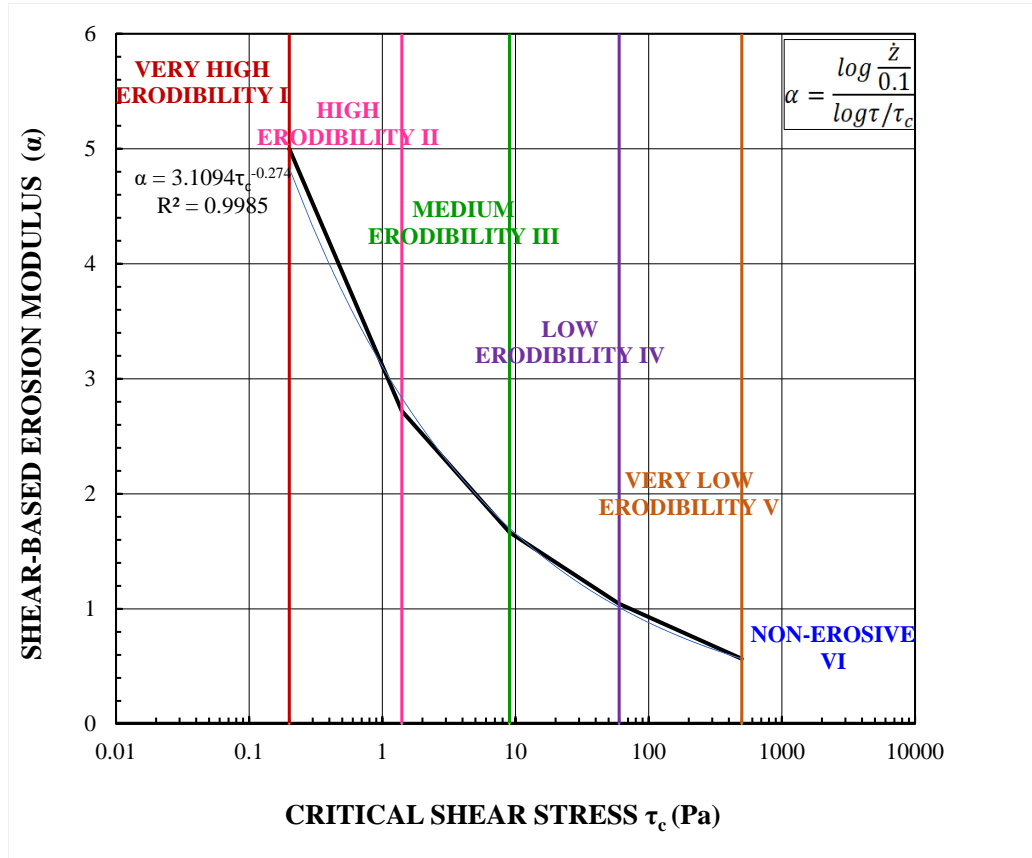


Figure 176. Shear-based erosion modulus (α) vs. critical shear stress (τ_c) in semi-logarithmic scale

The proposed new erosion model for shear stress has two classification charts:

- a. Normalized erosion rate versus normalized shear stress in logarithmic scale (Figure 175).
- b. Shear-based erosion modulus versus critical shear stress in semi-logarithmic scale (Figure 176).

8.4.2. Velocity

It is proposed the new model is also developed for velocity. Figure 177 shows the previous erosion classification chart (Briaud, 2011). The new model can be graphically presented as the normalized erosion rate versus the normalized velocity. The procedure to obtain the new velocity erosion chart is the same as for the shear stress and includes:

Use the previous erosion chart (erosion rate vs velocity in logarithmic scale) to find the equations of the boundaries between erosion categories. Use power model for each boundary line (Figure 177). The exponent of each equation would be velocity-based erosion modulus β .

- a. For each erosion category line, obtain the velocity (m/s) which corresponds to the erosion rate $\dot{z} = 1000$ mm/hr chosen as an arbitrary number.
- b. For each erosion category line, read the velocity from that chart corresponding to the erosion rate set as $\dot{z} = 0.1$ mm/hr.
- c. For each erosion category, find a ration of velocity over critical velocity $\frac{v}{v_c}$ and its logarithm.
- d. Take the erosion rate $\dot{z} = 1000$ mm/hr for the five erosion category lines.
- e. For each erosion category, find a logarithm of $\frac{\dot{z}}{0.1}$.
- f. Develop the erosion chart $\frac{\dot{z}}{0.1}$ vs. $\frac{v}{v_c}$ and show the boundary lines between erosion categories (Figure 178).

- g. Compute the erosion modulus β for each erosion category line and compare these numbers with the exponent of the previous power model (Figure 178).

Table 44 shows the results of calculations for obtaining the new velocity erosion chart.

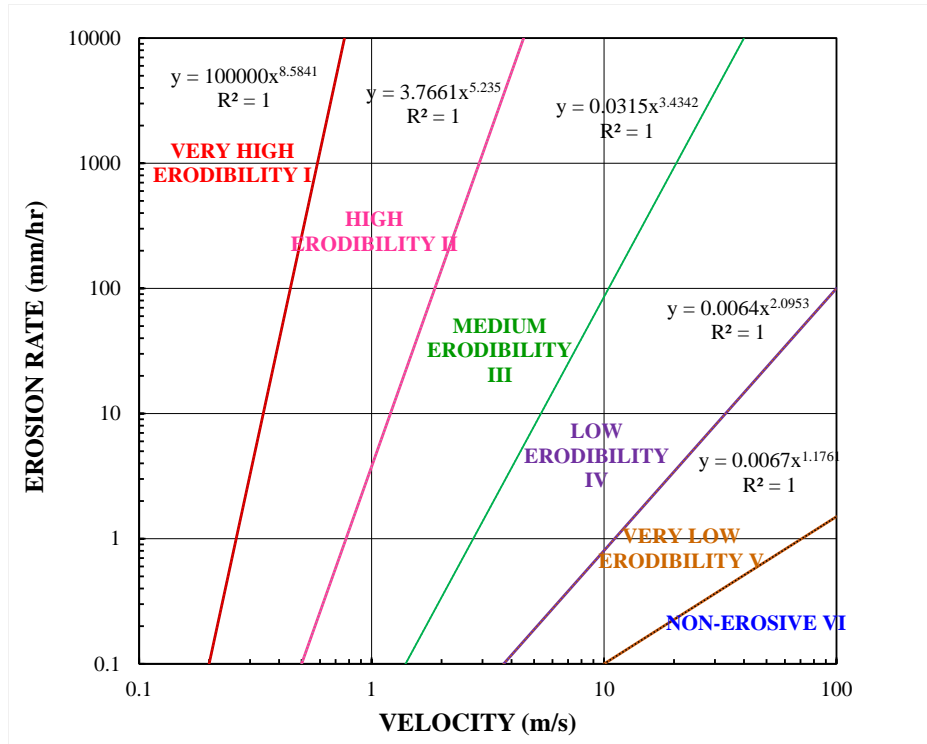


Figure 177. Erosion rate vs. velocity (modified from Briaud 2001)

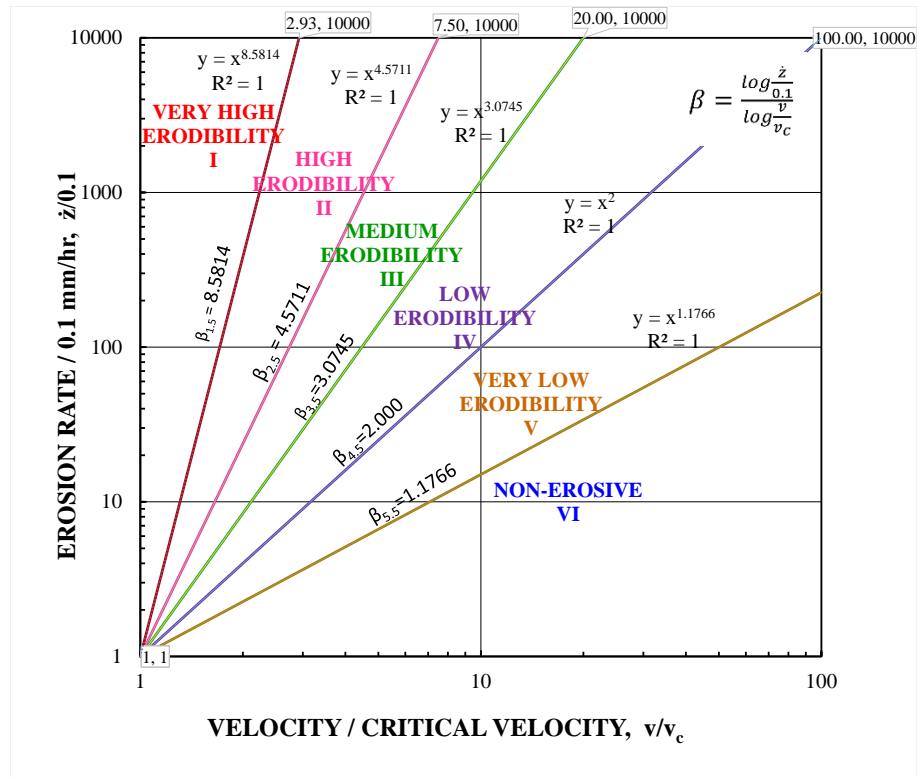


Figure 178. New erosion velocity chart

Table 44. Calculations for obtaining new erosion velocity chart

Category	v (m/s) for z-dot=1000 mm/hr	vc (m/s)	$\frac{v}{v_c}$	$\log \frac{v}{v_c}$	z-dot (mm/hr)	$\log \frac{z-dot}{0.1}$	Erosion modulus (β)	
							Computed	Obtained from the chart
I-II	2.93	0.20	2.93*	0.47	1000	4.00	8.581	8.581
II-III	96.42	0.50	5.81	0.76	1000	4.00	5.232	4.571
III-IV	6870.88	1.50	13.64	1.13	1000	4.00	3.525	3.074
IV-V	3891415. 9	3.80	79.34	1.90	1000	4.00	2.106	2.000
V-VI	2.778E+1 1	10.0 0	2510.0 0	3.40	1000	4.00	1.177	1.177

The new erosion function is shown in the Figure 178. It gives a relationship

between $\frac{z-dot}{0.1}$ and $\frac{v}{v_c}$ in a logarithmic scale. Note that the new erosion chart starts at $\frac{z-dot}{0.1} =$

1 and $\frac{v}{v_c} = 1$. The axes are non-dimensional. The boundaries lines split consecutive erosion categories (Figure 178). The slopes of the erosion line between categories are:

1. very high (I) and high erodibility (II) - $\alpha_{1.5} = 8.5814$;
2. high (II) and medium erodibility (III) - $\alpha_{2.5} = 4.571$;
3. medium (III) and low erodibility (IV) - $\alpha_{3.5} = 3.074$;
4. low (IV) and very low erodibility (V) - $\alpha_{4.5} = 2.000$;
5. very low erodibility (V) and non-erosive (VI) - $\alpha_{5.5} = 1.177$;

However, there is a need for a separate classification and erosion chart because the critical velocity is disappeared in the normalization process. An additional erosion chart showing velocity-based erosion modulus α versus critical velocity v_c can be drawn. The velocity-based erosion modulus β is the ratio of the logarithm of the erosion rate \dot{z} divided by a reference erosion rate arbitrarily chosen as 0.1 mm/hr to the logarithm of the velocity (v) divided by the critical velocity (v_c) (Eq. 39).

$$\beta = \frac{\log \frac{\dot{z}}{0.1}}{\log \frac{v}{v_c}} \quad (39)$$

The boundaries lines between erosion categories are the lines of constant critical velocity: $v_c = 0.2$ m/s; 0.5 m/s, 1.5 m/s, 3.8 m/s, 10 m/s. The black line on Figure 179 comes from the boundaries in Briaud erosion category chart.

Note that these boundary lines are vertical lines on semi-logarithmic scale (Figure 179). The velocity-based erosion modulus β decreases with an increase in critical velocity v_c as indicated on Figure 179.

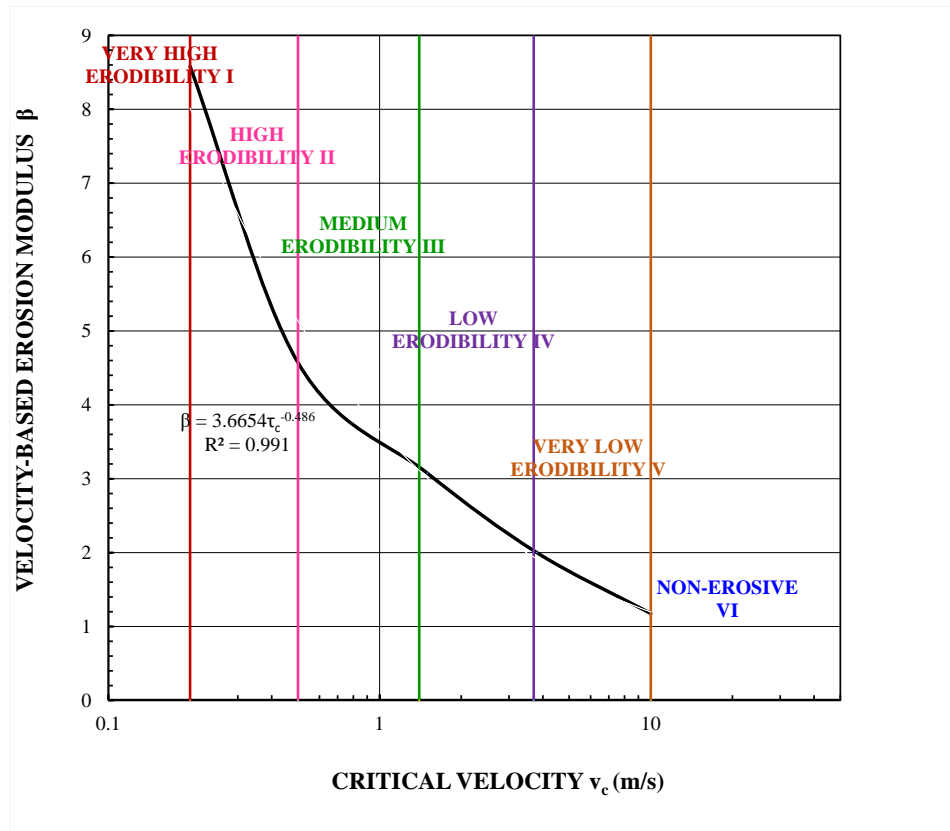


Figure 179. Velocity-based erosion modulus β vs. critical shear stress τ_c in semi-logarithmic scale

The proposed new erosion model for velocity has two classification charts:

- a. Normalized erosion rate versus normalized velocity in logarithmic scale (Figure 178).
- b. Velocity-based erosion modulus versus critical velocity in semi-logarithmic scale (Figure 179).

8.5. Erosion classification

The new erosion model proposed in this Section makes use of the soil erosion parameters such as:

1. Shear-based erosion modulus α
2. Velocity-based erosion modulus β
3. Critical shear stress τ_c
4. Critical velocity v_c

The new model allows to classify soil based on the parameters mentioned above. From the previous work (Arulanandan et al., 1980; Hanson and Cook, 2001), it was observed that there is a certain relationship between the erodibility coefficient and critical shear stress. It was concluded that the more erodible soils are typically associated with the steeper regression line on the erosion chart and may have higher critical shear stress compared to the soils which are less erodible and representing by a shallow slope on the erosion chart. The new model recognizes different nature and soil behavior when it comes to erosion and provides a better understanding of erosion phenomenon. Note that classification according to the critical shear stress is different from the classification according to the erosion modulus for the same soils. Table 45 illustrates the point the erosion classification based on shear-based erosion modulus α differs from the erosion classification for critical shear stress τ_c . Table 45 shows the range of critical shear stress τ_c and shear stress-based erosion modulus α for each erosion category. Table 46 shows the range of critical velocity v_c and velocity-based erosion modulus β for each erosion category. Note that the previous erosion model proposed by Briaud is used for soil classification based on shear stress and velocity. The ranges of erosion modulus α and β shown in Table 45 and Table 46 were obtained from the previous erosion chart proposed by Briaud.

The erosion modulus α and β are high for very high erodible soil and low for non-erodible soils which is opposite from the modulus of deformation used in geotechnical engineering to define how soils would deform under loading. Modulus of deformation is high for stiff soils and low for soft soils. The summary classification considering shear stress chart together with velocity chart is shown in Table 47. The shear stress and velocity classifications are more reliable than classification based on the erosion modulus α and β . The reason is that the critical shear stress and critical velocity are more clearly define than slope of the erosion function indeed the erosion function can exhibit many different shapes (Figure 180).

Table 45. Classification of soils based on new model (shear stress chart)

#	Category	Index	Range of Critical Shear Stress τ_c (Pa)	Estimated Corresponding Range of Erosion Modulus α
1.	Very High Erodibility	I	0.01 - 0.2	> 5.000
2.	High Erodibility	II	0.2 - 1.4	2.720 - 5.000
3.	Medium Erodibility	III	1.4 - 9.0	1.166 - 2.720
4.	Low Erodibility	IV	9.0 - 60.0	1.044 - 1.166
5.	Very Low Erodibility	V	60.0 - 500.0	0.566 - 1.044
6.	Non-Erosive	VI	> 500.0	< 0.566

Table 46. Classification of soils based on new model (velocity chart)

#	Category	Index	Range of Critical Velocity v_c (m/s)	Estimated Corresponding Range of Erosion Modulus β
1.	Very High Erodibility	I	0.1 - 0.2	> 8.5814
2.	High Erodibility	II	0.2 - 0.5	4.5711 - 8.5814
3.	Medium Erodibility	III	0.5 - 1.4	3.0745 - 4.5711
4.	Low Erodibility	IV	1.4 - 3.7	2.000 - 3.0745
5.	Very Low Erodibility	V	3.7 - 10.0	1.1766 - 2.000
6.	Non-Erosive	VI	> 10.0	< 1.1766

Table 47. Summary classification of soils based on new model (shear stress and velocity charts)

#	Category	Index	Velocity chart		Shear stress chart	
			Range of v_c (m/s)	Range of β	Range of τ_c (Pa)	Range of α
1.	Very High Erodibility	I	0.1 – 0.2	> 8.5814	0.01 - 0.2	> 5.000
2.	High Erodibility	II	0.2 – 0.5	4.5711 - 8.5814	0.2 - 1.4	2.720 - 5.000
3.	Medium Erodibility	III	0.5 – 1.4	3.0745 – 4.5711	1.4 - 9.0	1.166 - 2.720
4.	Low Erodibility	IV	1.4 – 3.7	2.000 - 3.0745	9.0 - 60.0	1.044 - 1.166
5.	Very Low Erodibility	V	3.7 – 10.0	1.1766 - 2.000	60.0 - 500.0	0.566 - 1.044
6.	Non-Erosive	VI	> 10.0	< 1.1766	> 500.0	< 0.566

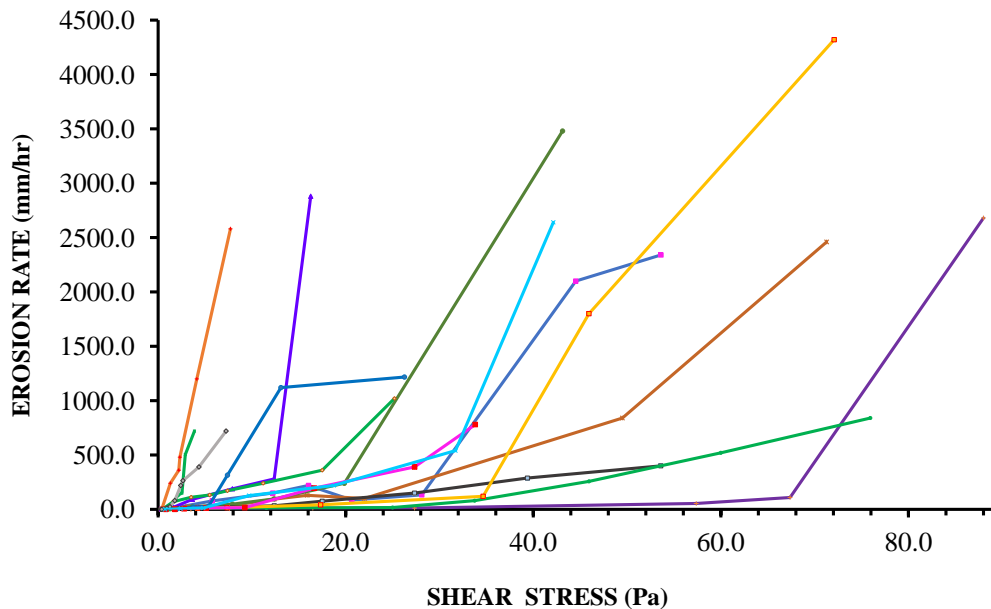


Figure 180. Different shapes of erosion function

Some soils exhibit very low erodibility or even no erosion up to a certain velocity and associated to this velocity shear stress, above which erosion progresses rapidly and significantly (Figure 180). This type of soil would have high critical shear stress and

high erosion rate (steep erosion slope on k_d versus τ_c chart). In reverse, some soils could have low critical shear stress and low erosion rate (moderate to almost flat surface of erosion function). More detailed analysis of soil erodibility applied to the different types of natural and improved soil is presented in Section 4.7, Section 5.4, Section 6.4, Section 7.4.

The approach to obtain the new erosion model considers all measurements taken during EFA testing. It has then limitation depending on the range of shear stresses applied during the test. Note that classification according to the critical shear stress and/or the critical velocity may be different from the classification according to the erosion modulus.

An engineer working on a project should consider the total erosion function and the range of shear stresses or velocity that the soil is to be subjected to. This range of shears stresses will define a more site-specific modulus for the calculations.

8.6. New erosion model for natural and improved soil

New erosion model is proposed to apply for a variety of natural soils including clay, silt, sand as well as for improved soils such as enzyme treated soil, lime treated soil, grass, and riprap. The model makes use of the entire erosion function. The description of the new erosion model and its parameters for each type of soil is presented below.

8.6.1. Clay

Figure 181 shows the new shear-based erosion classification chart for clay. It includes lean clay, silty clay, and sandy clay. Clay erodibility varies from Category I

(Very High Erodibility) to Category IV (Low Erodibility) with some points found in Category V at higher values of normalized shear stress when normalized erosion rate slow down (Very Low Erodibility). Erodibility of clay based on the shear stress new erosion chart corresponds well with erosion categories for the same clay obtained on a basis of the velocity chart. Figure 182 shows erosion categories for clay when the relationship between normalized erosion rate and normalized velocity is considered. Erodibility of clay is in Category I (Very High Erodibility) to Category IV (Low Erodibility). Note that the erosion curves on Figure 181 and Figure 182 are obtained for the points when $v/v_c \geq 1.0$ and $\dot{z}/0.1 \geq 1.0$. Therefore, they show soil behavior after erosion takes place.

The shear-based modulus versus critical shear stress for clay is shown on Figure 183. The black curve on Figure 183 shows the Briaud erosion boundaries which were obtained from the Briaud erosion chart. It demonstrates that the erosion modulus decreases with a critical shear stress which is intuitive. The erosion modulus α was obtained as an average of the slope calculated between the critical shear stress points and each point on the erosion curve. Those points come from the tests # 987-992, 994-1056 in the TAMU-Erosion database. The erosion modulus α of clay varies from 1 to 7. As it was mentioned in Section 8.5, the erosion classification based on critical shear stress is more reliable than on erosion modulus. The erosion modulus characterizes soil behavior after erosion is being initiated and progressed. Note that the erosion modulus is only obtained for the points at which $\tau/\tau_c > 1.0$ and $\dot{z}/0.1 > 1.0$. Considering values of critical shear stress shown on Figure 183 clay fits in Category II and Category III.

The velocity-based modulus versus critical velocity for clay is shown on Figure 184. Black curve on Figure 184 shows the Briaud erosion boundaries which were obtained from the Briaud erosion chart. This curve shows that erosion modulus decreases with a critical velocity which is intuitive. The erosion modulus β was obtained as an average of the slope calculated between the critical velocity points and each point on the erosion curve. Note that the erosion modulus is only obtained for the points at which $v/v_c > 1.0$ and $\dot{z}/0.1 > 1.0$. Those points come from the tests 987-992, 994-1056 in the TAMU-Erosion database. The values of erosion modulus β of clay varies from 2.5 to 11.5. Considering values of critical velocity shown on Figure 184, clay fits in Category II and Category III.

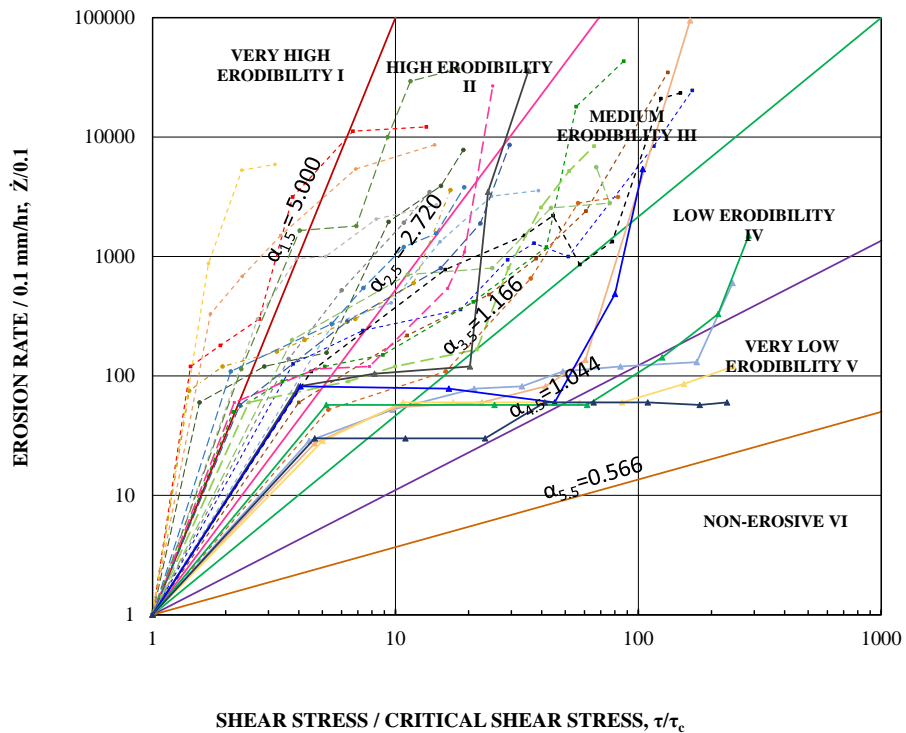


Figure 181. New shear-based erosion classification chart for clay

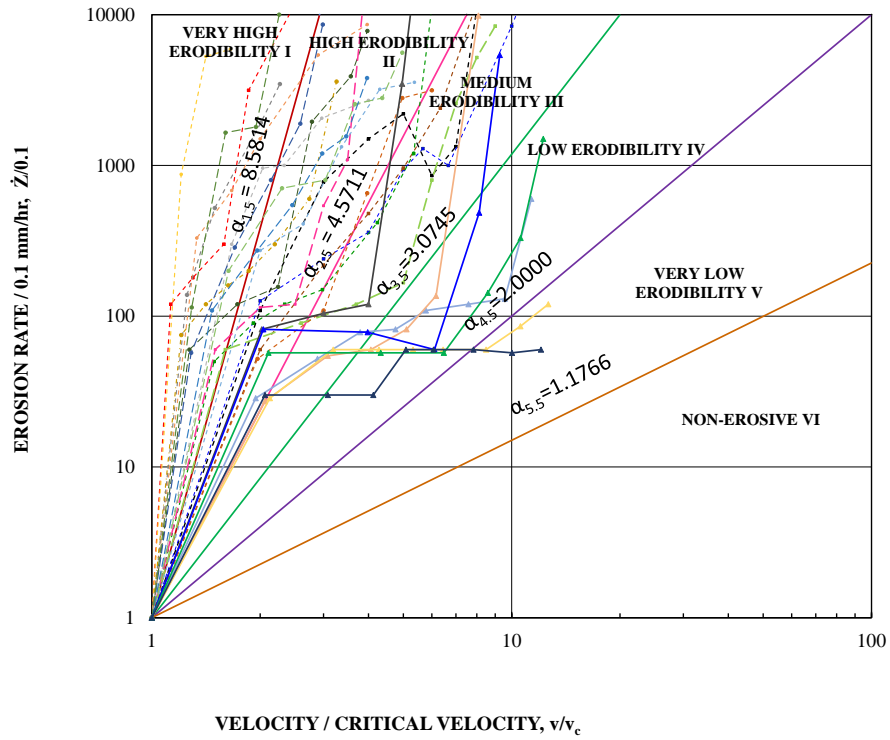


Figure 182. New velocity-based erosion classification chart for clay

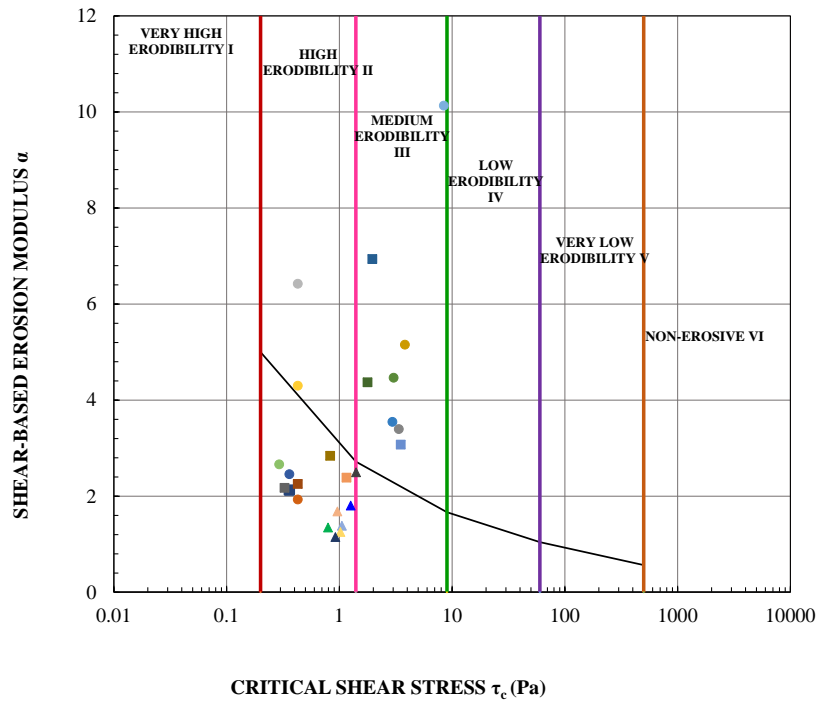


Figure 183. Shear-based erosion modulus (α) vs. critical shear stress (τ_c) in semi-logarithmic scale for clay

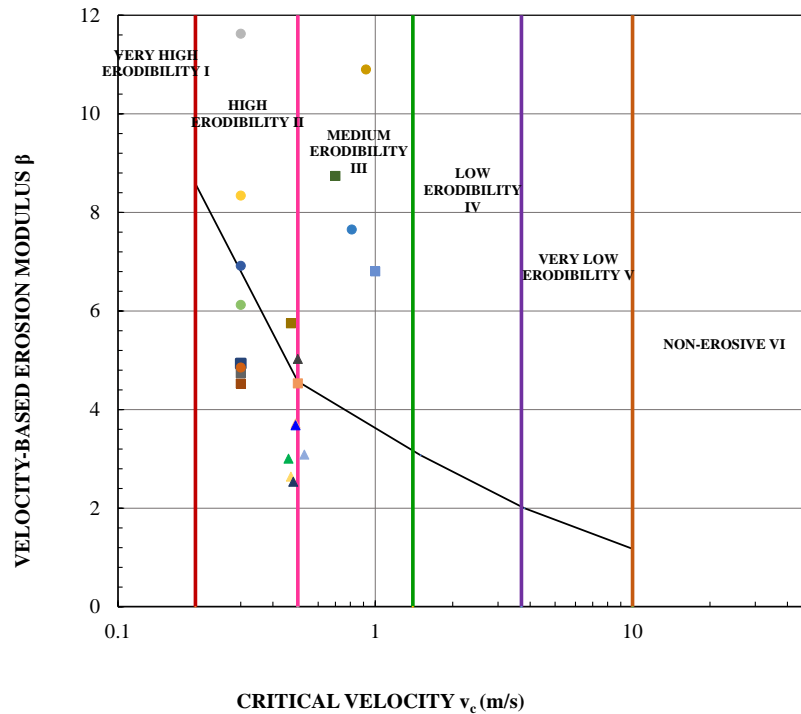


Figure 184. Velocity-based erosion modulus (β) vs. critical velocity (v_c) in semi-logarithmic scale for clay

8.6.2. Silt

Silt is found to be one of the most erodible soil. Figure 185 and Figure 186 show the new shear-based erosion classification chart and velocity-based erosion chart for silt which is in Category I (Very High Erodibility) to Category III (Medium Erodibility).

The shear-based modulus versus critical shear stress for clay is shown on Figure 187. The black curve on Figure 187 shows the Briaud erosion boundaries which were obtained from the Briaud erosion chart. It demonstrates that the erosion modulus decreases with a critical shear stress which is intuitive. The erosion modulus α was obtained as an average of the slope calculated between the critical shear stress points and each point on the erosion curve. Those points come from the tests # 999, 1000, 1004,

1025, 1030, 1033-1035, 1038, 1042, 1049, 1055 in the TAMU-Erosion database. The erosion modulus α of silt varies from 2 to 8. Considering values of critical shear stress shown on Figure 187, clay fits in Category II and Category III.

The velocity-based modulus versus critical velocity for clay is shown on Figure 188. Black curve on Figure 188 shows the Briaud erosion boundaries which were obtained from the Briaud erosion chart. This curve shows that erosion modulus decreases with a critical velocity which is intuitive. The erosion modulus β was obtained as an average of the slope calculated between the critical velocity points and each point on the erosion curve. Those points come from the tests # 999, 1000, 1004, 1025, 1030, 1033-1035, 1038, 1042, 1049, 1055 in the TAMU-Erosion database. The values of erosion modulus β of silt varies from 3 to 15. Considering values of critical velocity shown on Figure 188, clay fits in Category II and Category III.

The amount of silt particles has an impact on silt erodibility. Higher amount of silt particles in the soil, varying from 57.8 % to 60.2 % indicated for samples # 1030, 1033-1034 in the TAMU-Erosion database, corresponds to Category II (High Erodibility) soil using the shear stress classification on Figure 187. However, lower amount of silt particles, 42.5 % obtained for the sample # 1025, corresponds to Category II (Medium Erodibility) soil.

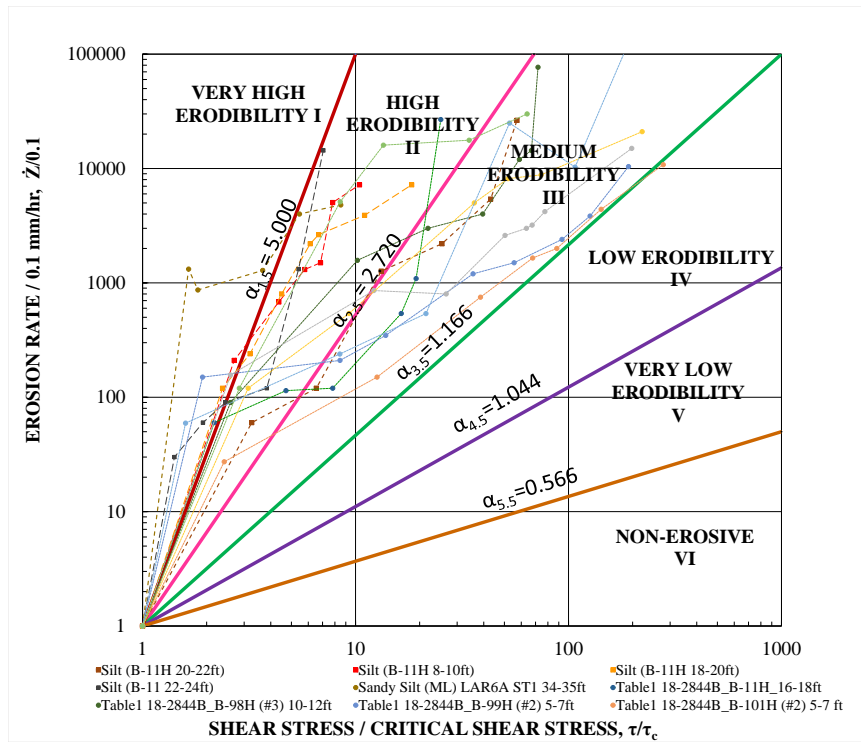


Figure 185. New shear stress-based erosion classification chart for silt

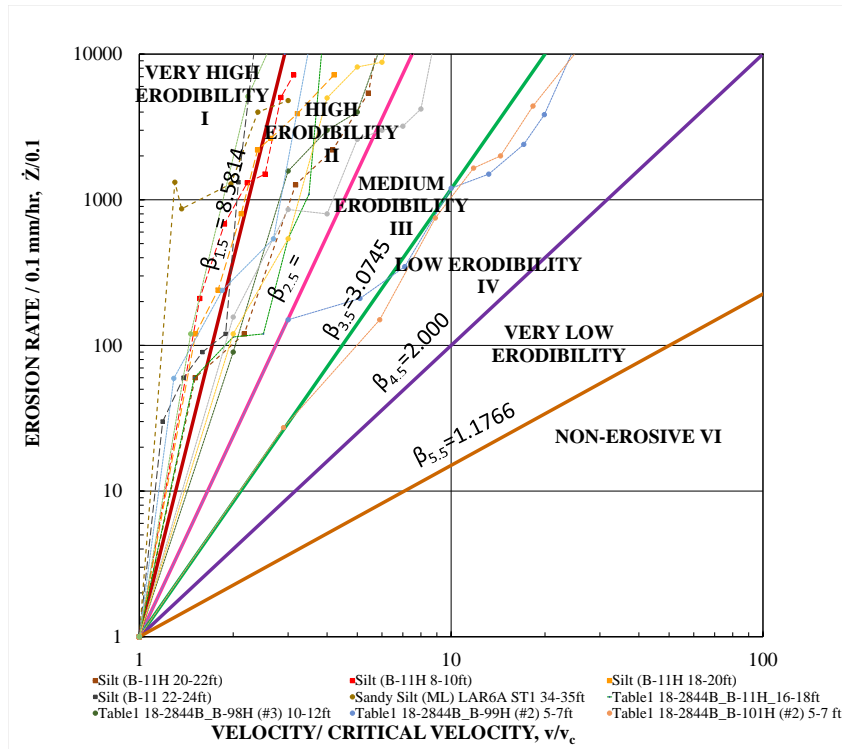


Figure 186. New velocity-based erosion classification chart for silt

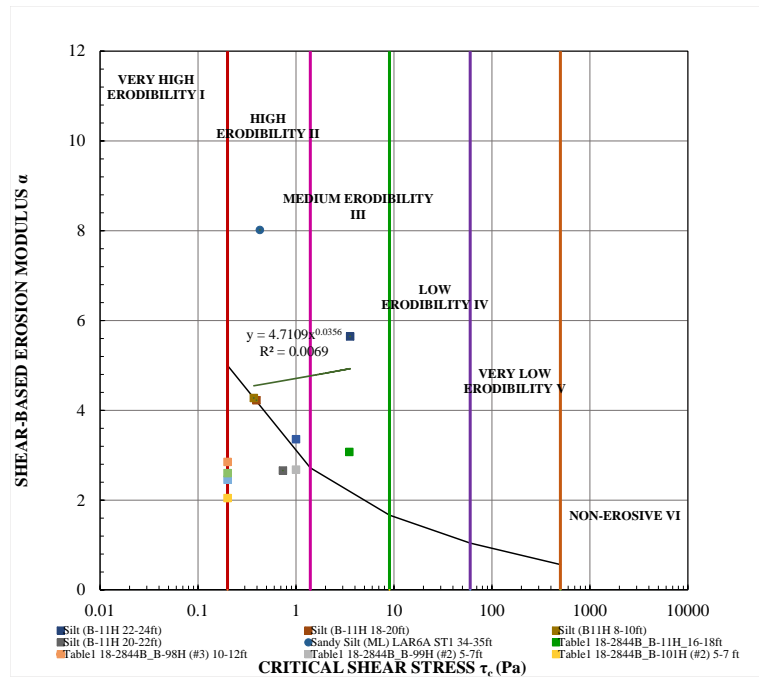


Figure 187. Shear stress-based erosion modulus (α) vs. critical shear stress (τ_c) in semi-logarithmic scale for silt

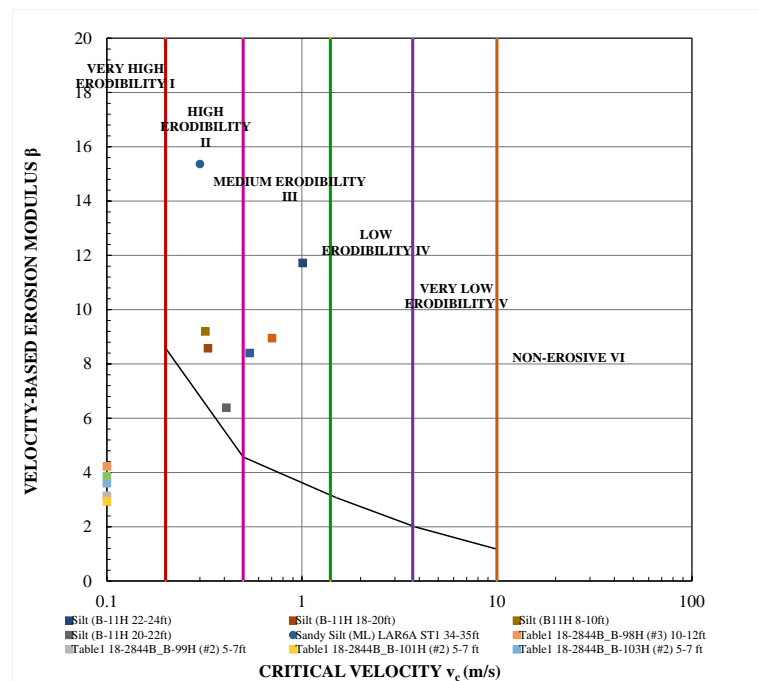


Figure 188. Velocity-based erosion modulus (β) vs. critical velocity (v_c) in semi-logarithmic scale for silt

8.6.3. Sand

All sand samples used for the new erosion model verification show high erodibility. The erosion curves on Figure 189 and Figure 190 are in Category I (Very High Erodibility) and Category II (High Erodibility). According to the critical shear stress and critical velocity charts Figure 191 and Figure 192, sand is in Category II (High Erodibility). Meanwhile, the erosion moduli α and β have a wide variation showing that the erosion slopes have different shapes, but the critical erosion parameters are very low: the critical shear stress for sand is $\tau_c < 1$ Pa and the critical velocity is $v_c < 0.3$ m/s.

It is worth to mention that the erosion moduli α and β were obtained as an average of the slope calculated between the critical shear stress and critical velocity points and each point on the erosion curve. Those points come from the tests # 1027, 1028, 1060, 1069-1085, 1087-1092 in the TAMU-Erosion database. The values of erosion modulus α varies from 2 to 9.5 and erosion modulus β varies from 4 to 18.5.

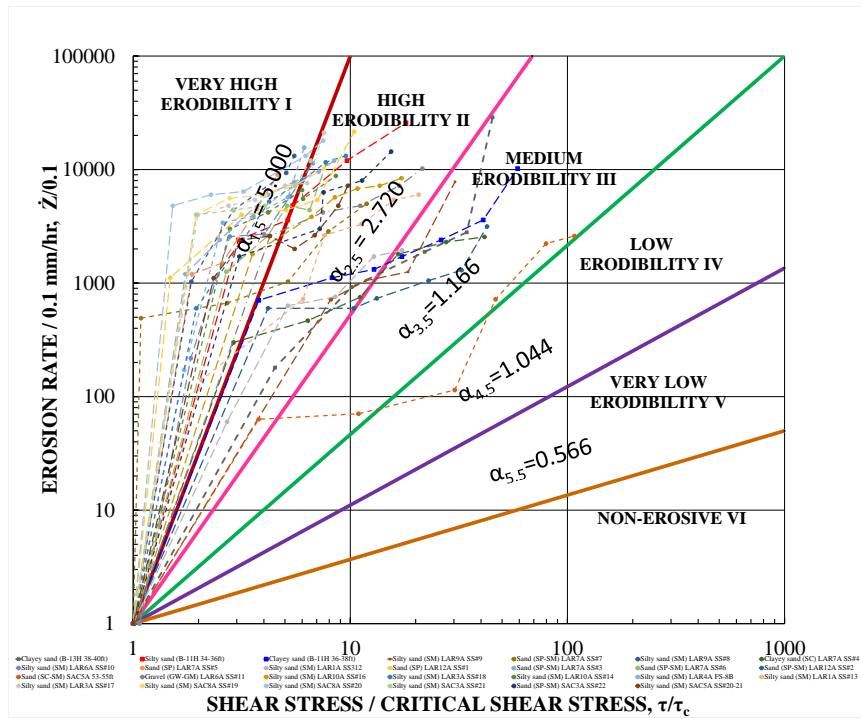


Figure 189. New shear stress-based erosion classification chart for sand

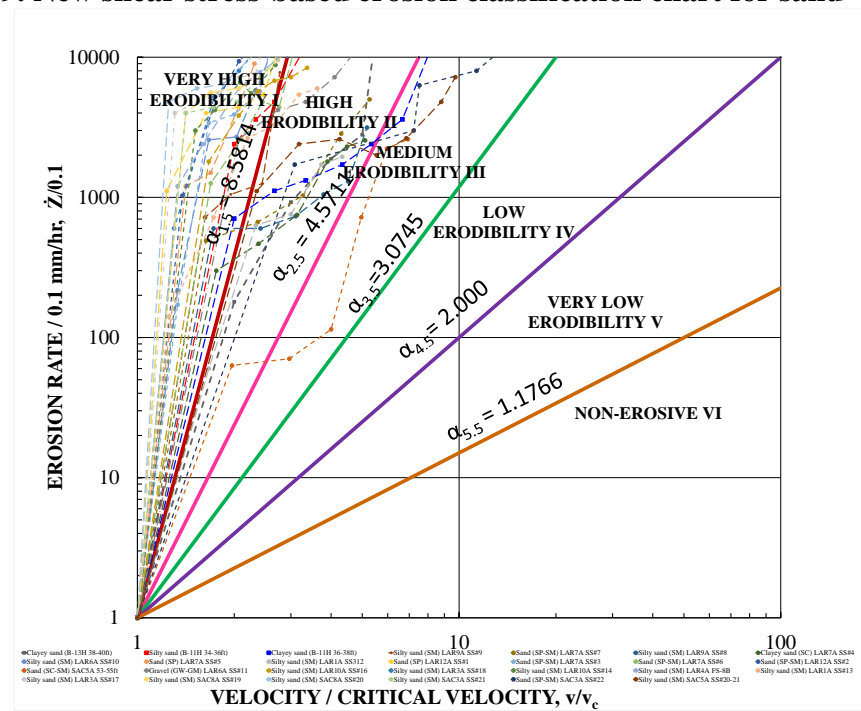


Figure 190. New velocity-based erosion classification chart for sand

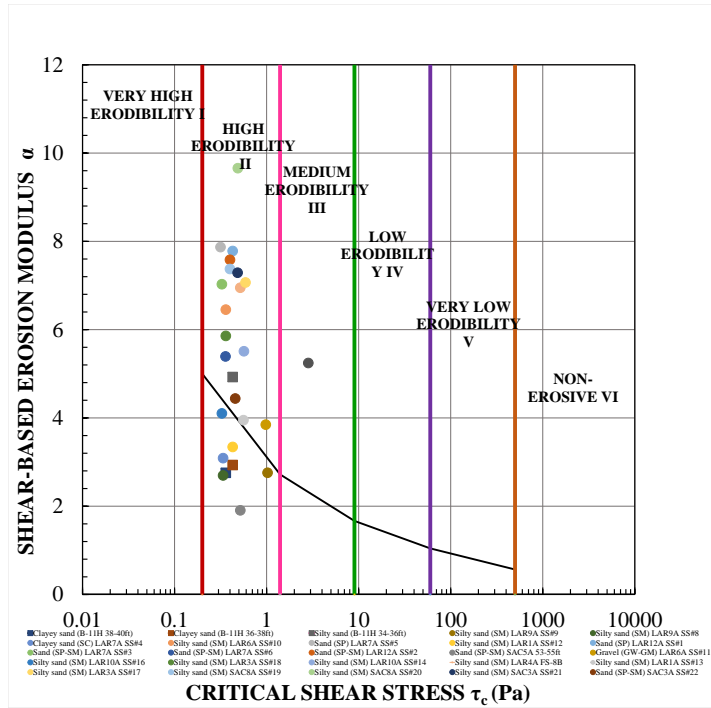


Figure 191. Shear stress-based erosion modulus (α) vs. critical shear stress (τ_c) in semi-logarithmic scale for sand

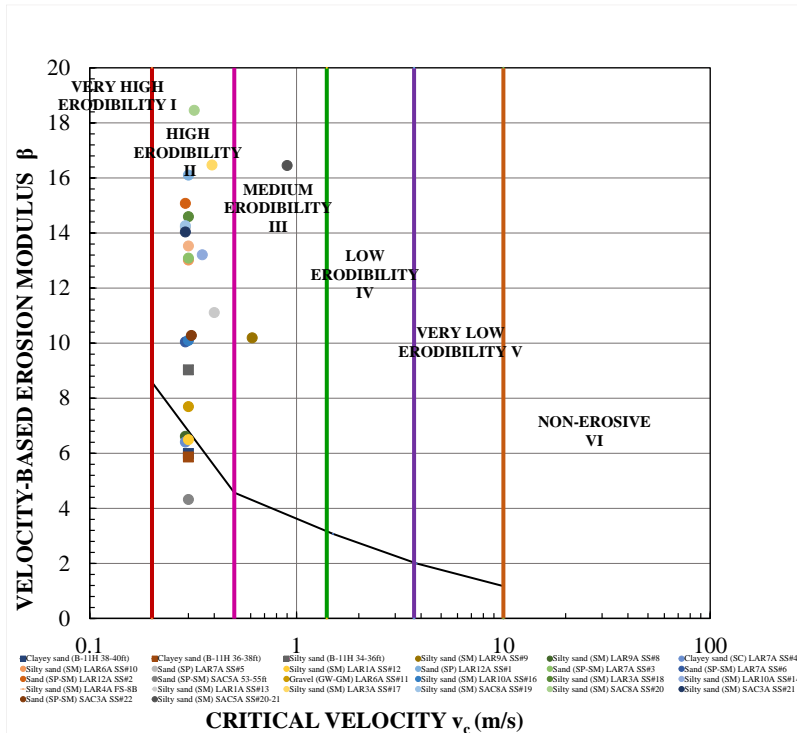


Figure 192. Velocity-based erosion modulus (β) vs. critical velocity (v_c) in semi-logarithmic scale for sand

8.6.4. Grass

The new model is proposed to use for grass. Figure 193 shows the new shear stress-based erosion classification chart for grass including Bermudagrass, St. Augustinegrass, Zoysiagrass, and Bahiagrass. Erodibility of grass varies from Category II (High Erodibility) to Category V (Very Low Erodibility). Figure 194 illustrates that considering velocity chart, grass is in Category I (Very High Erodibility) to Category IV (Low Erodibility).

Figure 195 and Figure 196 show the erosion modulus α versus critical shear stress and erosion modulus β versus critical velocity correspondingly. The erosion modulus for grass was obtained as an average of the slope calculated between the critical shear stress points or critical velocity points and each point on the erosion curve. Those points come from the tests # 1093-1136 in the TAMU-Erosion database. The black curve shows Briaud boundaries, and the green line is a trend line for grass. The curve for grass shows that erosion modulus increases with a critical shear stress or critical velocity which is counter intuitive. The reason is that once the grass mat is removed, erosion moves to a soil underneath the grass. The soil is subjected to high velocity and high shear stress therefore erosion is so dramatic. It is not a really grass modulus at the end of erosion curve but soil modulus at a high velocities and shear stress.

The erosion modulus α of grass varies from 1.5 to 9. The erosion modulus β is in a range of 3 to 18. As it was mentioned in Section 8.5, the erosion classification based on critical shear stress or critical velocity is more reliable than on erosion modulus. Considering values of thresholds (critical shear stress and critical velocity) shown on

Figure 195 and Figure 196, grass depending on a type and a variety, is in Category II and Category V. Overall, grass is more erosion resistant than base soil as it was demonstrated in Chapter 4.

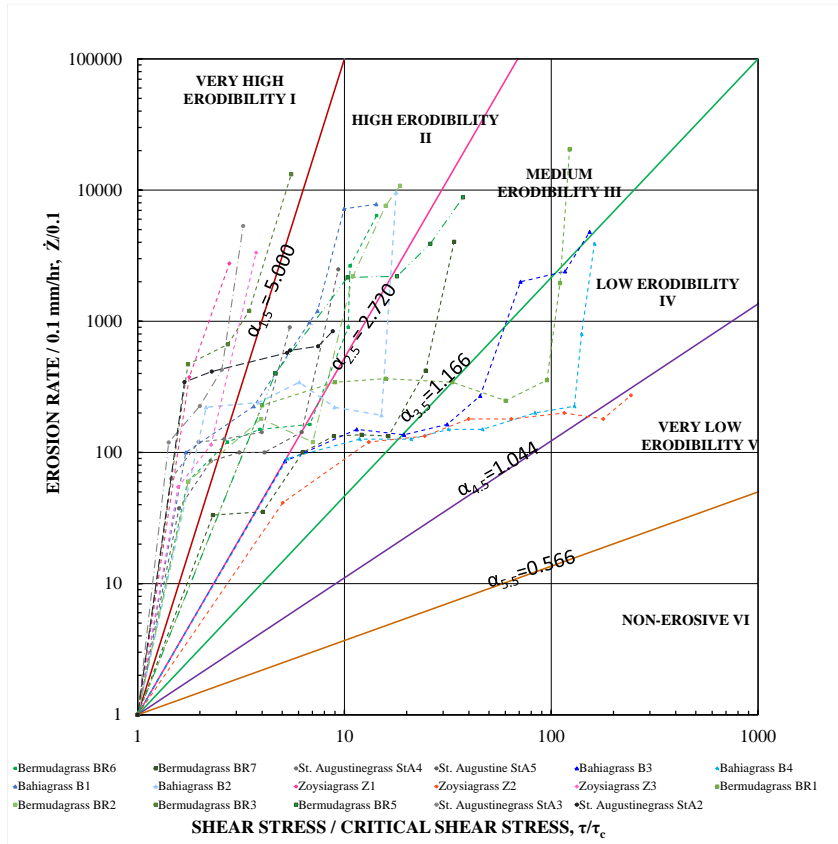


Figure 193. New shear stress-based erosion classification chart for grass

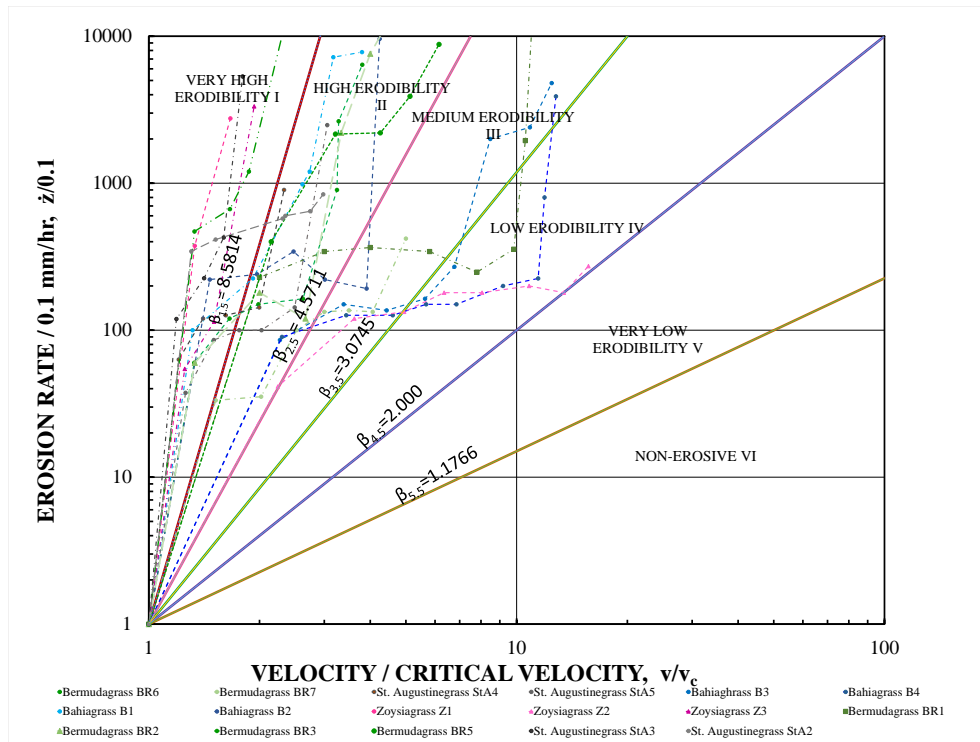


Figure 194. New velocity-based erosion classification chart for grass

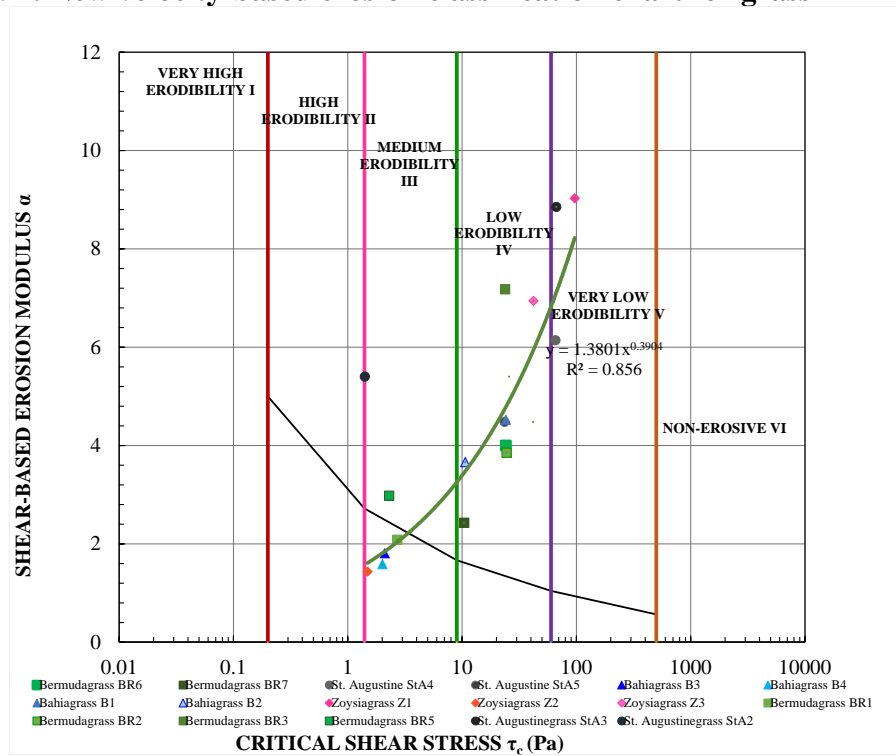


Figure 195. Shear stress-based erosion modulus (α) vs. critical shear stress (τ_c) in semi-logarithmic scale for grass

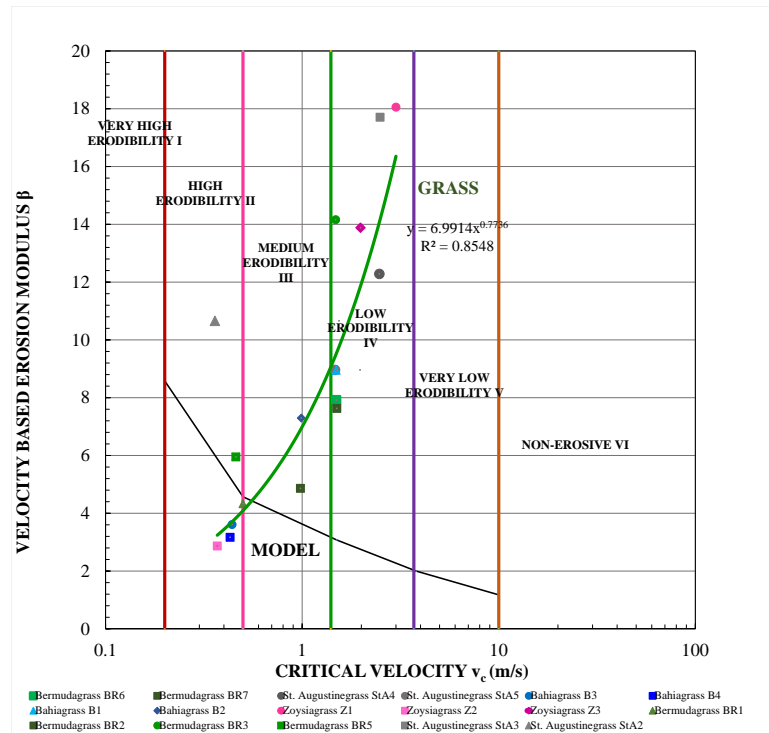


Figure 196. Velocity-based erosion modulus (β) vs. critical velocity (v_c) in semi-logarithmic scale for grass

8.6.5. Riprap

All “riprap” samples where gravel is used to reproduce riprap, were chosen for the verification of the new erosion model. The erosion curves on Figure 197 and Figure 198 are in Category I (Very High Erodibility) and Category II (High Erodibility) which shows the erosion behavior of riprap above the critical point when $v/v_c \geq 1.0$ and $z/0.1 \geq 1.0$. It means that once the critical point is reached, erosion progresses fast until riprap fails.

According to the critical shear stress and critical velocity charts (Figure 199 and Figure 200), riprap is in Category III (Medium Erodibility) and Category IV (Low

Erodibility). The erosion modulus α varies from 4 to 8 (Figure 199) and the erosion modulus β varies from 7.5 to 18 (Figure 200).

It is worth to mention that the erosion moduli α and β were obtained as an average of the slope calculated between the critical shear stress and critical velocity points and each point on the erosion curve. Those points come from the tests # 1237-1248 in the TAMU-Erosion.

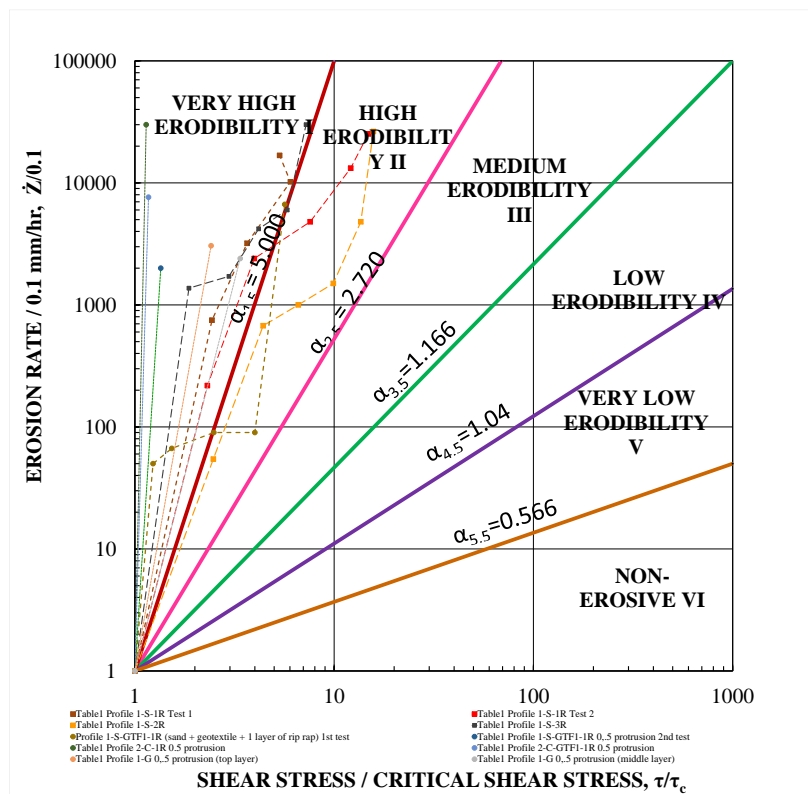


Figure 197. New shear stress-based erosion classification chart for riprap

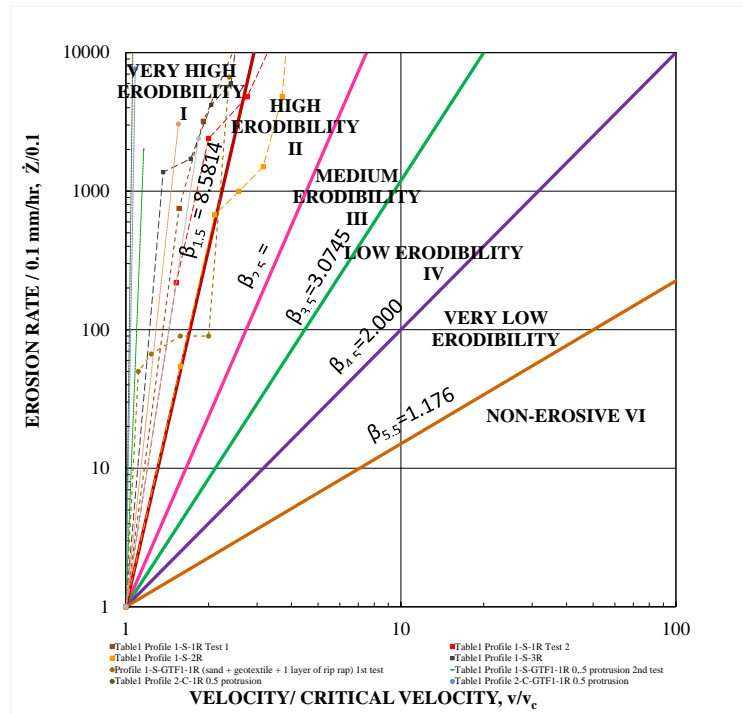


Figure 198. New velocity-based erosion classification chart for riprap

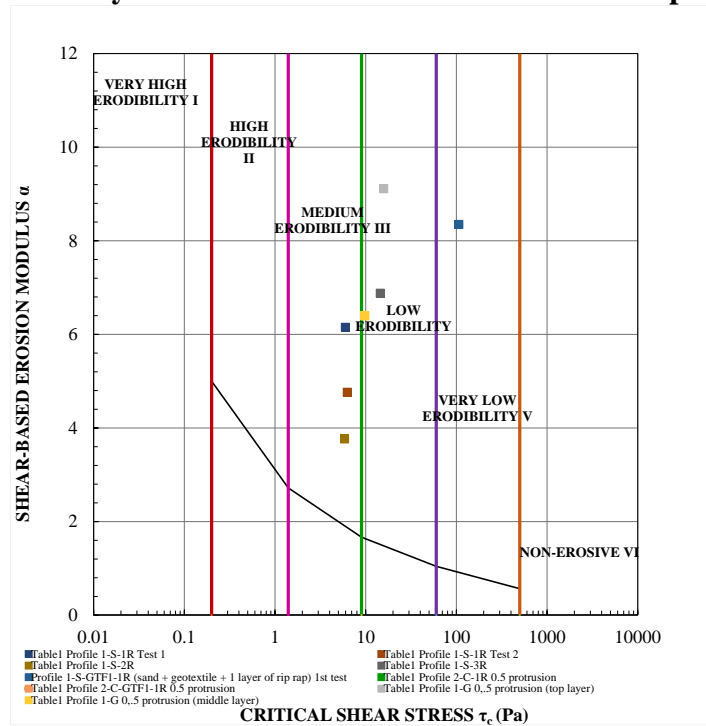


Figure 199. Shear stress-based erosion modulus (α) vs. critical shear stress (τ_c) in semi-logarithmic scale for riprap

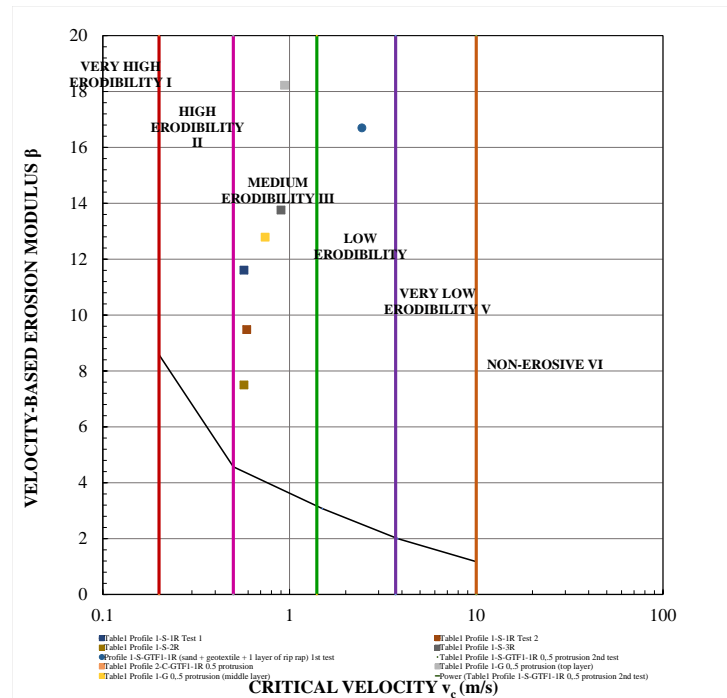


Figure 200. Velocity-based erosion modulus (β) vs. critical velocity (v_c) in semi-logarithmic scale for riprap

8.6.6. Enzyme treated soil

Enzyme-treated soil were chosen for the verification of the new erosion model.

The erosion functions on

Figure 201 and Figure 202 are in Category I (Very High Erodibility) and Category IV (Low Erodibility) which shows the erosion behavior of enzyme-treated soil above the critical point when $v/v_c \geq 1.0$ and $z/0.1 \geq 1.0$. It means that the enzyme-treated soil exhibits different erosion behavior showing that when the critical point is reached, erosion can progress fast as well as slow until soil fails. According to the critical shear stress and critical velocity charts (Figure 203 and Figure 204), enzyme-treated soil is in Category II (High Erodibility) and Category IV (Low Erodibility). The erosion modulus α varies from 1.5 to 5.5 and the erosion modulus β varies from 4 to 12.

It is worth to mention that the erosion moduli α and β were obtained as an average of the slope calculated between the critical shear stress and critical velocity points and each point on the erosion curve. Those points come from the tests # 1212-1236 in the TAMU-Erosion database.

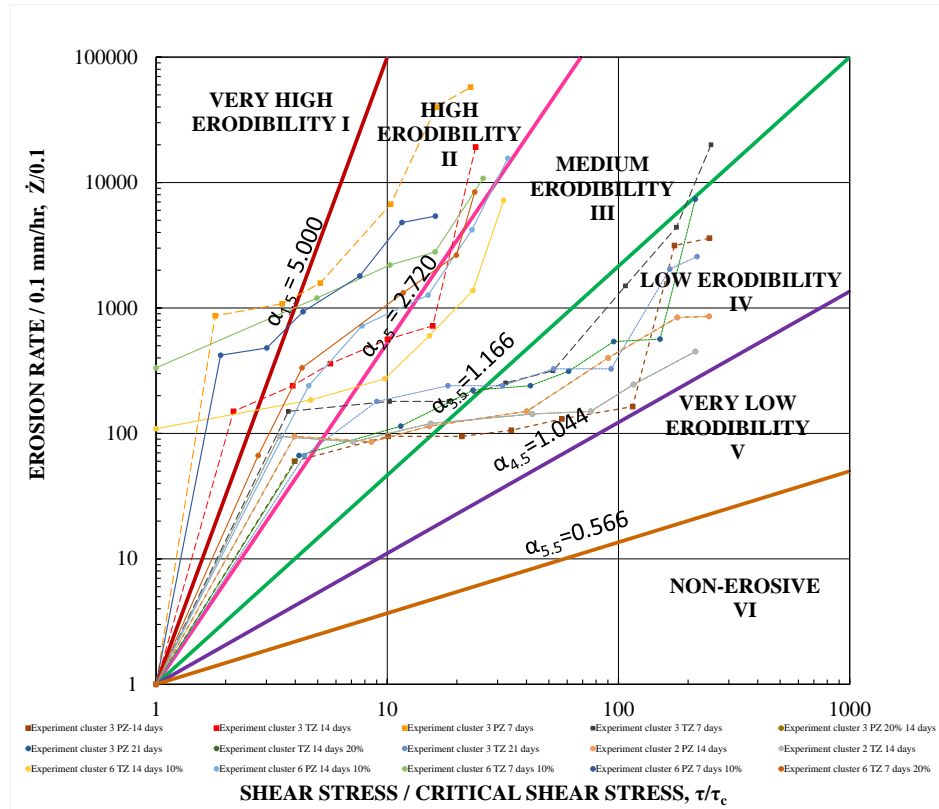


Figure 201. New shear stress-based erosion classification chart for enzyme treated soil

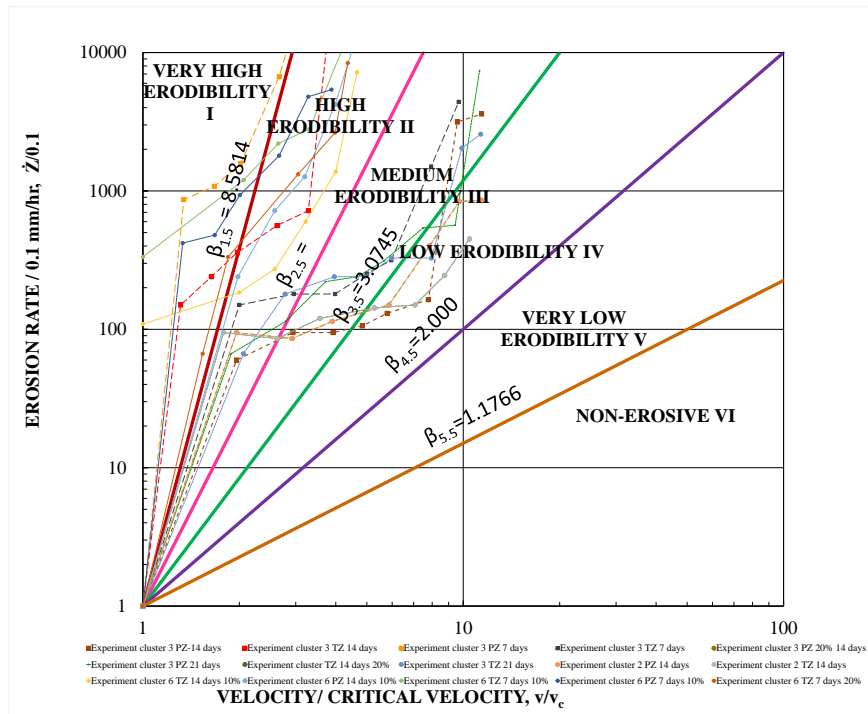


Figure 202. New velocity-based erosion classification chart for enzyme treated soil

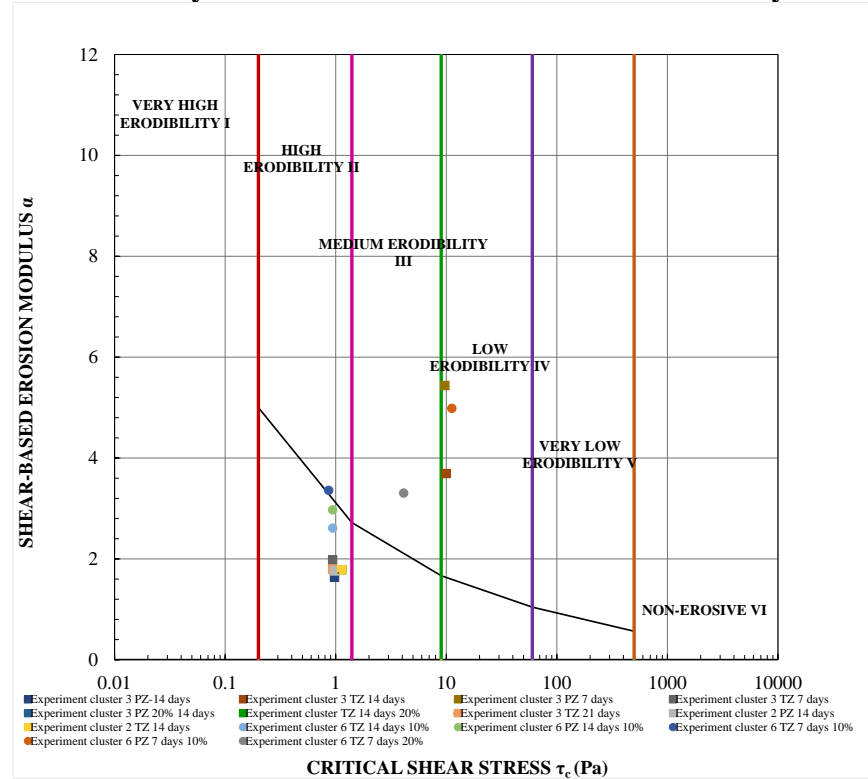


Figure 203. Shear stress-based erosion modulus (α) vs. critical shear stress (τ_c) in semi-logarithmic scale for enzyme treated soil

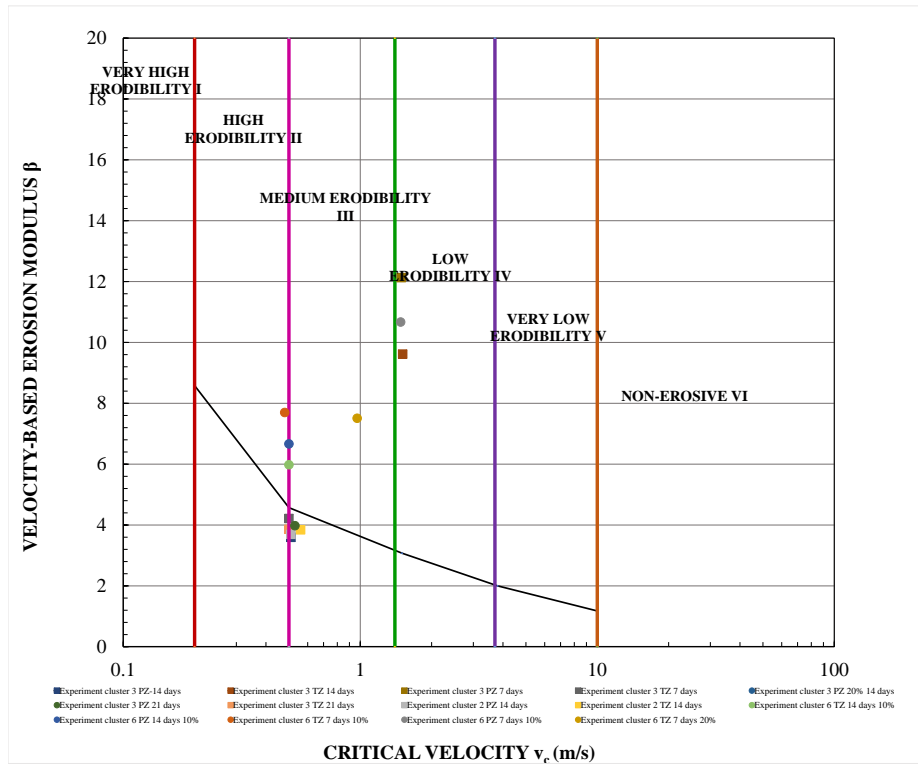


Figure 204. Velocity-based erosion modulus (α) vs. critical shear stress (τ_c) in semi-logarithmic scale for enzyme treated soil

8.6.7. Lime treated soil

Lime treated soil were chosen for the verification of the new erosion model. The erosion functions on Figure 205 and Figure 206 are in Category I (Very High Erodibility) and Category IV (Low Erodibility) which shows the erosion behavior of lime treated soil above the critical point when $v/v_c \geq 1.0$ and $\dot{z}/0.1 \geq 1.0$. It means that the lime-treated soil exhibits different erosion behavior showing that when the critical point is reached, erosion can progress fast as well as slow until soil fails. According to the critical shear stress and critical velocity charts (Figure 207 and Figure 208), enzyme-treated soil is in Category II (High Erodibility) and Category V (Very Low Erodibility). The erosion modulus α varies in a wide range from 1 to 13 and the erosion modulus β

varies from 5 to 26. The highest erosion modulus was obtained for the less erodible lime treated soil.

It is worth to mention that the erosion moduli α and β were obtained as an average of the slope calculated between the critical shear stress and critical velocity points and each point on the erosion curve. Those points come from the tests # 1202-1211 in the TAMU-Erosion database.

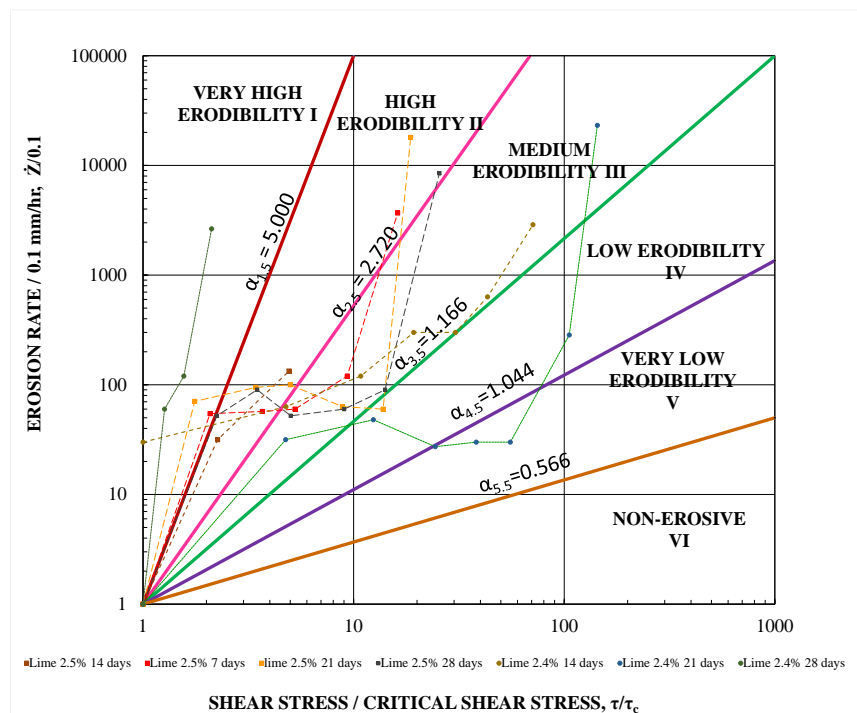


Figure 205. New shear stress-based erosion classification chart for lime treated soil

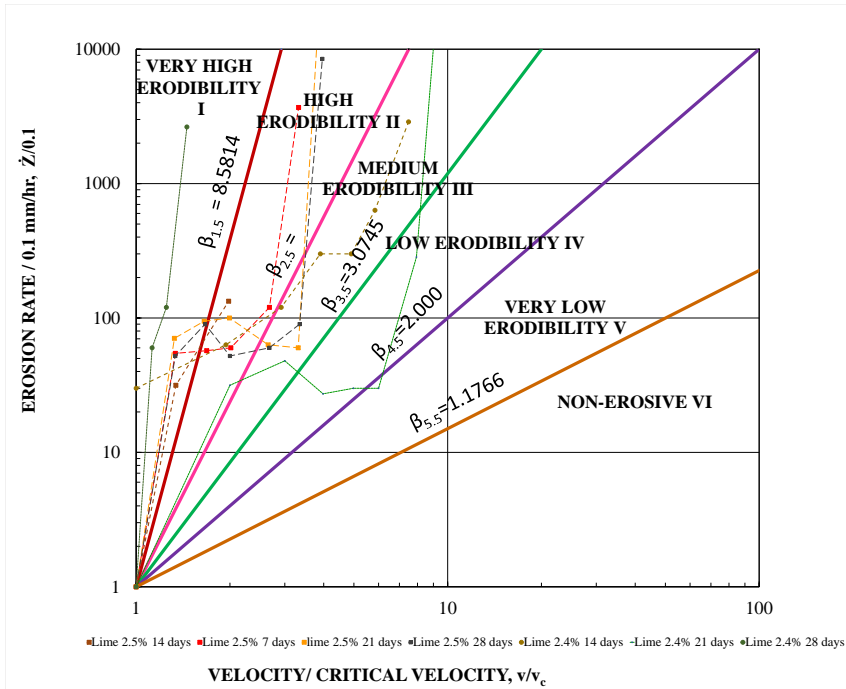


Figure 206. New velocity-based erosion classification chart for lime treated soil

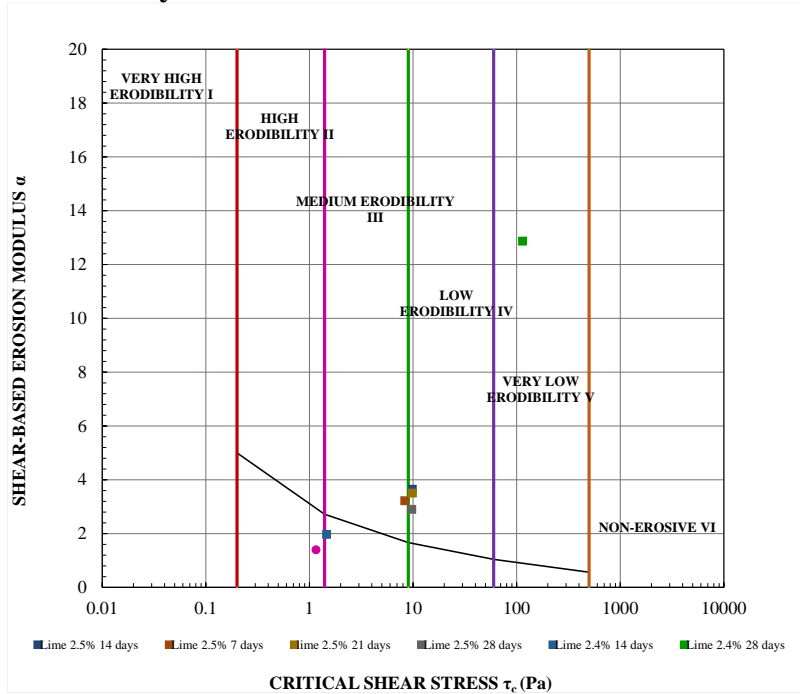


Figure 207. Shear stress-based erosion modulus (α) vs. critical shear stress (τ_c) in semi-logarithmic scale for lime treated soil

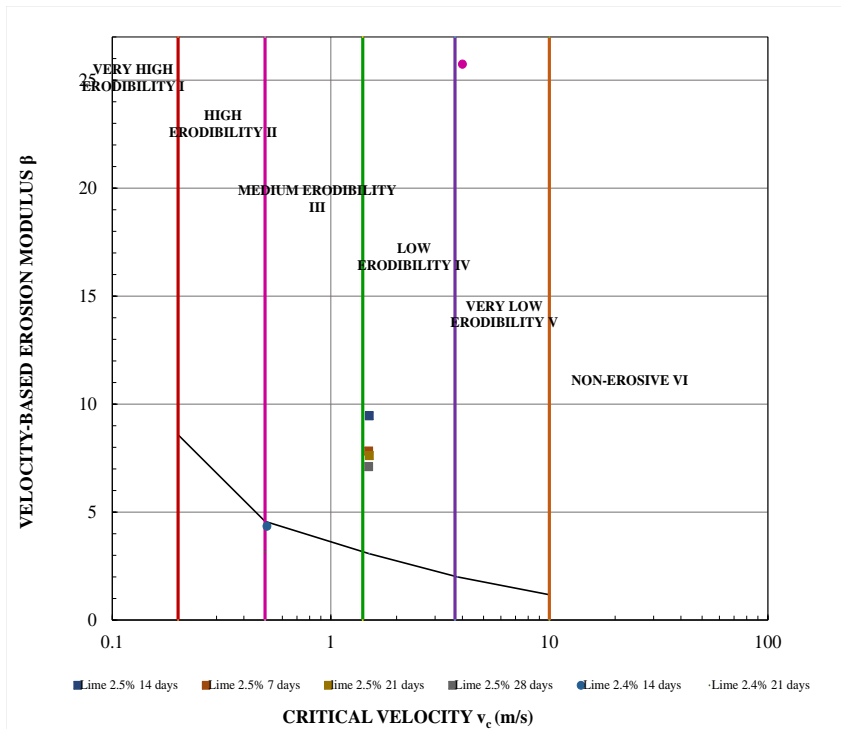


Figure 208. Velocity-based erosion modulus (α) vs. critical shear stress (τ_c) in semi-logarithmic scale for lime treated soil

8.7. Application of new erosion model

This chapter addresses the erosion aspect of the levees as they are overtopped by water. This chapter also develops a simple methodology (spreadsheet-level) for estimating a depth of erosion for levees, dams, embankments, and other similar structures. This methodology makes a use of the new erosion classification and the erosion modulus which were discussed in Section 8.5.

The numerical simulation performed by Dr. Chen (Briaud et. al., 2008) shows that the maximum velocity around the toe of the downstream levee surface is 12 m/s. The corresponding value of shear stress in the toe region of the downstream levee

surface is about 50–60 Pa. The maximum shear stress acts on the top of the levee and reaches 230 Pa (Figure 209).

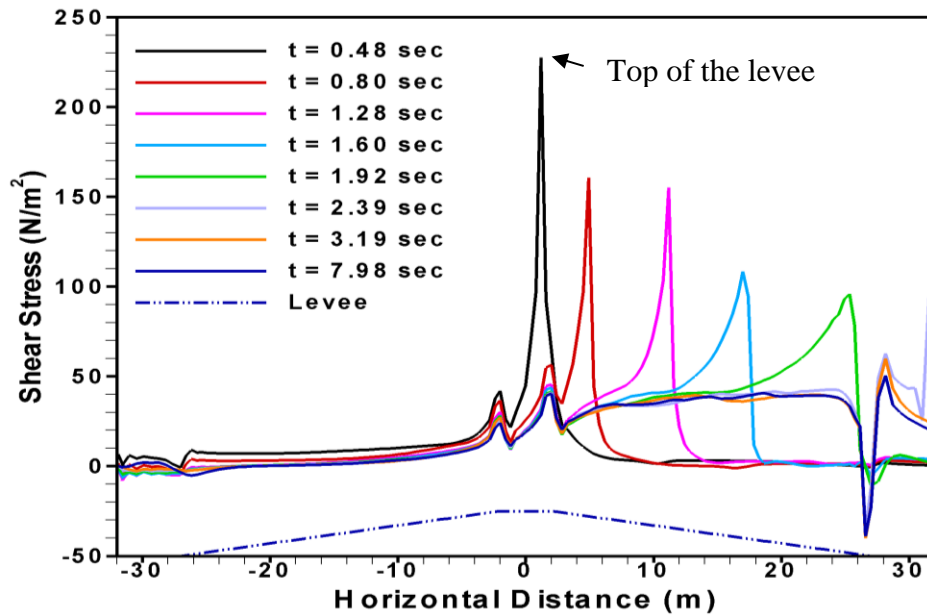


Figure 209. Shear stresses on levee surface (adapted from Briaud et al., 2008)

Note that overtopping of levees is not considered in levee design in the US. Flood return period used in Netherlands for levees design is 1/10,000 for most populated areas and 1/4,000 for less populated area. The probability of such a failure happening in any year is 0.0001 and 0.004 correspondingly (Silva et al., 2004). To compare, typical flood return period in the US for bridges design is 1/500 and 1/100 having annual exceedance probability of 0.2 % and 1 % correspondingly.

Hurricanes are large masses of wind and rain with various characteristics. The following numbers give an idea of hurricanes characteristics:

- a. Affected zone - 402 km (250 miles) in diameter
- b. Travel speed - 40 km/h (25 mph)

- c. Time on a levee or a bridge – around 10 hours
- d. Number of wave cycles - 6000

8.7.1. Prediction of levee erosion

New erosion model can be applied to predict levees erosion during a storm. It is used to calculate the depth of erosion by the end of the storm for a design case.

Problem statement. A soil erodibility is governed by the following model (new erosion model) (Eq. 40).

$$\frac{\dot{z} \text{ (mm/hr)}}{0.1 \text{ mm/hr}} = \left(\frac{\tau}{\tau_c} \right)^\alpha \quad (40)$$

where α is the shear stress-based erosion modulus. The erosion modulus α varies from 0.5 for very erosion resistant soils to 5 and more for very erodible soils (Section 8.5). The erosion modulus in this case is 2 (medium erodibility soil). The soil is needed to build a levee. Two design cases for overtopping erosion are being considered:

Scenario 1. The ratio of shear stress acting on the soil surface to critical shear stress $\frac{\tau}{\tau_c} = 3$ for a storm duration of 48 hours.

Scenario 2. The ratio of shear stress acting on the soil surface to critical shear stress $\frac{\tau}{\tau_c} = \frac{t(\text{hrs})}{6}$ for the first 24 hours of storm.

Scenario 3. The ratio of shear stress acting on the soil surface to critical shear stress $\frac{\tau}{\tau_c} = 8 - \frac{t(\text{hrs})}{6}$ for the next 24 hours.

For each design scenario, the depth of erosion of the levee by the end of the storm can be calculated by integration.

Scenario 1. The ratio of shear stress acting on the soil surface to critical shear stress $\frac{\tau}{\tau_c} = 3$ and a duration of the storm is 48 hours ($t = 48$ hours) (Figure 210).

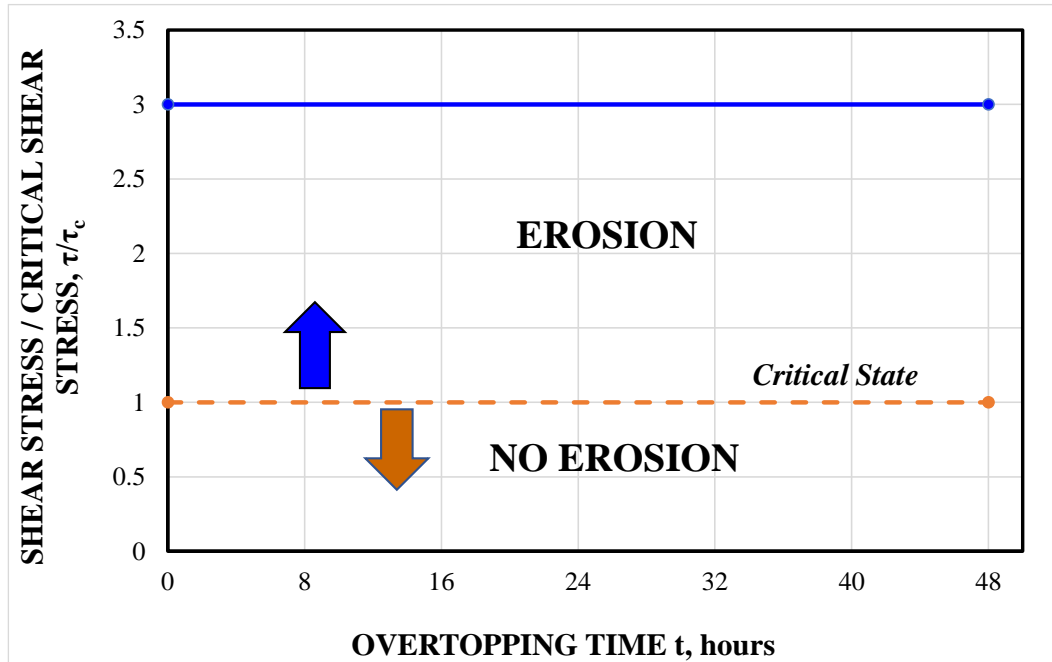


Figure 210. Shear stress over critical shear stress τ/τ_c versus time t

Solution. Differentiate a new erosion function with a respect to time:

$$\frac{dz}{dt} = 0.1\left(\frac{\tau}{\tau_c}\right)^2 \quad (41)$$

Replace a ration of $\frac{\tau}{\tau_c}$ with 3:

$$dz = 0.1 * 3^2 dt \quad (42)$$

Integrate a function dz from 0 to 48 hours:

$$\int_0^{48} dz = 0.9 \int_0^{48} dt = 0.9(48 - 0) \quad (43)$$

$$z = 43.2 \text{ mm}$$

The depth of erosion of the levee is 43.2 mm for a storm duration of 48 hours.

The corresponding erosion rate would be $\dot{z}=0.9$ mm/hr. The depth of erosion versus time of overtopping is plotted in

Figure 211. This example shows how the model allows the engineer to calculate the total erosion at the end of the storm. Note that in this case, there is only one cycle of loading and the shear stress is constant. The next example considers the effect of the rise and the fall of the storm.

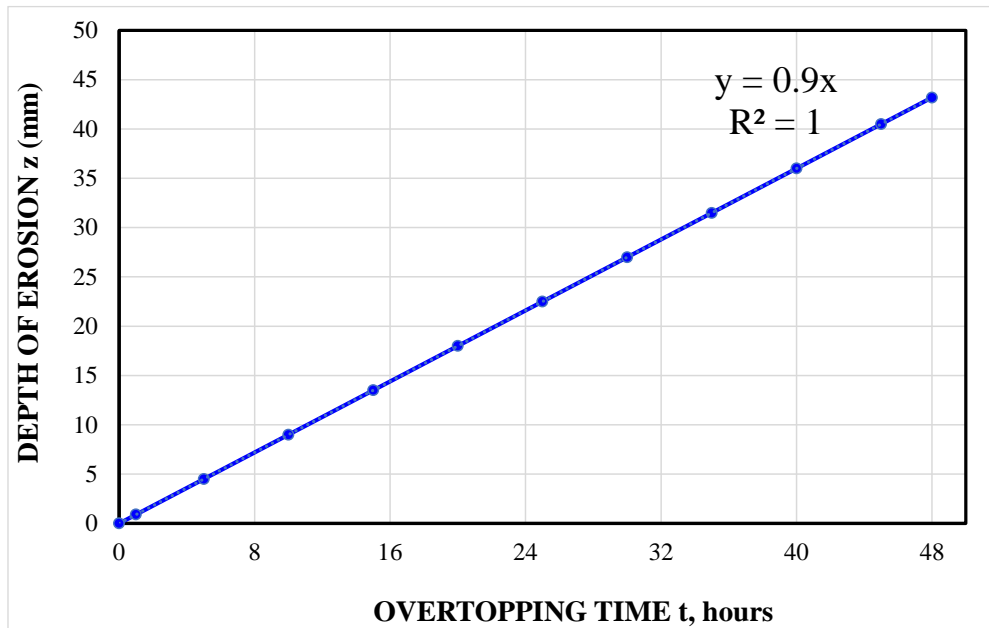


Figure 211. Depth of erosion versus overtopping time (Scenario 1)

Scenario 2. The ratio of shear stress acting on the soil surface to critical shear

stress $\frac{\tau}{\tau_c} = \frac{t(\text{hrs})}{6}$ for the first 24 hours of storm ($t < 24$ hours) (Figure 212).

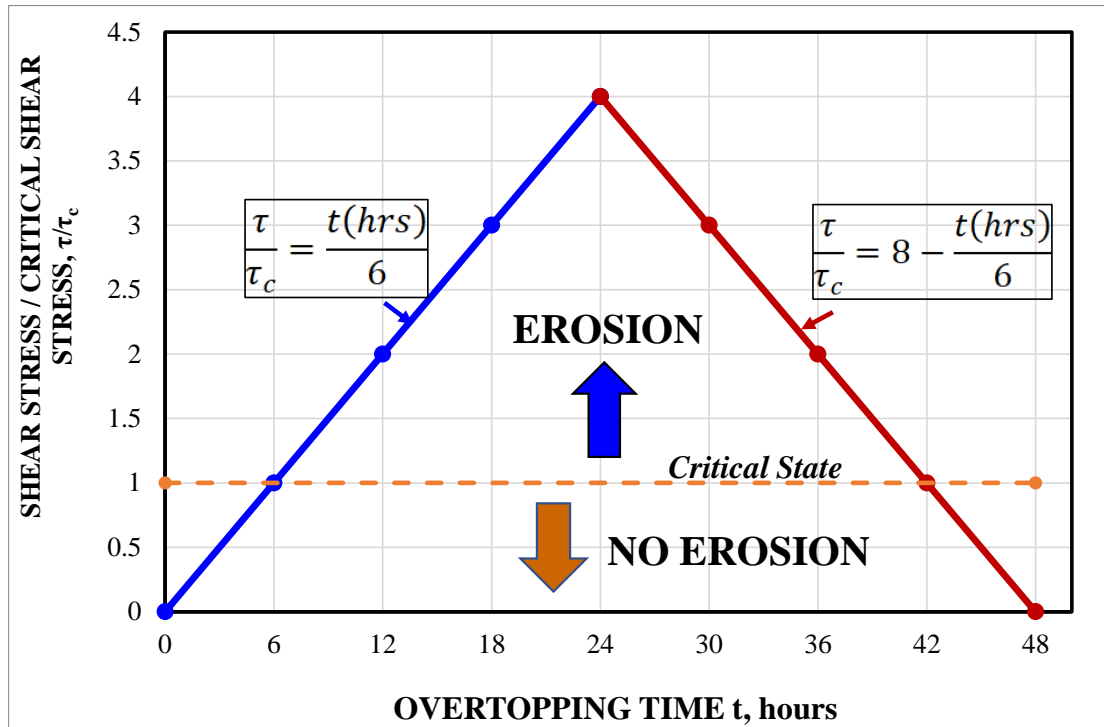


Figure 212. Shear stress / critical shear stress versus overtopping time (Scenario 2 and 3)

Solution. According to the definition, erosion does not take place or erosion can be neglected when shear stress acting on the soil-water flow interface is below critical shear stress ($\frac{\tau}{\tau_c} < 1$). Erosion initiates at the critical point $\frac{\tau}{\tau_c} = 1$; this condition is called critical state. Erosion progresses when acting shear stress is higher than critical shear stress, a soil can tolerate before starting to erode ($\frac{\tau}{\tau_c} > 1$). Therefore, for a given scenario with $\frac{\tau}{\tau_c} = \frac{t(hrs)}{6}$, erosion would not be observed the first 6 hours of a storm.

In a differentiated new erosion function, replace $\frac{\tau}{\tau_c}$ with $\frac{t(hrs)}{6}$:

$$\frac{dz}{dt} = 0.1\left(\frac{t}{6}\right)^2 \quad (44)$$

$$dz = 0.1 * \frac{t^2}{36} dt \quad (45)$$

Integrate a function dz from 6 to 24 hours (Eq. 46):

$$\int_6^{24} dz = \frac{0.1}{36} \int_6^{24} t^2 dt = \frac{0.1}{36} \left[\frac{t^3}{3} \right]_6^{24} = \frac{0.1}{36} \left(\frac{24^3}{3} - \frac{6^3}{3} \right) \quad (46)$$

$$z_1 = 12.6 \text{ mm}$$

The depth of erosion of the levee is 12.6 mm for a storm duration 24 hours (assuming no erosion is taking place for the first six hours). The corresponding erosion rate would be $\dot{z}=0.7$ mm/hr. The general equation for obtaining the depth of erosion z_1 at any time t corresponding to the model (Scenario 2) is:

$$z_1 = \frac{0.1}{36} \left(\frac{t^3}{3} - \frac{6^3}{3} \right) \quad (47)$$

Scenario 3. The ratio of shear stress acting on the soil surface to critical shear stress

$\frac{\tau}{\tau_c} = 8 - \frac{t(\text{hrs})}{6}$ for the next 24 hours of storm ($t = 24 - 48$ hours) (Figure 212).

In a differentiated new erosion function, replace $\frac{\tau}{\tau_c}$ with $8 - \frac{t(\text{hrs})}{6}$:

$$\frac{dz}{dt} = 0.1 \left(8 - \frac{t}{6} \right)^2 \quad (48)$$

$$dz = 0.1 \left(8 - \frac{t}{6} \right)^2 dt \quad (49)$$

$$dz = 0.1 \left(64 - 2 * 8 * \frac{t}{6} + \frac{t^2}{36} \right) dt = \left(6.4 - 0.267t + \frac{t^2}{360} \right) dt \quad (50)$$

Integrate a function dz from 24 to 42 hours (Note that at $\frac{\tau}{\tau_c} = 1$ no erosion is observed and, therefore, the corresponding time would be $t=42$ hours). The integration with a respect to time is set between 24 and 42 hours.

$$\int_{24}^{42} dz = \int_{24}^{42} \left(6.4 - 0.267t + \frac{t^2}{360} \right) dt = \left[6.4t - 0.267 \frac{t^2}{2} + \frac{t^3}{3 \cdot 360} \right]_{24}^{42} \quad (51)$$

$$z_2 = 115.2 - 0.267 \left(\frac{42^2}{2} - \frac{24^2}{2} \right) + \frac{42^3 - 24^3}{3 \cdot 360} = 115.2 - 0.267 \cdot 594 + 55.8$$

$$z_2 = 12.4 \text{ mm}$$

The total depth of erosion for a storm duration from 24 to 42 hours:

$$z_{total} = 25.0 \text{ mm}$$

The total depth of erosion of the levee is 25 mm for a storm duration 24 hours (assuming no erosion is taking place for the last six hours). The corresponding erosion rate would be $\dot{z}=0.7$ mm/hr. The general equation for obtaining the depth of erosion z_2 at any time t corresponding to the model (Scenario 3) is:

$$z_2 = 6.4t - 0.267 \left(\frac{t^2}{2} - \frac{24^2}{2} \right) + \frac{t^3 - 24^3}{3 \cdot 360} \quad (52)$$

Table 48 shows a change of erosion depth for different scenarios considered above. Figure 213 indicates the relationship between shear stress over critical shear stress and overtopping time.

Table 48. Depth of erosion of the levee for different cases

Scenario	Function of shear stress over critical shear stress $\frac{\tau}{\tau_c}$	Storm duration t (hours)	Time t corresponding to z	Depth of erosion of the levee z (mm)
A	$\frac{\tau}{\tau_c} = 3$	48	48	43.2
B	$\frac{\tau}{\tau_c} = \frac{t(\text{hrs})}{6}$	1 st 24	24	12.6
C	$\frac{\tau}{\tau_c} = 8 - \frac{t(\text{hrs})}{6}$	2 nd 24	18	12.4

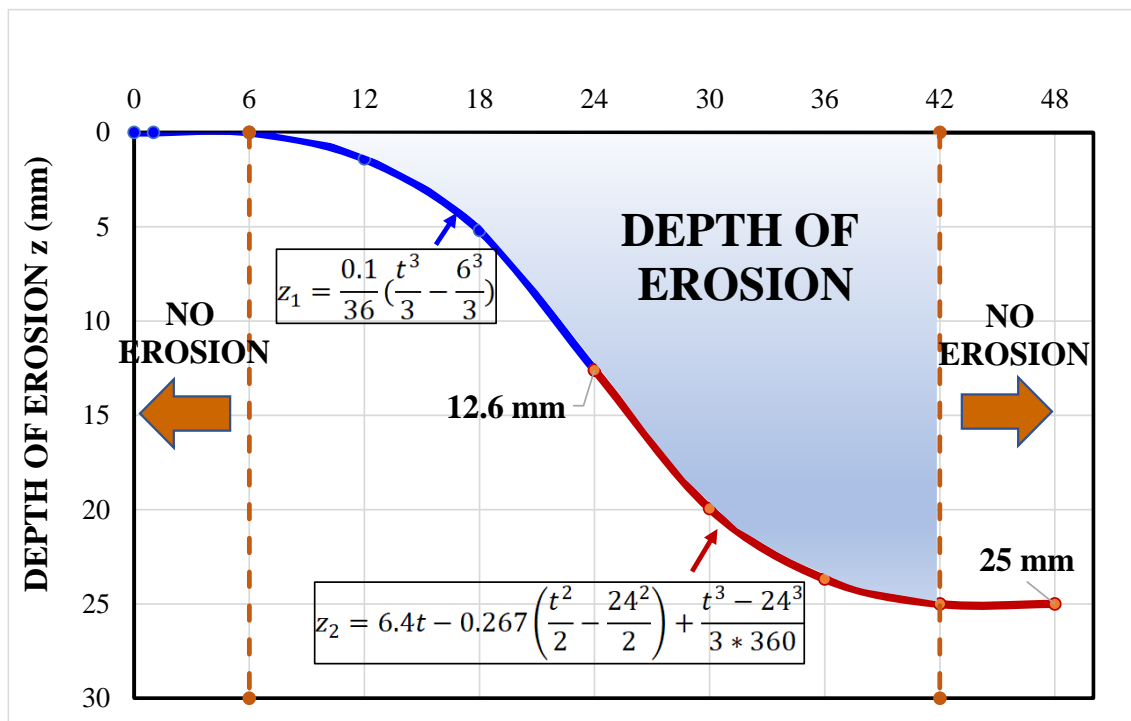


Figure 213. Depth of erosion versus overtopping time (Scenario 2 and 3)

The example presented above shows how the model allows the engineer to calculate the total erosion at the end of the storm. Note that in this case, there is only one cycle of loading. The next example considers the effect of the number of overtopping cycles created by waves.

8.7.2. Effect of overtopping cycling on erosion depth

A levee is overtopped by 5000 waves during a hurricane. Each wave generates a shear stress loading as shown on

Figure 214. The levee made of sandy soil of 5 m thick and covered with the grass of 0.05 m tall.

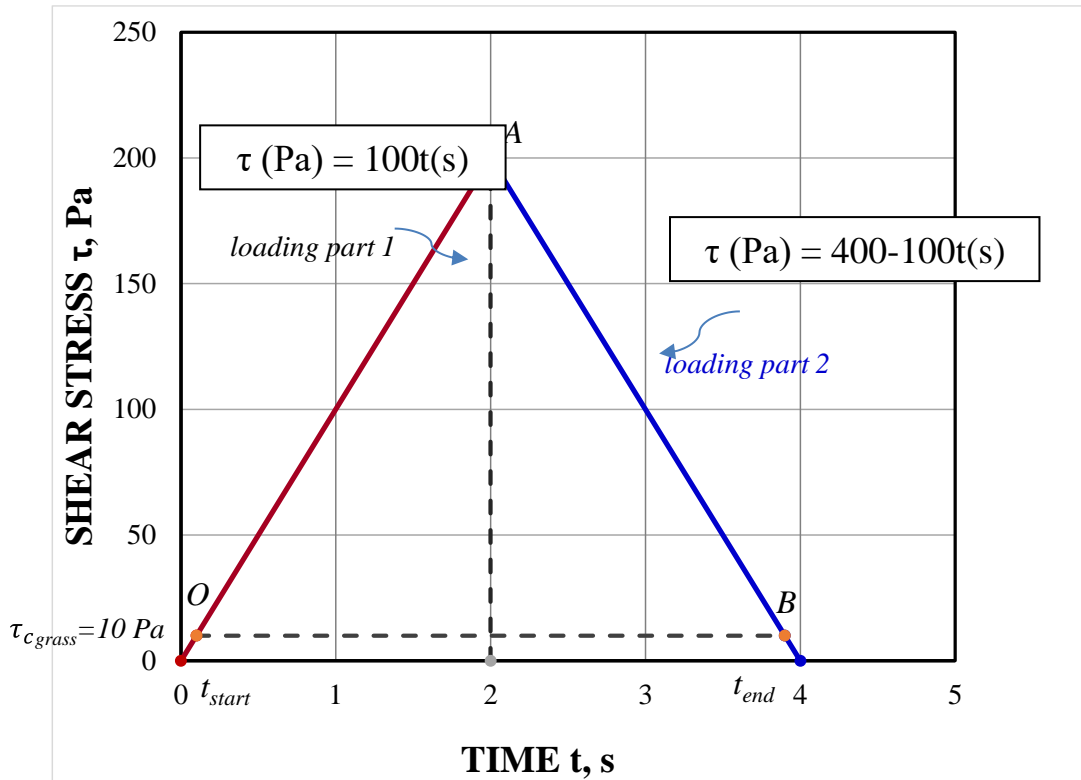


Figure 214. Shear stress vs. time (Scenario 2 and 3)

The erosion function of the levee is made of two components: grass and soil underneath. The erosion function for grass (for example, Bermudagrass) is shown below:

$$\frac{dz}{dt} = 0.1 \left(\frac{\tau}{\tau_c} \right)^2 \quad (53)$$

where τ is the shear stress, τ_c is the critical shear stress, $\tau_c = 10 \text{ Pa}$, $\alpha=2$.

The erosion function for soil is:

$$\frac{dz}{dt} = 0.1 \left(\frac{\tau}{\tau_c} \right)^3 \quad (54)$$

where τ_c is the critical shear stress, $\tau_c = 3 \text{ Pa}$, $\alpha=3$.

The depth of erosion of the levee can be obtained as follows.

8.7.3. Obtaining erosion depth for grass

When a levee is overtopped, erosion depth first is calculated assuming that only grass is being eroded. The following steps are considered:

Step 1. Find the equation for shear stress vs. time.

Step 2. Replace shear stress by function of time in erosion function. Define time corresponding to time when erosion of grass layer starts and ends. Note that there is no erosion when shear stress (τ) is less than critical shear stress (τ_c). Consider the loading part 1 so far only. For grass, considering the loading part 1 on

Figure 214, erosion starts at $\tau_c = 10 \text{ Pa}$ with corresponding time $t_{\text{start}} = t_1 = 0.1 \text{ s} = 0.1 / 3600 \text{ (hr)}$ and erosion ends at $\tau_c = 200 \text{ Pa}$ with corresponding time $t_{\text{end}} = t_2 = 2 \text{ s} = 2 / 3600 \text{ (hr)}$.

Step 3. Use the erosion function for grass and integrate for time t ($\tau_c = 10 \text{ Pa}$):

$$\frac{dz}{dt} = 0.1 \left(\frac{\tau}{10} \right)^2 = 0.1 \frac{1^2}{10^2} \tau^2 dt = \frac{1}{1000} \tau^2 dt \quad (55)$$

For the loading part 1: $\tau(\text{Pa})=100t(\text{s}) = 100*3600t \text{ (hr)}$

For the loading part 2: $\tau(\text{Pa})=400-100t(\text{s}) = 400-100*3600t \text{ (hr)}$

$$\text{and } dz = \frac{1}{1000} (100 * 3600)^2 dt \quad (56)$$

$$\text{and } \int_0^z dz = \int_{start}^{end} dz = \int_{0.1/3600}^{2/3600} \frac{1}{1000} (100 * 3600)^2 dt (hr) = \frac{100^2 * 3600^2}{1000} \left[\frac{t^3}{3} \right]_{0.1/3600}^{2/3600}$$

(57)

Step 4. Obtain the erosion depth z for one wave:

$$\text{so } z = \frac{100^2 * 3600^2}{1000 * 3 * 3600^3} (2^3 - 0.1^3) = 0.00741 \text{ mm}$$

Therefore, erosion depth of grass from O to A is $z=0.00741$ mm. By symmetry, erosion depth from A to B is $z=0.00741$ mm. The total erosion depth for grass from O to B is $z_{total} = 0.0148$ mm.

Step 5. Find the erosion depth for all wave cycle. Considering that there are 5000 waves during a hurricane and if the erosion functions do not change, the depth of erosion of grass is $z_{5000 \text{ waves}} = 5000 * 0.0148 = 74.07 \text{ mm} = 7.4 \text{ cm} = 0.074 \text{ m}$.

Step 6. Obtain a number of waves to erode grass. Considering the height of grass $h = 50 \text{ mm}$ and total erosion depth for one wave:

$$\frac{50 \text{ mm}}{0.0148 \text{ mm}} = 3378 \text{ waves will erode the grass layer completely. Note that erosion}$$

function is assumed to be constant during a hurricane.

8.7.4. Obtaining erosion depth for bare soil

After all grass is being eroded, erosion moves into the soil underneath. The following steps are considered:

1. Find the equation for shear stress vs. time.
2. Replace shear stress by function of time in erosion function. Define time corresponding to time when erosion starts and ends for grass and soil. Note that there is

no erosion when shear stress (τ) is less than critical shear stress (τ_c). Consider the loading part 1 so far only. For grass, considering the loading part 1 on

3. Figure 214, erosion starts at $\tau_c = 3$ Pa with corresponding time $t_{\text{start}} = t_1 = 3/100 = 0.03$ s = $0.03 / 3600$ (hr) and erosion ends at $\tau_c = 200$ Pa with corresponding time $t_{\text{end}} = t_2 = 2$ s = $2 / 3600$ (hr).

4. Use the erosion function for soil layer and integrate for time t ($\tau_c = 3$ Pa):

$$dz = 0.1\left(\frac{\tau}{3}\right)^3 = \frac{0.1}{27}\tau^3 dt = \frac{1}{270}(100 * 3600t \text{ (hr)})^3 dt \quad (58)$$

$$\int_0^z dz = \frac{100^3 * 3600^3}{270} \int_{\text{start}}^{\text{end}} \tau^3 dt = \frac{100^3 * 3600^3}{270} \left[\frac{t^4}{4} \right]_{0.03/3600}^{2/3600} \quad (59)$$

5. Obtain the erosion depth z for one wave:

$$\text{so } z = \frac{100^3 * 3600^3}{270 * 4 * 3600^4} (2^4 - 0.03^4) = 4.11 \text{ mm}$$

Therefore, erosion depth of soil from O to A is $z=4.11$ mm. By symmetry, erosion depth from A to B is $z=4.11$ mm. The total erosion depth of soil from O to B is $z_{\text{total}} = 8.22$ mm.

6. Find a number of waves needed to erode soil layer. If the thickness of soil layer is 5000 mm and the erosion depth of soil is 8.22 mm (assuming erosion function is constant), it needs 608 waves to erode soil layer completely.

8.7.5. Obtaining water velocity

To obtain the velocity at the downstream face toe of the levee, the energy conservation transfer principle is used. Energy is generally defined as a measure of an object's capability to do work. For a levee overtopping problem which is considered to

be an open-channel flow problem, potential and kinetic energy are of interest. The energy balance in an open-channel system is written as (Eq. 60 and Eq. 61):

$$E_A = E_B + \text{work done from A to B} \quad (60)$$

or

$$mgh_A + \frac{1}{2}mv_A^2 = mgh_B + \frac{1}{2}mv_B^2 + \text{work done from A to B} \quad (61)$$

where E_A is the energy at point A; E_B is the energy at point B.

For the levee problem, the components $\frac{1}{2}mv_A^2 = 0$ and $mgh_B = 0$ and $h_A=h$, where h is the height of the levee. Therefore, the Eq. 61 can be rewritten as:

$$mgh_A = \frac{1}{2}mv_B^2 + \text{work done from A to B} \quad (62)$$

The work done by the water overtopping the levee and flowing from point A at the crest of the levee to point B at the toe of the levee is (Figure 215) (Eq. 63):

$$\text{Work done from A to B} = E_{A \text{ beg.}} - E_{B \text{ end}} \quad (63)$$

The potential energy of an object of a mass m or capability of an object to perform work due to its position or elevation with respect to a reference elevation. If point B is taken as the datum, the potential energy at A is (Eq. 64):

$$E_{A \text{ beg}} = mgh = \rho Vgh = \rho z * 1 * 1 * gh \quad (64)$$

where g is gravitational acceleration, h is elevation of the center of mass of the object above the datum (in this case, h is the height of the levee), V is the rate of volume transfer, ρV is the rate of mass transfer. Therefore, the rate of potential energy transfer over the levee is (Eq. 65):

$$\text{Potential energy at A} = \rho zgh \quad (65)$$

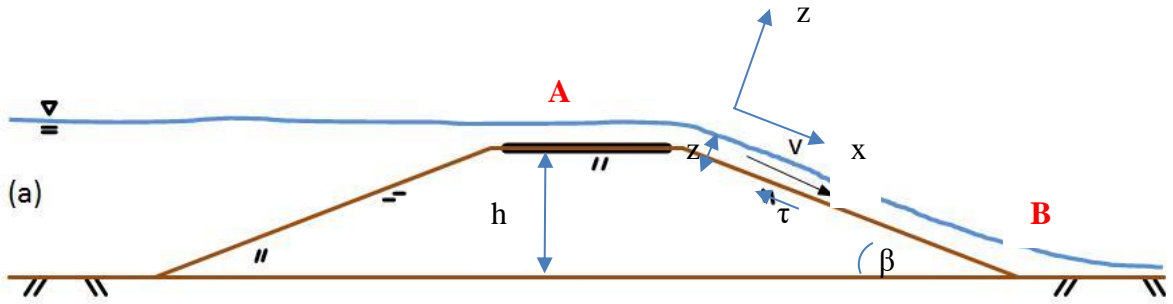


Figure 215. Levee overtopping problem (modified from Briaud, 2020)

A flowing water overtopping the levee has the capability of performing work which is referred as kinetic energy. The kinetic energy of a water mass m traveling with velocity v is defined as (Eq. 66 and Eq. 67):

$$E_{B\ end} = \frac{mv^2}{2} = \frac{\rho Vv^2}{2} = \frac{\rho z * 1 * 1 * v^2}{2} \quad (66)$$

$$Kinetic\ energy\ at\ B = \frac{\rho z v^2}{2} \quad (67)$$

The work done by the water between A and B is the work done by the friction at the soil water interface plus the internal energy dissipated in the water turbulence. This turbulence energy loss is neglected, and the elementary work done over the length of the levee dx , is (Eq. 68):

$$\tau(x) * 1 * 1 * dx \quad (68)$$

where τ is the shear stress at the water soil interface. From A to B that work is

$$Work\ done\ from\ A\ to\ B = \int_0^{h/\sin\beta} \tau(x) * 1 * 1 * dx \quad (69)$$

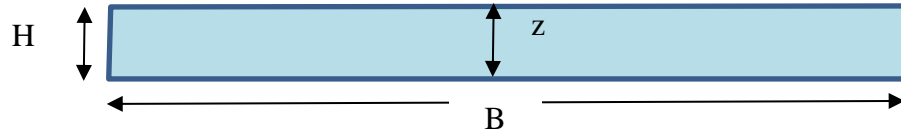
The hydraulic shear stress for open channel flow is (Eq. 70):

$$\tau = \gamma RS \quad (70)$$

where γ is the unit weight of water, R is the hydraulic radius defined as $R=A/P=z*1/1=z$, and S is the slope of the energy line. The slope of energy line S is given by Manning equation (Eq. 71):

$$S = \frac{n^2 v^2}{C_m^2 R^{4/3}} \quad (71)$$

where n is the Manning roughness coefficient (dimensionless) which depends on the surface material of the wetted perimeter of the channel (Chapter 4.1.2), v is the mean depth velocity, C_m is a constant which depends on the units ($C_m = 1$ for SI units, and 1.49 for American units). For a plane strain flow condition, R is equal to the water depth z : $R=A/P=HB/(B+2H)$, if $B \rightarrow \infty$, $R \rightarrow H$. which leads to:



$$\rho z g h - \frac{\rho z v^2}{2} = \rho z g \frac{n^2 v^2}{z^3} \frac{h}{\sin \beta} = \rho g \frac{n^2 v^2}{z^3} \frac{h}{\sin \beta} \quad (72)$$

$$\text{or} \quad v^2 \left(\frac{\rho z}{2} + \frac{\rho g n^2 h}{z^3 \sin \beta} \right) = \rho z g h \quad (73)$$

$$\text{or} \quad v^2 = \frac{z g h}{\frac{z}{2} + \frac{g n^2 h}{z^3 \sin \beta}} \quad (74)$$

$$\text{or} \quad v = \sqrt{\frac{g h}{\frac{1}{2} + \frac{g n^2 h}{z^4 \sin \beta}}} \quad (75)$$

The Eq. 75 gives the velocity at the toe of the overtopped side of the levee. As an example of velocity calculations, the following parameters are used: gravitational

acceleration $g = 9.81 \text{ m/s}^2$, height of the levee $h = 5.2 \text{ m}$, Manning roughness $n = 0.02$ (Section 4.2.2.), water overtopping depth $z = 0.3 \text{ m}$, levee slope angle $\beta = 10^\circ$.

The velocity v at the toe at the downstream face of the levee is in this case:

$$v = \sqrt{\frac{gh}{\frac{1}{2} + \frac{gn^2h}{z^{4/3}\sin\beta}}} = \sqrt{\frac{9.81 * 5.2}{\frac{1}{2} + \frac{9.81 * 0.02^2 * 5.2}{0.3^{4/3}\sin 10}}} = \sqrt{\frac{51.01}{0.50 + \frac{0.0204}{0.0349}}} = 6.87 \text{ m/s}$$

In the case of zero friction between the water and the soil (very smooth soil surface), $E_{A \text{ beg}} = E_{B \text{ end}}$ or $mgh = \frac{mv^2}{2}$, and the terminal velocity $v =$

$$\sqrt{2gh} = \sqrt{2 * 9.81 * 5} = 9.9 \text{ m/s.}$$

Note that the velocity at the downstream toe of the levee obtained by performing 2D numerical simulations with a very smooth levee surface was found to be 12 m/s (Briaud et al., 2008).

9. PREDICTION OF EROSION MOVEMENT (TAMU-PEM)

9.1. Existing knowledge on prediction of soil erosion

The prediction of erosion movement for levees, dams, bank erosion, scour etc. is an important practical problem to be solved. Many engineers have performed basic and applied research on the erosion movement of river meanders. The problem is typically not solved as movement as a function of time. In most cases, research relates to a meander movement per year as a function of various parameters such as bend radius, meander radius of curvature (Brice, 1982; Brice, 1983; Nanson and Hickin, 1986; Hudson and Kesel, 2000; Lagasse et al., 2004).

There are three groups of methods to predict erosion movement for a meander migration (Briaud and Montalvo-Bartolomei, 2017):

1. database and regression analysis methods
2. fundamental modelling methods
3. time sequence maps and extrapolation methods

Among the database and regression analysis methods are the following. Brice (1982) proposed a simple equation to obtain the average meander migration rate (\dot{M}_r , m/yr) which depends on the channel width (b, m) (Eq. 76):

$$\dot{M}_r = 0.01b \quad (76)$$

Nanson and Hickin (1986) suggested that the meander erosion rate would also depend on the radius of curvature of the meander (m). These two analytical methods

predict a constant rate of migration per year so the prediction versus time is a straight line.

Among fundamental modelling methods is TAMU-MEANDER developed by Briaud et al., 2007. The input to TAMU-MEANDER includes the three components of any erosion prediction process: geometry of the phenomenon, soil erodibility, water velocity and predicts the new location of the river (Briaud and Montalvo-Bartolomei, 2017).

The time sequence maps and extrapolation methods (Brice, 1982, 1983) include methods which assume that the erosion rate is constant over time regardless of the flow hydrograph which is not true.

Briaud and Montalvo-Bartolomei in 2014 suggested and in 2017 published the observation method to predict the future movement of river meanders based on their past behavior (Briaud and Montalvo-Bartolomei, 2017). The observation method for meander migration (OMM) makes use of the past movement and velocity history of the meander to back-calculate site specific erosion parameters. Those parameters serve as input to predict the movement of a point that would occur during a chosen future flood (e.g., 100-year flood). The 1% chance flood (100-year flood) and the associated river flow discharge Q_{100} are often used. The 100-year flow discharge Q_{100} (m^3/s) is the discharge that has a 1/100 probability of being equaled or exceeded in any given year. The OMM assumes that the soil to be eroded in the future will be similar to the soil which has been eroded during the period of observation. This method is based on the actual soil at the site and the actual geometry of the meander (Briaud and Montalvo-Bartolomei, 2017).

An example of meander migration (m) versus time (years) obtained from OMM is shown in Figure 216. The predicted migration of Brazos River with field velocity of 0.83 m/s correlates well with the observed data.

The Hydraulic Engineering Circular No. 18 HEC 18 “Evaluating Scour at Bridges” FHWA NHI 01-001 suggests a procedure how to obtain the scour depth during one event for a given flow velocity and a given pier or abutment geometry. The result of the procedure is a plot of total scour on a bridge cross section and a total scour prism that combines scour in the channel, scour at the abutments, and scour at the piers. It does not predict erosion movement versus time.

Considering limitations of existing methods used to predict erosion movement, the new method called TAMU-PEM (Prediction of Erosion Movement) is proposed and described below.

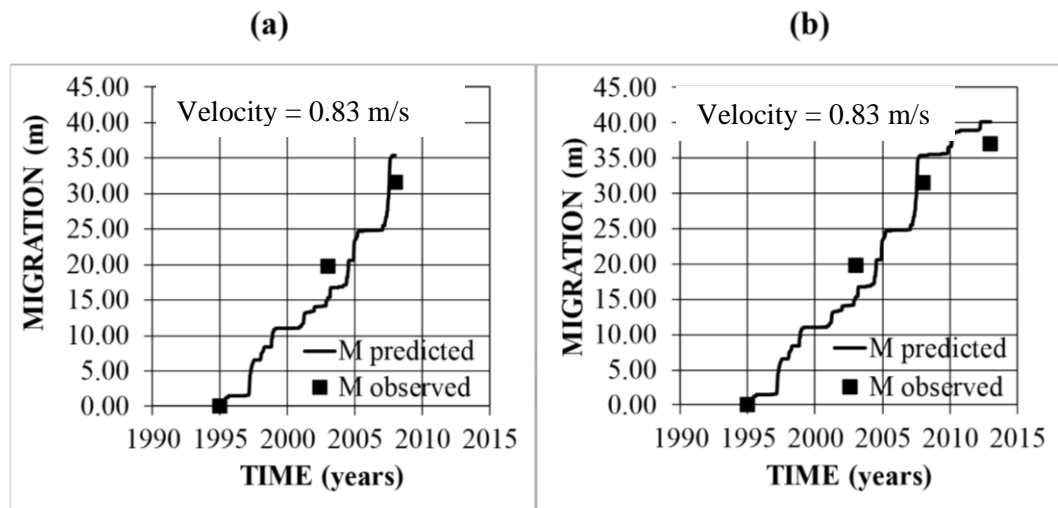


Figure 216. Brazos River verification of prediction with field critical velocity of 0.83 m/s. (a) first matching period, (b) second prediction period (adapted from Briaud and Montalvo-Bartolomei, 2014)

9.2. Procedure of TAMU-PEM (Prediction of Erosion Movement-Automated Excel Spread Sheet)

The goal of developing Excel spreadsheet (TAMU-PEM – Texas A&M University Prediction of Erosion Movement) is to be able to predict levee, dam or riverbank erosion including overtopping for different soils such as uniform soil, layered soils, grass and grass covered soils, and improved soils given the erosion functions for the soils and a velocity hydrograph for the flood. The output of TAMU-PEM is a chart showing erosion depth as a function of time. The TAMU – PEM can be used for uniform profiles made of uniform soils; in this case, there is a need to have one erosion function. However, for a multilayer soil profile, several erosion functions for each layer should be obtained and input in the spreadsheet. The TAMU-PEM manual described below is embedded in the Excel spreadsheet.

The procedure showing how to obtain the erosion movement by using TAMU-PEM is given below.

1. Input EFA erosion function point by point (erosion rate \dot{z} vs. velocity v or erosion rate \dot{z} vs. shear stress). An example of erosion function is shown in Figure 217.

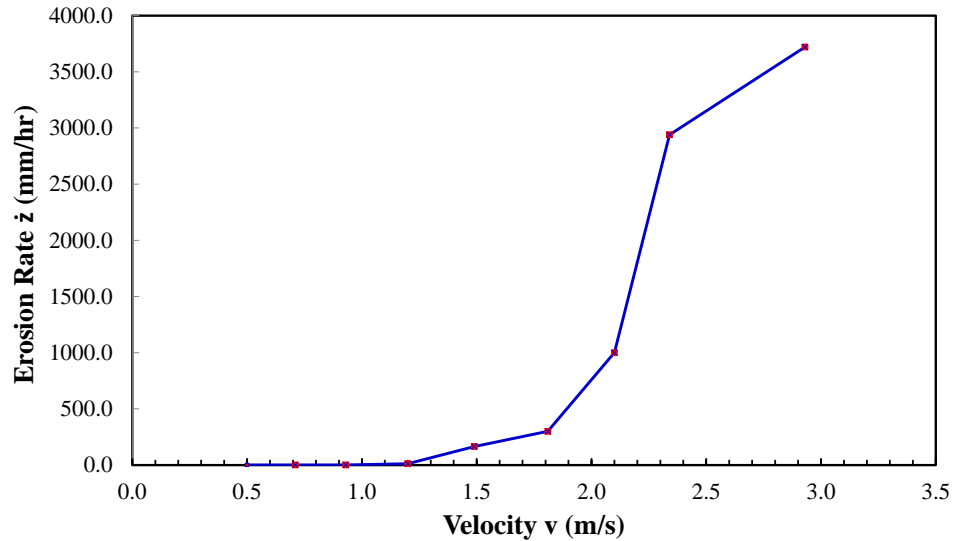


Figure 217. Erosion function (erosion rate vs. velocity)

2. Input flood velocity hydrograph or hydraulic shear stress hydrograph point by point for a given river location. The velocity hydrograph is a graph showing river velocity v (m/s) as a function of time t (hr) for a given period and location. The hydraulic shear stress hydrograph is a graph showing hydraulic shear stress at the water-soil interface τ (Pa) as a function of time t (hr) for a given period and location. Use a synthetic hydrograph if necessary or an observed (past) hydrograph. The procedure how to obtain an observed and a synthetic hydrograph is presented in Section 9.3.1 and 9.3.2. The example of velocity hydrograph is shown in Figure 217.

3. Decompose the velocity or shear stress hydrograph into a series of n constant velocity or shear stress steps for which v or τ is larger than v_c or τ_c . Time units equal one hour. The example of this step is given in Figure 218 for velocity hydrograph.

4. For each constant velocity or shear stress step where the velocity is v_i and the shear stress is τ_i , obtain a corresponding erosion rate \dot{z}_i from the erosion function.

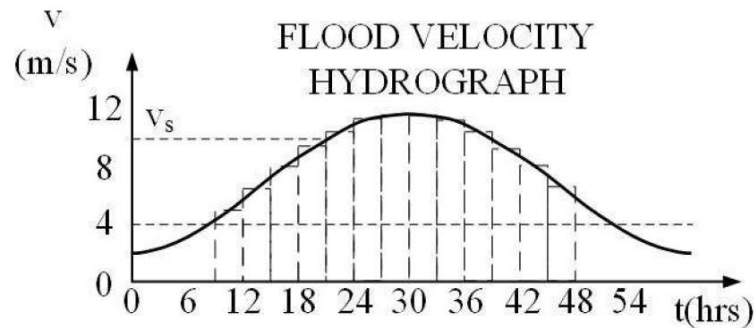


Figure 218. Velocity hydrograph (after Briaud, 2020)

5. Obtain the erosion function for the soil that is a subject to erosion. This can be done by erosion testing (e.g., EFA testing) or by using the erosion category chart based on soil classification. On the erosion function (\dot{z} vs. velocity or \dot{z} vs. shear stress), find the velocity v_b or the shear stress τ_b immediately below v_i or τ_i and the velocity v_a or the shear stress τ_a immediately above v_i or τ_i . Obtain the erosion rate \dot{z}_a and \dot{z}_b corresponding to v_a and v_b or τ_a and τ_b . The example of this step is shown in Figure 219 for velocity erosion curve. Steps 6 – 11 show the procedure for the velocity. The shear stress procedure is the same for steps 6 – 11; velocity should be replaced with shear stress.

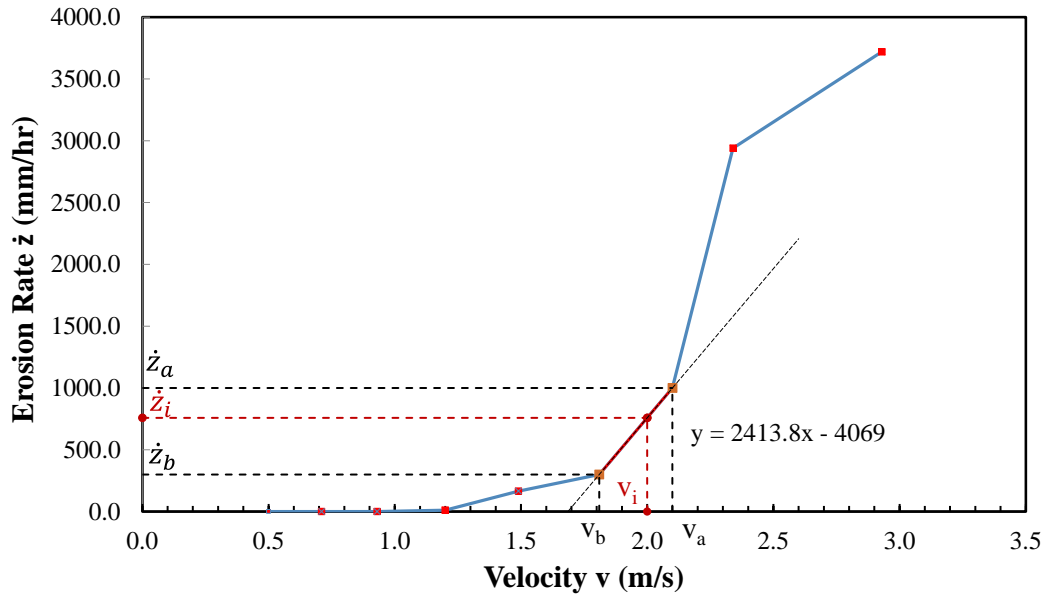


Figure 219. Erosion function (erosion rate vs. velocity) for SAC-5

$$\dot{z} = av + b \quad (77)$$

$$\dot{z}_a = av_a + b \quad (78)$$

$$\dot{z}_b = av_b + b \quad (79)$$

6. Write the equation of the straight line joining the points A and B.

Calculate the coefficients a and b for the straight line.

$$\dot{z}_a - \dot{z}_b = a(v_a - v_b) \quad (80)$$

$$a = \frac{\dot{z}_a - \dot{z}_b}{v_a - v_b} \quad (81)$$

$$\dot{z}_a = \frac{\dot{z}_a - \dot{z}_b}{v_a - v_b} v_a + b \quad (82)$$

$$b = \dot{z}_a - \frac{\dot{z}_a - \dot{z}_b}{v_a - v_b} v_a \quad (83)$$

$$b = \frac{\dot{z}_a(v_a - v_b) - (\dot{z}_a - \dot{z}_b)v_a}{v_a - v_b} = \frac{\dot{z}_b v_a - \dot{z}_a v_b}{v_a - v_b} \quad (84)$$

$$\dot{z} = \frac{\dot{z}_a - \dot{z}_b}{v_a - v_b} v + \frac{\dot{z}_b v_a - \dot{z}_a v_b}{v_a - v_b} \quad (85)$$

7. Calculate \dot{z}_i corresponding to v_i by using the equation developed in step 6 above.

$$\dot{z}_i = a v_i + b \quad (86)$$

$$\dot{z}_i = \Delta z_i / \Delta t_i \quad (87)$$

8. Compute the increase in erosion depth Δz_i (mm) during step Δt_i due to \dot{z}_i as

$$\Delta z_i = \dot{z}_i * \Delta t_i \quad (88)$$

9. Repeat steps 4-8 for all velocity steps to obtain $\Delta z_1, \Delta z_2, \dots, \Delta z_n$

10. Obtain the erosion depth as

$$z(t) = \sum_{i=0}^{i=n} \Delta z_i \quad (89)$$

11. Plot the curve $z(t_i)$ versus t_i .

If the shear stress procedure is used, the erosion depth can be obtained and the plot $z(t_i)$ versus t_i can be drawn. In the approach above, it is assumed that velocity is constant during a certain period of time and soil is uniform. It is also proposed to obtain water flow velocity from measured or predicted (synthetic) hydrograph.

9.3. Procedure to obtain velocity hydrograph

Velocity hydrograph can be obtained by using three different approaches:

1. Observed flood from the past which gives an observed (past) hydrograph
2. Predicted flood allowing to obtain a synthetic hydrograph
3. Synthetic/observed design hydrograph

9.3.1. Observed (past) hydrograph

This approach is to select a past hydrograph corresponding to a big flood on the river record and to predict the erosion movement when the soil is subjected to that flood. For doing this, the following procedure is proposed:

1. Find a big water event (flood) using the stream gages (for example the USGS website <https://waterwatch.usgs.gov>).
2. Choose an USGS gage close to the location of the interest.
3. Select a time domain over which the flow hydrograph is to be used for that gage (or a velocity hydrograph if available).
4. Run a program such as HEC-RAS (Hydraulic Engineering Center – River Analysis System) to transform a flow hydrograph into a velocity hydrograph if needed.
5. Draw a velocity hydrograph.

It should be noted that preparing a corresponding shear stress hydrograph requires advanced computation such as Computational Fluid Dynamics.

An Excel Spreadsheet has been developed to construct a velocity hydrograph by using the approach described above. Some examples are shown below. This approach is applied to the Lower American River and Sacramento levees.

1. The biggest flood on the Lower American River was in February 1986. For the example, a flood duration is taken from 15 February to 25 February 1986.
2. The gage USGS 11446500 on American River Fair Oaks CA, located on the riverbank of Lower American River in Sacramento, was chosen (Figure 220). Table 49 shows the data obtained from the stream gage.

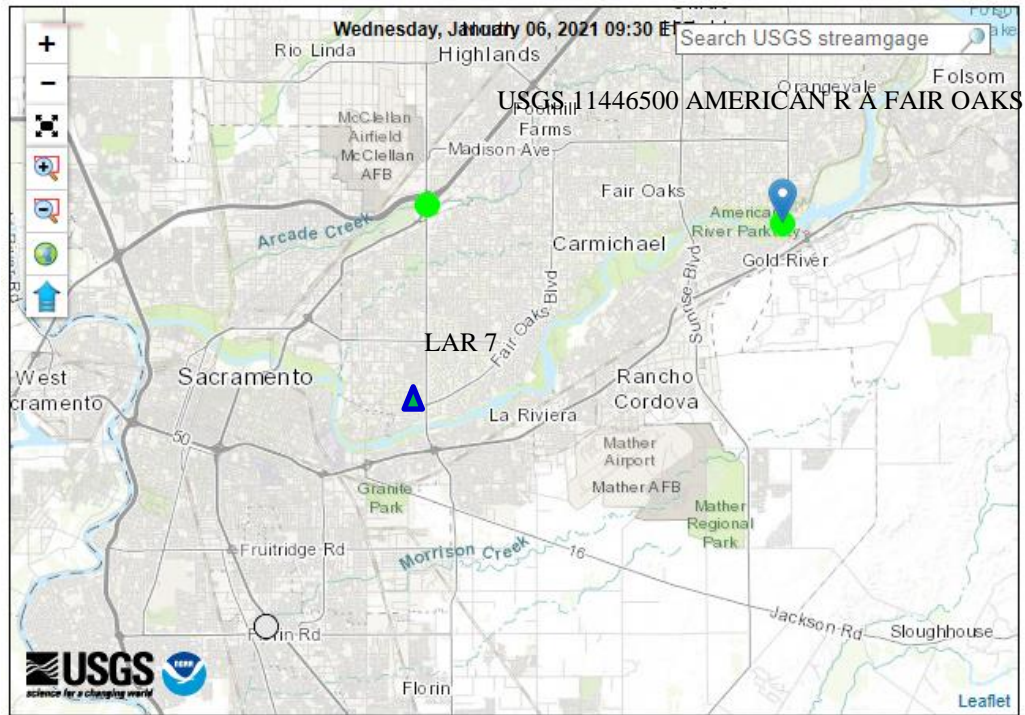


Figure 220. Map of Sacramento showing a location of the stream gage USGS 11446500 American River Fair Oaks gage, California (adapted from USGS website, accessed 2020)

Table 49. Discharge hydrograph for the stream gage USGS 11446500 American River Fair Oaks CA, USGS (15-25 February 1986)

Date	Time (hours)	Discharge (cfs)	Discharge (m ³ /s)
15	0	20,200	572.00
16	24	26,700	756.06
17	48	80,100	2268.18
18	72	124,000	3511.29
19	96	131,000	3709.51
20	120	114,000	3228.12
21	144	82,400	2333.31
22	168	47,400	1342.22
23	192	44,400	1257.27
24	216	31,700	897.64
25	240	22,700	642.79

3. The flow hydrograph for the chosen gage obtained from the USGS website is shown in Figure 221. The time domain was selected as 10-days showing the rise and the receding time. Each point on Figure 221 corresponds to the measurements taken daily starting February 15th and ending February 25th, 1986.

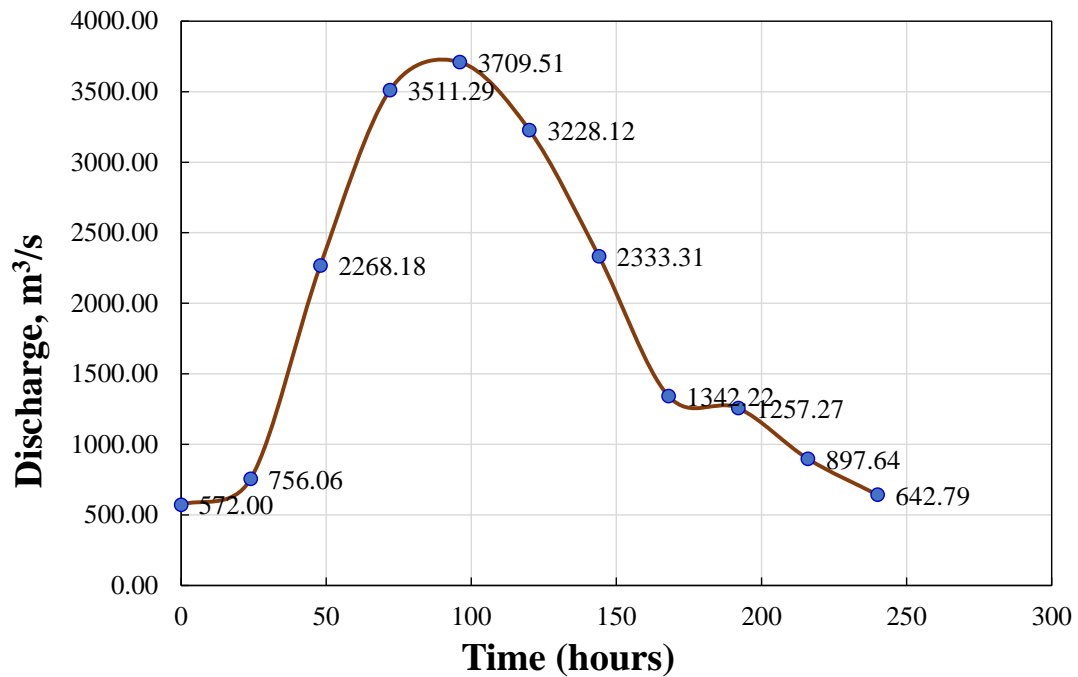


Figure 221. Flow hydrograph for the stream gage USGS 11446500 (modified from USGS website, accessed 2020)

4. Then a software program such as HEC-RAS can be used to transform the flow hydrograph into the velocity hydrograph. An example of the velocity hydrograph prepared for LAR-7 is shown in Figure 222.

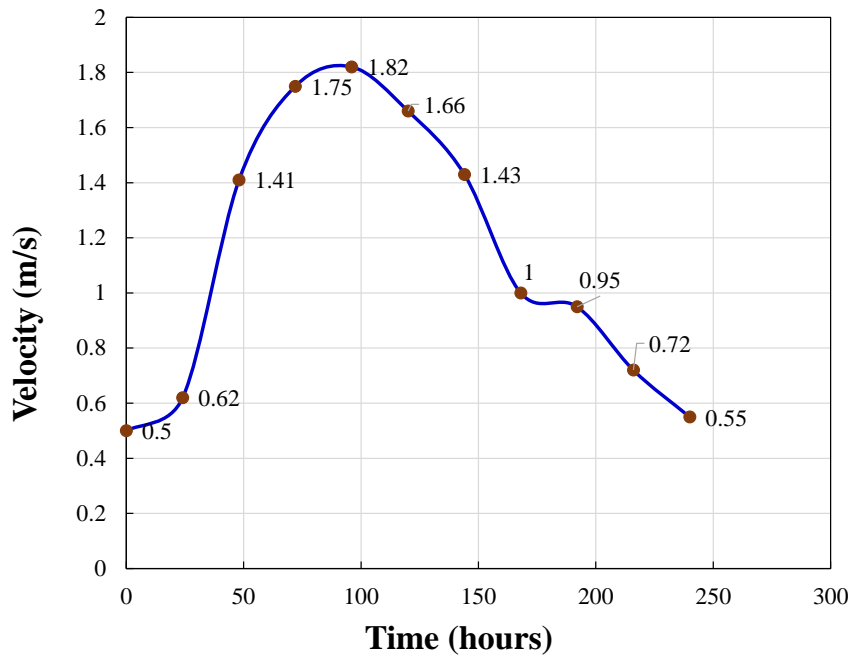


Figure 222. Velocity hydrograph for LAR-7

9.3.2. Synthetic hydrograph

This approach is to use a design flow corresponding to a selected recurrence interval and computation such as Hydrologic Engineering Center's River Analysis System (HEC-RAS) to obtain the relationship between the flow and the velocity and create a synthetic hydrograph. For doing this, the following procedure is proposed:

1. An engineer in charge should select a designed flood flow. For example, the design flood flow is $Q_{\text{design}} = 325$ -years flood meaning that a flood has a probability of $1/325$ to occur or to be exceeded in any given year.
2. To complete the hydrograph, a rise time of the flow should be selected as t_1 and the receding time is selected as t_2 . Time t_1 and t_2 are recommended as 1 or 2 days each. Then the hydrograph starts at time $t = 0$ and the corresponding value of flow, rises

to the design flow Q_{design} in a time t_1 and then decreases to the tail water level in a time t_2 . The flow hydrograph is completed by starting at $t = 0$ and ending at a normal flow at t_2 (Figure 223).

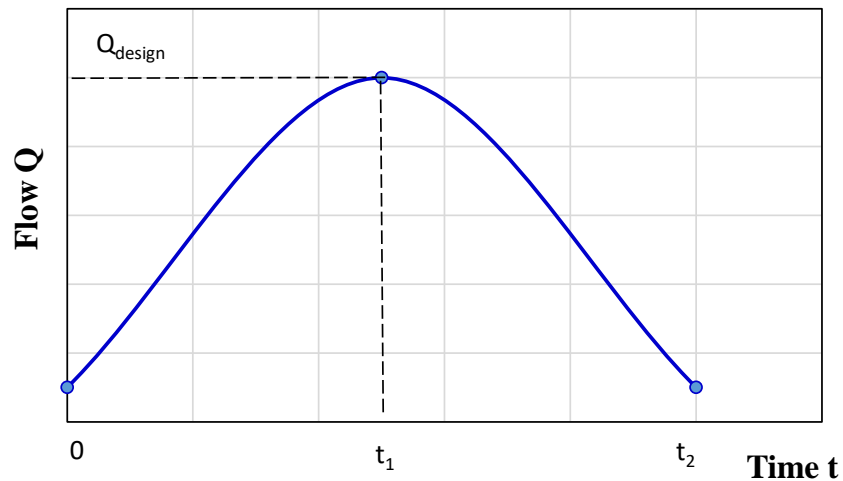


Figure 223. An example of synthetic flow hydrograph

3. Transform the flow hydrograph into the velocity hydrograph by using a software program such as HEC-RAS which gives the relationship between flow and velocity.

4. Draw the velocity hydrograph.

9.3.3. Synthetic/observed design hydrograph

This approach is a combination of a design flood, computation, and an observed (past) flow hydrograph. The following procedure is recommended:

1. An engineer in charge should select a designed flood flow. For example, the design flood is $Q_{\text{design}} = 325\text{-years flow}$.

2. The velocity versus discharge curve can be obtained by using a modelling tool like HEC-RAS. Table 50 shows the data obtained from the model developed by Matthew Weber (2020) for the Lower American River for LAR-7 (steady state runs). Figure 224 shows velocity vs. discharge for the same location. It was assumed that a hypothetical 325-year flood peaks at the flow of 4530.70 m³/s. It was found that the corresponding flow velocity is 2.088 m/s (Weber, personal communication, 2020).

Table 50. Discharge and velocity for LAR-7 (obtained from M. Weber, 2020)

Discharge (m ³ /s)	Depth (ft)	Depth (m)	Velocity (ft/s)	Velocity (m/s)
14.16	8.7	2.65	0.1	0.022
22.65	9.2	2.81	0.1	0.035
28.32	9.5	2.89	0.1	0.043
35.40	9.7	2.97	0.2	0.053
42.48	10.0	3.04	0.2	0.062
49.55	10.2	3.10	0.2	0.071
56.63	10.4	3.16	0.3	0.080
77.87	10.9	3.31	0.4	0.108
99.11	11.3	3.45	0.4	0.135
127.43	11.9	3.62	0.6	0.168
155.74	12.4	3.78	0.7	0.200
184.06	12.9	3.94	0.8	0.230
212.38	13.5	4.11	0.8	0.258
240.69	14.0	4.27	0.9	0.285
283.17	14.8	4.52	1.1	0.321
424.75	17.1	5.20	1.3	0.399
849.51	22.0	6.71	2.2	0.684
1274.26	25.6	7.82	3.2	0.962
1982.18	30.5	9.31	4.4	1.340
3256.44	36.0	10.99	5.5	1.667
4530.70	39.5	12.04	6.9	2.088

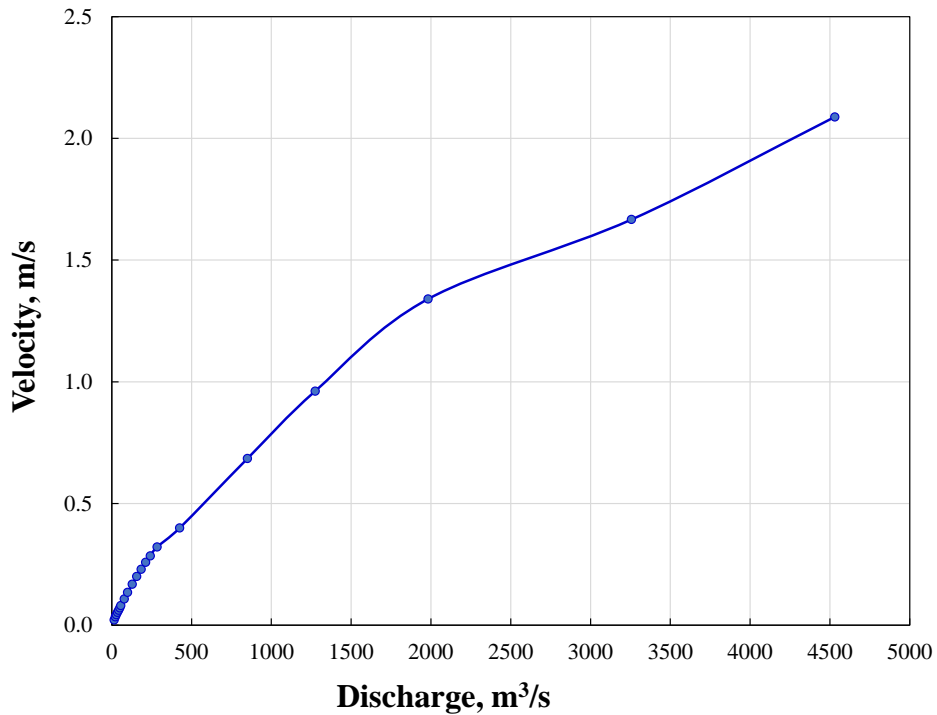


Figure 224. Velocity vs. discharge curve for LAR-7 (modified from M. Weber, received from Todd Rivas, 2020)

3. The flow hydrograph corresponding to a large flood is selected from the closest USGS gage. This gives flow versus time (See Figure 223).

4. The synthetic hydrograph is constructed by using the observed flow hydrograph of 3 above and multiplying all flows by the ratio of $Q_{\text{design}}/Q_{\text{max}}$. Flow Q_{design} is the design flow from 1 above and Q_{max} is the maximum flow observed during the selected flood from 3 above. This gives the synthetic flow hydrograph. For example, the maximum flow observed during the 1986 flood is $Q_{\text{max}} = 3709.51 \text{ m}^3/\text{s}$. The design flow is selected as $Q_{\text{design}} = 4530.70 \text{ m}^3/\text{s}$. The ratio of $Q_{\text{design}}/Q_{\text{max}}$ would be 1.22. Figure 225 shows the synthetic hydrograph.

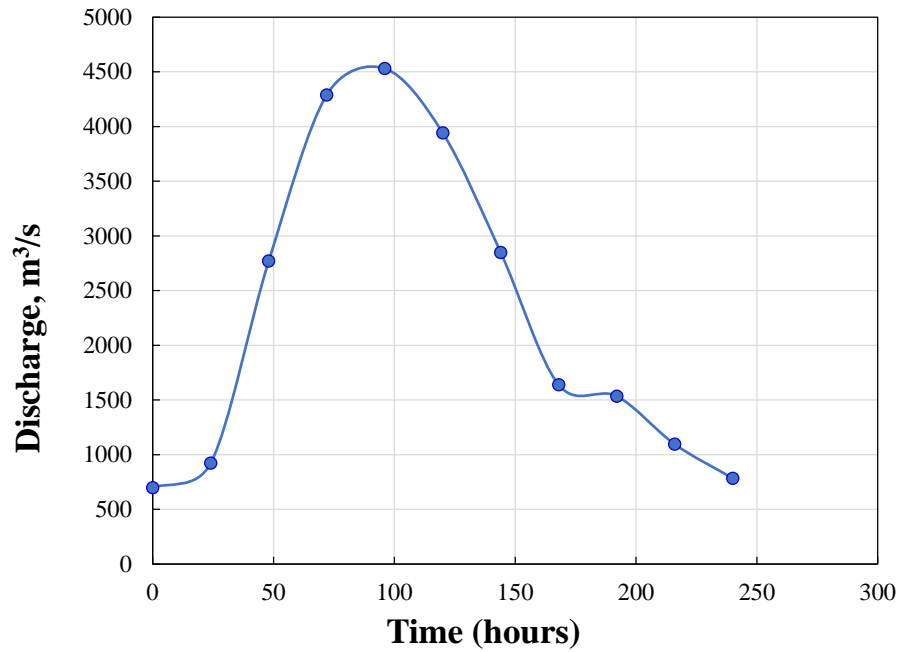


Figure 225. Synthetic flow hydrograph

5. The synthetic velocity hydrograph which corresponds to the synthetic flow hydrograph is constructed by using the velocity versus flow relationship in 2 above (Figure 224). Figure 226 illustrates the synthetic velocity hydrograph.

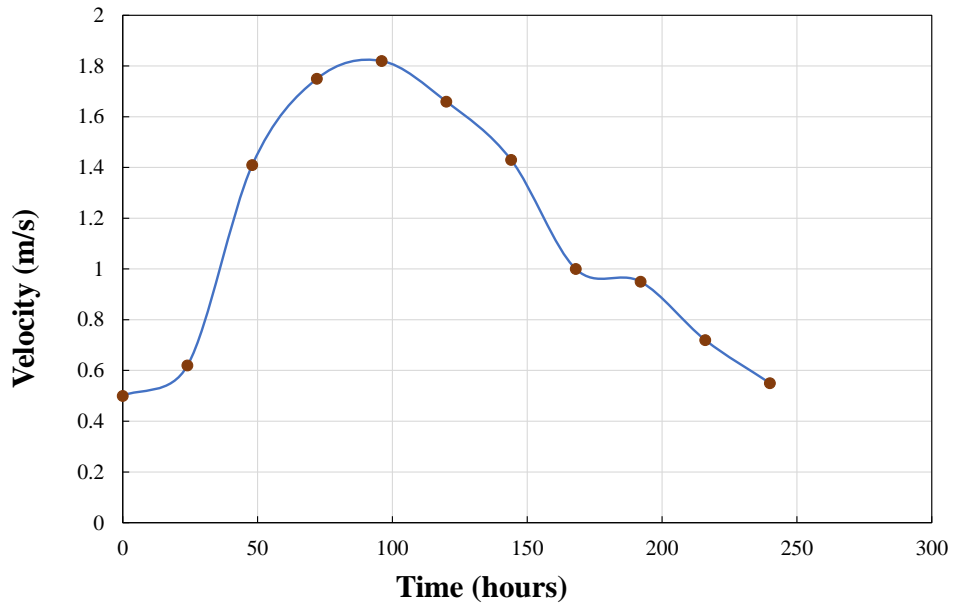


Figure 226. Synthetic velocity hydrograph

9.4. Prediction of erosion movement by using TAMU-PEM

Erosion movement can be obtained by running TAMU-PEM for different soils inputting the erosion curve and velocity hydrograph. TAMU-PEM has advantages and limitations. Among the advantages are simple calculations, use of erosion rate for a given soil and a velocity hydrograph for a given location, preliminary assessment of a magnitude of erosion during a potential event such as hurricane or flood. The limitation is that a levee or a dam is made of uniform soil with no layers. The erosion movement between the events is also neglected. However, the erosion movement can be obtained more precise knowing the soil profile along the direction of water flow for which the erosion movement is going to be predicted. Below, the examples of the erosion movement obtained for sand, silt, clay, improved soil, and grass.

Note that for all examples, the velocity hydrograph corresponds to the highest flood on the record of the Lower American River in February 1986. This event was a 225-years flood which had a probability of 1/225 to occur or to be exceeded in any year (225 return period).

9.4.1. Silty Sand

Sand is one of the most erodible soils. For the bare silty sand and the velocity hydrograph shown in Figure 227, the erosion movement using the erosion function shown in Figure 227 can extend 18 m for the first 24 hours at the water velocity of $v = 0.62$ m/s (Figure 226). Note that the event peak velocity is 1.9 m/s. The magnitude of erosion movement for silty sand is drastic and does not seem to be reasonable and

realistic. Note that levees are usually covered with vegetation which mitigate erosion as EFA testing indicates (Chapter 4).

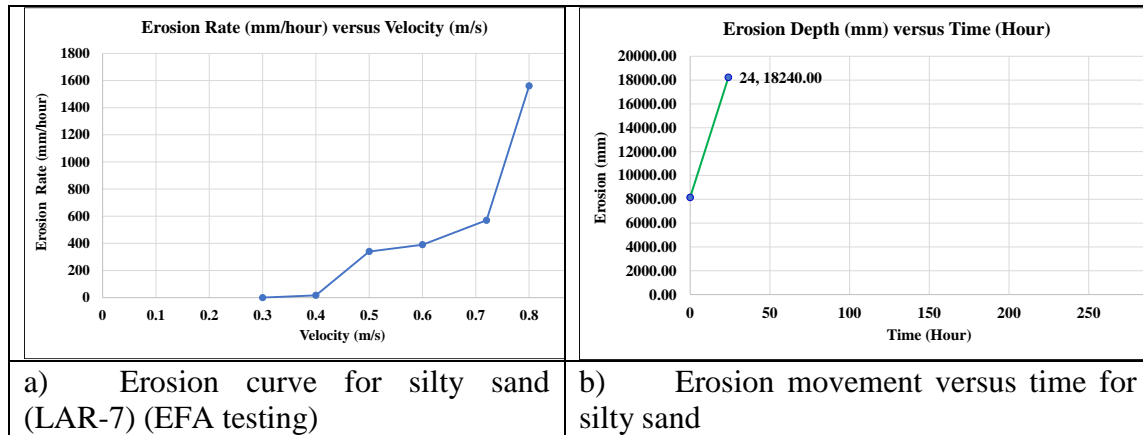


Figure 227. Erosion curve (a) and erosion movement (b) for silty sand

9.4.2. Clay

The erosion movement for the lean clay with the erosion function shown in Figure 228 and the velocity hydrograph shown in Fig. 6.8 is around 3 m for the first 24 hours at the water velocity of $v = 0.62$ m/s (Figure 226). The erosion movement obtained for clay is 6 times smaller when the movement calculated for silt. Note that the erosion movement versus time is obtained for the first 24 hours of event because clay resists erosion up to 1.2 m/s. Therefore, the entire erosion curve is considered in the erosion movement.

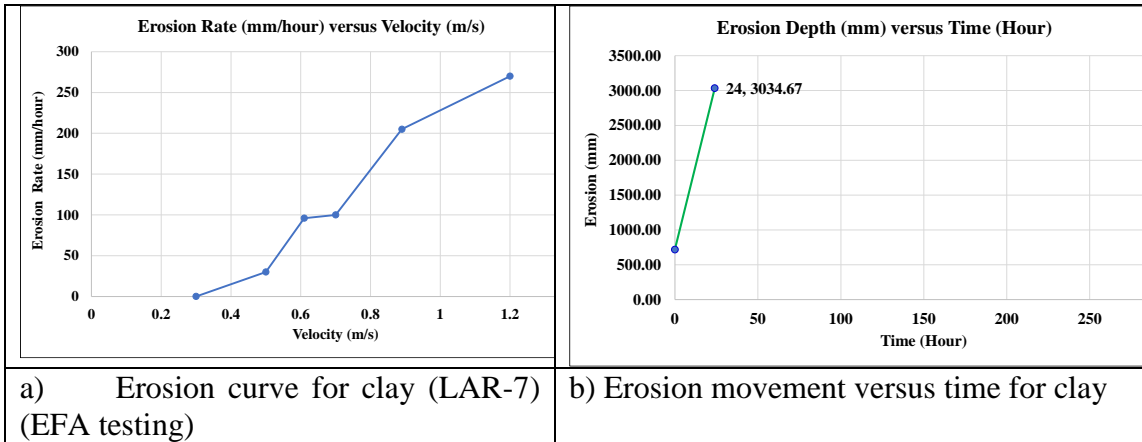


Figure 228. Erosion curve (a) and erosion movement (b) for clay

9.4.3. Silt

The erosion movement for the silty soil with the erosion curve shown on Figure 229 and the velocity hydrograph shown in Figure 226 is 4.8 m for the first 24 hours at the water velocity of 0.62 m/s. The silt can resist water velocity up to 2.1 m/s, the erosion movement during 10 days with the maximum water velocity for the event of $v = 1.9$ m/s is 16 m.

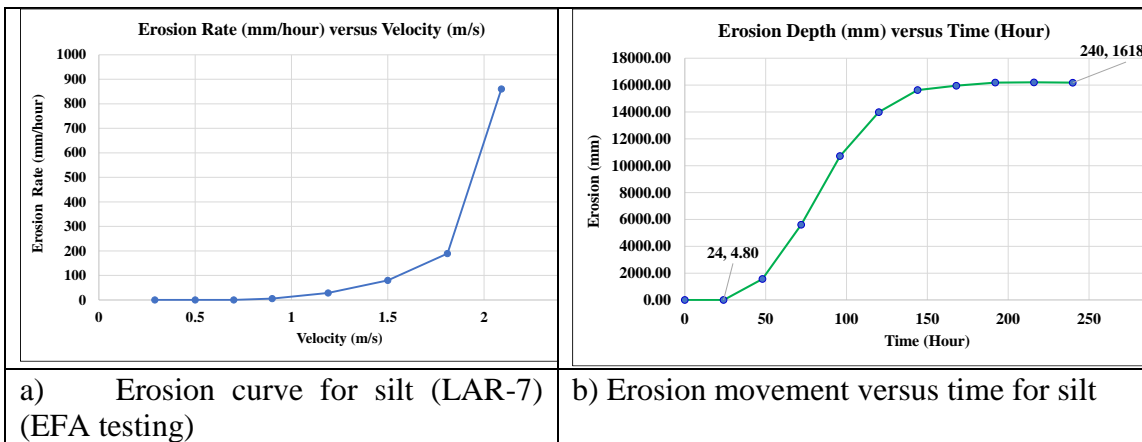


Figure 229. Erosion curve (a) and erosion movement (b) for silt

9.4.4. Bermudagrass

The erosion movement for Bermudagrass with the erosion function shown in Figure 230 and the velocity hydrograph shown in Figure 226 is around 0.25 m (25 cm) for the event duration of 10 days with the maximum velocity of $v = 1.9$ m/s (Figure 226). The erosion movement obtained for Bermudagrass is 64 times less than for the silt over the entire period (10 days). Note that EFA testing shows that Bermudagrass resists erosion up to the velocity of $v = 5.6$ m/s. Meanwhile, the maximum water velocity during the event is 1.9 m/s. The red circle on Figure 230 indicates the velocity range for which the erosion movement is predicted. Note that the erosion movement is obtained for a 225-years flood. For the case of the bigger flood or overtopping when water velocity can reach 10-12 m/s at the downstream toe of a dam, the erosion movement will be higher.

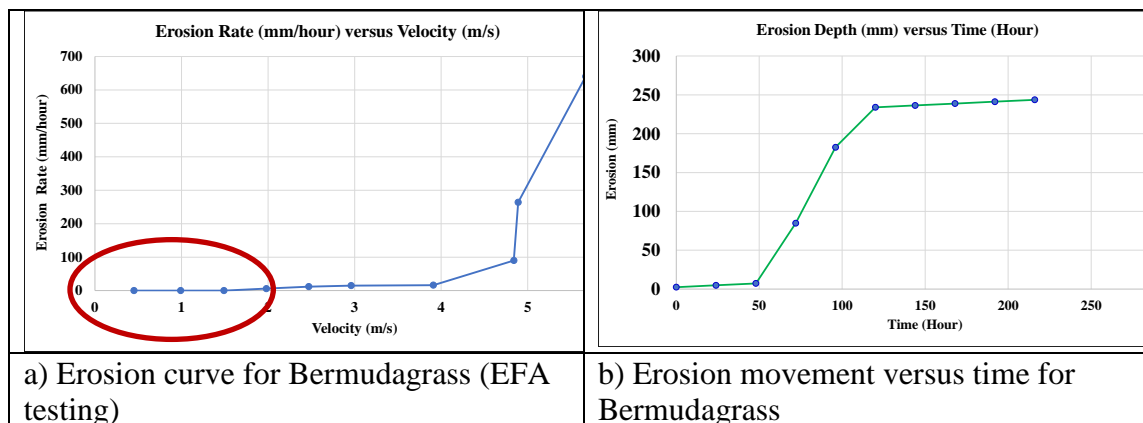


Figure 230. Erosion curve (a) and erosion movement (b) for grass

9.4.5. Enzyme-treated soil

The erosion movement for the enzyme-treated clayey sand with 14-days curing time (see Chapter 5, Section 5.4) with the erosion curve shown on Figure 231 and a 225-

years flood is 0.55 m (55 cm) for a 10-days long event with the maximum velocity of $v = 1.9$ m/s (Figure 231). The movement for the enzyme-treated clayey sand is 2 times higher than for the Bermudagrass.

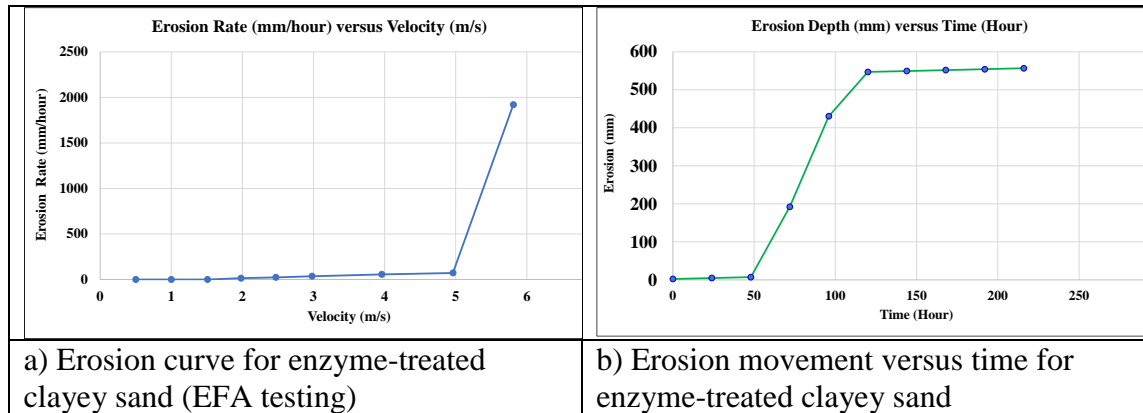


Figure 231. Erosion curve (a) and erosion movement (b) for enzyme treated clayey sand

9.4.6. Lime-treated soil

The erosion movement for the lime-treated soil of a 14-days curing time (see Chapter 6, Section 6.4) with the erosion function shown in Figure 232 and the 225-years flood is 0.13 m (13 cm) for a 10-days long event with the peak velocity of $v = 1.9$ m/s (Figure 226). The lime-treated soil shows less erosion movement compared to enzyme-treated soil and Bermudagrass. While considering lime-treatment for erosion mitigation, it should be noted that lime is not as environmentally friendly as enzymes and usually performs better in a dry warm climate. The red circle on Figure 232 indicates the velocity range for which erosion movement is predicted.

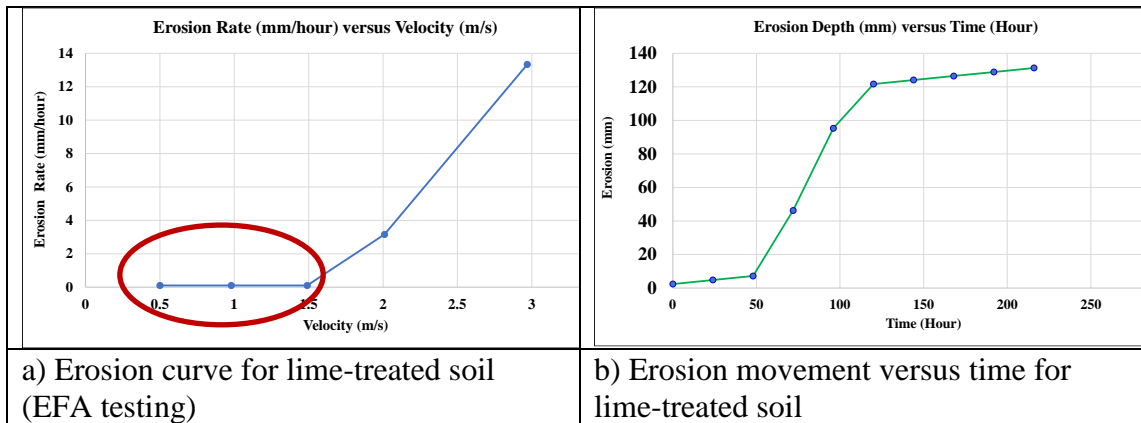


Figure 232. Erosion curve (a) and erosion movement (b) for lime treated soil

9.5. Comparison of efficiency of remedial measures

This section compares the erosion movement obtained for the remedial measures considered above. As Figure 233 indicates the minimum erosion movement is obtained for the lime-treated soil followed by Bermudagrass and the enzyme-treated soil. Therefore, lime treatment can be beneficially used to mitigate soil erosion (see Chapter 6, Section 6.4). However, lime is not as environmentally friendly as enzymes. Overall, all erosion mitigation techniques presented in this analysis, show a significant reduction in erosion movement compared to the non-treated soil. Engineers should decide on the erosion mitigation technique based on a soil type and composition, climate, purpose of construction or operating site.

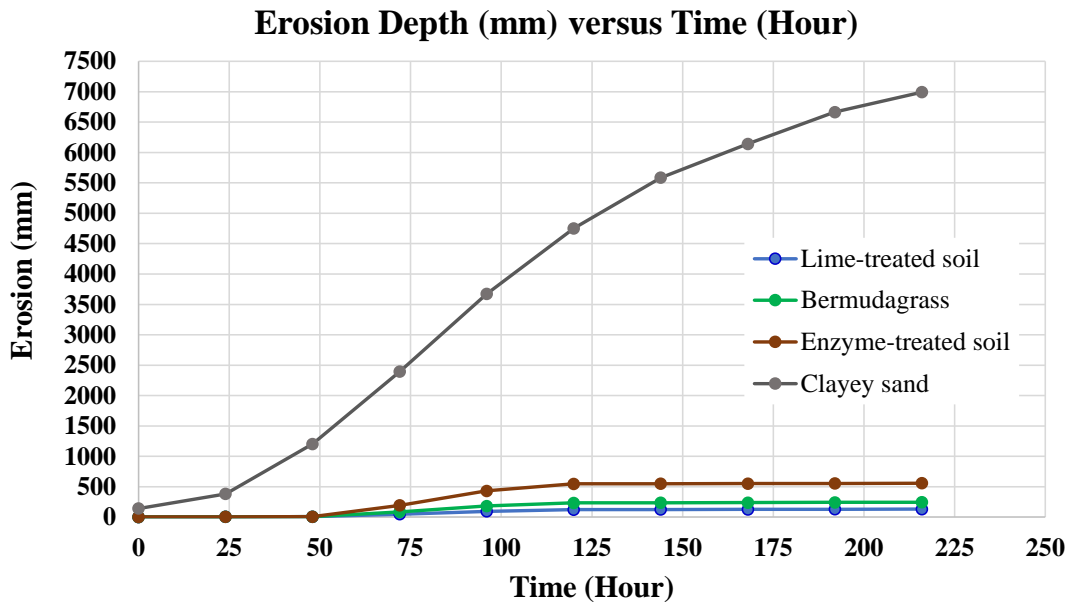


Figure 233. Erosion movement versus time for different remedial measures

Figure 233 shows that the remedial measures show to reduce soil erodibility by a factor varying between 15 and 70 depending on the measure.

9.6. Field calibration and scale factor

The erosion movement obtained by running TAMU-PEM is calibrated with the field measurements of erosion to be able to estimate the efficiency of the prediction. The approach presented in this Section is made use of available surveyed cross-sections for the Lower American River, the results of the HEC-RAS modelling, and the erosion functions obtained from EFA testing. Field measurement of ground surface elevations (NAVD 88) performed in 2006/2008 and in 2017 for LAR-7 on the Lower American River shows a ground movement presumably due to erosion taking place during this time. Figure 234 indicates that between 2008 and 2017 the site may have experienced up to about 6 meters (20 feet) of lateral erosion mostly at the riverbank. The results of the

numerical simulation performed by Chen (2020) shows that the shear stress along the riverbank is higher closer to the water surface. Also, the streamwise velocity in a river flows as maximum at the free surface.

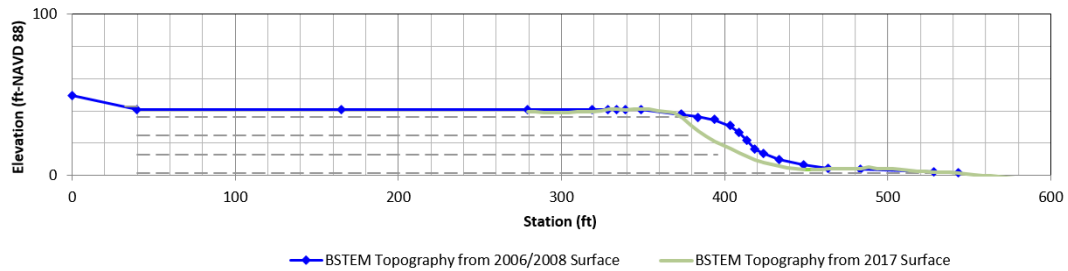


Figure 234. Simplified cross-section using the 2006/2008 topo surface and the 2017 surface for LAR 7 (Courtesy of Todd Rivas, USACE, Sacramento District, 2020)

The field measurement of erosion is compared with the results of TAMU-PEM for soil with no vegetation and covered with Bermudagrass assuming that the levee soil profile is uniform. Table 51 shows the results of the comparison. The predicted erosion movement for the silty sand is 18 m, for the silt – 16 m, for the clay – 3 m, and for Bermudagrass – 0.25 m. Then, the measured movement from 2008 to 2017 is 6 m. The results of TAMU-PEM and the field measurement do not match well. Site inspection performed in April 2019 showed that the riverbank was heavily vegetated. Therefore, to be able to create a field value of erosion movement assuming heavily vegetation, an Erosion Factor (EF) should be applied. The EF is calculated as the predicted erosion movement from TAMU-PEM for a bare soil with no vegetation divided by the predicted erosion movement from TAMU-PEM for Bermudagrass. For the case when the riverbank would be covered with Bermudagrass grown on a bare soil, the EF would be the follows:

- a. Bermudagrass on silty sand: $EF = 18/0.25 = 72$ times smaller than for a silty sand with no vegetation.
- b. Bermudagrass on silt: $EF = 16/0.25 = 64$ times smaller than for a silty soil with no vegetation.
- c. Bermudagrass on clay: $EF = 3/0.25 = 12$ times smaller than for a clayey soil with no vegetation.

Table 51. The erosion movement for different soils and grass (field and laboratory)

Type of Soil	Field Measurement	Erosion movement (m) from TAMU-PEM			
		Silty Sand	Silt	Clay	Bermudagrass
Erosion Movement	6	18	16	3	0.25

The erosion movement obtained from TAMU-PEM should be also compared with the field measurements if possible and reduced by a scale factor to be able to predict the erosion movement which can closely match the field measurements. For an example used above, if water velocity reaches more than 1.9 m/s, the magnitude of erosion movement would increase significantly.

10. TAMU-EROSION DATABASE

10.1. Existing knowledge on TAMU-Erosion database

The TAMU-Erosion was developed as a part of the National Cooperative Highway Research Program (Briaud et al., 2019) project at Texas A&M University in 2018 by Briaud and Shafii. Similar erosion databases have been proposed in France (Jean-Robert Courivaud, personal communication 2019). The TAMU-Erosion is a searchable Excel spreadsheet containing the information about soil erosion testing including erosion functions, erosion parameters and geotechnical properties of soils. The data in the database can be easily accessed, managed, modified, updated, controlled, and organized. This spreadsheet is a searchable tool, it allows the engineer to filter the data based on multiple criteria. In 2018, the database included near 1000 laboratory and field erosion tests results from the entire world.

The existing TAMU-Erosion suggests that the first approach to evaluate the erodibility of a desired site should be done through probing TAMU-Erosion. The user can find as many geotechnical properties information as possible including the USCS category, the AASHTO classification, the Atterberg limits, the unit weight, and the water content and filter the database with the goal of finding the soil samples that are like the target soil. Then, the obtained soil samples might be filtered with erosion tests including EFA, BET, PET, JET, and HET. The erodibility parameters such as critical velocity, critical shear stress, erosion rate and erosion function then can be obtained to preliminary estimate soil erodibility. Probing TAMU-Erosion helps the engineer to

estimate soil erodibility without running erosion tests. It should be noted that the TAMU-Erosion allows to preliminary estimate soil erodibility and cannot replace erosion testing on a desired soil. Figure 235 shows the introductory page of the TAMU-Erosion.





  	
PROGRAM	TAMU-Erosion
VERSION	BETA 1.0
DATE	August 2018
AUTHORS	Jean-Louis Briaud, Iman Shafii
PERFORMING ORGANIZATION	Texas A&M Transportation Institute (TTI)
SPONSOR	National Cooperative Highway Research Program
	
<p>What is the TAMU-Erosion? The TAMU-Erosion is a relational spreadsheet which allows the user to perform multi-conditional inquiries between the erodibility parameters and soil geotechnical properties.</p> <p>What does the TAMU-Erosion Incorporate? The TAMU-Erosion consists of near 1000 erosion tests. Around 750 erosion tests were collected from the literature review as well as by contacting researchers and organizations working on erosion around the entire world. Erosion data were extracted from technical reports, lab test results, field test results, and well-known journal/conference papers. In parallel with the erosion tests, the geotechnical properties of each tested sample, alongside with any information on the latitude and longitude location or origin of them were compiled. The data collected includes the results of commercially used erosion tests such as the Erosion Function Apparatus test (EFA), the Jet Erosion Test (JET), the Hole Erosion Test (HET), the Slot Erosion Test (SET), the Ex-situ Scour Test Device (ESTD), the Borehole Erosion Test (BET), the Rotating Erosion Testing Apparatus (RETA), the Sediment Erosion Rate Flume (SERF), the In-situ Scour Profile (ISEEP), and some large scaled flume tests. In addition to the aforementioned compiled data, around 250 erosion tests were performed during this project (NCHRP 24-43). These tests include the EFA, the JET, the HET, the PET, and the BET. Alongside with the erosion testing, all major geotechnical properties tests were conducted on each sample that was tested in any erosion device, and soil properties spreadsheets were generated for each sample.</p> <p>What does the TAMU-Erosion Do? The important characteristic of the TAMU-Erosion is its ability to bring a wide range of erodibility parameters together and compare them in a consistent fashion as proposed by Briaud (2008). The erodibility parameters which were selected to represent the erosion characteristics of a soil are the critical shear stress (τ_c), the critical velocity (v_c), the initial slope (E_v) of the "z versus v" curve, and the initial slope (E_s) of the "z versus τ" curve, and the erosion category (EC).</p>	

Figure 235. An image of the introductory page of TAMU-Erosion (TAMU-Erosion, 2021)

The existing TAMU-Erosion database has led to some improvements in predicting the erodibility of soils based on soil properties usually collected on geotechnical engineering projects. This database is useful for many engineers worldwide. The engineers worldwide have started to organize a global erosion database by exchanging

the information about erosion testing. The idea is to create an international erosion database in a consistent fashion as proposed by Briaud (2008) which would contain different erosion tests at different sites worldwide. This database aims to improve knowledge on soil erosion and then act correspondingly to reduce negative consequences of soil erosion. Therefore, there is a need to populate and improve the existing TAMU-Erosion database with new test results which were performed as a part of this dissertation including the ones on improved soils and grass.

10.2. Structure of TAMU-Erosion

The TAMU-Erosion structure is described in detail in the NCHRP 24-43 report (Briaud et al., 2019). The erosion test included in TAMU-Erosion are:

1. The Erosion Function Apparatus test (EFA)
2. The Jet Erosion Test (JET)
3. The Hole Erosion Test (HET)
4. The Slot Erosion Test (SET)
5. The Ex-situ Scour Test Device (ESTD)
6. The Borehole Erosion Test (BET)
7. The Rotating Erosion Testing Apparatus (RETA)
8. The Sediment Erosion Rate Flume (SERF)
9. The In-situ Scour Profile (ISEEP) and some large-scaled flume tests

Most of the tests are explained in Chapter 2, Section 2.2. The erosion tests input in TAMU-Erosion have been analyzed and introduced to the database in a consistent fashion as it was suggested by Briaud and Shafii (2018) (Briaud et al., 2019).

Figure 236 shows an example of the TAMU-Erosion Excel spreadsheet which allows to filter the data regarding the type of erosion test.

Record Number	Contact / Agency	Date Conducted / Service	Project Title / Service	Sample Name	Sample Depth	Soil Type	USCS Classification	AASHTO Classification	Natural / Marine	Erosion Test Type	Erosion Function	Erosion Category	k_s [mm/hr-m/s]	k_s [mm/hr-ft/s]	v_c [m/s]	v_c [ft/s]	Remarks on Erosion Test	General Comments
1	Brian Anderson / Auburn University, USA	4/15/2012	ALDOT	Bucatanne	-	Silt	ML with Sand	A-7.5 (S)	Natural	EFA	[Graphs]	2.25	11.21	4.20	0.30	0.41	Erosion plots are digitized	88.0
2	Brian Anderson / Auburn University, USA	4/6/2012	ALDOT	Yazoo	-	Sand	SM	A-5 (S)	Natural	EFA	[Graphs]	2.5	43.35	9.15	0.60	1.26	Erosion plots are digitized	57.0
3	Brian Anderson / Auburn University, USA	1/1/2012	ALDOT	Porter's Creek Clay	-	Silt	MH	A-5 (H)	Natural	EFA	[Graphs]	2.25	62.32	21.99	0.30	0.29	Erosion plots are digitized	62.0

Figure 236. An image of the TAMU-Erosion inventory page (TAMU-Erosion, 2021)

For each record in TAMU-Erosion, contact, data test, sample name, sample depth, soil type is presented. Each sample has been classified according to USCS and AASHTO classifications.

The erosion parameters selected to represent the erosion characteristics of a soil in TAMU-Erosion are:

1. The critical shear stress (τ_c)
2. The critical velocity (v_c)
3. The initial slope (E_v) of the "z" versus v" curve
4. The initial slope (E_τ) of the "z" versus τ " curve
5. The erosion category (EC)
6. Remarks on erosion tests

For some erosion tests, for example SERF and ESTD, the critical parameters are not presented because they were not obtained from the testing. However, the erosion functions were digitized and input in the database. This makes the database unique and useful for the engineers who are interested in the entire erosion curve showing erosion behavior of a soil in a range of velocity or shear stress.

The geotechnical parameters of a soil included in TAMU-Erosion are:

1. Soil plasticity including Liquid Limit, Plastic Limit, and Plasticity Index
2. Unit weight
3. Water content
4. Strength including Pocket Penetrometer Test, Tensile Strength, Unconfined Compression Strength, Undrained Strength by Vane Test
5. SPT N-value
6. Grain size parameters including D50, D10, D60, D30, coefficient of uniformity (C_u), coefficient of curvature (C_v), percent fines, percent clay, percent silt
7. Void ratio
8. Degree of saturation
9. Specific gravity
10. Others such as pH, salinity, organic content, soil activity, fluid temperature, electrical conductivity (parameters are given in some cases)

10.3. Advantages and limitations of TAMU-Erosion

The TAMU-Erosion has advantages and limitations summarized below. Among advantages of TAMU-Erosion are:

1. One of the first global erosion database containing near 1,250-1,300 erosion tests.
2. It includes the results of more than ten laboratory and field erosion test devices.
3. It is organized in a consistent fashion which makes it easy and convenient to compare the results between different tests.
4. It has erosion parameters including erosion curve as well geotechnical parameters which can be used to find any relationship between soil properties and its erodibility.
5. One can easy filter the data.
6. Can be useful for civil engineers particularly geotechnical and hydraulic engineers.
7. Excel spreadsheet can work with different software, for example, with Surfer® to map, model, and analyze the data.

The limitations of TAMU-Erosion are:

1. Some soil erosion and geotechnical parameters are missing especially for erosion tests performed by other organizations than Texas A&M University.
2. Sometimes soil type is shown in general like sand, clay, or silt with no grain size distribution.
3. Location of a sample might be missing which would not allow to accurately map for erosion.

10.4. New erosion tests

TAMU-Erosion has been updated with near 256 erosion tests including the tests performed as a part of this dissertation and the EFA tests run by the Erosion Testing Laboratory at Texas A&M University from August 2018 to June 2021. A total of 75 EFA tests out of 256 tests, performed on improved soils for this dissertation, were added in TAMU-Erosion. A total of 181 tests out of 256 were EFA tests were completed in the Soil Erosion Laboratory at Texas A&M University as additional research work on erosion. Table 52 shows the inventory of the EFA tests carried out as a research for this dissertation.

Table 52. The inventory of the EFA tests added to TAMU-Erosion

#	Type of soil	Number of tests	Type of test	Record number in TAMU-Erosion
1	Lime treated soil	10	EFA	1202-1211
2	Enzyme treated soil	25	EFA	1212-1236
3	Riprap	12	EFA	1237-1248
4	Grass	28	EFA	1093-1136
5	Sacramento, California	36	EFA	1057-1092
6	Sacramento, California	13	BET	1162-1174
7	Near Houston, Texas	32	EFA	976-986, 987-992, 1147-1149, 1150-1158, 1159-1161
8	Louisiana	90	EFA	994-1056, 1175-1201
9	Belgium	10	EFA	1137-1146

10.5. Improvement of TAMU-Erosion

The existing TAMU-Erosion has been improved by adding a procedure how to use the new erosion model and classification described in Chapter 8. In the existing TAMU-Erosion database, all the erosion data are analyzed for the five erodibility

parameters: τ_c , v_c , E_v , E_τ , and EC. Two new erosion parameters, shear-based erosion modulus α and velocity-based erosion modulus β , were added to the database. Note that the erosion moduli make use of the new erosion model presented in Chapter 8. The procedure describing how to obtain the erosion moduli is given below.

- 1) *Shear-based erosion modulus, α :*
 - a. Plot all the data points of the EFA shear stress curve in terms of normalized erosion rate $\frac{\dot{z}}{0.1}$ and normalized shear stress $\frac{\tau}{\tau_c}$ on the new erosion shear stress chart (Figure 237). The erosion rate of 0.1 mm/hour is chosen as an arbitrary assuming that erosion can be neglected. This plot is on logarithmic scale for both axes. The axes are non-dimensional.
 - b. Obtain the shear-based erosion modulus α as the ratio of the logarithm of the erosion rate \dot{z} divided by a reference erosion rate arbitrarily chosen as 0.1 mm/hr to the logarithm of the shear stress (τ) divided by the critical shear stress (τ_c).
 - c. Compute the mean value of the erosion modulus α .
 - d. Classify a soil according to the erosion chart on Figure 237 and its erosion modulus α shown on Figure 238.

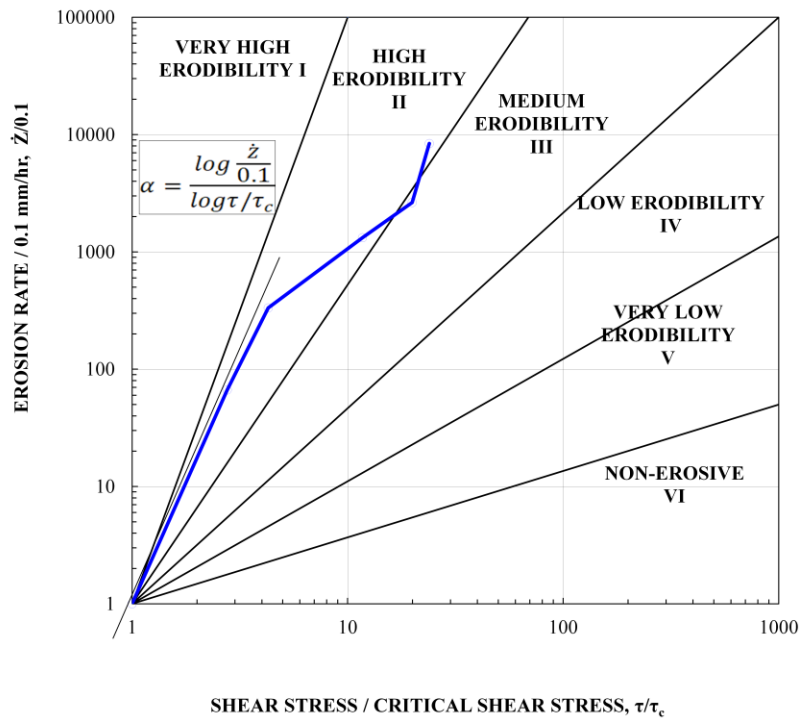


Figure 237. Normalized erosion rate versus normalized shear stress showing shear stress-based erosion modulus definition

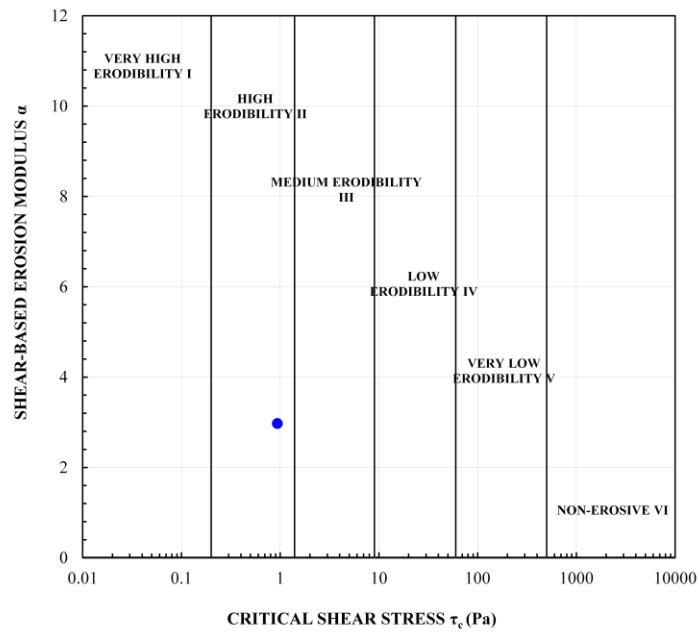


Figure 238. Shear stress-based erosion modulus versus critical shear stress

2) *Velocity-based erosion modulus, β :*

- e. Plot all the data points of the EFA velocity curve in terms of normalized erosion rate $\frac{\dot{z}}{0.1}$ and normalized velocity $\frac{v}{v_c}$ on the new erosion velocity chart (Figure 239). The erosion rate of 0.1 mm/hour is chosen as an arbitrary assuming that erosion can be neglected. This plot is on logarithmic scale for both axes. The axes are non-dimensional.
- f. Obtain the velocity-based erosion modulus β as the ratio of the logarithm of the erosion rate \dot{z} divided by a reference erosion rate arbitrarily chosen as 0.1 mm/hr to the logarithm of the velocity (v) divided by the critical velocity (v_c).
- g. Compute the mean value of the erosion modulus β .
- h. Classify a soil according to the erosion chart on Figure 239 and its erosion modulus β shown on Figure 240.

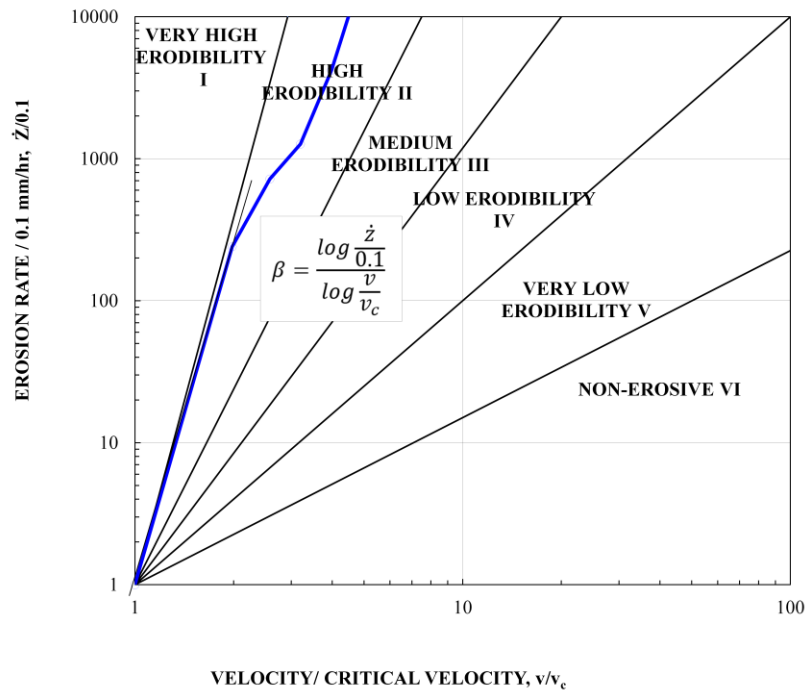


Figure 239. Normalized erosion rate versus normalized velocity showing velocity-based erosion modulus definition

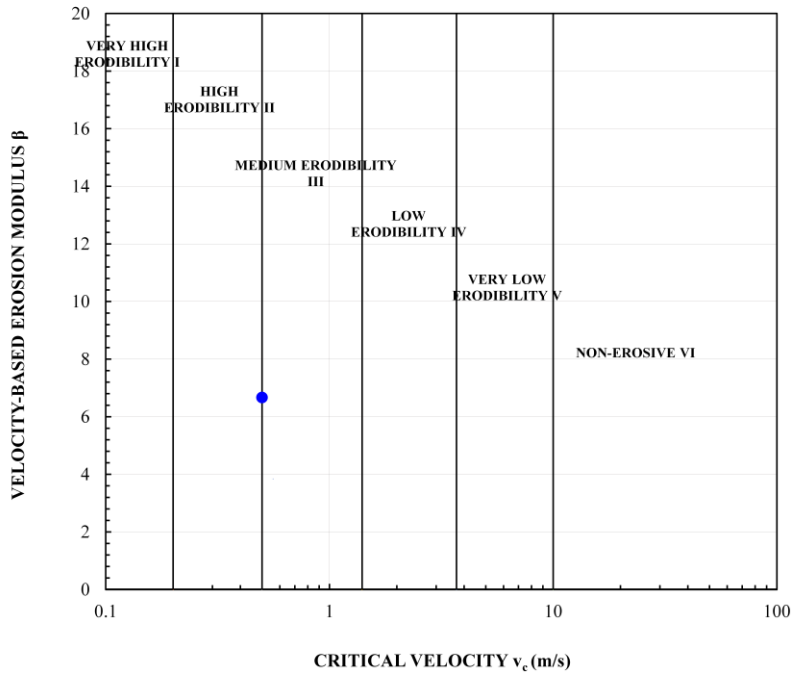


Figure 240. Velocity-based erosion modulus versus critical velocity

11. RISK MANAGEMENT FOR EROSION OF DAMS AND LEVEES

11.1. Databases on case histories

This section describes databases on case histories which were used to locate risk on the risk chart for dams, tailings dams, levees, and Harvey. The data on earth dams and levees are presented for the United States; tailing dams are the world data. Several databases described below were selected for this study. Some databases have a public access and can be downloaded from the websites. Some databases do not have a public access. The risk location for dams and levees is shown on the risk chart (See Section 11.2).

11.1.1. Earth dams

Case histories of failures of earth dams have been collected by the Association of State Dam Safety Officials (ASDSO) and presented in the Dam Safety Incident Database which can be found on the website <https://damsafety.org/incidents>. This database started as a cooperative effort between the Department of Homeland Security Dams Sector and ASDSO in 2010. The information in the database included:

- a. Location and date of construction.
- b. Mechanism of failure and its date.
- c. Number of fatalities.
- d. Economic damages in dollars on date of failure.
- e. Volume of soil released at failure.
- f. Dam parameters (height, maximum storage, surface area)

- g. Incident duration.
- h. References.

The latest version of the database updated on August 19, 2020, was used for this Chapter. Moreover, the ASDSO database was updated by adding more cases on earth dam failures by erosion and correcting the cost of the failures for inflation (\$US 2020). For example, Timberlake dam, Ka LoKo dam, Lawn Lake dam were added to the ASDSO database. The case histories then were selected for the last 50 years (1970-2020). The ASDSO database has 1084 case histories in total among which 391 cases reported as a failure. The failures related to erosion were selected. A total of 234 cases out of 391 failures are due to erosion. Among those 234 cases, 68 % were overtopping, 18 % were piping, and 14 % were other erosion. These are the cases that were used to identify the risk location for earth dams on the risk chart.

The total number of fatalities recorded in the database is 472. Among the major failures having the biggest numbers of fatalities are Buffalo Creek in 1972 (131 fatalities), Canyon Lake in 1972 (238 fatalities), Kelly Barnes in 1977 (39 fatalities), Lauren Run in 1977 (40 fatalities), and Teton dam in 1976 (11 fatalities). Note that Buffalo Creek is a coal mine dam, but it was included in the analysis. In the ASDSO database, the economic damage, in most cases, is given as a range. Thus, in this analysis the maximum value in US dollars as the failure cost was chosen for each case. The total cost of the 234 failures over 50 years is roughly 4.2 billion dollars (US 2020 dollars by correcting for inflation).

11.1.2. Tailing dams

Several attempts have been made to develop accurate databases on tailings dam failures including the ones by the Church of England (COE) tailings intervention program, Wise Uranium Project, World Mine Tailings Failures, The International Commission on Large Dams (ICOLD), the United States Committee on Large Dams (USCOLD), and the United Nations Environmental Program (UNEP). All these databases have limited information including inaccurate number of tailings dams due to underestimation of the number of inactive and abandoned facilities. There is no complete database of all historical failures. A description of each database is given below.

1. Wise Uranium Project compiled “Chronology of major tailing dam failure” (2021) starting in 1960 that can be found on the website <https://www.wise-uranium.org>. This database has 125 major failure cases worldwide and provides the follows:

- a. Location.
- b. Company.
- c. Type of incident.
- d. Volume of waste/tailings released.
- e. Impact such as fatalities and environmental impact.

2. World Mine Tailings Failures portfolio (2020) estimates that there are some between 29,000 – 35,000 tailing dams in the world. These numbers are very rough. The official data, presented in the portfolio, shows 19,214 tailing dams worldwide including 1625 tailings dams in the United States according to the USACE National

Inventory of Dams (2019). According to the database, a cumulative loss in 2019 is 2,762 lives (World Mine Tailings Failures portfolio, 2020).

3. ICOLD with a cooperation of USCOLD and UNEP have collected 221 case histories on tailing dam incidents potentially or directly leading to failure during the period of 1917 to 2000 (83 years). Not all failures occurred during that period have been reported in the database. However, each failure out of 221 is briefly described in Bulletin 121 “Tailing dam risk of dangerous occurrence”. Unfortunately, neither ICOLD nor USCOLD provides open public access to their databases. Moreover, the accurate number of tailing dam failures is difficult to obtain.

4. Center for science in public participation prepared a database of tailing dam failures from 1915 to 2016 that can be found on the website <http://www.csp2.org/tsf-failures-from-1915>. The database includes 289 failures worldwide with a total of 2454 fatalities. This database was updated with recent 24 failures (2016 to 2019) and 308 fatalities (World Mine Tailings Failures, 2019). The database can be found on the website <https://www.resolutionmineeis.us/sites/default/files/references/bowker-2019.pdf>.

11.1.3. Levees

The USACE has developed the National Levee Database covering some 40,000 km of levees in the USA. A subset of this database called the USACE levee portfolio covering some 23,000 km was studied in more details by the USACE. The databases are briefly described below.

1. The National Levee Database is a global searchable inventory of information about Nation's levees. It can be found on the website <https://levees.sec.usace.army.mil>. This database allowing to search a levee by a name and location includes:

- a. Length of levees.
- b. Number of levee structures and systems.
- c. Average age of levees.
- d. Potential consequences (property values in US dollars, population, buildings).

Unfortunately, the database does not provide the information on levees failures as well as number of fatalities and money lost needed to locate risk on the risk chart.

2. The USACE levee portfolio is the first summary report of the flood risks associated with levees (USACE Levee Safety Portfolio Report 2018). There are two major failure mechanisms considered in the portfolio:

- a. Levee overtopping with breach.
- b. Breach prior overtopping.

Both scenarios lead to a levee failure. It is recognized that levee overtopping with breach is the most common failure mechanism. About 40 % of levee systems fails due to overtopping with breach and approximately 32 % of failure is related to internal erosion (seepage and piping in embankment and foundation). Breach prior overtopping would have worse consequences in terms of lives loss and cost due to less advance warning as indicated by the USACE Levee Safety Portfolio Report 2018. Risk approach developed

by the USACE is based on fatalities, economic and environmental consequences. Six risk categories are identified including very high (1), high (2), moderate (3), low (4), very low (5), and no verdict (6). Among 23,000 km of the levees, about 13 % of levees are in high and very high risk. Those levees have a high potential to breach prior overtopping causing many fatalities and money lost if no actions are taken in advance. Approximately 60 % of the levees are in low category.

The USACE portfolio estimates that a probability of a levee overtopping for the majority of levee systems is between 1 % and 0.1 % meaning that an overtopping has a probability of 1/100 to 1/1000 to occur or to be exceeded in any given year. The USACE portfolio suggests that about 3.6 million people and \$400 billion in property value are behind the Nation's levees. The potential number of fatalities associated with a levee breach range from zero to more than 2,000.

11.2. Risk and risk chart

The goal of this section is to locate risk on the risk chart for earth dams, tailing dams, and levees. Risk definition and risk approach are given below. Risk can be categorized as preventable, strategic, and external (Crystal, Smith, 2016). Preventable risk can be monitored and controlled through rules, values, standards of practice, standard compliance tools and best management practices. For example, risk can be reduced through additional site investigations, monitoring, or applying a higher factor of safety. Preventable risk can allow to improve the resiliency of dams and levees with a goal to reduce the probability of failure or the consequences thereof. Strategic risk is a major factor in modern risk management that is focused on the most consequential and

significant risk. Strategic risk is aimed to help owners (e.g. Corp of Engineers) to make risk-informed decisions. External risk is the most uncontrolled risk because it is related to natural hazards (earthquakes, floods etc.). However, external risk can be reduced by minimizing the consequences of the event (for example, evacuating people).

In civil engineering, it is known that risk of an event is defined as the product of the probability of failure of an event times the value of the consequence of an event. The probability of failure P_f can be represented as the product of the probability of occurrence and/or exceedance of an event that might occur or be exceeded in any given one year $P(E)$, times the probability of failure if that event occurs $P(F/E)$. For example, the 350-years flood will be a flood which has a probability of 1/350 to occur or to be exceeded in any given year. The probability of failure is follows (Eq. 90).

$$P_f = P(E) \cdot P(F/E) \quad (90)$$

The annual risk R defined as the annual probability of failure P_f times the value of the consequence C in terms of lives lost and/or money lost (Eq. 91).

$$R = P_f \cdot C \quad (91)$$

Risk can be graphically represented on the risk chart which is also known as F-N Chart (F means frequency and N means the consequences) (Baecher and Christian, 2003). Figure 241 shows the risk chart first proposed by Whitman, then updated by Baecher and Christian, Gilbert, Briaud and others. The risk chart includes three components: the annual probability of failure, dollars lost, and fatalities. The annual probability of failure is plotted on the vertical axis and the value of the consequence is plotted on the horizontal axis. Figure 241 shows the risk chart for some major

engineering structures (foundations, bridges, open pit slopes) as well as for some other activities (plane crash, drill rigs, diseases) (Briaud et al. 2012; Briaud et al., 2014). The risk for engineering activities is shown as the ellipses associated with each activity. There are three lines in the risk chart also called risk tolerable curves representing equal risk along each line. The green solid line is associated with acceptable risk. The dashed blue line stands for medium risk. The dotted red line is unacceptable risk. The target risk levels are shown in Table 53.

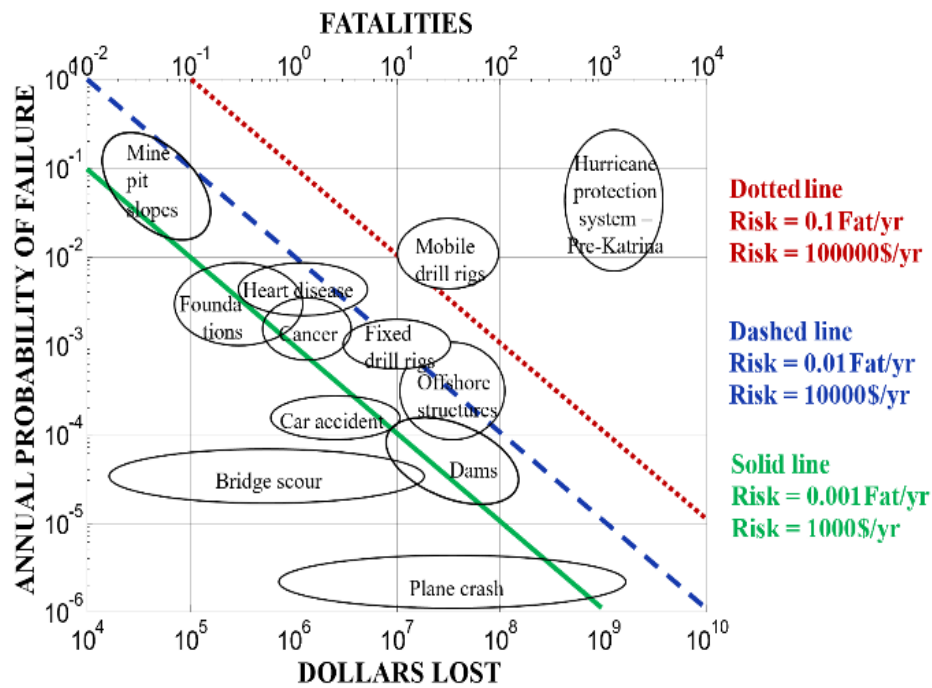


Figure 241. Civil engineering risk (adapted from Whitman 1984, Marr 1995, Christian, Baecher 2003, Briaud and Yao 2013, Gilbert 2017)

Table 53. Target risk levels for the United States (adapted from Briaud et al. 2012)

Risk Level	Risk (\$/yr)	Risk (fatalities/yr)
Acceptable	1,000	0.001
Medium	10,000	0.01
Unacceptable	100,000	0.1

Risk-informed decision should provide benefits of improved management of engineering structures. The USACE suggests to base risk-informed decision on a combination of the three major components: risk assessment, risk management, and risk communication (Figure 242). Risk assessment allowing to plan, can be based on risk location on the risk chart. Risk chart shows how tolerable risk is. A tolerable risk is a risk within a range that society can live with, but rather to keep under review and reduce it still further if possible (ICOLD 2002). It should be noted that tolerable risk is not constant. Risk management allows to apply management policies, procedures, and practices to identify, analyze, assess, treat, and monitor risk (ICOLD 2002). Risk communication is a process of the exchange of real-time information between risk experts and public involved with their health, economic or social well-being.

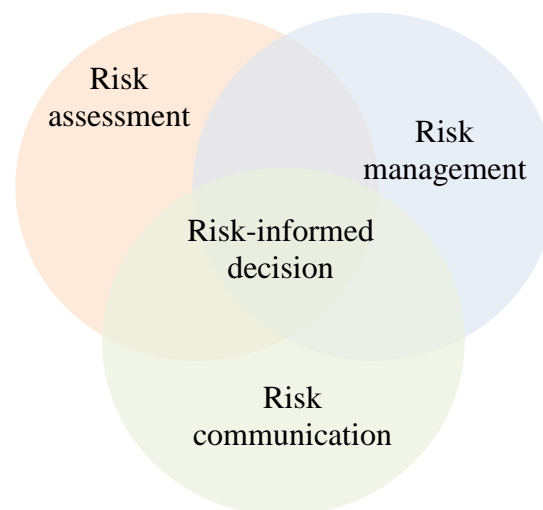


Figure 242. Risk framework (adapted from USACE Levee Safety Portfolio Report 2018)

11.2.1. General procedure to locate risk on risk chart

Several activities were selected to show their location on the risk chart. Among these activities are earth dams, tailing dams, and levees. The general step-by-step procedure for obtaining the risk location of a given activity on the chart was as follows:

Step 1. Define the failure (for example, earth dam failure).

Step 2. Collect information to determine the total number of failures F_t over n years (for example, 50 years). For doing that, the existing failure database can be used.

Step 3. Obtain the average annual number of failures F_a given by $F_a = F_t/n$ from the existing database.

Step 4. Collect information to determine the total number S of structures involved with the activity in the inventory (for example, total number of dams in the US). For doing that, use the official data such as National Inventory Database.

Step 5. Calculate the average annual probability of failure as $P_a = F_a/S$ and the range of P_a values for the study period (for example, 50 years).

Step 6. Collect the number of people that died for each documented failure for the period of n years. Add those up to obtain the total number of fatalities D over the period of n years and for F_t failures. For doing that, use the official data from the databases or from the published case histories.

Step 7. Determine the average number of fatalities X corresponding to one failure as D/F_t and the range of X values for the study period. Note that, because of the log scale, the ellipse created for each activity was bound by 0.01 fatalities if the lower bound was 0.

Step 8. Collect the consequence cost associated with each failure for the period of n years. Convert these values into US 2020 dollars by correcting for inflation. Add those up to obtain the total cost c of those failures over n years and for F_t failures.

Step 9. Compute the average cost C associated with each failure as c/F_t and the range of C values over the study period.

The location of the activity has coordinates of P_a and X on the fatality risk chart and P_a and C on the cost risk chart. The shape of the risk location is described as an ellipse, or a bubble usually stretched horizontally.

11.2.2. Procedure for risk location of earth dams

The data for the risk location of earth dams on the risk chart comes from the Dam Safety Incident Database described in Section 11.1. This database was analyzed over a fifty-year period (1970-2020) for incident type and frequency, number of failures, fatalities, economic consequences, and other relevant parameters.

Step 1. The case is earth dam failures.

Step 2. The total number of earth dam failures in the US during a 50-year period is $F_t = 234$.

Step 3. The average annual number of failures F_a given by $F_a = F_t/n = 234/50 = 4.68$.

Step 4. The total number of earth dams in the US is 91,457, 79,709 of which are earth dams (National Inventory of Dams, 2020).

Step 5. The average annual probability of failure as $P_a = F_a/S = 4.68/79,709 = 5.87 \cdot 10^{-5}$. The range of P_a values is minimum of $1.25 \cdot 10^{-5}$ to maximum of $7.03 \cdot 10^{-4}$ (for 50 years).

Step 6. The corresponding total number of fatalities for 50 years is 472.

Step 7. The average number of fatalities X corresponding to one failure is $X = 472/234 = 2.02$. The range of X values is minimum 0 (no fatalities) and maximum 234.

Step 8. The total cost c of the 234 earth dam failures over 50 years is 4,254.16 million dollars (US 2020 dollars by correcting for inflation). The total cost was estimated based on the Dam Incident Database (ASDSO, 2020a) and individual case histories published online (ASDSO, 2020b; 2020c).

Step 9. The average cost C associated with each failure is $c/F_t = 1.82 \cdot 10^7$ (US 2020 dollars). The range of C values over the 50-years period is minimum 10^5 and maximum $1.37 \cdot 10^9$ (US 2020 dollars).

The coordinates of the risk point are: annual probability 5.87×10^{-5} and 2 fatalities and probability 5.87×10^{-5} and cost 18.2 M\$. The mean value is illustrated as a green dot. The range of parameters is shown as a green ellipse on the fatality risk chart (Figure 243) and on the cost risk chart (Figure 244). The green, orange, and red lines on the charts correspond to constant low, medium and high-risk. Note that the coordinates of the constant risk lines were updated for dollars lost and the values of risk shown in

Table 54. The location of the earth dams on both risk charts indicates a low risk. However, assuming a range of fatalities and dollars lost (brown ellipse), risk can be medium (orange line).

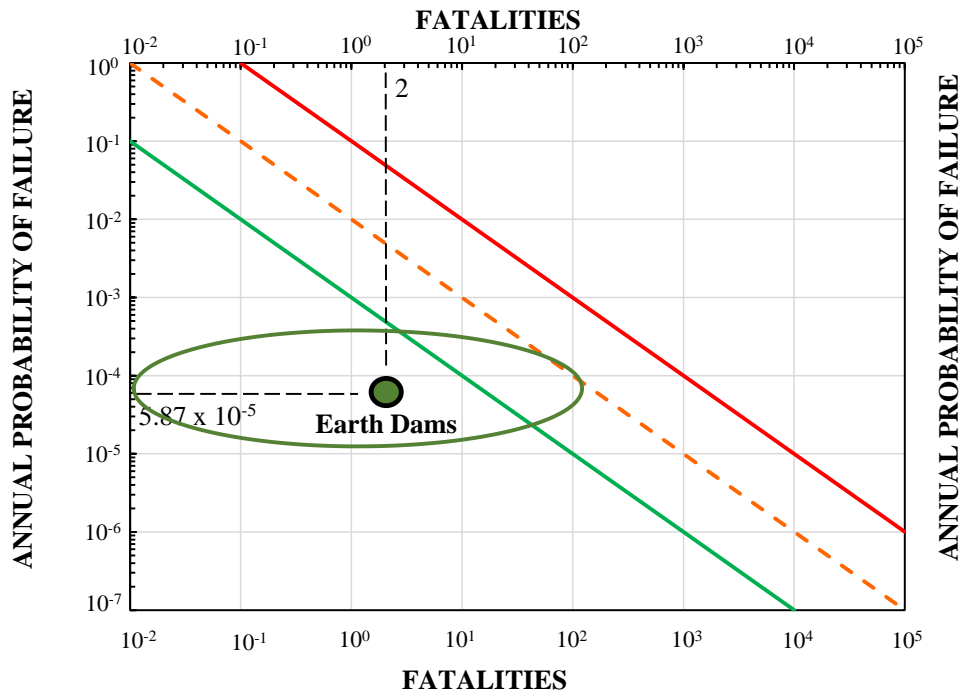


Figure 243. Risk chart for earth dams (for fatalities)

Table 54. Target risk levels for the United States (adapted from Timchenko, Shidlovskaya, Briaud, 2021)

Risk Level	Risk (\$/yr)	Risk (fatalities/yr)
Acceptable	10,000	0.001
Medium	100,000	0.01
Unacceptable	1,000,000	0.1

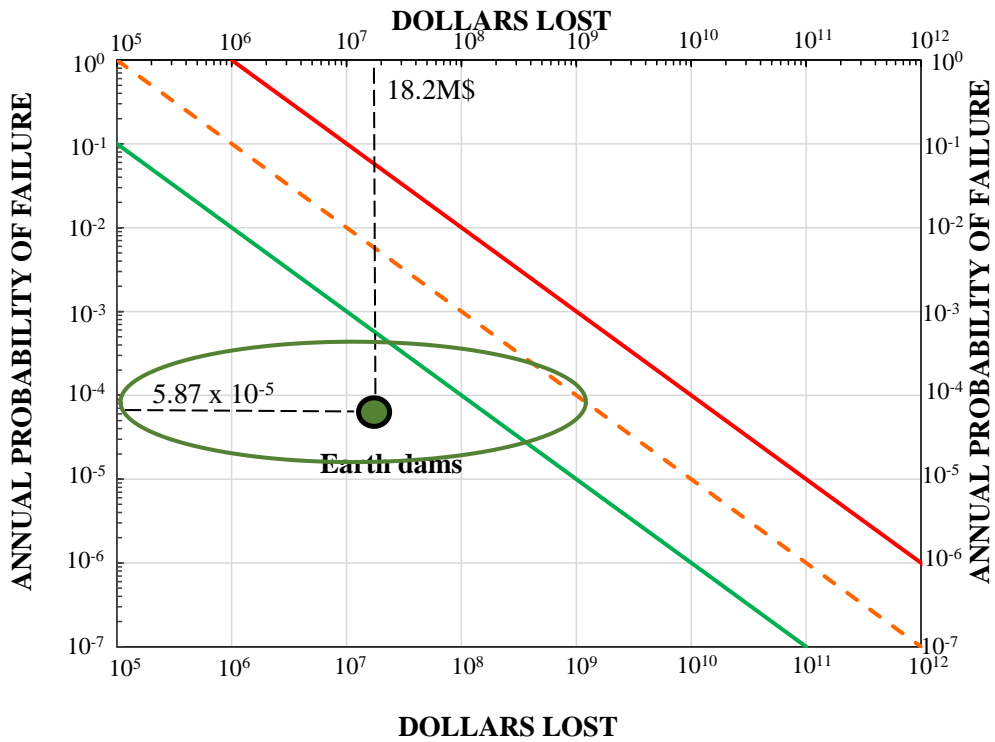


Figure 244. Risk chart for earth dams (for dollars lost)

11.2.3. Procedure for risk location of tailing dams

The procedure to locate the risk of tailing dam failures on the risk chart would be the same as for the earth dams. Two databases were used to locate the risk: World Mine Tailing Failures database and the Center for science in public participation database which seem to be similar.

Step 1. The case is tailing dam failures.

Step 2. The number of tailing dam failures worldwide during a 104-year period is $F_t = 313$ (World Mine Tailings Failures).

Step 3. The average annual number of failures F_a given by $F_a = F_t/n = 313/104 = 3.01$ if the number of failures is a sum of 289 (the Center for science in public

participation, 1915-2016) and 24 (World Mine Tailings Failures, 2016-2019). Some data suggests that 2 to 5 major tailings dam failures occur annually (Davies, 2002).

Step 4. One can assume a worldwide inventory of 19,214 tailings dams (the World Mine Tailings Failures Portfolio).

Step 5. The average annual probability of failure as $P_a = F_a/S = 3.01/19,214 = 1.57 \cdot 10^{-4}$. It should be noted that it is difficult to estimate the probability of tailing dam failures due to lack of data. Some data also indicates that the annual probability of failure is $5 \cdot 10^{-4}$ (USEPA, 2014).

Step 6. The corresponding total number of fatalities for 104 years is 2,762.

Step 7. The average number of fatalities X corresponding to one failure is $X = 2,762/313 = 8.82 \approx 9$.

The coordinates of the risk point on the risk chart are: annual probability 1.57×10^{-4} and 9 fatalities. The procedure cannot be applied for the cost because no total cost data could be found for all failures. The location of the risk point on the risk chart (annual probability versus fatalities) shown in Figure 245 is fraught with uncertainty because the data comes from multiple sources. However, the procedure described is valid and can be used if reliable and complete data can be found.

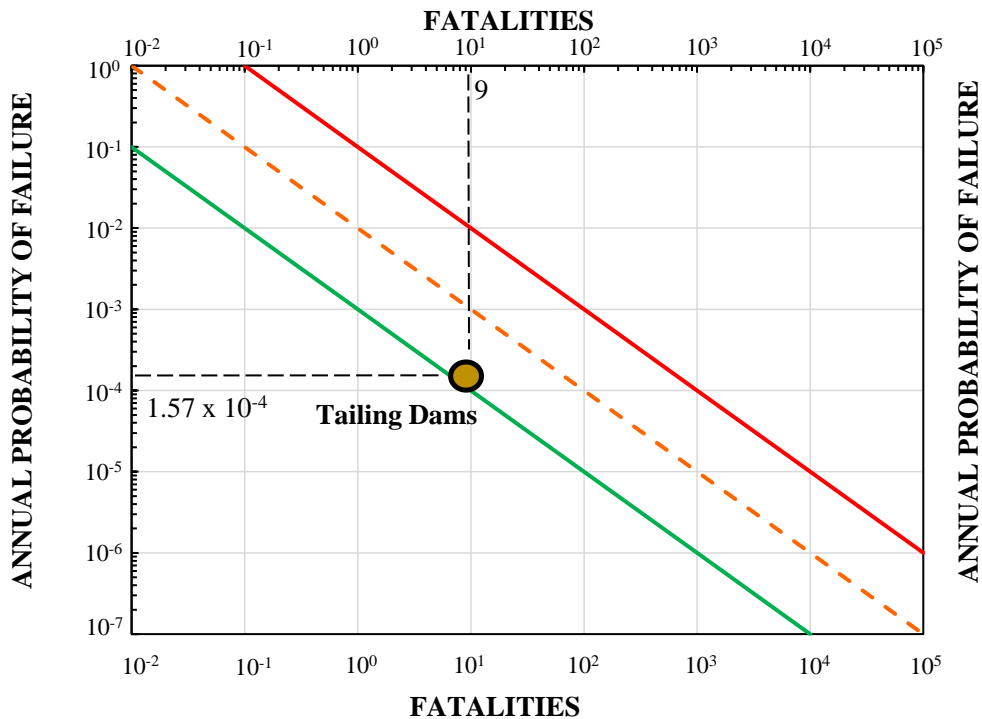


Figure 245. Risk chart for world tailing dams (annual probability versus fatalities)

11.2.4. Procedure for risk location of levees

The procedure followed for the dams and tailing dams can be followed for levees. Because no complete data could be found for levees, the risk point cannot be located on the risk chart. A hypothetical case is used to be able to show the location of risk on the risk chart.

Step1. The failure phenomenon is a levee breach (assume overtopping).

Steps 2 and 3. One can assume that the number of levee failures averages 20 per year and that the length of each failure (breach) is 50 meters.

Step 4. The total number of km of levees in the country is 40,000 (National Levee database).

Step 5. The annual probability of failure is therefore: $20 \times 50 / 40,000 = 2.5 \times 10^{-2}$.
². Note that the probability can also be estimated from the design flood. For example, a 100-year flood has a probability of 1/100 or 0.01 to occur or to be exceeded in any given year.

Step 6 and 7. Assume that an average of 100 fatalities occur for each failure.

Step 8 and 9. Assume that each failure leads to a cost \$10B.

Step 10. The coordinates of the risk points are: annual probability 2.5×10^{-2} and 100 fatalities and probability 2.5×10^{-2} and cost 10 B\$.

The risk chart for levees is shown in Figure 246 and Figure 247.

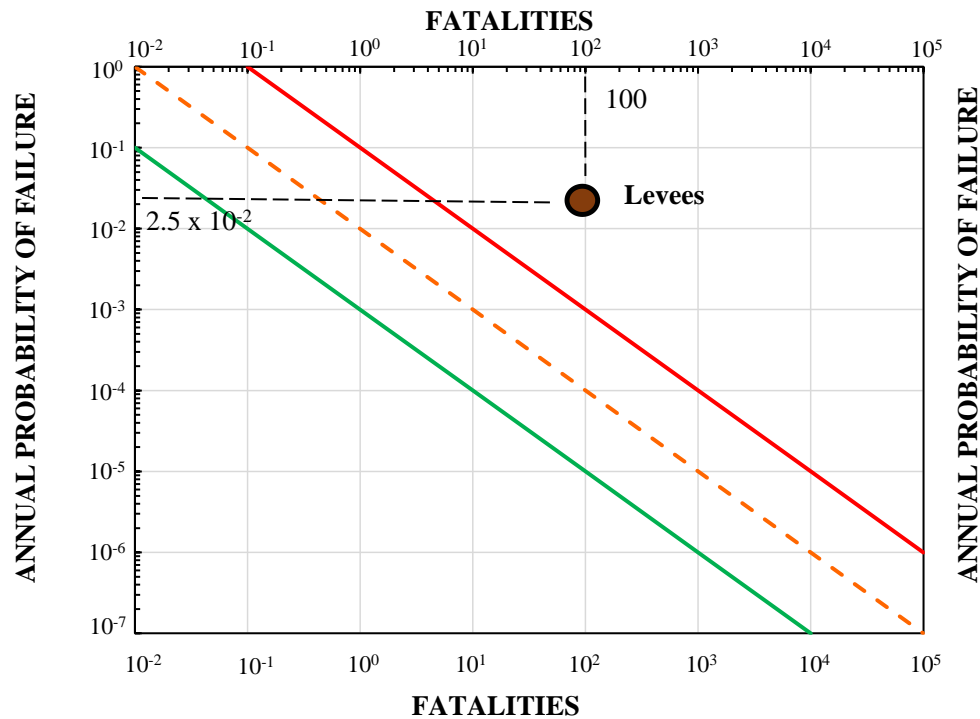


Figure 246. Risk chart for levees (annual probability versus fatalities)

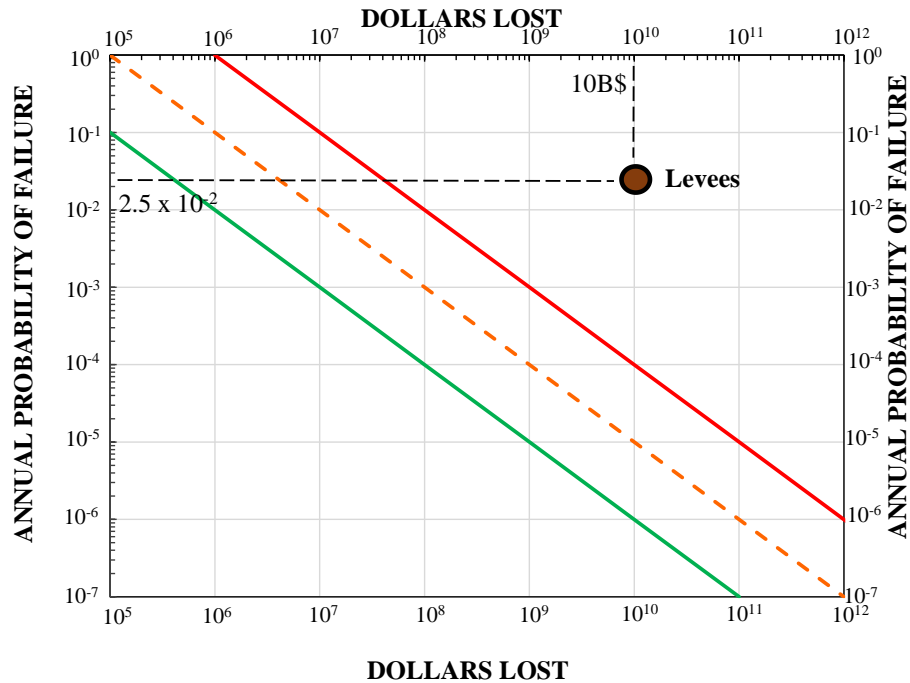


Figure 247. Risk chart for levees (annual probability versus dollars lost)

11.2.5. Procedure for risk location of a set of structures subjected to hurricane

This Section describes an approach to show risk for a set of structures subjected to a hurricane. For example, in 2017, Hurricane Harvey, one of the most catastrophic Category 4 storms ever hit the United States, caused at least 68 fatalities and \$133 billion (2021) in damage near Houston (Blake and Zelinsky, 2018). NOAA (2021) estimated that the occurrence interval for this event was more than 1,000 years or 0.1% chance to occur or to be exceeded in any given year. The data presented above was used to generate a point on the risk chart (Figure 248 and Figure 249). The coordinates of the point are: annual probability of 10^{-3} and 68 fatalities and annual probability of 10^{-3} and \$133 billion dollars lost.

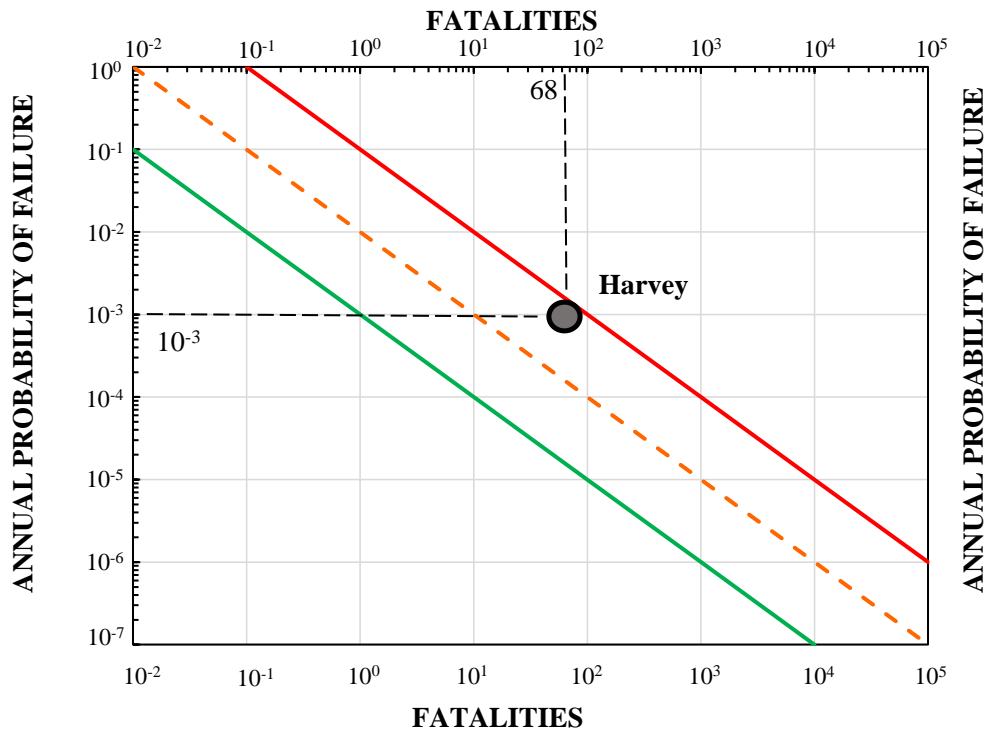


Figure 248. Risk chart for hurricane (annual probability versus fatalities)

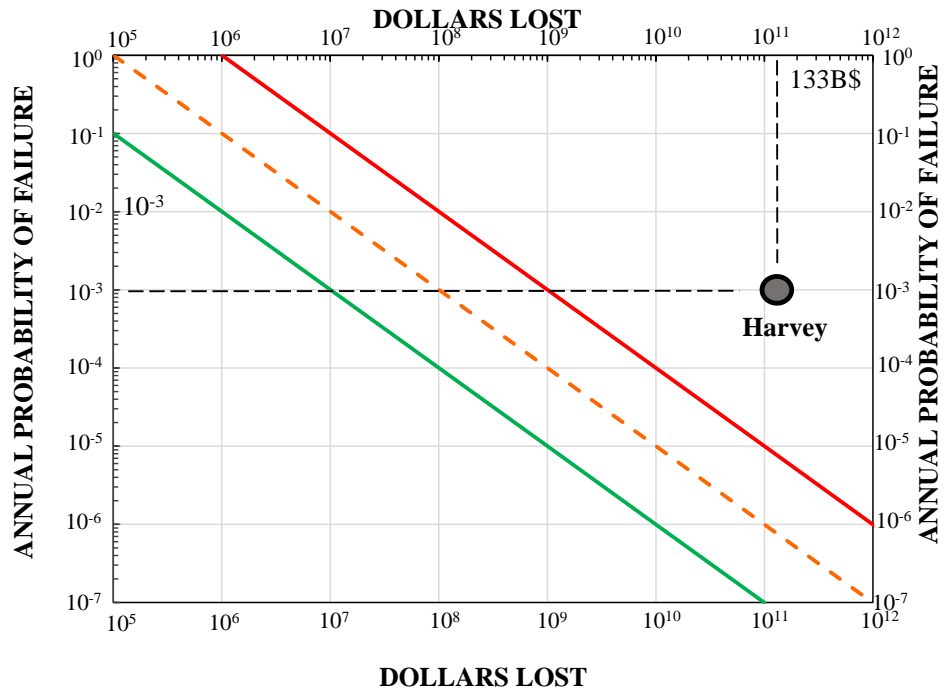


Figure 249. Risk chart for hurricane (annual probability versus dollars lost)

11.2.6. Summary risk chart for dams and levees

Risk chart can be presented as a comparison between different engineering structures used as examples in this Chapter (Figure 250 and Figure 251). One can make a risk-informed decision based on risk chart and also evaluate a way how to reduce risk to an acceptable level (See Section 11.4).

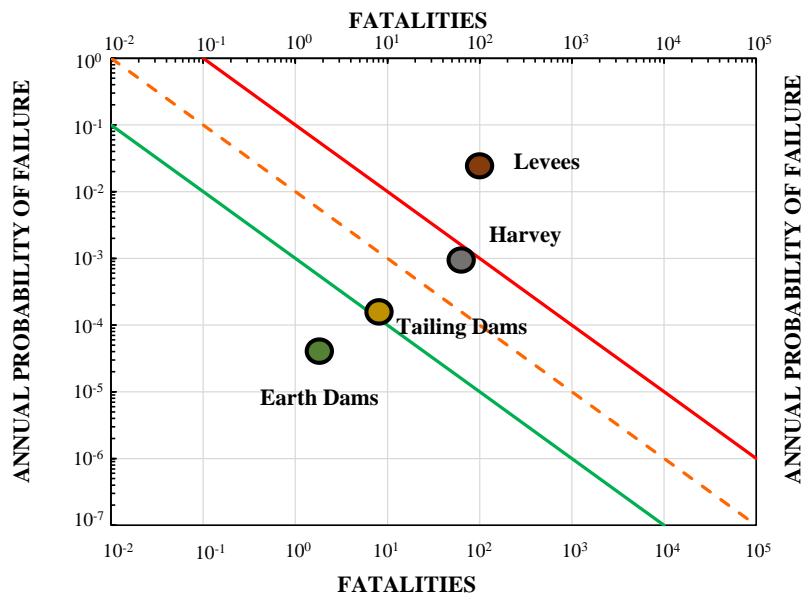


Figure 250. Summary risk chart for earth and tailing dams, levees, and hurricane (annual probability versus fatalities)

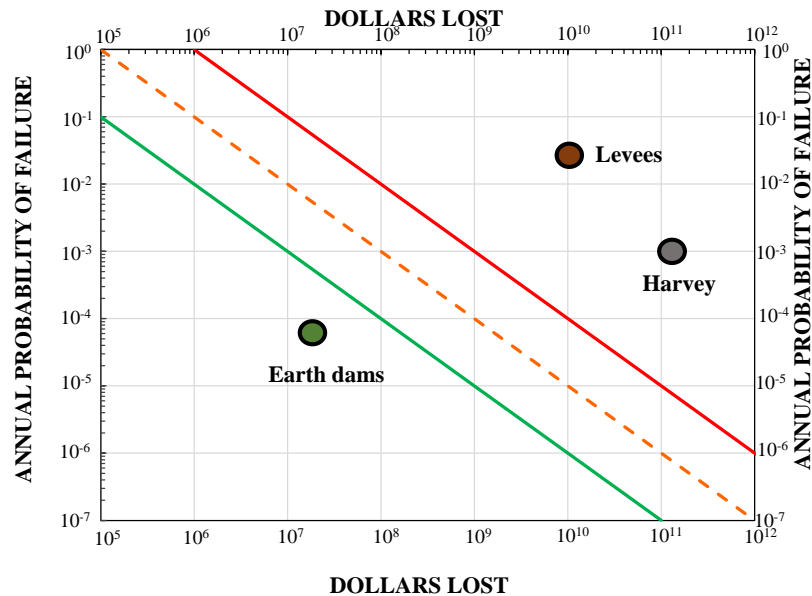


Figure 251. Summary risk chart for earth and tailing dams, levees, and hurricane (annual probability versus dollars lost)

11.3. Erosion risk category classification of dams

This Chapter describes a methodology to evaluate the erodibility of dams and levees by using the erosion categories. Proposed methodology makes use of erosion testing of soils, for example EFA testing, and the erosion model and chart developed by Briaud. The methodology is useful for zoned dams for which to obtain the erosion category of a dam is a challenge. Step-to-step procedure describing how to obtain the erosion categories presented below.

Step 1. Obtain erosion categories for different zones of a dam. The erosion testing is preferred, however, in some cases, the erosion categories of zones can be estimated based upon the soil description.

Step 2. Choose a reference line going through the dam. It is proposed to choose a horizontal line or a few lines cutting the dams through different erosion zones.

Step 3. Estimate the length of each zone through the lines or lines.

Step 4. Obtain dam erosion category as the weighted average of the zone's erosion categories. The weighted average would allow to evaluate dam erodibility considering erosion categories and dam geometry.

Step 5. On the erosion rate versus shear stress chart draw a line which corresponds to the estimated erosion category of the dam from the previous step. This line should be parallel to a boundary line.

A step-to-step procedure, described above, was applied for an example of a three-zoned dam (Figure 252). For each dam, the erosion categories were obtained by running the erosion tests. The length of each zone through the section AA is shown in the Figure 252. The weighted average of the zone's erosion categories is obtained as the following:

$$\text{Dam Erosion Category} = \frac{EC_{IV} * 17 (m) + EC_{III} * 100 (m) + EC_{IV} * 15 (m)}{17 (m) + 100(m) + 15(m)} = 3.2$$

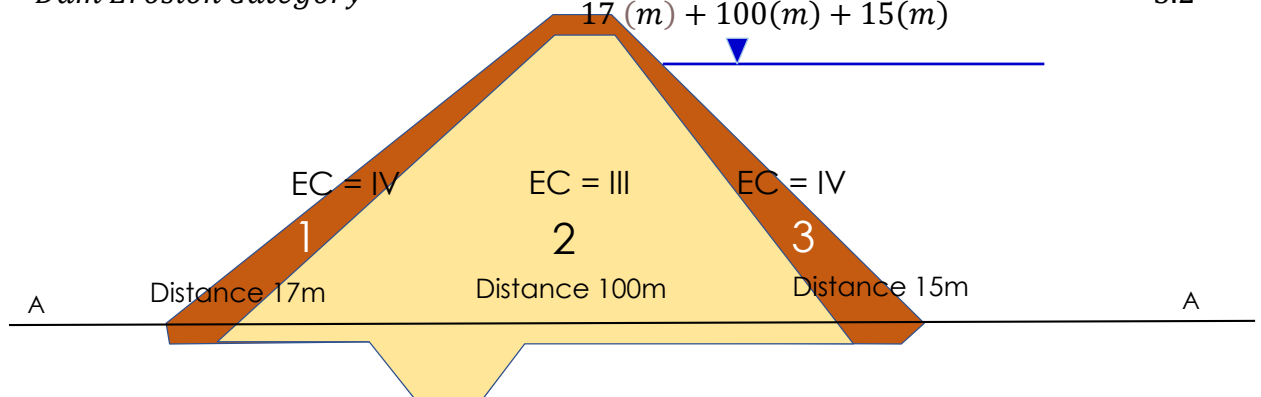


Figure 252. An example of a dam showing the erosion categories

The erosion category for the dam is 3.2. The assumption is the location of the reference horizontal section AA.

A step-by-step procedure was also performed for the Teton dam. Figure 253 shows Teton Dam cross section and the three arbitrary horizontal lines selected to obtain the weighted average erosion category for Teton Dam (after Briaud, 2021, personal communication). Table 55 shows the dam materials and their erosion categories. These erosion categories together with critical velocities were estimated based upon the material description in Seed and Duncan (1981). The calculations indicate that the weighted average of the erosion category according to the length of material exposed for that level are (Chedid et al., 2018):

- a. Section AA gave an EC = 2.5;
- b. Section BB gave EC = 2.6;
- c. Section CC gave EC = 2.7.

The weighted average erosion category of Teton dam is therefore obtained to be 2.6 or medium to high erodibility (Figure 253).

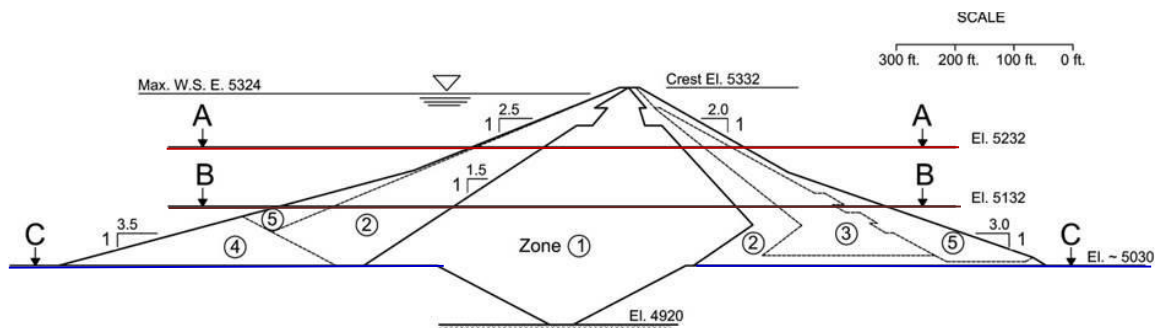


Figure 253. Cross section through Teton Dam (adapted from Seed and Duncan, 1981)

Note that the Teton Dam having an erosion category of 2.6 (medium to high erodibility) failed in 4 hours.

Table 55. Description of the Teton Dams zone materials with proposed erosion categories (adapted from Briaud, 2021)

Dam Zone Material	Description	Estimated critical velocity (m/s)	Erosion Category
Zone 1 (Core)	Silt with some clay, sand, and gravel	0.2	2
Zone 2	Selected sand, gravel and cobbles	1	3.1
Zone 3	Miscellaneous fill	0.5	2.5
Zone 4	Selected silt, sand, gravel, and cobbles	0.8	3
Zone 5	Rockfill	2	4

On the erosion rate versus shear stress chart draw a line which corresponds to the estimated erosion category of the dam from the previous step. This line should be parallel to a boundary line. The erosion chart on Figure 254 shows a blue line which corresponds to the erosion category of an example dam $EC = 3.24$ (Medium Erodibility) and a pink line which shows a Teton dam erosion category $EC = 2.6$ (Medium Erodibility).

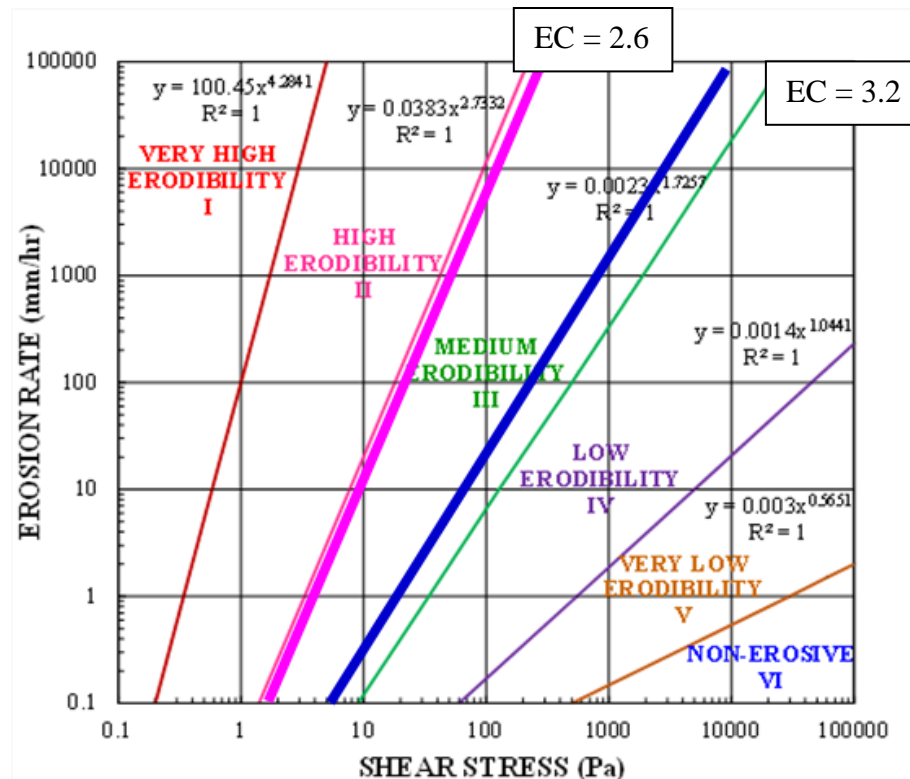


Figure 254. Erosion chart showing dams categories (adapted from Briaud, 2021)

A dam erosion limit showing a boundary between a failure and no failure might be useful on this chart. One can find case histories with a failure and no failure, estimate erosion category of each dam as a weighted category, show them on the chart and find a boundary on that chart between failure and no failure.

11.4. Recommendations for risk reduction

On the risk chart, risk can be reduced by lowering the probability of failure (P_f), or by lowering the consequence of failure such as dollars lost and fatalities or both. Some following solutions to reduce or minimize risk can be suggested. They all have advantages and limitations.

1. Increase the return period of the design flood within reasonable economical limits and therefore decrease the annual probability of failure. The probability of failure can only be reduced by understanding the weaknesses of the system (Crystal, Smith, 2016).
2. Decrease the cost of the consequence in terms of property loss. This is very difficult as houses and other engineering structures cannot be moved from a potentially flooding area.
3. Request that people evacuate their houses before large floods. This is very efficient in drastically decreasing the number of fatalities but could be costly from the point of view of the economy. Also, it is sometimes difficult to convince people to evacuate. Conveying the risk posed to the public is an important message to promote so that the public can make a risk informed decision.

12. CONCLUSIONS, RECOMMENDATIONS AND CONTRIBUTIONS TO NEW KNOWLEDGE

The conclusions and recommendations from the research work done are organized according to the chapters in the dissertation where contributions to new knowledge were accomplished.

12.1. Improvement of erosion testing and data reduction procedure

Chapter 3 describes the field and laboratory erosion testing performed on levee soils in Sacramento, California. A total of 36 EFA tests, 36 PET tests, and 13 BET test boreholes were performed at sites along the Lower American River and along the Sacramento River. The erodibility of the soils was classified according to an erosion classification chart which has 6 different levels with I being soils having “Very High Erodibility” and VI being “Non-Erodible” soils. Overall, the soils at the sites described mostly as silty sand, silt, and silty clay, belonged primarily in the erosion category II or “High Erodibility” according to the EFA tests results. The BET results tended to indicate less erodibility with most tests being concentrated in the erosion III category or “Medium Erodibility”. This may be due to the influence of sample disturbance on the laboratory measurements. The PET results, while intermediate, tended to agree more closely with the EFA results. However, the combination of BET, EFA, and PET provided a complementary assessment of soil erodibility.

The critical velocity measured in the EFA varied from 0.29 m/s to 1.5 m/s. The critical shear stress measured in the EFA varied from 0.293 Pa to 8.438 Pa. The slope of

the erosion function measured in the EFA (straight line regression in the natural space) varied from 1.328 mm/hr/Pa to 793.01 mm/hr/Pa. The critical shear stress inferred from the BET varied from 0.18 Pa to 18 Pa with the average of 2.9 Pa. The critical velocity inferred from the BET varied from 0.16 m/s to 1.5 m/s with the average of 0.53 m/s.

When comparing the results of the BET and the EFA, it was found that the critical shear stress inferred from the BET was on average 5.6 times higher than the critical shear stress measured in the EFA.

$$\tau_c(BET) = 5.6 \tau_c(EFA) \quad (92)$$

It is suggested that the higher τ_c value inferred from the BET is due to the advantage of testing the soil in its in-situ stress environment with the BET compared to having to contend with disturbance effects on the EFA results. As such it may be appropriate to shift the erosion function measured with the EFA to start at the BET inferred critical shear stress to get a more representative erosion function of the soil in-situ.

In terms of future development, it will be important to continue to develop the Borehole Erosion Test. Indeed, the BET potential is significant as a very valuable erosion profiling tool, a complement to laboratory erosion tests, and an in-situ calibration of laboratory data. The BET can be used in parallel with a few EFA tests to identify erodible layers. It will also be valuable to further develop erosion numerical simulations to use the entire measured erosion function rather than using the simplified linear model.

12.2. Mitigation of Erosion Using Grass

Based on the data presented in Chapter 4, the following conclusions and recommendations can be made regarding the erodibility of grass covered soils.

1. Grass is more erosion resistant than soil on the average. Overall, the presence of grass moves the erodibility of the soil surface by one category towards more erosion resistance on the erosion chart compared to the barren soil (Figure 255 and Figure 256). A summary of grass erodibility is shown in Table 28, Chapter 4.7.

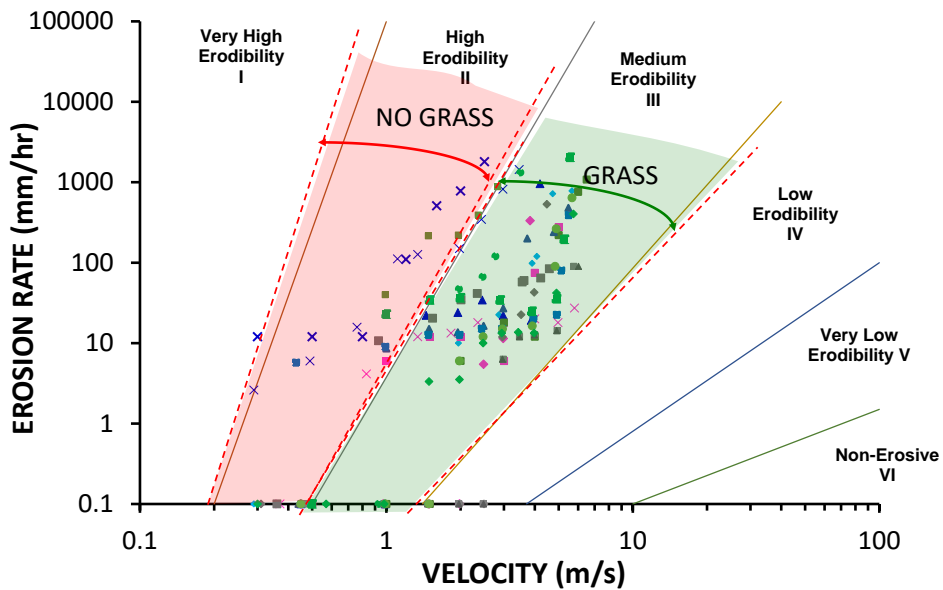


Figure 255. Summary of erosion rate versus velocity in logarithmic scale of grass

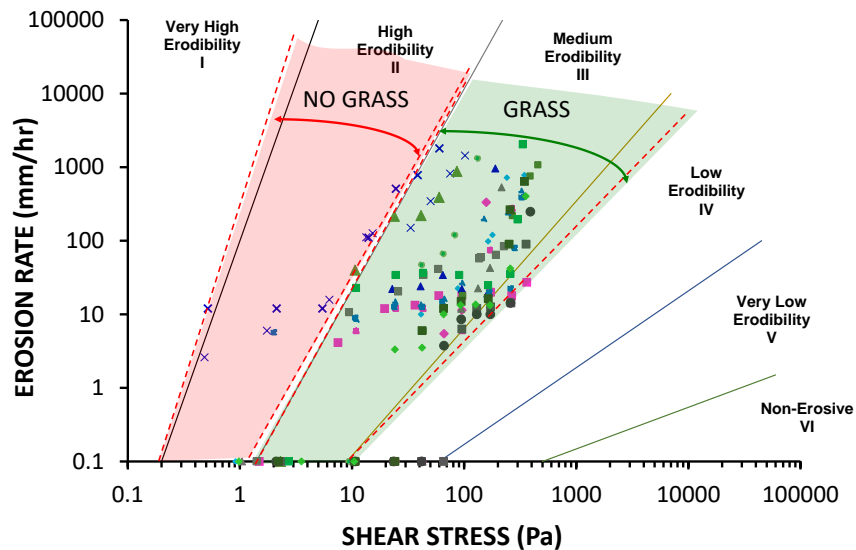


Figure 256. Summary of erosion rate versus shear stress in logarithmic scale of grass

2. The ratio between the grass critical velocity and the soil critical velocity or detachment velocity varies from 3 to 7 when considering average critical velocities for each type of grass and of bare soil.

3. The erodibility of a given type of grass varies depending on influencing factors.

4. The factors influencing the critical velocity of grass based on EFA testing are grass type, age, health, and coverage.

5. The following are the influence factors which were identified in the research:

- a. Type
- b. Age

- c. Health
 - d. Coverage
6. Once the grass mat is detached (failed), the soil below is still reinforced by the root system and this subsystem is still more resistant than the soil alone.
 7. If the grass is subjected to a first flood and is not detached (for example, tests on StA4 and Z2), that grass during a second erosion loading will not be as resistant as the first time if there is little time between floods. If there is enough time for the grass to reestablish itself then the second loading will be similar to the first loading (for example, Zoysiagrass tests).
 8. NDVI (Normalized Difference Vegetation Index) is not a good indicator of grass erosion resistance because the NDVI does not vary sufficiently from one case to the next. Coverage expressed in terms of percent cover seems to be a better indicator of grass erosion resistance.
 9. Four different types of grass were tested in the EFA. The results indicate that given the same age, Bermudagrass is the most resistant followed by St. Augustinegrass, Zoysiagrass, and Bahiagrass.
 10. The highest measured critical velocity of grass detachment in the EFA was 6.02 m/s for St Augustinegrass while the lowest measured critical velocity was 1.48 m/s (a case of dry brown Bermudagrass likely in a dormant state).
 11. For some grass, minor erosion corresponding to “cleaning” the grass mat from blades takes place at low velocity such as 0.4 m/s (BR1, BR5, B3, B4, Z1 and Z2).

However, for some grass (all St. Augustinegrass, Z3, BR6), erosion initiates only at 2.5 m/s.

12. For some grass, failure in the form of partial grass mat detachment, begins at low velocity (for example 1.48 m/s for BR5). However, for most grass samples, failure occurs at 4 m/s and higher. This is similar to the findings of Seijffert and Verheij (1985) who claimed that grass can resist up to a velocity of 2 m/s.

13. The erosion function of grass exhibits two thresholds. The first one corresponds to “cleaning” the grass of loose particles and dead blades of grass while the second corresponds to detachment of the grass mat. Between the first and second thresholds the erosion rate is usually small and constant.

14. The erosion function of the grass shows relatively low erosion rates until the detachment critical velocity is reached at which point the erosion rate increases rapidly (brittle behavior). This is quite different from typical soil erosion where the erosion rate increases gradually with the velocity (ductile behavior). This means that less time will be available between failure of the grass cover and drastic erosion than in the case of soil alone.

15. The advantages of grass as a countermeasure for erosion are
- a. Natural product which is environmentally friendly
 - b. Esthetically pleasing which increases property value
 - c. Reasonably economical
 - d. Low maintenance depending on the type except for mowing
 - e. Higher critical velocity than soil

f. Roots reinforce the soil

16. The limitations of using grass as a countermeasure are

a. Sensitive to seasons, rainfall and climate in general

b. Critical velocity is not sufficient for extreme events

c. It takes time to be established

17. The critical velocity of grass obtained in the EFA (2020) compared well with the few full-scale tests by Thornton et al. at Colorado State University (CSU) for USACE Jacksonville District in 2014; they also compared well with the results obtained by Van der Meer (2007) et al. in the Netherlands full-scale tests and with the results of a full-scale test performed by Thornton et al. at CSU for USACE New Orleans District in 2010.

18. The average shear stress corresponding to the grass mat failure observed in the EFA ($\tau_f = 230$ Pa) is much smaller than the average total cohesion of grass reinforcement soil ($c = 11000$ Pa) obtained by Armstrong in 2016 by running a direct shear test.

19. The EFA provides a much less expensive way to check how erosion resistant the grass will be for a given application. For example, a full-scale test may cost \$35,000 or more and an EFA test costs \$1500.

It is the recommendation of this study that grass is a successful product to control erosion in terms of its erosion performance and cost.

12.3. Mitigation of Erosion Using Enzymes

1. The summary erosion chart on Figure 257 and Figure 258 indicates that mixing the soil with enzymes moved the soil erodibility from Category II to Category III (Medium Erodibility).

2. The effectiveness of enzyme treatment depends significantly on the soil type and soil components. A reconstituted clayey sand (SC), a reconstituted silty sand (SM) and a natural silty and clayey sand (SM-SC) all treated with the same percentage of enzymes showed different erodibility and different degrees of erodibility improvement. The reconstituted soils are less erodible than the natural soil. The artificial soils are made of mineral particles with no organic matter. Meanwhile, the natural soil likely contains organic matter. Moreover, the presence of 19% silt particles in the natural soil and their absence in the artificially reconstituted soil could also have an impact on the soil erodibility. The soil mineralogy of the reconstituted and natural soils is also different and can be considered as a potential factor effecting soil erodibility.

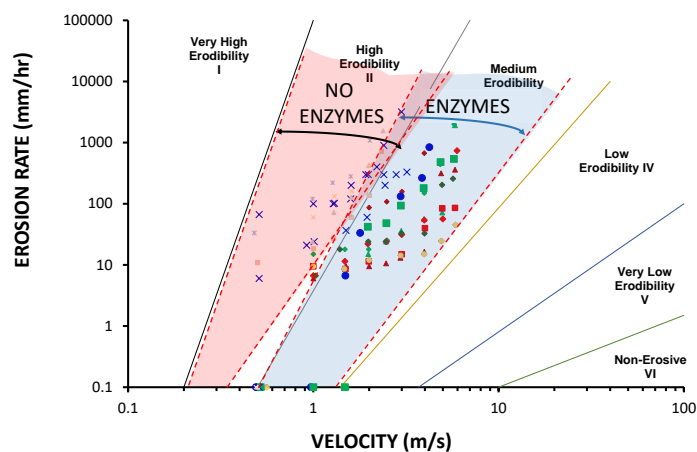


Figure 257. Summary of erosion rate versus velocity in logarithmic scale of enzyme-treated soil

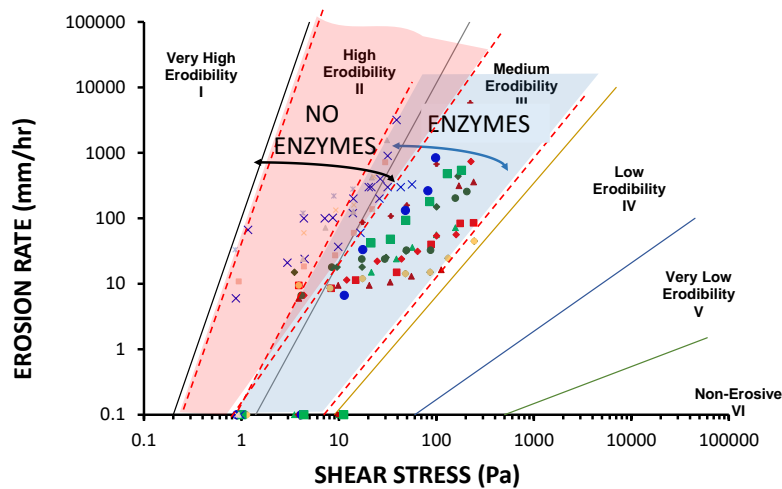


Figure 258. Summary of erosion rate versus shear stress in logarithmic scale of enzyme-treated soil

3. Both enzymes, PermaZyme and TerraZyme showed an improvement in the erosion resistance of reconstituted soils with 15 to 20 % of kaolinite clay particles.

4. The highest measured critical velocity of enzyme treated soil in the EFA was 2 m/s while the lowest measured critical velocity was 0.5 m/s.

5. The current study identified a suitable soil mixing ratio based on the optimum combination of clay and sand particles and water content that lead to less erosion compared to other soil mixtures. The least erosion for the kaolinite mixture was obtained for 15 % kaolinite clay particles, 50 % finer sand particles and 35 % coarser sand particles treated with TerraZyme and PermaZyme for 7, 14, 21, and 28 days.

6. Permazyme is a time-related enzyme; it showed an increase in critical velocity and critical shear stress during a cure time (7-14-21 days) for both reconstituted and natural soils.

7. TerraZyme-treated reconstituted soil exhibits no change in erodibility with an increase in cure time from 7 to 28 days. Meanwhile, TerraZyme-treated natural soil shows erosion improvement in time.

8. The soil reconstituted with 15% bentonite clay particles was more erosion resistant than the soil reconstituted with kaolinite particles; the erosion function for that bentonite sample is close to the same erosion category as the enzyme-treated soil with kaolinite.

9. The kaolinite reconstituted soil lost cohesion and erosion resistance when submerged in water for 7 hours. Applications should therefore be restricted to ephemeral flow conditions.

10. Linear erosion functions linking erosion rate to velocity or shear stress typically occur when the erosion is in terms of individual particle detachment. However, erosion by clusters of particles leads to nonlinear erosion functions.

11. The shape of the erosion functions, in many cases, show the importance of using the entire erosion curve rather than just the critical velocity, or the critical shear stress, and a linear erosion function. The entire erosion curve obtained from the erosion test allows the engineer to capture the erosion resistance of the material at different velocities and shear stresses with more precision and without bias.

12. An increase in the amount of clay particles from 10% to 20% reduces the soil critical velocity by a factor of two to three and moves the erosion function from high to medium erodibility on the erosion chart. Therefore, at least 20% of clay particles is recommended to beneficially decrease soil erodibility by using enzymes.

13. In some cases, for example Experiment cluster 7, one type of enzyme showed less erosion than another type of enzyme for the same soil and the same enzyme concentration.

14. Erosion testing of more combinations of soils and enzymes to encompass a wider range of materials and validating the laboratory results with field performance is recommended. The study has shown that enzymes are soil specific; their effect depends on many factors; therefore, laboratory and field erosion study should be performed prior to using enzymes at the site.

12.4. Mitigation of Erosion Using Lime

The results of the EFA tests show that the erodibility of lime-treated soil varies from the high erosion category to the low erosion category but is mostly located in the medium erosion category (Figure 259 and Figure 260). This study indicates that the magnitude of the improvement brought about by lime on the erosion resistance of a soil seems to be soil specific and depends not only on the soil type but also on the soil composition, presumably soil mineralogy, and the soil nature (artificially reconstituted or natural soil). The highest critical velocity of lime treated soil is 4 m/s while the lowest critical velocity is 0.5 m/s. Therefore, it is recommended that, if lime is to be used on a project to improve the soil resistance to erosion, preliminary tests on the soil samples be conducted in the laboratory to optimize the solution and evaluate the mixing process.

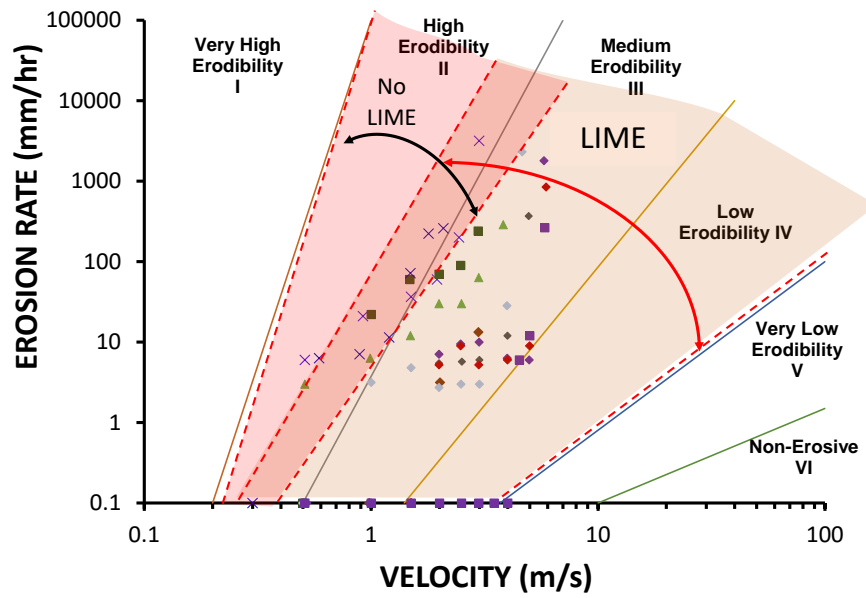


Figure 259. Summary of erosion rate versus velocity of the lime-treated soil

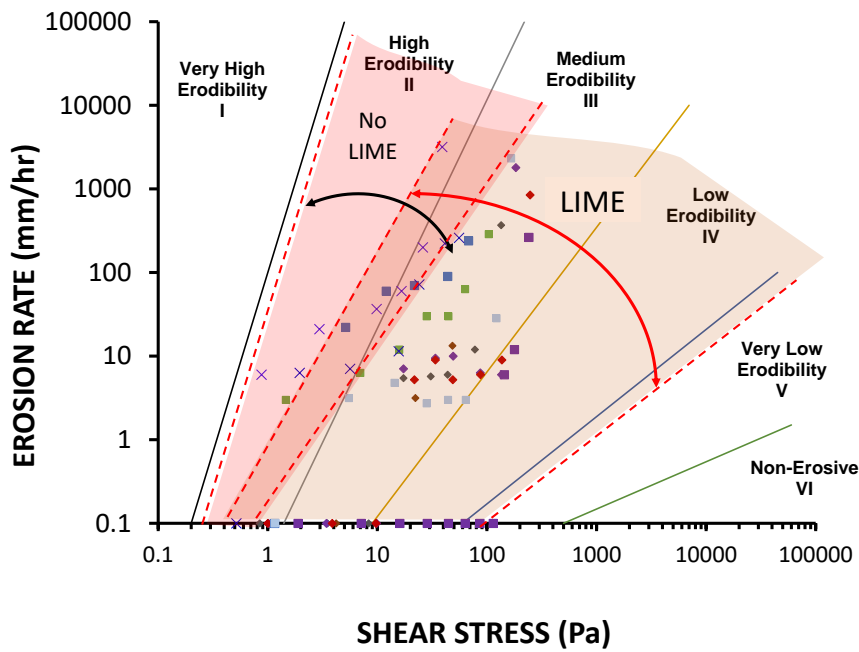


Figure 260. Summary of erosion rate versus shear stress of the lime-treated soil

12.5. Mitigation of Erosion Using Riprap

The following conclusion and recommendations on the use of gravel/riprap for erosion control are based on visual observations and data collected from EFA testing. Large gravel particles with $D_{50} = 30\text{mm}$ were used to represent riprap in the EFA; they were placed on the top of a sand or a clay layer with and without a geotextile filter.

1. Riprap can be beneficially used for erosion control. In the simulated EFA tests, the large gravel/riprap with a filter moves soil erodibility to medium, low, and very low erodibility. The gravel/riprap without a filter is in medium erodibility (Figure 261 and Figure 262).

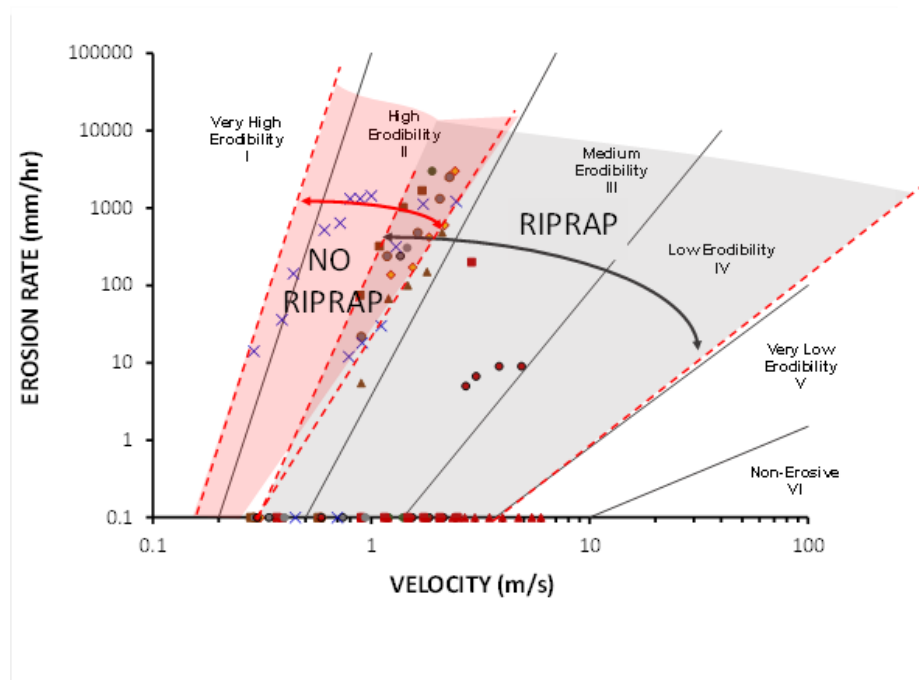


Figure 261. Summary of erosion rate versus velocity of riprap

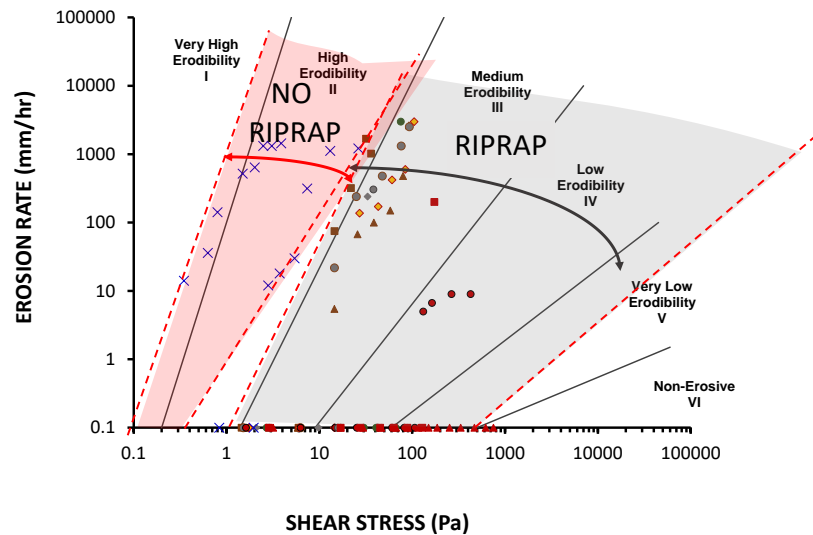


Figure 262. Summary of erosion rate versus shear stress of riprap

2. The effect of riprap, represented by a 30 mm diameter gravel, with no filter and with a geotextile filter on soil erosion was successfully studied and measured in the EFA under a wide range of velocity. The range of velocity varied from $v = 0.29$ m/s to $v = 6.5$ m/s.

3. One layer of gravel/riprap placed directly on top of sand does not prevent the erosion of the sand which is entrained through the voids in the gravel/riprap. The critical velocity of the sand under the gavel/riprap placed over it varies from $v_{cs} = 0.57$ m/s to $v_{cs} = 0.59$ m/s. The critical velocity of the sand without the gravel/riprap is $v_{cs} = 0.29$ m/s.

4. Increasing the thickness of the gravel/riprap to two or three layers slows down the erosion of the sand below the gravel/riprap but does not prevent it. The critical

velocity of the sand below three layers of gravel/riprap increases by up to 50% ($v_{cs} = 0.9$ m/s) compared to the case of one and two layers of gravel/riprap ($v_{cs} = 0.57 - 0.59$ m/s).

5. One layer of gravel/riprap placed directly on top of low plasticity clay does not prevent the erosion of the clay which is entrained through the voids in the gravel/riprap. Slight erosion of clay with the gravel/riprap on top occurs at $v_{cc} = 0.9$ m/s; erosion of the clay with no gravel/riprap is initiated at $v_{cc} = 0.7$ m/s.

6. The highest measured critical velocity of riprap in the EFA was 4.88 m/s for the case when the geotextile filter was used while the lowest measured critical velocity was 0.74 m/s (a case of riprap in a loose state).

7. Significant enhancement of the erosion resistance over the natural soil under a layer of gravel/riprap can only be achieved with a geotextile filter between the two. Placing a geotextile filter between the gravel/riprap and the sand increased the critical velocity of the system to $v_{cs} = 1.19$ m/s which is 4 times the critical velocity of sand by itself.

8. The arrangement of the gravel/riprap can have a significant influence on the critical velocity of the gravel/riprap. Indeed, a loose arrangement gave a critical velocity which was 4 times lower than the “wedged” arrangement. The critical velocity of the gravel/riprap with a “wedged” arrangement is $v_{cr} = 4.88$ m/s compared to a critical velocity $v_{cr} = 1.15$ m/s for the loose gravel/riprap arrangement. The critical velocity of the gravel/riprap based on full-scale field testing done by others is 1.5 m/s for a loose arrangement.

9. When the gravel/riprap is surrounded by a rigid wall (EFA steel tube), the critical velocity is high ($v_{cr} = 4.8$ m/s) and enclosing gravel/riprap inside a sheet pile wall may be a solution worth further consideration. It should be noted that the sheet pile can create a larger obstacle leading to a deeper scour hole.

10. Once the gravel/riprap gets detached, the geotextile filter fails due to uplift. This happens because the geotextile is not anchored in the soil below. In some cases, the geotextile filter remains in place until the last stone of the gravel/riprap gets detached up to a velocity of $v_{cr} = 4.88$ m/s. Even one gravel/stone can delay failure of the filter.

11. The geotextile filter appears to fail because of a combination of different factors such as inflow into the zone between the filter and the underlying soil and possible limitation of pressure relief through the geotextile layer.

12. It is concluded that a geotextile filter is needed as it prevents erosion of the natural soil below and gives full potential to the riprap.

12.6. Comparison between soil improvement methods

The comparison between soil improvement methods used in this study and their efficiency is presented below and based on three components: effectiveness, cost, and environmental impact. Each component is ranked from 1 to 3 meaning that 1 is a low grade, 2 is a moderate grade, and 3 is a high grade. The grade for effectiveness is based on the highest value of the critical velocity of the treated soil obtained in the EFA. The critical velocity of the treated soil varying from 0 – 2 m/s gives a grade of 1; the range of the critical velocity from 2 m/s to 4 m/s gives a grade of 2; and the range of the critical

velocity from 4 m/s to 6 m/s gives a grade of 3. The grade for cost is based on the cost of 1 m² of treated soil including installation cost. A cost from 0 to 30 \$/m² gives a grade of 3, a cost of 30 to 60 \$/m² gives a grade of 2 and a cost larger than 60 \$/m² gives a grade of 1. The grade for environment is more qualitative and based on the existing knowledge of how environmentally friendly the improving agent is. The impact factor of each improvement method is calculated as multiplication of those three components and gives a final grade shown in Table 56. The highest value of then impact factor is most desirable.

Table 56. Efficiency of soil improvement methods (based on three components)

Method	Impact Factor	Effectiveness	Cost	Environmental Impact
Grass	27	3	3	3
Enzymes	7.5	1	3	2.5
Riprap	7.5	3	1	2.5
Lime	6	2	3	1

1. **Improvement with grass.** Grass is found mostly in Category III (Medium Erodibility). The highest critical velocity of grass detachment is 6.02 m/s, therefore the grade for the effectiveness is 3. The cost of grass (Bermudagrass) is about of \$7-8 per 1 m² (Texas and California) (remodelingexpense.com) without installation. With an estimated cost of installation equal to \$15 per m², the total cost would be \$22 – \$23 per m². Therefore, the grade for cost is 3. The environment component has gotten the highest grade which is 3 as grass is environmentally friendly.

2. **Improvement with enzymes.** Enzyme has demonstrated that soil erodibility can be moved to Category III, which is Medium erodibility. However, the highest critical velocity in the EFA is 2 m/s which gives a grade of 1. The cost of

enzyme is about \$1.6 per 1 m² without installation. Adding an estimate of \$20 per m² for installation gives \$21.6 per m² in place. Therefore, the grade for cost is 3. Enzyme is environmentally friendly but not that friendly as grass which gives a grade of 2.5.

3. **Improvement with lime.** Lime has shown an ambiguous result in erosion control of soil; erodibility category varies from high to low. The highest critical velocity of lime treated soil in the EFA is 4 m/s, therefore the grade for effectiveness is estimated as 2. The cost of lime was estimated from the website stgec.org (Larry Cole, P.E. Carmeuse Lime and Stone Pittsburgh, PA) as \$3 per 1 m². Adding an estimate of \$20 per m² for installation gives \$23 \$ per m² in place. Therefore, the grade for cost is 3. Lime is not environmentally friendly that gives it a grade of 1 for the environment component.

4. **Improvement with riprap.** Riprap has indicated a wide scatter in erodibility, however the highest critical velocity is 4.88 m/s, therefore it gets a grade of 3 for effectiveness. The cost of riprap varies from \$89 to \$149 per 1 m² with installation which is not cost effective. The grade for cost is 1. The environment component gets a grade of 2.5 because it is not that beneficial as grass.

Table 56 shows the impact factor for all soil improvement methods used in this study. The highest impact factor is obtained for grass (27) followed by enzymes and riprap (7.5) and lime (6). Note that there are some assumptions and conditions used in calculating the impact factor, therefore, it is suggested to use that approach for preliminary estimates of the efficiency of soil improvement methods. It is recommended that erosion testing be performed on a site-specific basis of improved soil with a chosen agent.

12.7. Advantages and limitations of soil improvement for erosion mitigation

The advantages and limitations of each soil improvement method are shown in

Table 57.

Table 57. Advantages and limitations of soil improvement methods

Agent	Advantages	Limitations
Grass	<ol style="list-style-type: none"> 1. Environmentally friendly. 2. A variety of grass types to be used for levees and dams depending on the site and climate condition. 3. Erosion resistant up to high velocity (6.5 m/s). 	<ol style="list-style-type: none"> 1. Fast rate of erosion after grass failure (drastic erosion of subsoil). 2. Can go to a dormant state which reduces erosion resistance. 3. Can get sick (diseases). 4. Take time to get established
Enzymes	<ol style="list-style-type: none"> 1. Relatively wide application (roads, dams, levees, foundations). 2. Can be used in a variety of soils. 3. Environmentally friendly and biodegradable. 4. Higher dry density can be achieved with less compaction effort. 5. Improvement in erosion performance. 6. Cost effective; reduces construction cost. 7. Easy application. 	<ol style="list-style-type: none"> 1. Very soil specific. 2. Site condition specific. 3. Requires good mixture. 4. Wide range of improved soil properties including erosion functions and parameters. 5. In some cases, enzymes show ambiguous results or limited improvement. 6. Mixing well is important.
Lime	<ol style="list-style-type: none"> 1. Can increase erosion resistance and improve geotechnical properties of soil significantly. 2. Cost effective. 	<ol style="list-style-type: none"> 1. Limited application. 2. Limited by soil type. 3. Not environmentally friendly and not degradable. 4. slow acting (requires more than 28 days to cure). 5. Mixing well is important. 6. Not resistant to soaking for a long period of time.

Agent	Advantages	Limitations
Riprap	<ol style="list-style-type: none"> 1. Can be beneficially used for erosion control. 2. Environmentally friendly. 3. Easy to install. 	<ol style="list-style-type: none"> 1. Filter is needed to reduce soil erodibility. 2. Increase in riprap thickness does not reduce soil erosion. 3. Relatively expensive

12.8. New Erosion Model and Applications

Chapter 8 focused on the development of a new power law erosion model and its application. The new erosion model is:

$$\frac{\dot{z} \text{ (mm/hr)}}{0.1 \text{ mm/hr}} = \left(\frac{\tau}{\tau_c}\right)^\alpha \quad (92)$$

$$\frac{\dot{z} \text{ (mm/hr)}}{0.1 \text{ mm/hr}} = \left(\frac{v}{v_c}\right)^\beta \quad (93)$$

where \dot{z} is the erosion rate (mm/hr), 0.1 mm/hr is the erosion rate at which erosion is negligible, τ is the shear stress (Pa), τ_c is the critical shear stress (Pa), v is the velocity (m/s), v_c is the critical velocity (m/s), α and β are the slopes of the power law model in log-log coordinates.

The following conclusions can be proposed.

1. Classification according to the critical shear stress is separated from the classification according to the erosion modulus.
2. In the new erosion chart, critical velocity and critical shear stress corresponding to the initiation of erosion (soil detachment) are used which allows to trace erosion behavior of natural and improved soil, grass, and riprap above the critical point.

3. The erosion moduli obtained from the normalized erosion rate vs normalized shear stress or the normalized erosion rate vs normalized velocity log plots show erosion of natural or improved soil after the initiation of erosion.
4. It is proposed to classify a soil based on its critical shear stress τ_c and erosion modulus α . For example, and based on EFA testing, typically sand would have a low τ_c but a high α ; grass usually has a high τ_c but the erosion modulus can vary significantly.
5. The erosion modulus can be used to predict an erosion movement for levees and dams (See Section 12.9).

12.9. TAMU-Prediction of Erosion Movement (TAMU-PEM)

Chapter 9 described a procedure called TAMU-Prediction of Erosion Movement (TAMU-PEM) and automated in an excel spreadsheet developed as part of this research. The velocity hydrograph and the erosion function are used as input and the erosion movement as a function of time is the output. Prediction of erosion movement using TAMU-PEM were performed for sand, clay, silt, Bermudagrass, enzyme- and lime-treated soils as examples. A comparison between erosion movement for natural and improved soil was completed. The erosion movement obtained by running TAMU-PEM was calibrated with a field measurement on a Sacramento levee assuming heavily vegetation.

12.10. Improvement of TAMU-Erosion Database

Chapter 10 is dedicated to the description, updating, and improvement of the erosion spreadsheet developed by Briaud et al. (2019) and called TAMU-Erosion. The updating of the database consisted of uploading the 250 new tests performed in this study along with the corresponding geotechnical properties of the soil tested. TAMU-Erosion now has 1,250 documented erosion tests. The erosion properties include the erosion function, critical shear stress, critical velocity, initial slope of erosion rate vs velocity, initial slope of erosion rate vs shear stress, erosion category, and erosion modulus in the normalized log plots.

12.11. Risk Management for Erosion of Dams and Levees

The following conclusions refer to the work presented in Chapter 11.

1. Risk-informed decisions can be made based on the risk chart. On the proposed risk chart, the position of earth dams, tailing dams, levees, and Harvey are located. Figure 250 and Figure 251 show the summary risk charts for this category of structures.
2. A methodology to evaluate the erodibility of dams and levees is proposed by using the erosion categories on the erosion chart. A step-by-step procedure is described.
3. On the risk chart, risk can be reduced for levees and dams by
 - a. lowering the probability of failure (P_f), by considering a higher return period for the design flood for example.

- b. lowering the consequence in terms of fatalities by requesting early evacuation
- c. lowering the consequence in terms of cost.
- 4. For tailing dams, risk can be reduced by
 - a. abandoning the construction of the most dangerous types of tailing dam's construction called upstream dams. For example, the state of Minas Gerais, Brazil banned upstream tailings dams. Chile banned such dams in 1970.
 - b. develop an international standard for tailings dams and levees to be followed by the owners of these facilities.

12.12. Summary of contributions to new knowledge

The following is a summary of the perceived contributions to new knowledge in this doctoral research work. It is organized according to the set of objectives for the research.

OBJECTIVE I: Borehole Erosion Test.

1. Development of a detailed testing procedure for the BET which did not exist.
2. Development of a detailed data reduction procedure and a spread sheet for the BET including the missing shear stress aspect of the procedure.
3. Proposal of the shear-based equation for the BET data reduction.
4. Evaluation of the BET precision, advantages and drawbacks compared to other erosion tests (EFA) (mean, standard errors).
5. Extension of the Moody chart to very rough surfaces (relative roughness

$\varepsilon/D > 0.05$).

OBJECTIVE II: Soil Improvement.

1. Performance of EFA testing on grass, riprap, enzyme-treated and lime-treated soil to compare the results of the tests before and after treatment.
2. Obtaining erosion function and parameters from EFA testing such as critical velocity, critical shear stress, velocity-based erosion modulus, shear stress-based erosion modulus.
3. Evaluating the efficiency of erosion treatment for soils based on the EFA results.
4. Comparison, to the extent possible, of each soil improvement method between laboratory testing in the EFA with large scale field testing or field performance as published in the open literature of each soil improvement method.
5. Development of recommendations for using soil improvement methods for levees and dams depending on the purpose of usage, soil type, and site conditions (intensity of flood etc.).

OBJECTIVE III: New Erosion Model and Classification.

1. Proposal of a new power law model to improve on the current model shortcomings (for velocity and shear stress) and satisfy the non-linearity of the erosion functions.
2. Obtaining the relationship between erosion modulus and critical shear stress/critical velocity needed to strengthen the new model.
3. Preparation of new erosion classification charts consistent with the new

erosion model including a shear stress-based chart and a velocity-based chart.

4. Application of the new erosion model for different types of soil, improved soil, and materials.

5. Solution for some practical erosion problems as examples of the application of the new erosion function model (e.g., levee overtopping problem) by hand calculation or simple spread sheet.

OBJECTIVE IV: Prediction of Erosion Movement.

1. Development of the automated Excel Spread Sheet for obtaining the erosion movement and application to several examples.

2. Calibration of the results by comparing the prediction with a field performance considering the lab/field scale factor.

OBJECTIVE V: TAMU-Erosion Database.

1. Updating and improvement of the TAMU-Erosion spread sheet by increasing the number of tests in the spread sheet by more than 250 tests performed in the Texas A&M Erosion Laboratory from 2018 to 2021 including improved soils and grass.

OBJECTIVE VI: Risk Framework.

1. Identification of the risk associated with soil erosion of dams and levees and present the associated risk ellipses on the risk chart.

2. Developing a methodology to evaluate the erodibility of dams and levees by using the erosion categories.

REFERENCES

1. Abt, S.R. and T.L. Johnson, 1991. Riprap Design for Overtopping Flow. *Journal Hydraulic Engineering* 117(8): 959- 972, doi:
[http://dx.doi.org/10.1061/\(ASCE\)0733-9429\(1991\)117:8\(959\)](http://dx.doi.org/10.1061/(ASCE)0733-9429(1991)117:8(959)).
2. Abt, S.R., M.S. Khattak, J.D. Nelson, J.F. Ruff, A. Shaikh, R.J. Wittler, D.W. Lee, and N.E. Hinkle, 1987. Development of Riprap Design Criteria by Riprap Testing in Flumes: Phase 1. U.S. Nuclear Regulatory Commission Report NUREG/CR-4651, May, 109 pp., Washington, D.C.
3. Al-Madhhachi, A.T., Hanson, G.J., Fox, G.A., Tyagi, A.K., Bulut, R. 2013. Measuring soil erodibility using a laboratory mini jet. *American Society of Agricultural and Biological Engineers*. Vol. 56(3), pp. 901-910.
4. Almajed, A., Tirkolaei, H. K., Kavazanjian, E., & gi, N. 2019. Enzyme Induced Biocementated Sand with High Strength at Low Carbonate Content. *Scientific reports*, 9(1), [1135]. <https://doi.org/10.1038/s41598-018-38361-1>.
5. Almajed, A.A. 2017. Enzyme Induced Carbonate Precipitation (EICP) for Soil Improvement. Doctoral Dissertation. Arizona State University.
6. American Society of Civil Engineers (ASCE). 2017 Infrastructure Report Card. <https://www.infrastructurereportcard.org/> Accessed in 2020-2021.
7. American Society of Civil Engineers (ASCE). 2021 Infrastructure Report Card. <https://www.infrastructurereportcard.org/> Accessed in 2021.
8. Application of Enzyme Induced Carbonate Precipitation (EICP) for Channel Lining and Repair, Low Volume Road Stabilization, Embankment Construction, and

- Erosion Control. USBR. Research and Development Office Science and Technology Program (Final Report) ST-2019-1840-01. Principal Investigator: Angel Gutierrez et al. Research Topic: Repair and Maintenance. 2019.
9. Armstrong B. 2016. Acoustic Behavior of Soil Reinforced with Grass Roots. Thesis of master's degree. University of Mississippi.
 10. Arulanandan, K. and Perry, E.B. 1983. Erosion in relation to filter design criteria in earth dams. Journal of the Geotechnical Engineering Division, ASCE. 109(GT5), pp. 682-698.
 11. Arulanandan. K, Gillogly, E., Tully, R. 1980. Development of a quantitative method to predict critical shear stress and rate of erosion of natural undisturbed cohesive soils (Technical Rep. GL-805) US Army of Engineers' Waterway Experiment Station, Vicksburg, Mississippi (1980).
 12. ASCE 2021. Report Card for America's Infrastructure. Levees | ASCE's 2021 Infrastructure Report Card.
 13. Association of State Dam Safety Officials (ASDSO). 2020. <<https://damsafety.org/>>
 14. Association of State Dam Safety Officials (ASDSO). 2020. Lessons Learned from Dam Incidents and Failures. <<https://damfailures.org/lessons-learned/>>
 15. ASTM D5852. 2007. Standard test method for erodibility determination of soil in the field or in the laboratory by the jet index method (withdrawn 2016). ASTM International, West Conshohocken, PA, 2007.
 16. ASTM Standard D1587/D1587M – 15. Standard Practice for Thin-Walled Tube Sampling of Fine-Grained Soils for Geotechnical Purposes.

17. ASTM Standard WK67195, 2019, "New Test Method for Measuring the Erosion Function of a Soil," ASTM International, Ballot D18.06(21-02), In Balloting, www.astm.org.
18. Baecher, G., and Christian J. 2003. Reliability and statistics in geotechnical engineering, John Willey & Sons, United Kingdom.
19. Bennadi, A., Herrier, G., Lesueur, D. 2016. Lime treated soil erodibility investigated by EFA erosion testing. Conference Paper · September 2016. DOI: 10.1201/9781315375045-67.
20. Bergendahl and Kerenyi. 2016. In-situ Scour Testing Device. Patent N0. US 9,322,142 B2. 2016. The U.S. Federal Highway Administration (FHWA).
21. Blake, E. S., and D. A. Zelinsky, 2018: National Hurricane Center tropical cyclone report: Hurricane Harvey (AL092017). NOAA/NWS, 77 pp., www.nhc.noaa.gov/data/tcr/AL092017_Harvey.pdf.
22. Bloomquist, D., Sheppard, D., Schofield, S., Crowley, R. 2012. "The Rotating Erosion Testing Apparatus (RETA): A Laboratory Device for Measuring Erosion Rates versus Shear Stresses of Rock and Cohesive Materials," Geotechnical Testing Journal 35, no. 4 (2012): 641-648. <https://doi.org/10.1520/GTJ104221>.
23. Briaud J.-L., 2013, "Geotechnical Engineering: Unsaturated and Saturated Soils", John Wiley and Sons, New York, 1000 pages.
24. Briaud J.-L., Chedid M., Chen H.C., Shidlovskaya A. 2017. The Borehole Erosion Test, Journal of Geotechnical and Geoenvironmental Engineering, ASCE, Reston, Virginia, USA, Vol 143 Issue 8.

25. Briaud J.-L., Chedid M., Shidlovskaya A. 2016. “The Borehole Erosion Test”, Proceedings of the 8th International Conference on Scour and Erosion (Oxford, UK, 12-15 September 2016), Eds. John Harris, Richard Whitehouse, Sarah Moxon, CRC Press, Taylor and Francis.
26. Briaud J.L., Chen, H.C., Govindasamy, A.V., Storesund, R. 2008. Levee Erosion by Overtopping in New Orleans during the Katrina Hurricane. *Journal of Geotechnical and Geoenvironmental Engineering*, 134(5): 618-632.
27. Briaud J.-L., Shafii I., Chen H.C., Medina-Cetina Z., 2019, “Relationship Between Erodibility and Properties of Soils”, NCHRP Research Report 915, The National Academies Press. <https://doi.org/10.17226/25470>, National Cooperative Highway Research Program; Transportation Research Board; National Academies of Sciences, Engineering, and Medicine.
28. Briaud J.-L., Ting F., Chen H.C., Cao Y., Han S.-W., Kwak K., 2001, “Erosion Function Apparatus for Scour Rate Predictions”, *Journal of Geotechnical and Geoenvironmental Engineering*, Vol. 127, No.2, pp. 105-113, Feb. 2001, ASCE, Reston, Virginia.
29. Briaud, J. L. 2008. Case histories in soil and rock erosion: Woodrow Wilson Bridge, Brazos River Meander, Normandy Cliffs, and New Orleans Levees, The 9th Ralph B. Peck Lecture, *Journal of Geotechnical and Geoenvironmental Engineering*, Vol. 134(10), ASCE, Reston Virginia, USA.

30. Briaud, J. L., Bernhardt, M., Leclair, M. 2012. The pocket erodometer test: development and preliminary results. *Geotechnical Testing Journal*, Vol. 35, No. 2, Paper ID GTJ102889.
31. Briaud, J. L., Chen, H. C., Kwak, K., Han, S., Ting, F. 2001. Multiflood and multilayer method for scour rate prediction at bridge piers, *Journal of Geotechnical and Geoenvironmental Engineering*, Vol. 127(2), pp. 114-125, Feb. 2001, ASCE, Reston, Virginia.
32. Briaud, J. L., Ting, F. C. K., Chen, H. C., Gudavalli, R., Perugu, S., Wei, G. 1999. SRICOS: Prediction of scour rate in cohesive soils at bridge piers, *Journal of Geotechnical and Geoenvironmental Engineering*, Vol. 125(4), pp. 237-246, April 1999, ASCE, Reston, Virginia.
33. Briaud, J. L., Ting, F., Chen, H.C., Cao, Y., Han, S.-W., Kwak, K., 2001, Erosion function apparatus for scour rate predictions, *Journal of Geotechnical and Geoenvironmental Engineering*, Vol. 127(2), pp. 105-113, Feb. 2001, ASCE, Reston, Virginia.
34. Briaud, J.L. 2011. Erosion testing of high-performance turf reinforcement mat (HPTRM) levee strengthened samples. Summary Report for Jackson State University Levees (JSU-P2-1).
35. Briaud, J.-L., Gardoni P., Yao C. 2012. Bridge Scour Risk. Proceedings of the Sixth Conference on Scour and Erosion ICSE-6 Paris - August 27-31, 2012.
36. Briaud, J.-L., Gardoni P., Yao C. 2014. Statistical, Risk, and Reliability Analyses of Bridge Scour. *Journal of Geotechnical Engineering* 140(2): 04013011(10).

37. Briaud, J.-L., Montalvo-Bartolomei, A. 2017. Meander migration: the observation method. *Canadian Geotechnical Journal*. 2017.
38. Brice, J.C. 1982. "Stream Channel Stability Assessment," Report No. FHWA/RD-82/021. Federal Highway Administration, Washington, DC, USA, p.41.
39. Brice, J.D. 1983. "Factors in Stability of Relocated Channels," *Journal of Hydraulic Engineering*, ASCE, Vol. 109, No. 10, pp. 1298-1313.
40. Center for science in public participation. Tailing dam failures database from 1915. Downloaded 5 June 2021. <http://www.csp2.org/tsf-failures-from-1915>.
41. Chalmers, D.R. and McAfee, J. Turfgrass selection for Texas. *Ecological Turf Tips*. Agrilife Extension. Texas A&M Agrilife Extension Service. Texas A&M University. Downloaded from <https://cdn-ext.agnet.tamu.edu/wp-content/uploads/2018/10/L5519-turfgrass-selection-for-texas-ecological-turf-tips.pdf>.
42. Chang, D.S., Zhang, L.M. 2011. A Stress-controlled Erosion Apparatus for Studying Internal Erosion in Soils *Geotechnical Testing Journal*, Vol. 34, No. 6. pp. 1-12.
43. Chapius, R. P. and Gatien, T. 1986. An improved rotating cylinder technique for quantitative measurements of the scour resistance of clays. *Canadian Geotechnical Journal*. 23. pp 83-87.
44. Charles I., Herrier, G., Chevalier, C., Durand E. 2012. An experimental full-scale hydraulic earthen structure in lime treated soil. ICSE6 Paris.
45. Chedid, M., Shafii, I., Briaud, J. L., 2018. Erosion Tests on the Teton Dam Soils. The 9th International Conference on Scour and Erosion, Taipei, Taiwan.

46. Chek, A., Crowley, R., Ellis, T.E., Durnin, M., Wingender, B. 2021. Evaluation of Factors Affecting Erodibility Improvement for MICP-Treated Beach Sand. *Journal of Geotechnical and Geoenvironmental Engineering*. Vol. 147, Issue 3 (March 2021) [https://doi.org/10.1061/\(ASCE\)GT.1943-5606.0002481](https://doi.org/10.1061/(ASCE)GT.1943-5606.0002481)
47. Chen, Y.H., Cotton, G.K., 1988. Design of roadside channels with flexible linings. US Department of Transport. Report No. FHWA-IP-87-7.
48. Crystal, C. and Smith, M. 2016. Risk management and decision making as related to mill tailings disposal. *Proceedings of Risk and Resilience Mining Solutions, 2016* November 14-16, 2016, Vancouver, Published by InfoMine, @ 2016 InfoMine, ISBN, 978-1-9881-85-00-2.
49. Davies, M. P. 2002. Tailings impoundment failures: are geotechnical engineers listening? *Geotechnical News*. September: 31–36.
50. Dean, R.G., Rosati, J.D., Walton, T.L., Edge, B.L. 2010. Erosional equivalences of levees: Steady and intermittent wave overtopping. *Ocean Engineering*. Volume 37, Issue 1, January 2010, Pages 104-113. <https://doi.org/10.1016/j.oceaneng.2009.07.016>.
51. DeJong, J.T., Fritzsche, M.B. and Nusslein, K. 2006. Microbial induced cementation to control sand response to undrained shear. *ASCE J Geotech Geoenviron. Eng* 132, 1381– 1392.
52. DeJong, J.T., Martinez, B.C., Mortensen, B.M., Nelson, D.C., Waller, J.T., Weil, M.H., Ginn, T.R., Weathers, T. et al. 2009. Upscaling of bio-mediated soil

- improvement. Proceedings of the 17th International Conference on Soil Mechanics and Geotechnical Engineering, Alexandria, Egypt.
53. DeJong, J.T., Mortensen, B.M., Martinez, B.C. and Nelson, D.C. 2010. Bio-mediated soil improvement. *Ecol Eng* 36, 197– 210.
54. DeJong, J.T., Soga, K., Banwart, S.A., Whalley, W.R., Ginn, T., Nelson, D.C., Mortensen, B.M., Martinez, B.C. et al. 2011. Soil engineering in-vivo: harnessing natural biogeochemical systems for sustainable, multi-functional engineering solutions. *J R Soc Interface* 8, 1– 15.
55. Dr J.W. van der Meer. 2007. Design, construction, calibration and use of the wave overtopping simulator. Version: v3.3. For CUR on behalf of ComCoast and Rijkswaterstaat. Project number: 04i103.
56. Dunn, I. S. 1959. Tractive resistance of cohesive channels. *Journal of Soil Mechanics and Foundations Division, ASCE*, pp. 1–24.
57. Eli, R.N., Gray, D.D. 2008. Hydraulic Performance of a Steep Single Layer Riprap Drainage Channel. *Journal of Hydraulic Engineering*. Volume 134. Issue 11.
58. [Europe and China with most cases of dam failure in mining sites after 2000 \(911metallurgist.com\)](#)
59. Fell R., Fry J.J. 2007. *Internal Erosion of Dams and their Foundations*. Taylor and Francis Group, London, UK.
60. FHWA Hydraulic Engineering Circular 23 (HEC-23) – Bridge Scour and Stream Instability Countermeasures: Experience, Selection, and Design Guidance (<https://www.fhwa.dot.gov/engineering/hydraulics/pubs/09111/09112.pdf>)

61. Fleming, R.; Sills, G.; Stewart, E.: Lime Stabilization of Levee Slopes. 1992. In: Proceedings of the second interagency symposium on stabilization of soils and other materials, LA, pp. 5-15 to 5-22.
62. Frizell, K.H., J.F. Ruff, and S, Mishra. 1997. "New riprap design criteria to prevent embankment dam failure during overtopping." Proc. ASDSO Dam Safety '97, Pittsburg, PA. September 8, 1997.
63. Frizell, K.H., Ruff, J.F., Mishra, S. 1998. Simplified design guidelines for riprap subjected to overtopping flow. pp. 301-312
64. Gabr, M., Caruso, C., Key, A., Kayser, M. 2013. Assessment of in situ scour profile in sand using a jet probe. Geotechnical Testing Journal, Vol. 36(2).
65. Gao, Y.F., Hang, L., He, J., Chu, J. 2018. Mechanical behavior of biocemented sands at various treatment levels and relative densities. Acta Geotech.
66. Gao, Y.F., Tang, X.Y., Chu, J., He, J. 2018. Microbial induced calcite precipitation for seepage control in sandy soil. Geomicrobiol. J.
67. Garver, L.L. 1987. Canal Repair Techniques Using Lime-Stabilized Soil, Lime for Environmental Uses, ASTM STP931, pp.115-120.
68. Ghebreiyessus, Y. T., Gantzer, C. J., Alberts, E. E., Lentz, R. W. 1994. Soil erosion by concentrated flow: shear stress and bulk density. Transactions of the ASAE. Vol. 37(6), pp. 1791-1797.
69. Gibbs, H. J. 1962. A study of erosion and tractive force characteristics in relation to soil mechanics properties. US Department of the Interior, Bureau of Reclamation, Division of Engineering Laboratories, Soils Engineering Report No. EM-643.

70. Gilbert, R.B. 2017. Beyond protecting the public from risk. *The Bridge* 47(1), 30-35
71. Gutschick, K.A. 1978. Lime stabilization under hydraulic conditions. 4th lime congress Hershey (PA). 1–20.
72. Gutschick, K.A. 1985. Canal lining stabilization proves successful., *Pit & Quarry*: 58–60.
73. Haaland, SE. 1983. "Simple and Explicit Formulas for the Friction Factor in Turbulent Flow". *Journal of Fluids Engineering*. 105 (1): 89–90.
doi:10.1115/1.3240948.
74. Ham, S., Kwon, T., Chang, I., Chung, M. 2016. Ultrasonic P-Wave Reflection Monitoring of Soil Erosion for Erosion Function Apparatus, *Geotechnical Testing Journal* 39, no. 2 (2016): 301-314. <https://doi.org/10.1520/GTJ20150040>.
75. Ham, S-M., Chang, I., Noh, D.H., Kwon, T-H. 2018. Improvement of Surface Erosion Resistance of Sand by Microbial Biopolymer Formation. *Journal of Geotechnical and Geoenvironmental Engineering*. Volume 144 Issue 7 - July 2018.
76. Ham, S-M., Chang, I., Noh, D.-H., Kwon, T-H., Muhunthan, B. Improvement of Surface Erosion Resistance of Sand by Microbial Biopolymer Formation *J. Geotech. Geoenviron. Eng.*, 2018, 144(7): 06018004.
77. Hamdan, N. 2015. Applications of Enzyme Induced Carbonate Precipitation (EICP) for Soil Improvement. PhD thesis, Arizona State University, Tempe, Arizona.
78. Handbook of Channel Design for soil and water conservation. Soil Conservation Center. United States Department of Agriculture. Washington D.C., 1954.

79. Hanson, G. J. 1990. Surface erodibility of earthen channels at high stresses. Part I – Open channel testing. Transactions of the ASAE, Vol. 33, Issue 1, pp. 127-131.
80. Hanson, G. J. 1991. Development of a jet index to characterize erosion resistance of soils in earthen spillways. Trans. ASAE. General Edition, Vol. 34(5), pp. 2015-2020. ISSN 00012351.
81. Hanson, G. J., Cook, K. R. 2004. Apparatus, test procedures, and analytical methods to measure soil erodibility in situ. Applied Engineering in Agriculture. American Society of Agricultural Engineers. ISSN 0883-8542. Vol. 20(4), pp. 455-462.
82. Hanson, G. J., Hunt, S. L. 2007. Lessons learned using laboratory JET method to measure soil erodibility of compacted soils. Applied Engineering in Agriculture. American Society of Agricultural and Biological Engineers ISSN 0883-8542. Vol. 23(3), pp 305-312.
83. Hanson, G. J., Robinson, K. M., Temple, D. M. 1990. Hydraulic Engineering – Proceedings of the 1990 National Conference. pp. 525-530. ISBN 0872627748.
84. Hanson, G. J., Simon, A., Cook, K. R. 2002. Non-vertical jet testing of cohesive streambank materials. ASAE Annual International Meeting / CIGR XVth World Congress. Paper Number: 022119.
85. Hanson, G.J., and Simon, A. 2001. Erodibility of cohesive streambeds in the loess area of the Midwestern USA, Hydrological Processes, Vol. 15(1), pp. 23-38.
86. Harkes, M.P., van Passen, L.A., Booster, J.L., Whiffin, V.S., van Loosdrecht, M.C. 2010. Fixation and distribution of bacterial activity in sand to induce carbonate precipitation for ground reinforcement. Ecol. Eng. 36(2), 112-117.

87. Herrier G., Bonelli S. 2015. Internal erosion resistance of soils treated with lime: An evolutive benefit. Scour and Erosion – Cheng, Draper & An (Eds). Taylor & Francis Group, London, 978-1-138-02732-9. 73-80.
88. Herrier G., Lelong G V., Lesueur D., et al. 2012. Soil treatment for dikes, SOTREDI final report, Lhoist Eds. Limelette, Belgium, pp. 1–103.
89. Herrier G., Lsueur D., Puiatti D., et al. 2012. “Lime treated soils as an erosion-resistant material for hydraulic earthen structures”, 6th International Conference on Scour and Erosion, Paris, France, pp. 97–104, 27–31 August 2012.
90. Hewlett, H.W.M., Boorman, L.A., Bramley, M.E. 1987. Design of reinforced grass waterways; CIRIA Report 116; Construction and Industry Research and Information Association; London, UK.
91. Hoang, T., J. Alleman, B. Cetin, K. Ikuma, and S. G. Choi. 2018. Sandy and Silty-Sand Soil Stabilization using Bacterial Enzyme Induced Calcite Precipitation (BEICP). Canadian Geotechnical Journal.
<http://www.nrcresearchpress.com/doi/abs/10.1139/cgj-20180191#.W9nGE-JOmUk>.
IPCC.
92. Howard, A. K., Bara J. P. 1976. Lime Stabilization on Friant-Kern Canal, U.S. Bureau of Reclamation, Report No. REC-ERC-76-20, Denver, CO, 61 p.
93. <https://www.epa.gov/climate-indicators/climate-change-indicators-coastal-flooding>.
94. <https://www.fema.gov/hazard-mitigation-assistance>.
95. <https://www.history.com/news/hurricane-katrina-levee-failures>
96. <https://www.turfalyzer.com/turf-analyzer>. Accessed 2020.

97. <https://www2.usgs.gov>
98. Hudson, P.F., Kesel, R.H. 2000. Channel migration and meander-bend curvature in the lower Mississippi River prior to major human modification. *Geology* 2000; 28 (6): 531–534. doi: [https://doi.org/10.1130/0091-7613\(2000\)28<531:CMAMCI>2.0.CO;2](https://doi.org/10.1130/0091-7613(2000)28<531:CMAMCI>2.0.CO;2)
99. Huesker. <https://mediacache1.bgflux.com/86/67/3f74-8ca6-477d-bf30-8d28ec6f20a4/soiltain-pp-105-105-dw.pdf>. Assessed June 2021.
100. Hughes, S. A. 2007. Estimation of overtopping flow velocities on earthen levees due to irregular waves. CHETN Technical Notes Collection. ERDC/CHL CHETN-III77. Vicksburg, MS: U.S. Army Engineer Research and Development Center. <http://chl.erd.usace.army.mil/chetn>
101. Hughes, S.A., Thornton, C.I. 2015. Tolerable Time-Varying Overflow on Grass-Covered Slopes. *J. Mar. Sci. Eng.* 2015, 3, 128-145; doi:10.3390/jmse3010128.
102. Ikuma, K. 2018. Use of Biocementation for Slope Stabilization of Levees. Final Report. Iowa State University.
103. Indraratna, B., Muttuvel, T., Khabbaz, H., Armstrong, R. 2008. Predicting the erosion rate of chemically treated soil using a process simulation apparatus for internal crack erosion. *J. Geotech. Geoenviron. Eng.* 134(6), 837-844.
104. Jiang, N-J., Soga, K. 2019. Erosional behavior of gravel-sand mixtures stabilized by microbially induced calcite precipitation (MICP). *Soils and Foundations*. Volume 59, Issue 3, June 2019, pp. 699-709.

105. Kandiah, A., Arulanandan, K. 1974. Hydraulic erosion of cohesive soils. Transportation Research Record No. 497.
106. Kavak, A., Baykal, G. 2012. Long-term behavior of lime-stabilized kaolinite clay. *Environ Earth Sci.* 66:1943–1955 DOI 10.1007/s12665-011-1419-8.
107. Kavazanjian, E., Iglesias, E., & Karatas, I. 2009. Biopolymer soil stabilization for wind erosion control. In *Proceedings of the 17th International Conference on Soil Mechanics and Geotechnical Engineering: The Academia and Practice of Geotechnical Engineering* (pp. 881-884). (Proceedings of the 17th International Conference on Soil Mechanics and Geotechnical Engineering: The Academia and Practice of Geotechnical Engineering; Vol. 1). <https://doi.org/10.3233/978-1-60750-031-5-881>
108. Kavazanjian, E., Karatas, I. 2008. Microbiological Improvement of the Physical Properties of Soil. 6th International Conference on Case Histories in Geotechnical Engineering, Arlington, Virginia, August 2008.
109. Kayser, M. 2014. Investigation of Soil Erodibility using In Situ Erosion Evaluation Probe (ISEEP). PhD dissertation, North Carolina.
110. Khan L.I. and M. Sarker. 1993. Enzyme Enhanced Stabilization of Soil and Fly Ash. *Fly Ash for Soil Improvement. ASCE GSP 36.* New York. 1993. 43-58.
111. Khan, T.A., Taha, M.R., Khan, M.M., Shah, S.A., Aslam, M.A., Waqar, A., Khan, A.R., Waseem, M. 2020. Strength and Volume Change Characteristics of Clayey Soils: Performance Evaluation of Enzymes. *Minerals* 2020, 10, 52.

112. Knodel, P. C. 1987. Lime in canal and dam stabilization, US Bureau of Reclamation, Report No GR-87-10, 21 p.
113. Lagasse, P. F., Zevenbergen, L.W., Spitz, W. J., and Thorne, C.R. 2004. "Methodology for predicting channel migration." NCHRP web only document 67 (Project 24-16), TRB Washington DC, USA.
114. Le Runigo, B., Ferber, V., Cui, Y-J., Cuisinier, O., Deneele, D. 2011. Performance of lime-treated silty soil under long-term hydraulic conditions. *Engineering Geology*, Elsevier, 2011, 118 (1-2), pp.20-28.
10.1016/j.enggeo.2010.12.002. hal-00574328.
115. Lefebvre, G., Rohan, K., Douville, S. 1985. Erosivity of natural intact structured clay: Evaluation. *Canadian Geotechnical Journal*. Vol. 22, pp. 508-517.
116. Levees | ASCE's 2021 Infrastructure Report Card.
117. Lime-treated soil construction manual. Lime stabilization & lime modification. National Lime Association. 2004.
118. Little D.L. 1995. Handbook for Stabilization of Pavement Subgrades and Base Courses with Lime, Kendall/Hunt. Publishing Company, Dubuque, Iowa, 1995.
119. Little, D. 1999. Evaluation of structural properties of lime stabilized soils and aggregates. Volume 1. Summary of findings.
120. Lyle, W. M., Smerdon, E. T. 1965. Relation of compaction and other soil properties to erosion resistance of soils. *Transactions of the ASAE*. Vol. 8(3), pp. 419-422. 284-298.

121. McNeil, J., Taylor, C., Lick, W. 1996. Measurements of Erosion of Undisturbed Bottom Sediments with Depth. *Journal of Hydraulic Engineering*. June 1996. Vol. 122 (6), pp. 316-324.
122. Mississippi River breaches Pin Oak levee in Winfield, flooding homes in Lincoln County, Missouri | cbs8.com
123. Mitchell, J.K. and Santamarina, J.C. (2005) Biological Considerations in Geotechnical Engineering. *J Geotech Geoenviron Eng* 131, 1222– 1233.
124. Montalvo Bartolomei, A.M. 2014. “Observation method to predict meander migration and vertical degradation of rivers”, Master of Science thesis, Zachry Dpt. of Civil Engineering, Texas A&M University, College Station, Texas, USA, pp.153.
125. Montoya, B. M., J. Do, and M. M. Gabr. 2018. “Erodibility of microbial induced carbonate precipitation-stabilized sand under submerged impinging jet.” In *Proc., IFCEE 2018*, 19–28. Reston, VA: ASCE.
126. Moody, L.F. (1944). "Friction Factors for Pipe Flow". *Transactions of the ASME*. 66 (8): 671–684.
127. Moore, W. L., Masch, F. D., Jr. 1962. Experiments on the scour resistance of cohesive sediments. *Journal of Geophysical Research*, Vol. 67(4), pp. 1437-1449.
128. Moriwaki, Y. and Mitchell, J. K., 1977. "The Role of Dispersion in the Slaking of Intact Clay," *Dispersive Clays, Related Piping, and Erosion in Geotechnical Projects*, ASTM STP 623, J. L. Sherard and R. S. Decker, Eds., American Society for Testing and Materials, pp. 287-302.

129. Mortensen, B.M., Haber, M.J., DeJong, J.T., Caslake, L.F., and Nelson, D.C. "Effects of Environmental Factors on Microbial Induced Calcium Carbonate Precipitation" *Applied Microbiology*, 2011, Vol. 111, Issue 2, pp. 338-349.
130. Muguda, S, Nagaraj, H.B. 2019. Effect of enzymes on plasticity and strength characteristics of an earthen construction material. *Geo-Engineering* (2019) 10:2 <https://doi.org/10.1186/s40703-019-0098-2>. 14 p.
131. Munson, Bruce R., Young, Donald F., Okiishi, Theodore H., Huebsch, Wade W. 2009. *Fundamentals of Fluid Mechanics, Sixth Edition*. John Wiley & Sons, Inc. ISBN 978-0470-26284-9.
132. Nanson, G.C., and Hickin, E.J. 1986. "A statistical analysis of bank erosion and channel migration in western Canada", *Geological Society of America Bulletin*, v.97, p. 497-504.
133. National Levee Database, <https://levees.sec.usace.army.mil/#/>
134. Nerinx N., Bonelli S., Puiatti D., Herrier G., Fry J.J., Tourment R., Nicaise S. 2016. *Impact of Lime Treated Soils Performance on Design of Earthfill Dams and Dykes. Appropriate technology to ensure proper Development, Operation and Maintenance of Dams in Developing Countries* © SANCOLD, ISBN 978-0-620-71042-8.
135. NOAA. "Hurricane Harvey," https://www.nhc.noaa.gov/data/tcr/AL092017_Harvey.pdf. Page 7. Accessed June 6, 2021.
136. Perma-Zyme. *Substrata. Safety Data Sheet*. 2020.

137. Perry J.P. 1977. Lime treatment of dams constructed with dispersive clay soil. Transactions of the ASAE. 20:1093–1099.
138. Phillips, J.V., and Tadayon, S. 2006. Selection of Manning’s roughness coefficient for natural and constructed vegetated and non-vegetated channels, and vegetation maintenance plan guidelines for vegetated channels in central Arizona: U.S. Geological Survey Scientific Investigations Report 2006–5108, 41 p.
139. Pooni, J., Giustozzi F., Robert, D., Setunge, S., O'Donnell, B. 2019. Durability of enzyme stabilized expansive soil in road pavements subjected to moisture degradation. Transportation geotechnics 21 (2019). 100255.
140. Rajoria, V., Kaur, S. (2014). A Review on stabilization of soil using bio-enzyme. International Journal of Research in Engineering and Technology. Volume: 03 Issue: 01 | Jan-2014. P. 75-78. eISSN: 2319-1163 | pISSN: 2321-7308.
141. Richards, K., Reddy, K. 2010. True Triaxial Piping Test Apparatus for Evaluation of Piping Potential in Earth Structures. Geotechnical Testing Journal 33(1).
142. Rivas, T., AuBuchon, J., Shidlovskaya, A., Langendoen, E.D., Work, P., Livsey, D., Timchenko, A., James, K., Briaud, J.-L. Risk-informed levee erosion countermeasure site selection and design in the Sacramento area. Part 1 and Part 2. 10th International Conference on Scour and Erosion (ICSE). 2021.
143. Roberts, J.D., Jepsen, R.A., James, S.C. 2003. Measurement of Sediment Erosion and Transport with the Adjustable Shear Stress Erosion and Transport Flume. Journal of Hydraulic Engineering. Nov. 2003. Vol. 129(11), pp. 862-871.

144. Sahoo, S., Sridevi, G., Raman, C.V., Raju, B.V. 2018. Soil Stabilization Using Bio-Enzyme. *International Journal of Pure and Applied Mathematics*. Volume 118 No. 24 2018. ISSN: 1314-3395 (on-line version) url: [http://www.acadpubl.eu/hub/Special Issue](http://www.acadpubl.eu/hub/Special%20Issue).
145. Saini, V., and Vaishnava, P., 2015, "Soil stabilization by using TerraZyme", *International Journal of Advances in Engineering and Technology*, ISSN: 22311963.
146. Salifu, E., E. MacLachlan, K. R. Iyer, C. W. Knapp, and A. Tarantino. 2016. "Application of microbially induced calcite precipitation in erosion mitigation and stabilization of sandy soil for foreshore slopes: A preliminary investigation." *Eng. Geol.* 201 (Feb): 96–105. <https://doi.org/10.1016/j.enggeo.2015.12.027>.
147. Salim, S., Jayarathe, R., Wijeyesekera, C. 2011. Soil protrusion apparatus for erosion rate prediction with smooth and rough sediment beds. *Advances in Computing and Technology*. The School of Computing, Information Technology and Engineering, 6th Annual Conference 2011.
148. Santamarina, C., Torres-Cruz, L.A., Bachus, R.C. 2019. Why coal ash and tailings dam disasters occur. *Science* 364 (6440), 526-528. DOI: 10.1126/science.aax1927. <http://science.sciencemag.org/content/364/6440/526>.
149. Santoni, R. L., J. S. Tingle, and M. Nieves. 2005. Accelerated Strength Improvement of Silty Sand with Nontraditional Additives. In *Transportation Research Record: Journal of the Transportation Research Board*, No. 1936, Transportation Research Board of the National Academies, Washington, D.C., 2005, pp. 34–42.

150. Santoni, R. L., J. S. Tingle, and S. L. Webster. 2002. Stabilization of Silty Sand with Nontraditional Additives. In *Transportation Research Record: Journal of the Transportation Research Board*, No. 1787, Transportation Research Board of the National Academies, Washington, D.C., 2002, pp. 61–70.
151. Schery, R.W. 1973. *A perfect lawn, the easy way*. New York: Macmillan. viii, 294 pages: illustrations; 24 cm.
152. Seed, H.B., and Duncan, J.M. 1981. “The Teton dam failure – a retrospective review.” *Proc. of 10th Int. Conf. Soil Mechanics and Found. Eng.*, 3: 219-238.
153. Seijffert, J. W., and Verheij, H. 1999. Grass covers and reinforcement measures, Chapter 14, Rijkswaterstaat, Hydraulic Engineering Division, Delft, The Netherlands, 289–302.
154. Shafii I., Shidlovskaya A., Briaud J.-L. 2018. Investigation into the Effect of Enzymes on the Erodibility of a Low-Plasticity Silt and a Silty Sand by EFA Testing. *Journal of Geotechnical and Geoenvironmental Engineering*. ASCE, ISSN 1090-0241.
155. Shafii, I., Briaud, J.-L., Chen, H.C., Shidlovskaya, A., 2016, “Relationship between soil erodibility and engineering properties”, *Proceedings of the 8th International Conference on Scour and Erosion* (Oxford, UK, 12-15 September 2016), Eds. John Harris, Richard Whitehouse, Sarah Moxon, CRC Press, Taylor and Francis.

156. Shaikh, A., Ruff, J. F., Charlie, W.A. and Abt, S.R. 1988. Erosion rate of dispersive and nondispersive clays. *Journal of Geotechnical Engineering*. Vol. 114(5), pp. 589-600.
157. Shan, H., Shen, J., Kilgore, R., Kerényi, K. 2015. Scour in cohesive soils. US Department of Transportation, Federal Highway Administration. Publication No. FHWA-HRT-15-033.
158. Sheppard, D.M., Bloomquist, D., Slagle, P.M. 2006. Rate of erosion properties of rock and clay. Developed for the Florida Department of Transportation. UF Project 00030890 (4554013-12).
159. Sheppard, D.M., Odeh, M., Glasser, T. 2004. Large scale clear-water local pier scour experiments. *Journal of Hydraulic Engineering*. Vol. 130, No. 10. ISSN 0733-9429/2004/10-957.
160. Sherard, J. C., Dunnigan, L. P., and Talbot, J. R. (1984). "Basic properties of sand and gravel filters." *J. Geotech. Engineering*, 110(6), 684–700.8zn*J. Geotech. Engrg.*
161. Sherard, J. L., Dunnigan, L. P., Decker, R. S. and Steele, E. F. 1976. Pinhole test for identifying dispersive soils. *Journal of Geotechnical Engineering Division, ASCE*. Vol. 102, pp. 69-85.
162. Shidlovskaya, A., Briaud, J.-L., Chedid, M., Keshavarz, R., 2016, "Erodibility of soil above the groundwater level: some test results", *Proceedings of the 3rd European Conference on Unsaturated Soils – "E-UNSAT 2016"*, (Paris, France,

- September 12-14, 2016), P. Delage, Y.-J. Cui, S. Ghabezloo, J.-M. Pereira and A.-M. Tang (Eds.), Presse des Ponts et Chaussees.
163. Shidlovskaya, A.V., Shafii, I., Briaud, J.-L. Enzyme Treatment of Soil for Erosion Control. Conference of the European Group-Internal Erosion of Dams, Dikes and Levees and Their Foundations 27th Annual Meeting. Vancouver. Canada. 20 June 2019 (accepted for publication).
164. Silva, W., Dijkman, J., Loucks, D. 2004. Flood management options for the Netherlands. *Intl. J. River Basin Management* Vol. 2, No. 2 (2004), pp. 101–112.
165. Stapledon, D.; MacGregor, P.; Bell, G.; Fell, R. 2005. *Geotechnical Engineering of Dams*, Taylor & Francis Eds.
166. stgec.org (Larry Cole, P.E. Carmeuse Lime and Stone Pittsburgh, PA)
167. Storesund R, Bea RG, Huang Y. (2010) Simulated wave-induced erosion of the Mississippi River–Gulf Outlet Levees during Hurricane Katrina. *J Waterw. Port Coast Ocean Eng.* 136(3):177–189.
168. Taha, M.R., Khan, T.A., Jawad, I.T., Firoozi, A.A., Firoozi, A.A. 2013. Recent experimental studies in soil stabilization with bio-enzymes-a review. *Electronic Journal of Geotechnical Engineering.* January 2013.
169. Tailings dam risk of dangerous occurrences. Lessons learnt from practical experiences. International Commission on Large Dams (ICOLD), United Nations Environment Program (UNEP), Bulletin 121, 2001.
170. TAMU-EROSION database. 2020-2021.
171. TerraZyme. Nature Plus Inc. Dosage Guidelines and Lab Preparation. 2020.

172. The Hydraulic Engineer Circular (HEC 18). 2012. “Evaluating Scour at Bridges”
FHWA NHI 01-001.
173. The LawnInstitute, 2020.
<https://www.thelawninstitute.org/pages/education/lawn-maintenance/let-your-turfgrass-go-dormant/>
174. Thompson, R.F., Wattier, C.M., Liggett, R.R., and Truax, R.A. 2014. Estimation of Potential Scour at Bridges on Local Government Roads in South Dakota, 2009–12. Scientific Investigations Report 2013–5233. US Department of Interior, US Geological Survey.
175. Thornton, C.I., Hughes, S.A., Scholl, B.N., Youngblood, N. 2014. Full-Scale Wave Overwash Resiliency Testing of Dikes and Embankments on Florida Sandy Soils. CSU. Prepared for U.S. Army Corps of Engineers, Jacksonville District Jacksonville, Florida.
176. Thornton, C.I., Scholl, B.N., Abt, S.R. 2010. Wave Overtopping Simulator Testing of Proposed Levee Erosion Protection Methods. Prepared for United States Army Corps of Engineers, New Orleans District. CSU, 2010.
177. Timchenko A., Shidlovskaya, A., Briaud, J.-L. Tolerable risk chart. Proceedings of the 20th International Conference on Soil Mechanics and Geotechnical Engineering, Sydney 2021.
178. Tingle J.S., Santoni, R.L. 2003. Stabilization of Clay Soils with Nontraditional Additives. Transportation Research Record 1819 Paper No. LVR8-1136. P. 72-84.

179. Tingle, J.S., Newman, J.K., Larson, S.L., Weiss, C.A., Rushing, J.F. 2007. Stabilization Mechanisms of Non-traditional Stabilizers. In Transportation Research Record: Journal of the Transportation Research Board, No. 1989, Vol.2, Transportation Research Board of the National Academies, Washington, D.C., pp. 59–67.
180. Trammel, M. 2004. Laboratory apparatus and methodology for determining water erosion rates of erodible rock and cohesive sediments. MS thesis to the University of Florida.
181. U.S. Army Corps of Engineers, “National Inventory of Dams,” 2020 partial update. (Accessed December 09, 2020).
182. U.S. Army Corps of Engineers, “U.S. Army Corps of Engineers Levee Portfolio Report: A Summary of Risks and Benefits Associated with the USACE Levee Portfolio,” March 2018.
183. USEPA (U.S. Environmental Protection Agency). 2014. An Assessment of Potential Mining Impacts on Salmon Ecosystems of Bristol Bay, Alaska. Region 10, Seattle, WA. EPA 910-R-14-001.
184. USGS Publication Repository. <https://pubs.usgs.gov>
185. Van Paassen, L. A. 2009. Biogrout: Ground Improvement by Microbially Induced Carbonate Precipitation. Delft University of Technology.
186. Velasquez R., M.O. Marasteanu, R. Hozalski & T. Clyne. 2005. Preliminary Laboratory investigation of Enzyme solutions as a soil stabilizer. Research Report MN/RC-2005-25. University of Minnesota, USA.

187. Wahl, T. L., Regazzoni, P. L., Erdogan, Z. 2009. Practical improvements for the Hole Erosion Test. 33rd IAHR Congress, Vancouver, BC, Canada.
188. Wahl, T.L. 2010. A Comparison of the Hole Erosion Test and JET Erosion Test. Joint Federal Interagency Conference on Sedimentation and Hydrologic Modeling June 27 - July 1, 2010 --- Las Vegas, NV.
189. Wan, C. F., Fell, R. (2004). Investigation of rate of erosion of soils in embankment dams. *Journal of Geotechnical and Geoenvironmental Engineering*. Vol. 130(4), pp. 373-380.
190. Wan, C. F., Fell, R. 2002. Investigation of internal erosion and piping of soils in embankment dams by the slot erosion test and the hole erosion test. UNICIV Report R-412. The University of New South Wales.
191. Whitehead, E., Schiele, M., Bull, W. 1976. A guide to the use of grass in hydraulic engineering practice, CIRIA Technical Note 71. Construction and Industry Research and Information Association: London, UK.
192. Whitehead, E., Schiele, M., Bull, W. A guide to the use of grass in hydraulic engineering practice, CIRIA Technical Note 71. Construction and Industry Research and Information Association: London, UK, 1976.
193. Whitman, R.V. 1984. Evaluating calculated risk in geotechnical engineering. *Journal of Geotechnical engineering* 110(2), 143-188.
194. WISE. World Information Service on Energy Uranium Project (<http://www.wise-uranium.org/mdaf.html>) as of June 5, 2021.

195. World mine tailings portfolio 2021. World Mine Tailings Failures—from 1915 – supporting global research in tailings failure root cause, loss prevention and trend analysis.